

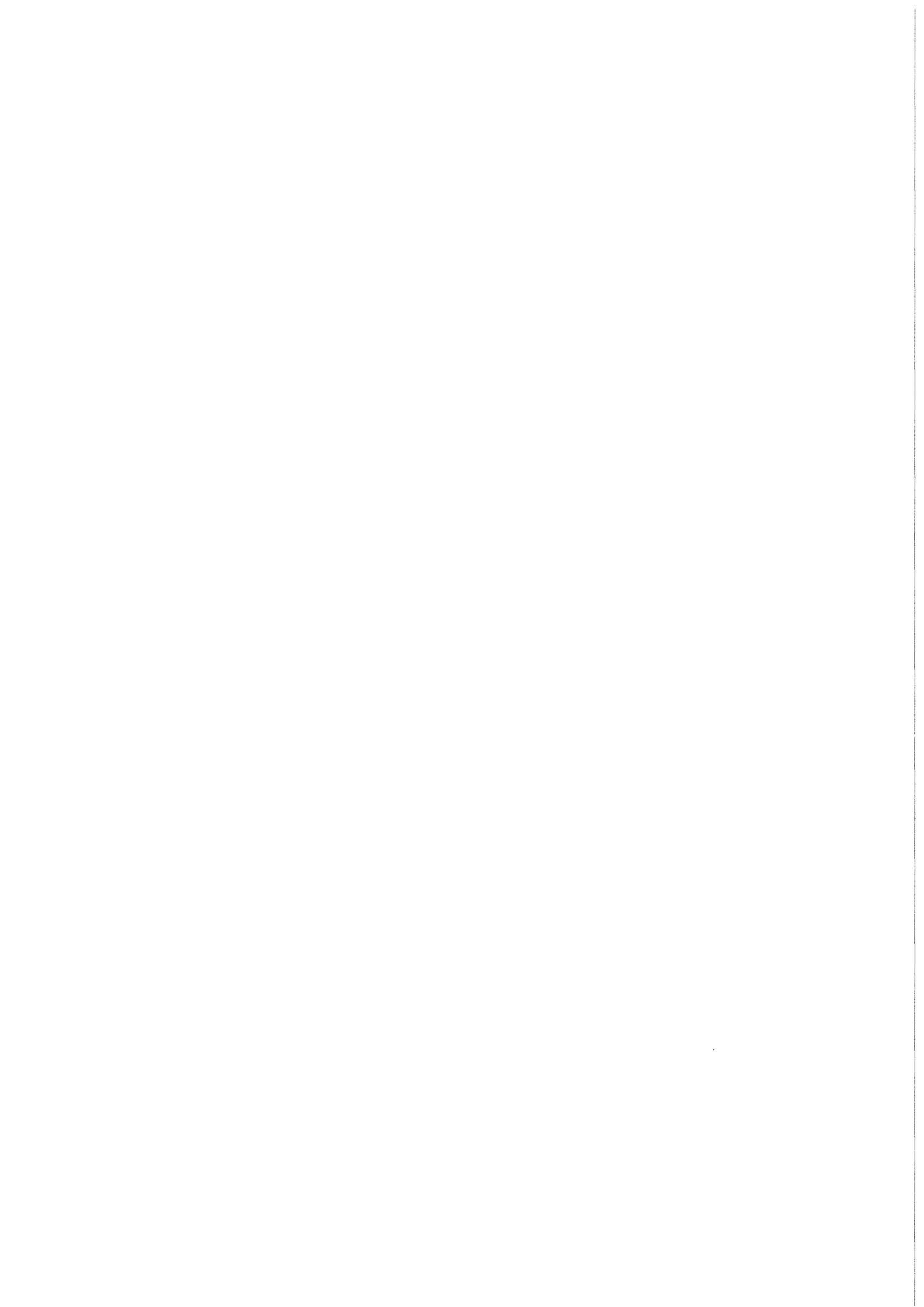
KfK 4279  
IWGFR/64  
August 1987

# **Fission and Corrosion Products Behavior in Primary Circuits of LMFBR's**

**Proceedings of an  
International Atomic Energy Agency  
Specialist's Meeting  
International Working Group on Fast Reactors  
Karlsruhe, Federal Republic of Germany,  
May 5 - 8, 1987**

**Editors:  
H. Feuerstein, A. W. Thorley  
Hauptabteilung Ingenieurtechnik**

**Kernforschungszentrum Karlsruhe**



**KERNFORSCHUNGSZENTRUM KARLSRUHE  
HAUPTABTEILUNG INGENIEURTECHNIK**

**KfK 4279  
IWGFR/64**

**FISSION AND CORROSION PRODUCTS BEHAVIOR  
IN PRIMARY CIRCUITS OF LMFBR's**

**Proceedings of an  
International Atomic Energy Agency Specialists' Meeting  
International Working Group on Fast Reactors  
Karlsruhe, Federal Republic of Germany, May 5-8, 1987**

**Editors: H. Feuerstein  
A.W. Thorley\***

**Kernforschungszentrum Karlsruhe GmbH, Karlsruhe**

**\*UKAEA, Risley Nuclear Power Development Laboratory**

Als Manuskript vervielfältigt  
Für diesen Bericht behalten wir uns alle Rechte vor

Kernforschungszentrum Karlsruhe GmbH  
Postfach 3640, 7500 Karlsruhe 1

ISSN 0303-4003



**Meeting Chairman:** H. Feuerstein,  
Kernforschungszentrum Karlsruhe  
Hauptabteilung Ingenieurtechnik

**Co-Chairmen:** H.H. Stamm,  
Kernforschungszentrum Karlsruhe,  
Institut für Radiochemie

K.Ch. Stade,  
Kernkraftwerk Betriebsgesellschaft,  
Fast Breeder Reactor KNK-II

**Scientific Secretary  
of IWGFR:** V. Arkhipov,  
International Atomic Energy Agency,  
Vienna

## CONTENTS

|   | page |
|---|------|
| 1. Agenda   | 3    |
| 2. Participants   | 5    |
| 3. Summary, Conclusions and Recommendations   | 9    |
| 4. Papers:  | 15   |
| N. Aoki, K. Wada, M. Uotani, N. Yokota,<br>J. Horie, N. Nakao;<br>Evaluation of Corrosion Products Behavior<br>in Pool Type FBRs  | 17   |
| Yu.G. Bobkov, I.A. Efimov, Yu.I. Zagoroul'ko,<br>E.I. In'utin, E.E. Konovalov, A.I. Lastov, A.G. Zikunov;<br>Radionuclides Behaviour in Sodium Coolant                              | 41   |
| R. Borsari, J.P. Hairion;<br>P.S.1. Experiment<br>Release and Behaviour of Fission Products and<br>Fuel inside a Sodium-Irradiation Loop  | 61   |
| W.F. Brehm, R.P. Colburn, H.P. Maffei, W.P. Stinson,<br>W.L. Bunch, A. Bechtold;<br>Corrosion and Fission Products in Primary Systems<br>of Liquid Metal Cooled Reactors in the USA | 75   |
| R. Clerc, J. Guidez, P. Maux, P. Michaille, J. Misraki, D. Msika;<br>The French Experience concerning the Contamination<br>of the LMFBRs  | 93   |
| R. Clerc, J. Guidez, P. Michaille, J. Misraki;<br>"Bilan des Mesures de Contamination Effectuees<br>a Phenix au 1er Avril 1987"   | 141  |
| N. Hanebeck, R. Tusche, D. Msika, J. Misraki, R. Allegre;<br>The Development of Cesium Traps for Commercial<br>Sodium-Cooled Fast Breeder Reactors                                  | 187  |
| K. Iizawa, T. Kikuchi, I. Nihei, J. Horie;<br>Calculational Model and Code for Corrosion Products<br>Transfer in Sodium Systems   | 191  |
| K. Iizawa, S. Suzuki, M. Tamura, S. Seki, T. Hikichi;<br>Study on Radioactive Corrosion Products Behaviour<br>in Primary Circuits of JOYO   | 227  |

|   |     |
|---|-----|
| R.P. Kapoor, D.S. Mitragotri, G. Periaswami;<br>Programme of Work at Indira Gandhi Centre for<br>Atomic Research (IGCAR) regarding Activity Transport<br>in Sodium Systems                                | 257 |
| V.D. Kizin, V.V. Konyashov;<br>Calculated Model of Radioactive Fission and Corrosion<br>Product Accumulation and Distribution in a Fast Reactor<br>Sodium Coolant Circuit                                 | 271 |
| V.D. Kizin, N.V. Krasnoyarov, V.I. Polyakov, E.K. Yakshin;<br>Study of Radionuclide Distribution in BOR-60  | 285 |
| L. Mason, E.A. Trevillion, N.S. Morrison, K.B. Steele, T.H. Green;<br>Measurements of Fission Products and Activated Corrosion<br>Products in the Primary Sodium Circuit of the Prototype<br>Fast Reactor | 297 |
| M.A. Mignanelli, P.E. Potter;<br>On the Chemistry of Defective Fuel Pins in LMFBRs  | 321 |
| V.I. Polyakov;<br>Methods for Measurement of Gamma-Emitting Nuclide<br>Activities in a Fast Reactor Circuit   | 349 |
| H.H. Stamm, K.Ch. Stade;<br>Filtration Experiments of the KNK II Primary Sodium   | 367 |
| H.H. Stamm, K.Ch. Stade;<br>Radiochemical Surveillance of KNK Primary Sodium  | 385 |
| H. Taki, K. Hata, K. Iizawa;<br>Transport Behavior of Cs and I in Sodium Vapor Trap   | 419 |
| A.W. Thorley;<br>Fission and Corrosion Product Behaviour in Primary<br>Circuits of LMFBR's  | 433 |
| N. Yokota, Sh. Shimoyashiki, J. Horie;<br>Precipitation Mechanism of Corrosion Products<br>Released from Type 304 Stainless Steel in Liquid Sodium  | 469 |

A G E N D A

Monday, May 4 1987

19.30 Informal meeting of the participants

Tuesday, May 5 1987

9.00 OPENING ADDRESS

W.Marth  
Head of the Fast Breeder Project (PSB),  
Nuclear Research Center Karlsruhe  
V.Arkipov  
Scientific Secretary of the IWGFR,  
IAEA, Vienna

9.30 - 11.45 SESSION 1: CORROSION PRODUCTS  
Chairman W.F.Brehm

Source Term of Radioactive Corrosion Products,  
Mass Transfer and Deposition, Diffusion into  
Steel, Particles: Formation and Behavior,  
Removal of Corrosion Products by Traps,  
(Decontamination)

12.00 Lunch

13.30 - 14.45 SESSION 2: FISSION PRODUCTS  
Chairman P.Michaille

Background Level, Release from Breached Fuel  
Pins, Influence of Chemical Reactions,  
Deposition and Redissolution, Transport to the  
Covergas (Rare Gases and Alkaline Metals),  
Aerosols, Tritium, Removal from Sodium by Traps

15.00 Visit of KNK-II  
Organized by H.Richard and K.Ch.Stade

18.30 Reception  
(Bus to the hotel at 20.30)

Wednesday, May 6, 1987

9.00 - 11.45 SESSION 3: FUEL  
Chairman P.E.Potter

Release from Breached Fuel Pins, Chemistry of  
the Release, Oxygen Levels in Sodium, Deposition  
of Fuel, Carbide Fuel

12.00 Lunch



## **PARTICIPANTS**

### **Federal Republic of Germany**

H. Feuerstein (Meeting Chairman)  
Kernforschungszentrum Karlsruhe  
GmbH  
Postfach 3640  
D-7500 Karlsruhe

N. Hanebeck  
INTERATOM GmbH  
Postfach  
D 5060 Bergisch-Gladbach 1

K. Ch. Stade, (Co-Chairman)  
Kernkraftwerk Betriebsgesellschaft  
GmbH  
KNK-II  
D-7514 Eggenstein-Leopoldshafen

H.H. Stamm, (Co-Chairman)  
Kernforschungszentrum Karlsruhe  
GmbH  
Postfach 3640  
D-7500 Karlsruhe

### **France**

J. Guidez  
CEA  
B.P. 171  
F 30205 Bagnols sur Ceze  
CEDEX

P. Michaille  
Div. Études et Développement des  
Réacteurs  
Centre d'Etudes Nucléaires de  
Cadarache  
B.P. 1  
F 13115 Saint Paul lez Durance

Mrs. J. Misraki  
Div. Études et Développement des  
Réacteurs  
Centre d'Etudes Nucléaires de  
Cadarache  
B.P. 1  
F 13115 Saint Paul lez Durance

### **India**

R.P. Kapoor  
Techn. Services Superintendent (FBTR)  
Indira Gandhi Centre for Atomic  
Research  
Kalpakkam 603 102 Tamil Nadu

### **Italy**

R. Borsari  
ENEA  
Via Martiri di Monte Sole 4  
Bologna

P. Cecchi  
ENEA  
Via Martiri di Monte Sole 4  
Bologna

### **Japan**

K. Iizawa  
Power Reactor and Nuclear Fuel  
Development Co, Tokyo  
4002 Narita-cho, Oarai-machi  
Higashi Ibaraki-gun, Ibaraki-ken  
311-13 Japan

H. Taki  
Omiya Technical Institute  
Mitsubishi Atomic Power Industry Ltd.  
1-297 Kitabukuro-machi  
Omiya-shi, Saitama-ken  
330 Japan

N. Yokota  
Energy Research Laboratory  
Hitachi, Ltd.  
1168 Moriyama-cho  
Hitachi-shi, Ibaraki-ken  
316 Japan

United Kingdom

P.E. Potter  
UKAEA  
Harwell Laboratory  
Chemistry Division  
Oxfordshire, OX11 0RA

A.W. Thorley  
UKAEA  
Risley Nuclear Power  
Development Laboratory  
Risley, Warrington  
Cheshire, WA3 6AT

E.A. Trevillion  
UKAEA  
Dounreay Nuclear Power  
Development Establishment  
PFR Division  
Thurso, Caithness  
KW14 7TZ

USA

W. F. Brehm  
USDOE  
Westinghouse Hanford Laboratory  
P.O. Box 1970  
W/C 53, Richland, WA 99352

USSR

J.G. Bobkov  
Inst. of Physics and Power Engineering  
Obninsk

E.K. Jakshin  
Scientific and Research Institute  
of Atomic Reactors  
Dimitrovgrad

J.I. Zagorulko  
Inst. of Physics and Power Engineering  
Obninsk

CEC

H. Blank  
Commission of the European  
Communities  
Joint Research Center Karlsruhe  
P.O. Box 2340  
D-7500 Karlsruhe  
FRG

H.J. de Nordwall  
Commission of the European  
Communities  
dg xii/d/2  
200 Rue de la Loi  
B 1049 Brussels  
Belgium

IAEA

V. Arkhipov  
Scientific Secretary IWGFR  
International Atomic Energy Agency  
Wagramerstr. 5  
P.O. Box 100  
A 1400 Vienna  
Österreich

Observers

Venkata Subramani, S.C.R.,  
Kalpakkam, India

N.P. Bhat,,  
Kalpakkam, India

G. Petzold, SBK, FRG

S. Jacobi, KfK, FRG

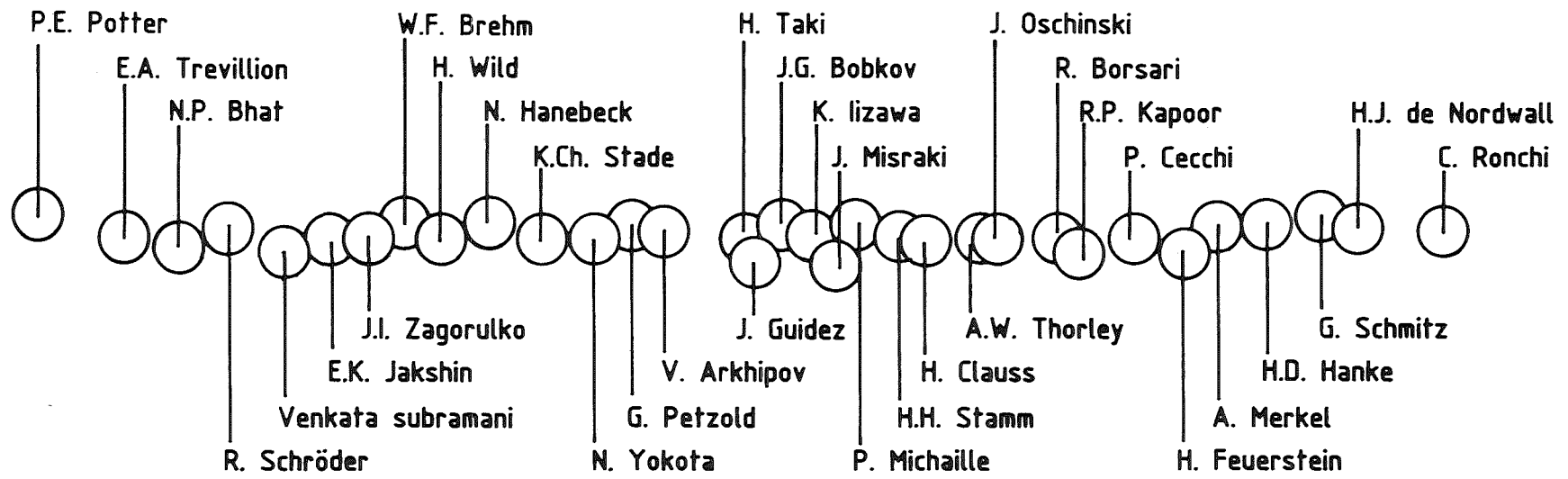
H. Wild, KfK, FRG

G. Schmitz, KfK, FRG

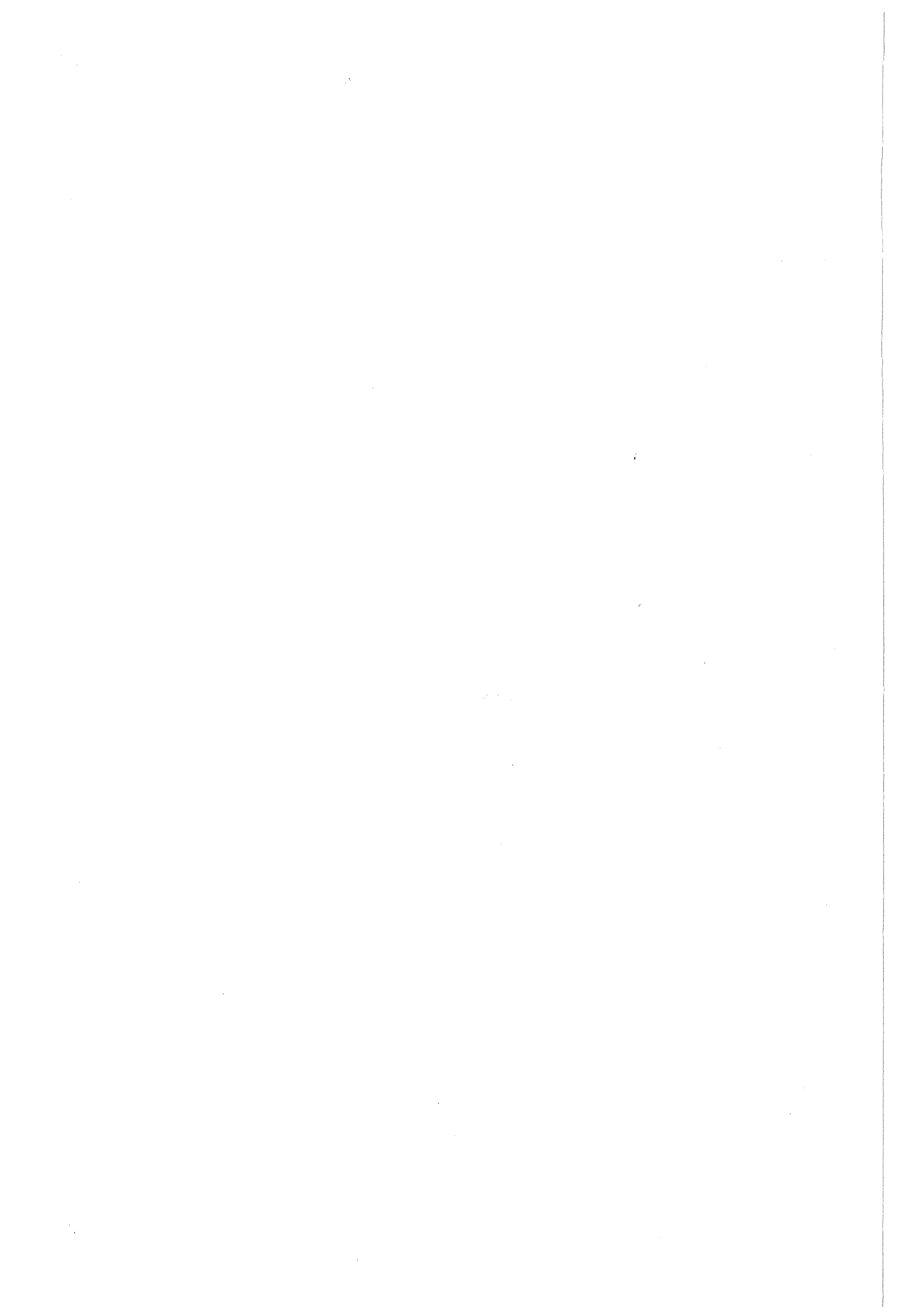
J. Wagner,  
Interatom, FRG

A. Merkel,  
Interatom, FRG

C. Ronchi,  
CEC-Karlsruhe, FRG







FISSION AND CORROSION PRODUCTS BEHAVIOUR IN PRIMARY CIRCUITS OF LMFBR's  
KARLSRUHE, 5-8 MAY 1987

**SUMMARY, CONCLUSIONS AND RECOMMENDATIONS**

1. Corrosion and Mass Transfer of Corrosion Products

For source term estimates the delegates considered that the corrosion of stainless fuel cladding is now reasonably well understood. Mass-transfer studies undertaken in the mock up loops and other test systems, since the Dimitrovgrad meeting, have identified that 60Co can be retained in the corrosion zone and that 54Mn release is enhanced by diffusion from the substrate of the corroding steel. Also similar experiments have shown that the deposition of 60Co is enhanced at the hot-end of a simulated IHX while the deposition of 54Mn increases at the cold-end.

Reactor experiments performed in Phenix using samples placed in the IHX also indicate a decrease in Co level and an increase in Mn level from the hot to the cold parts of the IHX. This finding is consistent with model predictions. It should also be noted that the Phenix measurements also include values for the distribution of 63Ni for the first time. However, because the distribution of this element is different to 54Mn it is thought that co-precipitation of these two elements may not be occurring in the cooler parts of the IHX.

Experience from KNK and loop studies have shown evidence of particles circulating in flowing sodium environments. Although the source of some of the particles in KNK is not known, it appears that in the loop systems particles can originate by oxidation of steel surface, generally downstream of the high temperature part of the system, or by precipitation. The delegates agreed that the effect of particles on mass-transfer corrosion model predictions requires further assessment, especially as current models are based on dissolved species.

New evidence from BR-10 has shown that both 60Co and 54Mn can adsorb onto and penetrate into stainless steel pipework at moderate temperatures (350-430°C) after 120,000 hrs reactor operation. This observation could influence decontamination procedures when active components are removed from operating systems. KNK experience also indicates that alloys such as Stellite, Colmonoy and other high Co materials can attract 54Mn and influence decontamination procedures.

For the control of 54Mn the US have now demonstrated in EBR2 and in FFTF that expanded surfaces of pure nickel installed in an assembly above the fuel pins effectively removes this element from sodium systems. No operating difficulties, caused by flow or temperature instabilities, were recorded during the testing of seven assemblies in reactor environments. The traps proved to be capable of removing 54Mn from the entire circuit as well as from the underlying fuel assembly, implying that a smaller number of traps can be installed above the core to control the level of 54Mn. Despite this promising development there are no plans to install traps on operating systems, although some consideration is being given to their possible use on MONJU.

2. Fission Products

All delegates agreed that the main fission product of concern was 137Cs. French experience in Rapsodie indicated that about half the caesium was

trapped in the two primary cold traps and 17% was estimated to be in the sodium aerosols. This latter high level could be due however to the high gas flow rates used in Rapsodie. The total amount of caesium measured in all parts of the reactor was in satisfactory agreement with estimated amounts of release from fuel examinations.

Measurement undertaken in PFR and the Siloe PS1 experiment indicate that <sup>137</sup>Cs release fractions were about 40% (early PFR failures) and 70% respectively. Release fractions obtained in Siloe for <sup>131</sup>I and <sup>132</sup>Te were about 4%, <sup>95</sup>Zr and <sup>103</sup>Ru about 0.2% and <sup>140</sup>Ba about 1%. In the Siloe experiments some of the <sup>140</sup>Ba was not released in the same way as fuel, but was released as a pre-cursor. By contrast Zr, Ru and some of the Ba were released in a way similar to the fuel. The cold trap effectively removed both iodine and tellurium but a smaller fraction of Cs. Results from advanced mixed oxide fuel pins installed in BOR-60 also showed lower release fractions for this nuclide, compared to UO<sub>2</sub> fuel used earlier. However, recorded release rates in the range 20-70%, were thought to be dependent upon a number of factors.

The partition coefficient\* for <sup>137</sup>Cs between sodium and reactor surfaces in BOR-60 has increased from an earlier value of about 0.7 to 2 (0.3 on BN350). The increase was thought to be due to continuous ingress of small amounts of oil into the reactor. Distribution coefficients on steel were considered by the Soviet delegates to be associated with physical adsorption phenomena whereas with graphite the adsorption was considered to be chemical in nature. It was also noted that the removal of oxygen from sodium decreased the amount of Cs deposited onto stainless surfaces at low Cs concentrations.

Experience on reactor systems has identified that Cs may cause high radiation levels in cover gas spaces as well as in cold-trap regions, thus causing operating problems in both parts of the system. However, the use of reticulated vitreous carbon (RVC) and certain porous carbonaceous materials to remove this contaminant, in both experimental loop and the reactor system, has been successfully demonstrated. Nevertheless, there are indications that contamination of sodium cooled surfaces by oil or carbon species may promote situations where Cs may be difficult to remove.

Tritium balance measurements made on PFR are now providing good agreement between estimated and literature values for fission yield. There was no evidence to suggest that hot traps were required for tritium removal due to the high efficiency of the cold trap in removing this element. There were also no operating difficulties in any reactors resulting from release of tritium. However, requalification of cold traps containing tritium still requires further investigation.

### 3. Fuel

Experience with failed pins in reactor systems - additional to those reported at the Dimitrovgrad meeting - have not identified any major operating problems and generally speaking the amount of fuel entering the primary sodium is low. Experimental work started in the UK since the Dimitrovgrad meeting has now improved our knowledge of chemical reactions between sodium

---

\*Partition coefficient defined as  $\frac{\text{curies/cm}^2 \text{ (surface)}}{\text{curies/cm}^3 \text{ (bulk sodium)}}$

and fuel and the way such reactions could lead to the contamination of primary circuits. The delegates noted with interest the presentation made by Mr Kapoor regarding the use of carbide fuel in the Fast Breeder Test Reactor (FBTR) at Kalpakkam.

#### 4. Measuring Techniques and Analytical Procedures

Sampling techniques involving dip samplers, overflow methods and multi-purpose samplers are now being used to extract samples from liquid sodium systems. Statistical treatment of results obtained from KNK has identified that better reproducibility is obtained with those radionuclides that are readily soluble in sodium. Selected crucible materials have to be used for certain elements and materials ranging from Ta, Ni, stainless steel, quartz and Pyrex are being used. To obtain more representative results certain countries prefer to dissolve the sodium before measurement.

Methods to study the behaviour of particles in primary sodium systems by using filter assemblies are being investigated. It was noted that the design and location of filtering devices in sodium systems is important if sampling techniques are to be successful. Also isokinetic samplers are required if the measurements are to be representative.

Dose rate measurement using thermo-luminescent dosimeters (TLD's) are now being undertaken on certain reactors. Reliable measurements have been obtained using TLD's up to temperatures of 250°C. Higher temperature detectors are now under development.

#### 5. Reactor Experience

Since the Dimitrovgrad meeting seven new plants have been commissioned providing approximately 100 reactor-years operation. These systems have not identified a major irradiation/contamination problem. Also means of removing the major radionuclides from these systems with on-line devices have been established.

Sodium samples removed from operating reactor systems show increasing levels of Cs reflecting fuel failures in operating cores. The presence of certain elements, eg Zn in KNK, were either found to be peculiar to the reactor system, or their origins were difficult to establish (Ag, Sb). Corrosion product levels (Mn, Co) in the sodium measured during different periods of reactor operation were found to be small and variable. Direct and indirect evidence for the presence of radioactive particles in primary sodium has been found in sodium samples and during vault scans. It also appears that particles containing Mn and Co may be collecting on the bottom of the reactor vessel below the diagrid.

Measurements of  $^{54}\text{Mn}$ ,  $^{58}\text{Co}$ ,  $^{60}\text{Co}$  in different reactor systems have identified different distributions of these elements on component surfaces. Direct gamma measurements on the IHX of Phenix were consistent with predicted behaviour, namely, most  $^{54}\text{Mn}$  deposits in the lower temperature part of the unit. In-contrast JOYO showed a more or less homogeneous distribution of  $^{54}\text{Mn}$  in both hot- and cold-leg pipework, while  $^{60}\text{Co}$  was relatively more prevalent in the cold leg of BOR-60.

Dose rates measured on pipework were in the range 20-500 mR/hr for some reactor systems. Higher dose rates, several R's/hr, were found however, in more important components such as the IHX, pumps, at the sodium-gas interface within the components, and in the aerosol filter. Although the major

contaminant in the cover-gas spaces was  $^{137}\text{Cs}$ , small amounts of both  $^{54}\text{Mn}$  and  $^{60}\text{Co}$  were also identified. However, Cs transfer to the cover-gas can be prevented by trapping techniques using RVC and similar control can also be applied to  $^{54}\text{Mn}$  through the use of nickel traps (see earlier).

It was recognised by the delegates that all LMFBR's were now operating with failed fuel-pins. The delegates agreed however, that the question concerning acceptable numbers of failed pins could only be answered by continuing plant operation and the analysis of proper constraints. It was apparent that confidence in operating systems with failed pins was now being generated in most countries, however, the delegates thought it was too early, at this stage, to specify an acceptable number.

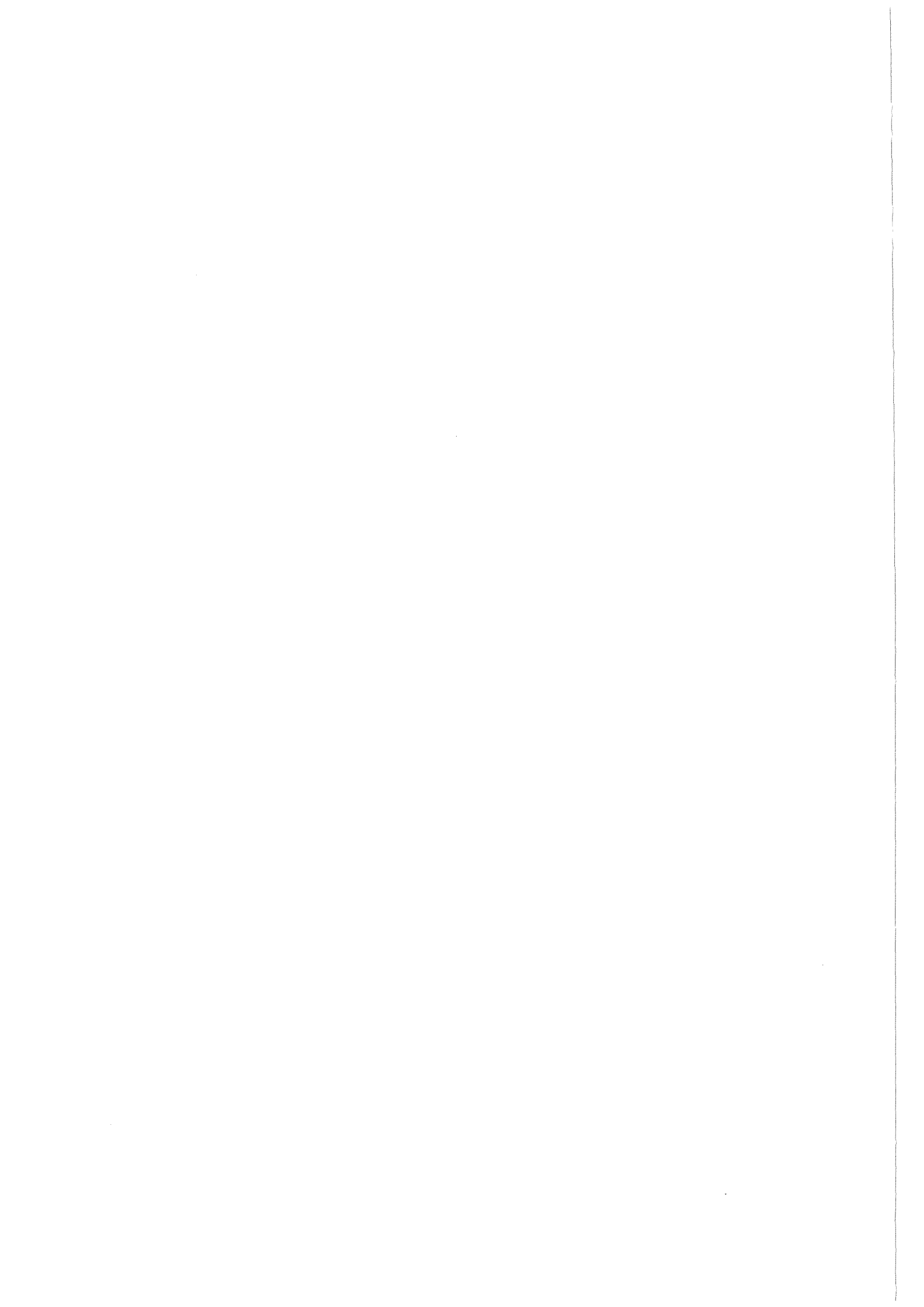
#### 6. Codes and Models

Since the Dimitrovgrad meeting models describing fission gas release, fission product behaviour and the mass-transfer behaviour of corrosion products have been developed by most countries. In addition some codes were being applied to evaluate corrosion product behaviour and control in future LMFBR's. Although in the case of the mass-transfer of corrosion products the results from some reactor systems were within a factor of 2 to 5 of estimated values, the agreement was not so good for FFTF and PFR. However, since Dimitrovgrad the understanding of the role of certain model parameters has improved. A model related to particle behaviour in water and gaseous environments is now being studied in the UK to see whether it can be applied to sodium systems. Also in the UK a model to predict the likely consequences of fuel clad failure on circuit contamination levels is being developed (see section 3).

#### 7. Recommendations

1. Because  $^{54}\text{Mn}$  appears to be readily released from fuel element cladding a better understanding is required of the way it deposits in sodium systems. Current estimates of behaviour are based on mass-transfer coefficients which are perhaps not correct. The interaction of Mn with other dissolved species, eg Ni, is also important in this context.
2. For modelling purposes, better values for the retention of Co isotopes within the core are required, especially as this would give more **reliable** estimated levels of radioactivity in components such as the IHX and pumps. Examination of fuel elements removed from reactors would assist in obtaining this information.
3. More data on activity levels and nuclide deposition rates and the boundary conditions at the depositing interface are required from reactor systems to improve the validity of existing codes for radioactive material transport. The effect of particles on code predictions also requires further investigation. Also the development of codes to predict the source term for failed fuel situations is needed so that better estimates of the total radioactivity released to the primary coolant can be provided.
4. As changes in the composition of fuel cladding to achieve higher burn-ups could introduce changes in both source term values and estimates of the deposition behaviour of the corroding species; mass-transfer studies in support of alternative cladding alloys should endeavour to provide the necessary inputs to existing codes so that they can be modified to suit future designs.

5. To eliminate discrepancies which may arise due to differences in sampling techniques, standardisation of sampling methods should be investigated so that better comparisons can be made of values obtained from different reactor systems. This should also include standardisation of on-line monitors such as plugging meters, oxygen meters, hydrogen meters and tritium meters. It is also important that reactor design and operating programmes cater for the taking of representative and reproducible samples (as distinct from ad-hoc samples) from the coolant so that a better understanding can be obtained of the behaviour of various radioactive species in operating plant. Improved methods of obtaining samples of particulates need to be developed.
6. To improve our understanding of Cs behaviour, work is required to:
  - a. obtain better partition data for equilibrium for Cs between steel surfaces and sodium and the rate at which this is achieved. The measurements should include the effect of surface composition and condition, total carbon content, oxygen level, bulk corrosion/deposition rate and flow/geometry regimes.
  - b. assess the impact, on the overall caesium balance, of losses to the cover gas and associated surfaces and to the primary cold trap.
  - c. establish means for removing caesium from the surfaces of carbon contaminated components. This part of the investigation should be linked to consideration of the treatment and disposal of the decontamination solution - which will contain other nuclides as well as caesium.
  - d. establish ways of disposing of caesium traps.
7. For insoluble fission products attention should be given to:
  - a. The source term and fractional release and whether failures are randomly distributed.
  - b. The form of insoluble FPs following release. If these are present as oxides what can be said about particle size and its effect on the liquid phase mass transfer coefficient since values used so far are based on molecular diffusion through the boundary layer. Also, are there other resistances or transfer in the reverse direction, which can govern the overall deposition process?
8. Fuel-sodium reaction studies should be continued to obtain a quantitative understanding of the factors affecting release of fission product species from failed fuel during operation and storage. Also fuel pin behaviour in operating reactors should be controlled; in case increased contamination occurs when higher burn-ups are reached.
9. The delegates suggested that the next meeting on fission and corrosion products behaviour in LMFBR's should be held in four years time.



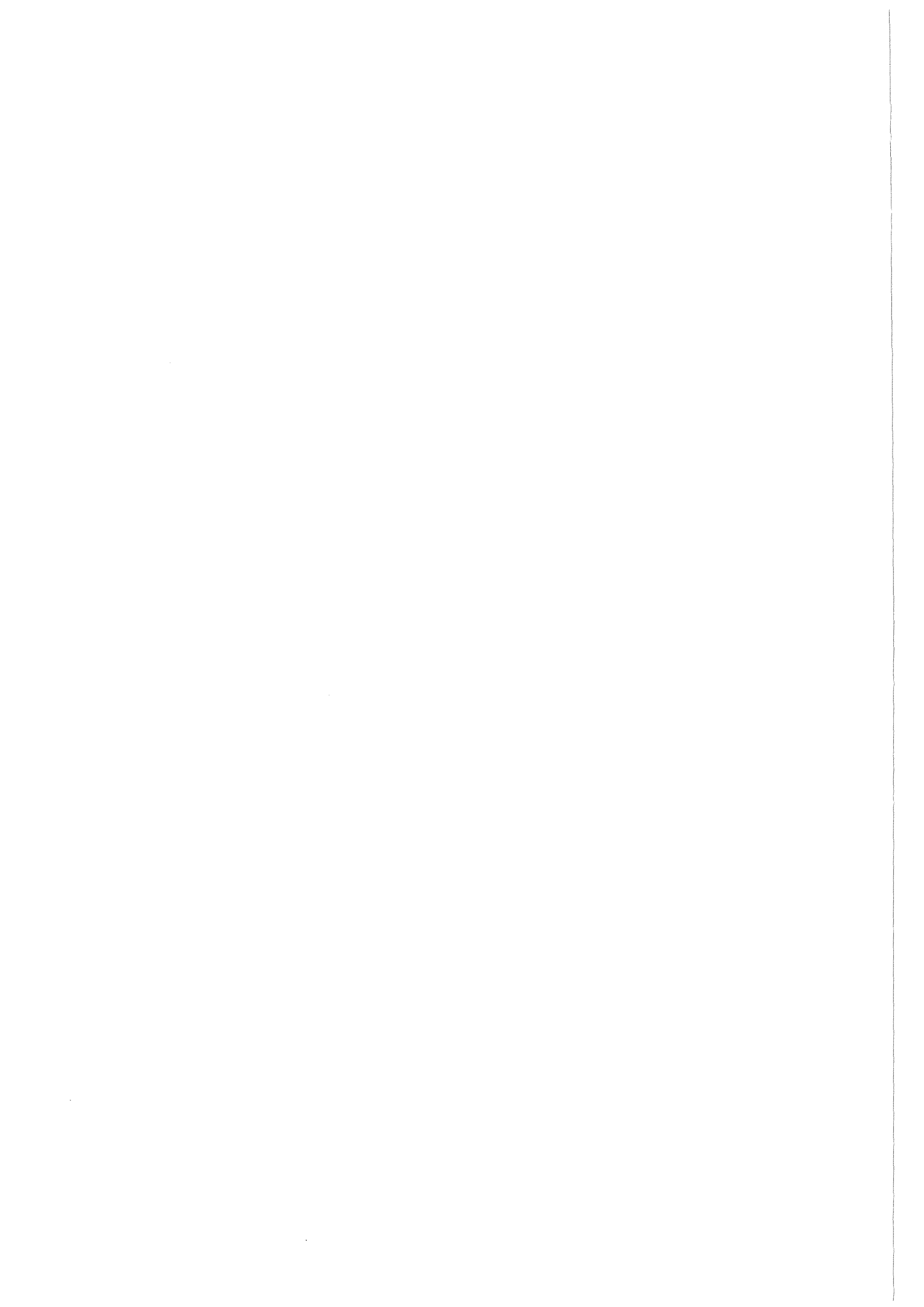
## PAPERS

### **General remarks:**

**20 papers were presented during the Specialists' Meeting. Most of these papers report items belonging to more than one session. Therefore the papers were not arranged by sessions, but rather by an alphabetic order of the authors.**

**The papers are reproduced as received from the participants.**





Evaluation of Corrosion Products Behavior in Pool Type FBRs

Norichika Aoki \*  
Kunihisa Wada \*  
Masaki Uotani \*  
Norikatsu Yokota \*\*  
Junnosuke Horie \*\*\*  
Noboru Nakao \*\*\*\*

- \* Central Research Institute of Electric Power Industry (CRIEPI)  
11-1, Iwato Kita 2-chome Komae-shi, Tokyo, 201 Japan  
\*\* Energy Research Laboratory, Hitachi, Ltd.  
1168 Moriyama-cho, Hitachi-shi, Ibaraki-ken, 316 Japan  
\*\*\* Hitachi Division, Hitachi Engineering Co., Ltd.  
3-2-1 Saiwai-cho, Hitachi-shi, Ibaraki-ken, 317 Japan  
\*\*\*\* Hitachi Works, Hitachi, Ltd.  
3-1-1 Saiwai-cho, Hitachi-shi, Ibaraki-ken, 317 Japan

Abstract

A computer program "CYGNUS" has been developed to evaluate the distribution of radioactive corrosion products in the primary cooling system of pool type FBRs.

Processes of release and deposition were described in three steps: (1) diffusion through structural materials, (2) absorption and desorption on the interface between structural materials and liquid sodium, and (3) diffusion through a lamina layer of sodium flow. Transportation of radioactive corrosion products along the sodium flow direction was also described by using two elements as a node and a segment. The node was a point having functions of branching and mixing of sodium flow. The segment corresponded to a place, like piping and components, where release and deposition of corrosion products occurred on the surface.

By using "CYGNUS", generation and distribution of radioactive corrosion products were calculated after a 5-year operation of a 1000MWe pool type reactor, designed by Hitachi, Ltd. Sodium flow patterns in the pool were calculated using a program of three-dimensional thermal hydraulic behavior analysis. In the hot plenum, the main sodium flow occurred towards the intermediate heat exchangers (IHXs), away from the core outlet and the branch flows occurred towards the outer walls of the IHXs and pumps. Similar sodium flow patterns were found in the cold plenum. Distribution of deposited corrosion products was very much affected by sodium flow patterns. Deposition amounts of  $^{54}\text{Mn}$  and  $^{60}\text{Co}$  on the surface were lower along the sodium flow direction, from the core outlet. Deposition fractions of  $^{54}\text{Mn}$  and  $^{60}\text{Co}$  in the IHXs were obtained as rather

high values in comparison with their proportional surface area in the total primary cooling system area.

## 1. Introduction

Radiated fuel claddings and structural materials in an FBR core are corroded by liquid sodium and various radioactive corrosion products are released into liquid sodium of primary cooling system. These corrosion products are transported by sodium flow and they deposit on the surfaces of piping and components. Therefore, it is very difficult to maintain components of the primary cooling system, and it becomes important to evaluate the extent of corrosion, the amounts of radioactive corrosion products in the core, and their deposition distribution in the primary cooling system.

Evaluations of corrosion product behavior in the primary cooling system of loop type FBRs have been done<sup>(1), (2)</sup>. In this type FBRs, sodium in the primary loop has a piston flow. However, in pool type FBRs, for which evaluations are limited, much of the sodium is contained in the hot and cold plenum, between the core and Intermediate Heat Exchangers(IHXs) or the IHXs and pumps. Therefore, sodium flow easily mixes and branches. It is very important to consider complicated flow patterns for evaluation of radioactive corrosion products behavior in pool type reactors. This report describes a computer program "CYGNUS" and results calculated by it on a 1000 MWe pool type reactor, after five years of operation.

## 2. Computer program "CYGNUS"

The program can deal with up to 20 nuclides in corrosion products; 11 nuclides of stable corrosion products and 9 nuclides of radioactive species. Activation reactions are shown in Table 1. Stable nuclides do not contribute to the dose rate, but they must be included in calculations of mass balance and concentrations of corrosion products in sodium. In the core, neutron energies can be divided into 30 groups. Furthermore, the amounts of activated nuclides in the core structural materials are calculated by division into a maximum of 50 regions. Diffusion of nuclei and corrosion of fuel claddings are influenced significantly by temperature. Therefore, cladding surface temperatures were calculated using the temperature of sodium and power densities of fuel claddings. Deposition regions are divided along the sodium flow direction. Amounts of corrosion products released and deposited are calculated. Concentrations of radionuclides at given regions in the core are obtained for consideration of the refueling cycle scheduling.

A calculation model of corrosion and deposition of each corrosion product species is shown in Fig.1. Mass transfer between structural material and sodium is considered to be in the three steps as reported by Kuhn<sup>(3)</sup> and Polley et al.<sup>(4)</sup>:

- (1) diffusion through structural material to the surface;
  - (2) absorption and desorption in the interface between structural material and sodium;
- and

(3) diffusion, through lamina flow, from the surface of structural material to bulk sodium.

These steps are described using mass flux as follows:

$$J = D \left( \frac{\partial C}{\partial x} \right)_{x=0} \pm u C_i \quad \dots\dots\dots (1)$$

$$J = k_d C_i - k_a C'_i \quad \dots\dots\dots (2)$$

$$J = k(C'_i - C') \quad \dots\dots\dots (3)$$

where

$J$  : mass flux

$D$  : diffusion coefficient in structural material

$C$  : concentration of corrosion products in structural material

$k_d$  : desorption coefficient

$k_a$  : absorption coefficient

$k$  : mass transfer coefficient in sodium

$C_i$  : concentration in surface of structural material

$C'_i$  : concentration in the sodium interface between the structural material and sodium

$C'$  : concentration in sodium

$u$  : corrosion rate.

In this case, a necessary condition is that the three mass fluxes are equal to each other. Then,  $J$  and  $C'_i$  are eliminated from equations (1)-(3).

$$D \left( \frac{\partial C}{\partial x} \right)_{x=0} = \left( \frac{K}{\beta} \mp u \right) C_i - K C' \quad \dots\dots\dots (4)$$

where

$K$  : overall mass transfer coefficient

$$K = \frac{k k_a}{k + k_a} \quad \dots\dots\dots (5)$$

$\beta$  : distribution coefficient

$$\beta = \frac{k_a}{k_d} \quad \dots\dots\dots (6)$$

Assuming that the surface reaction is very fast in comparison to diffusion in sodium,  $K$  is nearly equal to  $k$ . The distribution coefficient is defined as a ratio of the absorption coefficient to the desorption coefficient between solid and liquid (structural material and sodium). These values are uniquely determined for the structural material as a function of temperature. A diffusion equation of the radionuclides in the structural material is obtained, for consideration of their velocity in the interface between the structural material and sodium,

$$\frac{\partial C}{\partial x} = D \frac{\partial^2 C}{\partial x^2} + u \frac{\partial C}{\partial x} - \lambda C + R \quad \dots\dots\dots (7)$$

where

$\lambda$  : decay constant of radionuclide

$R$  : activation rate of radionuclide.

An analytical solution of equation (7) is obtained when the following boundary and initial conditions are used:

$$C = C_0 \text{ at } t = 0. \quad \dots\dots\dots (8)$$

The mass flux  $J$  is obtained using  $C_i$  in the surface of the structural material, based on the calculated results of the concentration profile in the material. Concentrations of corrosion products along the sodium flow direction are obtained from mass balance as follows:

$$\pi \left(\frac{d}{2}\right)^2 \cdot v \cdot d \cdot C' = J \cdot \pi \cdot d \cdot dy \quad \dots\dots\dots (9)$$

and using equations (3) and (9),

$$\frac{\partial C'}{\partial y} = \frac{4K}{d \cdot v} \left( \frac{C_i}{\beta} - C' \right) \quad \dots\dots\dots (10)$$

where

$y$  : sodium flow direction

$d$  : equivalent diameter

$v$  : velocity of sodium.

Concentrations of radionuclides along the sodium flow are determined using equation (10).

### 3. Mixing and branching model

In pool type reactors, sodium flows in three dimensions. Two elements are introduced as a node and a segment to deal with complicated, three-dimensional flow patterns. The segment is defined as a place, like pipings and components, where corrosion products are released and deposited on the surface and the node is a point

having functions of mixing and branching sodium flow. A solution method for the mixing and branching model is shown in Fig.2.

The sodium flow is not always connected to the next node. Therefore, a given segment  $i$  is assigned the node number  $j$  of inflow and the node number  $k$  of outflow,

$$S(i, j, k). \quad \dots\dots\dots (11)$$

At the segment outlet, concentrations of corrosion products in sodium are passed to the next segment. The node is a change point for concentrations of the corrosion products, by mixing sodium which flows from the upstream segments. Concentrations of corrosion products are calculated to get the average concentration of each segment having the same  $k$  number,

$$C'_i = \frac{\sum C'_k f_k}{\sum f_k} \quad \dots\dots\dots (12)$$

where

- $C'_i$  : concentration of corrosion product in the segment  $i$
- $C'_k$  : concentration of corrosion product in the outlet of segment  $k$
- $f_k$  : sodium flow rate from segment  $k$  to segment  $i$ .

4. Surface area of deposition

A cross section of sodium flow in pool type reactors has a complicated shape. Therefore, it is represented as two shapes, a square and a circle. The actual area where corrosion or deposition occur is marked by the oblique lines in Fig.3.

For the square

$$S_1 = \eta_1 \times (\pi \times d) \times l \quad \dots\dots\dots (13)$$

For the circle

$$S_2 = \eta_2 \times 2 \times (a + b) \times l \quad \dots\dots\dots (14)$$

where

- $S_1, S_2$  : actual deposition area
- $\eta_1, \eta_2$  : ratios of actual deposition area to defined area
- $d$  : equivalent diameter
- $a, b$  : sides of the square
- $l$  : segment length.

5. Evaluation of corrosion product distribution

5.1 Configuration of pool type reactor

A distribution of radioactive corrosion products was calculated using the pool type reactor, designed by Hitachi, Ltd. The cross-section of the hot plenum is shown in Fig.4. Main characteristics are shown in Table 2.

## 5.2 Calculation conditions

The operation pattern, as shown in Fig.5, was a 360-day operation followed by a 70-day shutdown. The generation and deposition of radioactive corrosion products were calculated after about a 5-year operation.

Configuration of an axially heterogenous core is shown in Fig.6. The core was divided into 15 regions in the axial and radial direction as shown in Fig.7.

Sodium flow patterns in the pool type reactor were calculated using a computer program "THERVIS" for three-dimensional thermal hydraulic behavior analysis<sup>(5)</sup>. A simple, example flow pattern calculated for the pool type reactor is shown in Fig.8. Detailed flow patterns in the hot and cold plenums are shown in Figs.9 and 10. In the hot plenum, the main sodium flow occurred toward the IHXs, away from the core outlet, and the branch flow occurred toward the outer wall of the IHXs and pumps. Sodium flow patterns were similar in the cold plenum. Based on these calculated flow patterns, the deposition areas were divided into 49 regions; 21 regions in the hot plenum, 7 regions in the IHX and 21 regions in the cold plenum as shown in Figs.11-14.

## 6. Results and discussion

The distributions of  $^{54}\text{Mn}$  and  $^{60}\text{Co}$  were calculated and these results are shown in Fig.15. The fractions of radionuclides deposited are shown in Table 3. The deposition densities of  $^{54}\text{Mn}$ , as shown in Fig.15, became higher in the hot plenum and lower along the sodium flow direction. In the hot plenum, the sodium flow from the core was branched to each region, and had the same concentrations of corrosion products. Therefore, each deposition density became nearly the same. In the cold plenum, the sodium flow from the IHX was also branched to each region and the deposition densities became the same. The differences between deposition densities in the hot plenum were caused by the differences of sodium flow velocity. The slower the velocity was, the thicker the lamina flow layer became. Therefore, if sodium velocity was slow, the diffusion distance between the sodium bulk and the deposition wall became longer and the deposition rate became slower. The deposition densities of corrosion products were dependent on the concentration gradient between the sodium bulk and the deposition wall. In the IHX which had a large deposition surface area, corrosion products deposited easily in the upstream sodium, having higher concentrations of corrosion products. Therefore, the deposition densities were reduced along the sodium flow direction, corresponding to the reduction of corrosion product concentrations in the same direction. For  $^{54}\text{Mn}$  deposited in the primary cooling system, 70% was concentrated on the IHXs which represent about 70% of the total deposition area in the pool type reactor.

The distribution of  $^{60}\text{Co}$  differed from that of  $^{54}\text{Mn}$ . The inlet region of the IHXs is larger than the other regions. In the IHXs, the deposition densities were lower along the sodium flow direction, the same as for  $^{54}\text{Mn}$ , but the  $^{60}\text{Co}$  concentration in sodium was about 1/3 times smaller than that of  $^{54}\text{Mn}$ . Of the total deposition amount, 80% of the  $^{60}\text{Co}$  was concentrated on the IHXs.

## 7. Conclusion

A computer program "CYGNUS" has been developed to evaluate the distribution of radioactive corrosion products in the primary cooling system of pool type FBRs.

Processes of release and deposition were described in three steps: (1) diffusion through structural materials, (2) absorption and desorption on the interface between structural materials and liquid sodium, and (3) diffusion through a lamina layer of sodium flow. Transportation of radioactive corrosion products along the sodium flow direction was also described by using two elements as a node and a segment. The node was a point having functions of branching and mixing of sodium flow. The segment corresponded to a place, like piping and components, where release and deposition of corrosion products occurred on the surface.

By using "CYGNUS", generation and distribution of radioactive corrosion products were calculated after a 5-year operation of a 1000MWe pool type reactor, designed by Hitachi, Ltd. Sodium flow patterns in the pool were calculated using a program for three-dimensional thermal hydraulic behavior analysis. In the hot plenum, the main sodium flow occurred toward the intermediate heat exchangers (IHXs), away from the core outlet, and the branch flow occurred toward the outer walls of the IHXs and pumps. In the cold plenum, similar sodium flow patterns were found. Distribution of deposited corrosion products was very much affected by sodium flow patterns. Deposition amounts of  $^{54}\text{Mn}$  and  $^{60}\text{Co}$  on the surface were lower along the sodium flow direction, away from the core outlet. Deposition fractions of  $^{54}\text{Mn}$  and  $^{60}\text{Co}$  in the IHXs were obtained as higher values in comparison with the IHX surface area relative to the total primary cooling system area.

## References

- (1) C.E.Erdman, et al. : Nucl.Safety,16(1975), p.43.
- (2) M.H.Cooper, et al. : Nucl. Eng. Design, 32(1975), p.246.
- (3) W.H.Kuhn : Conf. 760503-P1,(1976), p.280.
- (4) M.V.Polley, et al. : J. Nucl. Mater. 75(1978), p.226.
- (5) M.Yamakawa, et al.:Proceeding of CNS/ANS InternationalConference on Numer. Meth. in Nucl. Eng., (1983), vol.1, p.949.



Table 1 Nuclear reactions

| Radionuclide      | Reaction                                      |
|-------------------|---|
| $^{51}\text{Cr}$  | $^{50}\text{Cr} (n, \gamma) ^{51}\text{Cr}$   |
|                   | $^{52}\text{Cr} (n, 2n) ^{51}\text{Cr}$       |
|                   | $^{54}\text{Cr} (n, \alpha) ^{51}\text{Cr}$   |
| $^{54}\text{Mn}$  | $^{54}\text{Fe} (n, p) ^{54}\text{Mn}$        |
|                   | $^{55}\text{Mn} (n, 2n) ^{54}\text{Mn}$       |
| $^{55}\text{Fe}$  | $^{54}\text{Fe} (n, \gamma) ^{55}\text{Fe}$   |
| $^{59}\text{Fe}$  | $^{58}\text{Fe} (n, \gamma) ^{59}\text{Fe}$   |
| $^{58}\text{Co}$  | $^{58}\text{Ni} (n, p) ^{58}\text{Co}$        |
|                   | $^{59}\text{Co} (n, 2n) ^{58}\text{Co}$       |
| $^{60}\text{Co}$  | $^{59}\text{Co} (n, \gamma) ^{60}\text{Co}$   |
|                   | $^{60}\text{Ni} (n, p) ^{60}\text{Co}$        |
| $^{65}\text{Zn}$  | $^{64}\text{Zn} (n, \gamma) ^{65}\text{Zn}$   |
| $^{124}\text{Sb}$ | $^{123}\text{Sb} (n, \gamma) ^{124}\text{Sb}$ |
| $^{182}\text{Ta}$ | $^{181}\text{Ta} (n, \gamma) ^{182}\text{Ta}$ |

Table 2 Configuration of pool type reactor

|                     |                               |
|---------------------|-------------------------------|
| Electric power      | 1,000 MWe                     |
| Shape core          | axially heterogeneous core    |
| Number of component | pump 4<br>IHX 8               |
| Core temperature    | outlet 530 °C<br>inlet 380 °C |
| Sodium inventory    | 3,000 m <sup>3</sup>          |

Table 3 Deposition ratios of  $^{54}\text{Mn}$  and  $^{60}\text{Co}$

| Region      | Area<br>cm <sup>2</sup>      | $^{54}\text{Mn}$                      |                | $^{60}\text{Co}$                      |                |
|-------------|------------------------------|---------------------------------------|----------------|---------------------------------------|----------------|
|             |                              | Density<br>$\mu\text{Ci}/\text{cm}^2$ | Amount<br>Ci   | Density<br>$\mu\text{Ci}/\text{cm}^2$ | Amount<br>Ci   |
| Hot plenum  | $1.38 \times 10^7$<br>(14.7) | 22.5                                  | 311<br>(28.0)  | 4.09                                  | 56.4<br>(16.7) |
| IHX         | $6.45 \times 10^7$<br>(68.8) | 12.1                                  | 778<br>(70.0)  | 4.19                                  | 270<br>(80.0)  |
| Cold plenum | $1.50 \times 10^7$<br>(16.0) | 1.45                                  | 21.8<br>( 1.9) | 0.72                                  | 10.8<br>( 3.2) |
| Pump        | $4.37 \times 10^5$<br>( 0.5) | 1.37                                  | 0.6<br>( 0.1)  | 0.78                                  | 0.34<br>( 0.1) |
| Total       | $9.37 \times 10^7$<br>( 100) | 11.8                                  | 1111<br>( 100) | 3.61                                  | 338<br>( 100)  |

( ) indicates ratio(%).

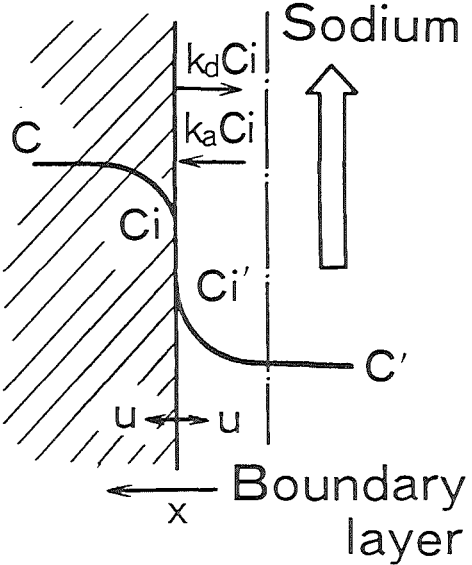
| Mass flux           | Basic equation   |  |
|---------------------|--|--|
| Material to surface | $J = D \left( \frac{\partial C}{\partial x} \right)_{x=0} \pm uC_i$ <p>+ : corrosion      - : deposition</p> |  |
| Surface reaction    | $J = k_d C_i - k_a C_i'$   |  |
| Surface to bulk     | $J = k (C_i' - C')$  |  |

Fig. 1 Mass transfer model of corrosion products

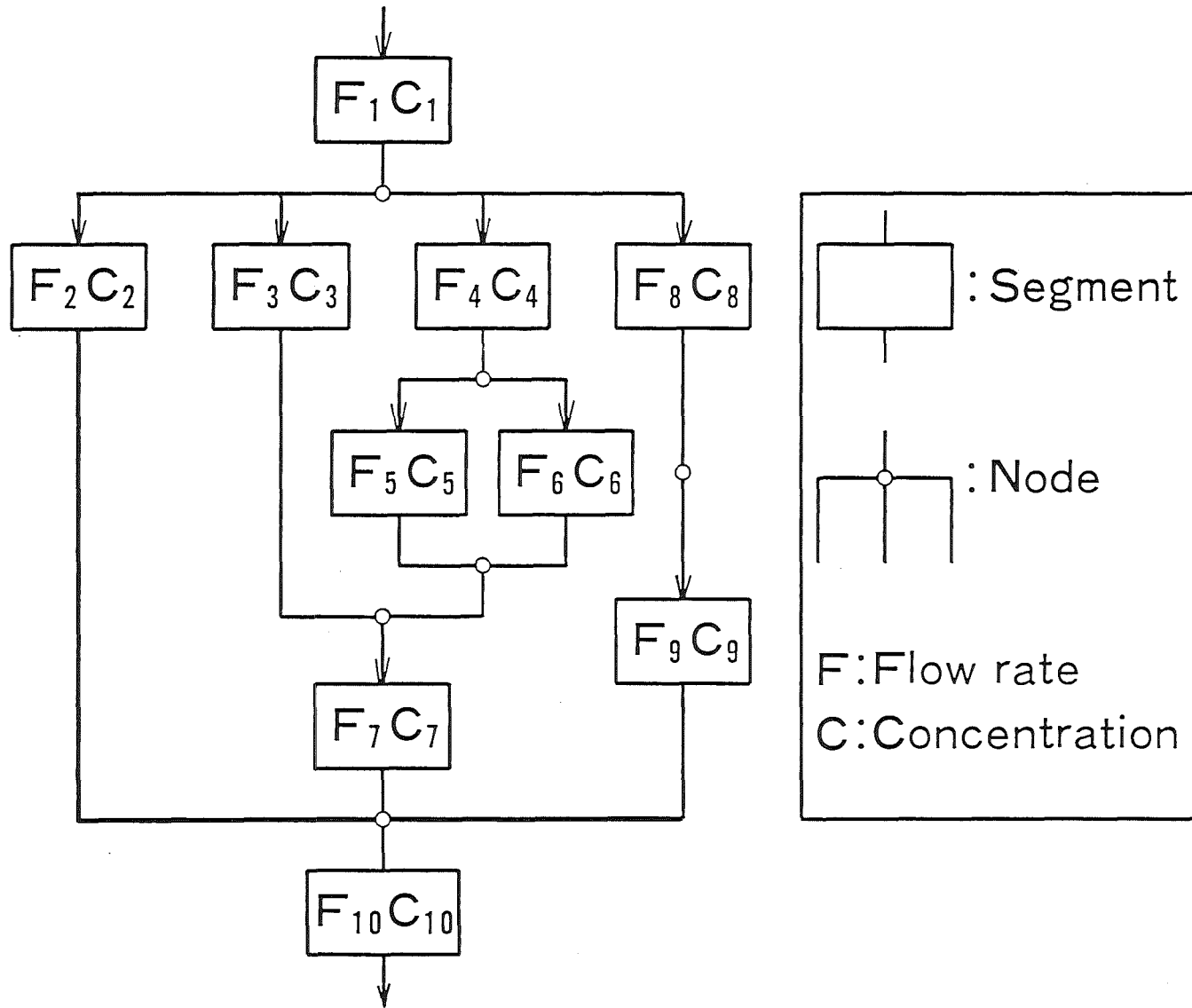


Fig. 2 Transfer model to consider mixing and branching flow

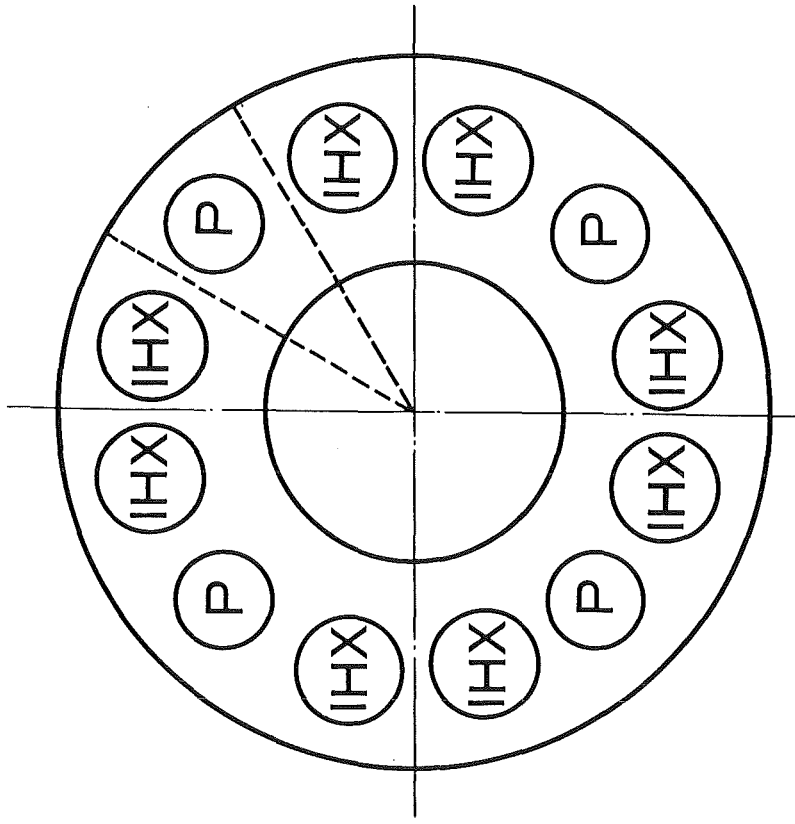


(i) Square

(ii) Circle

oblique line : actual deposition or corrosion area

Fig. 3 Cross-section of sodium flow



P : Pump

IHX : Intermediate heat exchanger

Fig. 4 Cross-section of hot plenum

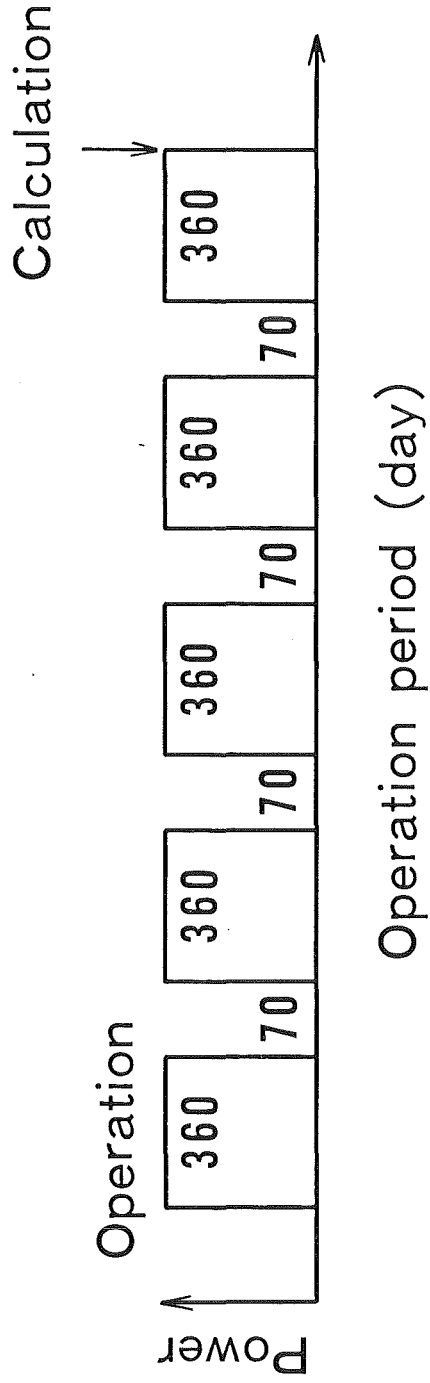


Fig. 5 Operation pattern



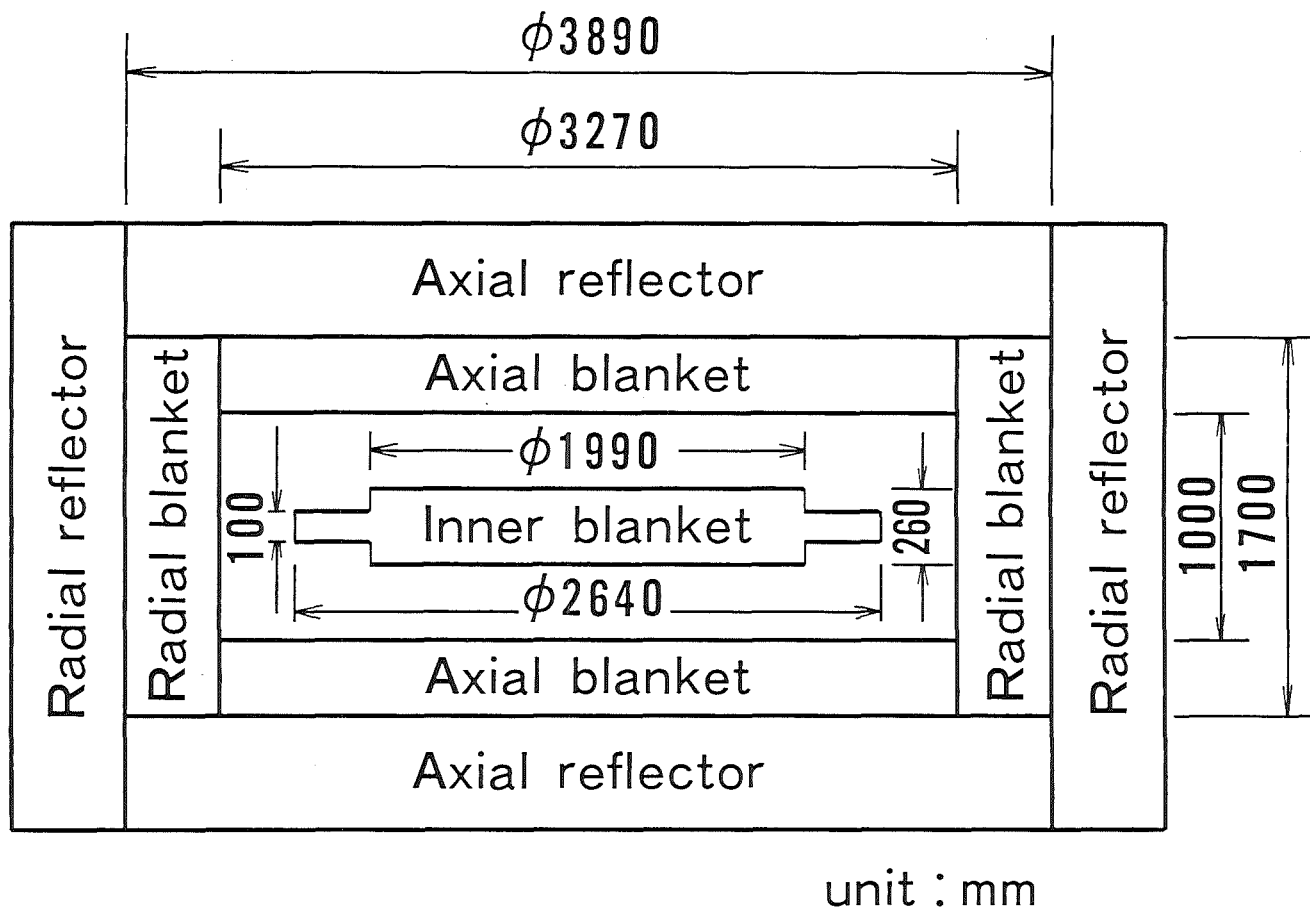


Fig. 6 Configuration of core

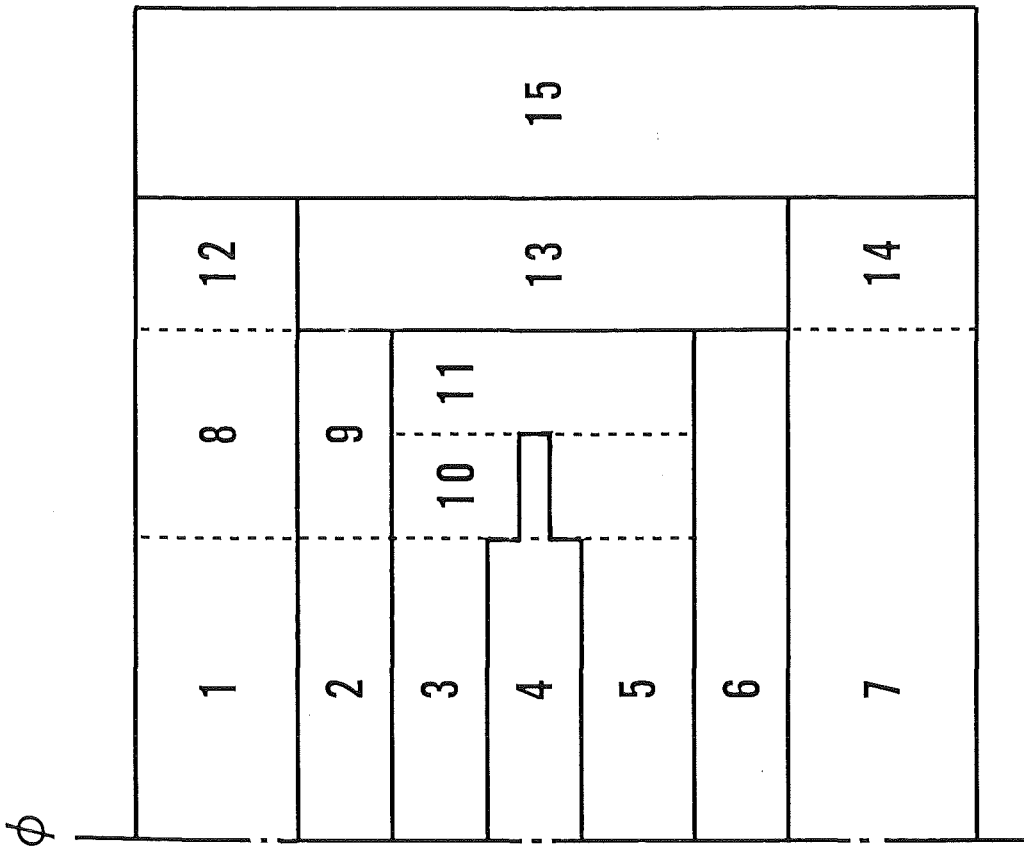
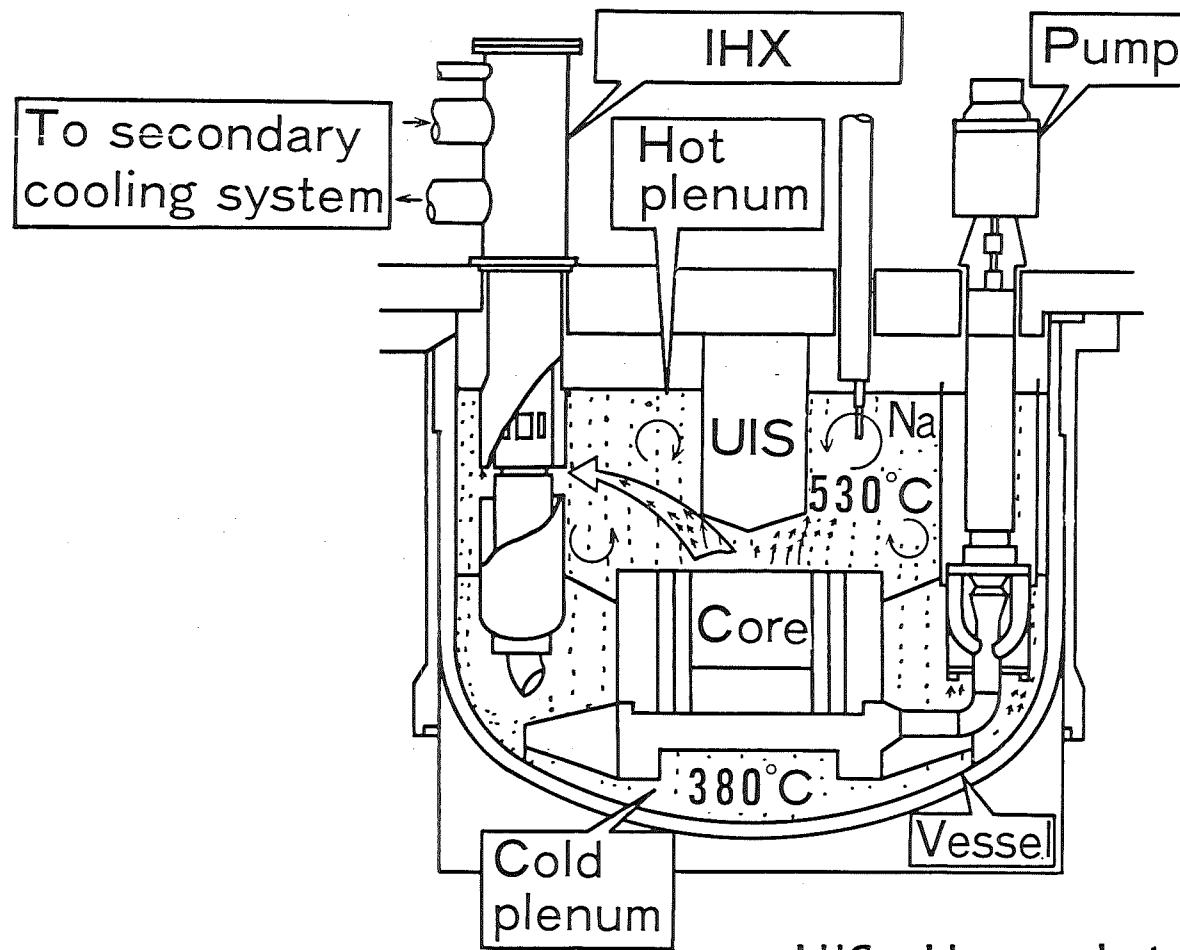
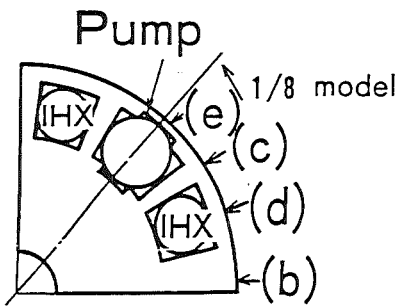


Fig. 7 Division in core

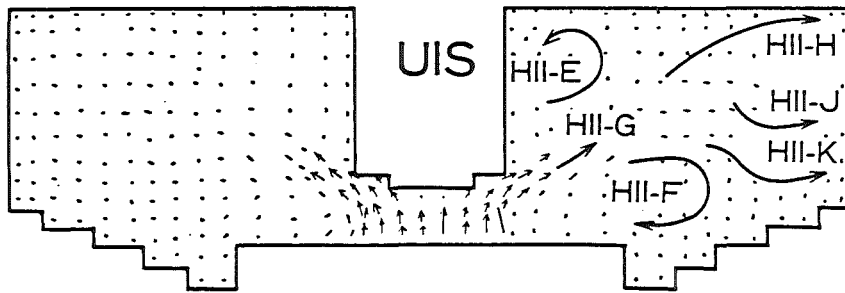


UIS : Upper Internal Structure

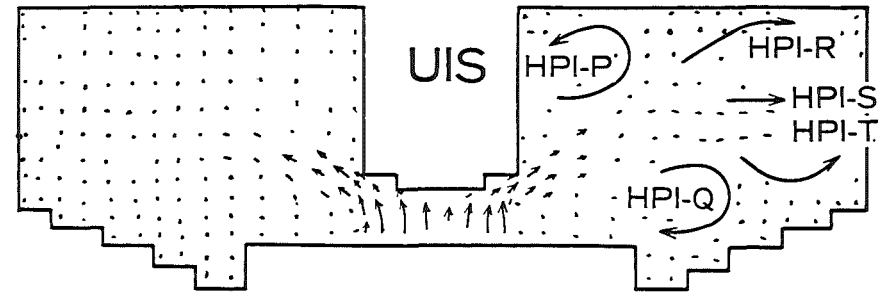
Fig. 8 Configuration of pool type reactor and flow pattern of sodium



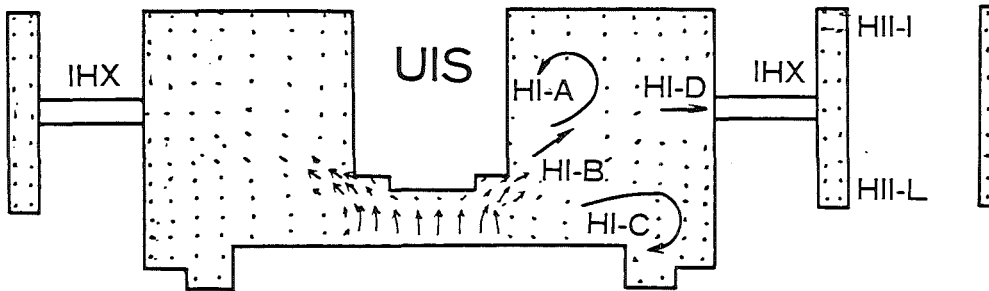
(i) Calculation points



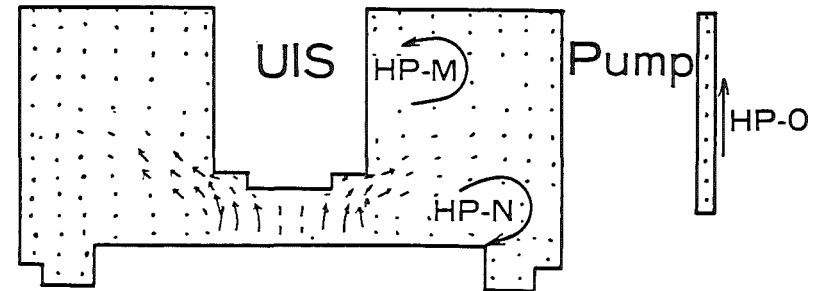
(ii) Flow at point (b)



(iii) Flow at point (c)



(iv) Flow at point (d)



(v) Flow at point (e)

Fig. 9 Flow patterns of sodium in hot plenum for perpendicular cross-section



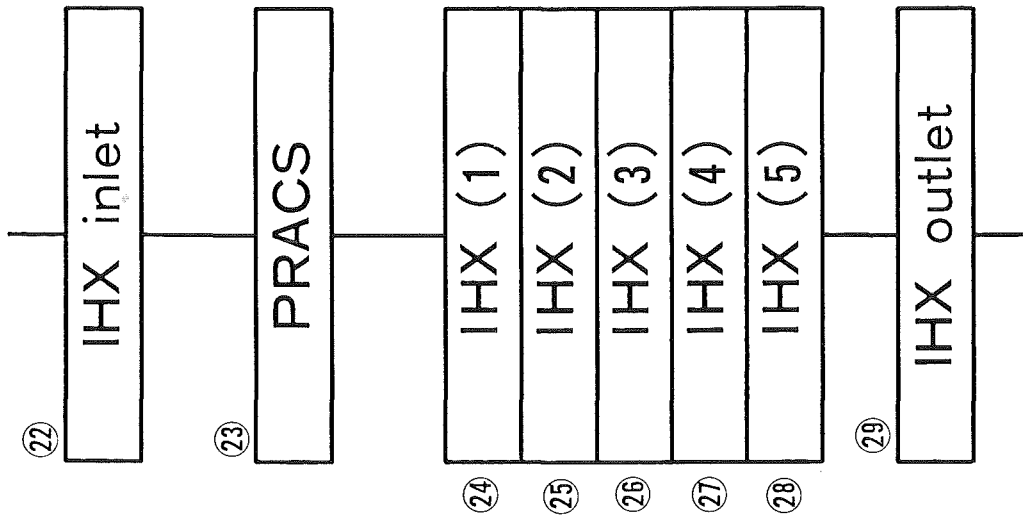


Fig. 12 Division of sodium flow patterns in IHX

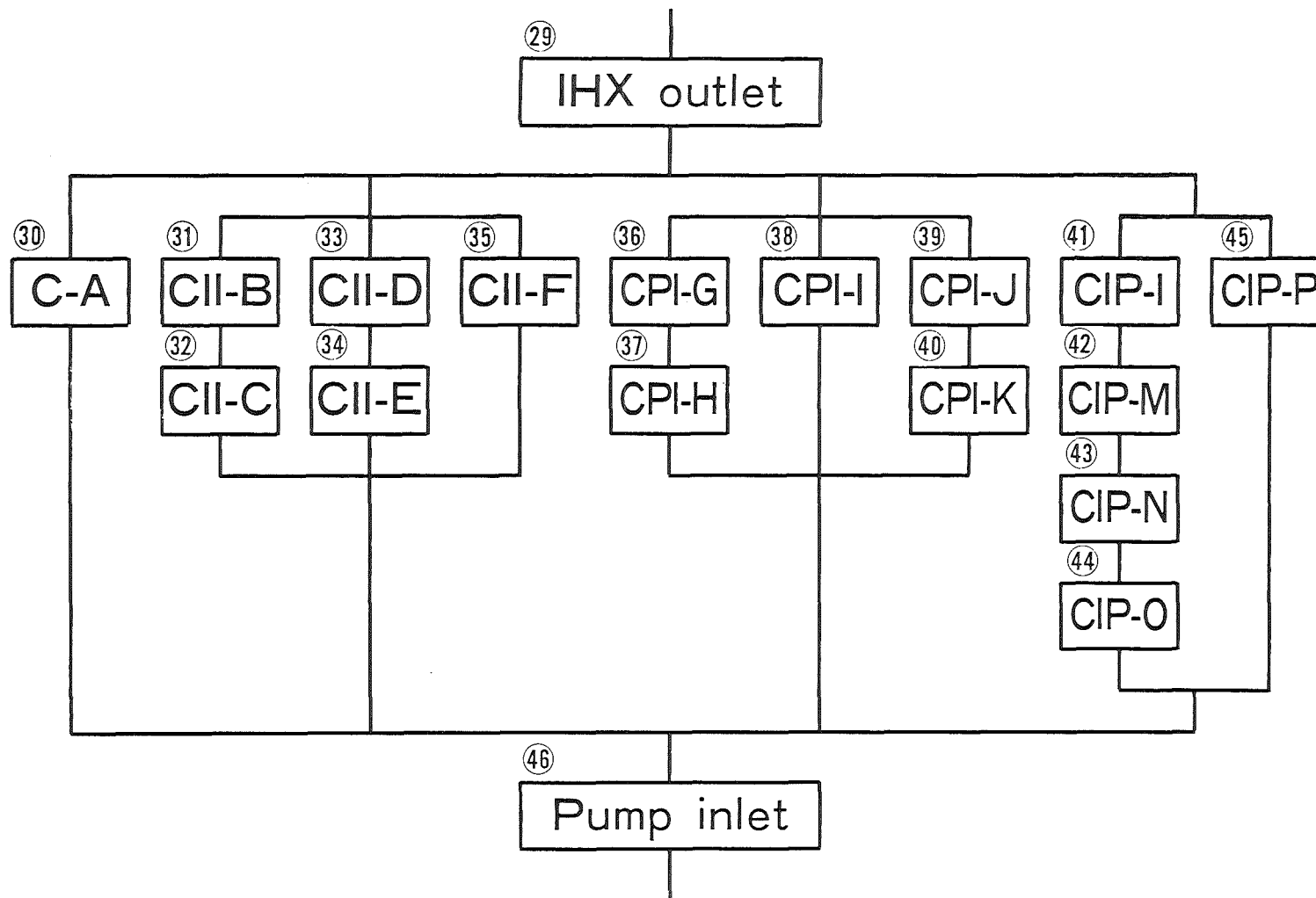


Fig. 13 Division of sodium flow patterns in cold plenum

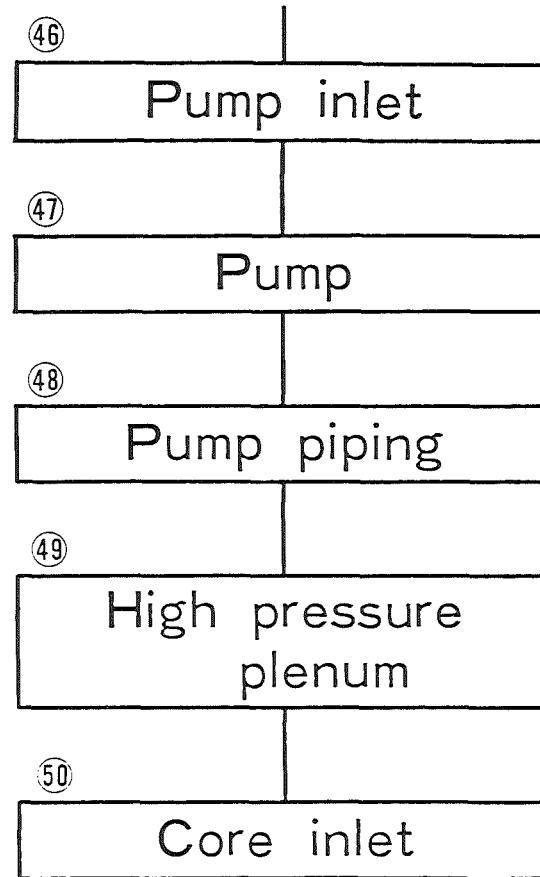


Fig. 14 Division of sodium flow patterns from pump inlet to core inlet



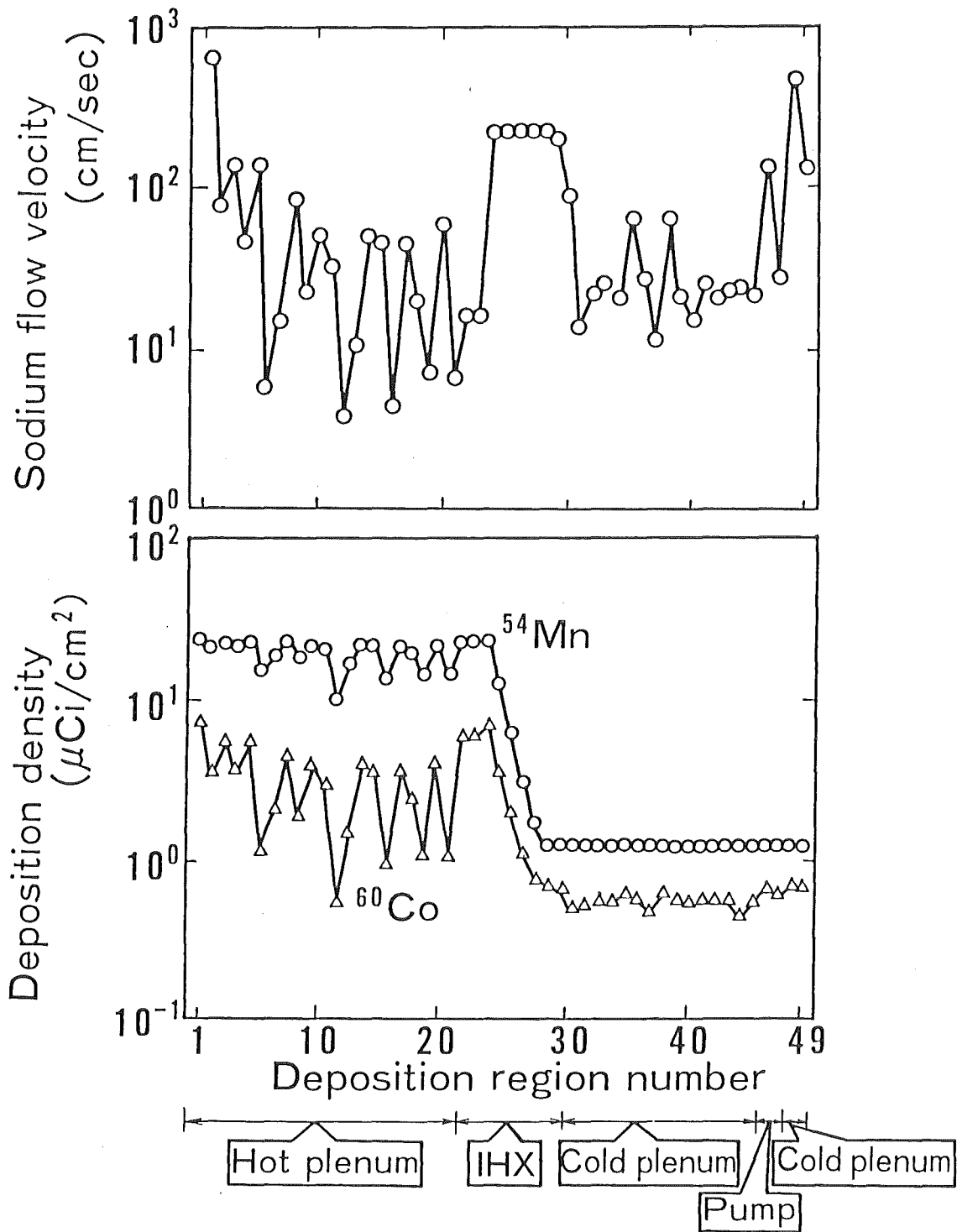


Fig. 15 Deposition distributions of  $^{54}\text{Mn}$  and  $^{60}\text{Co}$  in pool type reactor and sodium flow velocities

Yu.G. Bobkov, I.A. Efimov, Yu.I. Zagoroul'ko,  
E.I. In'utin, E.E. Konovalov, A.I. Lastov,  
A.G. Zikunov

RADIONUCLIDES BEHAVIOUR IN SODIUM COOLANT

Institute of Physics and Power Engeneering,  
Obninsk, USSR

SUMMARY

Results of investigation of cesium, manganese, cobalt radionuclides sorption from sodium by various materials are presented.

The data are given on the release of volatile fission products at operation with fuel elements claddings having natural and artificial failures on the reactor BR-10 and with vented fuel elements on the reactor BN-600.

The discription is given of deposeted cesium, manganese, niobium and lanthanum distribution along the hight of removed unit of BN-600 primary circulation pump in the initial state and after its vapour - water washing.

## INTRODUCTION

Development of the power industry on the basis of Fast Reactors with sodium coolant is determined in many respects by successful decision of the problems, linked with safe maintenance of the power stations and environment protection.

Among these problems an important part concerns the deactivation of primary circuits equipment and pipelines as well as purification of sodium coolant from the radioactive contaminations.

Activity of the primary sodium coolant is defined by the activation product of sodium and its impurities, activated corrosion and fission product. The sources of ingress of fuel and its fission product into primary sodium coolant are either fuel pins claddings surface contaminations or failed fuel pins claddings.

Procedures and methods of purification and decontamination are chosen with regard to many factors and, in no lesser extent are defined by the state of radioactive impurities in sodium and the processes of their deposition on the primary circuit surfaces.

The distinct peculiarity of the systems sodium - radionuclides impurities is very low mass concentration of the majority of radionuclides in sodium. It excludes possibility of solid phases precipitation at the expense of crystallization processes as well as due to radionuclides interaction with other impurities, for example, with oxygen.

Under such circumstances the character of radionuclides deposition on the surfaces of circulatory loop is defined by adsorption and adhesion processes. Besides the study of sorption processes is of great significance in understanding of such important problems as evaluation of the bulk ingress into primary circuit of radioactive impurities generated in active zone, the state and nature of species of radionuclides in circulatory loop, an interpretation of the results obtained in the course of sodium analysis for radionuclides etc.

The first section of the this report contains description of the results obtained in investigation of cesium, manganese and cobalt radionuclides sorption on the surfaces of various

materials . Here, as a rule laboratory experiments are described. In the next two sections the results of investigation are reviewed on the release of volatile fission product at operation with natural and artificial pins claddings defects on the reactor BR-10 and with vented fuel pins on the reactor BN-600.

An important information on the behaviour of radionuclides in sodium coolant may be obtained in the study of their distribution on the primary circuit equipment surfaces. In the last section of this report are given results of investigation of cesium, manganese, niobium and lanthanum radionuclides deposition on the surfaces of the removed unit of BN-600 primary circuit circulation pump.

#### 1. SORPTION OF CESIUM, MANGANESE AND COBALT RADIONUCLIDES ON THE VARIOUS MATERIALS.

Analysis of the properties of radionuclides - fission product in sodium coolant indicates that about 80 % of gamma-ray exposure of the primary circuit equipment and pipelines is due to the cesium-137 gamma radiation /1/. The next by their influence on the radiation conditions are manganese and cobalt radionuclides - activated product of structural materials components.

It is convenient to describe the sorption of the radionuclides by means of the equilibrium distribution coefficients, characterizing radionuclides partition between sodium and sorbents

$$K = A_s / A_1 \quad , \quad (1)$$

where  $A_1$  ( $\text{Bq}/\text{m}^3$ ) - volume specific activity in sodium,  $A_s$  ( $\text{Bq}/\text{m}^3$ ) or  $A_s$  ( $\text{Bq}/\text{kg}$ ) - respectively, surface or mass specific activities of radionuclides in sorbents. Depending on the choice of the activity units, respectively surface distribution coefficient  $K_s$  or mass distribution coefficient  $K_m$  are used.

An investigation on the sorption of cesium-137 by stainless steel X18H10T was carried out. The experiments were performed in the nonisothermal conditions using sealed steel ampulas filled with sodium during time period sufficient for equilibrium distribution of radionuclide. Results of these experiments are illustrated by the curves in the fig. 1-3. The course of the

curves in fig. 1 and 3, as well as calculated values for the heat of sorption  $\Delta H = (15 + 30)$  kJ/mol indicate, that cesium deposits on the steel surface from sodium according to mechanism of physical sorption. Preliminarily exposed for some time into sodium steel surface weaker adsorbs cesium and especially in the range of low cesium concentration. Cesium sorption is weakly dependent on the temperature conditions of these exposures. Decrease of oxygen concentration in sodium by means of zirconium gettering reduces cesium sorption in the range of low cesium concentrations ( $\sim 10^{-6}$ % mass); on the other hand with increase of cesium concentration in sodium up to  $10^{-3}$ % mass this effect was not noted. Results of this investigation explain the contradictions in the data obtained by the other authors /2-5/, taking into account the probable influence of such factors as cesium and oxygen concentration in sodium, temperature, the state of steel surface.

It is of practical interest to obtain data on the distribution of cesium radionuclides between sodium and other solid phases initially present in the coolant (f.e. suspension of carbon bearing impurities) or specially introduced into the sodium for the purpose of its purification (f.e. graphite, applied in cesium traps).

Advantage of graphite as compared with others cesium sorbents are illustrated in the fig. 4. It is notable from the course of the curves that interaction of chemical nature takes place between cesium-137, graphite and alumogel, moreover up to the temperature  $\sim 300$  °C there is an activated chemisorption.

Sintered nickel up to the temperature  $380$  °C adsorbs cesium according to mechanism of physical sorption like st. steel. Above this temperature an activated chemisorption begins to be notable. High sorption ability of carbonaceous material in comparison with others sorbents is illustrated by the data in the table 1. The most acceptable materials for cesium traps, taking into account their mechanical strength and sorption ability, are pyrographites and vitreous carbon. It follows from the temperature dependencies of distribution coefficients represented in fig. 5, that optimal working temperature for graphites is about  $300$  °C. The region below this temperature corresponds to activated chemical processes. Over the indicated temperature value the interaction is lowered in correspondence with thermodynamics calculations. An interac -

tion of this kind is typical for the processes with chemical sorption as their mechanism, or as applied to graphites - adsorption with chemical bonding between the reacted components.

Nowadays application of the graphites for the purification of FBR's sodium coolant from cesium radionuclides may be considered as completely satisfactory. It is necessary to note, however, that such important ecological problem as regeneration and storage of the cesium traps after their use is not still solved.

Cesium radionuclides transfer processes in primary circuit are defined probably by the presence in the sodium of suspended carbon bearing particulate phase, which may be considered as sorbent distributed in the coolant volume. In the fig. 6 the measurements results are given on the distribution of Cs-137 in reactor BR-10 primary sodium samples after their centrifugation. Most probable explanation of the noted partition in the system sodium - cesium is generation of the graphitides due to the interaction of cesium with carbon particles.

Radiation conditions on the primary circuits of reactor are dependent also on the presence of manganese and cobalt radionuclides. In the sodium samples manganese and cobalt radionuclides as a rule are not identified. Being generated in active zone of reactor these radionuclides are transferred by the coolant and deposited on the surfaces of structural materials due to the sorption processes. The data on the temperature dependence of this process are contradictory /6/. In the fig. 7 the results are given on the investigation of Mn-54 sorption by various materials. The experiments were performed in the ampulas with convective mixing of sodium. Similar results were obtained when investigating distribution coefficients of the Co-60 with the same materials (fig. 8).

During formation of radionuclides deposition on the metallic surfaces two simultaneous processes take place : sorption of radionuclides and their diffusion into the metall. At long contact of sodium coolant with metalls the diffusion processes distort equilibrium distribution of the radionuclides between sodium and structural materials. In this case distribution coefficients values are overstated in comparison with their equilibrium values, especially in the region of high temperature. The other cause which may be referred to for the explanation of cobalt and manganese radionuclides distribution coefficient temperature

dependence is activated chemisorption. In order to determine the controlling mechanism it is necessary to investigate radionuclides sorption at higher temperature. In the fig. 9 are presented the results of the measurements of cesium, manganese and cobalt penetration into steel, obtained at the analysis of reactor BR-10 primary pipelines samples.

## 2. GASEOUS FISSION PRODUCT RELEASE STUDY ON RESEARCH REACTOR

Research reactor BR-10 is used for a long time for study of fuel elements with natural cladding failures.

In the absence of failed pins delay neutron flux in sodium and activity of gaseous fission product (GFP) depend linearly on power. Delay neutron flux depends weakly on sodium temperature. In the primary coolant are practically absent Cs-138, Cs-136, I-131, Zr-95, as well as Xe-135m is absent in cover gas. An appearance of failed pin in active zone with fuel sodium contact is followed by emergence in the sodium isotopes Cs-136, Cs-138, I-131, I-132. Simultaneously activities of Cs-137 and La-140 increase  $\sim 10$  times. In the table 2 are given mean values of GFP release as a function of the fuel burn-up.

For description of coolant degassing process and the dynamics of GFP accumulation in reactor cover gas simple linear equations with one empirical parameter are used. Mean value of delay time of GFP in primary sodium coolant of reactor BR-10 is evaluated to be 1 - 3 h.

Experiments on the fuel elements with naturally defected claddings give a number of useful results, but make some difficulties in their interpretation due to the uncertainties in location, type and sizes of the defect.

In order to make clear some problems, linked with interpretation of the signals of the failed claddings detection system some experiments with different size and form claddings artificial defects were performed on the reactor BR-10. The investigations were carried out with usual fuel elements with fresh nitride fuel (90 % enrichment). Artificial defects were made in the pins claddings. The results, obtained in these experiments are represented in the table 3.

Delay neutron precursors (DNP) and GFP releases as

functions of sodium temperature in the range 200 - 400 °C and reactor power (500 - 800 kWt) were studied. It was established that DNP release depends strongly on the defect location along the pins height, fuel cladding gap and defect size. When defect was located on the fuel level, with increase of its surface there was growth of either GFP or DNP release. However, the GFP and DNP release growth is late in comparison with the rate of defect's size. As it follows from the comparison of GFP release values the main parameter determining gas release through the defect, located on the fuel level is defect prolongation along the pins claddings. Moreover, defect may be in the form of several separate holes (two holes with diameter 1 mm produce the same GFP release as the fissure 50 mm × 0,2 m). Dependence of the fission product release of this kind on the defect prolongation is not characteristic for DNP release. Moreover it was found that two holes with diameter 1 mm produced the same delay neutron flux as one hole with diameter 1 mm. The next parameter determining release of fission product from the failed fuel element is value of the gap between fuel and cladding. Decrease of this gap drop down both GFP and DNP release. Growth of Kr - isotopes activity has no explanation.

### 3. REACTOR BN-600 EXPERIENCE

#### 3.1. Radiation safety conditions

Starting June 1981 reactor BN-600 operates every microcampaign with gas-type pins defects. The number of defected pins never overcomes 0.1 % of their total amount.

Usually, gas-type fuel elements failures were observed after 5 + 6 % h.a. fuel burn-up. In the cases when the operation with the fuel assemblies having gas-type failures was continued the delay neutrons signals at the finish of separate microcampaigns were detected after 6 - 7 % h.a. fuel burn-up.

Experimental value of Na-24 specific activity in primary circuit while reactor's operation is equal to  $7.5 \cdot 10^{11}$  Bq/kg, and of Na-22 -  $3 \cdot 10^7$  Bq/kg at the beginning of 1987. Activity of Cs-137 during reactor's operation is about  $1.5 \cdot 10^8$  Bq/kg. After reactor shut down it becomes 20 + 30 % lower. Sodium isotopic composition, recalculated to the moment of sodium sampling



is represented in the table 4. In the absence of failed pins the activity of reactor gas is on the Ar-41 activity level and averages of about  $5.3 \cdot 10^6$  Bq/l. Up to the finish of microcampaign it increases in factor 100. Maximum cover gas activity during all period of reactor operation was detected to be of  $4.8 \cdot 10^9$  Bq/l.

### 3.2. Investigation on the radionuclides deposition on the surface of removal unit of primary circuit pump

At the replacement of the primary circuit pump's removal unit some investigation was performed on the radionuclides deposition on its surfaces. The measurements were carried out before and after vapour washing of the unit. Deposition samples were taken by means of spirit-moistened tampons from the area of  $100 \text{ cm}^2$ . Location of samples taking is shown in the fig. 10. In the fig. 10 also the distribution of the Cs, Mn, Nb and La radionuclides deposition along the height of the pump removal unit before the vapour-water washing is represented. Activity measurements were performed in the period of two months after reactor shut down. Specific activity of Cs deposition on the surface in gas environment approximately 10 times higher than one on the surface, located under sodium level. Likewise Mn-54 deposition is higher on the sodium flown about surface. Concentration of Mn-54 increases sharply in the places, where the sodium velocity is higher. This trend could be also observed for the deposition of others nuclides. It was estimated that approximately 10 % of the total amount of Cs contained in primary circuit sodium deposited on the surfaces under the sodium level and about 2 % deposited on the surfaces in gas environment. Equilibrium distribution coefficient of Cs-137 in the system was found to be about of 0.3 cm.

After vapour-water washing the sampling was repeated. The best cleaning result was achieved for the surfaces in gas environment. Activity of Cs on this surface drops down approximately 100 times.

For the surfaces under sodium level disactivation coefficient is about  $10 \pm 40$  for Cs,  $2 \pm 40$  for La and Nb,  $2 \pm 8$  for Mn. Gamma radiation dose rate was decreased  $5 \pm 10$  times on the surfaces located under sodium level and  $200 \pm 250$  times on the surfaces in gas environment.

REFERENCES

1. Konovalov E.E., Lastov A.I., Otstavnov P.S. Chemistry of the Sodium Coolant. Nuclear Fuel's and its Fission Product Impurities in Sodium Coolant of Fast Reactors: Preprint FEI N 1362, Obninsk, 1982.
2. Sagava N. et al. - J. Nucl. Sci. Technol., v.12, N 7, 1975, p.413.
3. Shimojama H. et al. Fission Products Deposition in a Stainless Steel Sodium System. - Specialists Meeting on Fission and Corrosion Product Behaviour in Primary Circuits of LMFBR's, Dimitrovograd, USSR, September 8-11, 1975. Summary Report, p.96.
4. Colburn R.P. - Trans. Am. Nucl. Soc., 1971, v.14, N 2, p.626.
5. Cooper M.N., Taylor G.R. - Nucl. Technol., 1971, v.12, N 9, p. 83.
6. Polyakov V.I., Krasnojarov N.V. Purification of Sodium Coolant of FBR from Radioactive Impurities: Review of information. NIIAR, Dimitrovograd, 1982.
7. Kizin V.D., Krasnojarov N.V., Polyakov V.I., Sobolev A.M. Behaviour of Cesium's Nuclides at Purification of Sodium Coolant by means of Cold Traps and specially designed Traps: Preprint NIIAR-33 (548), Dimitrovograd, 1982.

Table 1.

Equilibrium distribution coefficients of Cs-137 in the systems "sodium - carbonaceous materials" and "sodium - adsorbents" at 300 °C.

| Materials being tested                      | $K_m, m^3 \cdot kg^{-1}$ |
|---|--------------------------|
| Activated carbons (various brands)          | 2.2 + 4.3                |
| Vitrious carbon                             | 4.5                      |
| Graphite tissue                             | 2.8                      |
| Graphite ARV                                | 6.3 (250 °C)             |
| Reactor grade graphite                      | 0.72                     |
| Isotropic pyrographite with low density     | 3.1                      |
| Isotropic pyrographite with high density    | 1.9                      |
| Anisotropic pyrographite with high density  | 0.86                     |
| Graphite MPG-8                              | 8.3 (230 °C)             |
| Graphite MPG-6                              | 23.0                     |
| Alumogel AG-1100                            | 0.40                     |
| Zeolites (various brands)                   | 0.22 + 0.28(250°C)       |
| Sintered nickel (with pores size of 12 mcm) | 0.01                     |

Table 2.

Relative GFP release from the failed fuel element (PuO<sub>2</sub>) at different fuel burn-up values. (% of the amount accumulated in fuel element)

| Fuel burn-up, % h.a. | Xe-133    | Xe-135      | Kr-85m | Kr-88 | Kr-87 |
|----------------------|-----------|-------------|--------|-------|-------|
| 8.62                 | 0.5 ± 0.2 | 0.1 ± 0.2   |        |       |       |
| 10.92                | 0.3 ± 0.2 | 0.07 ± 0.04 |        |       |       |
| 12.88                | 1.5 ± 1.0 | 0.57 ± 0.4  | 0.3    | 0.2   | 0.04  |
| 14.15                | 1.7 ± 1.4 | 0.63 ± 0.5  | 0.34   | 0.38  | 0.13  |

Table 3.

Specific activity of gaseous fission product (mBq/l) and delayed neutrons detectors count rate at irradiation of the fuel elements with artificial defects.

| Nuclide          | Types of the defects                                     |   |  |  |   |
|------------------|--|---|--|--|---|
|                  | Orifice with diameter 1mm in the center of the fuel pole | Orifice with diameter 1mm, 5 mm below the fuel pole | Two orifices with diameter 1 mm on the distance 50mm, in the center of fuel pole | Fissure 50 mm x 0.3 mm, in the center of the fuel pole Without gap between cladding and fuel | Fissure 50 mm x 0.2 mm in the center of fuel pole |
| Xe-133           | 170  | 37  | 207  | 107  | 163   |
| Xe-135           | 7.1  | 30  | 143  | 93   | 158   |
| Kr-85m           | 2.5  | 0.13  | 7.3  | 8.9  | 7.0   |
| Kr-88            | 4.0  | 0.25  | 13.1   | 17.5   | 12.1  |
| Kr-87            | 2.7  | 0.22  | 9.4  | 11.1   | 9.3   |
| Delayed neutrons | 570  | 580   | 540  | 1670   | 2580  |

Table 4.

Radionuclides composition in reactor BN-600 primary circuit sodium.

| Radionuclides | Activity, Bq/kg          |
|---------------|--------------------------|
| Na-22         | $2.6 \cdot 10^7$         |
| Cs-137        | $1.5 \cdot 10^8$         |
| Cs-134        | $5 \cdot 10^7$           |
| Cs-136        | $2 \cdot 10^6$           |
| I -131        | $(0.7 + 1.3) \cdot 10^7$ |
| Sb-124        | $1.5 \cdot 10^5$         |

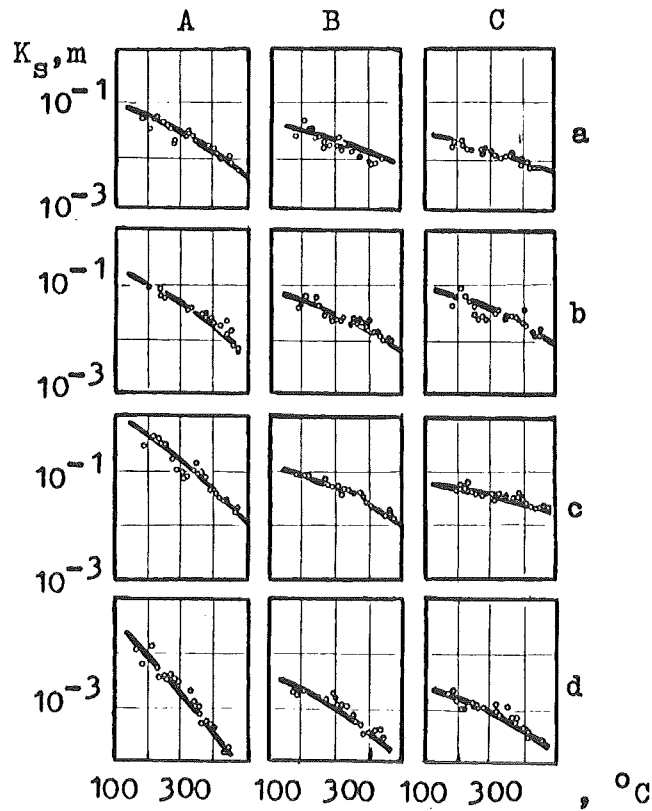


Fig. 1. Distribution coefficients of Cs-137 between sodium and st. steel X18H10T in dependence on the starting cesium concentration and steel surface preliminary exposure conditions in sodium.  
 A - without preliminary exposure of steel in sodium, B - preliminary exposure of steel in sodium at  $260^{\circ}\text{C}$  during 120 hr, C - preliminary exposure of steel in sodium at  $400^{\circ}\text{C}$  during 120 hr;  
 a, b, c, d - cesium concentration correspondently  $1 \cdot 10^{-3}$ ,  $1 \cdot 10^{-4}$ ,  $1 \cdot 10^{-5}$  and  $1 \cdot 10^{-6}$  % mass.

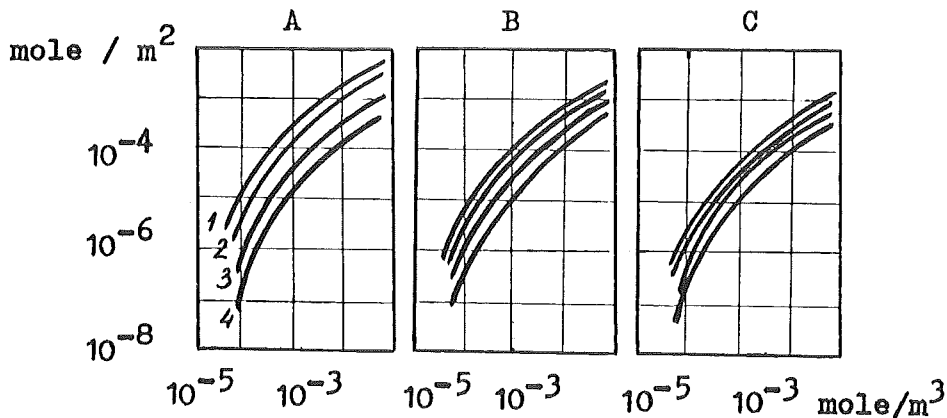


Fig. 2. Sorption isotherms of Cs-137 by st. steel from liquid sodium.  
 A - without preliminary exposure of steel in sodium, B - preliminary exposure of steel at  $260^{\circ}\text{C}$  during 120 hr, C - preliminary exposure of steel in sodium at  $400^{\circ}\text{C}$  during 120 hr;  
 1 -  $200^{\circ}\text{C}$ , 2 -  $300^{\circ}\text{C}$ , 3 -  $400^{\circ}\text{C}$ , 4 -  $500^{\circ}\text{C}$ .

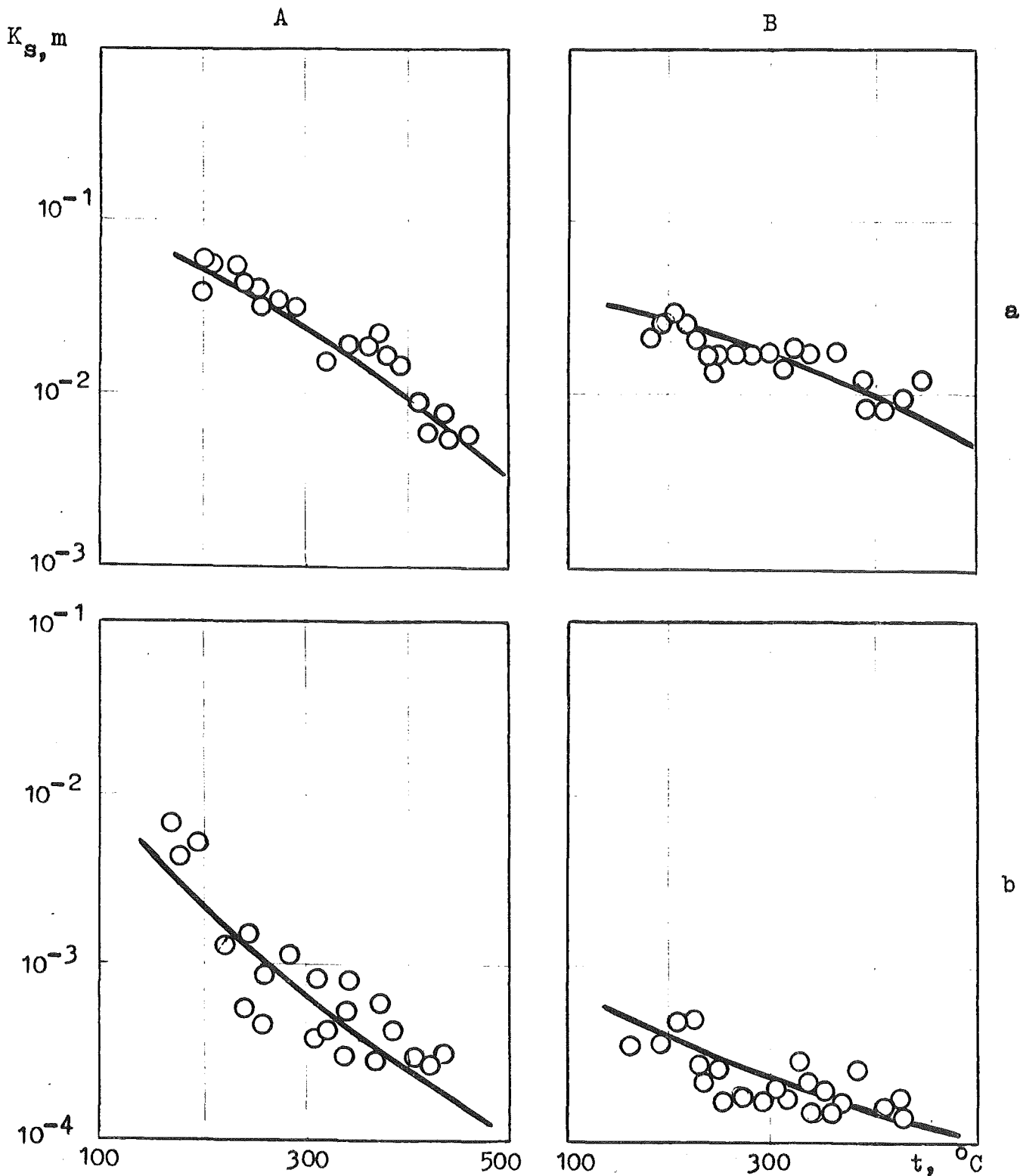


Fig. 3. Distribution coefficients of Cs-137 between deoxidized sodium and st. steel X18H10T in dependence on the starting cesium concentration and preliminary steel surface exposure conditions in sodium.

A - without preliminary exposure of steel in sodium,  
 B - preliminary exposure of steel in sodium at 260°C during 120 hr;

a, b - cesium concentration correspondently  $1 \cdot 10^{-3}$  and  $1 \cdot 10^{-6}$  % mass.

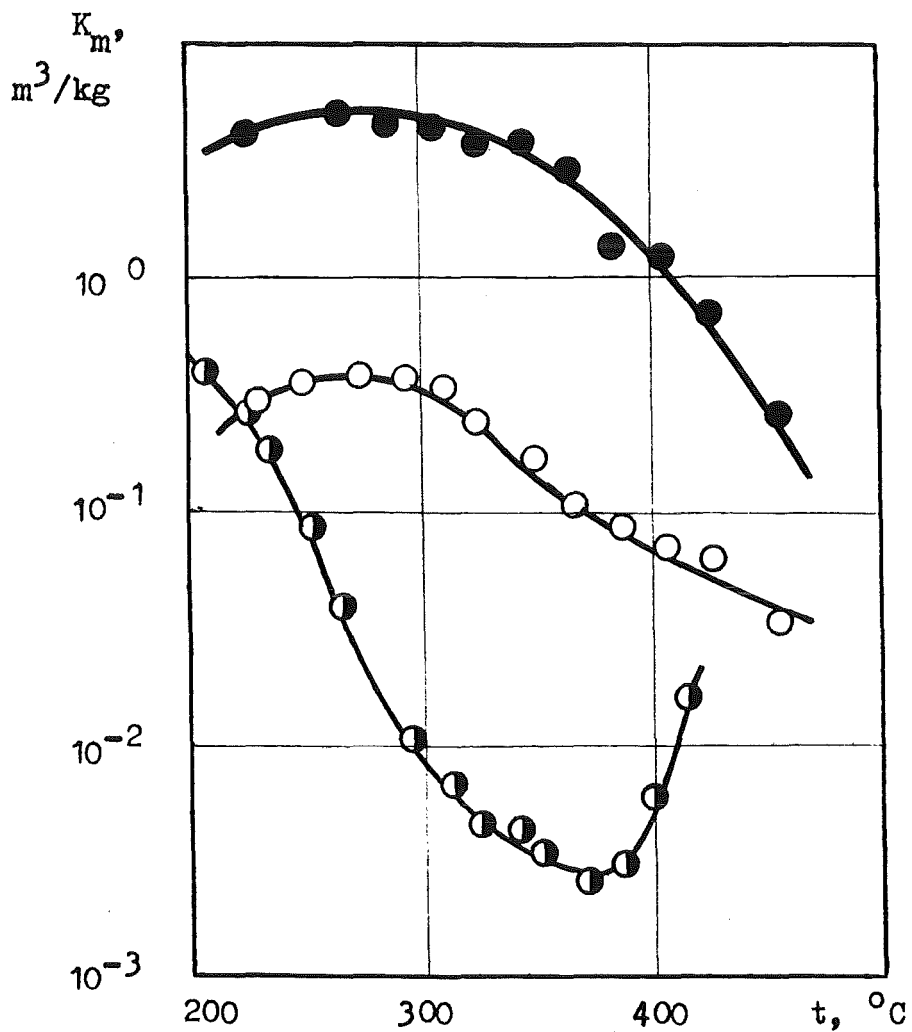


Fig. 4. Distribution coefficients of Cs-137 between sodium and: isotropic pyrographite PGI ( $\rho = 2,2 \text{ g}\cdot\text{cm}^{-3}$ ) - (-●-); alumogel AG-1100 - (-○-); sintered nickel with pores size of 12 micrometers - (-◐-).

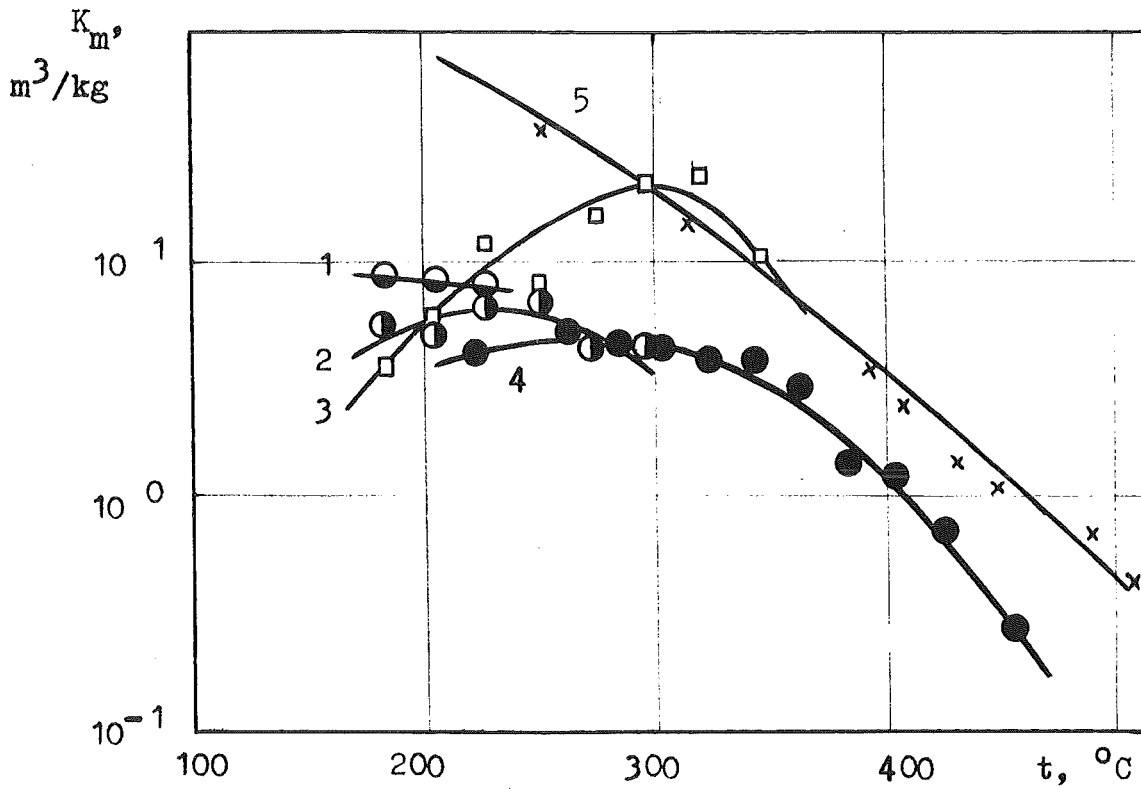


Fig. 5. Distribution coefficients of Cs-137 between sodium and graphites.

The data of this work: 1 (-○-) - MPG-8,

2 (-●-) - Su-2000, 3 (-□-) - MPG-6,

4 (-●-) - isotropic pyrographite ( $\rho = 2,2\text{g}\cdot\text{cm}^{-3}$ ).

The data of the work /7/: 5 (-x-).



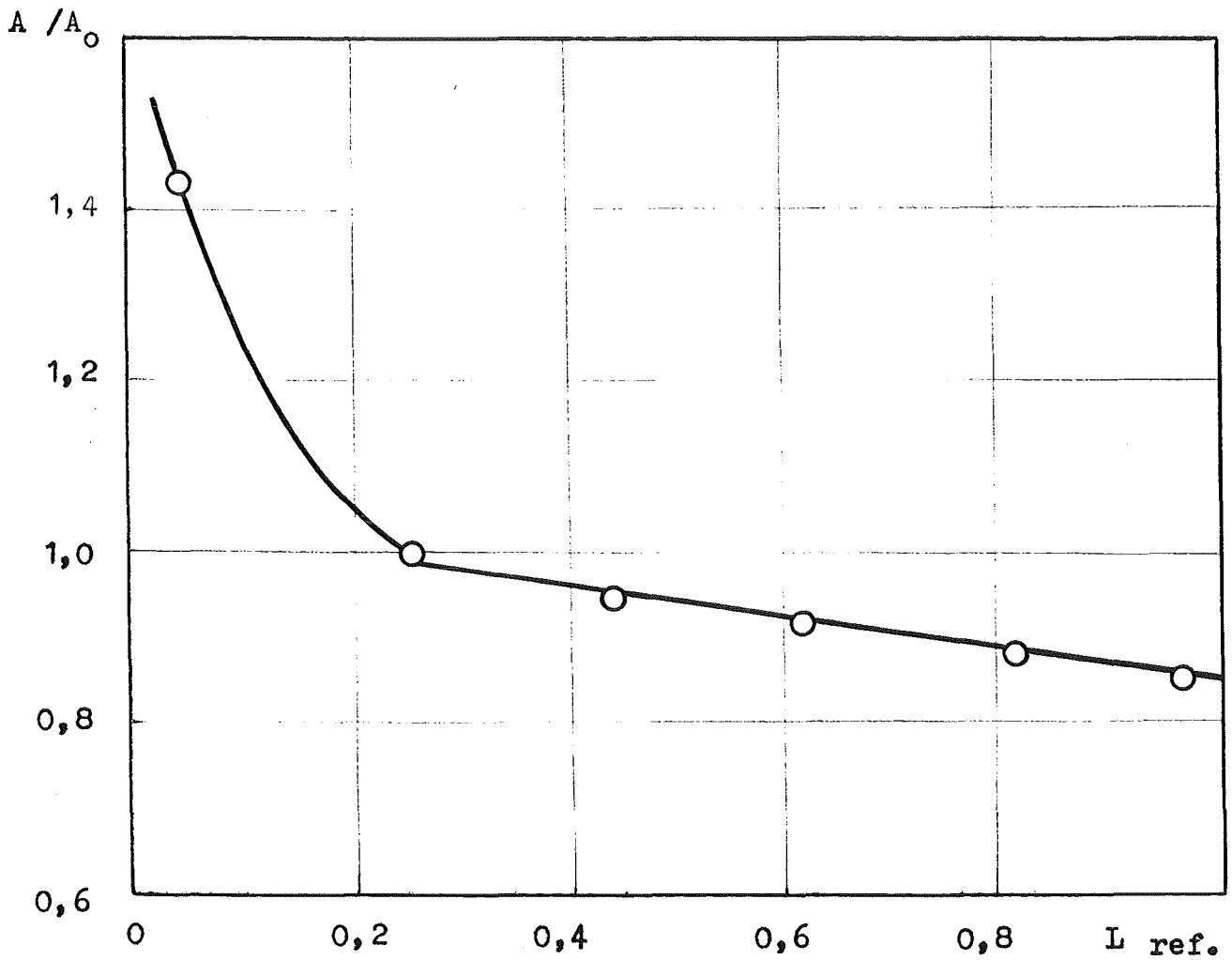


Fig. 6. Distribution of Cs-137 over the length of capillary tube, filled with reactor BR-10 primary sodium after centrifugation ( $6000 \text{ r}\cdot\text{min}^{-1}$ ) at  $150^\circ\text{C}$  during 45 min.  $A$  - specific activity over capillary length,  $A_0$  - starting specific activity.

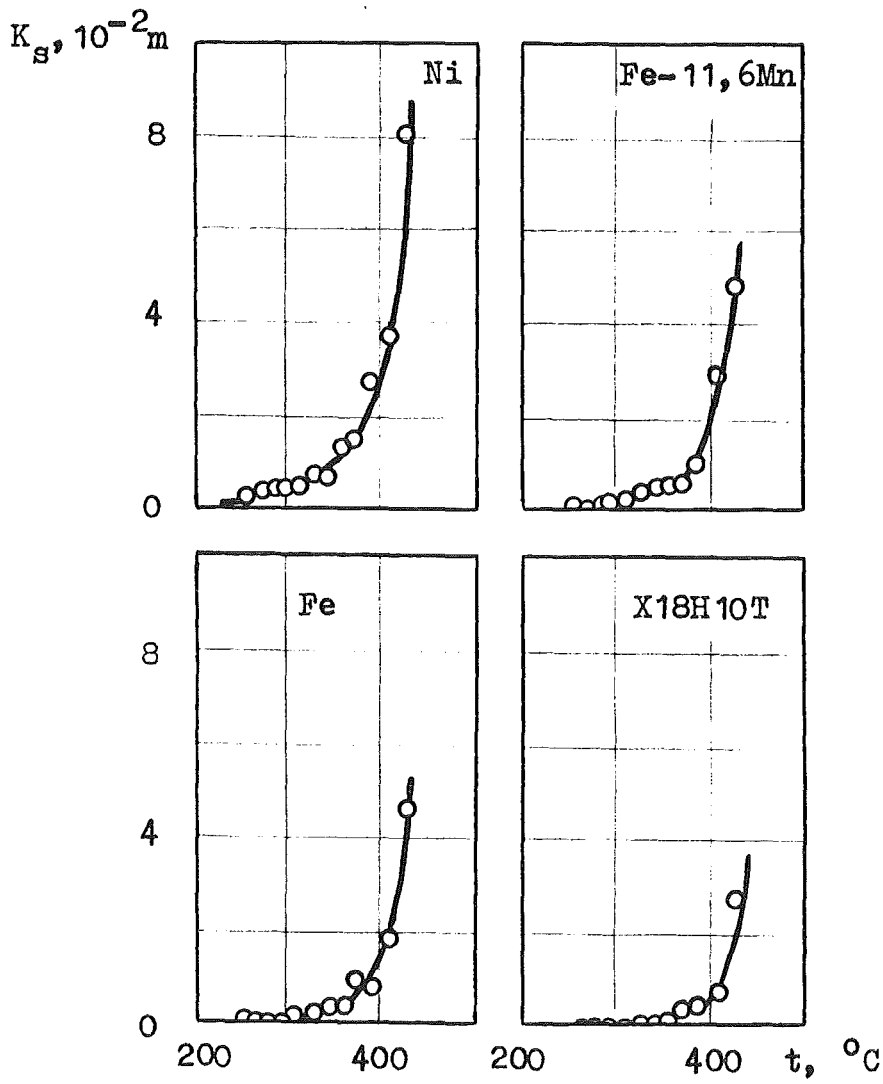


Fig. 7. Distribution coefficients of Mn-54 between sodium and various solid materials.

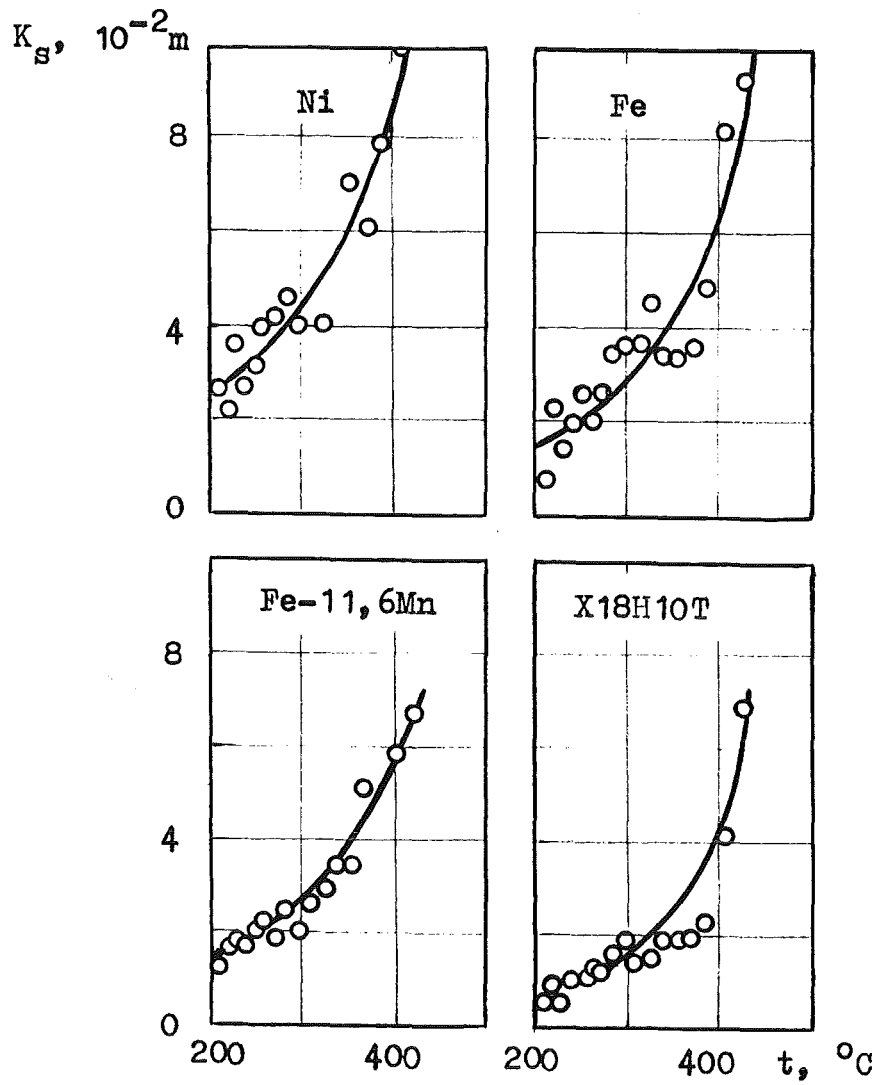


Fig. 8. Distribution coefficient of Co-60 between sodium and various materials.

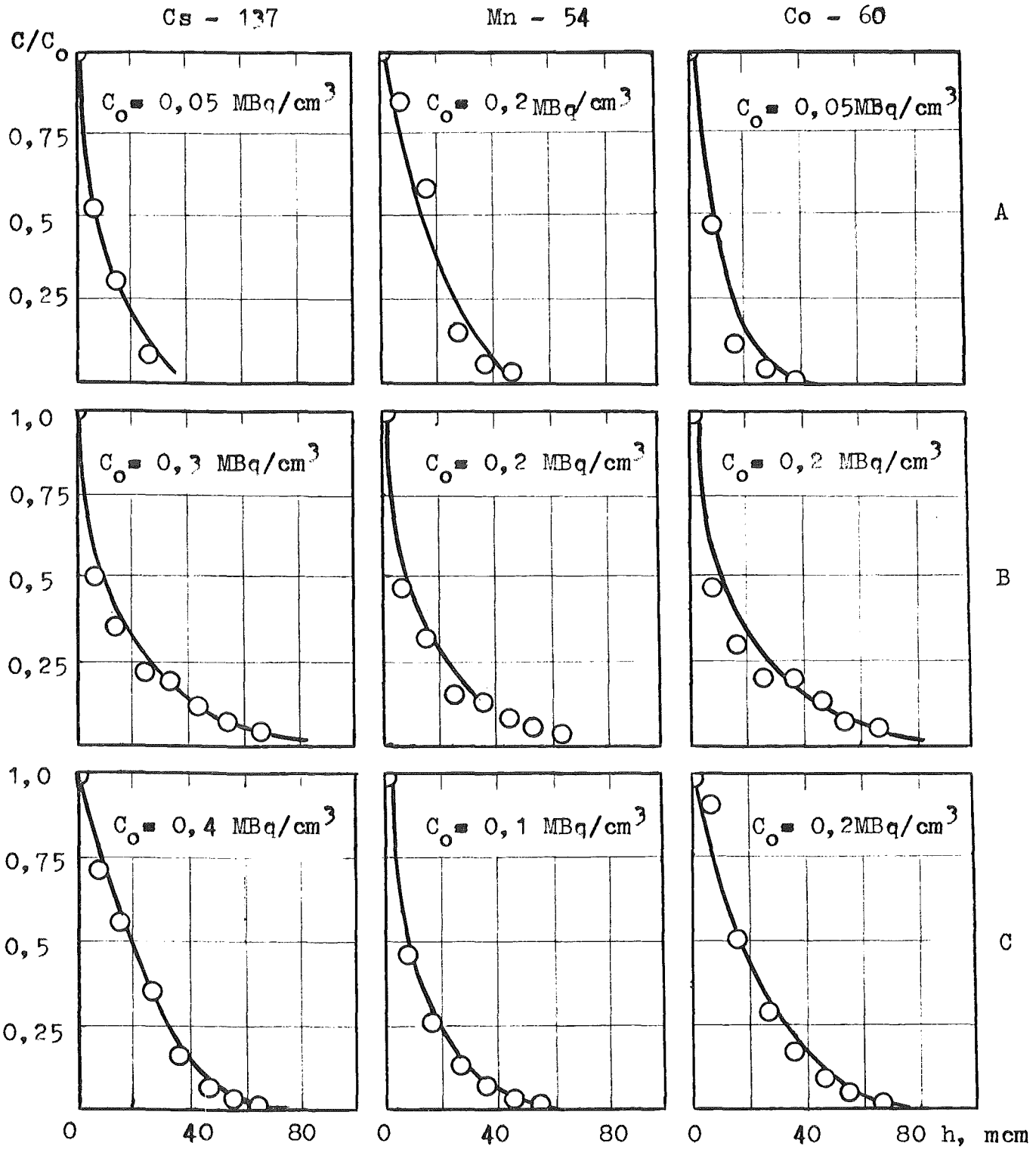


Fig. 9. Distribution of Cs-137, Mn-54, Co-60 on the wall thickness of reactor BR-10 primary pipeline various sections after 120000 hr of operation.

A - outlet collector (430 °C), B - big thermocompensator (430 °C), C - small thermocompensator (350 °C).

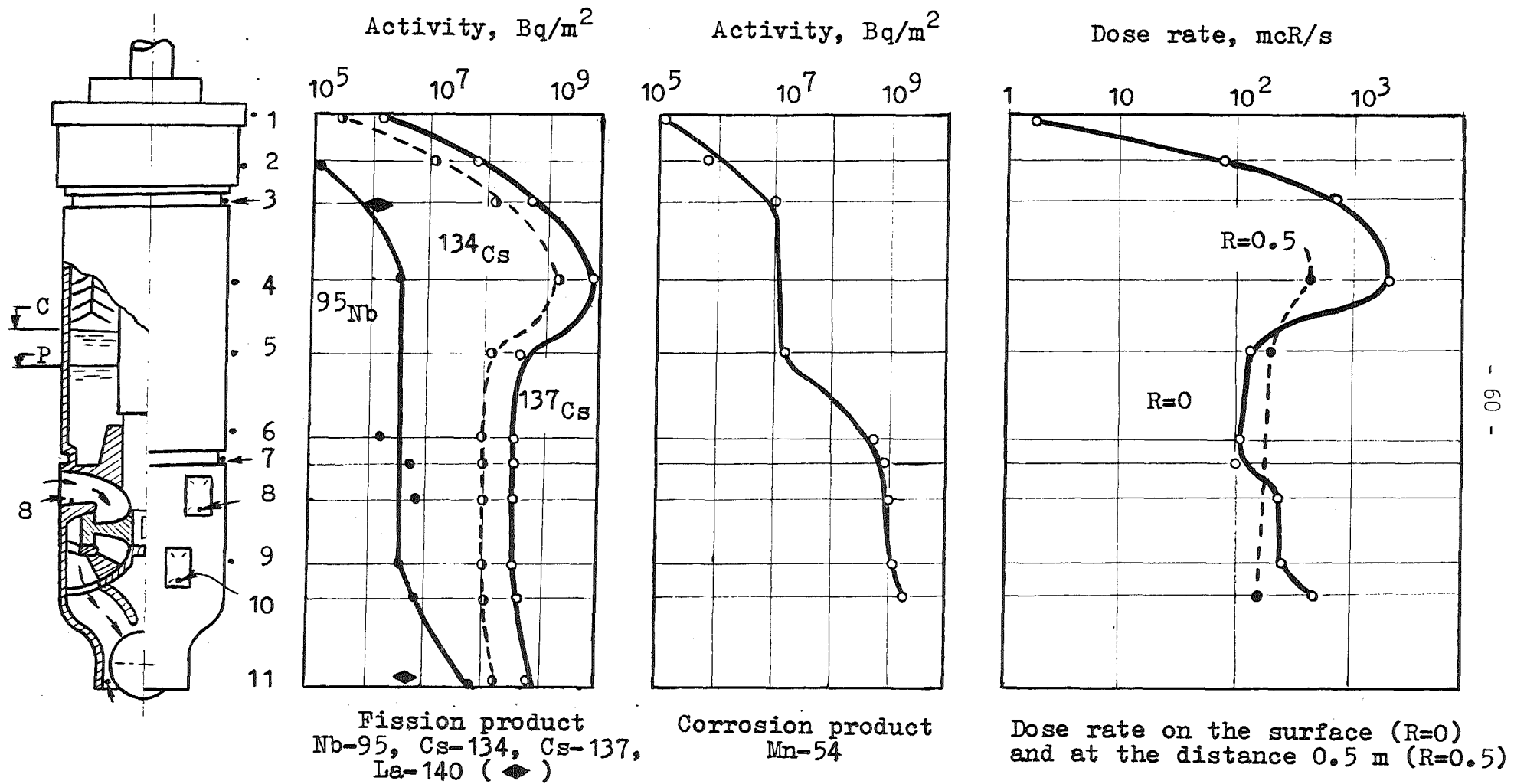


Fig. 10. Radioactive depositions and gamma-radiation distribution over surface of the primary pump's removed unit before and after vapour-water washing.

Designations : C - inoperative sodium level, P - operative sodium level.

P.S.1. EXPERIMENT.

RELEASE AND BEHAVIOUR OF FISSION PRODUCTS AND FUEL INSIDE A  
SODIUM-IRRADIATION LOOP.

R.Borsari, ENEA-Bologna, Italy

J.P.Hairion, CEA-Grenoble, France

I - INTRODUCTION

The P.S.1. experiment has been carried out in SILOE reactor at Grenoble in the frame of a joint experimental program among CEA, ENEA, KFK.

The main objectives of the experiment were:

- pin failure evolution;
- localisation and characterisation of a failure in a power plant;
- contamination by fission products and fuel of the irradiation device.

Only the last point will be discussed in this paper.

II - EXPERIMENT

The test was performed in a closed sodium-loop (FIGURE 1) which consisted of a main circuit driven by thermopumps with a forward leg, where was set the fuel pin, placed beside the reactor core, and a back leg joint by a upper and a lower "U" shape, and a derivative secondary circuit driven by a induction pump.

In the secondary circuit were set up two sensible volumes to allow, by means of fission chamber, the analysis of the fission products emitters of delayed neutrons, an oxides trap, made of steel wool, and a expansion vase to compensate for the sodium thermic dilation and to sample fission gas.

The main geometrical data are:

primary loop length = 455 cm

primary loop sodium content = 1028 cm<sup>3</sup>

secondary loop sodium content(at 560 C) = 852 cm<sup>3</sup>

trap sodium content = 59 cm<sup>3</sup>

FIGURE 1 shows also some temperatures mesured along the device.

It must be pointed out that the cold spot in the back leg is just before the neutron flux zone because in that zone there is a slight increase of the temperature due to the gamma power dissipation and the electric heating.

The main characteristics of P.S.1 pin before irradiation were:

$\varnothing_e = 8.65$  mm ;

$\varnothing_i = 7.50$  mm ;

Cladding material 15/15 Ti (coldworked, annealed) ;

$\varnothing_e(\text{pellet}) = 7.27$  mm ;

$\varnothing_i(\text{pellet}) = 2.$  mm ;

$\text{PuO}_2 / (\text{U} + \text{Pu})\text{O}_2 = 13.09$  .

The pin was preirradiated in PHENIX up to a burn-up of about 11 at.‰.

To adapt the pin to the device the lower expansion plenum was

suppressed and the pin was pressured up to  $4 \times 10^6$  Pa with helium.

The pin was irradiated in Siloe reactor during three cycles, in all for about 20 days; the primary failure happened after 6 irradiation days, the secondary failure after 10 irradiation days.

A gamma-scanning facility, placed beside the wall of the reactor-pool, allowed at the end of every irradiation cycle to measure the quantities of the different fission products gamma-emitters along the device.

### III - RESULTS

The main questions investigated were:

- a) evaluation of the fuel-tracer character for certain fission products (F.P.);
- b) balance of released for the different fission products and for the fuel;
- c) distribution along the device of the fission products related to the sodium volume and the temperature distribution during operation;
- d) effectiveness of the oxide trap in relation to the different fission products.

#### III-a FUEL TRACER FISSION PRODUCTS

The  $^{95}\text{Zr}$  and the  $^{103}\text{Ru}$  are strictly tracers of the escaped fuel; this conclusion relies upon:

- The distributions of  $^{95}\text{Zr}$  and  $^{103}\text{Ru}$  are nearly identical



all over the loop (compare FIGURE 2 and FIGURE 3).

- The distributions of the two F.P. in the trap show a heap in the inlet side (hot side) in opposite of all other F.P. that show a complementary distribution (heap in the cold side); this distribution can be explained as a filter effect of the steel wool over the fuel particles (FIGURE 4 shows the distribution of  $^{95}\text{Zr}$  in the trap).

- The ratios  $^{95}\text{Zr}/^{103}\text{Ru}$ , between the quantities measured along the loop and created inside the pin, are very close.

The  $^{140}\text{Ba}$ , instead, can be estimated to be released for 1 part as bound to the fuel and for 7 parts as free fission product.

### III-b BALANCE OF RELEASE

In the TABLE 1 is shown the balances of release for some fission products, at the end of irradiation.

To estimate the precision of the results it must be noticed that the sodium has been analysed to an extent of 67% in the primary loop and 24% in the secondary loop, an extrapolation over the total sodium volume was made; for the aerosol present in the expansion vase no measurements were available.

Therefore the release rates for the gaseous and volatile fission products could be wrong in shortage.

### III-c DISTRIBUTIONS

The  $^{134}\text{Cs}$  and the  $^{137}\text{Cs}$  have a concentrations in the sodium (atoms/mm<sup>3</sup> of cavity) uniform along the loop; therefore they

appear to be mostly dissolved in the sodium.

This statement has been also proved with a gamma-scan, carried out at the end of irradiation, over the transfer vase (FIGURE 1) where was poured the sodium of the loop: about 70% of the total Cesium escaped has been found again in the transfer vase; in the steel wool of the trap, on the contrary, where the ratio surface/volume is very high, the Cesium did not move.

Their distributions in the trap are sensitive to the temperature, with a heap on the cold side (outlet side).

FIGURE 5 gives the distribution of  $^{134}\text{Cs}$ .

FIGURE 6 gives a detailed distribution of  $^{134}\text{Cs}$  in the trap.

The  $^{131}\text{I}$  and the  $^{132}\text{Te}$  are mostly deposited over the device structures; their distributions are strictly related to the temperature-distribution, with important heaps in the colder zones.

The FIGURE 7 gives the distribution of the  $^{132}\text{Te}$ .

It must be pointed out that the difference of temperature between the coldest point in the primary loop and the temperature in the near points is just few degrees.

The fuel lost by the pin is entirely deposited over the structures; this statement has been proved by carrying out a reirradiation of the empty loop (without the fuel pin) and by analysing, by gamma-scan, the fissile matter reactivated.

The distribution shows also a temperature-dependence: the accumulations are stronger in the colder parts.

### III-d TRAP EFFECTIVENESS

The inlet and outlet temperatures of the cold trap, made by steel wool, were respectively 440 C and 350 C, the temperature at the top of the pin was 560 C.

The TABLE 2 gives the concentration-ratios: trap/primary loop and trap/secondary loop, at the end of the last irradiation cycle.

It goes out (see TABLE 2) that the effectiveness of the trap for  $^{131}\text{I}$  and  $^{132}\text{Te}$  is largely predominant in comparison to the other nuclides.

#### IV - CONCLUSIONS

Due to the large provoked breach, the fuel loss was very important (about 1 g.); certainly this quantity of fuel loss is not completely representative for a natural failure.

Nevertheless the consistency of the fuel-release and beside that of the fission products, have permitted a more accurate study of their behaviours out of the pin.

The following conclusions can be drawn from the P.S.1. test:

- Zirconium and Ruthenium are strictly fuel-tracers.
- The Cesium released is uniformly dissolved in the sodium, a small fraction is deposited over the walls of the device and it cannot be removed when the sodium is taken off.
- All others F.P. analysed and fuel released are mostly deposited over the device structures with stronger heaps in the colder zones; the temperature-dependence is very marked for Iodine and Tellure.
- The balances of release are in good agreement with the results of previous experiments; the release of Cesium is always to an important extent.
- The effectiveness of the trap, made of steel wool, is far highest for Iodine and Tellurium, but, on the contrary, negligible for Cesium.

Because of this last fact and the important amount of Cesium release, the removal of Cesium from the primary sodium is pointed out as the predominant problem in the long term Run Beyond Cladding Breach.

This point needs to be investigated in future experiments.

TABLE 1

Balance at the end of irradiation

| nuclide | escape rates<br>(released/born) |
|---------|---------------------------------|
| 95 Zr   | 0.196%                          |
| 103 Ru  | 0.201%                          |
| 140 Ba  | 1.15 %                          |
| 134 Cs  | 62.6 %                          |
| 137 Cs  | 68.6 %                          |
| 131 I   | 4.34 %                          |
| 132 Te  | 3.11 %                          |

TABLE 2

Ratios of the concentration trap/loop1 and trap/loop2  
at the end of irradiation

| nuclide | $\frac{\text{atoms/mm}^3(\text{trap})}{\text{atoms/mm}^3(\text{loop1})}$ | $\frac{\text{atoms/mm}^3(\text{trap})}{\text{atoms/mm}^3(\text{loop2})}$ |
|---------|--|--|
| 131 I   | 479.   | 1419.  |
| 132 Te  | 1170.  | 1862.  |
| 134 Cs  | 2.22   | 2.22   |
| 137 Cs  | 2.16   | 2.16   |
| 140 Ba  | 0.68   | 2.89   |

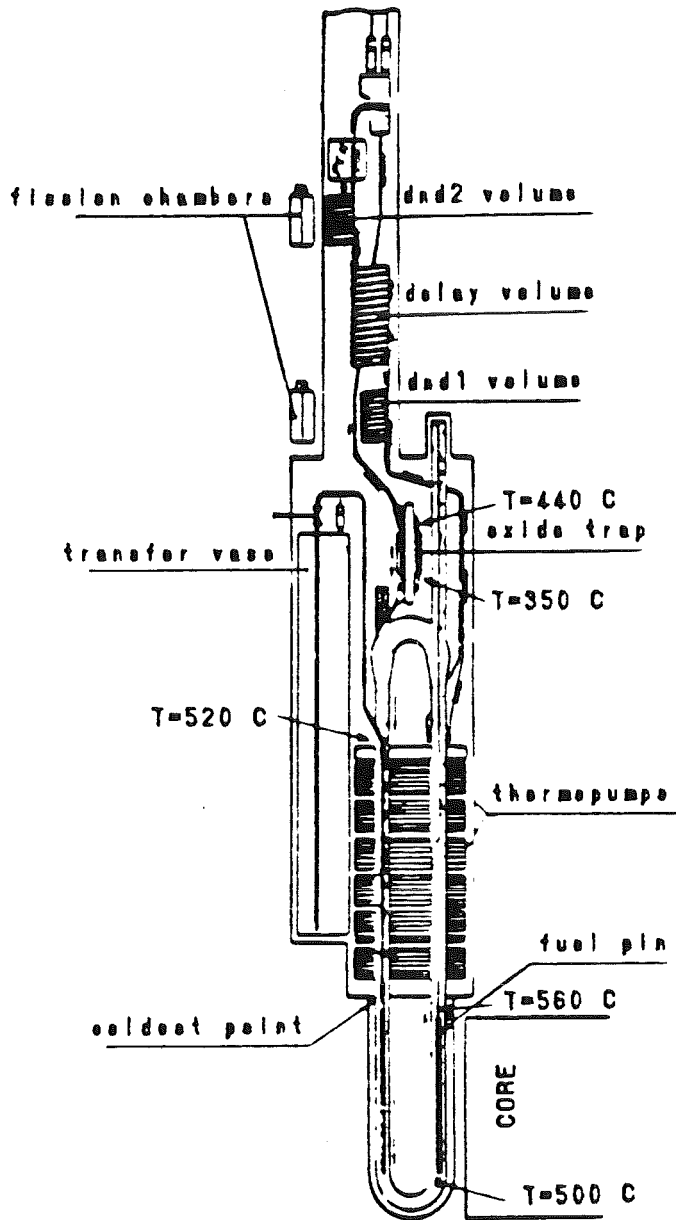


FIGURE 1

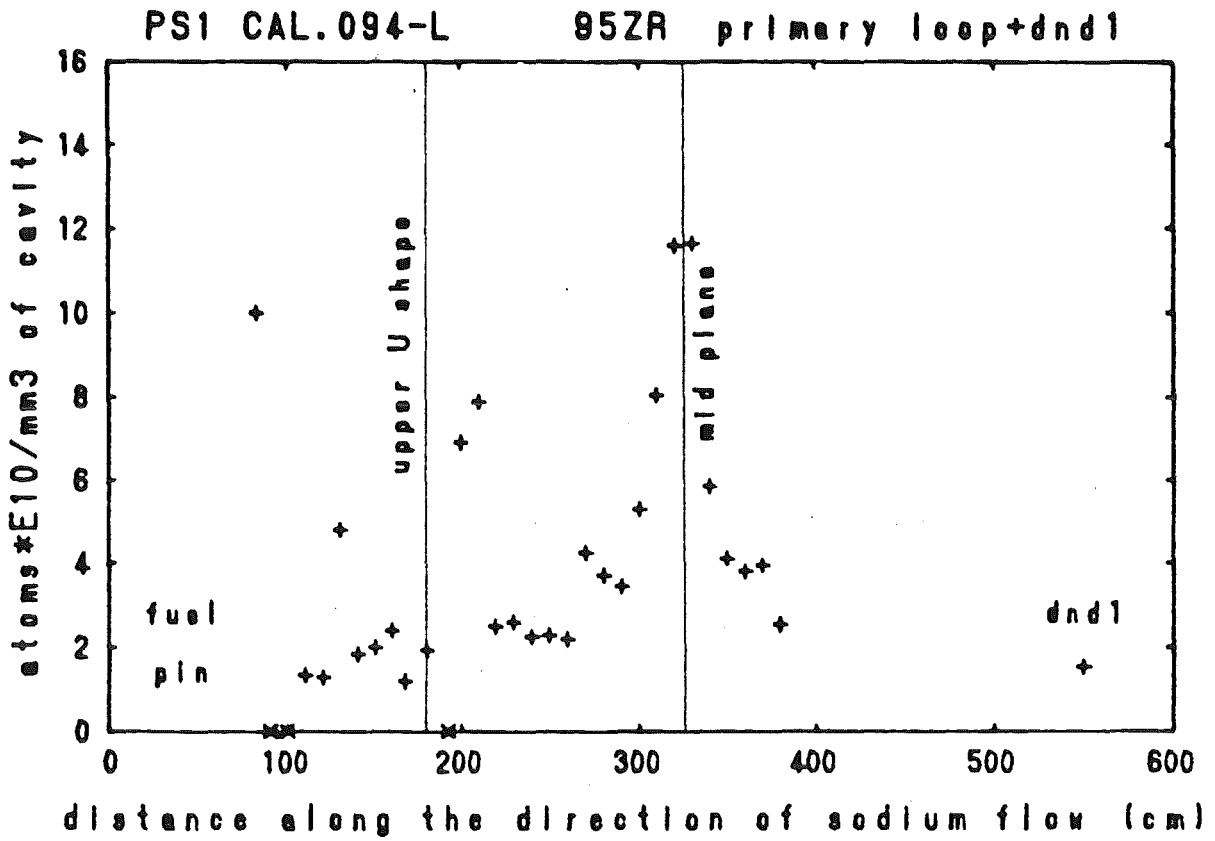


FIGURE 2

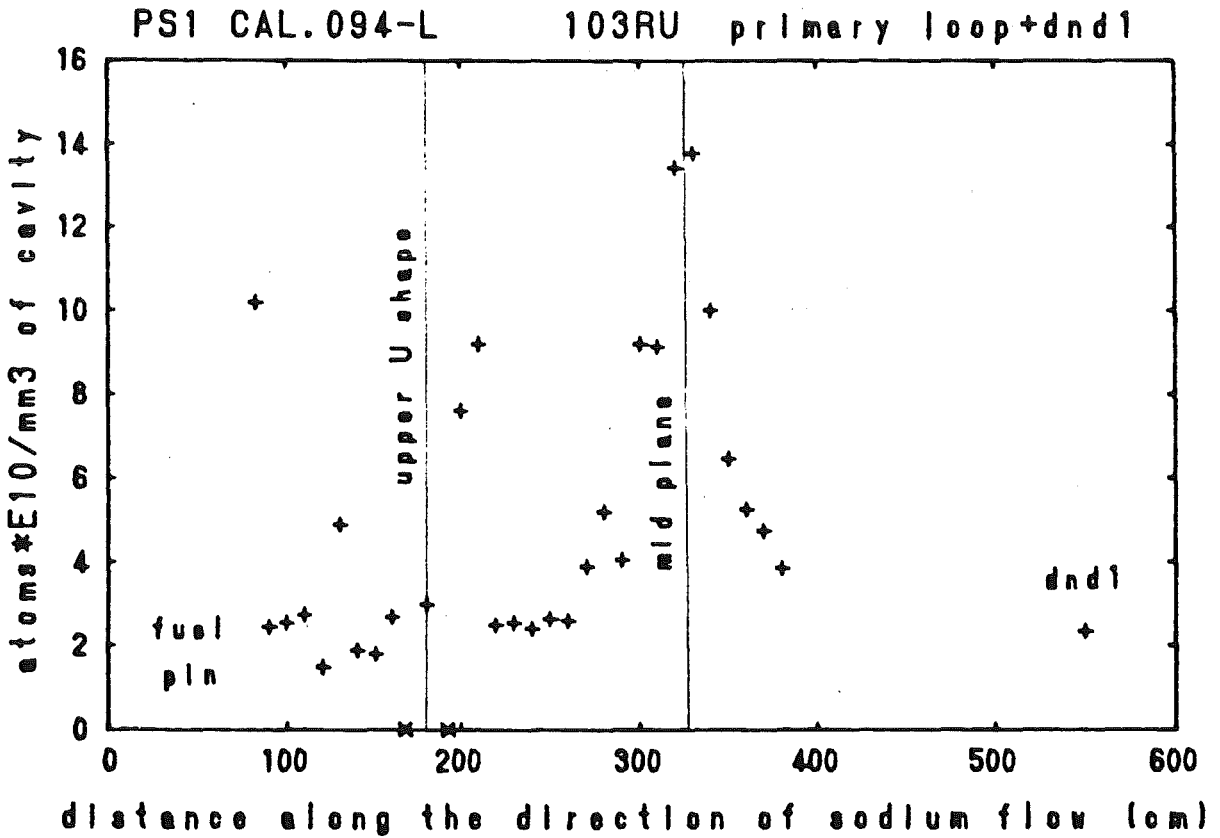


FIGURE 3

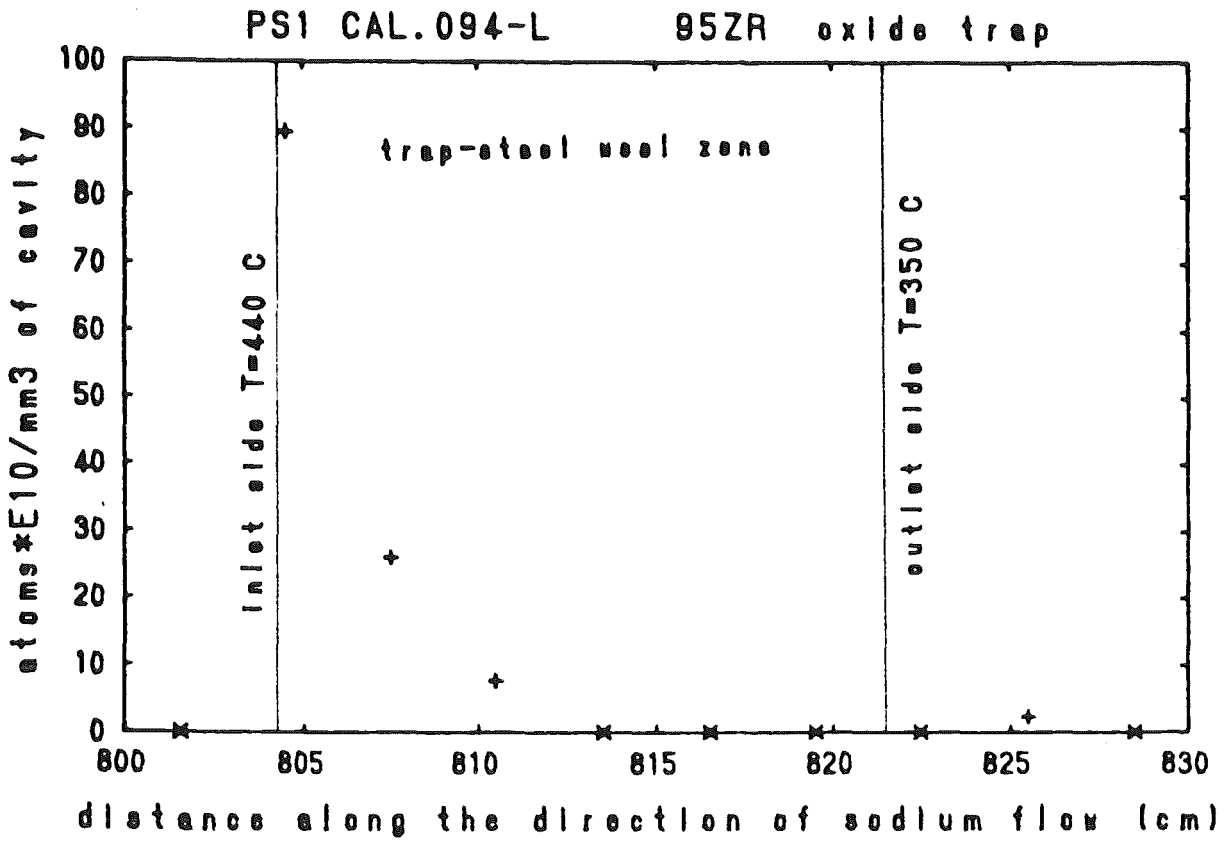


FIGURE 4

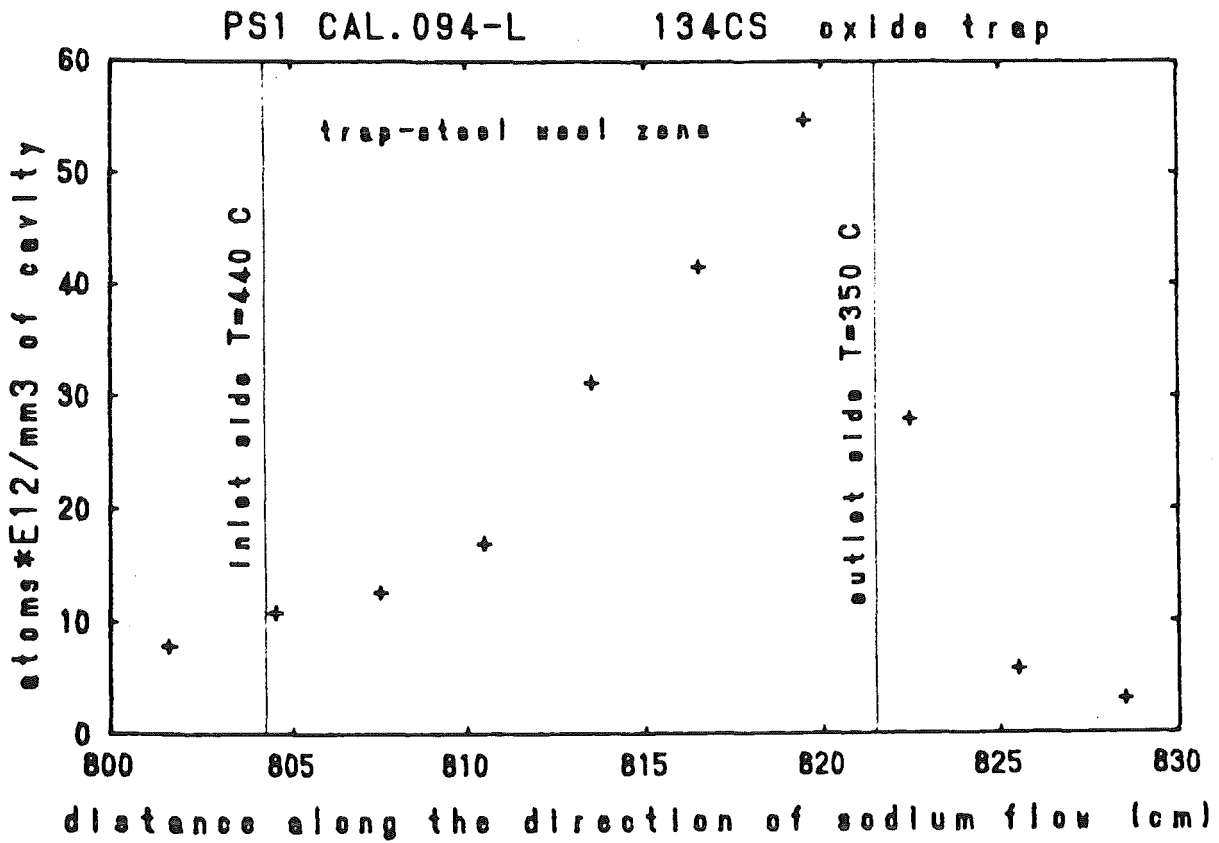


FIGURE 6



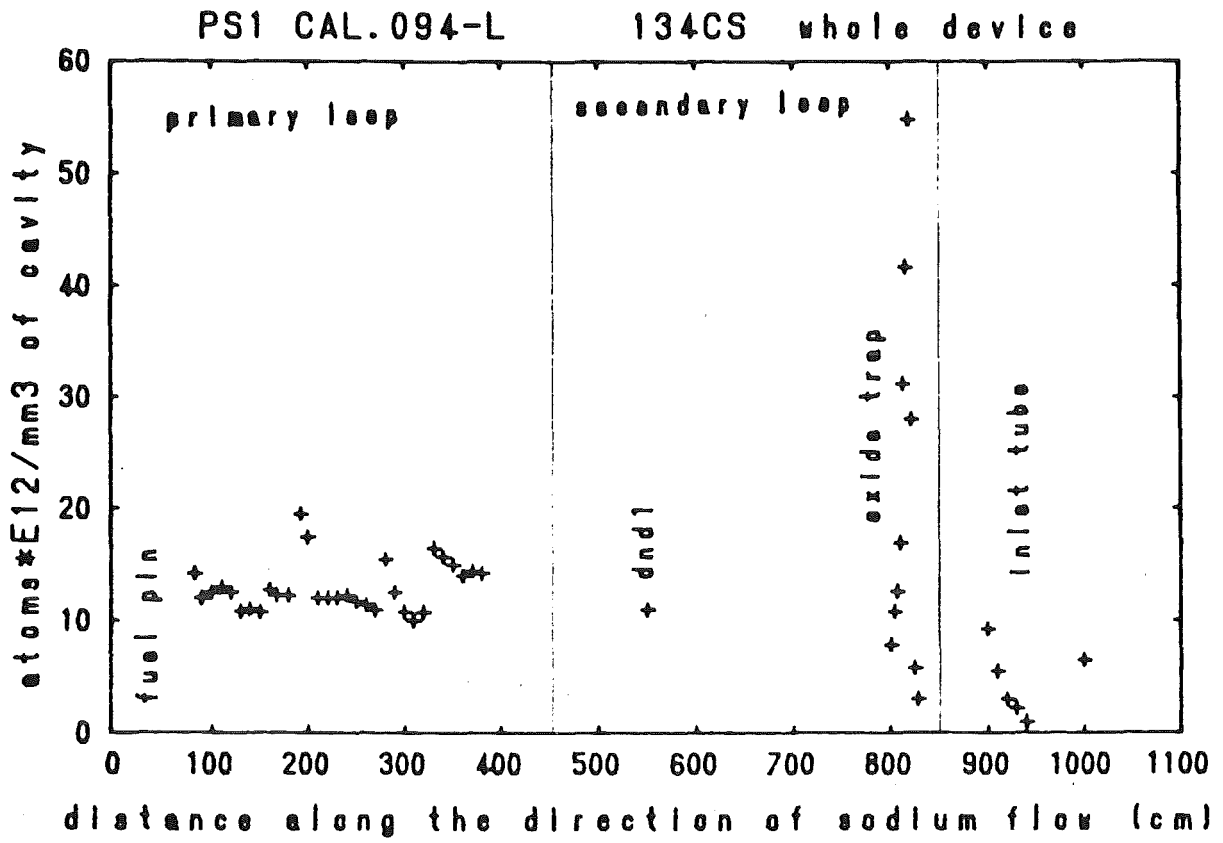


FIGURE 5

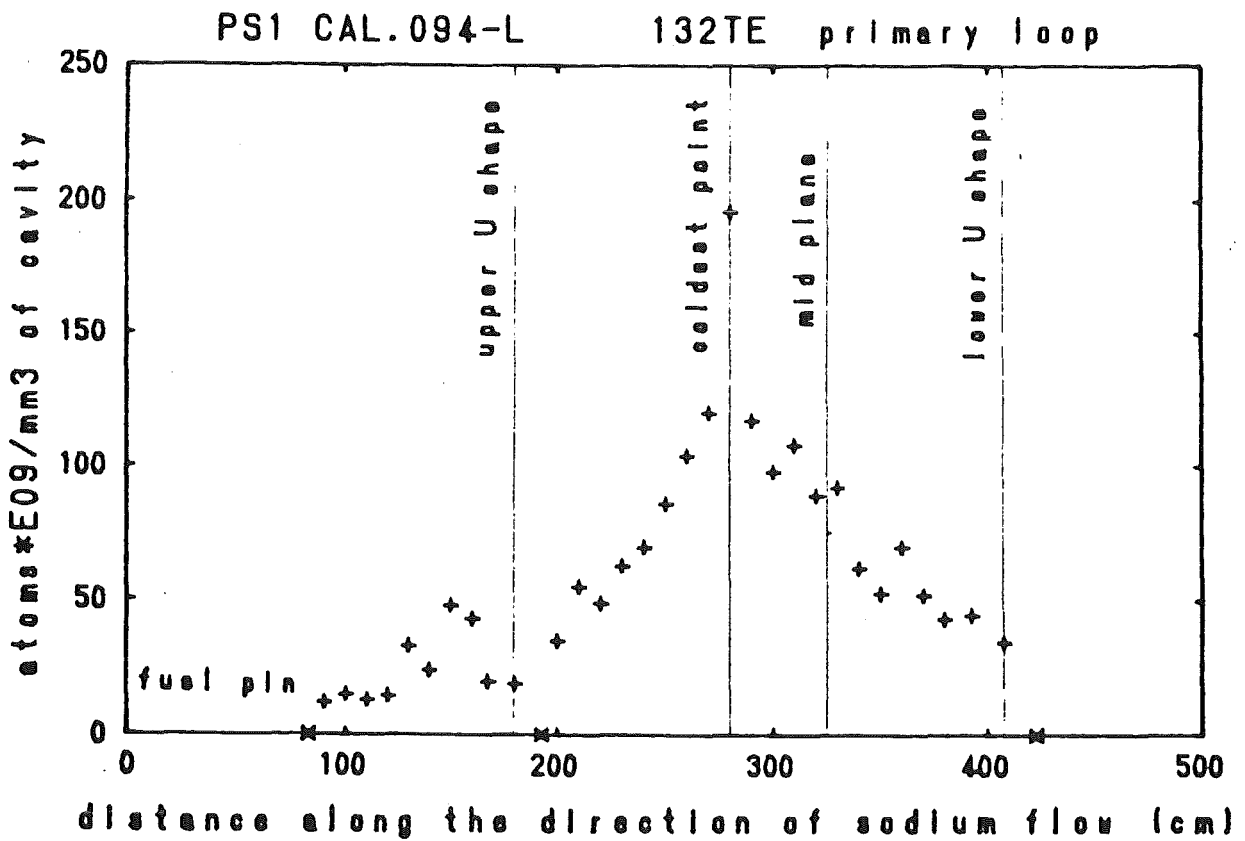


FIGURE 7

REFERENCES

/1/ Veyrat - Dupont - Rousseau

"FAST REACTOR IRRADIATION FACILITIES IN THE REACTOR  
DEPARTEMENT OF Grenoble Nuclear Research Centre".

Conference of fast and thermal fission reactor experiment - 8  
april 1982 - Salt Lake City.



HEDL-SA-3689 FP

CORROSION AND FISSION PRODUCTS IN PRIMARY SYSTEMS  
OF LIQUID METAL COOLED REACTORS IN THE USA

W.F. Brehm, R.P. Colburn, H.P. Maffei, W.P. Stinson

W.L. Bunch, R.A. Bechtold

Westinghouse Hanford Company  
Richland, Washington, USA

W.H. Olson

Argonne National Laboratory-West  
Idaho Falls, Idaho

IAEA/IWGFR Specialists' Meeting on Fission  
and Corrosion Products in Primary Systems of  
LMFBR's  
May, 1987

Karlsruhe, Federal Republic of Germany

**COPYRIGHT LICENSE** — By acceptance of this article, the publisher and/or recipient acknowledges the U.S. Government's right to retain a nonexclusive, royalty-free license in and to any copyright covering this paper.

**HANFORD ENGINEERING DEVELOPMENT LABORATORY** — Operated by the Westinghouse Hanford Company, P.O. Box 1970, Richland, WA, a subsidiary of the Westinghouse Electric Corporation, under U.S. Department of Energy Contract No. DE-AC06-76FF02170.

## INTRODUCTION

This paper presents a summary of the work in the USA to support the measurement and control of radionuclides in primary systems of liquid metal cooled reactors. The efforts to characterize and control the ingress of radioactive corrosion and fission products, fuel particles, and radioactivity in gas systems have been quite successful in the USA. Several recent papers attest to the degree of contamination control that has been achieved. (Refs. 1,2,3)

## CORROSION PRODUCTS

Transport Studies. The laboratory studies on transport of radioactive corrosion products were concluded several years ago and the summary was reported at the Karlsruhe symposium in 1981. (Ref. 4) The work showed that manganese-54 was released preferentially into sodium from stainless steel, that oxygen content of sodium in the range 0.003 to 2.5 wppm (vanadium wire equilibration measurement) did not affect the release of the manganese, and that the manganese deposited preferentially on nickel surfaces at all positions in test rigs (hot leg or cold leg), or preferentially in the cold leg if no nickel-rich surface were present. Cobalt-60, on the other hand, was preferentially retained in the stainless steel; the release was a function of oxygen in sodium at 0.5 and 2.5 wppm but no decrease in cobalt-60 release was obtained by decreasing the oxygen level to 0.003 wppm. The temperature dependence of cobalt release was less marked than that of manganese release in the temperature range 538°C. to 604°C. Iron was the only major constituent of stainless steel to show a release dependency on oxygen content, verifying the theory of Weeks and Isaacs (Ref. 5). There was correlation on individual specimens in this test program between iron release and cobalt release, suggesting that the cobalt is released as part of an iron-rich particle. The fate of these particles, which according to Weeks and Isaacs are probably an iron (cobalt)-sodium-oxygen compound on the steel surface, is not known; it is possible that they dissolve in the sodium stream once detached from the surface. Cobalt deposited preferentially in the hot legs of the test systems downstream from the release points and did not show any preferential deposition on nickel surfaces.

The results of this work were used to update the calculational model for predicting the distribution of radioactive material in FFTF. The release and deposition patterns of the radioactive corrosion products in FFTF are similar, but with significant differences, to those observed in the test loops; this point will be discussed in detail later in the paper.

Radionuclide Trap Development. Again, the laboratory and in-reactor test program has been completed on devices to remove manganese from flowing sodium. (Refs. 6 and 7) The work showed that pure nickel, at any location in the main circuit, was effective at removing manganese from sodium. Six tests in EBR-II and one in FFTF were completed; these

tests showed that operation of a nuclide rolled-sheet trap above the fuel pins is completely feasible from a safety standpoint. The EBR-II tests also showed that one trap removed three to four times the amount of manganese than was release from the fuel assembly beneath it. The inference to be drawn from this result is that (1) the manganese circulates in the sodium and is not completely deposited in the first pass, (2) it would not be necessary to equip all fuel assemblies with a nuclide trap. Perhaps only the outer rows or the reflector assemblies need to be so equipped.

However, the complication and added costs of fitting fuel assemblies have thus far made nuclide traps unattractive. Feasibility studies of nickel-plating the upper part of the fuel pins (even though such a test was done in EBR-II), or adding diffusion barriers such as molybdenum or nickel aluminide to the fuel pin surface have shown these concepts to be equally unattractive.

#### FISSION PRODUCTS AND TRITIUM

Fission Product Laboratory Studies. The affinity of cesium for various forms of pure carbon has been known for quite some time; in the USA the pioneering work of Olson resulted in a device for removal of cesium from sodium being tested in the laboratory and then installed on EBR-II. (Ref 8) Subsequent laboratory testing by Colburn (Ref. 9) showed that it would be feasible to operate such a device on-line if need be, rather than only during periods of reactor shutdown. The cesium removal trap on EBR-II has operated effectively since its installation in 1978. (Ref. 10)

Tritium Control. A thorough review of tritium control technology, and predictive methods for use on large sodium-cooled reactors was made by McGuire and Renner (Ref. 11) in 1978; in summary, the presence of oxide barriers on stainless and ferritic steel surfaces exposed to the environment, primary cell atmospheres, or to the water side of a steam generator eliminates much of the tritium diffusion outward. The tritium that remains in the primary and secondary sodium circuits is removed by co-precipitation with sodium hydride in the cold traps on both primary and secondary circuits. The on-line hydrogen meter (Ref. 12) has been modified by addition of scintillation chambers to serve as an on-line tritium meter; these have operated successfully on EBR-II for many years. (Refs 10 and 13) Neither FFTF nor EBR-II has reported any particular problems with tritium release or control.

#### ANALYTICAL PROCEDURES AND SAMPLING METHODS

Methods for sampling and analysis for EBR-II and FFTF have been described in previous reports (Refs. 10 and 14); there have been no new developments in analytical procedures since then. Particle formation in FFTF sodium is suggested based on results of trace metal determinations. Iron, chromium, and nickel concentrations in the samples vary from <0.1 ppm to 44 ppm without apparent other pattern.

If nickel rather than tantalum sampling cups are used for obtaining FFTF sodium samples, measurable amounts of Mn-54 and Zn-65 are found adhering to the sample cup.

### REACTOR EXPERIENCE

Nuclide Concentrations and Behavior - EBR-II. Table 1 shows the nuclides found in the primary system of EBR-II. Sodium-24 activity in the primary system reaches a level of 104 MBq/g (2.8 mCi/g), it of course decays away in about fourteen days so is not a factor in plant maintenance. The sodium-22 activity reaches an equilibrium value of 5 kBq/g (140 nCi/g).

With the exception of the Sb-124, the combined radioactivity from the activation products of sodium impurities has remained less than that of sodium-22. The Sb-124 reached a maximum level of 21 kBq/g (570 nCi/g), and was introduced to the sodium as a result of failure of an antimony capsule in an antimony/beryllium neutron source in 1984. It has since decayed away. The other nuclides resulted from activation of tin and bismuth spilled into the sodium from the eutectic seals of the rotating plugs. The tin concentration has slowly built up in the sodium to about 100 wppm, since the tin is very soluble in sodium and does not segregate to system surfaces nor precipitate in the cold trap. Bismuth, on the other hand, is removed by the cold trap; the bismuth concentration in sodium is 2 to 5 wppm. The major activation product of bismuth is alpha-emitting polonium-210, fortunately the deposition of bismuth in the cold trap keeps the circulating inventory in the sodium low and retards Po-210 buildup. The antimony is much less soluble than tin, and deposited in the cold trap causing temporary radiation levels near the trap as high as 30 R/hr.

The material activation/activated corrosion product nuclides detected are Mn-54, Cr-51, Co-58, Co-60, and Ta-182. Of these, only Mn-54 is present in significant quantities. It is readily transported through the primary circuit and is the dominant gamma-emitting nuclide on all components that have been removed from the primary system for maintenance. The cobalt-60 and chromium-51 are thought to be the result of in-situ activation rather than transported corrosion products. The Ta-182 comes from the activation of tantalum which was used to clad the antimony capsules in the neutron-source assemblies, and from tantalum impurities in other alloys. Since 1969, the tantalum has diminished. Radioactivity from all these materials, including Co-58, although sometimes detectable, is insignificant compared to the Mn-54.

Fission products have been introduced into the sodium from cladding breaches. Through 1975, there were very few breaches and these were removed from the reactor as soon as they were located. Since then, however, selected experimental fuel subassemblies with breached cladding have undergone irradiation testing lasting from several days to several weeks. The significant sodium-soluble fission products are Cs-134, Cs-137, H-3 (tritium), and I-131. Of course, the tritium diffuses readily through the fuel cladding and is released into the

sodium without cladding breach. Until 1978, the cesium isotopes were the major cause for concern. Cesium collected in the cold trap; in addition because of its higher vapor pressure it is preferentially found in cover gas spaces where it deposits on cool surfaces, increasing maintenance problems. By 1978 the Cs-134 and Cs-137 concentrations had reached 1.67 kBq/g (45 nCi/g) and 13 kBq/g (351 nCi/g) respectively. At that time the carbon-filled trap was installed. Intermittent operation of the trap since then has maintained the total cesium isotope inventory below 1.2 kBq/g (32 nCi/g).

Iodine isotopes also segregate to the cold trap and other cool surfaces. Their contribution to the overall radioactive burden is minimal, however, because of their short half-lives.

Tritium is found in low concentrations, below those that present any operation and maintenance problems, in plant systems from the primary sodium to the condenser cooling water.

The principal sodium-insoluble fission product found on primary sodium components is the beta-emitter Sr-90. The shorter-lived Sr-89 is also present, but at much lower levels of activity. The strontium is probably present in the coolant as a result of the release and transport of sodium-soluble precursors Rb-90, Kr-90, and Br-90, with decay to strontium occurring in the primary sodium, followed by deposition on the primary surfaces. Little or no strontium was found on primary pump removed in 1971, prior to the start of the run-beyond clad-breach test program. However, considerable strontium was found on the primary pump removed in 1982, resulting in a beta dose rate of 1 to 10 R/hr.

A behavior similar to that for Sr-90 is theorized for Ba-140/La-140. Its precursors are Cs-140, Xe-140, and I-140, with half-lives ranging from 0.86 to 65 sec. These nuclides can transport from the fuel to the bulk sodium before they completely decay. Barium and lanthanum are both insoluble in sodium and plate out on component surfaces.

Other sodium-insoluble fission products, such as Zr-95/Nb-95 and Ce-141, have not been found in significant quantities in the primary sodium.

EBR-II Radiation Levels. Both primary sodium pumps have been removed from the primary tank for maintenance. The #1 pump, serviced in 1971, showed a peak gamma activity of 150 mR/hr, practically all Mn-54, at a distance of about 0.3 m. The #2 pump, removed in 1982, showed a combined beta-gamma activity of up to 10 R/hr, and a peak gamma activity of 500 mR/hr, at a distance of 0.3-0.45 m.

Background radiation levels in the general area of the sodium service piping outside the primary tank are 20-50 mR/h with hot spots of 100-200 mR/h. Radiation levels adjacent to the original cold-trap crystallizers were 2-10 R/hr. Except for the antimony capsule failure



mentioned earlier, radiation levels adjacent to the smaller, integrally-shielded cold-trap crystallizer have been <100 mR/hr.

It is worth noting that the average radiation exposure for plant workers has declined steadily since 1977, despite the removal of the pump with the high radiation level, and the aggressive run-beyond-clad-breach programs.

FFTF Nuclides and Concentrations. Table 2 shows the maximum concentrations of nuclides in the sodium. The sodium-22 level is at present is about 20kBq/g (0.55 mCi/g), it has been higher when the reactor was operating at 400 mWt and with long uninterrupted cycles. Figure 1 shows the amount of sodium-22 compared to the predicted amount. It can be seen that the agreement is good, especially during the early operation of the plant.

A plot of Cs-134 and Cs-137 activity is shown in Figure 2. The level is decreasing, suggesting a removal mechanism of some kind. Smears from two floor valves showed greatly enhanced concentration of cesium relative to sodium. The presence of Cs-136 (halflife 13.1 days) at an apparent equilibrium level (about 0.037 kBq/g or 1 nCi/g) has been observed after months have elapsed since the last leaking fuel assembly. A possible explanation for the equilibrium is the presence of Cs-135 (halflife  $10^6$  years), which would circulate undetected until neutron activation to Cs-136.

Alpha activity in FFTF has been detected; the alpha energies fit three nuclides: Po-210, U-232, or Am-243. Of these, Po-210 was considered the most likely in the absence of other precursors of the uranium decay chain. Since Po-210 can be formed by neutron activation of bismuth, very small traces of bismuth in the sodium (measured <0.01 to 0.02 wppm) was considered the source of this activity. Periodic measurements were made over an eight month period to obtain a curve fit which confirmed the identity of the alpha emitter as Po-210.

Cesium Trap in FFTF. The cesium concentration, as noted, has been increasing in the primary sodium as a result of several fuel pin failures and has reached a maximum concentration of 7.4 Kbbq/g or 200 nCi/g. This concentration in primary sodium is not significant compared to the manganese and sodium nuclides, but the high vapor pressure of cesium results in its transport into the cover gas space where it condenses on cool surfaces and is concentrated several orders of magnitude higher than what is seen in the sodium. This has resulted in increased difficulty cleaning refueling equipment and is making maintenance of equipment exposed to the cover gas increasingly difficult. Recent work on a control rod drive mechanism (CRDM) showed a hot spot of 2.5 R/hr at the surface. The predicted radiation level was 100 mR/hr from activation of the metal.

The installation of a cesium trap in the primary sodium loop will reduce the continued transport and deposition of cesium to the cover gas space. It is a modified spare closed loop cold trap, with the

stainless steel mesh removed and replaced with Reticulated Vitreous Carbon. It will be operated on an "as needed" basis at a temperature 150° to 175°C, when sodium analysis indicates a high concentration of cesium in sodium. Figure 3 shows a schematic of the trap.

Radiation Levels in FFTF from Corrosion Products. Measurements have continued on the periscope hole for radiation levels, and the surveillance holes for nuclide gamma spectra, as described in Reference 7. The results are shown in Fig. 4. There are several interesting points to make about the data of Fig. 4.

The gamma radiation reported on Fig. 4 is from Mn-54 only. The sodium-22 and cesium-137 contributions have been subtracted from the total. No Co-60 or Co-58 has been found, despite predictions of 10-20 mR/hr contribution from these isotopes. The Co-60, especially, should be detectable since it has a higher gamma energy than any of the other nuclides. This result indicates that the cobalt-60 is not being released at the predicted rate, or is not being transported to the heat transport system. Analyses from wash water from the fuel cleaning station indicate Co-60 on the fuel assemblies and in the adherent sodium.

SP-307 is in a hot leg location (See Figure 5). The radiation level measured there is consistently only about one-third of what is predicted, indicating more rapid transport of Mn-54 through the heat transport system.

The radiation levels at SP-303, which view both hot leg and cold leg locations, and SP-308, a cold leg location, were fairly close to predictions for over a year, but recently have risen to considerably more than predicted. There appears to be a leveling off.

We as yet have no good explanation for the lack of cobalt isotopes, nor the increase in Mn-54 levels above what was predicted. The reactor operating cycles (times and temperatures) are fairly close to the ones used in making the calculations from the predictions.

The cesium-137, although present in measurable amounts in the heat transport system, is not contributing significantly to the radiation levels except on components in the cover gas space. No measurements of radiation levels in the cold trap vault have been made.

The measurements are continuing at each reactor outage. As mentioned, the sodium-22 contribution to the radiation level is near 300 mR/hr depending on the location in the cell, fairly close to the predicted level.

Despite the radiation level of nearly 1R/hr from the combination of Na-22 and Mn-54, an entry has been made into the equipment cells when the reactor was down, to repair some instrumentation. This job was accomplished without excessive radiation exposure to the staff.

ACKNOWLEDGMENT

This work was sponsored by the United States Department of Energy under contract numbers DE-AC06-76FF02170 and W-31-109-ENG-38.

## REFERENCES

1. W. H. Olson, "The Impact of Radionuclides on Maintenance of Experimental Breeder Reactor II", Proc. Int. Meeting on Nuclear Power Plant Maintenance, Salt Lake City, March 1986
2. M. L. Grygiel and C. G. McCargar, "The Replacement of an Electromagnetic Primary Sodium Sampling Pump in the Fast Flux Test Facility", HEDL-SA-3292-FP, presented as in Ref. 1.
3. R. A. Bechtold et al., "Reactor Cover Gas Monitoring at the Fast Flux Test Facility", HEDL-SA-3589-FP, Presented at IAEA Specialists' Meeting on Fast Reactor Cover Gas Purification, Richland, September 1986
4. W. F. Brehm and R. P. Anantatmula, "Corrosion Product Release into Sodium from Austenitic Stainless Steel", in Material Behavior and Physical Chemistry in Liquid Metal Systems, ed. Borgstedt, Plenum Press, New York, (1982)
5. J. R. Weeks and H. S. Isaacs, Advances in Corrosion Science and Technology, 3 (1973) pp 1-66.
6. J. C. McGuire and W. F. Brehm, Nuclear Technology 48, (1980), p 101-9.
7. H. P. Maffei et al., "Measurement and Control of Radioactive Material Transport in the FFTF", in Proc. Third Int. Meeting on Liquid Metal Engineering and Technology, Thomas Telford Ltd, London (1985).
8. W. H. Olson and W. E. Ruther, Nuclear Technology 46, (1979) p. 318.
9. R. P. Colburn and H. P. Maffei, "Cesium Behavior and Control in Sodium Systems", in Proc. Second Int. Conf. on Liquid metal Technology in Energy Production, Richland, April 1980, CONF-800401.
10. C. R. F. Smith et al., "Sodium Technology Experience at EBR-II - 1976 to 1980", in CONF-800401.
11. J. C. McGuire and T. A. Renner, Atomic Energy Review, 16, 4 (1978), p 657.
12. D. R. Vissers et al., Nuclear Technology 12 (1971) p 218
13. M.M. Osterhout, "Operating Experience with On-Line Meters at Experimental Breeder Reactor II (EBR-II)", in CONF-800401.
14. R. A. Bechtold et al., "Experience with Chemistry Monitoring Systems at FFTF", as in Ref 7.

TABLE 1 EBR-II NUCLIDES

| <u>NUCLIDES</u>  | <u>HALF-LIFE</u> | <u>MAXIMUM ACTIVITY</u><br><u>Curies/g</u> |
|--|------------------|--|
| <u>Activation products of sodium:</u>                    |                  |  |
| <sup>22</sup> Na   | 2.6 y            | 1.4 x 10 <sup>-7</sup>                     |
| <sup>24</sup> Na   | 15 h             | 2.97 x 10 <sup>-3</sup>                    |
| <u>Activation products of sodium impurities:</u>         |                  |  |
| <sup>110m</sup> Ag                                       | 252 d            | 3.5 x 10 <sup>-9</sup>                     |
| <sup>113</sup> Sn/ <sup>113m</sup> In                    | 115 d/99m        | 8.8 x 10 <sup>-8</sup>                     |
| <sup>117m</sup> Sn                                       | 14 d             | 5.4 x 10 <sup>-8</sup>                     |
| <sup>124</sup> Sb  | 60.2 d           | 5.7 x 10 <sup>-7**</sup>                   |
| <sup>125</sup> Sb  | 2.73 y           | 1.6 x 10 <sup>-8</sup>                     |
| <sup>210</sup> Po  | 138 d            | 2.0 x 10 <sup>-10</sup>                    |
| <u>Material activation/activated corrosion products:</u> |                  |  |
| <sup>51</sup> Cr   | 27.7 d           | ---***                                     |
| <sup>54</sup> Mn   | 313 d            | 4.3 x 10 <sup>-9</sup>                     |
| <sup>58</sup> Co   | 70.8 d           | 1.3 x 10 <sup>-8</sup>                     |
| <sup>60</sup> Co   | 5.27 y           | 6.2 x 10 <sup>-10</sup>                    |
| <sup>182</sup> Ta  | 115 d            | ---***                                     |
| <u>Sodium-soluble fission products:</u>                  |                  |  |
| <sup>3</sup> H   | 12.3 y           | 3.0 x 10 <sup>-6+</sup>                    |
| <sup>131</sup> I   | 8.04 d           | 3.0 x 10 <sup>-7</sup>                     |
| <sup>134</sup> Cs  | 2.06 y           | 4.3 x 10 <sup>-8</sup>                     |
| <sup>137</sup> Cs  | 30.2 y           | 3.5 x 10 <sup>-7</sup>                     |
| <u>Sodium-insoluble fission products:</u>                |                  |  |
| <sup>89</sup> Sr   | 50.5 d           | 2.0 x 10 <sup>-8</sup>                     |
| <sup>90</sup> Sr/ <sup>90</sup> Y                        | 29 y/64 h        | 8.9 x 10 <sup>-9</sup>                     |
| <sup>140</sup> Ba/ <sup>140</sup> La                     | 12.8 d/40.2 h    | 2.8 x 10 <sup>-8</sup>                     |

- \* Most <sup>134</sup>Cs comes from activation of <sup>133</sup>Cs which results from the decay of the mass-133 fission products
- + Unusually high due to Li - containing experiments
- \*\* Due to Sb/Be neutron source failure
- \*\*\* Observed on components removed from reactor, never in sodium.

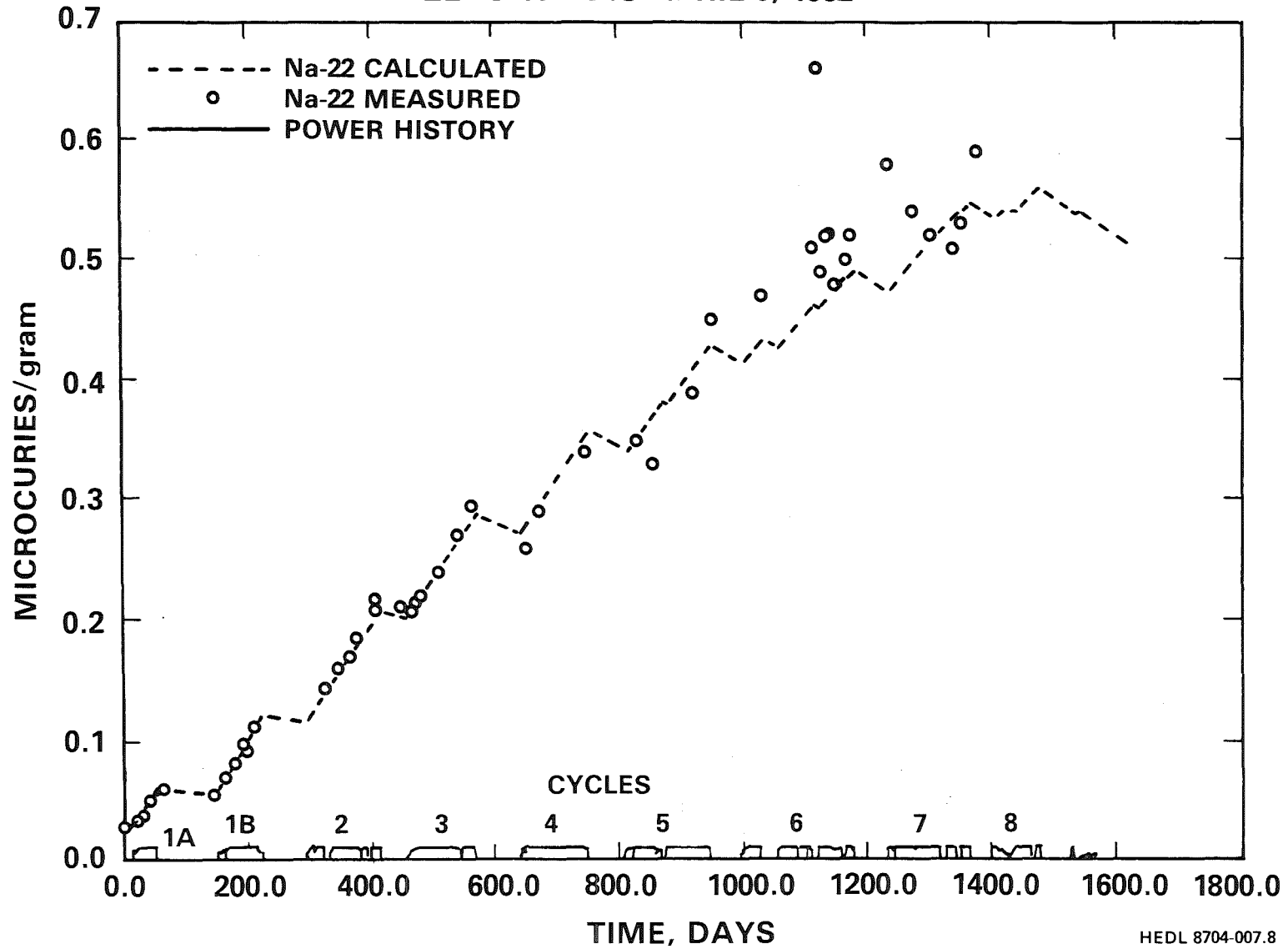
TABLE 2 MAXIMUM FFTF PRIMARY SODIUM ACTIVITY (1985)

| <u>NUCLIDE</u> | <u>HALF-LIFE</u> | <u>ACTIVITY (Ci/gm)</u>  |
|----------------|------------------|--------------------------|
| Na-24*         | 15 hr            | $1.00 \times 10^{-2}$    |
| Na-22          | 2.6 yr           | $5.9 \times 10^{-7}$     |
| H-3            | 12 yr            | $3.0 \times 10^{-7}$     |
| Rb-86          | 18.7 d           | $9.1 \times 10^{-8}$     |
| Au-198*        | 2.7 d            | $\sim 3. \times 10^{-8}$ |
| Cs-136         | 13 d             | $2.1 \times 10^{-7}$     |
| Cs-137         | 30 yr            | $2.2 \times 10^{-7}$     |
| I-131*         | 8 d              | $4.9 \times 10^{-8*}$    |
| Te/I-132       | 78 hr/2.3 hr     | $1.7 \times 10^{-8}$     |
| Co-58*         | 71 d             | $1.4 \times 10^{-9}$     |
| Mn-54*         | 313 d            | $4.1 \times 10^{-9}$     |
| Sb-124         | 60 d             | $7.0 \times 10^{-10}$    |
| Sn-113         | 115 d            | $<3.0 \times 10^{-8}$    |
| Ag-110m        | 253 d            | $\sim 3 \times 10^{-9}$  |
| Cs-134*        | 2.0 y            | $1.5 \times 10^{-7}$     |
| Sb-125         | 2.73 y           | $\sim 2 \times 10^{-9}$  |
| C-14*          | 5730 y           | $<1 \times 10^{-9}$      |
| Po-210*        | 138.4 d          | $\sim 7 \times 10^{-13}$ |

\*Observed/measured infrequently.

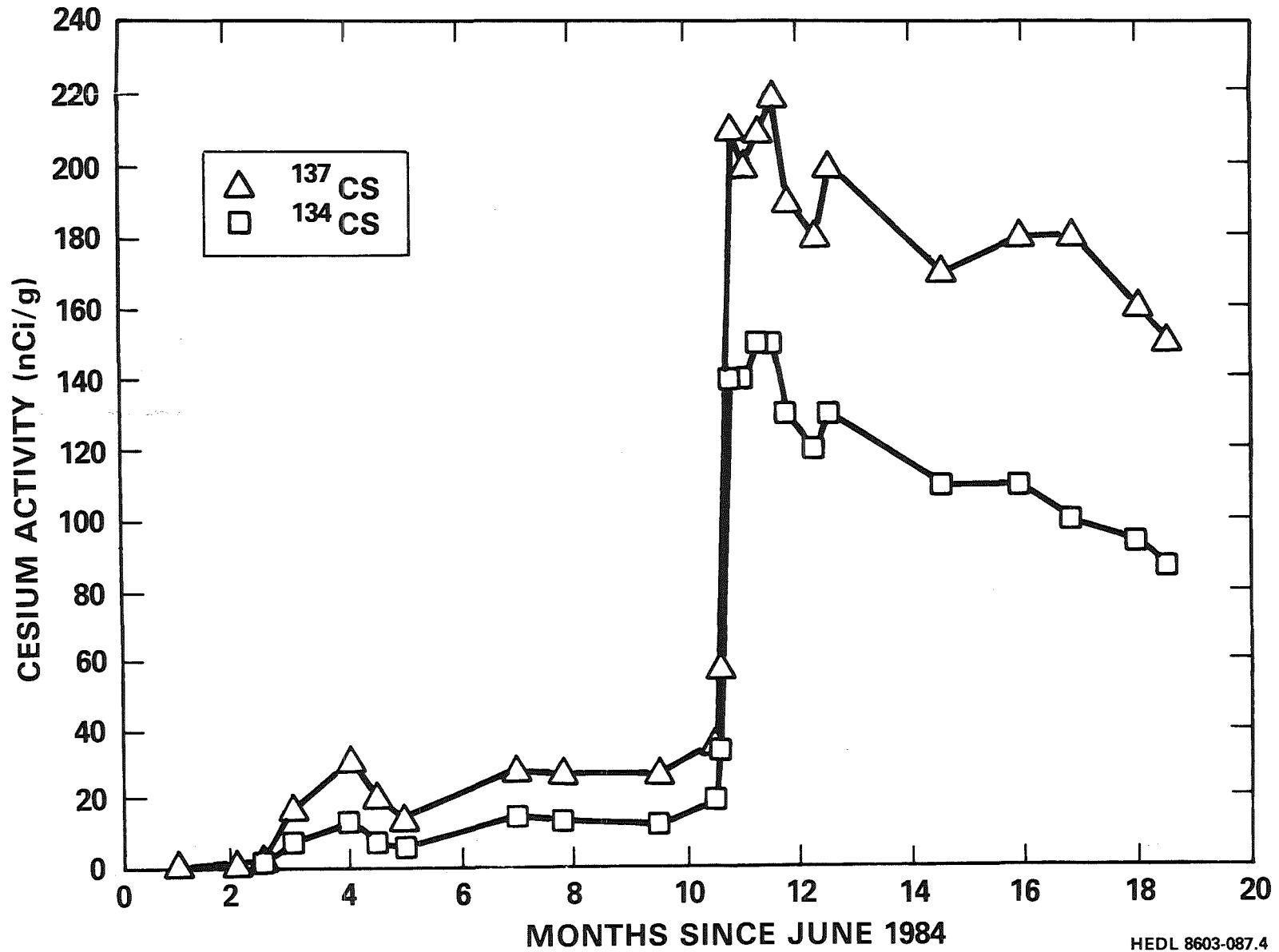
# FIGURE 1 – FFTF PRIMARY SODIUM ACTIVITY

SEPTEMBER 9, 1986  
ZERO TIME IS APRIL 6, 1982



HEDL 8704-007.8

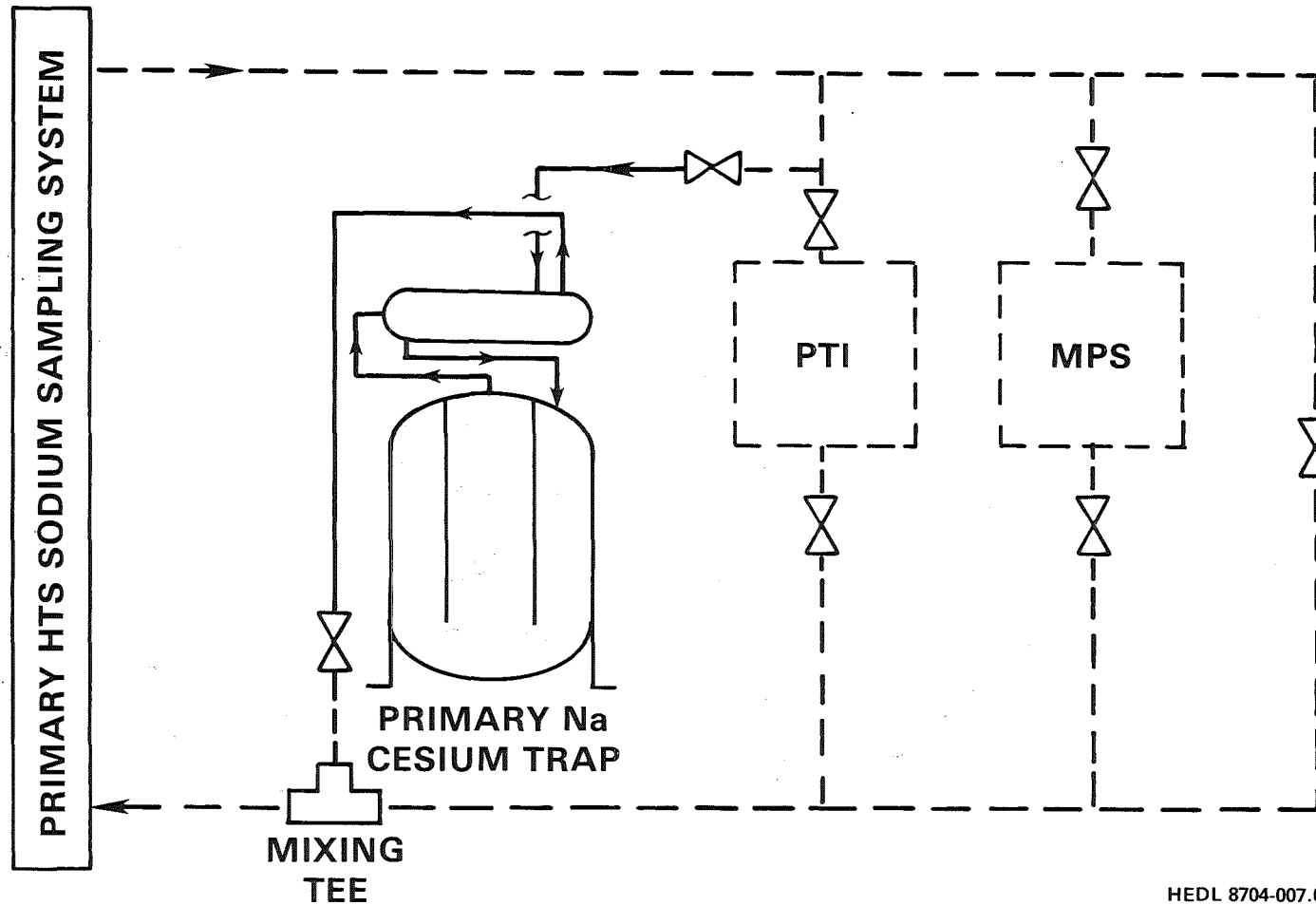
# FIGURE 2 — FFTF CESIUM ACTIVITY



HEDL 8603-087.4



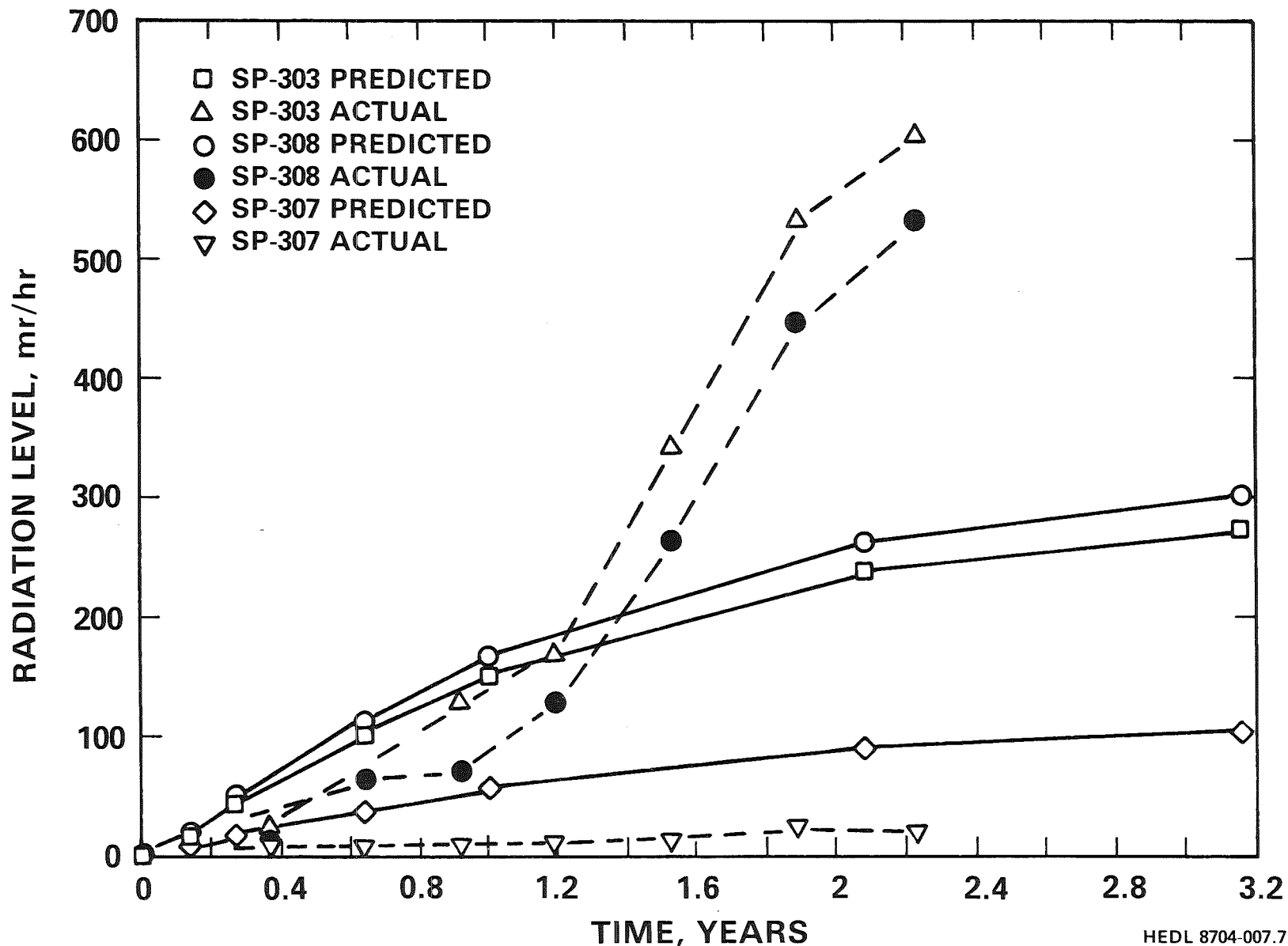
# FIGURE 3 – FFTF REACTOR PRIMARY CESIUM TRAP



HEDL 8704-007.6

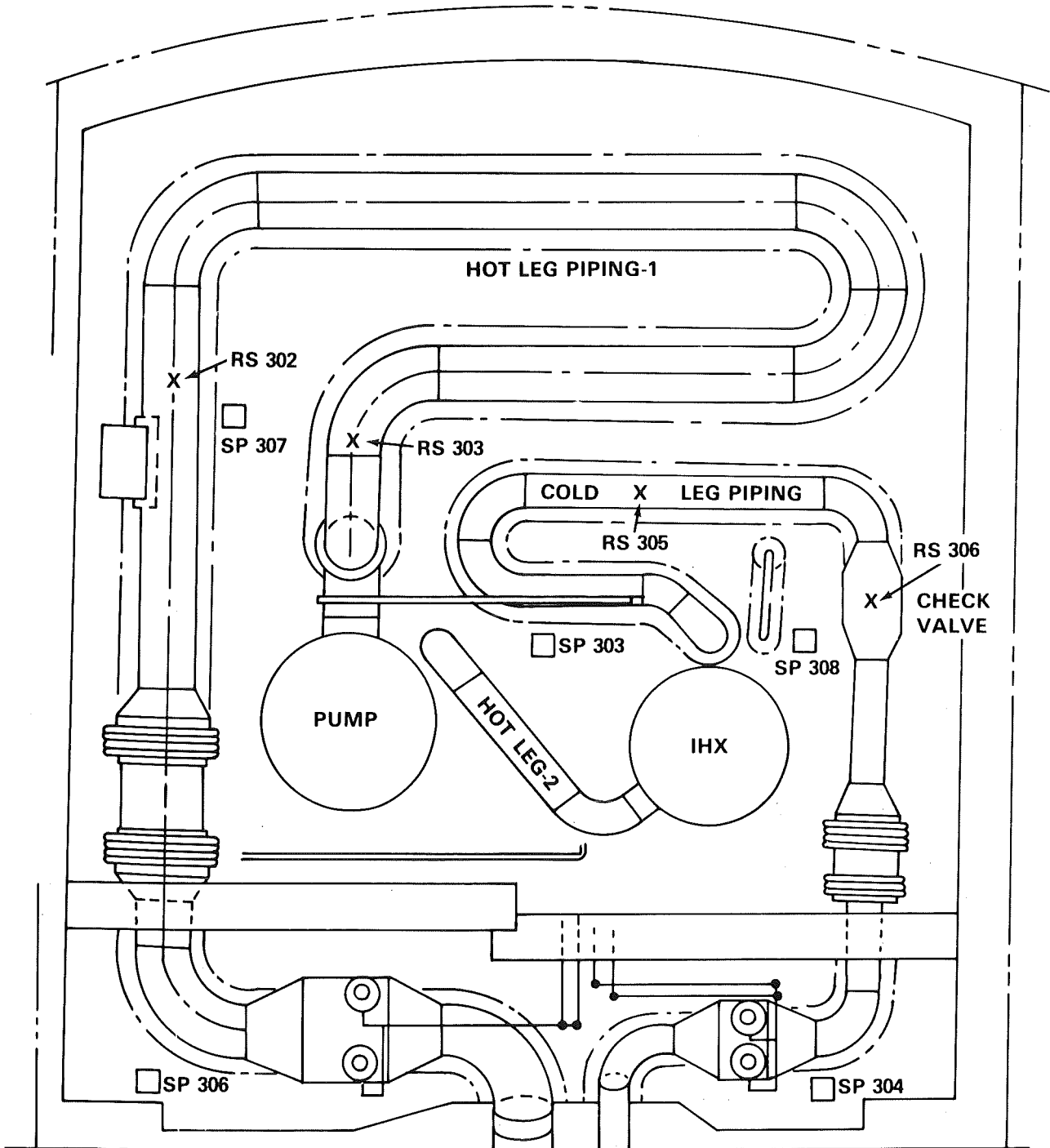
# FIGURE 4 — FFTF RADIATION LEVEL BUILDUP

PREDICTED AND ACTUAL COMPARED



HEDL 8704-007.7

# FIGURE 5 — PLAN VIEW OF FFTF-HTS CELL LAYOUT



X = SURVEILLANCE HOLE  
□ = PERISCOPE HOLES

# COMPARISON OF EBR-II AND FFTF

- SODIUM ISOTOPE ACTIVITIES COMPARABLE
- CORROSION PRODUCT ACTIVITIES COMPARABLE
- CESIUM ACTIVITY IN FFTF APPROACHING MAXIMUM CESIUM ACTIVITY FOUND IN EBR-II BEFORE INSTALLATION OF TRAP. CESIUM TRAP TO BE INSTALLED ON FFTF

HEDLM 8704-007.22

# COMPARISON OF EBR-II AND FFTF (CONTINUED)

- MORE IODINE AND INSOLUBLE FISSION PRODUCT ACTIVITY IN EBR-II SODIUM, BECAUSE OF THE MUCH LARGER NUMBER OF FUEL PIN BREACHES
- MUCH HIGHER Po-210 ACTIVITY IN EBR-II BECAUSE OF BISMUTH-TIN ROTATING PLUG. THIS ALSO ACCOUNTS FOR PRESENCE OF TIN IN EBR-II
- HIGHER TRITIUM IN EBR-II BECAUSE OF Li CONTAINING EXPERIMENTS. SIMILAR EXPERIMENTS PLANNED FOR FFTF

**THE FRENCH EXPERIENCE CONCERNING  
THE CONTAMINATION OF THE LMFBRs**

**R. CLERC<sup>1</sup>, J. GUIDEZ<sup>1</sup>,  
P. MAUX<sup>2</sup>  
P. MICHAILLE<sup>3</sup>, J. MISRAKI<sup>3</sup>, D. MSIKA<sup>3</sup>**

<sup>1</sup> CEA/IRDI/DERPE/SCPx, C.E.N. Marcoule

<sup>2</sup> CEA/IRDI/DERPE/SEER, C.E.N. Cadarache

<sup>3</sup> CEA/IRDI/DEDR/DRNR/STRA, C.E.N. Cadarache

IWGFR SM/CONTAMINATION.

Session 1 : Expériences de filtration du sodium primaire - Réacteur RAPSODIE - FORTISSIMO.

Session 2 : Bilan d'activité en  $^{137}\text{Césium}$  du circuit primaire - Réacteur RAPSODIE - FORTISSIMO.

Session 3 : Prélèvement de sodium par le procédé Tasténa.

Session 4 : Mesures de contamination sur les composants du réacteur RAPSODIE - FORTISSIMO.

Session 5 : Bilan des mesures de contamination effectuées sur le réacteur PHENIX.

Session 6 : Modèles et codes utilisés en France.

**ABSTRACT : Notional position**

With respect to the problems related to the contamination of the primary circuits of LMFBRs, the French position based on the experience of RAPSODIE and PHÉNIX can be summarized as follows:

- The corrosion products of the fuel clads that contaminate the components are essentially  $^{54}\text{Mn}$ , mostly deposited in the cold parts of the circuits (pumps, lower part of the IHXs, and in a minute fraction in the cold traps). In the operating conditions of the French reactors: at low oxygen concentration, this contamination remains at low levels, compatible with a removal by decontaminating agents without great difficulty, when it is necessary to repair the component. In particular, few particles were observed after filtration of the primary sodium of RAPSODIE; no overheatings of the subassemblies of PHÉNIX were related to blockages by particles.
  
- The major consequence of the cladding failures is the release of fission products, either gaseous, or soluble in the sodium. In the French operating conditions, a very efficient monitoring of the delayed neutron precursors enables to shut down the reactor prior to an eventual escape of fissile material. Concerning the contamination of the cover gas, the levels of contamination by fission products remain at PHÉNIX well below the contamination by the  $^{23}\text{Ne}$  (activation product). Concerning the contamination of the primary sodium, the major contaminant measured at PHÉNIX is  $^{137}\text{Cs}$ ; the levels are, here also, well below the activation products ( $^{24}\text{Na}$ ,  $^{22}\text{Na}$ ). Furthermore, the  $^{137}\text{Cs}$  appears to be trapped for about 50% of the released inventory in the cold trap of RAPSODIE. A carbonaceous trap was used to decontaminate the sodium of RAPSODIE during the decommissioning, and such traps will also be used to decontaminate the sodium of the transportation cans of the defected subassemblies from SUPER PHÉNIX to ISAI.
  
- Tritium is not a major problem on the LMFBRs: the release rates to the environment when the reactor is in operation are well below those of the PWRs. However, it can make more difficult the regeneration of the secondary cold traps, when they are filled with sodium hydride and oxide.
  
- In the view that the contamination problems of the LMFBRs are only of minor importance for the normal operation of the reactor (the dimensioning is performed on the activation products), simple models and codes are sufficient to cope with the evaluations needed for a project. The experience of PHÉNIX allowed to validate them in an acceptable range of precision.



IWGFR SM/CONTAMINATION

EXPERIENCES DE FILTRATION  
DU SODIUM PRIMAIRE  
REACTEUR RAPSODIE - FORTISSIMO

-----

1/ Après les opérations de vidange normales du circuit primaire de RAPSODIE, des poches de sodium sont restées en différents endroits du circuit.

En particulier, quelques centaines de litres de sodium devaient être retenues autour du sommier ; en fait, cette masse de sodium s'est vidangée d'elle-même vers le bas de la tuyauterie d'entrée de la cuve du réacteur et s'est donc retrouvée dans la partie basse du "Saxo".

Dans le cadre du "bilan matières fissiles" effectué sur le réacteur RAPSODIE, il était intéressant de déterminer la quantité et l'activité en isotopes de l'Uranium et du Plutonium contenus dans cette fraction de sodium primaire restée en fond de cuve et de mettre en évidence, par comparaison avec les résultats d'analyses du sodium primaire effectuées au cours du fonctionnement du réacteur, un éventuel phénomène d'"enrichissement par dépôt".

2/ DEROULEMENT DE L'OPERATION DE VIDANGE.

Une opération de vidange spéciale de cette masse de sodium a donc été prévue par DERPE-SEER ; cette vidange devant être réalisée à une température de sodium relativement basse, il a été décidé de déterminer les isotopes d'Uranium et de Plutonium après filtration sur poral et récupération des particules filtrées.

3/ TRAITEMENT DU PORAL.

Après circulation du sodium sur le poral et vidange du sodium résiduel, l'ensemble de filtration a été traité au laboratoire STRA/LCPC. Le poral a été sorti du système et traité selon le mode opératoire décrit en annexe 1.

A la fin de cette première étape, ont été obtenues d'une part, la solution d'hydrolyse du sodium, d'autre part, les particules recueillies sur le filtre en papier.

.../...

Ces particules, après comptage gamma ont été soumises à une procédure de dissolution dont le mode opératoire est décrit en annexe 2.

Sur les fractions différentes ainsi obtenues, des dosages d'émetteurs gamma (spectrométrie) et d'émetteurs alpha (spectrométrie) ont été réalisés. Ces derniers ont été effectués par le laboratoire SPR/Rad après, dans certains cas, séparation préliminaire au LCPC.

#### 4/ RESULTATS.

On ne donnera, dans ce paragraphe, que les résultats totaux.

Il faut noter que la répartition des radionuclides entre particules filtrées sur papier et solution n'a pas de signification : en effet, l'objectif de cette étude étant la détection de matière fissile, nous avons utilisé dans la procédure de récupération des particules retenues sur le poral une solution d'acide nitrique qui a modifié la répartition des activités en entraînant en solution des radionuclides.

##### 4.1 Débit de dose mesuré sur l'ensemble de filtration.

Après vidange du sodium résiduel, on a relevé un débit de dose de 40 mrads/h au contact du calorifuge.

Le calcul prévisionnel de débit de dose avait abouti à 42 mrads/h à 5 cm du poral.

L'accord est donc très bon entre résultats calculés et mesurés.

##### 4.2 Masse des particules.

Les particules séparées par application du mode opératoire décrit ont été pesées. On a observé une masse de 0,0783 g pour un volume de sodium filtré de 380 litres. Cette masse de particules est vraisemblablement sous évaluée pour les raisons exprimées en tête de ce paragraphe.

Les précédentes opérations de filtration du sodium primaire de RAPSODIE avaient été pratiquées réacteur en fonctionnement, à l'aide de frittés métalliques disposés dans des ensembles de filtration mis en Cellule B 11.

Le tableau ci-après rappelle l'ensemble des résultats obtenus.

| <u>ESSAIS</u>                                   | <u>1er</u>            | <u>2ième</u>          | <u>Cet essai</u>         |
|---|-----------------------|-----------------------|--------------------------|
| date  | 25.10.77              | 18.05.78              | 10.08.84                 |
| fritté  | acier                 | nickel                | acier                    |
| seuil d'arrêt                                   | 8 µm                  | 5 µm                  | 20 µm                    |
| sodium filtré                                   | sodium primaire cuve  | sodium primaire cuve  | poche de sodium résiduel |
| volume filtré                                   | 1000 l                | 5000 l                | 380 l                    |
| température du sodium                           | 400 °C                | 440 °C                | 180 °C                   |
| masse des particules                            | < 1 mg                | 6 mg                  | 78 mg                    |
| masse des particules rapportée au volume filtré | < 1 mg/m <sup>3</sup> | 1,2 mg/m <sup>3</sup> | 206 mg/m <sup>3</sup>    |

On voit le net "enrichissement" en particules dans le sodium restant après vidange totale de la cuve.

.../...

#### 4.3 Activités en radionuclides émetteurs gamma.

Les activités totales mesurées sont, au 5.09.84 :

|        |                   |                 |    |
|--------|-------------------|-----------------|----|
| 22 Na  | (2,04 $\pm$ 0,17) | 10 <sup>5</sup> | Bq |
| 54 Mn  | (1,43 $\pm$ 0,04) | 10 <sup>6</sup> | Bq |
| 60 Co  | (1,6 $\pm$ 0,1)   | 10 <sup>5</sup> | Bq |
| 134 Cs | (2,14 $\pm$ 0,08) | 10 <sup>6</sup> | Bq |
| 137 Cs | (1,08 $\pm$ 0,03) | 10 <sup>8</sup> | Bq |

Comme il n'y a pas enrichissement en 22 Na, on peut calculer à partir de l'activité mesurée et de l'activité en 22 Na du sodium primaire, la masse de sodium retenu dans les pores du fritté d'acier.

Au 5.09.84, l'activité du sodium primaire est (6,89  $\pm$  0,15) 10<sup>3</sup> kBq de 22 Na par kg de sodium ; il y avait donc 0,0296  $\pm$  0,0038 kg de sodium sur le poral.

Cette valeur permet d'établir le tableau suivant :

| <u>RADIONUCLIDES</u> | <u>CONTAMINATION Na</u><br><u>PRIMAIRE</u><br>au 5.09.84<br><br>kBq / kg<br>(Tasténa R 269) | <u>CONTAMINATION PORAL</u><br><u>+ Na</u><br>au 5.09.84<br><br>kBq / kg |
|----------------------|---|---|
| 54 Mn                | non mesurable   | $(4,8 \pm 0,5) 10^4$  |
| 60 Co                | non mesurable   | $(5,1 \pm 0,6) 10^3$  |
| 134 Cs               | $(6,6 \pm 0,3) 10^2$  | $(7,2 \pm 0,8) 10^4$  |
| 137 Cs               | $(3,2 \pm 0,15) 10^4$   | $(3,65 \pm 0,40) 10^6$  |

On note donc sur l'ensemble de filtration de fortes activités ; elles sont explicables par le double phénomène de concentration de ces radionuclides dans le sodium restant dans le fond de cuve après vidange du sodium à une température  $< 400^\circ\text{C}$  suivie du dépôt de ces mêmes radionuclides sur la surface du poral, dépôt favorisé par une circulation de sodium à basse température.

L'enrichissement pour le césium est de l'ordre de 100.

#### 4.4 Activités en radionuclides venant de la matière fissile.

Les activités mesurées en isotopes de l'uranium et du plutonium, rapportées à la masse de sodium sont donc :

|                                |  |
|--------------------------------|--|
| 239 + 240 Pu                   | 4,2 Bq / kg de sodium                      |
| 238 Pu                         | 0,84 Bq / kg de sodium                     |
| équivalent 241 Pu              | 120 Bq / kg de sodium                      |
| 234 U                          | $\sim 5,5 \cdot 10^{-3}$ Bq / kg de sodium |
| 235 + 236 U                    | non mesurable                              |
| 238 U                          | non mesurable                              |
| U total $2 \cdot 10^{-8}$ g/kg | $< \text{masse} < 4 \cdot 10^{-8}$ g/kg    |

présence de 241 Am et 242 Cm.

.../...

En 239 + 240 Pu, l'activité mesurée correspond aux plus faibles et dernières activités qui ont pu être mesurées dans le sodium primaire sur des prélèvements Tasténa (5 Bq/kg en 1974).

Quant aux isotopes de l'Uranium, les activités en concentrations observées sont nettement inférieures à celles mesurées sur le sodium primaire des prélèvements Tasténa ( $10^{-3}$  g/kg au maximum en 1972 et 1973).

241 Am et 242 Cm ont déjà été décelés dans le sodium primaire.

## 5/ CONCLUSIONS.

L'examen du contenu du poral ayant servi à la filtration du sodium primaire resté dans le bas du Saxo a conduit à l'observation d'une masse de particules équivalente à environ 200 mg/m<sup>3</sup>.

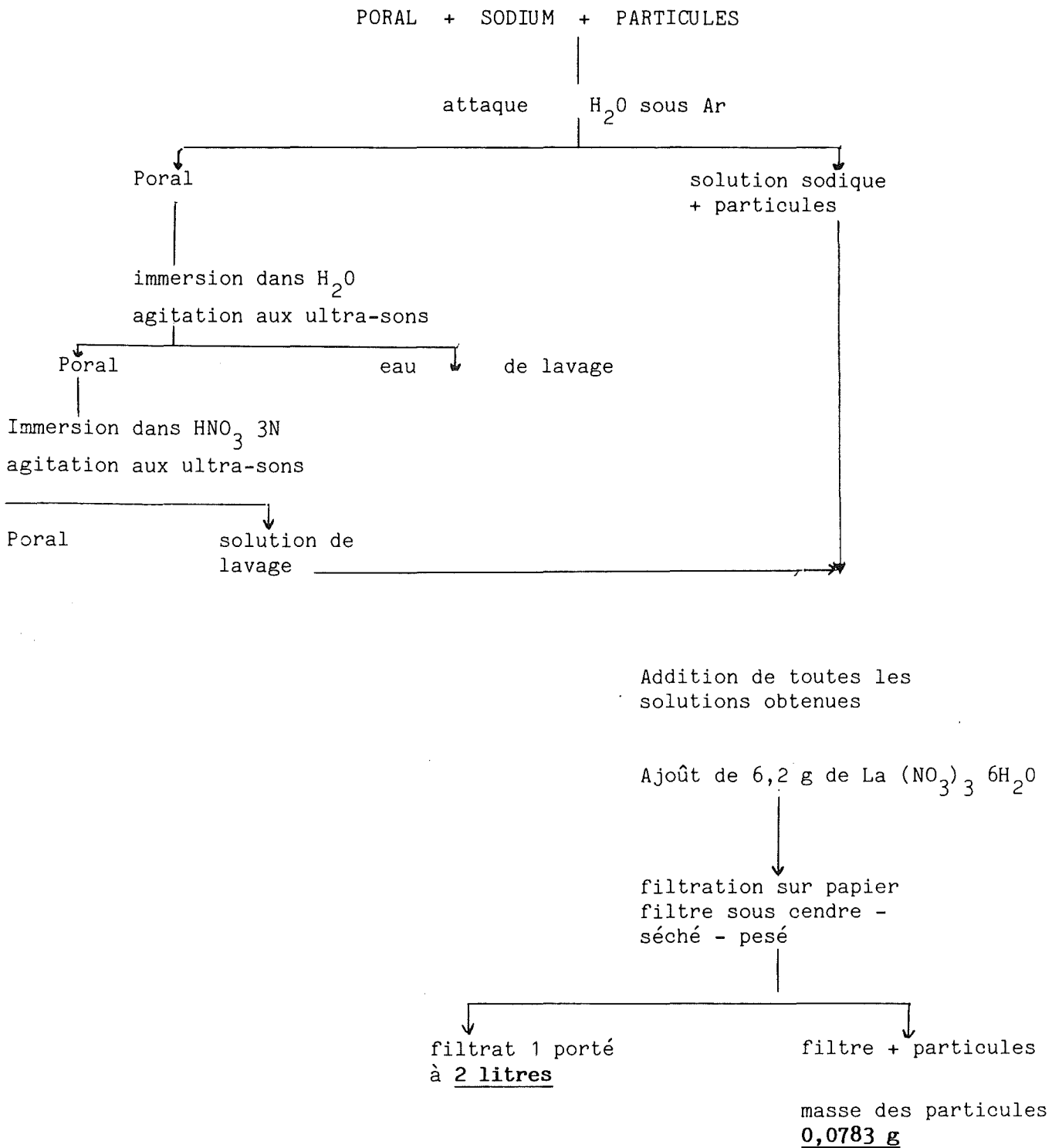
Les activités en isotopes du matériau fissile mesurées sur ces particules sont soit du même ordre (cas du Plutonium), soit beaucoup plus faible (cas de l'Uranium) que les activités mesurées dans le sodium primaire par les échantillons Tasténa.

Par contre, les activités gamma mesurées, rapportées au volume du sodium filtré, sont nettement supérieures à celles mesurées dans les Tasténa.

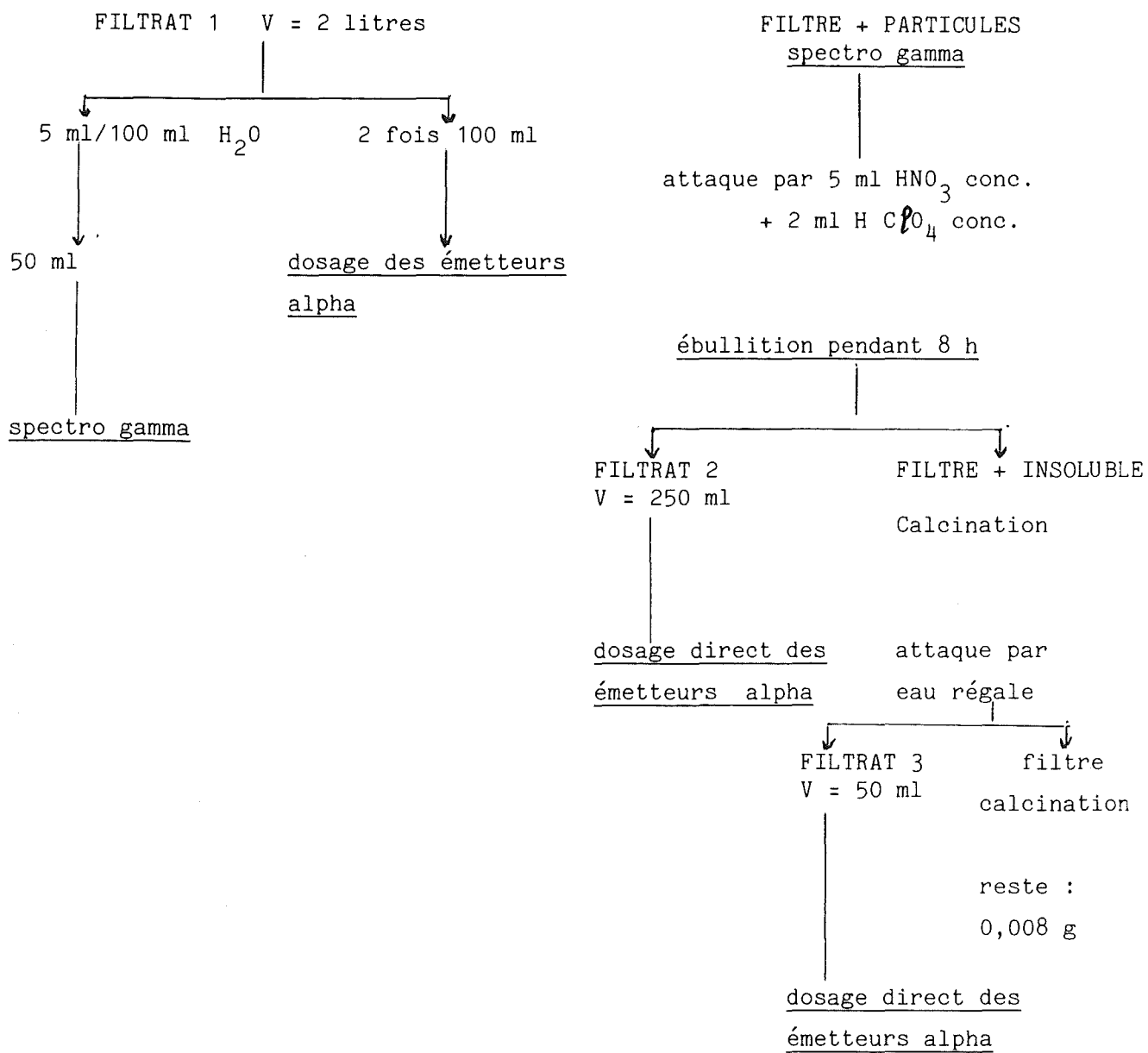
On peut donc supposer que les particules filtrées sont constituées essentiellement de produits de corrosion et de produits de fission.

.../...

ANNEXE 1



ANNEXE 2





IWGFR SM/CONTAMINATION

BIAN D'ACTIVITE EN 137 CESIUM  
DU CIRCUIT PRIMAIRE DE RAPSODIE

Les différentes mesures associées aux opérations de démantèlement du réacteur nous ont permis de dresser un premier bilan de la répartition de l'activité en 137 Cs.

Le tableau suivant précise les différentes zones de mesure et indique la valeur de l'activité et la méthode utilisée pour obtenir cette valeur.

| Localisation                           | Activité en 137 Cs TBq | Méthode   |
|--|------------------------|---|
| 1 Sodium après l'opération d'épuration | 0,18                   | Analyse du Na   |
| 2 Réservoir de stockage                | 0,54                   | Interprétation des débits de dose   |
| 3 Premier piège à Cs                   | 1,7                    | Interprétation des débits de dose + interprétation des mesures Na en amont et aval du piège |
| 4 Deuxième piège à Cs                  | 0,18                   | Idem  |
| 5 Piège froids                         | 4,18                   | Spectrométrie $\gamma$  |
| 6 Faux assemblages pièges à Cs         | 0,48                   | Spectrométrie $\gamma$  |
| 7 Echangeurs + pompes                  | 0,13                   | Spectrométrie $\gamma$  |
| 8 Dépôts d'aérosols dans le circuit    | 1,48                   | Estimation  |

Parmi ces valeurs, certaines sont connues avec plus de certitude que d'autres. L'activité en 137 Cs dans les dépôts n'est pas issue d'une mesure : ce n'est qu'une estimation réalisée à partir d'une masse supposée de dépôt à laquelle on a appliqué le facteur d'enrichissement des dépôts d'aérosols vis-à-vis du 137 Cs.

Les valeurs issues des mesures effectuées sur les pièges froids sont également entachées d'une grande erreur et nous avons en ce moment d'autres mesures en cours pour préciser ces activités.

Néanmoins, ce premier bilan arrive à 8,87 TBq de  $^{137}\text{Cs}$   
dont 3,21 TBq (36%) dans la totalité du sodium primaire ayant participé  
à toute la vie du réacteur (1 + 2 + 3 + 4 + 6 + 7)  
4,18 TBq (47%) dans les pièges froids (5)  
1,48 TBq (17%) dans les dépôts d'aérosols (8).

Nous avons voulu comparer ce terme puits au terme source.

Après recensement de toutes les ruptures de gaine répertoriées, la quantité totale de  $^{137}\text{Cs}$  émis par les ruptures est évaluée à 6,4 TBq.

Ces 6,4 TBq (source) sont à comparer aux 8,87 TBq (puits).

Nous estimons que l'accord est correct.

## IWGFR §M/CONTAMINATION

### PRELEVEMENT DE SODIUM PAR LE PROCEDE TASTENA

-----

Le suivi de la qualité du sodium des circuits d'un réacteur, aussi bien primaire que secondaire, peut apporter des informations sur le fonctionnement du réacteur et aider à la compréhension de mécanismes tels que celui du transfert de contamination.

Un des moyens d'assurer ce suivi est de prélever des échantillons de sodium et d'en extraire, par l'analyse chimique, l'information recherchée.

Le dispositif TASTENA permet le prélèvement direct d'échantillons dans les diverses installations d'une centrale, en particulier dans la cuve du réacteur, pendant le fonctionnement ou à l'arrêt.

#### Impuretés dosables dans un échantillon prélevé par TASTENA.

Toutes les impuretés susceptibles d'être présentes dans le sodium d'un circuit ne peuvent pas être dosées dans un échantillon prélevé par TASTENA. Les impuretés telles que Oxygène, Hydrogène, Carbone ne sont pas dosables ; en effet, le prélèvement n'est pas conditionné ni traité en étant complètement protégé d'une pollution.

Les métaux tels que l'Argent, le Zinc, l'antimoine, l'étain, le plomb, le calcium, un élément tel le Silicium qui sont partiellement solubles dans le sodium sont dosables.

La présence de métaux comme les métaux de transition (Fer, Chrome, Nickel, Manganèse) dont la solubilité dans le sodium est très faible, est une information difficile à obtenir.

En ce qui concerne les radionuclides, les produits de fission tels que les iodes et les césiums sont couramment dosés ; le tritium entre dans cette même catégorie ainsi que les produits d'activation (22 Na, 24 Na, 65 Zn, 110 mAg).

Les produits d'activation corrodés, 54 Mn, 51 Cr, 58 Co, 60 Co, 59 Fe sont soumis à la même observation que celle citée plus haut pour les métaux de transition.

Quant aux isotopes de l'Uranium et du Plutonium, l'expérience que nous avons montrerait que la représentativité de l'échantillon prélevé par TASTENA est douteuse.

.../...

### Conditions d'utilisation.

Quant on aborde le problème de représentativité, il faut préciser les conditions dans lesquelles sont prélevés les échantillons par le dispositif TASTENA.

La température du sodium ainsi échantillonné doit être  $\geq 400^{\circ}\text{C}$ . Il arrive que cette condition ne soit pas respectée, on juge alors de la représentativité du prélèvement en fonction de l'information recherchée (exemple  $^{22}\text{Na}$  dans le sodium contenu dans la cuve du barillet, température maximale  $200^{\circ}\text{C}$ ).

Le sodium doit également être brassé (pompes en fonctionnement).

Le godet utilisé pour le prélèvement est élaboré avec un matériau pur (nickel 200), lavé et dégraissé correctement avant utilisation.

Pour chaque prélèvement, le godet mis en jeu est neuf.

### Description du dispositif.

Les figures 1 et 2 décrivent d'une part le godet de prélèvement et l'ensemble du dispositif et d'autre part les différentes opérations que nécessite un prélèvement.

### Utilisation du dispositif TASTENA sur les réacteurs français : quelques exemples.

Les trois réacteurs RAPSODIE, PHENIX et SPX1 ont été et sont équipés du dispositif TASTENA aussi bien sur le circuit primaire que sur les circuits secondaires en ce qui concerne les deux plus récents réacteurs.

On a pu ainsi mesurer les iodes et césiums produits de fission, de période courte, émis dans le sodium primaire par les ruptures de gaine de RAPSODIE et de PHENIX ; la contamination en  $^{137}\text{Césium}$  est suivie régulièrement à l'aide des échantillons prélevés par TASTENA. Ces derniers ont également permis de faire les mesures nécessaires à la compréhension du comportement du tritium.

On a pu aussi déterminer la concentration d'éléments polluants le sodium à la suite d'une situation incidentelle (exemples :

- chute du joint Sn - Bi dans le sodium primaire de RAPSODIE,
- présence de Sb due à une rupture d'une source de neutrons (Sb - Be) à PHENIX,

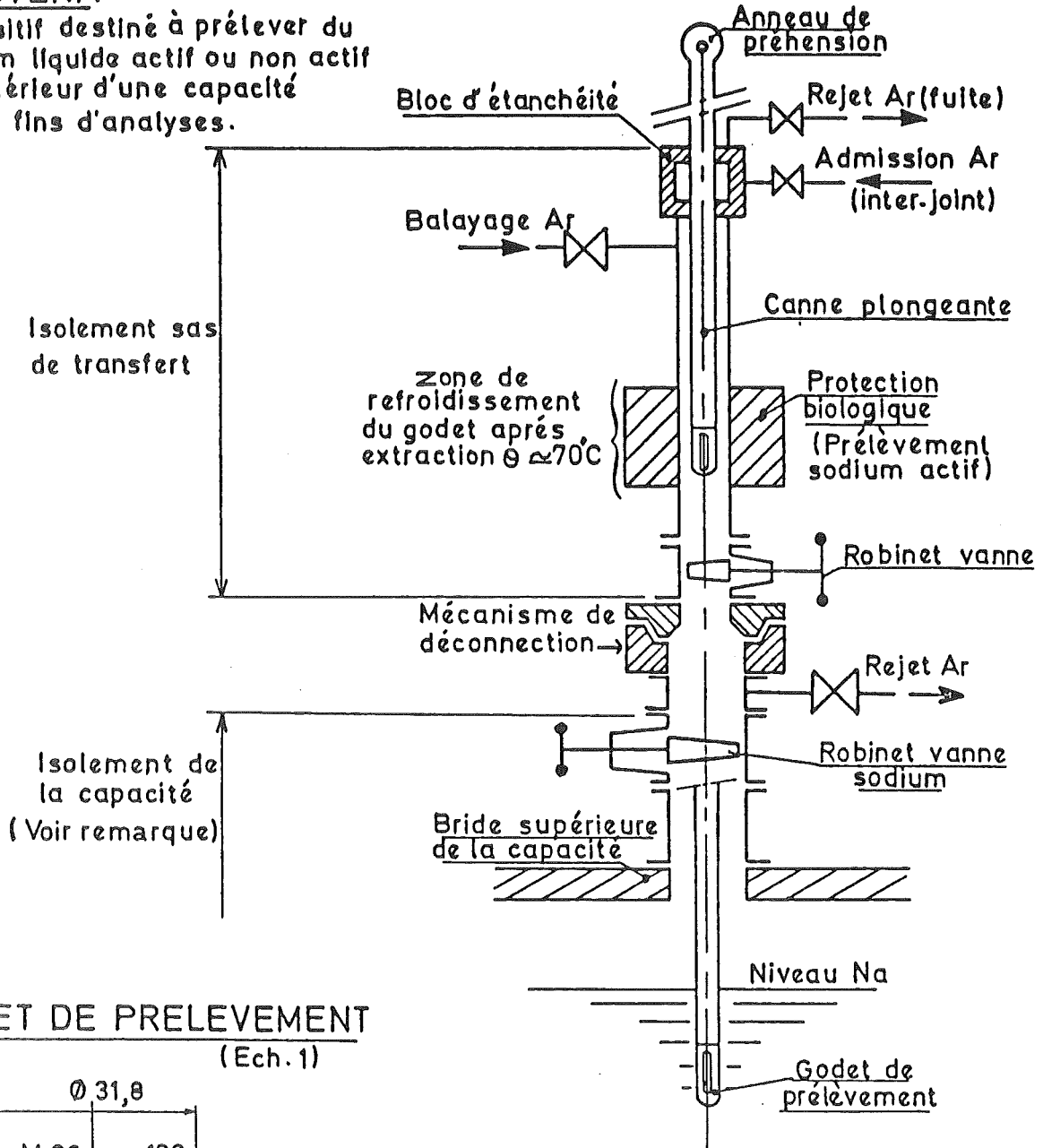
- mesure de la concentration en  $^{198}\text{Au}$ , traceur du sodium lors des essais de la mise en évidence de la fissure de la cuve primaire de RAPSODIE).

Le dispositif TASTENA implanté sur la Centrale SPX1 a déjà été utilisé. Lors des essais de montée en température et après avoir atteint le palier à 395°C, il a permis de prélever des échantillons de sodium primaire et de sodium secondaire.

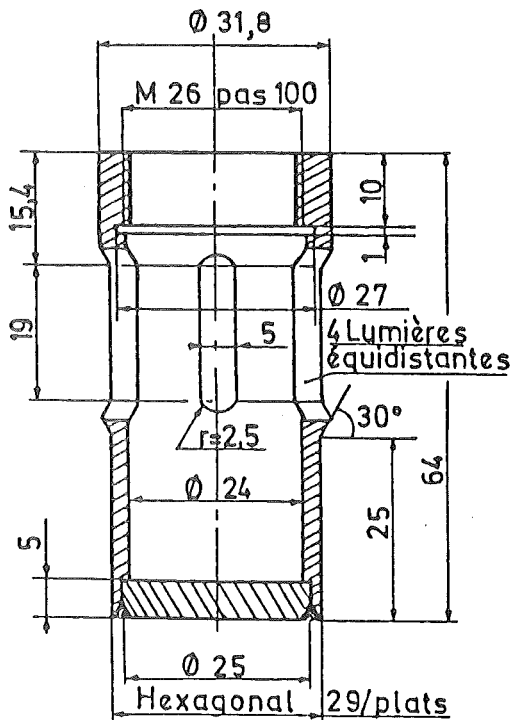
L'analyse de ces échantillons a été orientée vers la détermination du "point zéro" de la qualité du sodium vis-à-vis des éléments suivants : Calcium, Silicium, Zinc, Etain, Plomb ; on en a profité pour mesurer les concentrations en Fer, Chrome et Manganèse.

# TASTENA

Dispositif destiné à prélever du sodium liquide actif ou non actif à l'intérieur d'une capacité à des fins d'analyses.



## GODET DE PRELEVEMENT (Ech. 1)



### Remarque:

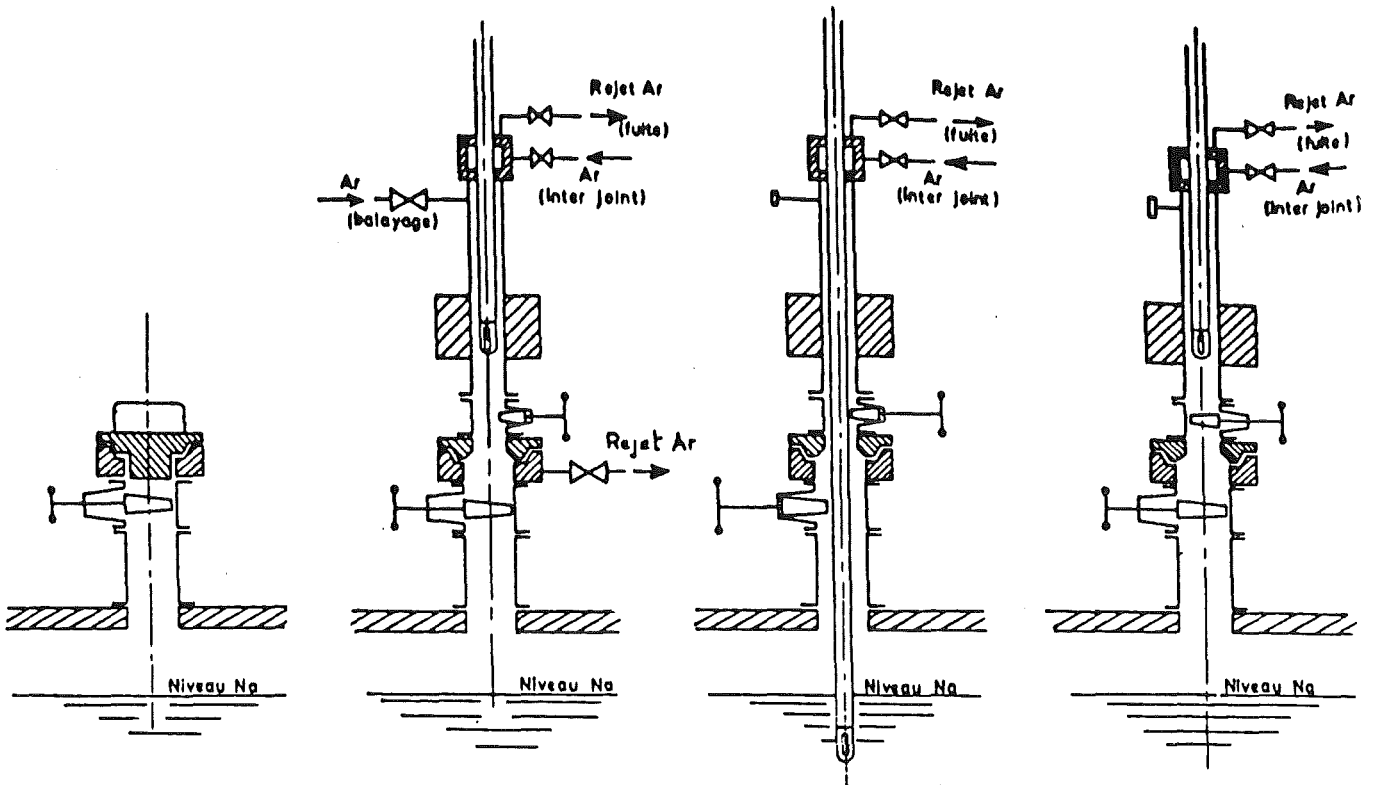
Sur le réacteur un bouchon obture le canal de prélèvement au dessus du robinet vanne sodium.

Sur les circuits d'essais le bouchon est remplacé par un robinet vanne argon.

Matériau : Nickel 200

Usinage: ∇ poli intérieur et extérieur ainsi que les lumières. Moucher les angles vifs.

|      |        |          |                     |            |
|------|--------|----------|---------------------|------------|
| CEA. | DR.NR. | S.T.R.S. | Recommandation N°10 | Figure n°1 |
|------|--------|----------|---------------------|------------|



**POSITION D'ATTENTE**

- Un bouchon obture le canal de prélèvement sur la capacité.

**PHASE I**

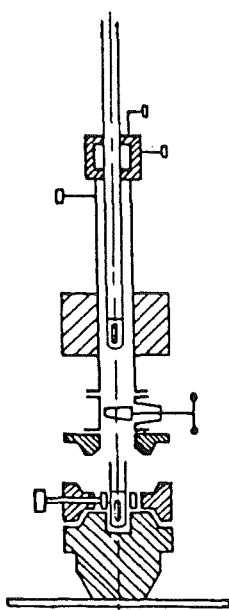
- Verrouillage du sas de prélèvement sur le canal.  
- Balayage argon du sas.

**PHASE II**

- Prélèvement Na

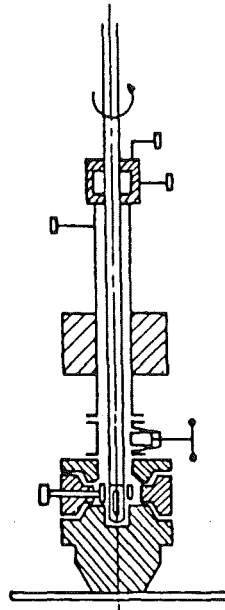
**PHASE III**

- Refroidissement naturel du godet.  
- Désolidarisation du sas de prélèvement du canal.



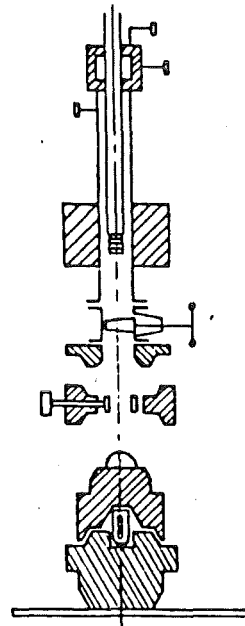
**PHASE IV**

- Mise en place du sas de prélèvement sur le chateau équipé du mandrin (mors ouverts)



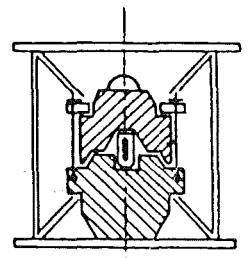
**PHASE V**

- Déverrouillage du godet de prélèvement à l'aide du mandrin (mors fermés)



**PHASE VI**

- Dépose du sas de prélèvement et du mandrin (mors ouverts)  
- Mise en place du couvercle.



**PHASE VII**

- Verrouillage du chateau.

IWGFR SM/CONTAMINATION

MESURES DE CONTAMINATION  
SUR LES COMPOSANTS  
RAPSODIE - FORTISSIMO  
-----

Le réacteur RAPSODIE-FORTISSIMO est maintenant à l'arrêt et en opération de démantèlement.

Les principaux composants ont été extraits et leur contamination a été mesurée à l'aide de différentes méthodes.

On trouvera ainsi dans ce qui suit les résultats de ces mesures. Toutes les valeurs d'activité ont été calculées au 3 janvier 1982, date d'arrêt du réacteur ; les essais réalisés pendant le premier trimestre 1983 sont considérés comme peu importants vis-à-vis de la contamination. Les mesures ayant été effectuées à partir de 1984, les radiocontaminants de période courte n'ont pas été décelés.

La dernière vidange des circuits primaires a été effectuée le 20 avril 1983 ; les mesures de contamination reflètent donc la vie des composants : périodes de fonctionnement en puissance, arrêts chauds, arrêts froids, vidanges.

1/ **POMPES PRIMAIRES.**

Les deux pompes Nord et Sud ont été extraites et lavées.

La pompe Nord a été démantelée, la contamination surfacique a pu être mesurée sur des échantillons découpés en différentes zones.

1.1 **Temps de fonctionnement.**

La pompe Nord a travaillé 106 124 heures en sodium dont 12.800 avec le profil de température donné figure 1 et 53.980 heures avec les températures données en figure 2.

La pompe Sud a travaillé 82.200 heures en sodium dont 53.980 heures avec le profil de température figure 2.

.../...



## 1.2 Mesures de débit de dose.

Ces mesures ont été effectuées sur la pompe Nord au moment de son extraction à travers le sas de la hotte de manutention soit à environ 50 cm.

Le tableau 1 montre les différents points de mesure et les valeurs de débits de dose.

## 1.3 Contamination des eaux de lavage.

Le lavage a eu pour objectif d'éliminer le sodium. Des échantillons d'eaux ont été prélevés à chaque étape du lavage. Le tableau 2 donne les résultats de la contamination mesurée sur ces solutions de lavage. Le radiocontaminant majeur est le <sup>137</sup>Césium.

## 1.4 Mesures de contamination surfacique.

Des échantillons ont été découpés en des zones indiquées sur les figures 3, 4, 5 et 6. Les résultats obtenus sont donnés tableau 3.

## 1.5 Contamination totale de la pompe.

Il est difficile de calculer la contamination totale de la pompe à partir des résultats de contamination surfacique car d'une part, il est difficile de calculer la surface géométrique d'une pompe et d'autre part, certaines parties de la pompe sont élaborées avec des matériaux bruts de fonderie ou simplement forgés et ont ainsi une surface réelle inconnue mais certainement supérieure à leur surface géométrique apparente.

Néanmoins, on a tenté de calculer la contamination totale de la pompe en utilisant sa surface géométrique évaluée à 14 m<sup>2</sup>.

On a ainsi - tableau 4 - une estimation de la contamination de la pompe par les principaux radionuclides, en ce qui concerne la partie immergée en sodium.

.../...

## 2/ ECHANGEURS INTERMEDIAIRES (E.I).

Le même type d'analyses a été réalisé sur l'E.I Sud.

### 2.1 Temps de fonctionnement.

Il a travaillé environ 53.980 heures avec le profil de températures présenté en figure 7.

### 2.2 Mesures des débits de dose.

Ils ont été mesurés dans les mêmes conditions que celles de la pompe Nord - tableau 5 - mais 200 jours avant celles réalisées sur la pompe. Aussi, peut-on dire que les débits de dose mesurés sur l'E.I et la pompe sont voisins.

### 2.3 Contamination des eaux de lavage.

Malheureusement le volume d'eau utilisée pour une des phases de lavage n'a pas été mesuré, aussi est-il difficile de calculer la contamination des solutions de lavage.

Nous avons considéré une valeur maximale que pouvait atteindre ce volume et le tableau 6 donne la contamination mesurée dans les eaux de lavage (par excès).

### 2.4 Contamination surfacique.

Les échantillons sont prélevés dans la virole dans les zones situées sur les figures 7, 8, 9 et 10. Les résultats obtenus sont donnés tableau 7.

### 2.5 Contamination totale.

En ce qui concerne la zone de l'E.I.S immergée en sodium, sa surface est de 113,5 m<sup>2</sup>, ce qui fait pour les principaux radionuclides des activités totales citées tableau 8.

.../...

## 2.6. Comparaison Pompe - Echangeur.

Les radiocontaminants principaux des zones en sodium sont  $^{54}\text{Mn}$  et  $^{137}\text{Cs}$ .

Le  $^{137}\text{Cs}$  se retrouve surtout dans les eaux de lavage. On note que pour des surfaces de contact très différentes, les niveaux de contamination sur la pompe et l'échangeur sont identiques.

Dans les zones en Argon, la présence de  $^{137}\text{Cs}$  s'explique, après lavage, par la présence de dépôts carbonés.

Des radiocontaminants comme le  $^{90}\text{Sr}$  et les émetteurs  $\gamma$  sont présents sur les deux composants.

## 3/ PIEGES FROIDS.

### 3.1 Temps de fonctionnement.

Le piège froid 300 a fonctionné 84.443 heures ; le 400 n'a fonctionné que 22.008 heures.

### 3.2 Mesures.

Les mesures ont été effectuées par spectrométrie  $\gamma$  à l'aide de canaux percés dans la protection de plomb et servant de collimateurs; A partir des résultats de ces spectrométries, une estimation des activités totales contaminant les pièges a été réalisée - tableau 9 -.

Le  $^{137}\text{Cs}$  est de loin le radiocontaminant le plus important des pièges.

.../...

**4/ CONCLUSIONS : COMPARAISON DE LA CONTAMINATION MESUREE SUR LES DIFFERENTS COMPOSANTS.**

Le tableau 10 récapitule les activités mesurées sur les composants.

Cette contamination est due d'une part aux produits de corrosion activés, essentiellement  $^{54}\text{Mn}$ , d'autre part à un produit de fission, le  $^{137}\text{Cs}$ .

On note que la contamination en  $^{137}\text{Cs}$  de la pompe et de l'échangeur intermédiaire, que l'on retrouve uniquement dans les eaux de lavage, est négligeable vis-à-vis de celle des pièges froids.

Quant à la contamination par le  $^{54}\text{Mn}$ , on retrouve des activités d'un même ordre de grandeur sur pompe, échangeur intermédiaire et pièges froids.

Il ne faut pas oublier que ces mesures de contamination ont été réalisées en fin de vie du réacteur, alors que celui-ci avait eu de longues périodes de fonctionnement sans puissance ; il est possible que ces arrêts aient eu comme conséquence une redistribution de la contamination en  $^{54}\text{Mn}$ .



POMPES PRIMAIRES

CONTAMINATION DES SOLUTIONS DE LAVAGE .

ACTIVITES AU 03.01 1982

| Radioéléments | PPNa 200<br>Bq               | PPNa 100<br>Bq            |
|---------------|------------------------------|---------------------------|
| 3H            | non mesuré                   | $(1,96 \pm 0,07)10^9$     |
| 22 Na         | $(3,12 \pm 0,7)10^6$         | $(2,88 \pm 0,6)10^6$      |
| 54 Mn         | $(2,50 \pm 0,06)10^9$        | $(5,70 \pm 0,15)10^9$     |
| 60 Co         | $(2,60 \pm 0,26)10^7$        | $(2,35 \pm 1,3)10^7$      |
| 134 Cs        | $(1,23 \pm 0,40)10^9$        | $(1,34 \pm 0,07)10^9$     |
| 137 Cs        | $(3,70 \pm 0,11)10^{10}$     | $(4,10 \pm 0,20)10^{10}$  |
| 239 + 240 Pu  | $1,72 \cdot 10^5$            |                           |
| 238 Pu        | $3,01 \cdot 10^4$            |                           |
| 241 Am        | # $5,5 \cdot 10^4$           | Emetteurs de # qq. $10^3$ |
| 242 Cm        | # $9,5 \cdot 10^3$           |                           |
| 244 Cm        | # $1,3 \cdot 10^2$           |                           |
| U total       | $8,3 \cdot 10^{-4} g$        |                           |
|               | (traces 234 U, 235 U, 238 U) |                           |
| 90 Sr         | non recherché                | ed                        |

Les incertitudes sur les volumes de lavage ne sont pas connues, mais sont certainement importantes.

TABEAU 2

PP NORD  
 CONTAMINATION SURFACIQUE APRES LAVAGE  
 ACTIVITES EN kBq/m<sup>2</sup> au 3/01/82

---

| Radiocontaminants                   | Lanterne<br>d'aspiration | Zone sodium<br>jupe entretoise |                        |                        |
|-------------------------------------|--------------------------|--------------------------------|------------------------|------------------------|
|                                     |                          | zone marnage                   | zone argon             |                        |
| <sup>3</sup> H                      | # 5,23.10 <sup>2</sup>   | # 1,96.10 <sup>3</sup>         | # 6,54.10 <sup>2</sup> | # 7,85.10 <sup>2</sup> |
| <sup>54</sup> Mn                    | 7,26.10 <sup>5</sup>     | 6,78.10 <sup>5</sup>           | 6,53.10 <sup>5</sup>   | 2,13.10 <sup>5</sup>   |
| <sup>60</sup> Co                    | 1,88.10 <sup>3</sup>     | n.d                            | n.d                    | n.d                    |
| <sup>63</sup> Ni                    | 5.10 <sup>3</sup>        | 2,1.10 <sup>3</sup>            | < 10 <sup>3</sup>      | < 10 <sup>3</sup>      |
| <sup>90</sup> Sr(+ <sup>90</sup> y) | 3,15.10 <sup>3</sup>     | n.m                            | n.m                    | n.m                    |
| <sup>94</sup> Nb                    | 1,7.10 <sup>1</sup>      | 1,2.10 <sup>2</sup>            | 9.10 <sup>2</sup>      | < 11                   |
| <sup>125</sup> Sb                   | traces                   | traces                         | traces                 | nd                     |
| <sup>134</sup> Cs                   | traces                   | traces                         | traces                 | 1.10 <sup>4</sup>      |
| <sup>137</sup> Cs                   | 6,59.10 <sup>3</sup>     | 2,46.10 <sup>4</sup>           | 6,7.10 <sup>4</sup>    | 2,34.10 <sup>4</sup>   |
| <sup>239</sup> + <sup>240</sup> Pu  | 9                        | n.m                            | n.m                    | n.m                    |
| <sup>238</sup> + <sup>241</sup> Am  | 6                        | n.m                            | n.m                    | n.m                    |
| <sup>238</sup> U                    | < 6                      | n.m                            | n.m                    | n.m                    |

TABLEAU 3

PP NORD  
 CONTAMINATION TOTALE  
 ACTIVITES EN Bq au 3.01.82

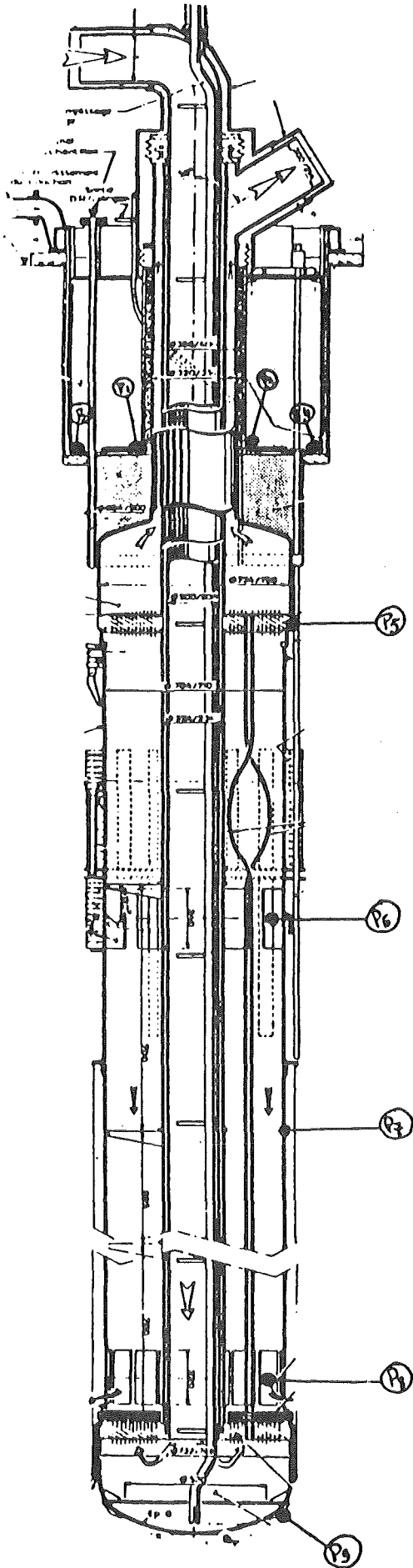
| Radiocontaminants                | Lavage               | Pompe              | Contamination totale     |
|----------------------------------|----------------------|--------------------|--------------------------|
| $^3\text{H}$                     | $1,96 \cdot 10^9$    | # $7,3 \cdot 10^6$ | $2 \cdot 10^9$           |
| $^{54}\text{Mn}$                 | $5,7 \cdot 10^9$     | $9,8 \cdot 10^9$   | $1,55 \cdot 10^{10}$     |
| $^{60}\text{Co}$                 | $2,35 \cdot 10^7$    | $2,6 \cdot 10^7$   | $4,95 \cdot 10^7$        |
| $^{63}\text{Ni}$                 | n.m                  | $4,97 \cdot 10^7$  | $\approx 5 \cdot 10^7$   |
| $^{90}\text{Sr}(+^{90}\text{Y})$ | n.m                  | $4,4 \cdot 10^7$   | $\approx 4,5 \cdot 10^7$ |
| $^{137}\text{Cs}$                | $4,10 \cdot 10^{10}$ | $1,4 \cdot 10^8$   | $4,1 \cdot 10^{10}$      |
| émetteurs $\alpha$               | # $10^3$             | # $2 \cdot 10^5$   | # $2 \cdot 10^5$         |

TABLEAU 4



E . I . S .

DÉBITS DE DOSE AVANT LAVAGE



60 mrads/h , le 06.03.1985

30 mrads/h , le 06.03.1985

90 mrads/h ; le 06.03.1985

TABEAU 5

ECHANGEUR INTERMEDIAIRE SUD  
CONTAMINATION DES SOLUTIONS DE LAVAGE Bq  
au 3.01.87

-----

|                    |                |
|--------------------|----------------|
| $^3\text{H}$       | non mesuré     |
| 22 Na              | $2,31.10^7$    |
| 54 Mn              | $3,47.10^9$    |
| 60 Co              | $1,88.10^8$    |
| 90 Sr(+ 90 y)      | n.m            |
| 134 Cs             | $8,53.10^8$    |
| 137 Cs             | $2,14.10^{10}$ |
| émetteurs $\alpha$ | n.m            |

TABLEAU 6

ECHANGEUR INTERMEDIAIRE SUD  
 CONTAMINATION SURFACIQUE APRES LAVAGE  
 kBq/m<sup>2</sup> au 3.01.82

-----

| Radiocontaminants | zone Na froid         | zone Na médian        | zone Na chaud        | zone de marnage      | zone Argon           |
|-------------------|-----------------------|-----------------------|----------------------|----------------------|----------------------|
| 3H                | # 6,5.10 <sup>2</sup> | # 7,4.10 <sup>1</sup> | n.m                  | n.m                  | n.m                  |
| 54 Mn             | 3.10 <sup>5</sup>     | 2,18.10 <sup>5</sup>  | 2,44.10 <sup>5</sup> | 2,05.10 <sup>5</sup> | 5,98.10 <sup>4</sup> |
| 60 Co             | 2,7.10 <sup>3</sup>   | 2,75.10 <sup>3</sup>  | 4,81.10 <sup>3</sup> | 2,41.10 <sup>3</sup> | 8,4.10 <sup>3</sup>  |
| 63 Ni             | 8,1.10 <sup>3</sup>   | 7,2.10 <sup>3</sup>   | n.m                  | n.m                  | < 10 <sup>3</sup>    |
| 90 Sr(+ 90 y)     | 1,55.10 <sup>3</sup>  | 1,61.10 <sup>3</sup>  | n.m                  | n.m                  | 8,4.10 <sup>2</sup>  |
| 134 Cs            | < 221                 | ≤ 17                  | 1,27.10 <sup>3</sup> | 5,1.10 <sup>2</sup>  | 9,29.10 <sup>3</sup> |
| 137 Cs            | 4,78.10 <sup>3</sup>  | 1,26.10 <sup>3</sup>  | 3,08.10 <sup>4</sup> | 1,11.10 <sup>4</sup> | 2,4.10 <sup>5</sup>  |
| 239 + 240 Pu      | 1,1.10 <sup>1</sup>   | 1.10 <sup>1</sup>     | n.m                  | n.m                  | 3                    |
| 241 + 238 Pu      | 5                     | 5                     | "                    | "                    | 2                    |

TABLEAU 7

ECHANGEUR INTERMEDIAIRE S

CONTAMINATION TOTALE

Bq au 3.01.82

-----

| Radiocontaminants  | Lavage               | Echangeur           | Contamination totale |
|--------------------|----------------------|---------------------|----------------------|
| 3 H                | n.m                  |                     | -                    |
| 54 Mn              | $3,47 \cdot 10^9$    | $3,4 \cdot 10^{10}$ | $3,75 \cdot 10^{10}$ |
| 60 Co              | $1,88 \cdot 10^8$    | $4,26 \cdot 10^8$   | $6,14 \cdot 10^8$    |
| 63 Ni              | n.m                  | $9,1 \cdot 10^8$    | # $10^9$             |
| 90 Sr(+ 90 y)      | n.m                  | $1,82 \cdot 10^8$   | # $2 \cdot 10^8$     |
| 134 Cs             | $8,53 \cdot 10^8$    | n.m                 | -                    |
| 137 Cs             | $2,14 \cdot 10^{10}$ | $1,36 \cdot 10^9$   | $2,27 \cdot 10^{10}$ |
| émetteurs $\gamma$ | n.m                  | # $1,7 \cdot 10^6$  | # $1,7 \cdot 10^6$   |

TABLEAU 8

**PIEGES FROIDS**  
**CONTAMINATION TOTALE**

Bq

| Radiocontaminants | PF Na 300<br>15.01.82 | PF Na 400<br>24.11.78 |
|-------------------|-----------------------|-----------------------|
| 22 Na             | $4,5 \cdot 10^9$      | $7,7 \cdot 10^9$      |
| 54 Mn             | $1 \cdot 10^{10}$     | $1,4 \cdot 10^{10}$   |
| 60 Co             | # $3,7 \cdot 10^8$    | $3,1 \cdot 10^8$      |
| 110 mAg           | $5,9 \cdot 10^8$      | $9,8 \cdot 10^8$      |
| 113 Sn            | $6,4 \cdot 10^9$      | $1,6 \cdot 10^{10}$   |
| 124 Sb            | $4,9 \cdot 10^{11}$   |                       |
| 134 Cs            | $5,4 \cdot 10^{10}$   | $2,4 \cdot 10^{11}$   |
| 137 Cs            | $1,28 \cdot 10^{12}$  | $2,90 \cdot 10^{12}$  |

TABLEAU 9

CONTAMINATION TOTALE (Bq)  
 EN <sup>137</sup>Cs ET EN PRODUITS D'ACTIVATION  
 CORRODES DES COMPOSANTS

-----

| Radiocontaminants | Pompe N<br>3.01.82   | E.I.S<br>3.01.82     | Piège froid 300<br>15.1.82 | Piège froid 400<br>24.11.78 |
|-------------------|----------------------|----------------------|----------------------------|-----------------------------|
| 54 Mn             | $1,55 \cdot 10^{10}$ | $3,75 \cdot 10^{10}$ | $1 \cdot 10^{10}$          | $1,4 \cdot 10^{10}$         |
| 60 Co             | $4,95 \cdot 10^7$    | $6,14 \cdot 10^8$    | # $3,7 \cdot 10^8$         | $3,1 \cdot 10^8$            |
| 124 Sb            | -                    | -                    | $4,9 \cdot 10^{11}$        | -                           |
| 134 Cs            | -                    | -                    | $5,4 \cdot 10^{10}$        | $2,4 \cdot 10^{11}$         |
| 137 Cs            | $4,1 \cdot 10^{10}$  | $2,27 \cdot 10^{10}$ | $1,28 \cdot 10^{12}$       | $2,90 \cdot 10^{12}$        |

TABLEAU 10







# POMPE PRIMAIRE

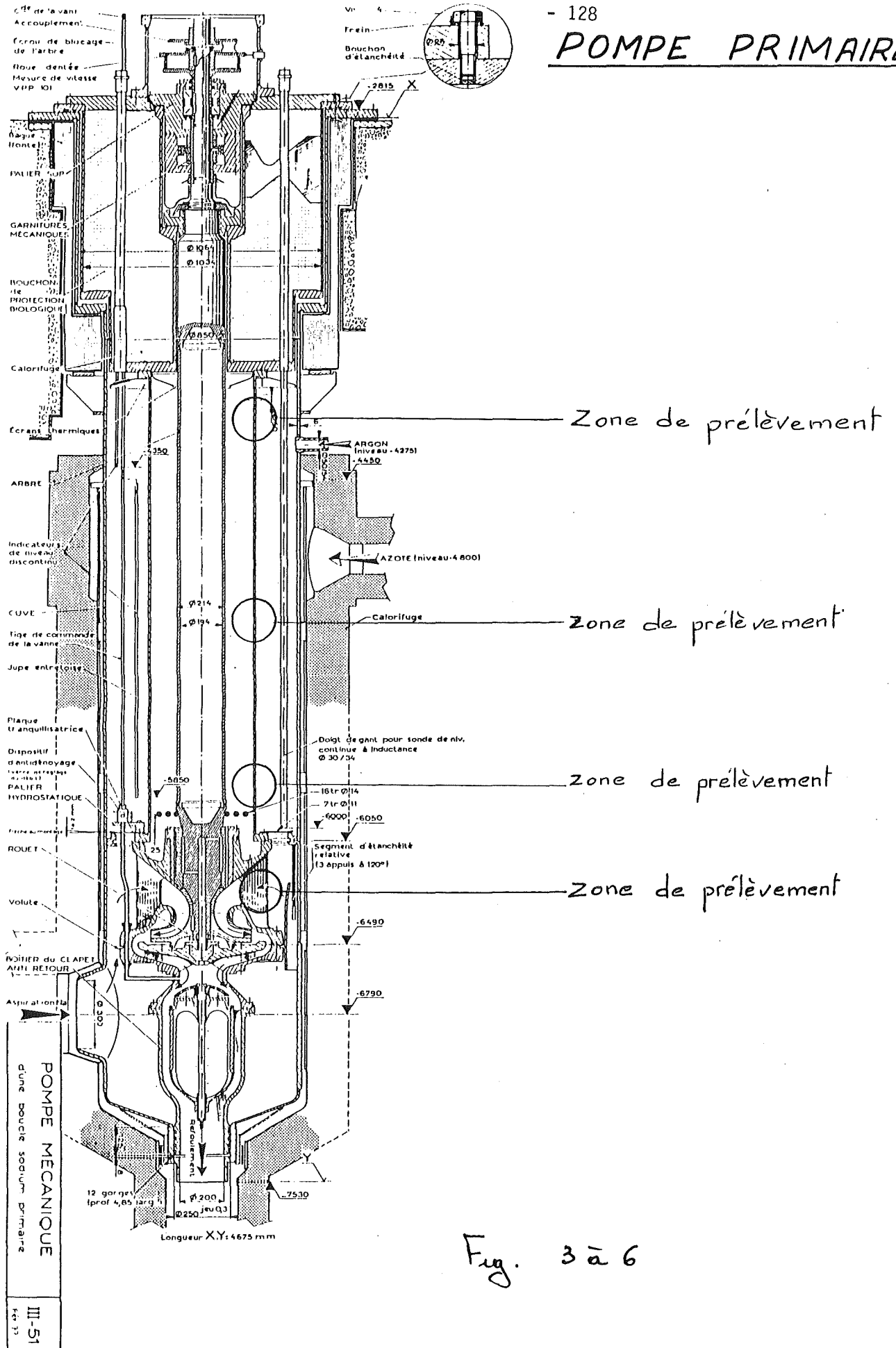
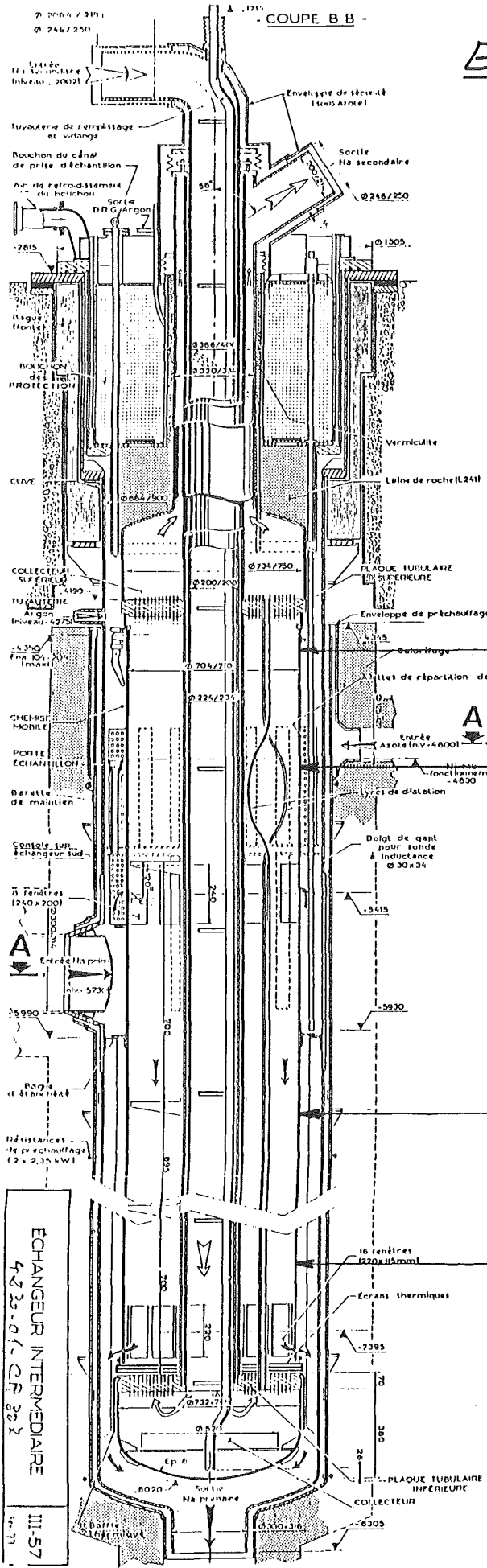


Fig. 3 à 6



# ECHANGEUR INTERMEDIAIRE SUD (E.I.S.)



} zone de prélèvement

} zone de prélèvement

} zone de prélèvement

} zone de prélèvement

} zone de prélèvement

ECHANGEUR INTERMEDIAIRE  
4-23-07-CP 202  
III-57  
12-71

Fig. 7 à 10

## **Introduction**

The models and codes used in France to describe the repartition of the contamination in a LMFBR are characterized by :

- their simplicity ;
- the fact that they are drawn from the direct experience of the reactors (RAPSODIE, PHÉNIX) ;
- their aim: to dimension new reactors of commercial size (SUPER PHÉNIX, RNR 1500).

They are used in the following fields:

- dimensionning of the protections (handling casks, etc);
- dimensionning of the effluents processing;
- aid to the operator (prediction of the contamination).

## **CONTAMINATION OF THE COVER GAS [1]**

### **Contamination by the activation products**

In addition to  $^{23}\text{Ne}$  which is the predominant species when the reactor is operating,  $^{41}\text{Ar}$  and  $^{37}\text{Ar}$  were measured at PHÉNIX .

#### ◆ $^{23}\text{Ne}$ ( $T_{1/2} = 38 \text{ s}$ )

Current measurements show an activity of  $5 - 7 \text{ TBq/m}^3$  in the cover gas of PHÉNIX. This low value compared to the production can only be explained by an important delay ( $T_{1/2} \approx 50-80 \text{ min}$ ) assumed for coalescence of the atoms and their degassing at the sodium-gas interface.

#### ◆ $^{41}\text{Ar}$ ( $T_{1/2} = 110 \text{ min}$ )

The activity of  $^{41}\text{Ar}$  extrapolated from RAPSODIE to PHÉNIX (direct activation of the cover gas) proved to be underestimated by several orders of magnitude in comparison to the measured  $1,5 \text{ GBq/m}^3$ . To explain this discrepancy, it was first assumed that the cover gas of the pumps could be carried along by the vortex and activated when flowing through the core. Recent calculations showed that the potassium content of the sodium ( $\approx 200 \text{ ppm}$ ) was sufficient to account for all the  $^{41}\text{Ar}$  activity measured, by (n,p) reaction on  $^{41}\text{K}$  (present for 6,9 % of natural potassium ).

The delay constant of argon was analysed during a fast shut down of the reactor: after a small peak, the activity decreases with an exponential asymptote (Fig. 6.1). It is interpreted by the use of two delay constants: a nominal constant when the reactor is in operation, and a higher constant at the moment of the shut-down (possibly due to a more rapid coalescence of the bubbles when the sodium is cooling down).

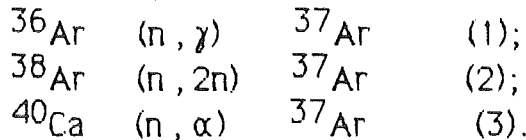
The adjustment of the calculated curve to the measured values yielded a nominal constant of  $2,4 \cdot 10^{-4} \text{ s}^{-1}$  ( $T_{1/2} = 48 \text{ min}$ ), and a shut-down degassing constant about 3 times higher.

The fact that the nominal degassing constant has a comparable value as the one assumed for  $^{23}\text{Ne}$  is in favour of a similar mechanism of formation: activation of single atoms, rather than activation of argon bubbles for which one could expect a higher degassing constant.

◆  $^{37}\text{Ar}$  ( $T_{1/2} = 35 \text{ d}$ )

It has been measured by gas sampling at a level of  $0,2 \pm 0,03 \text{ GBq/m}^3$  in the cover gas of PHÉNIX.

The possible formation reactions are:



Calculation of direct activation of  $^{36}\text{Ar}$  in the cover gas yields a value  $3 \cdot 10^8$  times lower than measured. Supposing gas carrying (e.g. by the vortex of the pumps) with a flowrate estimated from  $^{41}\text{Ar}$  measurements yields a value 3000 times lower than measured.

Reaction (2) does not take place in the cover gas, since it requires high energy neutrons. It should presumably be insufficient to account for the measured value in the case of gas carrying.

On the other hand, calculation with reaction (3) and a sodium content of 5 ppm of calcium - which is the high limit specified for "nuclear grade" sodium - yields  $0,16 \text{ GBq/m}^3$ , close to the measured value.

◆ **conclusion:**

These measurements and interpretations show that:

- in the case of a pool-type reactor, the direct activation of the cover gas is negligible in comparison to the activation of the sodium and of its impurities;
- the half-delay time of PHÉNIX for simple atoms is about 1 h, with a good consistency between the 3 activation products.

We estimate that this value could also be used for the fission gases produced in a similar way, that is by single atoms, from tramp fuel for example.

### **Contamination by the fission products**

The activity of the cover gas due to fission gases has the form of peaks, as if the gases were mostly released by the cladding failure under the form of sporadic bubbles. Contrarily to the activation gases, it can be considered in that case that the degassing of the gas bubble at the sodium-argon interface is instantaneous. Since no measured peak reaches a value corresponding to the total release of the inventory of the pin, it can be assumed that some delay exists however. Actually, it is well known that the fuel ceramic is very fractured, with voids that are only partially interconnected. Moreover, a compound layer (of cesium uranates) fills the gap between clad and fuel, which restricts a direct emptying of the pin. In the model developed below, we consider for these reasons that the limiting step is the release from the pin.

#### **Model and code BOUFFON:**

The fuel pin is schematized by a simple envelope (cladding) filled with gas under pressure, and all the delays are converted to an equivalent micro-leak on the cladding (cylinder of length equal to the depth of the cladding). The radioactive species contained in the plenum are expelled by the pressure of the stable gases. The regime of leakage is transitory for the low burn-ups and laminar for the higher burn-ups reached at PHÉNIX.

The calculation of the gases available for the leakage at the failure time are obtained as follows:

The released fraction of the stable gases versus the burn-up is obtained from the examination of the fuel irradiated in RAPSODIE and PHÉNIX. Concerning the released rates of the radio-xenons and krytons, data are available from in loop measurements at SILOÉ. They can also be obtained by adjustment of the measured contamination curves from PHÉNIX, where  $^{133}\text{Xe}$ ,  $^{135}\text{Xe}$ ,  $^{135\text{m}}\text{Xe}$ ,  $^{87}\text{Kr}$ ,  $^{85\text{m}}\text{Kr}$  are continuously monitored: on a set of 5 curves of activity, the best fit is searched for:

- a common value for the equivalent diameter of the hole,
- 5 individual release rates for the radioactive species.

An example of such a simulation is given on Fig. 6.2 : the best fit of the calculated curves with regard to the measured values is obtained with an equivalent diameter of 7  $\mu\text{m}$  (current values found at RAPSODIE: 1 to 4  $\mu\text{m}$ ); the apparent release rates are:

$$^{133}\text{Xe} : 7\% ; ^{135}\text{Xe} : 4\% ; ^{135\text{m}}\text{Xe} : 7\% ; ^{87}\text{Kr} : 5,5\% ; ^{85\text{m}}\text{Kr} : 11\% .$$

At present, no physical meaning is attributed to these values, that show no correlation with the decay constant.

## CONTAMINATION BY THE TRITIUM

The adaptation of the Kumar's model to PHÉNIX was presented by TIBI [2].

Some modifications were brought to the method of calculation of the permeation coefficient: integration of the permeation rate law along the IHXs and steam generators permitted to reduce the gap between the measured and calculated values.

Recent PHÉNIX measurements of the tritium and hydrogen (by the use of a primary hydrogenmeter) sources proved that the first estimated values from PHÉNIX were highly overestimated.

Although the fit between measurements and calculations was greatly improved by these modifications, we think that a complete comprehension of the phenomena will only be possible by measuring continuously the tritium concentrations in primary and secondary circuits with a tritiummeter.

## CONTAMINATION OF THE COMPONENTS BY CORROSION PRODUCTS

The model (drawn from General Electric works) and the code CORONA were presented in [3].

From a review of the available international work on austenitic corrosion rates and some additional work performed by Mr. P. BAQUÉ at C.E.N. Cadarache on the Mass Brothers loop (Fig. 6.3), a new corrosion model was built to account particularly for the operational conditions of the French breeder reactors: a high purity of the sodium as regards the oxygen concentration.

### ◆ Influence of oxygen:

The dispersion of the proposed laws around 1 as exponent of the oxygen concentration leads us to take :

$$dm/dt \propto [O] \quad (* \text{ is employed for "proportional to"})$$

It must be emphasized that this is valid only on a limited range, because at high oxygen concentrations the corrosion process is modified.

### ◆ Influence of the sodium velocity:

Although the existence of an asymptote of the corrosion rate was reported for increasing sodium velocity, we still keep the General Electric law:

$$dm/dt \propto V_{Na}^{0,435} .$$

### ◆ Influence of the temperature:

The Arrhenius type law was not observed in Mass Brothers. On the contrary, the existence of a temperature threshold, under which the corrosion of austenite does not take place, was noticed (this threshold seems to decrease slightly with the time: from 550°C [t = 0] to 535°C [t = 25 000 h]).

For the first year of corrosion, the following rate law fits well with the results:

$$dm/dt \propto \exp(-150/(t-544))$$

**IWGFR SM/contamination - French experience - models & codes - p.5**

---

◆ **Influence of the down-stream effect:**

From the preceding consideration, only the fuel cladding is concerned by the corrosion. Because of the increase of the sodium temperature all along the core, the downstream effect is neglected.

◆ **Influence of the time:**

2 periods are considered in the corrosion phenomenon:

\* during the first period, the dissolution of the superficial ferritised layer ( $\propto t$ ) and the diffusion of the elements through the ferritised layer ( $\propto t^{1/2}$ ) take place simultaneously;

\* during the second period, a steady state is reached, and the corrosion is equivalent to a dissolution of the austenite ( $\propto t$ ).

The time needed to reach the steady-state varies from some weeks to some years depending on the oxygen concentration and the sodium velocity.

**Application to PHÉNIX:** results of calculation of the loss of surfacic mass for various times and temperatures for a 316 type steel:

**1st case : t = 1 year**

| $\theta(^{\circ}\text{C}) \setminus \Delta m \text{ (mg/cm}^2\text{)}$ | Fe   | Cr   | Ni   | Mo   | Mn   | total |
|--|------|------|------|------|------|-------|
| 650  | 1,48 | 0,94 | 0,71 | 0,06 | 0,07 | 3,26  |
| 620  | 0,84 | 0,53 | 0,41 | 0,03 | 0,05 | 1,87  |
| 600  | 0,34 | 0,30 | 0,23 | 0,01 | 0,03 | 0,92  |

**2nd case : t = 2 years**

| $\theta(^{\circ}\text{C}) \setminus \Delta m \text{ (mg/cm}^2\text{)}$ | Fe   | Cr   | Ni   | Mo   | Mn   | total |
|--|------|------|------|------|------|-------|
| 650  | 2,95 | 1,43 | 1,05 | 0,11 | 0,12 | 5,67  |
| 620  | 1,68 | 0,82 | 0,62 | 0,06 | 0,08 | 3,27  |
| 600  | 0,68 | 0,47 | 0,36 | 0,03 | 0,05 | 1,61  |



The corrosion model of BAQUÉ was installed into the CORONA code at the place of the corrosion equations of General Electric. The new code CORNAC (corrosion by Na of the activation products) was applied to 2 IHXs of PHÉNIX having run during about 800 EFPD. The calculations by both codes yield very close results (within  $\pm 10\%$ ) for  $^{54}\text{Mn}$ , which represents 95% (or more) of the deposited activity; but for the cobalts, CORNAC yields much closer value than CORONA, as shown on the following table.

| (calc/mes) ratios | $^{54}\text{Mn}$ | $^{60}\text{Co}$ | $^{58}\text{Co}$ | $^{51}\text{Cr}$ |
|-------------------|------------------|------------------|------------------|------------------|
| CORONA            | 1                | 20 ÷ 2           | 10               | 1                |
| CORNAC            | 1                | 1,5              | 1                | 1                |

### CONTAMINATION OF THE PRIMARY SODIUM

No particular model is used for the fission products, except for iodine and cesium for which the cold trap efficiency has been measured in PHÉNIX. The efficiency was reported to be close to 1 for the iodine [4]; for the cesium, the value  $4 \cdot 10^{-3}$  was measured.

---

[1] P. MICHAILLE & R. CLERC, IAEA/IWGFR Specialists' Meeting on Fast Reactor Cover Gas Purification, HEDL, Richland, WA (USA) 24-26 sept 1986

[2] A. TIBI, J. MISRAKI & D. FÉRON, Liquid metal engineering and technology, 3rd Int. Conf. Oxford (GB) 9-13 april 1984

[3] L. COSTA, R. de FRÉMONT, J. C. MOUGNIOT, D. MSIKA, IAEA/IWGFR Specialists' Meeting on Fission and corrosion product behaviour in primary circuits of LMFBR's, Dimitrovgrad (URSS) 8-11 sept 1975

[4] C. BERLIN & J. C. CAUVIN, *ibid.*

Fig. 6.1 : Degassing curve of  $^{41}\text{Ar}$  at PHÉNIX

O : measured values ; — : adjusted curve

**Expression of the adjusted curve:**

$t = 0$  : shut-down

$y = [\text{volumic activity}(t)] / [\text{volumic activity}(t = 0)]$  can be expressed :

$$y = \exp(-a*t) + k*a/(c-a) * [\exp(-a*t) - \exp(-c*t)] \quad \text{where:}$$

$$a = KD + DB/VK ; c = KA1 + KD ; k = KA1/KA0$$

$KD$  : decay constant of  $^{41}\text{Ar}$  ;

$DB$  : sweeping flowrate of the cover gas ;

$VK$  : volume of the cover gas ;

$KA0$  ( $KA1$ ) : degassing constant before (after) shutdown

**Adjusted values:**

$$KA0 = (2,4 \pm 0,2) \cdot 10^{-4} \text{ s}^{-1}$$

$$KA1 = (7 \pm 2) \cdot 10^{-4} \text{ s}^{-1}$$

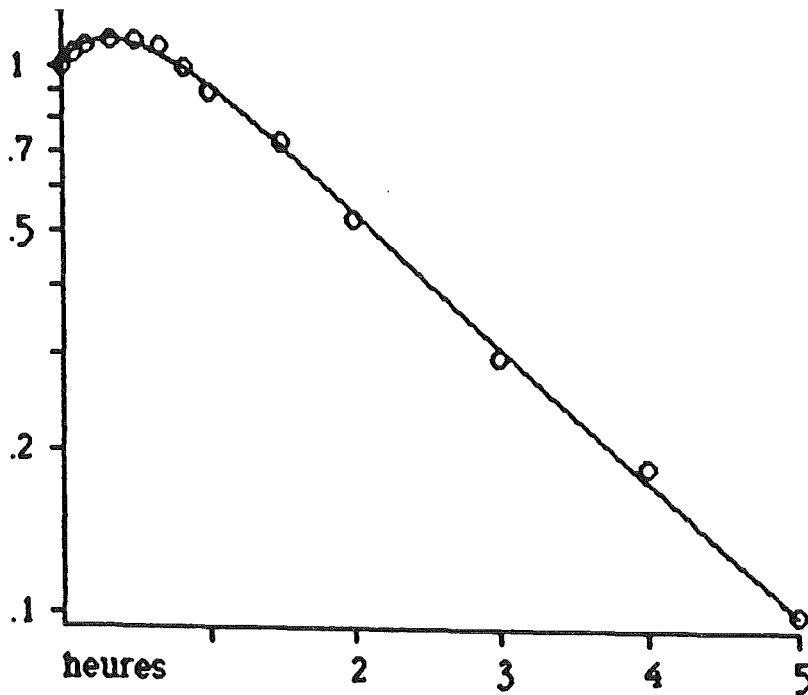


Fig. 6.2 : Adjustment of the parameters on a set of activity curves on a typical release of PHÉNIX

measurements :  $\circ$  :  $^{133}\text{Xe}$  ;  $\circ$  :  $^{135}\text{Xe}$  ;  $\bullet$  :  $^{85\text{m}}\text{Kr}$  ;  $\blacksquare$  :  $^{87}\text{Kr}$  ;  $+$  :  $^{135\text{m}}\text{Xe}$   
adjusted curves : — with similar symbols for distinction

The fitting was performed on the first 6 hours of release. The figure below suggests that after that time, a small burst occurred. See values of the parameters in the text.

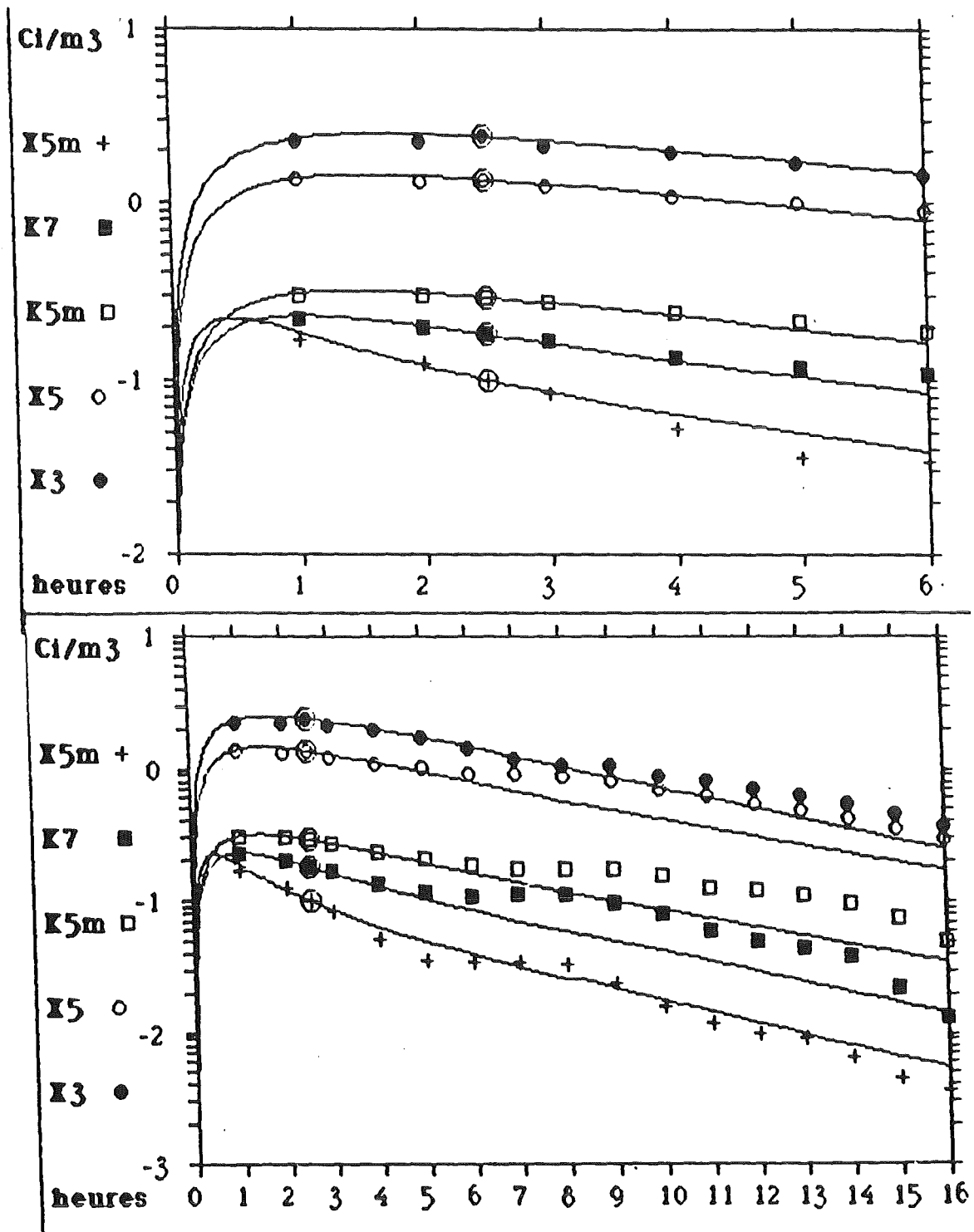
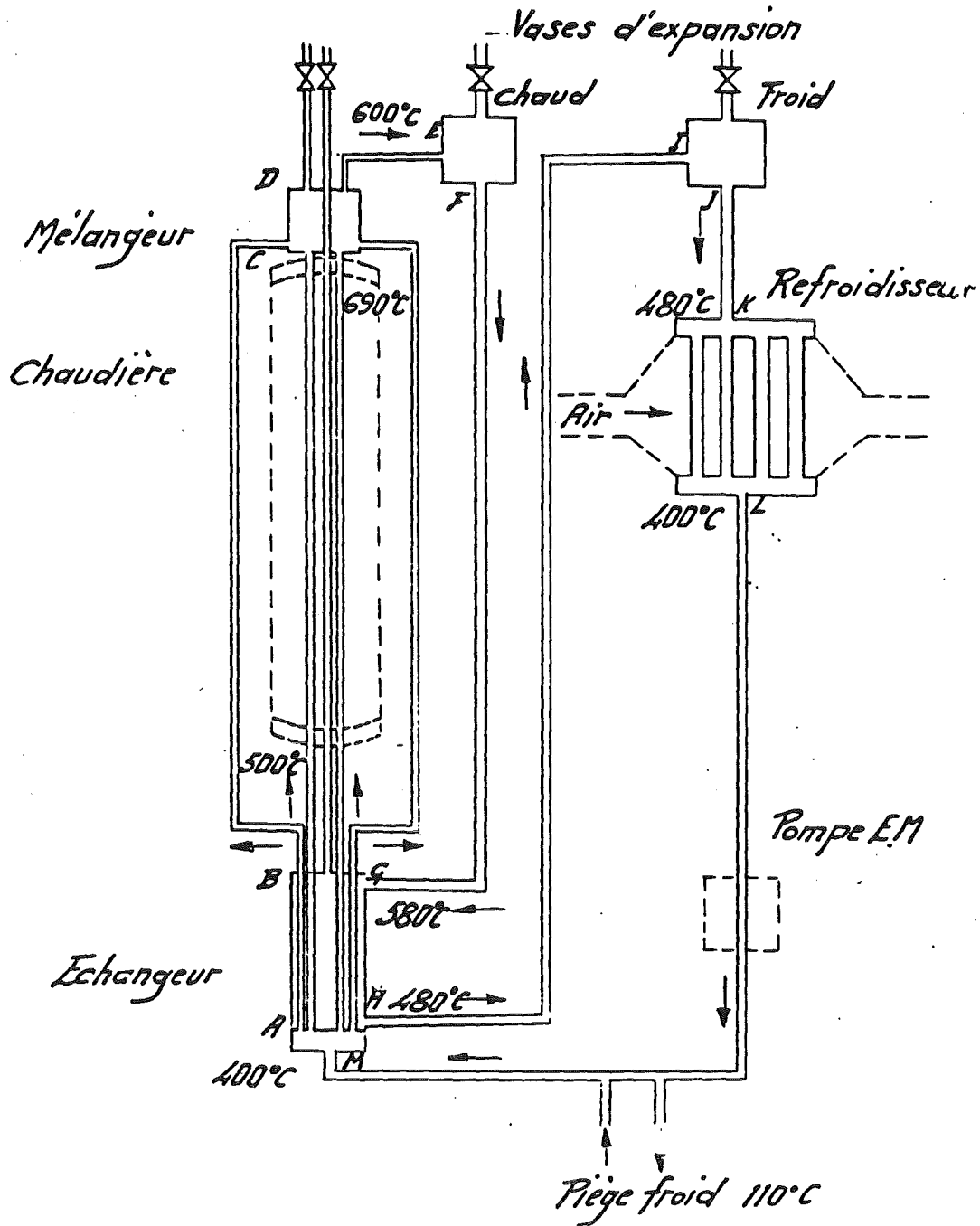


Fig 6.3 : Scheme of the MASS BROTHERS loop

The surface ratio deposition/corrosion ( $\approx 50$ ) and the temperature distribution is representative of PHÉNIX. The sodium velocity is 0,895 m/s in the heater ( $\varnothing = 0,5$  cm) and 0,03 m/s in the mixing zone.





" BILAN DES MESURES DE CONTAMINATION EFFECTUEES  
A PHENIX AU 1er AVRIL 1987 " -

R. CLERC - J. GUIDEZ  
P. MICHAILLE - J. MISRAKI

Centrale PHENIX  
DRNR/STRA

SOMMAIRE

- 1 - BUT DE LA NOTE
- 2 - MESURES DE CONTAMINATION SUR E.I ET POMPES
- 3 - MESURES TASTENA
- 4 - MESURES PIEGE FROID PRIMAIRE
- 5 - MESURES LRG/DRG
- 6 - MESURES TRITIUM
- 7 - CONCLUSION

## 1 - BUT DE LA NOTE

Dans un réacteur rapide, un certain nombre de produits actifs se créent en fonctionnement :

- soit par activation (du sodium, de l'argon, des impuretés initiales, des produits de corrosion ultérieurs, etc...),
- soit occasionnellement par relâchement des ruptures de gaine,
- soit par "pollution des assemblages" (fission de la matière fissile polluant les soudures en cours de fabrication),
- soit, pour le tritium, par une production continue dans le coeur.

Ces produits entraînent une contamination de l'ensemble du bloc réacteur.

Le but de cette note est de faire au 01.04.1987 un bilan de l'ensemble des mesures de contamination effectuées depuis l'origine à PHENIX :

- sur les EI,
- sur les pompes,
- sur le piège froid primaire,
- par les tastenas,
- par la LRG/DRG,
- par les mesures tritium.



Une première interprétation de ces mesures est effectuée pour dégager les grandes lignes de l'expérience Phénix dans ce domaine.

## 2 - MESURES DE CONTAMINATION SUR LES POMPES ET LES ECHANGEURS INTERMEDIAIRES

### 2.1 Mouvement des pompes et E.I à PHENIX

Les pompes et les E.I. ont été plusieurs fois sortis et décontaminés à Phénix.

La Figure 1 résume les mouvements des pompes depuis 1973 et la Figure 2 le mouvement des échangeurs.

Ces opérations ont permis à chaque fois d'effectuer des bilans de contamination de ces composants.

### 2.2 Mesures de contamination sur les pompes primaires

Des bilans de contamination ont été effectués sur trois pompes :

- la pompe A lavée et décontaminée en Octobre 1976 (date de sortie du réacteur Juillet 1976),
- la pompe B lavée et décontaminée en Janvier 1982 (sortie du réacteur Octobre 1981),
- la pompe D lavée et décontaminée en Mars 1983 (sortie du réacteur Février 1983).

Les méthodes de lavage et de décontamination ont varié d'une pompe à l'autre ; mais pour ces trois pompes, plusieurs prélèvements d'échantillons ont été effectués pendant les opérations de prélavage, de lavage des différentes parties de la pompe et de leur décontamination.

Tous ces échantillons ont été mesurés par spectrométrie gamma.

Les résultats de ces mesures sont les suivants.

#### 2.2.1 Radiocontaminants mis en évidence

Les produits d'activation ( $^{22}\text{Na}$  et  $^{65}\text{Zn}$ ) et les produits de fission ( $^{137}\text{Cs}$  accompagné du  $^{134}\text{Cs}$ ) sont présents dans les eaux de lavage.

On retrouve les produits d'activation corrodés ( $^{51}\text{Cr}$ ,  $^{58}\text{Co}$ ,  $^{54}\text{Mn}$  et  $^{60}\text{Co}$ ) dans les solutions de lavage et essentiellement dans les solutions de décontamination.

#### 2.2.2 Contribution des radiocontaminants à la contamination totale

Le Tableau 1 permet de voir la participation de chaque radiocontaminant à la contamination totale de chaque pompe.

#### 2.2.3 Conclusion

Le  $^{54}\text{Mn}$  représente à lui seul plus de 97 % de la contamination totale des pompes primaires.

Les produits d'activation et de fission peuvent être considérés comme négligeables.

### 2.3 Echangeurs intermédiaires

Un plus grand nombre d'échangeurs intermédiaires a été extrait du réacteur. De plus, nous avons pu diversifier les moyens de mesure de la contamination déposée sur ces composants.

#### 2.3.1 Eprouvette témoin de contamination

Deux échangeurs intermédiaires de Phénix sont équipés d'une éprouvette témoin de contamination : le D et le G.

**TABLEAU 1**  
CONTRIBUTION DES RADIOCONTAMINANTS  
A LA CONTAMINATION TOTALE  
DES POMPES PRIMAIRES

| POMPES   | A                                  | B                               | D                               |
|--|------------------------------------|---------------------------------|---------------------------------|
| Temps de fonctionnement  | 20.800 h                           | 48.700 h                        | 70.000 h                        |
| Date de sortie   | 07.1976                            | 10.1981                         | 02.1983                         |
| Date de mesure   | 10.1976                            | 01.1982                         | 03.1983                         |
| Radiocontaminants  |                                    |                                 |                                 |
| Produits d'activation<br>22 Na<br>+<br>65 Zn                       | présents<br><br>non mesurés        | 0,03 %                          | 0,01 %                          |
| Produits de fission<br>137 Cs<br>+<br>134 Cs                       | 0,2 %                              | 0,2 %                           | 0,2 %                           |
| Produits d'activation corrodés<br>51 Cr<br>54 Mn<br>58 Co<br>60 Co | 99,8 %<br><br>dont 97,7 %<br>54 Mn | 99,8 %<br><br>(97,6 %<br>54 Mn) | 99,8 %<br><br>(98,3 %<br>54 Mn) |

L'éprouvette équipant l'échangeur G descend jusqu'au niveau de la plaque tubulaire inférieure alors que celle de l'échangeur D s'arrête en haut de la fenêtre de sortie du sodium.

### 2.3.1.1 Description du dispositif témoin de contamination de l'échangeur G

Le dispositif témoin de contamination se présente comme suit : (Figure 3) à la place d'un tube d'échange de la couronne externe du faisceau se trouve une gaine-fourreau réalisée dans la même nuance d'acier que le faisceau tubulaire (316 L), d'une longueur d'environ 10.195 mm et d'un diamètre 12-14 mm.

Cette gaine est bouchée à sa base et comporte de part et d'autre d'une double courbure correspondant au niveau de la fenêtre d'entrée, une série de lumières diamétralement opposées et qui sont destinées à assurer le passage du sodium à l'intérieur de la gaine.

Les lumières de 40 mm x 6 mm sont espacées entre elles de 80 mm.

On introduit dans cette gaine l'éprouvette témoin de contamination proprement dite : c'est une tige en 316 L également, de 4 mm de diamètre et 8.676 mm de longueur sur laquelle sont enfilés, sur une hauteur d'environ 6.910 mm, 106 tronçons de tube ( $\phi$  : 5 - 7 mm, longueur : 60 mm) séparés par des entretoises ( $\phi$  : 11,2 mm, hauteur : 5 mm) ; à l'extrémité inférieure de la tige se trouve un embout de diamètre maximum 10 mm et de hauteur 14 mm ; la butée supérieure a un diamètre maximum de 10 mm, une hauteur de 10 mm (Figure 4).

L'ensemble est surmonté d'un bouchon faisant protection biologique.

Les tronçons de tube que nous nommerons par la suite échantillons, embouts et bouchon sont tous de la même nuance d'acier, celle des tubes d'échange de l'échangeur : 316 L.

La tige a été dégraissée au formaldéhyde diméthyl acétate alors que les échantillons et entretoises ont subi le même prétraitement (passivation) que l'échangeur.

#### 2.3.1.2 Déroulement de l'expérience

L'éprouvette a donc été introduite en réacteur en même temps que l'échangeur G en Mai 1980 pendant la campagne de manutention située entre le 19 et le 20ème cycle d'irradiation.

Elle a été extraite le 24 Juin 1984 en fin de 31ème cycle. L'échangeur lui-même a été sorti du réacteur en Janvier 1985 en fin de 32ème cycle, soit peu de temps après l'extraction de l'éprouvette.

Ainsi, du 15.05.1980 au 16.01.1985, l'échangeur G a totalisé :

- 41 014 heures en sodium primaire,
- 16.997 heures de fonctionnement du réacteur à 3 GV,
- 4.058 heures de fonctionnement à 2 GV/3,
- 36.154 heures en sodium secondaire.

On peut considérer que l'éprouvette elle-même a totalité environ :

- 36.070 heures en sodium primaire,
- 14.902 heures de fonctionnement à 3 GV,
- 4.058 heures de fonctionnement à 2 GV.

Après son extraction, l'éprouvette a été démantelée et chaque échantillon a été seulement nettoyé par un bain d'alcool éthylique.

### 2.3.1.3 Mesures effectuées

#### Spectrométrie gamma des échantillons

Tous les échantillons ont été mesurés par spectrométrie  $\gamma$ .

La Figure 5 est un exemple de spectre obtenu.

Les radioéléments dont la présence a été mise en évidence sont  $^{51}\text{Cr}$ ,  $^{54}\text{Mn}$ ,  $^{58}\text{Co}$ ,  $^{59}\text{Fe}$ ,  $^{60}\text{Co}$  et  $^{182}\text{Ta}$ .

L'activité gamma devient très faible à partir de l'échantillon 96. Huit échantillons ont été totalement décontaminés afin de transférer toute la radioactivité en solution et ainsi, puisque l'ensemble de spectrométrie  $\gamma$  est étalonné pour une géométrie de comptage en milieu liquide, de déterminer le coefficient d'étalonnage à appliquer aux mesures des échantillons.

On obtient ainsi la Figure 6 donnant en fonction du numéro de l'échantillon, l'activité de chacun d'entre eux pour les différents radionuclides.

Les activités sont exprimées en Becquerels et calculées à la date d'arrêt du réacteur précédant l'extraction de l'éprouvette, c'est-à-dire le 26.04.1986.

#### Dosages du $^{63}\text{Ni}$

Le  $^{63}\text{Ni}$  est un produit d'activation du nickel qui a 100 ans de période et qui se désintègre en émettant uniquement un rayonnement  $\beta^-$  de faible énergie  $\beta^-$  maximum. Son dosage nécessite un mode opératoire particulier et il n'a été possible de la pratiquer que sur un petit nombre d'échantillons.

On peut voir sur la Figure 6 les quelques valeurs d'activité en  $^{63}\text{Ni}$  obtenues.

#### 2.3.1.4 Interprétation des résultats de mesure

Nous considérons que la présence des radionuclides observés est dûe essentiellement au dépôt de produits d'activation corrodés.

Les activités dues à l'irradiation neutronique au niveau de l'échangeur sont considérées comme négligeables. Les résultats des essais de décontamination, afin de déterminer les coefficients d'étalonnage confirment ceci puisque l'on a atteint des rendements de décontamination voisins de 100 %.

La Figure 6 montre la répartition des différents radio-contaminants le long de l'éprouvette :

- prédominance du  $^{54}\text{Mn}$ ,
- profils identiques pour  $^{51}\text{Cr}$ ,  $^{58}\text{Co}$ ,  $^{60}\text{Co}$  et semble-t-il  $^{63}\text{Ni}$ ,
- forte contamination en  $^{54}\text{Mn}$  vers le bas de l'éprouvette,
- contamination relativement constante le long de l'éprouvette pour  $^{51}\text{Cr}$ ,  $^{58}\text{Co}$ ,  $^{60}\text{Co}$  et  $^{63}\text{Ni}$ .

En ce qui concerne le  $^{54}\text{Mn}$ , nous avons tracé les activités mesurées sur chaque échantillon en fonction de la répartition de température le long d'un tube de la couronne extérieure (Figure 7).

La contamination atteint un palier vers  $490 - 500^\circ\text{C}$ . Pour la région comprise entre  $350^\circ$  et  $500^\circ\text{C}$ , nous avons porté le logarithme de l'activité en  $^{54}\text{Mn}$  exprimée en  $\text{Bq}/\text{cm}^2$  en fonction de l'inverse de la température exprimée en Kelvin ; on obtient une droite (Figure 8).

La contamination en  $^{54}\text{Mn}$  dans cette région 350 - 500° C suit une loi représentée par :

$$A_{\text{Bq/cm}^2} = 6,425 \cdot 10^{-5} e^{\frac{15.317}{T_K}}$$

### 2.3.2 Spectrométrie $\gamma$ directe

Soit au moment de l'extraction du réacteur (uniquement pour le F (première fois) et le E), soit surtout au moment de l'introduction en puits de lavage, certains E.I. ont subi des mesures par spectrométrie  $\gamma$  directe.

Onze points de mesure ont été répartis le long de la zone immergée en sodium ; une sonde  $\gamma$  (Ge - Li puis Ge - Hp) a été placée face à ces onze points de mesure, derrière un des hublots du sas de manutention.

Dans ce hublot, la diode a été placée au contact de collimateurs qui visaient les points de mesure.

Le traitement des mesures se résume ainsi :

- établissement du coefficient de rendement de la diode à l'aide d'une source ponctuelle d'Eu 152 étalon vue à travers les collimateurs utilisés,
- établissement du coefficient de géométrie par application du programme Mercure IV, à une source représentant la partie tubulaire de l'échangeur (activité supposée homogène dans tout le volume source).

Les valeurs de contamination ainsi calculées sont connues avec une incertitude d'au moins 30 %.



Ces mesures par spectrométrie  $\gamma$  directe nous permettent de confirmer les profils de contamination déjà observés (Figures 9, 10, 11, 12) et de souligner que pour tous les échangeurs, les radiocontaminants les plus importants sont  $^{54}\text{Mn}$ ,  $^{51}\text{Cr}$ ,  $^{58}\text{Co}$  et  $^{60}\text{Co}$  ; les  $^{59}\text{Fe}$  et  $^{137}\text{Cs}$  n'ayant pas été mis en évidence de manière mesurable.

### 2.3.3 Mesures des échantillons de solutions de lavage et de décontamination

Comme pour les pompes, des échantillons des solutions de chaque étape de lavage et de décontamination ont été prélevés et mesurés par spectrométrie gamma.

Les résultats de ces mesures sont connus à  $\pm 20\%$ .

Le Tableau 2 décrit la contribution des radiocontaminants à la contamination totale des échangeurs intermédiaires.

On retrouve les mêmes résultats que ceux observés pour les pompes primaires :

- la contribution des produits d'activation corrodés est de plus de 99 %, le radiocontaminant le plus abondant étant  $^{54}\text{Mn}$ ,
- la participation des produits de fission et des produits d'activation peut être considérée comme négligeable.

### 2.3.4 Conclusion

Les mesures effectuées sur les échangeurs ont permis de confirmer les résultats obtenus sur les pompes.

Les différents moyens de mesure utilisés ont permis en particulier de mieux comprendre les lois de "déposition" du  $^{54}\text{Mn}$  en fonction de la température.

TABLEAU 2  
CONTRIBUTION DES RADIOCONTAMINANTS  
A LA CONTAMINATION TOTALE DES E.I.

| E.I.                                 | A                         | F                         | C                         | B                         | D                         | E                         | F                           | G                           | C                        |
|--------------------------------------|---------------------------|---------------------------|---------------------------|---------------------------|---------------------------|---------------------------|-----------------------------|-----------------------------|--------------------------|
| Temps total en sodium h              | 42.351                    | 33.462                    | 40.986                    | 42.569                    | 38.683                    | 34.961                    | 25.983                      | 41.014                      | 58.164                   |
| Date de sortie                       | 11.1977                   | 11.1976                   | 09.1977                   | 10.1977                   | 06.1977                   | 01.1977                   | 05.1980                     | 01.1985                     | 07.1984                  |
| Date de mesure                       | 12.1977                   | 12.1976                   | 09.1977                   | 12.1977                   | 07.1977                   | 01.1977                   | 12.1980                     | -                           | -                        |
| Etat à la mise en oeuvre             | Neuf                      | Neuf                      | Neuf                      | Neuf                      | Neuf                      | Neuf                      | Décontaminé                 | Neuf                        | Décontaminé              |
| P.A.<br>22Na + 65 Zn                 | 0,01 %                    | 0,01 %                    | 0,01 %                    | 0,01 %                    | 0,03 %                    | 0,02 %                    | 0,01 %                      | -                           | -                        |
| P.F.<br>137Cs (+ 134Cs)              | 0,3 %                     | 0,2 %                     | 0,3 %                     | 0,3 %                     | 0,35 %                    | 0,4 %                     | 0,02 %                      | -                           | -                        |
| P.A.C.<br>51Cr, 58Co, 54 Mn<br>60 Co | 99,9 %<br>(84 %<br>54 Mn) | 99,7 %<br>(84 %<br>54 Mn) | 99,8 %<br>(80 %<br>54 Mn) | 99,9 %<br>(83 %<br>54 Mn) | 99,8 %<br>(99 %<br>54 Mn) | 99,7 %<br>(96 %<br>54 Mn) | 99,8 %<br>(98,8 %<br>54 Mn) | 100 %<br>(~ 100 %<br>54 Mn) | 100 %<br>(94 %<br>54 Mn) |

### 3 - MESURES TASTENA

#### 3.1 Description du "Tastena"

Le dispositif TASTENA permet le prélèvement direct d'échantillons dans les diverses installations d'une centrale, en particulier dans la cuve du réacteur, pendant le fonctionnement ou à l'arrêt.

#### Impuretés dosables dans un échantillon prélevé par TASTENA

Toutes les impuretés susceptibles d'être présentes dans le sodium d'un circuit ne peuvent pas être dosées dans un échantillon prélevé par TASTENA. Les impuretés telles que Oxygène, Hydrogène, Carbone ne sont pas dosables ; en effet, le prélèvement n'est pas conditionné ni traité en étant complètement protégé d'une pollution.

Les métaux tels que l'Argent, le Zinc, l'Antimoine, l'Etain, le Plomb, le Calcium, un élément tel le Silicium qui sont partiellement solubles dans le sodium sont dosables.

La présence de métaux comme les métaux de transition (Fer, Chrome, Nickel, Manganèse) dont la solubilité dans le sodium est très faible, est une information difficile à obtenir.

En ce qui concerne les radionuclides, les produits de fission tels que les iodes et les césiums sont couramment dosés ; le tritium entre dans cette même catégorie ainsi que les produits d'activation (22 Na, 24 Na, 65 Zn, 110 mAg).

Les produits d'activation corrodés, 54 Mn, 51 Cr, 58 Co, 60 Co, 59 Fe sont soumis à la même observation que celle citée plus haut pour les métaux de transition.

Quant aux isotopes de l'Uranium et du Plutonium, l'expérience que nous avons, montrerait que la représentativité de l'échantillon prélevé par TASTENA est douteuse.

#### Conditions d'utilisation

Quand on aborde le problème de représentativité, il faut préciser les conditions dans lesquelles sont prélevés les échantillons par le dispositif TASTENA.

La température du sodium ainsi échantillonné doit être  $\geq 400^{\circ} \text{C}$ . Il arrive que cette condition ne soit pas respectée ; on juge alors de la représentativité du prélèvement en fonction de l'information recherchée (exemple  $^{22} \text{Na}$  dans le sodium contenu dans la cuve du barillet, température maximale  $200^{\circ} \text{C}$ ).

Le sodium doit également être brassé (pompes en fonctionnement).

Le godet utilisé pour le prélèvement est élaboré avec un matériau pur (nickel 200), lavé et dégraissé correctement avant utilisation.

Pour chaque prélèvement, le godet mis en jeu est neuf.

#### Description du dispositif

Les Figures 13 et 14 décrivent d'une part le godet de prélèvement et l'ensemble du dispositif et d'autre part les différentes opérations que nécessite un prélèvement.

### 3.2 Résultats de mesure

Environ 160 prélèvements de sodium primaire ont été effectués, utilisant la méthode TASTENA. Ils ont tous été exécutés quand le sodium était chaud (température > 400° C) et brassé par les pompes primaires, ce qui assure une représentativité correcte à l'échantillonnage.

Tous les creusets utilisés pour les prélèvements sont neufs. Ils sont élaborés en Nickel pur, après la récupération du sodium, on peut facilement récupérer le <sup>137</sup>Cs déposé sur les parois internes et l'incorporer au résultat final.

Les valeurs d'activité sont issues d'un dosage spécifique des radiocésiums.

La Figure 15 montre l'évolution de la contamination du sodium primaire au cours du fonctionnement du réacteur.

On voit que la contamination en <sup>137</sup>Cs du sodium primaire est faible, nettement inférieure à l'activité en <sup>22</sup>Na (environ  $2,2 \cdot 10^4$  kBq/ kg actuellement), après 10 ans de fonctionnement.

En partie supérieure du graphe, sont notées les différentes ruptures décelées au cours du fonctionnement :

- les ruptures de catégorie 1 sont celles ayant entraîné un arrêt du réacteur sur émission de neutrons retardés,
- les ruptures de catégorie 2 regroupe les ruptures "gaz" présentant un défaut sur la colonne fissile,
- les ruptures de catégorie 3 sont les ruptures "gaz" dont le défaut n'est pas sur la colonne fissile.

On voit que l'augmentation de l'activité en  $^{137}\text{Cs}$  correspond à la présence de ruptures de type 1 aussi bien que de type 3 dans le coeur du réacteur.

Il nous reste maintenant à corréler les quantités de  $^{137}\text{Cs}$  relâchées dans le sodium en fonction de la taille du défaut et du temps de séjour de l'élément rupté en réacteur.

### 3.3 Conclusion

Les mesures TASTENA ont permis de suivre de manière quantitative (sans problème d'étalonnage), les évolutions de contamination du sodium primaire de Phénix (en particulier les évolutions du césium en fonction des ruptures de gaine).

## 4 - MESURES SUR LE PIEGE FROID PRIMAIRE

### 4.1 Rappels sur le piège froid primaire

La Figure 16 donne une vue du piège froid primaire de PHENIX.

C'est le même piège froid qui est en fonctionnement depuis le démarrage du réacteur en 1974.

Les conditions de fonctionnement habituelles sont  $Q = 10 \text{ m}^3/\text{h}$  et température point froid =  $115^\circ \text{C} \pm 5^\circ \text{C}$ .

Sauf cas particuliers (essais ou arrêt du débit sur l'ensemble du circuit sodium primaire), le piège froid primaire est en permanence en fonctionnement.

#### 4.2 Emplacement des mesures/Mode de mesure

Des mesures peuvent être effectuées avec collimateurs, par une diode en spectro  $\gamma$  à 4 altitudes différentes du piège (voir Schéma N° 1).

En fait, le point 1 est au niveau des tuyauteries d'entrée, le point 3 est au niveau du knit (dans le tiers partie basse) mais gêné par la présence de poutres IPN et le point 4 est en partie basse du piège au niveau du béton.

Dans ces conditions, le point de mesure le plus représentatif est le point 2 qui se trouve au niveau tiers partie haute du knit et n'est pas gêné par les structures environnantes.

C'est donc de cet emplacement qu'ont été effectuées toutes les mesures présentées.

En fonctionnement du réacteur, la présence du sodium 24 rend toute mesure totalement impossible (bruit de fond trop important).

Il faut au moins 7 jours d'arrêt (du réacteur ou du piège) pour que les mesures soient faisables et utilisables. Toutes les mesures présentées sont donc faites à 250° C réacteur (ou piège) à l'arrêt depuis au moins une semaine.

Le signal de la diode est influencé par des facteurs géométriques propres à l'emplacement de mesure et au collimateur utilisé. Pour étalonner la diode on part donc du principe que la concentration du sodium 22 est identique dans tout le sodium du réacteur (y compris la surface libre où est effectué le prélèvement Tastena et le sodium du circuit primaire).

En partant de cette hypothèse les mesures Tastena de sodium 22 permettent de recalibrer les valeurs données par la diode.

#### 4.3 Rappel des "produits" en suivi

Outre le sodium 22 (période 2,6 ans), on suit par ces mesures :

- le Manganèse 54 (période 313 jours) qui est le principal responsable de contamination des composants (produit d'activation corrodé),
- le Césium qui a l'avantage d'avoir une bonne solubilité en sodium (possibilité de mesure par Tastena) et de n'être produit que par les ruptures de gaines.

Le Césium 136 a une période courte (13 jours) et a l'intérêt d'être très représentatif des ruptures de gaine (montée et décroissance rapides). Par contre les mesures doivent être faites très tôt.

Le Césium 134 et 137 ont des périodes plus longues (2,1 et 30 ans). Les mesures peuvent donc être faites avec retard (Tastena) et présentent un aspect "cumulatif".

D'autres corps (Co 60, Zn 65,...) sont également suivis mais l'intérêt est moindre.

L'Iode 131 (période 8 jours) a une période comparable au Césium 136 et se trouve lui aussi représentatif des ruptures de gaine ; mais il faut tenir compte de son piégeage dans le piège froid.



#### 4.4 Résultats de mesure

Le Tableau ci-joint montre à titre d'exemple les résultats de mesure obtenus en Janvier 1985 sur :

- le dernier Tastena,
- le piège froid primaire/collimateur N° 2,
- une mesure par diode, au niveau du bloc DND/G situé à l'entrée du circuit auxiliaire de sodium primaire,

Ces mesures sont en  $\mu\text{Ci/g}$  et ont été recalées sur la mesure en sodium 22 du Tastena primaire.

| TYPE MESURE                        | Na 22               | Cs 137              | Cs 134              | Mn 54             | Co 60             | Zn 65               |
|------------------------------------|---------------------|---------------------|---------------------|-------------------|-------------------|---------------------|
| "Tastena" primaire                 | $5,4 \cdot 10^{-1}$ | $4,5 \cdot 10^{-2}$ | $9 \cdot 10^{-3}$   |                   |                   |                     |
| "DND/G"                            | $5 \cdot 10^{-1}$   | $2,3 \cdot 10^{-2}$ | $4,8 \cdot 10^{-3}$ | $7 \cdot 10^{-1}$ | $1 \cdot 10^{-3}$ |                     |
| Piège "froid" primaire<br>Cell. C2 | $5 \cdot 10^{-1}$   | 50                  | 8,5                 | 2,4               |                   | $2,6 \cdot 10^{-1}$ |

La Figure 17 ci-joint montre à titre d'exemple les résultats de mesure obtenus sur l'Année 1981 et les positions de rupture de gaine correspondants.

La Figure 18 donne l'évolution des mesures effectuées sur le piège froid et les Tastenas de 80 à 86.

#### 4.5 Interprétation

Il faut d'abord, durant toute l'interprétation, rester conscient de l'aspect qualitatif des mesures obtenues.

Certains points apparaissent cependant :

- la concentration au sodium 22 est à l'équilibre actuellement (presque à l'équilibre après 2 périodes),
- les évolutions rapides (montée et décroissance) du Césium 136 permettent de suivre ponctuellement une rupture de gaine (voir évolutions sur la figure N°17),
- l'aspect "cumulatif" des ruptures de gaine pour le Césium 137, est visible sur la figure N°18 ,
- l'enrichissement très important de la teneur en Césium au niveau du piège semble montrer un effet de piégeage sélectif. (Le signal Césium 137 mesuré est environ 20 fois plus fort que le signal Mn 54 dans le piège, alors qu'il est de 1000 à 10000 fois plus faible sur un composant avant décontamination),
- le signal Mn 54 est relativement faible. Une hypothèse possible est que le Mn 54 se dépose trop rapidement dans les parois du collecteur froid et à l'entrée du circuit auxiliaire primaire sodium pour pouvoir aller se déposer dans le piège.

#### 4.6 Conclusion

Les mesures effectuées sur le piège froid doivent être interprétées avec prudence (difficultés de mesures, problèmes d'étalonnage, etc...). En particulier elles sont toujours effectuées après une semaine d'arrêt à 250° C avec des possibilités de lessivage et de redistribution dans le piège.

On peut cependant en retenir une totale inversion des mesures Césium 137/Mn 54 par rapport aux mesures effectuées sur les composants. Il semblerait bien qu'à la température de fonctionnement du point froid piège ( $\sim 120^\circ \text{C}$ ), il y ait enrichissement ou piégeage du césium.

## 5 - MESURES LRG/DRG

### 5.1 Contamination par pollution

Le comptage global effectué au niveau de la DND est affecté en dehors des ruptures des gaines par la pollution des assemblages et par d'autres facteurs plus faibles ( $\gamma$  du Na 24, neutrons de fuites, bruit de fond électronique, etc...).

Ce comptage a baissé depuis l'origine d'environ 160 coups/sec (dont environ 130 attribuables à la pollution) à environ 50 c/s (dont environ 30 attribuables à la pollution).

Il y a donc eu baisse dans le temps de la contamination par pollution, due à un changement des conditions de fabrication des assemblages.

Les mesures LRG confirment cette baisse de pollution.

Pour les mesures DRG gaz, la pollution de l'ordre de  $10^{-4} \text{ Ci/m}^3$  est masquée par l'Argon 41 (environ  $4 \cdot 10^{-2} \text{ Ci/m}^3$ ) et son évolution est alors difficilement mesurable.

### 5.2 Contamination du sodium par ruptures de gaines

Après déchargement des assemblages ruptés, nous avons toujours observé un retour à un comptage normal.

Aucune contamination du sodium par matière fissile n'a donc pu être observée et imputée à des ruptures de gaine.

### 5.3 Contaminations gaz

En fonctionnement nominal 3 corps entraînent en particulier une contamination gaz :

- Le Néon 23

L'activité correspondante du ciel de pile est très importante (estimée à environ 150 Curie/m<sup>3</sup>). Mais sa période est si courte (38 sec) que cette production n'est pas gênante.

En particulier, il suffit pour les mesures de prévoir un temps de transit suffisant pour qu'il n'y ait pas de perturbations.

- L'Argon 41

Période 110 min. L'activité correspondante du ciel de pile est de 4 à 5.10<sup>-2</sup> Ci/m<sup>3</sup>.

- L'Argon 37

Période 35 jours. L'activité correspondant au ciel de pile est de 10<sup>-3</sup> Ci/m<sup>3</sup>.

Les ruptures de gaine produisent en continu un relâchement (entre 10<sup>-1</sup> et 10<sup>-4</sup> Ci/m<sup>3</sup>) dont la valeur varie suivant de nombreux paramètres (taille de la fissure, pression du gaz, etc...).

Sur des ruptures de gaines franches les valeurs maximales fugitives atteintes ont été de 5 Ci/m<sup>3</sup> dans le ciel de pile (équivalent 133 XE).

Il faut rappeler que l'épuration du gaz de couverture permet d'éviter toute pollution externe à la centrale. Les rejets sont donc théoriquement négligeables (efficacité de piégeage supérieure à  $10^4$ ). Le piégeage et stockage du Xénon 133 sont en particulier très efficaces vu sa faible période (5,3 jours). Ceci se traduit d'ailleurs par des rejets très faibles de la centrale (environ 1700 curies sur 14 ans), les valeurs données étant d'ailleurs dues en grande partie au bruit de fond des appareils de mesure à la cheminée.

#### 5.4 Conclusion

Les contaminations mesurées par le système LRG/DRG sont très faibles et décroissantes par "pollution des assemblages", indétectables en pollution par matière fissile après rupture de gaine, nettes en contamination gaz (fonctionnement nominal ou rupture de gaine), mais sans effet sur les rejets de la centrale qui restent très faibles ( $< 0,5$  Curies/jour).

### 6 - MESURES TRITIUM

Il y a une production neutronique continue du tritium au niveau du B4C des barres de commande et par fission ternaire.

Ce tritium reste essentiellement en phase liquide et sa présence est indécélable en phase gazeuse (argon de couverture).

Par contre, il diffuse au niveau des E.I et des G.V. et on le retrouve en bout de chaîne dans l'eau du circuit IPE.

La plus grosse partie ( $> 98$  %) reste piégée dans les pièges froids primaire et secondaire, où le piégeage s'effectuerait en co-précipitation avec l'hydrogène.

Le suivi de l'évolution des teneurs en tritium a alors nécessité un code de calcul prenant en compte l'ensemble des phénomènes (termes source hydrogène et tritium, coefficients de perméation hydrogène et tritium à travers les E.I. et les G.V., conditions de fonctionnement des pièges froids primaire et secondaire, etc...).

Les mesures de tritium peuvent être effectuées dans le circuit eau par prélèvement et comptage. En sodium, les opérations sont beaucoup plus complexes : prélèvement par Tastena et mesures ultérieures par dissolution.

Un essai d'arrêt du piège froid primaire fin 1986 a permis avec 4 prélèvements Tastena de donner par comparaison avec le code de calcul une première estimation du terme source de tritium à Phénix d'environ 0,03 mg/h.

La Figure 19 montre la comparaison entre le calcul de l'évolution de la concentration tritium durant l'essai (arrêt, puis redémarrage du piège froid) et les 4 points de mesure obtenus par Tastena primaire.

Des essais restent en cours pour préciser les valeurs du terme connu et les coefficients de perméation à travers E.I et G.V.

La contamination entraînée par le tritium reste donc essentiellement localisée au niveau des pièges froids primaire et secondaire (quelques milliers de Ci/an).

## 7 - CONCLUSION

Cette note présente une synthèse permettant de se faire une première idée :

- sur la contamination des composants (pompes et E.I) et sur les paramètres importants pour cette contamination,
- sur la production tritium et les phénomènes de diffusion,
- sur les contaminations par ruptures de gaine,
- sur les contaminations par pollution et activation,
- sur les phénomènes de piégeage et leurs rapports avec la contamination.

L'expérience Phénix est alors particulièrement intéressante à plusieurs titres.

- D'abord parce que le réacteur est en fonctionnement depuis 1974.

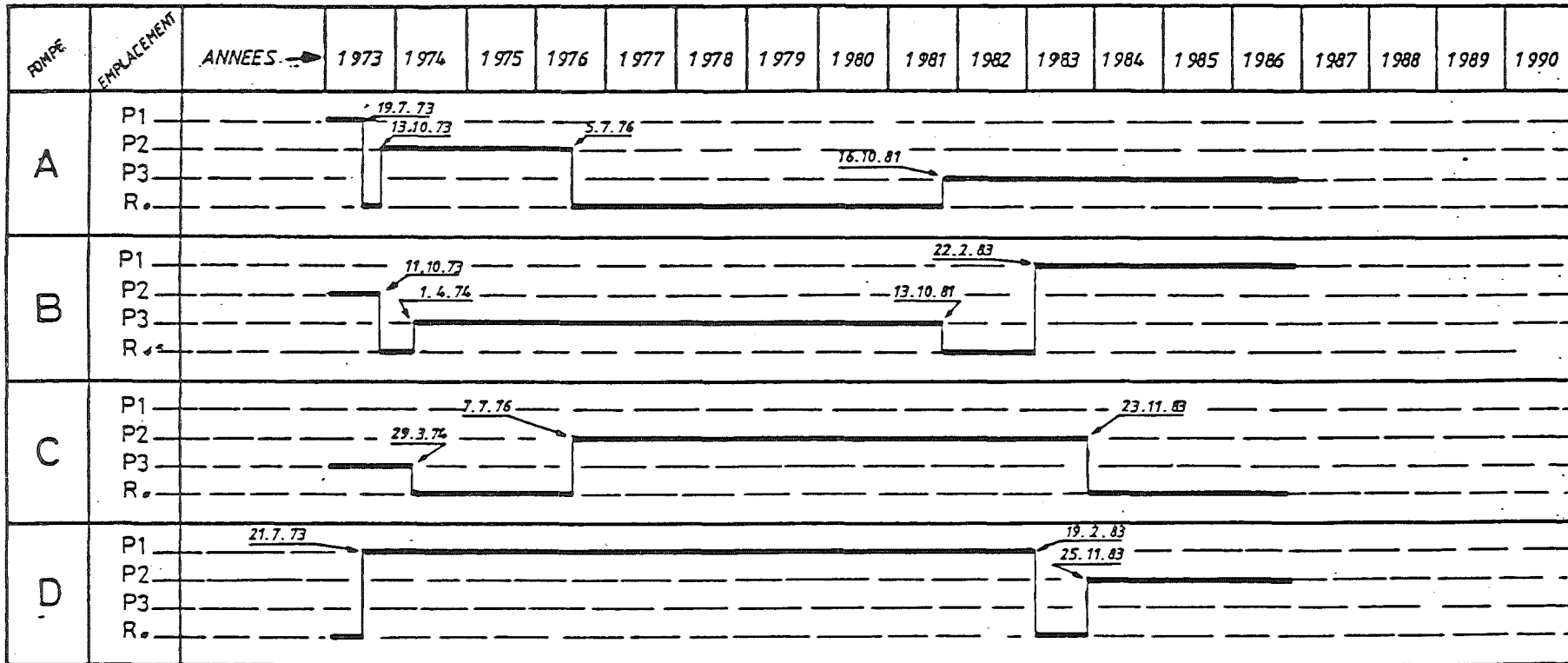
- Ensuite parce que de nombreux composants ont été sortis depuis cette date.

- Enfin parce que des calculs prévisionnels sont particulièrement difficiles à faire dans ce domaine et que l'expérience du premier réacteur rapide en fonctionnement est alors irremplaçable.

Il faut cependant garder à l'esprit que l'expérience Phénix n'est pas directement transposable à d'autres réacteurs rapides et que de nombreux paramètres externes doivent être pris en compte pour tenter d'éventuelles interpolations (niveau retenu pour l'arrêt du réacteur par rupture de gaine, composition des matériaux, impuretés du sodium, fabrication des assemblages, température du circuit sodium primaire, type et mode de fonctionnement du piège froid, etc, etc,...).

Centrale PHENIX  
Service Physique  
Essais - Statistiques

• R = Reserve



- 10.01.73 = REACTEUR EN SODIUM
- 01.02.73 = PREMIERE MISE EN SERVICE DES POMPES PRIMAIRES (A.B.C) SUR MOTEUR AUXILIAIRE.
- 12.02.73 = 300 tr/mn
- 14.02.73 = 600 tr/mn
- 26.02.73 = 700 tr/mn

Figure N°1 - MOUVEMENT DES POMPES PRIMAIRES PHENIX  
( de 1973 à 1987 )



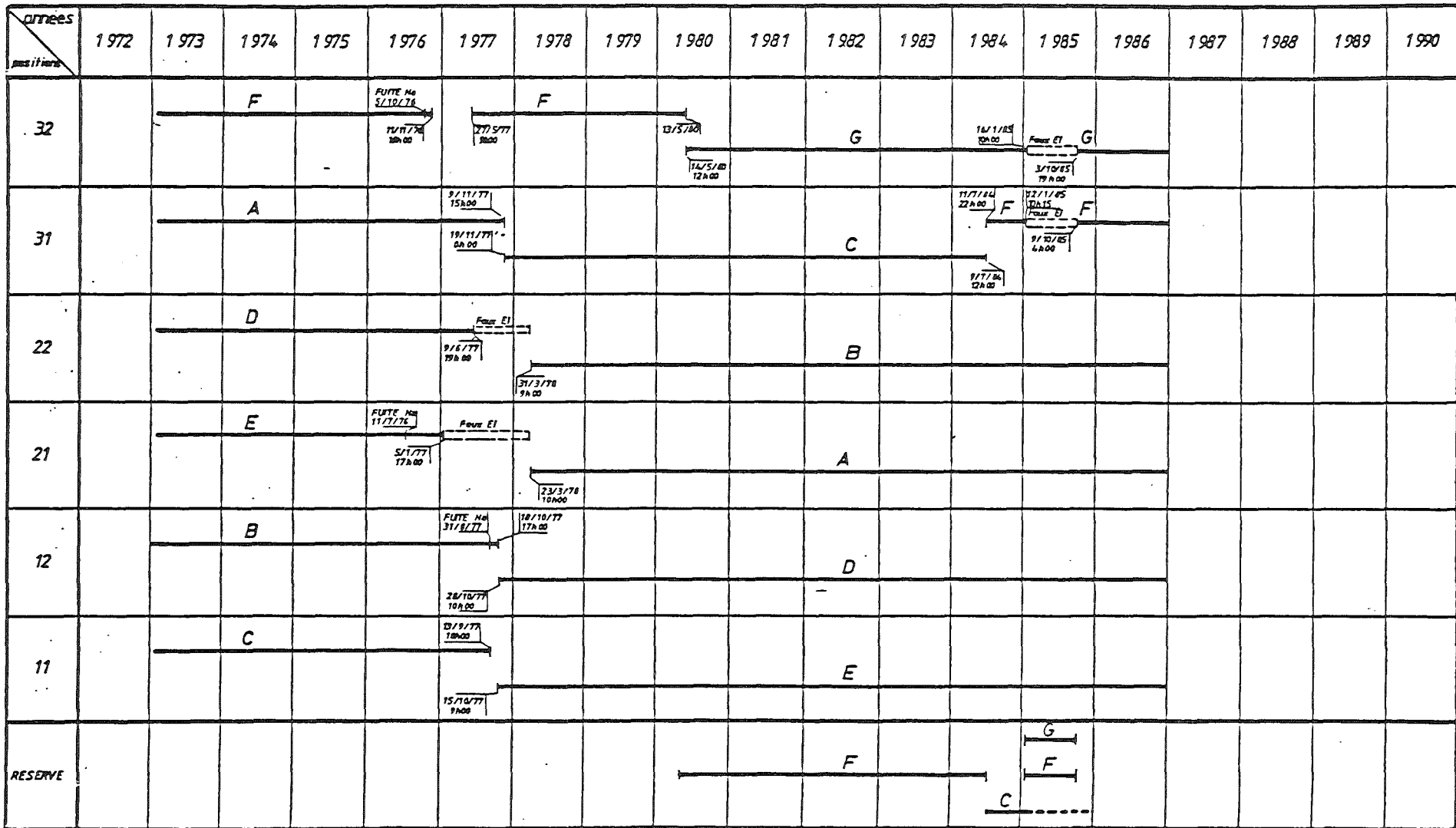


Figure N°2 - MOUVEMENT DES ECHANGEURS PHENIX  
( de 1973 a 1987 )

Figure N°3 - SITUATION DE L'EPROUVETTE DANS L'ECHANGEUR

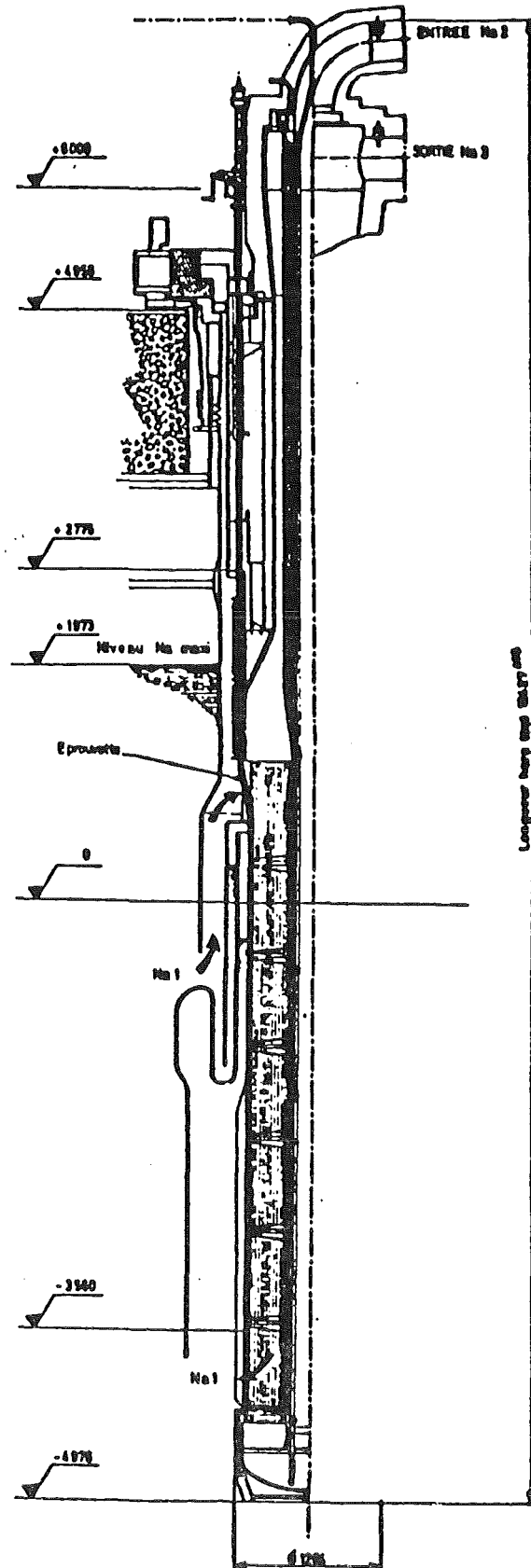


Figure N°4 - DESCRIPTIF DE L'EPROUVETTE DE CONTAMINATION

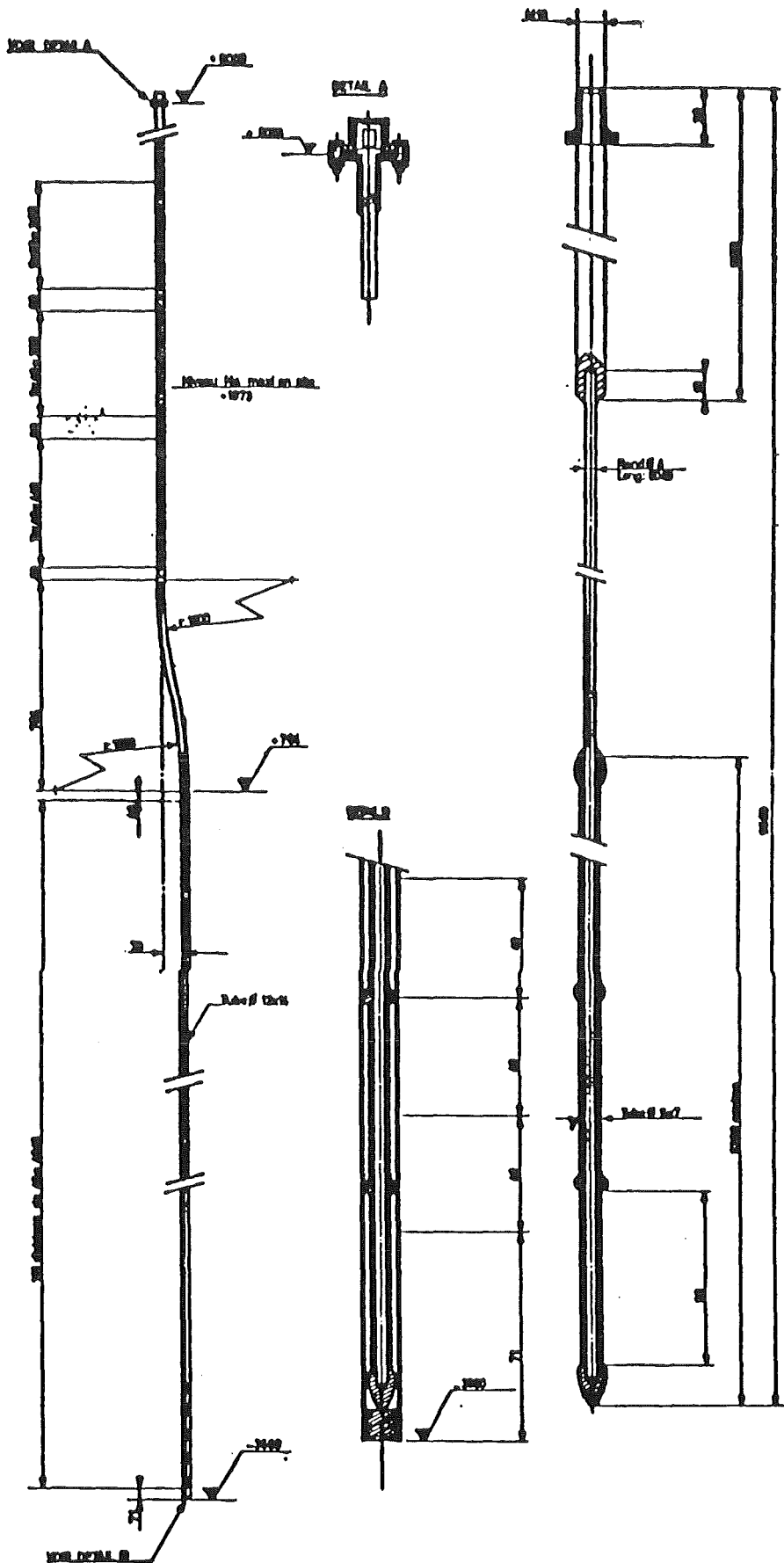


Figure N°5 - PROFIL SPECTRE GAMMA . ECHANTILLON N°17 SUR L'EPROUVETTE DE CONTAMINATION DE L'EI "G" DE PHENIX

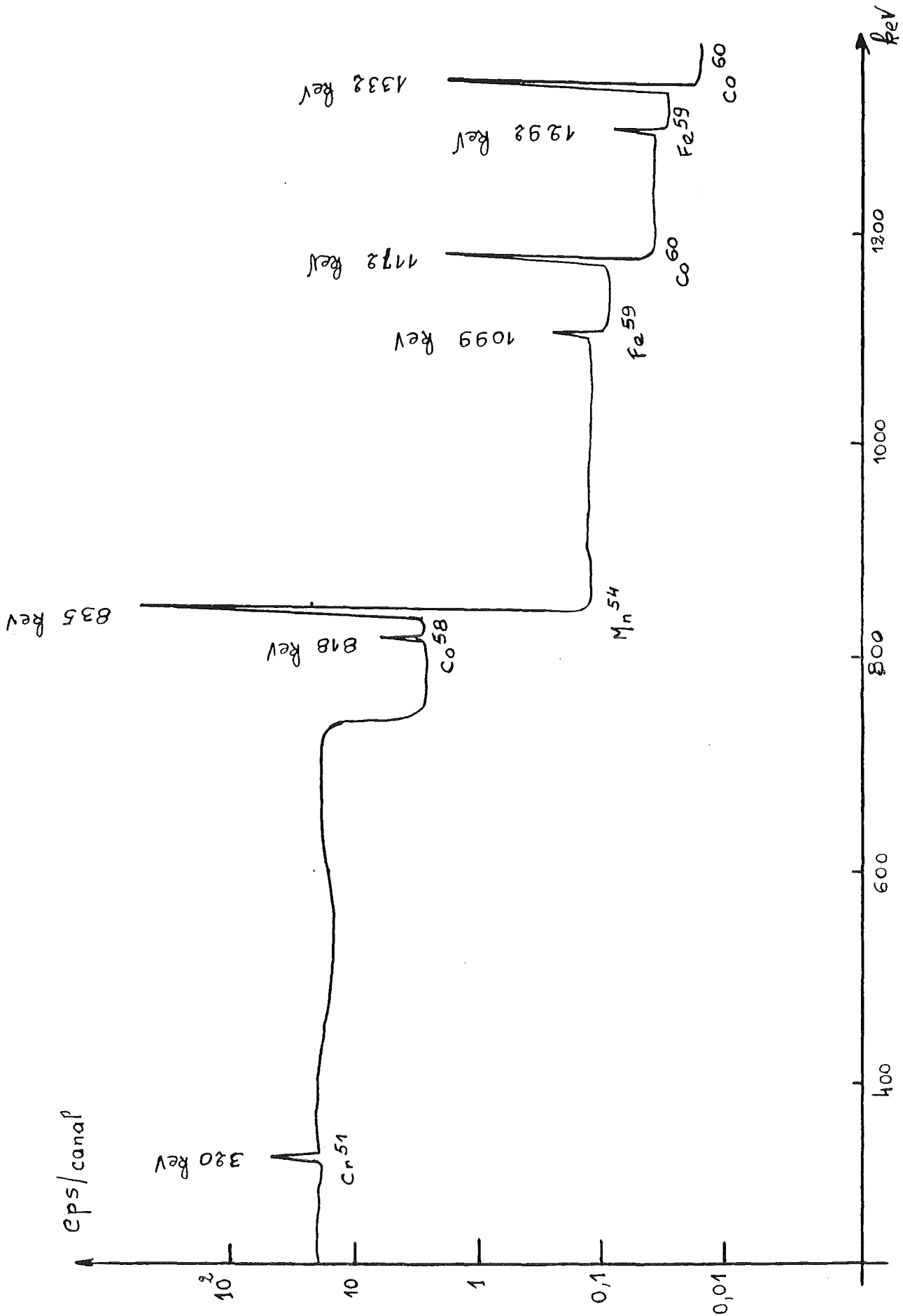


Figure N°6 - EVOLUTION DES ACTIVITES LE LONG DE L'EPROUVETTE.

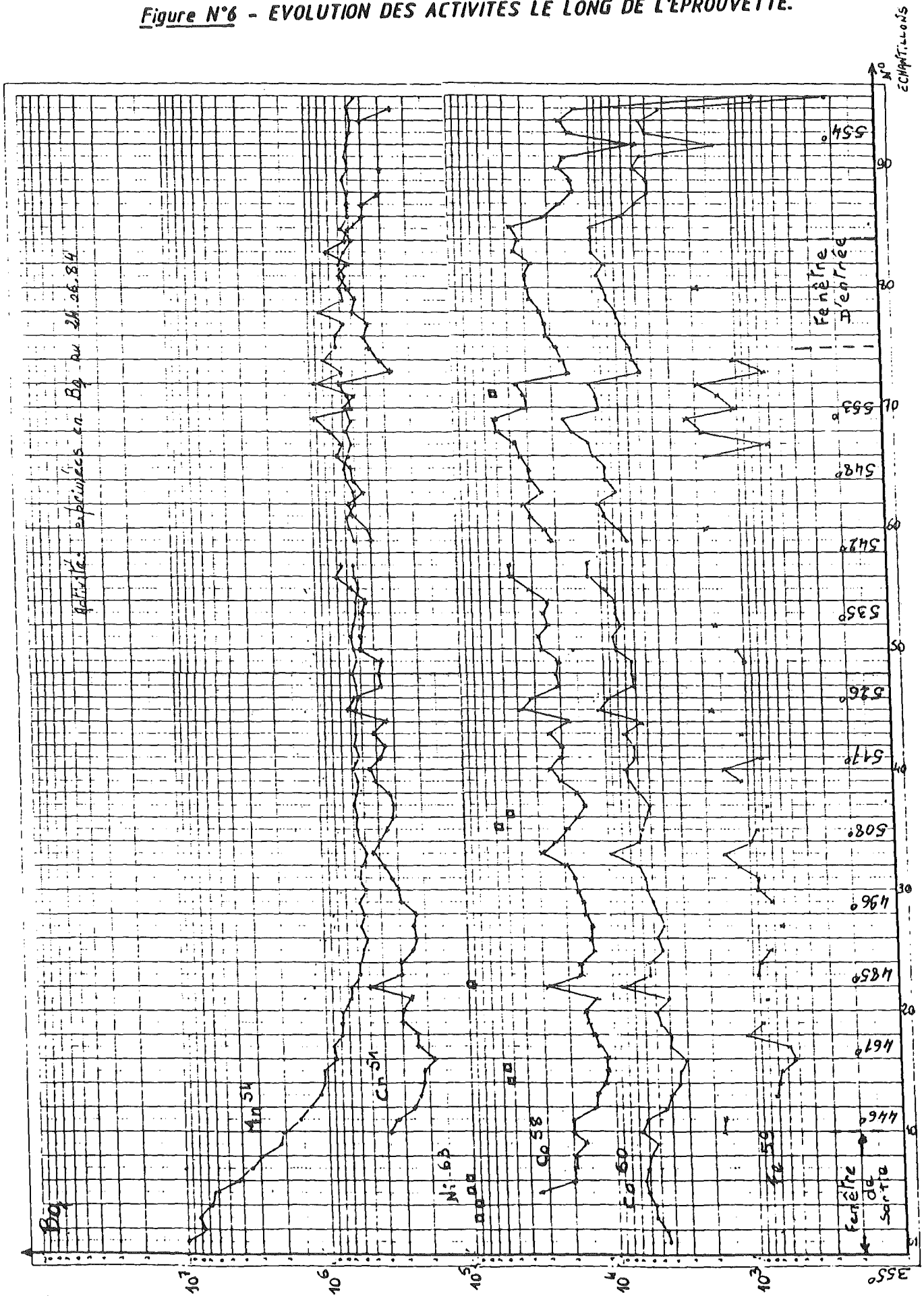


Figure N°7 - EVOLUTION DE L'ACTIVITE  $Mn^{54}$  LE LONG DE L'EI

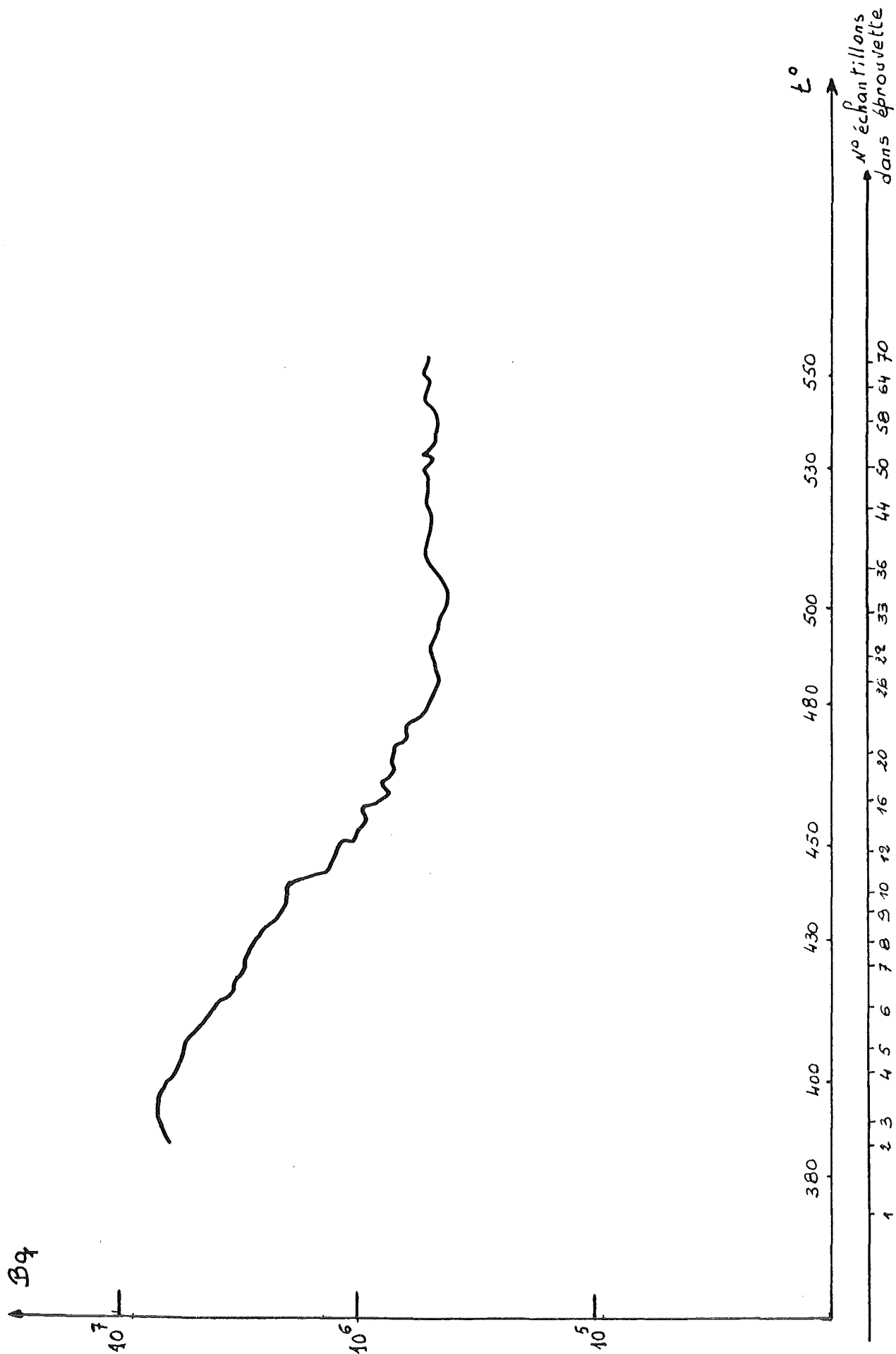


Figure N°8 - EVOLUTION DE L'ACTIVITE  $Mn^{54}$  EN FONCTION DE LA TEMPERATURE.

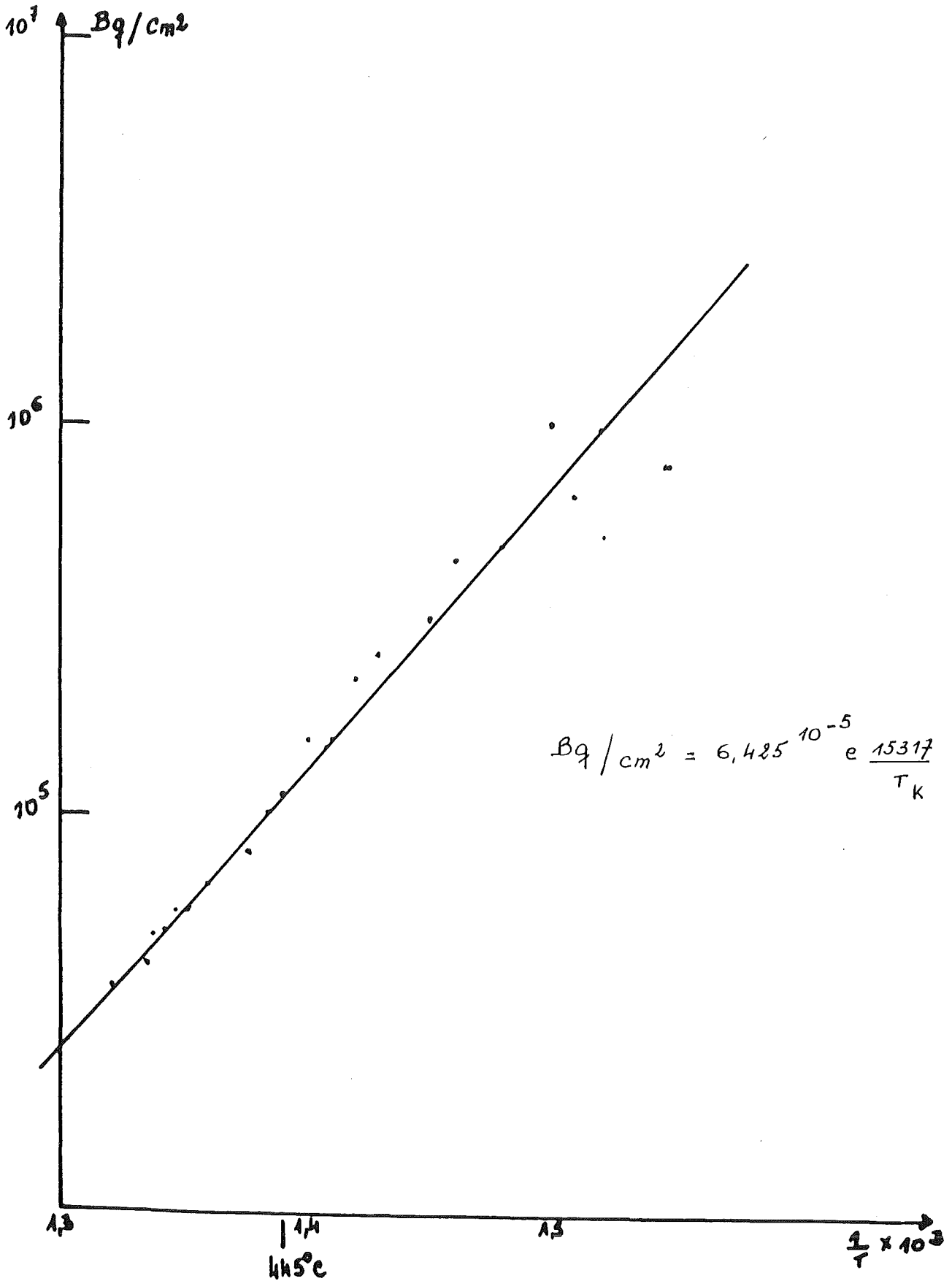


Figure N°9 - EVOLUTION DES ACTIVITES  $Mn^{54}/Co^{58}$  ET  $Co^{60}$  LE LONG DE L'EI "E".

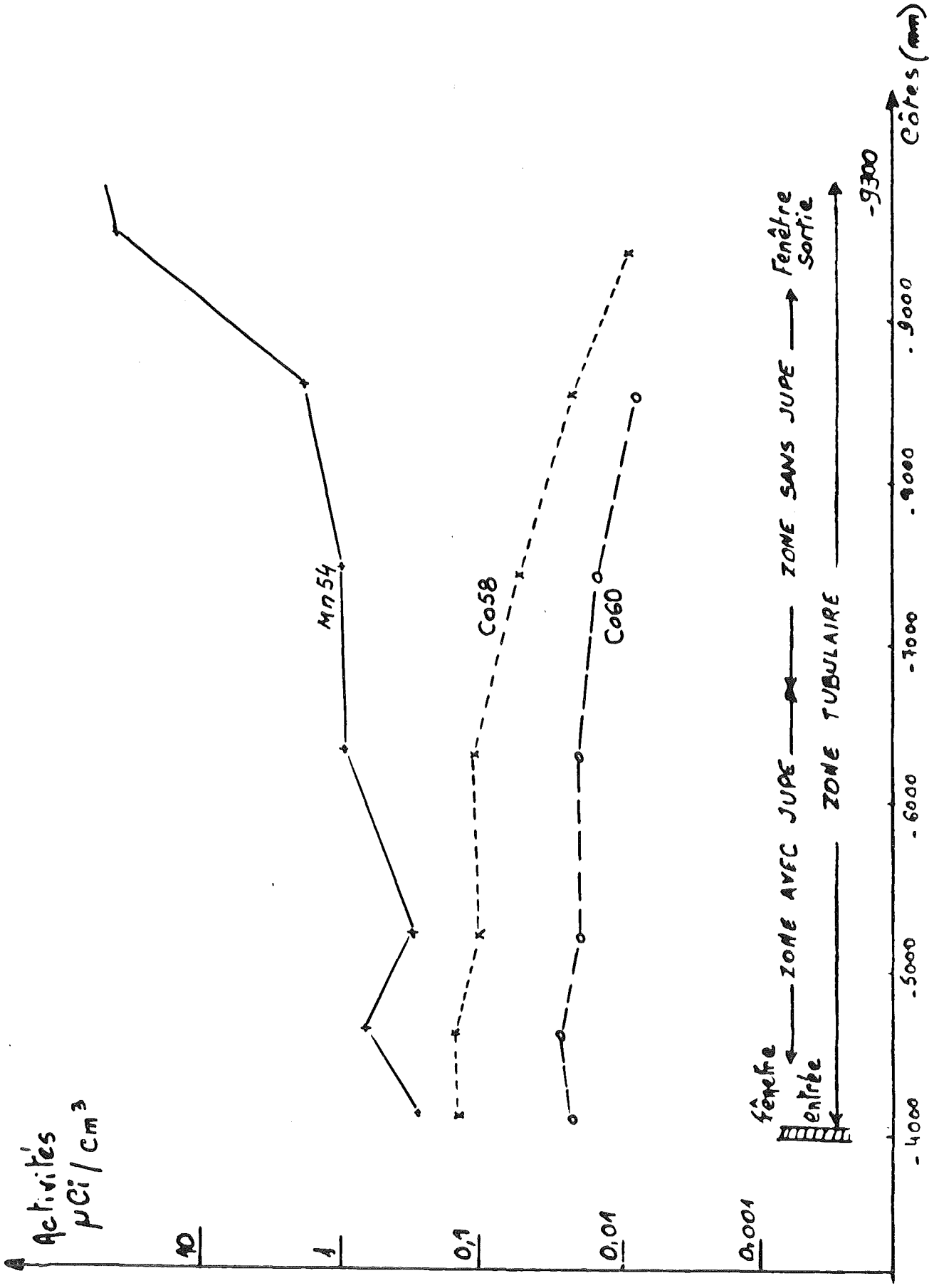




Figure N°10 - EVOLUTION DES ACTIVITES  $Mn^{54}/Co^{58}$  ET  $Co^{60}$  LE LONG DE L'EI "F".

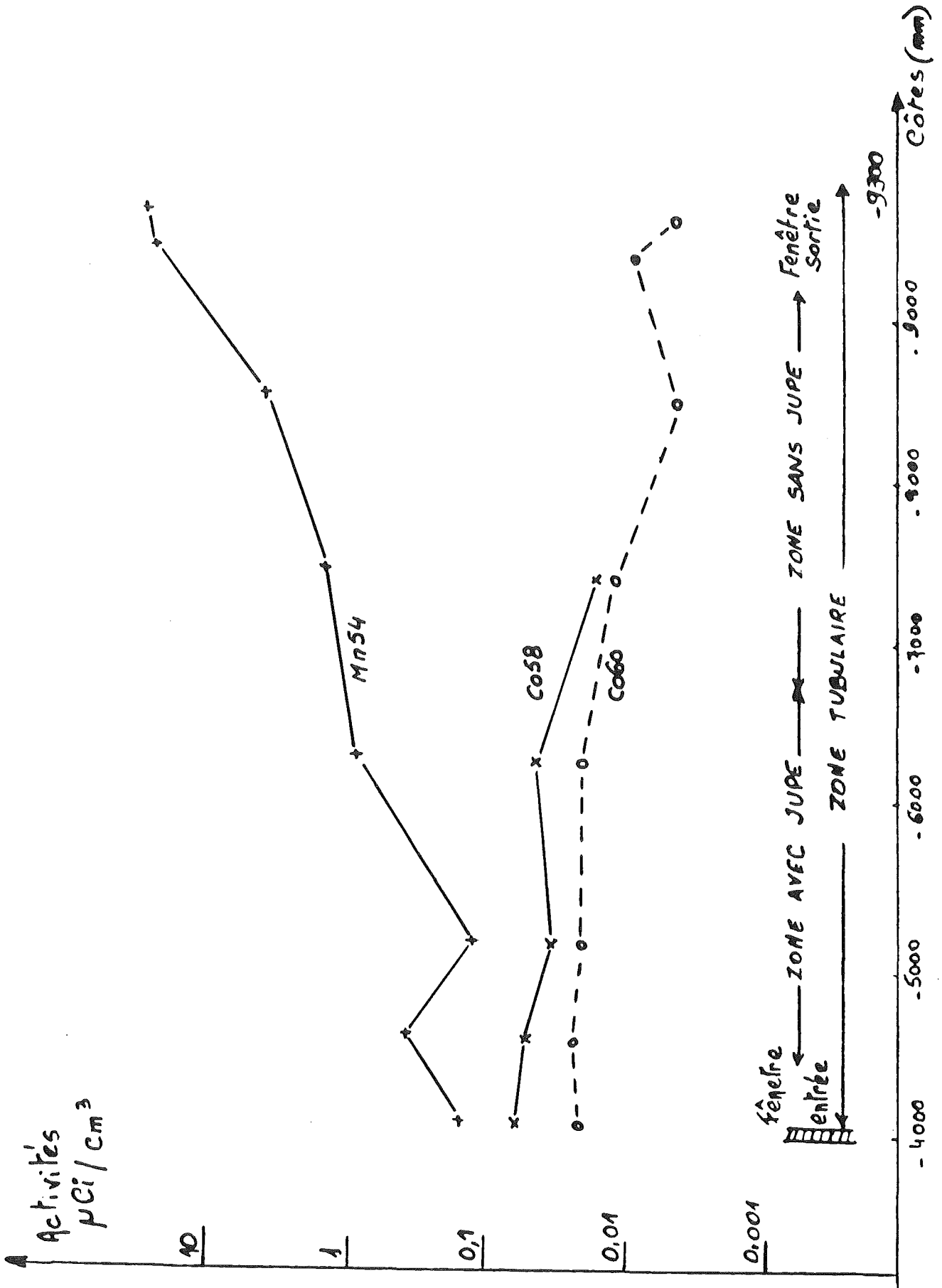


Figure N°11 - EVOLUTION DES ACTIVITES  $Mn^{54}/Co^{58}$  ET  $Co^{60}$  LE LONG DE L'EI "B".

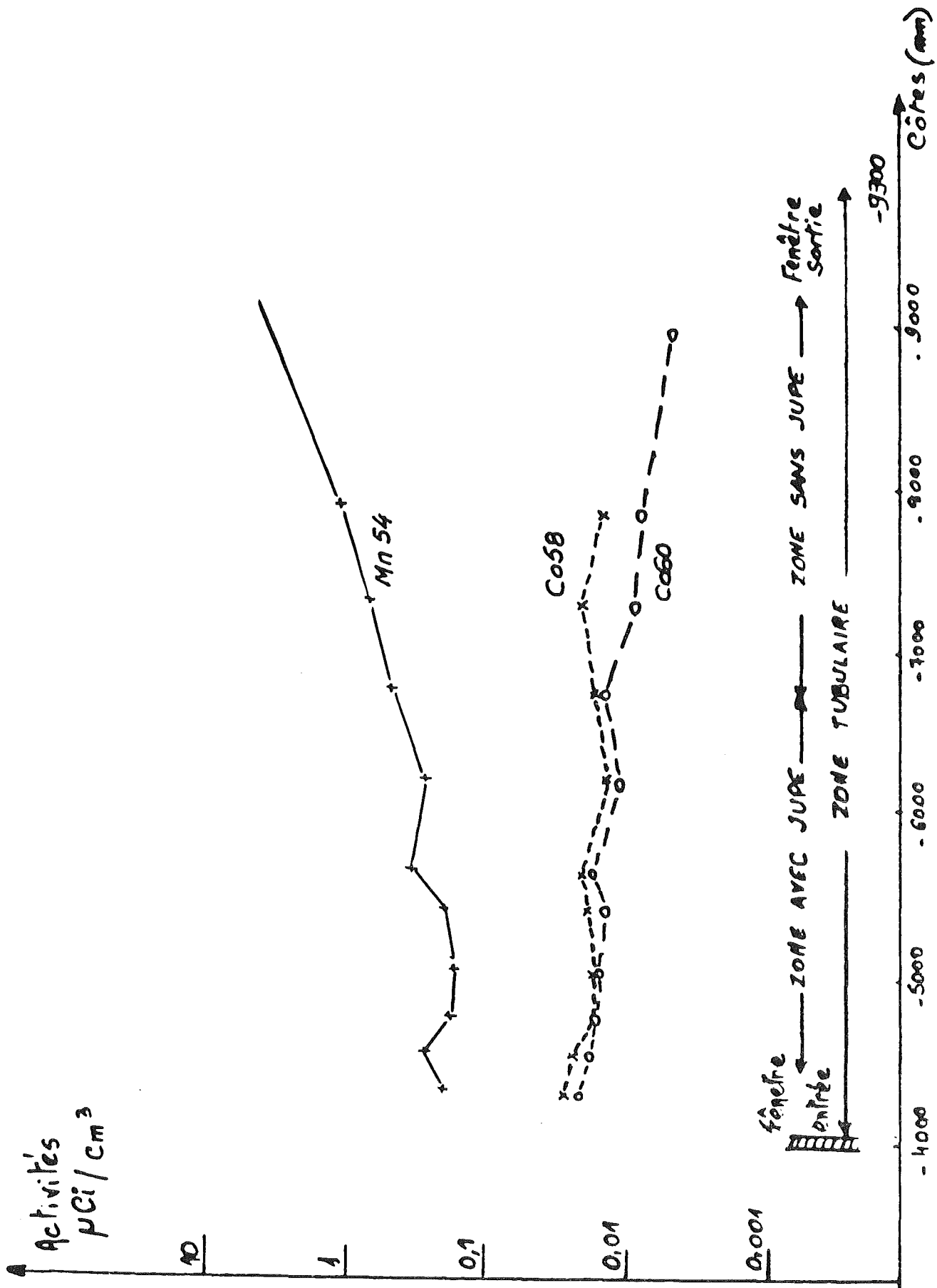


Figure N°12 - EVOLUTION DES ACTIVITES  $Mn^{54}/Co^{58}$  ET  $Co^{60}$  LE LONG DE L'EI "G".

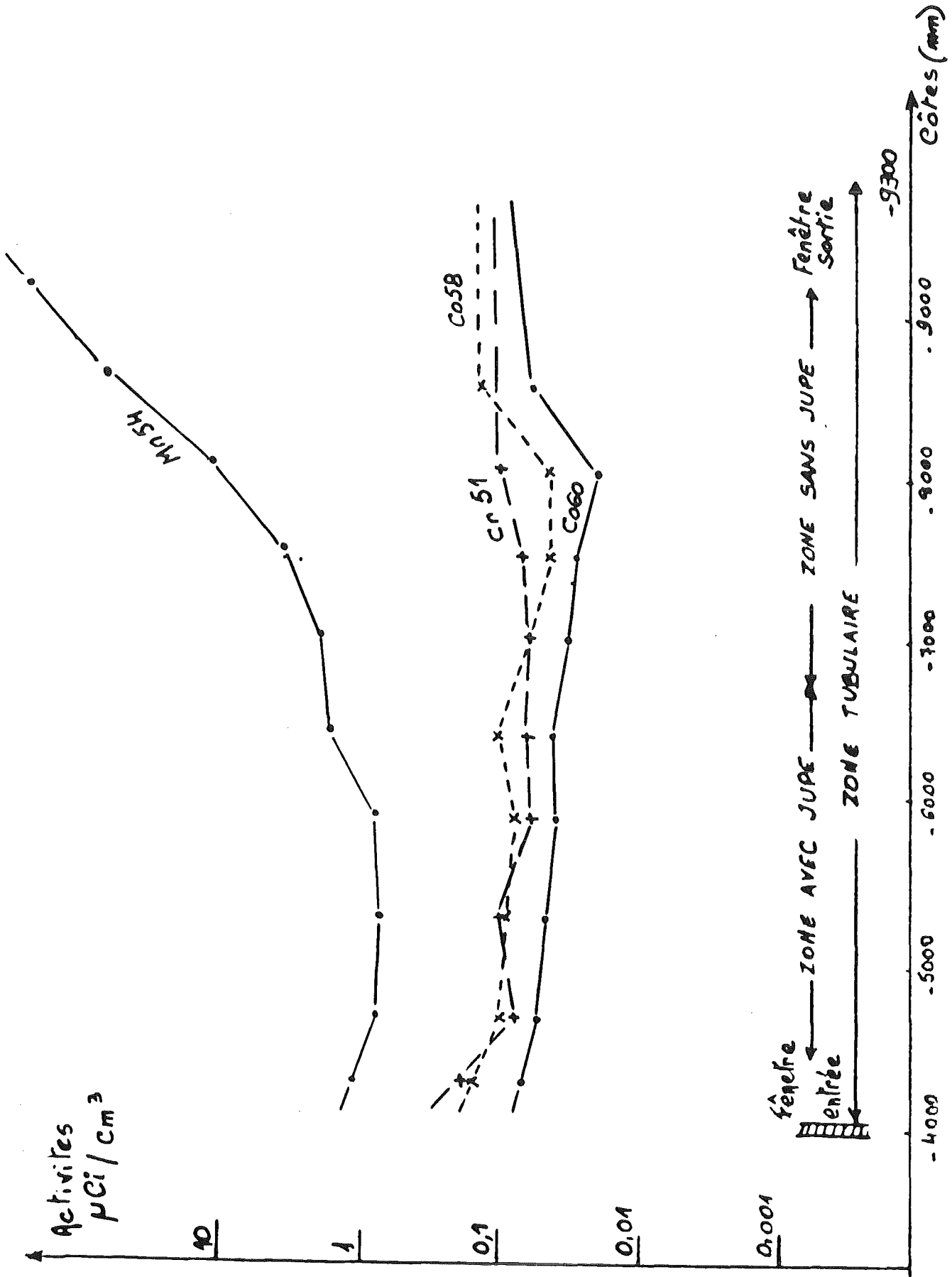
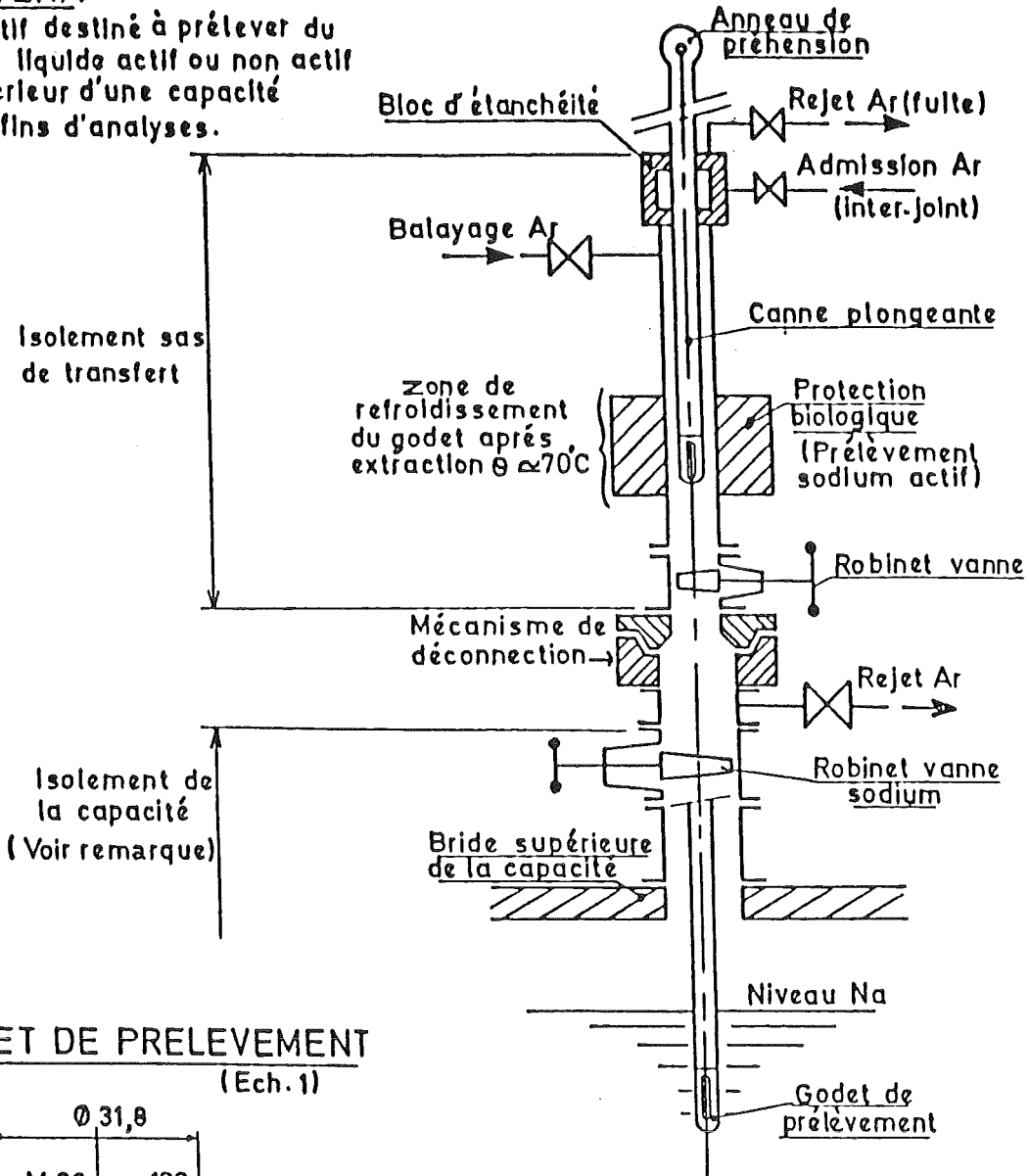


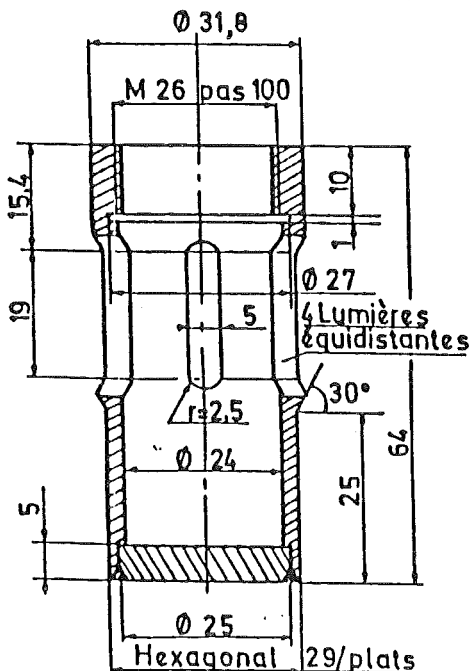
Figure N°13 - DESCRIPTIF DU DISPOSITIF "TASTENA".

### TASTENA

Dispositif destiné à prélever du sodium liquide actif ou non actif à l'intérieur d'une capacité à des fins d'analyses.



### GODET DE PRELEVEMENT (Ech. 1)



#### Remarque:

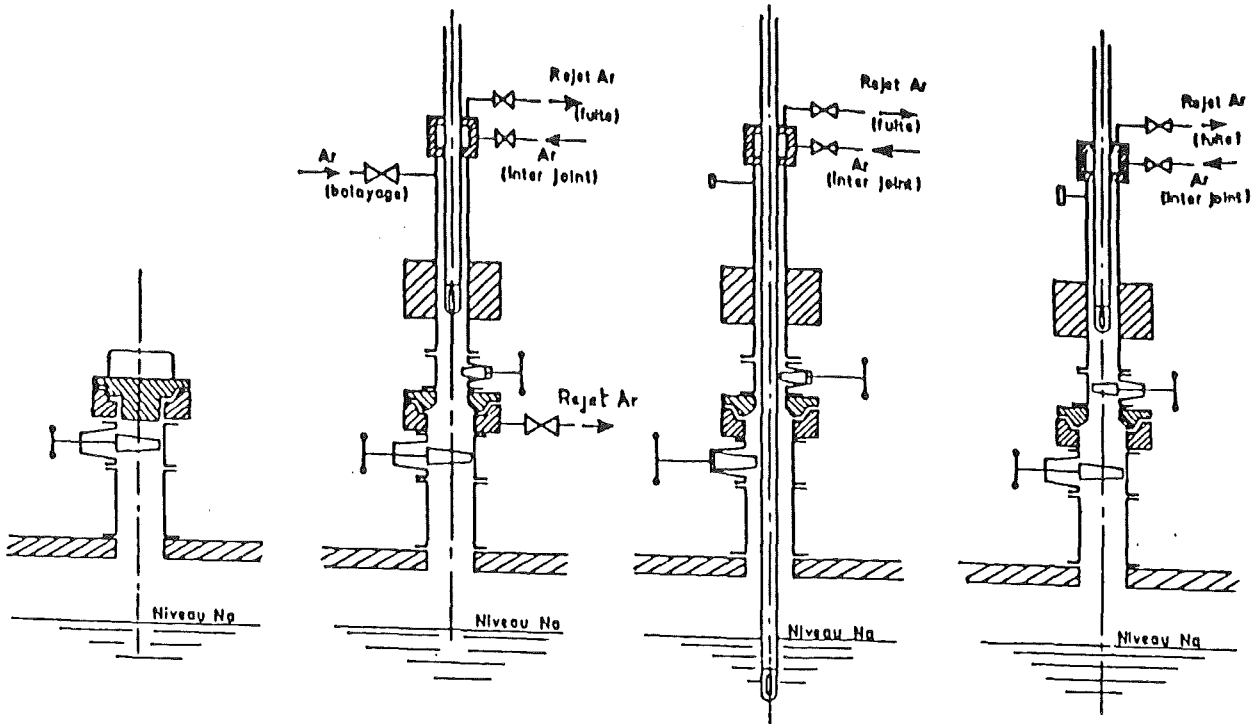
Sur le réacteur un bouchon obture le canal de prélèvement au dessus du robinet vanne sodium.

Sur les circuits d'essais le bouchon est remplacé par un robinet vanne argon.

Matériau : Nickel 200

Usinage:  $\nabla$  poli intérieur et extérieur ainsi que les lumières. Moucher les angles vifs.

Figure N°14 - DESCRIPTIF DU MODE OPERATOIRE DU "TASTENA".



**POSITION D'ATTENTE**

- Un bouchon obture le canal de prélèvement sur la capacité.

**PHASE I**

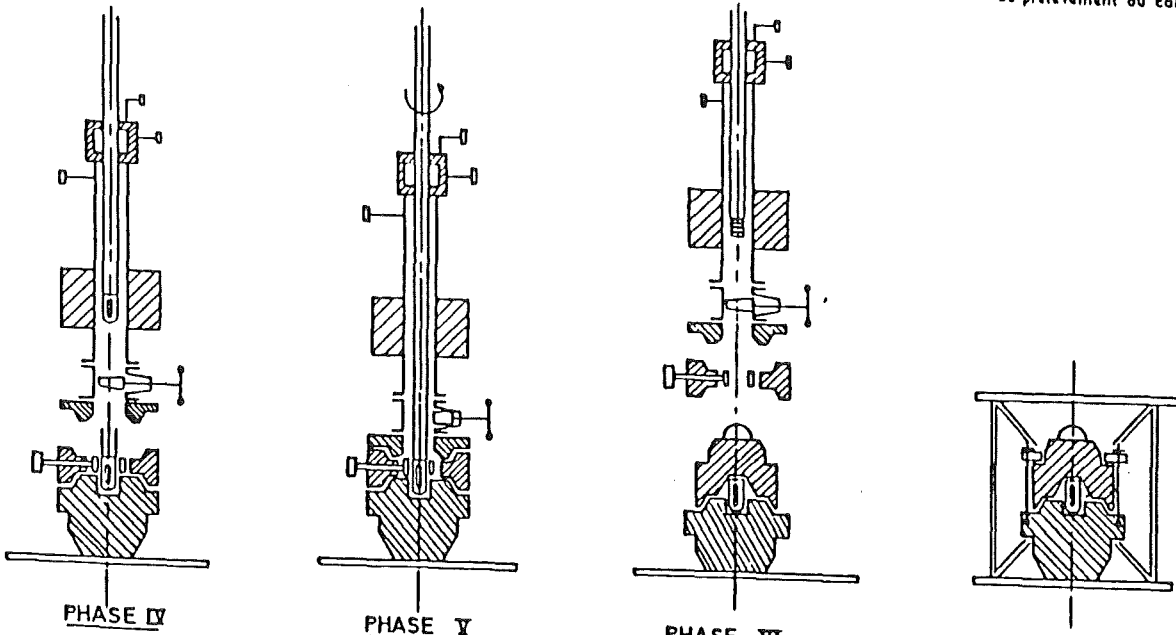
- Verrouillage du sas de prélèvement sur le canal.
- Balayage argon du sas.

**PHASE II**

- Prélèvement Na

**PHASE III**

- Refroidissement naturel du godet.
- Désolidarisation du sas de prélèvement du canal



**PHASE IV**

- Mise en place du sas de prélèvement sur le chateau équipé du mandrin. (mors ouverts)

**PHASE V**

- Déverrouillage du godet de prélèvement à l'aide du mandrin. (mors fermés)

**PHASE VI**

- Dépose du sas de prélèvement et du mandrin. (mors ouverts)
- Mise en place du couvercle.

**PHASE VII**

- Verrouillage du chateau.

Figure N°15 - EVOLUTION DE L'ACTIVITE EN  $^{137}\text{Cs}$   
DU SODIUM PRIMAIRE.

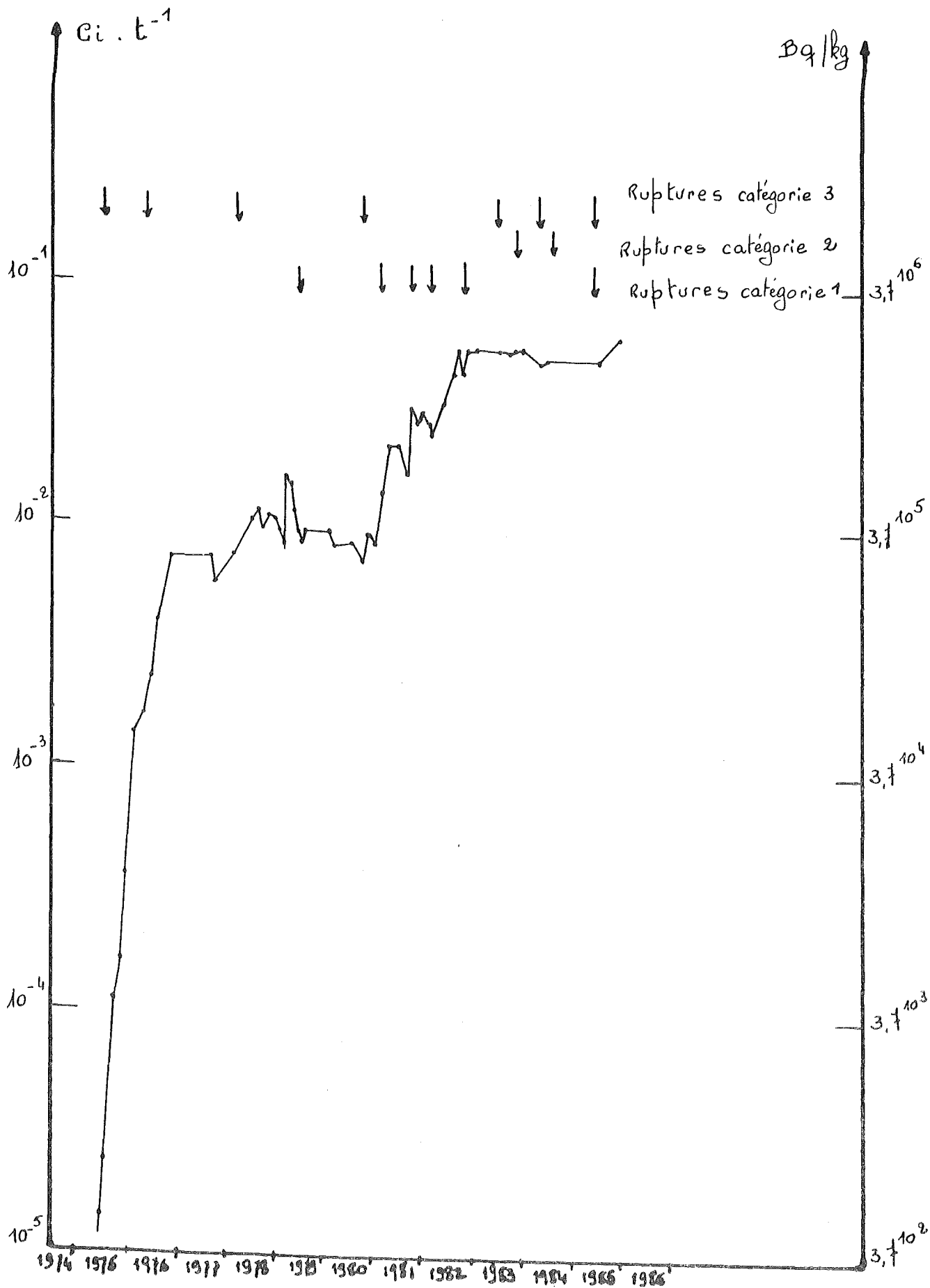


Figure N°16 - VUE EN COUPE D'UN PIEGE FROID CIRCUIT PRIMAIRE.

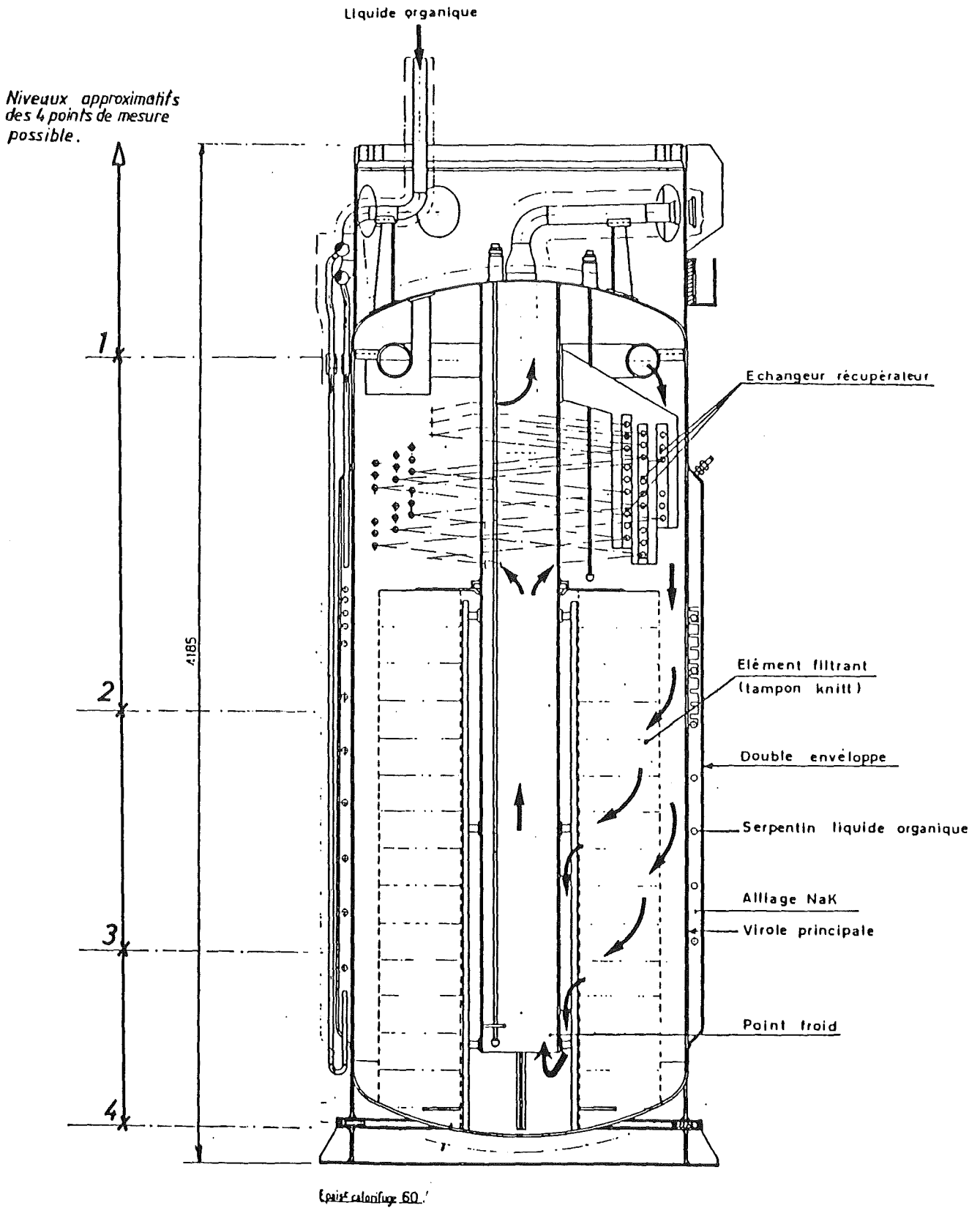


Figure N°17 - EXEMPLE DE SUIVI EN 1981 DES MESURES PIEGE FROID PRIMAIRE.

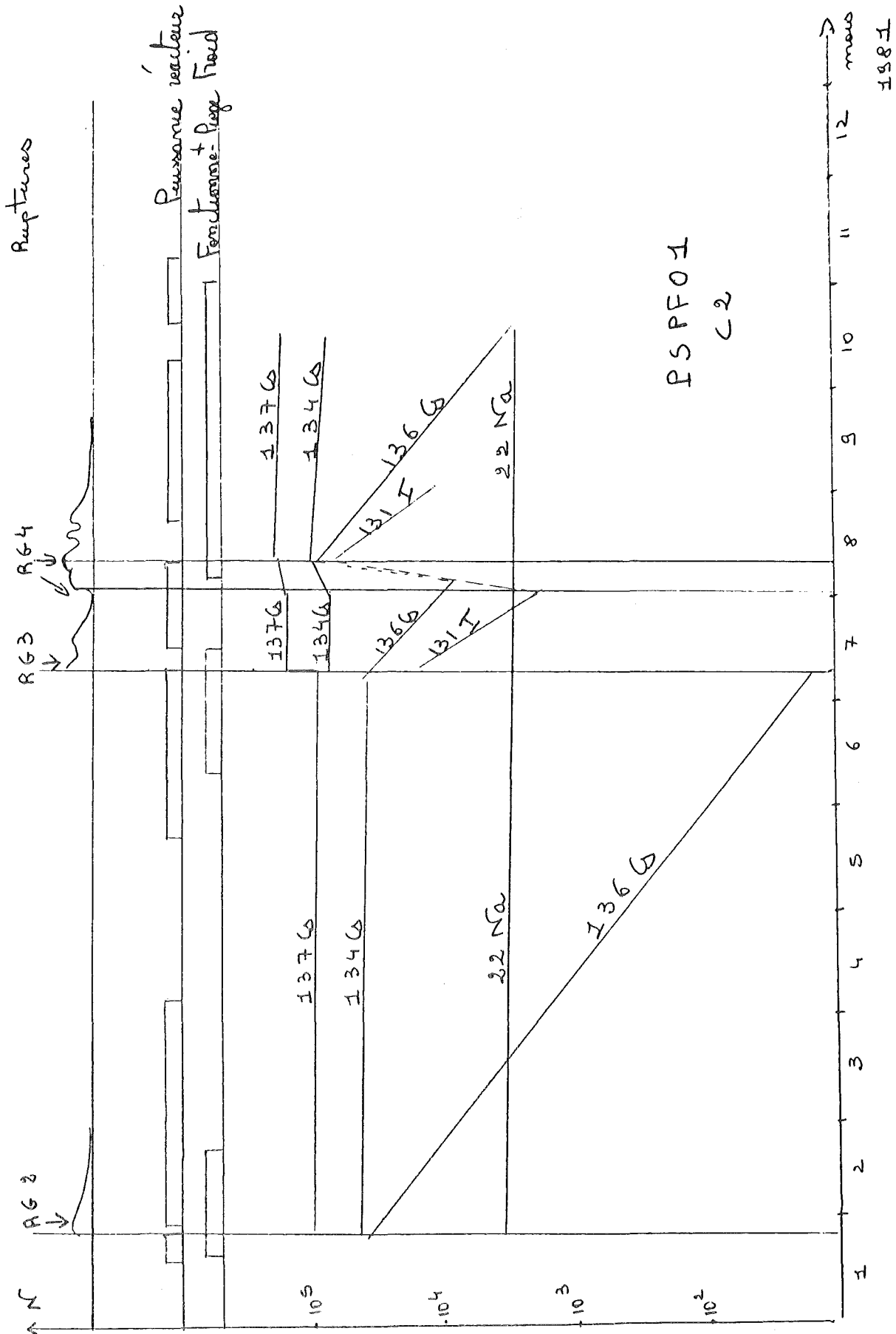




Figure N°18 - EVOLUTION DE 80 A 86 DES MESURES D'ACTIVITE PIEGE FROID PRIMAIRE.

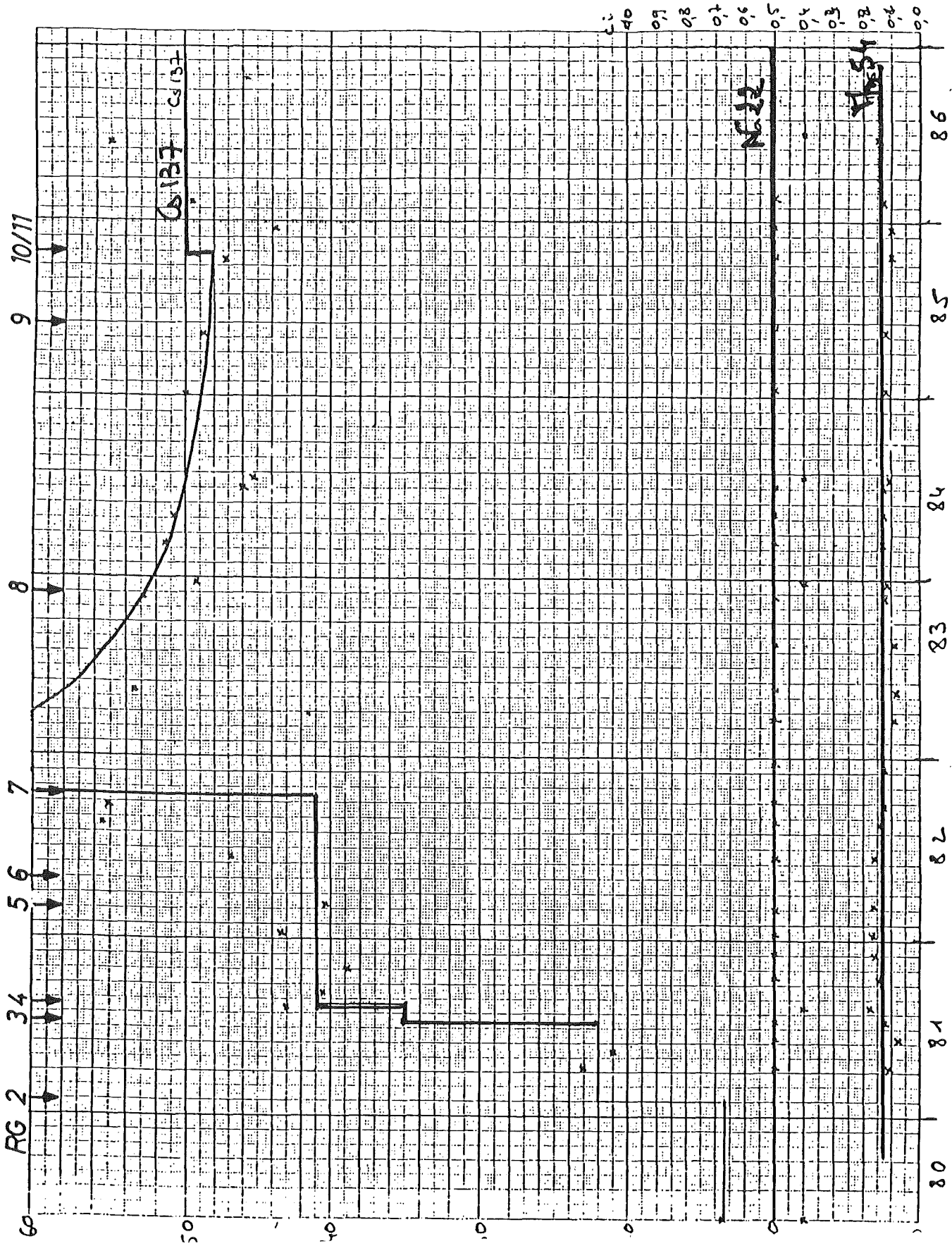
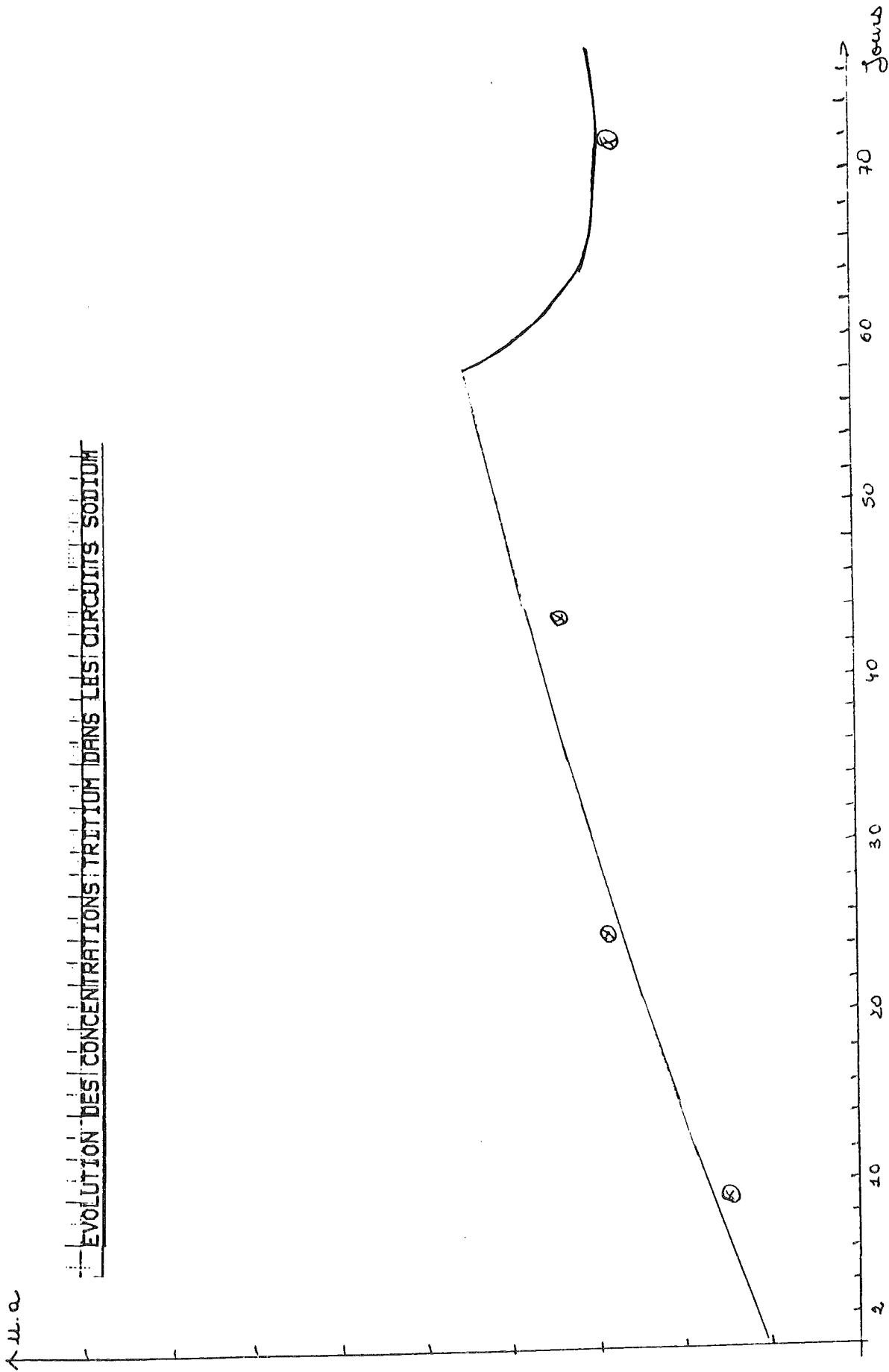
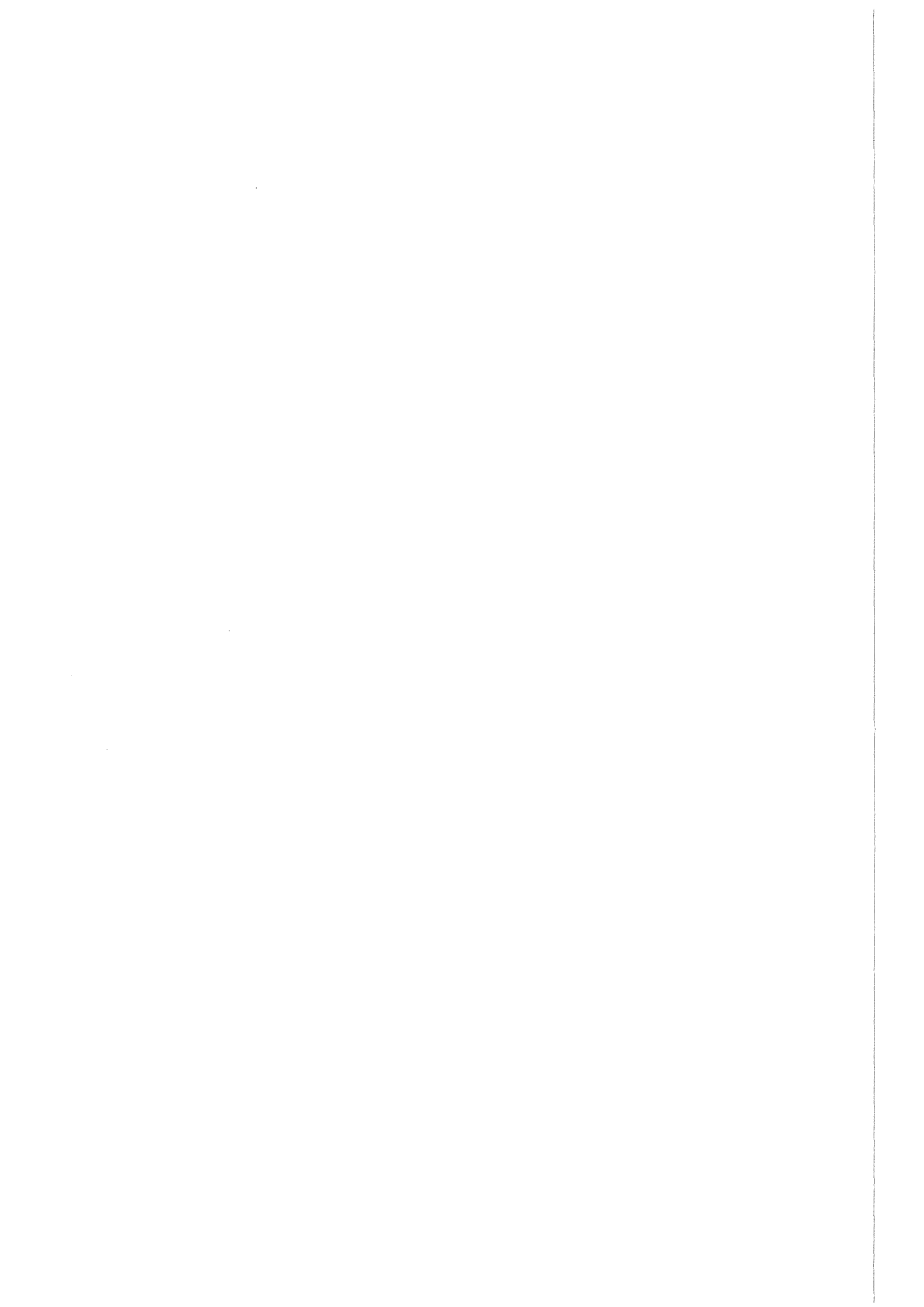


Figure N°19 - COMPARAISON MESURES/CALCUL DES EVOLUTIONS DE CONCENTRATION TRITIUM PRIMAIRE DURANT LE 38<sup>ème</sup> CYCLE.





IWGFR Specialists Meeting  
on Fission and Corrosion Products Behavior  
in Primary Circuits of LMFBRs  
Karlsruhe, FRG, May 1987

The Development of Cesium Traps for Commercial Sodium-Cooled Fast Breeder Reactors

N. Hanebeck, R. Tusche  
Interatom GmbH, Bergisch Gladbach, FRG

D. Msika, J. Misraki, R. Allegre  
CEA, Cadarache, France

Operating experience with defective fuel rods in operating sodium-cooled reactors has shown that, of the released fission products, cesium makes the greatest contribution to the coolant activity. As is known today, the cesium activity can be significantly reduced by means of traps containing carbonaceous materials in certain modifications which are installed in the primary sodium purification system.

By means of experiments in KNK, Rapsodie and other reactors it has been possible to demonstrate the basic function of this purification method under certain operational conditions. However, these tests did not indicate how a trap suitable for reactor use would behave in the case of a high cesium inventory in the coolant or, above all, whether it would be capable of significantly lowering the cesium level below that of Na-22 in the case of certain preloading.

Such a field testing possibility was offered by Rapsodie at CEA in Cadarache. Within the scope of the decommissioning program, approx. 50 Ci of radioactive cesium were removed from 40 t of primary sodium. 90 % of the activity in the coolant was due to Cs-137 with a half-life of 30 a. The remainder was mainly caused by Na-22 and Cs-134.

The trap which was designed and supplied by Interatom was installed and operated by CEA in a special purification loop above the sodium dump tank. The operating program was agreed on by both parties.

The trap concept is such that a system, which is completely mounted in a rig including shielding and electrical heaters, is installed on site. In order to guarantee flexible test operation and to be prepared for any unexpected problems, the actual sorbent system and the particle filter are separate units. One trap and one filter are available as replacement parts. The most important data and operational parameters of the system are as follows:

Sorbent material in cylindrical form:

Porous glassy carbon type

RVC 2 x 1 - 100 S from American production

Length of sorbent zone: 25 cm

Cross-section of cylinder: 102 cm<sup>2</sup>

Design value trap capacity: 50 Ci sorbent volume: 2.5 l

Weight of trap section

incl. lead shielding: 630 kg

Filter assemblies:

Fineness 25  $\mu$ m

Filter surface 0.37 m<sup>2</sup>

Weight per assembly incl.

lead shielding: 160 kg

Sodium flow during  
pumping operation:

1.0 m<sup>3</sup> h<sup>-1</sup>

Sodium temperature:

200 °C

The purification loop with sodium sampling installations and radioactivity measuring facilities allowed continuous monitoring of the trapping behaviour over the entire test period. In addition, it was possible to directly measure the distribution of the loading within the sorbent from the outside. The temporal distribution of concentration in the trap provided important information on sorption kinetics in relation to the flow.

With trap No. 1, the Cs activity was lowered by about a factor of 12, and the level was therefore close to the Na-22 level. Sorption equilibrium was attained; there was no further significant reduction of the Cs level in sodium.

As the transfer of sodium to an external tank was planned in any case, the sodium was subjected to post-purification in trap No. 2 during this operation. For reasons relating to licensing this was only performed at a sodium temperature of 130 °C and, due to the resulting known less favourable trapping kinetics, only at a flow of some 100 lh<sup>-1</sup>.

The Cs activity then dropped underneath that of Na-22 approximately by a factor of 2, thus allowing the primary sodium from Rapsodie to be reused as reactor grade sodium without any significant problems. The loaded traps are initially stored in their own lead shieldings as radioactive waste.

All in all the tests have shown that the cesium problem in sodium-cooled reactors can be well controlled with a sorption trap, and that trap capacities are available which permit the concentration of large quantities of radioactive species within an extremely small space.

CESIUM TRAPS RAPSODIE

ACTIVITIES BEFORE OPERATION TRAP NO. 1:

|        |      |                     |
|--------|------|---------------------|
| NA-22  | 5.72 | KBQ G <sup>-1</sup> |
| Cs-134 | 1.64 | "                   |
| Cs-137 | 103  | "                   |

AFTER OPERATION TRAP NO. 1:

|        |      |                     |
|--------|------|---------------------|
| NA-22  | 5.71 | KBQ G <sup>-1</sup> |
| Cs-134 | 0.13 | "                   |
| Cs-137 | 8.33 | "                   |

Cs-137 LEVEL DECREASED BY 92 %.

---

ACTIVITIES DURING OPERATION TRAP NO. 2:

|        |      |                     |
|--------|------|---------------------|
| NA-22  | 5.70 | KBQ G <sup>-1</sup> |
| Cs-134 | 0.10 | "                   |
| Cs-137 | 6.8  | "                   |

---

ACTIVITIES IN EXTERNAL TANK (37 T NA)

|        |                        |  |
|--------|------------------------|--|
| NA-22  | 2.1 · 10 <sup>11</sup> | Bq                                     |
| Cs-134 | 1.1 · 10 <sup>9</sup>  | < ACTIVITY < 3.6 · 10 <sup>9</sup> Bq  |
| Cs-137 | 9.4 · 10 <sup>10</sup> | < ACTIVITY < 2.5 · 10 <sup>11</sup> Bq |

## Calculational Model and Code for Corrosion Products Transfer in Sodium Systems

Katsuyuki Iizawa\*, Takao Kikuchi\*  
Isao Nihei\* and Junnosuke Horie\*\*

\* O-arai Engineering Center,  
Power Reactor and Nuclear Fuel Development Corporation,  
4002 Narita-cho, O-arai-machi, Higashi Ibaraki-gun,  
Ibaraki-ken, 311-13 Japan

\*\* Hitachi Division, Hitachi Engineering Co. Ltd.,  
3-2-1 Saiwai-cho, Hitachi-shi, Ibaraki-ken, 317 Japan



Abstract

Models have been developed to predict radioactive CP behaviour in an LMFBR. In this work, the solution-precipitation model developed by M.V. POLLEY and G. Skyrme, and by W.L. Kuhn is shown to interpret the transport of radioactive CPs such as  $^{54}\text{Mn}$  and  $^{60}\text{Co}$  in experimental sodium loops. A computer code for LMFBRs is developed. According to this model, mass transfer in sodium systems is characterized in four steps : (a) solid state diffusion in steel and surface loss or gain by solution or precipitation, respectively, (b) mass transfer across the sodium-steel interface, (c) mass transfer across the liquid viscous boundary sublayer, and (d) mass transfer in the circulating sodium, with release or deposition at surfaces. Analytical expressions for the concentrations in steel and bulk sodium, and the mass fluxes, are given for CP release or deposition in experimental sodium loops or LMFBR primary circuits.

The parameters needed to predict LMFBR radioactive CP behaviour are obtained by fitting the model to the release rates and distribution of deposits in experimental sodium loops. Analysis of the downstream effect for  $^{60}\text{Co}$  deposition confirms the tentative suggestion of the previous workers that the mechanism controlling  $^{60}\text{Co}$  transfer is diffusion through the boundary sublayer in the flowing sodium. On the other hand, analysis of  $^{54}\text{Mn}$  deposition suggests that the controlling mechanism for this nuclide is probably an intermediate case between diffusion-control in the liquid and reaction-control at steel surfaces.

The super-stoichiometric release of  $^{54}\text{Mn}$  and the sub-stoichiometric release of  $^{60}\text{Co}$  are interpreted from their model parameters as being likely related to their solubilities in sodium.

The computer code developed for this model is named PSYCHE, and can be applied to estimating radioactive CP behaviour and resulting radiation fields near the piping and components in loop type LMFBR primary circuits.

## Introduction

During the operation of an LMFBR (Liquid Metal Fast Breeder Reactor), radioactive isotopes are produced in the reactor core by  $(n, \gamma)$  and  $(n, p)$  reactions on the constituent elements of stainless steel fuel cladding and subassembly wrappers. The most important isotopes are  $^{54}\text{Mn}$ ,  $^{60}\text{Co}$ ,  $^{58}\text{Co}$ ,  $^{51}\text{Cr}$ , and  $^{59}\text{Fe}$ . A small but significant fraction of the radioisotopes is released both by corrosion (i.e. surface loss) of the activated cladding and by solid state diffusion of isotopes out of the cladding into the circulating sodium. The released radioisotopes transfer with the sodium and deposit in the piping and components of the primary circuit. The deposited isotopes can cause radiation fields near the piping and components which greatly complicate maintenance procedures and contribute significantly to radiation exposures of plant personnel.

R & D work has been conducted at PNC to determine the magnitude and distribution of the radiation fields near the primary circuits of the experimental fast reactor JOYO and the prototype FBR MONJU. The first task is to characterize radioisotope release and distribution in order to evaluate potential control methods, and to estimate the radiation fields so that the maintenance procedures can be developed. For this purpose a calculational model and code for estimating the transfer of radioactive CPs in LMFBR primary circuits, and predicting the resulting radiation fields, has been developed.

The transfer of radioactive CPs in sodium shows some striking aspects as reported by previous workers [1, 2], as follows :

- (a) Sodium loop experiments have shown that species are either selectively leached or retained in the steel, (for example,  $^{54}\text{Mn}$  release is super-stoichiometric, while  $^{60}\text{Co}$  is sub-stoichiometric) and that the concentration at the steel surface is either reduced or increased, respectively, accompanied by diffusion towards or away from the surface. Similarly, CPs are known to diffuse into the steel following deposition.
- (b) It has been observed that the release or deposition rate of species decreases with distance downstream in an isothermal section of experimental sodium loops.
- (c) Brehm [2] showed that the release of  $^{60}\text{Co}$  and  $^{58}\text{Co}$  was sensitively influenced by the oxygen concentration in the sodium, but that of  $^{54}\text{Mn}$  was not.

In our attempt to explain these observations, we will assume that transfer between steel and sodium is mainly due to the solution and precipitation of atomic or molecular species, rather than the detachment and sticking of large particles. Thus, release and deposition calculations require solution of the diffusion equation in the steel, with boundary conditions at the moving sodium-steel interface which can be obtained from mass transfer theory. This solution - precipitation model for radioactive CP transfer in LMFBR's has been investigated by Polley [4], Kuhn [5] and others.

Ideally a complete mass balance around the circuit is required for each CP, i.e. the quantity released or deposited and the concentration in the sodium at all positions in the circuit as a function of time. However, in practice the analysis is extremely complex if release and deposition should be correlated exactly on the mass conversion law and unless it is assumed that the concentration in the sodium is independent of time.

Kuhn [5] presented a model for calculating release of radioactive CPs from LMFBR cores. His analytical solution could be applied to the case of highly leached species, since the zero concentration in sodium at the surface was assumed. Polley [4] treated both release and deposition of active species for the general case of an LMFBR and gave an analytical expression. However, in his treatment also the concentration in the bulk sodium was taken to be either zero or independent of time for release and deposition calculations, respectively. Using Polley's boundary conditions and assuming that the concentration in the bulk sodium is independent of time, the present work derives expressions in differentiated form for release and deposition calculations of stable and active species. The expressions are applicable to the general case of sodium loop experiments or LMFBRs. A simple mass balance around the circuit is taken into consideration in a numerical procedure for release and deposition calculations. Thus, it is expected to improve appreciably the zero concentration assumption which would give overestimates for the release of radioactive CPs in both LMFBR primary circuits and experimental sodium loops. The apparent difference between the dependence on the oxygen concentration in sodium of the release of active cobalt isotopes and  $^{54}\text{Mn}$  is investigated, assuming that the adsorbed oxygen at the steel surface would activate the dissolution of species into sodium, for  $^{60}\text{Co}$  and  $^{58}\text{Co}$  in particular.

Parameters needed to predict the transfer of radioactive CPs in an LMFBR can be evaluated by fitting the model to experimentally determined

release rates from activated cladding, and the distribution of radioactive deposits. Data used in this work was obtained primarily from the AMTL experiments [1] at PNC and elsewhere [3]. It is assumed that mass transfer coefficients, the interfacial velocity and the radioisotope production rate are constants. Diffusion in the steel is characterized by a single diffusion coefficient independent of depth. Grain boundary diffusion and possible formation of a second phase at the surface (e.g. ferrite, intermetallic compounds) are not specifically treated. This effective diffusion coefficient incorporates lattice and grain boundary diffusion.

A computer code for calculating radioactive CP transfer in LMFBR primary circuits, and the resulting radiation fields exterior to the reactor piping and components, has been developed. The code is named PSYCHE (Program System for Corrosion Hazard Evaluation). The system comprises analysis codes for transfer of the corroded species of interest in LMFBR primary circuits and experimental sodium loops, and for the radiation fields in the HTS of an LMFBR. The modified QAD-CD code is applied to radiation field calculations. Using PSYCHE, the calculated radioactive CP distribution and radiation fields in the primary circuit of the experimental fast reactor JOYO were compared with those measured. It was found that the ratio of calculated to measured values are from 0.5 to 2 for  $^{54}\text{Mn}$  and  $^{60}\text{Co}$  distribution in the piping, and from 0.6 to 1.3 for dose rate distribution [12]. We consider that this gives an appropriate estimation.

### Calculational Model

The basic idea for mass transfer of the species of interest between steel and sodium in a solution - precipitation model is shown in Fig. 1. The driving force for mass transfer of the constituent elements of steel between steel and sodium may be attributed to the difference between their chemical activities in steel and sodium. Following this model, mass transfer of the species in sodium loop is characterized by four steps :

- (a) solid state diffusion in the steel and surface loss or gain by solution or precipitation, respectively.
- (b) mass transfer at the sodium - steel interface,
- (c) mass transfer across the liquid viscous boundary sublayer,
- (d) mass transfer with the circulating sodium, followed by release or deposition at the surface.

The mass fluxes for step (a) to (c) are, respectively, for net release [Fig. 1(a)]

$$J = D \frac{\partial C}{\partial x} \Big|_{x=0} \pm u C_i \left( \begin{array}{l} + \text{ bulk corrosion} \\ - \text{ bulk deposition} \end{array} \right), \quad (1)$$

$$J = k_s C_i - k_p 'C_i' \quad \text{or} \quad K_s C_i \theta' - K_p 'C_i', \quad (2)$$

$$J = k' (C_i' - C'), \quad (3)$$

where  $C$  and  $C'$  are the concentration in the steel and bulk sodium, respectively, (the subscript  $i$  indicating interfacial values at  $x = 0$ ),  $\theta'$  is the dimensionless oxygen concentration in sodium (i.e. the actual oxygen concentration divided by the reference oxygen concentration),  $u$  is the magnitude of the interfacial velocity,  $k'$  is the mass transfer coefficient for diffusion through the viscous sublayer, and  $K_s$  and  $k'_p$  are the solution or precipitation kinetic constants, respectively.

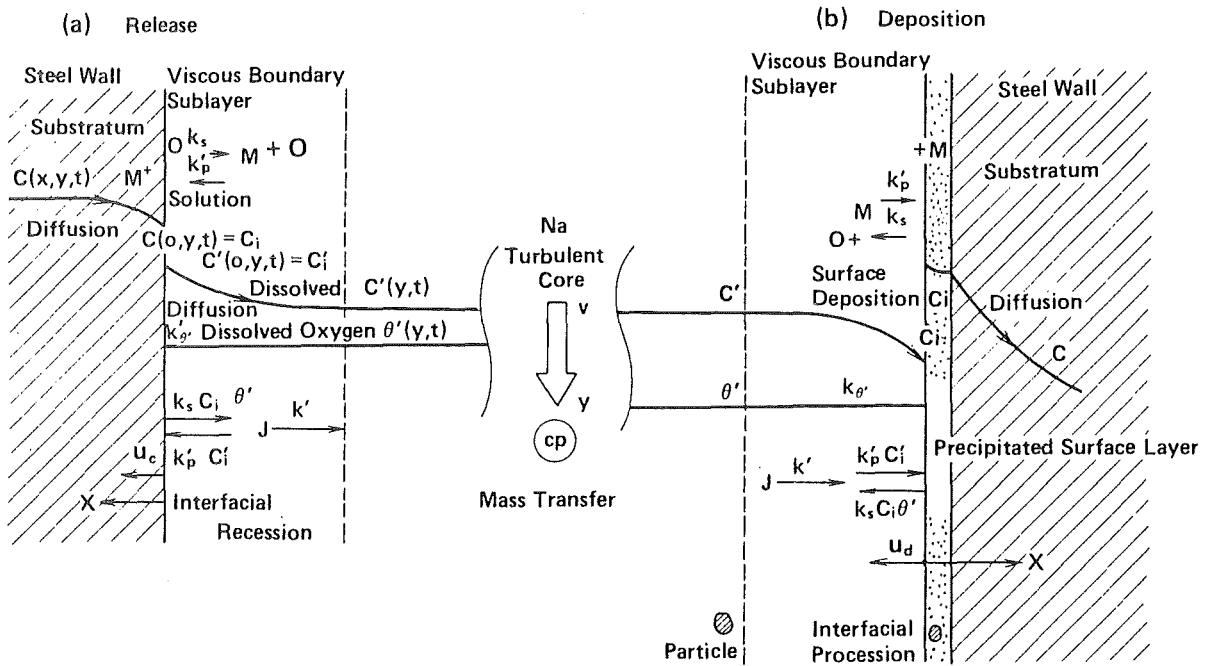


Fig. 1 Mass Transfer between Steel and Flowing Sodium (Solution-Precipitation Model).

For net deposition the relationships of  $J$  are identical but opposite in sign [Fig. 1(b)]. In eq.(2) the first expression is applied to strongly leached species such as manganese isotopes and the second expression to weakly leached species such as cobalt isotopes. The free energy change in dissolution of weakly leached species from the steel surface,  $-\Delta G$ , is influenced more strongly by adsorbing oxygen at the steel surface. The dissolution of these species appears to be linearly proportional to the oxygen concentration. This behaviour is not observed for strongly leached species. This assumption is compatible with the experimental loop or plant data, as shown in the next section.

Eliminating  $C_i'$  from eqs. (2) and (3) yields

$$J = K' \left( \frac{C_i}{\beta \text{ or } \beta'} - C' \right) \quad (4a)$$

for release, or

$$J = K' \left( C' - \frac{C_i}{\beta \text{ or } \beta'} \right) \quad (4b)$$

for deposition, where

$$K' = k'k'_p / (k' + k'_p) \quad (5)$$

$$\text{and } \beta = k'_p/k_s \text{ or } \beta' = \beta/\theta' \quad (6)$$

are the overall mass transfer coefficient and the chemical partition parameter, respectively. A boundary condition similar to Polley's is obtained by equating (1) and (4a), as in eq.(7),

$$D \frac{\partial C}{\partial x} \Big|_{x=0} = \left( \frac{K'}{\beta \text{ or } \beta'} \mp u \right) C_i - K'C' \begin{pmatrix} - \text{bulk corrosion} \\ + \text{bulk deposition} \end{pmatrix} \quad (7)$$

which is applicable to either release or deposition.  $X$  is the depth from the surface into the steel.

For release the diffusion equation in the steel for the most general case (release of active species in LMFBR cores) is

$$D \frac{\partial^2 C}{\partial x^2} \pm u \frac{\partial C}{\partial x} - \lambda C + R = \frac{\partial C}{\partial t} \begin{pmatrix} + \text{bulk corrosion} \\ - \text{bulk deposition} \end{pmatrix}, \quad (8)$$

where R is the production rate of the species by neutron activation and  $\lambda$  is the decay constant of the radioisotope. This  $\lambda$  should be replaced by  $\lambda + \int \sigma \phi dE_n$  for nuclides such as  $^{58}\text{Co}$  or  $^{181}\text{Ta}$  with large neutron cross sections. Now,  $\sigma$  is the neutron capture cross section of the nuclide of interest and  $\phi$  is the neutron flux,  $\sigma\phi$  being integrated over the neutron energy spectrum. For sodium loop experiments using preirradiated specimens  $R = 0$ . For stable species in all cases  $R = 0$  and  $\lambda = 0$ . The corrosion case is indicated by the plus sign and deposition by the minus sign. For most sodium loop experiments the surface of activated specimens is subjected to bulk corrosion. For LMFBR cores deposition occurs on the surface of fuel pin cladding in the cold plenum, while corrosion occurs on the surface of cladding in the bundle and hot plenum as the temperature increases.

For deposition the diffusion equation for active species in the steel which is applicable to experimental sodium loops and to LMFBR circuits, is

$$D \frac{\partial^2 C}{\partial x^2} \pm u \frac{\partial C}{\partial x} - \lambda C = \frac{\partial C}{\partial t} \left[ \begin{array}{l} + \text{ bulk corrosion} \\ - \text{ bulk deposition} \end{array} \right] \quad (9)$$

For stable species  $\lambda = 0$ . The significance of the sign pair ( $\pm$ ) in the equation is similar to that for the release case. For hot leg piping of experimental sodium loops or LMFBR circuits, the bulk corrosion case probably becomes important.

The interfacial boundary condition is, for either release or deposition [eq.(7)],

$$D \left. \frac{\partial C}{\partial x} \right|_{x=0} = \left[ \frac{K'}{\beta \text{ or } \beta'} \mp u \right] C_i - K' C', \left[ \begin{array}{l} - \text{ bulk corrosion} \\ + \text{ bulk deposition} \end{array} \right] \quad (10)$$

In the following analysis the general procedure is to calculate the concentration profile in the steel by solving the relevant diffusion equation (eq.(8) or (9)) for this condition at the sodium-steel interface, and assuming the steel to be of infinite thickness. This assumption can be seen to be appropriate for diffusion of metallic species, i.e. substitutional alloying elements of low diffusivity in the steel, but is perhaps not suitable for species with higher diffusivity in thin walled structures, for example carbon in fuel cladding. Carbon is of concern because of problems of structural integrity caused by its transfer. The initial

condition is

$$C = C_0 \quad \text{or} \quad 0 ; \quad t = 0, \quad (11)$$

where  $C_0$  is the concentration of active or stable species in the steel at  $t = 0$ . For release of active species in experimental sodium loops or LMFBR cores the initial condition is  $C = C_0$ . In the present work the mass conversion law which is considered, is expressed by the following equation :

$$\frac{\partial C'}{\partial y} = 4 \frac{K'}{vd} \left( \frac{C_i}{\beta \text{ or } \beta'} - C' \right), \quad (12)$$

where  $v$  is the sodium velocity,  $d$  is the equivalent hydrodynamic diameter of the flow path, and  $y$  is the distance along the region of interest, measured along the flow path with zero position at the entry to the region. The concentration of species in the bulk sodium,  $C'$ , is assumed to be zero at the starting time of operation, i.e. at  $t = 0$ .  $C'$  is calculated approximately from eq. (12) by considering the release or deposition at each region in the system, assuming that the concentration is independent of time during each time step. Precision of this calculational procedure has been examined by varying the time step interval. It has been found to give reasonable results.

The appropriate equation for diffusion in the steel for release or deposition [eq.(8) or eq.(9)] must be solved with the boundary condition at  $x = 0$  given by eq.(10), the initial condition at  $t = 0$  by eq.(11), and the mass conservation law by eq.(12). The solution can be obtained analytically by Laplace and inverse Laplace transformation [6], assuming that the concentration of species in the bulk sodium is independent of time, except for radioactive decay of active species in sodium loop experiments. The resulting expressions for the concentrations of species in the steel and bulk sodium, and the mass fluxes, are tabulated in Table 1 for release and deposition. Some points of interest regarding these solutions are as follows.

(a) For sodium loop experiments it is found that the solution for the corrosion of active species differs from that for stable species only by the radioactive decay term,  $e^{-\lambda t}$ . (b) The mass flux of active deposition in sodium loop experiments or LMFBR circuits is expressed by  $K\eta C'$ , where  $\eta$  is the deposition coefficient for retaining active species



at the steel surface. Since  $\eta$  is a function of  $D$ ,  $K'$ ,  $\beta$  or  $\beta'$ ,  $u$ ,  $x$  and  $t$ , but not of  $y$ , the overall mass transfer coefficient,  $K'$ , can be obtained from analysis of the downstream effect for deposition of active species in isothermal sections in sodium loops. (c) Mass flux of stable or active corrosion in experimental loops becomes  $uC_0$  or  $uC_0e^{-\lambda t}$  asymptotically, respectively, as  $t$  approaches infinity, where  $C_0$  is the initial concentration in the steel, i.e. the concentration of species at infinite depth. This means that the magnitude of the interfacial velocity for bulk corrosion,  $u_c$ , can be obtained from the steady state corrosion rate in stable or active mass transfer tests in experimental sodium loops.

#### Comparison with Data on Corrosion Products Transfer in Sodium Loop

In this section we describe the determination of the solution-precipitation model parameters needed to predict LMFBR radioactive CP transfer. They can be evaluated by fitting the model to the experimentally determined release rates and the distribution throughout the loop for active or stable species. For their evaluation in this work the data obtained from the AMTL-I [1] and -II at PNC, the STCL at HEDL [3] were used. The model parameters given below are described in the cgs unit system.

A number of investigations have been conducted on solid state diffusion of alloying elements in steel. Smith and Hales [7] reported the diffusivity of chromium and manganese in Type 316 stainless steel at relatively high temperature for annealing steel. The lattice or grain boundary diffusion coefficient is given for each element in the steel in their work. Extrapolated to the temperature of interest for an LMFBR, the Smith & Hales correlation predicts a lattice diffusion coefficient which is an order of magnitude below the apparent values obtained from an analysis of the  $^{60}\text{Co}$  concentration profile in the Type 316 deposition specimen, sampled from the AMTL-I tubing, or of the  $^{54}\text{Mn}$  concentration profiles in the Type 304 or 316 deposition specimens reported by Anantatmula [8] using a similar model, as shown in Fig. 2. Our results or Anantatmula's are rather well represented by Kuhn's expression. We do not know the cause of the discrepancy. It may be caused by an unknown factor in our analysis ; e.g., the deposition rate in the precipitated layer on the specimen surfaces, or the partial formation of a ferrite phase. Reasoning from the results shown in Fig. 2 or 3, we expect the difference due to kind of element

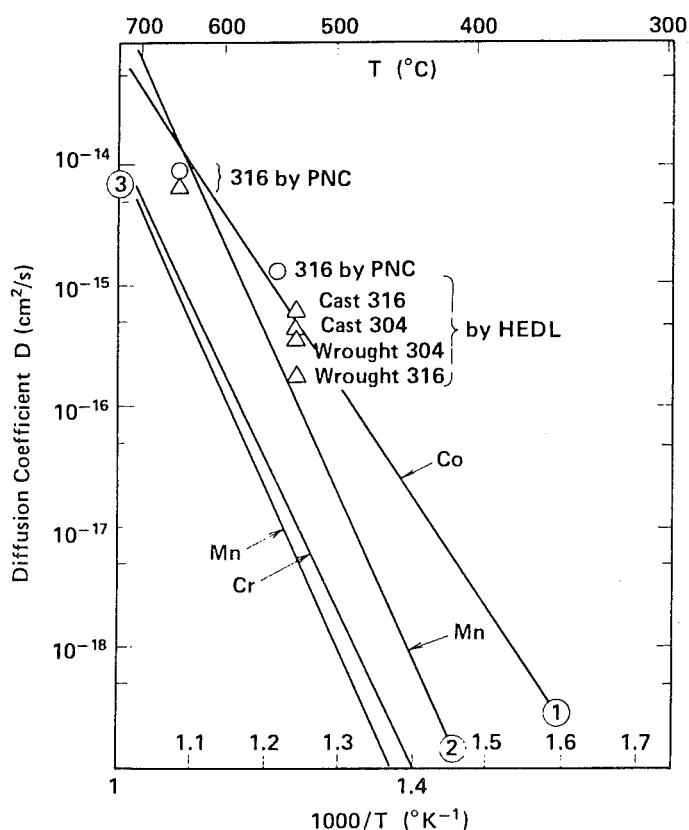


Fig. 2 Diffusion Coefficient of Manganese, Chromium or Cobalt in Stainless Steel.

- ① : Estimated by Our Work
- ② : Proposed by W.L. Kuhn [ 5 ]
- ③ : Proposed by A.F. Smith [ 7 ]
- : Experimental Values of Co [ 1 ]
- △ : Experimental Values of Mn [ 8 ]

should be small for not only chromium, manganese and cobalt but also iron and nickel. The effective diffusion coefficient used in the present work is an apparent lattice diffusion coefficient obtained from the result for  $^{60}\text{Co}$  in the AMTL-I,

$$D = 1.32 \times 10^{-4} \exp(-42.1/RT), \tag{13}$$

where R is the gas constant,  $1.987 \times 10^{-3}$  Kcal/deg.mol.

The overall mass transfer coefficient for the species of interest is obtained from an analysis of the sodium flow velocity dependence of the downstream effect for deposition of active species in experimental sodium loops. The analysis of the  $^{60}\text{Co}$  deposition measurements in the AMTL-I confirms Polley's tentative suggestion [4] or Newson's result [9] that the mechanism controlling  $^{60}\text{Co}$  deposition is diffusion through the boundary sublayer in the flowing sodium, i.e.,  $K' \approx k'$ . On the other hand, the

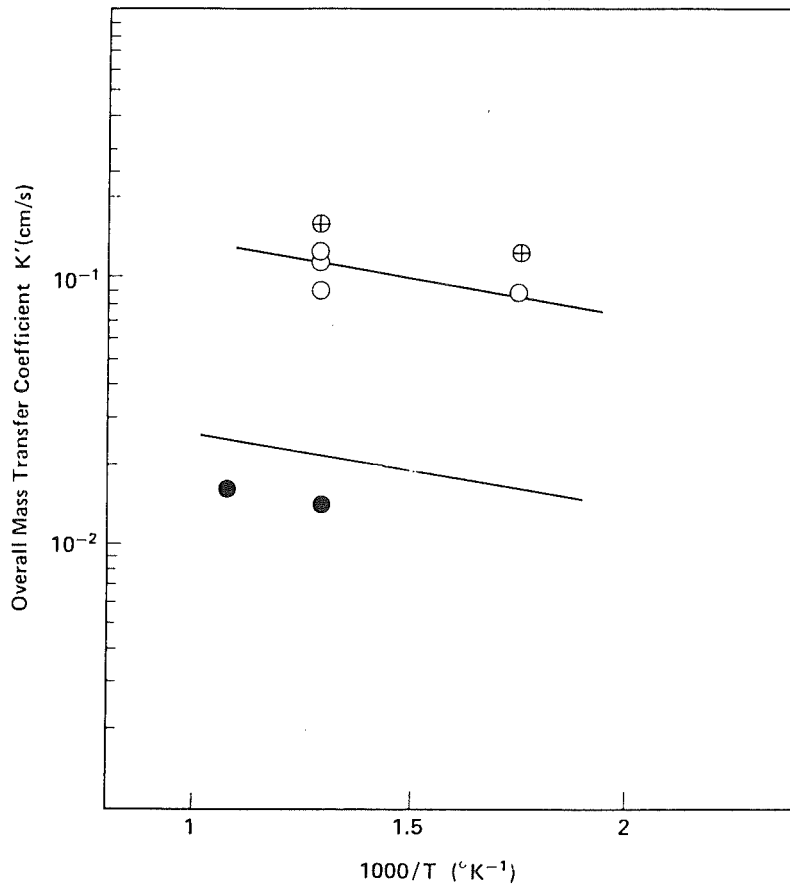


Fig. 3 Temperature and Flow Dependence of Overall Mass Transfer Coefficient of  $^{60}\text{Co}$  ( $\circ$ : 90 cm/s,  $\bullet$ : 18 cm/s) or  $^{58}\text{Co}$  ( $\oplus$ : 90 cm/s) Obtained from Deposition Down Stream Analysis in Flowing Sodium.  
 —: Calculated Curves Using Eqs. (15) and (16)

$^{54}\text{Mn}$  deposition measurements in the AMTL-I and -II suggests that its controlling mechanism is probably an intermediate case between the limiting cases, i.e. diffusion-control in the liquid or reaction-control at the steel surface. Thus the overall mass transfer coefficient of  $^{54}\text{Mn}$  requires evaluating  $K'_p$ .

For radioactivity deposition in an experimental sodium loop with sodium velocity  $v$  in a pipe of bore  $d$ , the decay-corrected mass flux is

$$J_L \cdot \exp(\lambda t) = K'_p C'(0,0) \exp\left(-\frac{4K'}{v} \frac{L}{d}\right), \quad (14)$$

where  $J_L$  is mass flux of the species at  $y = L$  and  $t$ , and  $C'(0,0)$  is the concentration at  $y = 0$  and  $t = 0$ . A plot of  $\ln J_L$  against  $L/d$  should yield a straight line of negative slope equal to  $4 K'/v$ . Fig. 3 shows plots of  $K'$

against  $1/T$  on log/linear coordinates for both  $^{60}\text{Co}$  and  $^{58}\text{Co}$  deposition at temperatures of  $300^\circ$ ,  $500^\circ$  and  $650^\circ\text{C}$ , and sodium velocities of 18 cm/s and 90 cm/s. These experimentally derived values are compared with values of mass transfer coefficient,  $k'$ , calculated from the wellknown equation given by Treybal [10], which defines the diffusion controlled mass transfer coefficient through the boundary sublayer in the flowing sodium as

$$k' = 0.023 \text{ Re}^{0.83} \text{ Sc}^{1/3} D'/d, \quad (15)$$

where  $\text{Re}$  and  $\text{Sc}$  represent the Reynolds and Schmidt numbers, respectively, and  $D'$  the diffusivity of the species in liquid sodium. Fig. 3 shows that the experimental  $K'$  values are relatively well expressed by  $k'$  calculated from equation (15) above. This means that the mass transfer of cobalt isotopes between steel and sodium is controlled by diffusion through the boundary sublayer in the flowing sodium, i.e.  $K' \approx k'$ . The diffusivity of cobalt in liquid sodium,  $D'$ , is obtained from fitting equation (15) to the experimental  $K'$  values as

$$D' = 5.1 \times 10^{-4} \exp(-0.032/k_B T), \quad (16)$$

where  $k_B$  is the Boltzmann constant,  $8.617 \times 10^{-5} \text{ eV/deg}$ . This result agrees reasonably well with Newson's value [9]. We use this expression for all the species of interest.

The analysis of the  $^{54}\text{Mn}$  deposition measurements in the AMTL-I results in overall mass transfer coefficients whose values at  $300^\circ$ ,  $500^\circ$  and  $650^\circ\text{C}$  indicate little dependence on the sodium velocity of 18 cm/s or 90 cm/s. This suggests that the mechanism controlling  $^{54}\text{Mn}$  deposition may be the intermediate case mentioned before. Fig. 4 shows plots of  $K'/k'$  against  $k_p'/k'$  on linear/log coordinates. Since  $k_p'/k' = X(T) d^{0.17} / v^{-0.83}$ , where  $X(T) = k_p' \cdot v^{1.16} / 0.023 D'^{1.33}$ , the experimental value of  $K/k'$  could be examined by plotting it against the corresponding logarithmic value of  $d^{0.17} v^{-0.83}$ . Since  $k_p'/k' = 1$  at  $K/k' = 0.5$ ,  $X(T)$  is given by the reciprocal of the  $d^{0.17} v^{-0.83}$  value at  $K/k' = 0.5$ . The experimental  $K/k'$  values for  $^{54}\text{Mn}$  deposition in the AMTL-I and -II are plotted against their  $d^{0.17} v^{-0.83}$  values at temperatures of  $300^\circ$ ,  $400^\circ$ ,  $500^\circ$  or  $650^\circ\text{C}$  in Fig. 5. Although the experimental correlations scatter appreciably, the  $X(T)$  values for  $^{54}\text{Mn}$  which give  $k_p'$  can be tentatively found from the theoretical curves. Following the analysis described above, the overall mass transfer

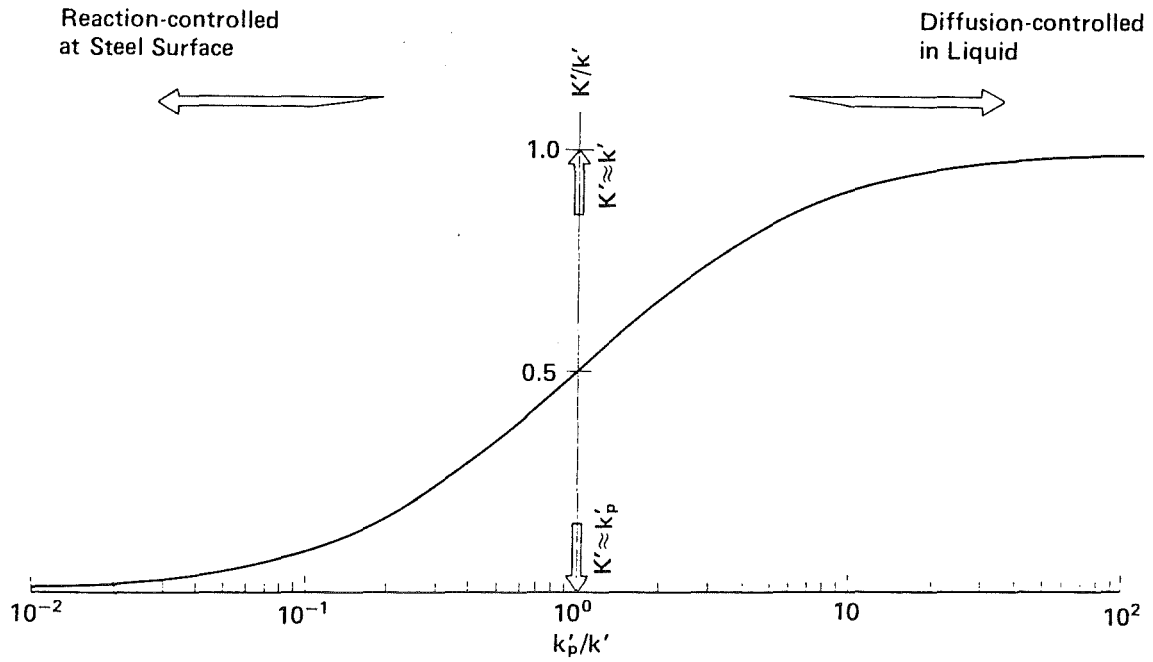


Fig. 4 Correlation between Overall Mass Transfer Coefficient and Rate Controlling Step.

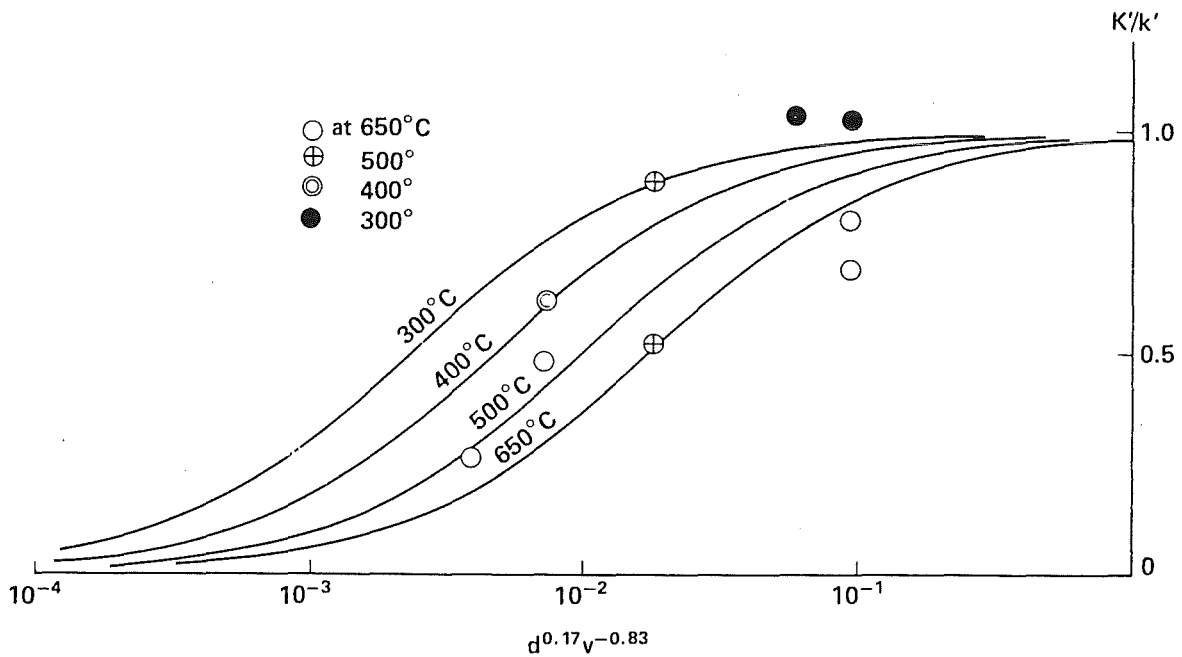


Fig. 5 Correlation between Overall Mass Transfer Coefficient Normalized by Mass Transfer Coefficient in Sodium and Power Term of Reciprocal Sodium Velocity for  $^{54}\text{Mn}$ .  
—: Adjusted Theoretical Curve

coefficient for  $^{54}\text{Mn}$  is expressed as

$$K' = k'k'_p / (k' + k'_p) \quad (17a)$$

$$k'_p = 5.05 \times 10^{-3} \exp(3.46/RT), \quad (17b)$$

$$k' = 0.023 \text{ Re}^{0.83} \text{ Sc}^{1/3} D'/d; \quad (17c)$$

$$D' = 5.1 \times 10^{-4} \exp(-0.032/k_B T). \quad (17d)$$

Manganese-54 transfer between steel and sodium becomes controlled by reaction at the steel surface as the temperature is increased at a given  $v$  and  $d$ , or as the sodium velocity is increased at a given temperature.

For the bulk corrosion case, the surface recession rate,  $u_c$ , approaches a constant value in stable or active mass transfer tests in experimental sodium loops after exposing the steel in sodium for several thousand hours. In the present work a correlation of the corrosion rate of type 316, 304 or 321 given by Maruyama [11] at PNC is applied to our calculation. This rate is expressed as a function of temperature, oxygen concentration in sodium and a downstream factor for isothermal regions. The correlation is independent of sodium velocity above about 2 m/s, in agreement with the other literature.

$$u_c = 3.17 \times 10^{-12} O_{x'}^{0.803} \exp(12.63 - 22.0/RT - 0.00591 L/d), \quad (18)$$

where  $O_{x'}$  is the oxygen concentration in ppm and the downstream factor is defined as the distance,  $L$ , down the isothermal section divided by the hydraulic diameter,  $d$ . Fig. 6 shows the correlations of the sodium corrosion rate of steel in steady state reported by some investigators as a function of temperature at 2 ppm of oxygen concentration, 6 m/s of sodium velocity and  $L/d = 0$ . Maruyama's value is appreciably higher rather than Thorley's and the other's, except for Bagnall's, which shows a higher temperature dependence.

For the bulk deposition case the interfacial velocity,  $u_d$ , is the procession rate of the wall due to deposition of stable and active corrosion products onto the steel surface. In this work the procession rate is tentatively given from an analysis of the active deposition profile of  $\text{Co}^{60}$  or  $\text{Mn}^{54}$  along the nonisothermal piping system in the AMTL experiment,

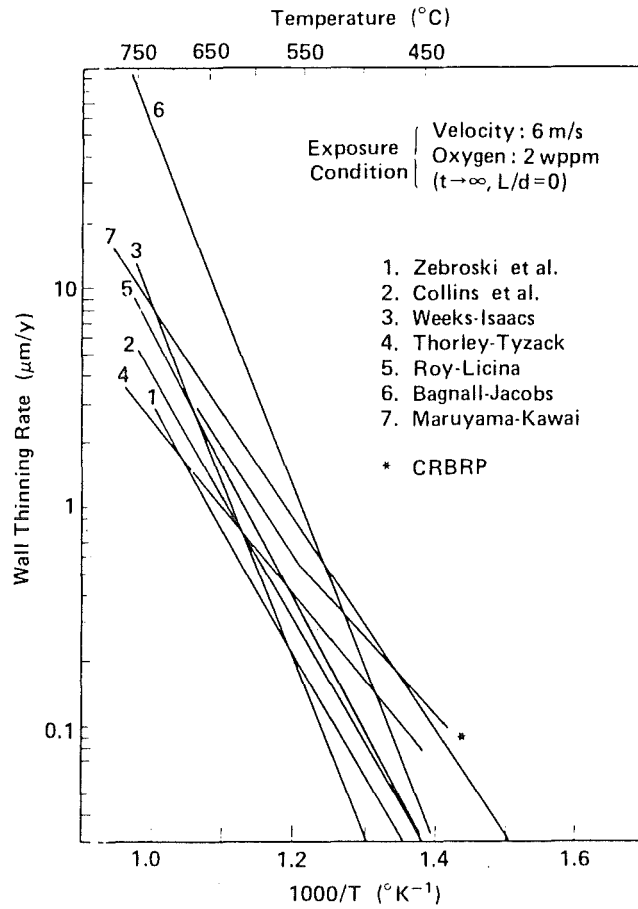


Fig. 6 Temperature Dependence of Steady State Wall Thinning Rate of Type 304 or 316 Stainless Steel Exposed in Sodium.

with a maximum sodium temperature of 659°C and oxygen concentration of 12 ppm :

$$u_d = 3.17 \times 10^{-14} \times 4.02 \exp(2.29/RT) \quad (19)$$

It seems that this correlation can be applied to the analysis of an LMFBR primary circuit as a standard which would likely be corrected with a factor.

In the present work the chemical partition parameter for  $^{54}\text{Mn}$  or  $^{60}\text{Co}$  was determined by fitting a calculation by the model to the activity profiles along the nonisothermal loop system in the AMTL-I experiment, using the other parameters above mentioned. The appropriateness of the parameter to an analysis for the JOYO primary circuit was examined [12]. It was found that a correction was required for  $^{60}\text{Co}$  but not for  $^{54}\text{Mn}$ .

The chemical partition parameters are for  $^{54}\text{Mn}$

$$\beta = 1.58 \times 10^9 \exp(2.13/RT), \quad (20)$$

and for  $^{60}\text{Co}$

$$\beta'\theta' = 9.93 \times 10^9 \exp(1.69/RT), \quad (21a)$$

$$\theta' = O_{x'}/12. \quad (21b)$$

$O_{x'}$  is the sodium oxygen concentration in ppm. The value of  $O_{x'}$  in the AMTL-I experiment was 12 ppm. It was found that the expressions above are satisfactory for both release and deposition of  $^{54}\text{Mn}$  or  $^{60}\text{Co}$ . However, these correlations are given tentatively, leaving the opportunity for improvement using measurement results for radioactive CP transfer in LMFBR primary circuits.

Fig. 7 and 8 show comparisons of the fraction released to the initial inventory for  $^{54}\text{Mn}$  and  $^{60}\text{Co}$ , plotted against sodium exposure time. Experimental data was obtained in the AMTL-II and theoretical values from the solution - precipitation model calculation using the model parameters above mentioned. The activated cladding specimens which had been exposed in sodium were reduced in thickness by 150  $\mu\text{m}$  from the non-exposed inner side, to enhance the release fraction of the species of interest. The experimental values are moderately well reproduced by the calculated correlations. Figs. 9 and 10 show the experimental and calculated concentration profiles in the cladding specimens for stable Mn or  $^{60}\text{Co}$ , respectively. The experimental values for Mn or  $^{60}\text{Co}$  were obtained from experiments in the AMTL-II or the STCL, respectively [3]. This agreement between observation and calculation is satisfactory. The observed deposition profile for  $^{54}\text{Mn}$  and  $^{60}\text{Co}$  along the AMTL-I loop system is plotted against the distance downstream from the active source in Fig. 11, as is the calculated profile. The result for  $^{60}\text{Co}$  is reproduced better than that for  $^{54}\text{Mn}$  by the calculation. However, the strikingly different deposition behaviour of  $^{54}\text{Mn}$  and  $^{60}\text{Co}$  is well demonstrated. From these results it is seen that the deposition distribution of  $^{54}\text{Mn}$  is primarily governed by the temperature profile along the sodium system, while the distance downstream from the active source is a very important factor for the  $^{60}\text{Co}$  deposition distribution. This indicates that stable or active cobalt species are more likely than manganese to deposit onto steel in sodium. The difference in deposition characteristics between manganese and cobalt may be attributed



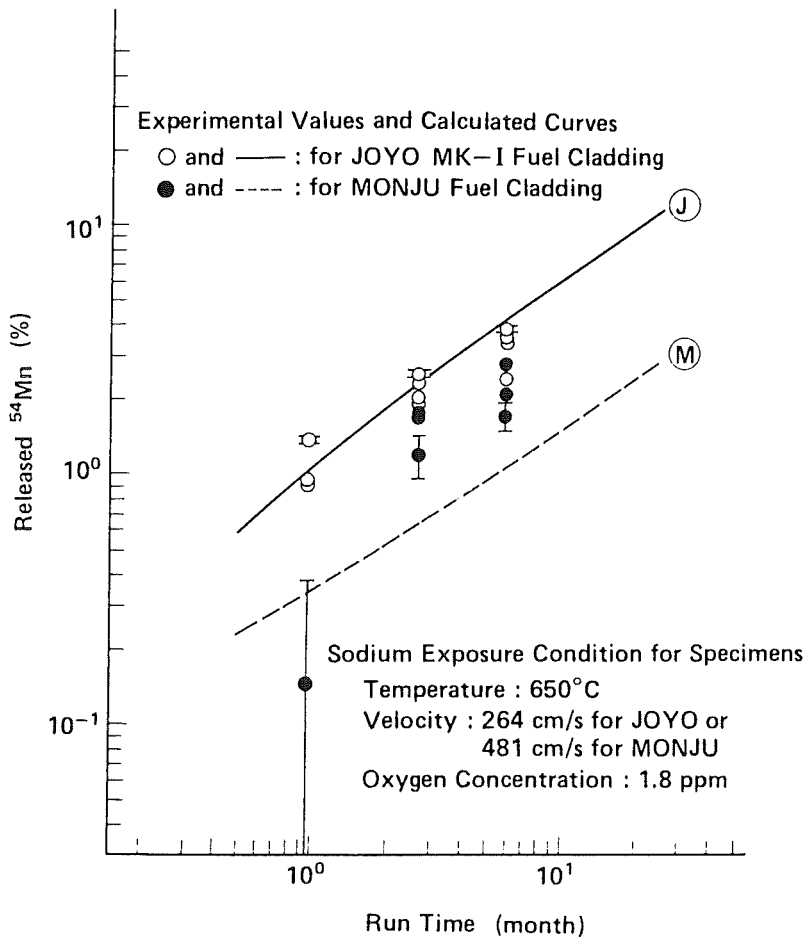


Fig. 7 Comparison between Experimental and Calculated Variation of Released  $^{54}\text{Mn}$  with Sodium Exposure Time.

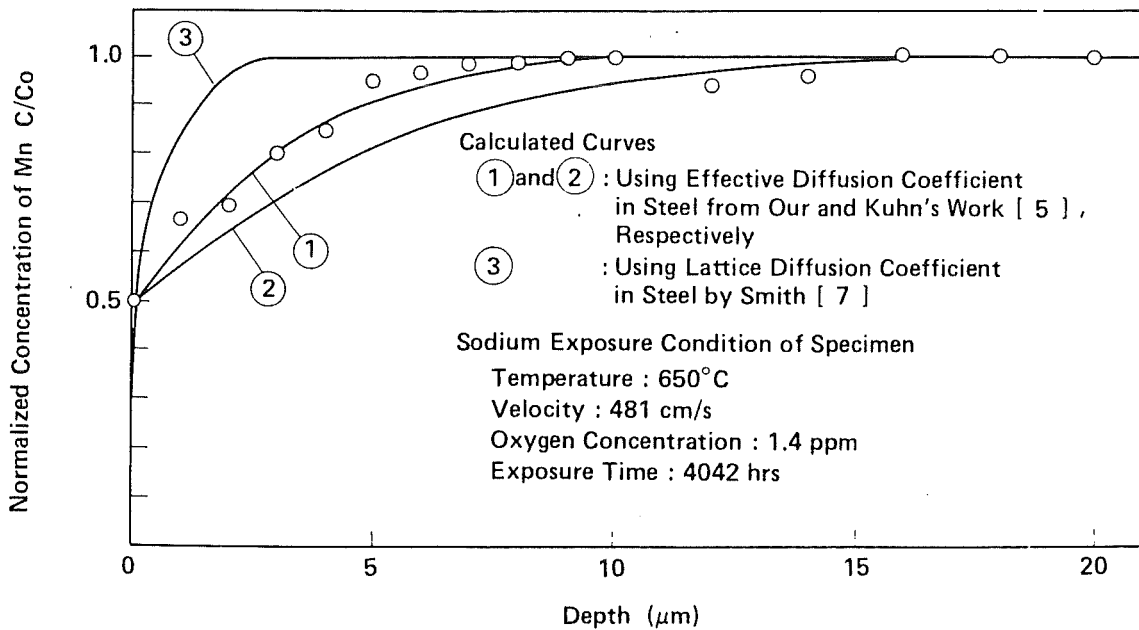


Fig. 9 Comparison between Experimental and Calculated Concentration Profile of Manganese in Type 316 Fuel Cladding Specimen for MONJU.

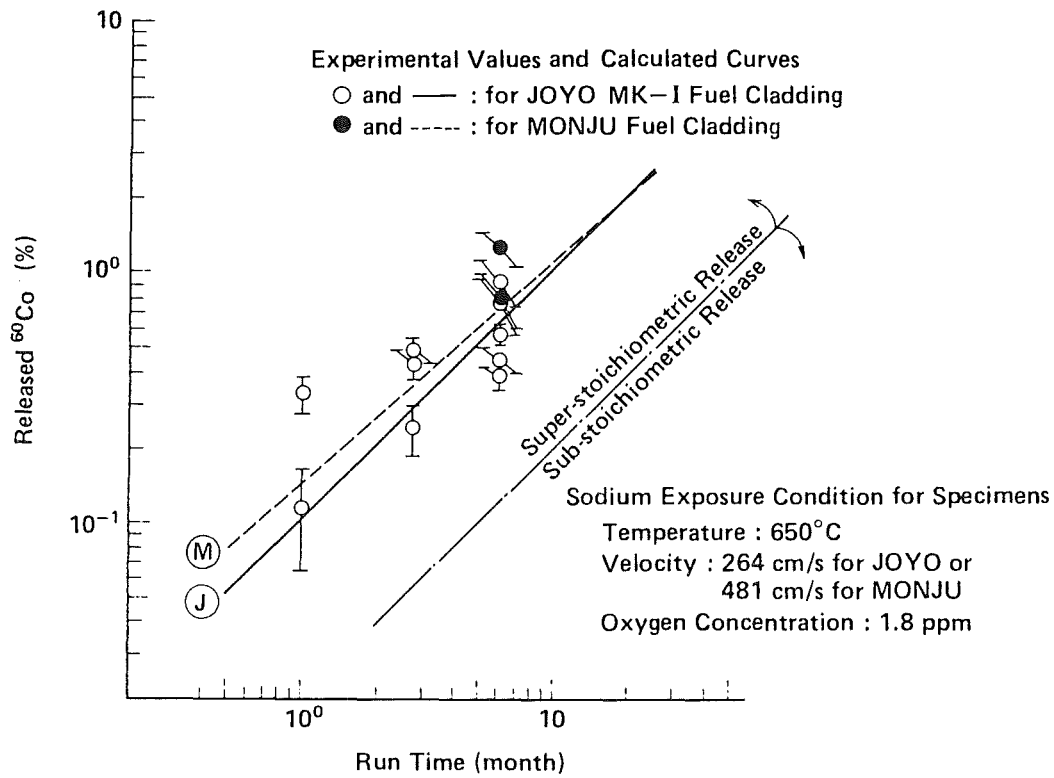


Fig. 8 Comparison between Experimental and Calculated Variation of Released  $^{60}\text{Co}$  with Sodium Exposure Time.

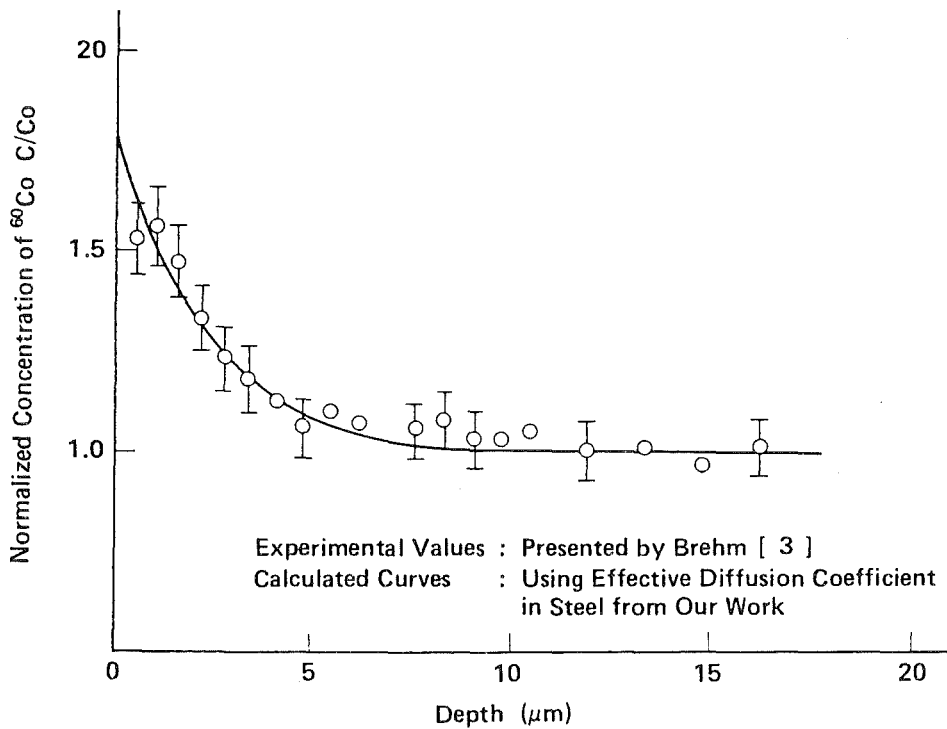


Fig. 10 Comparison between Experimental and Calculated Concentration Profile of  $^{60}\text{Co}$  in Type 316 Fuel Cladding Specimen for FFTF.

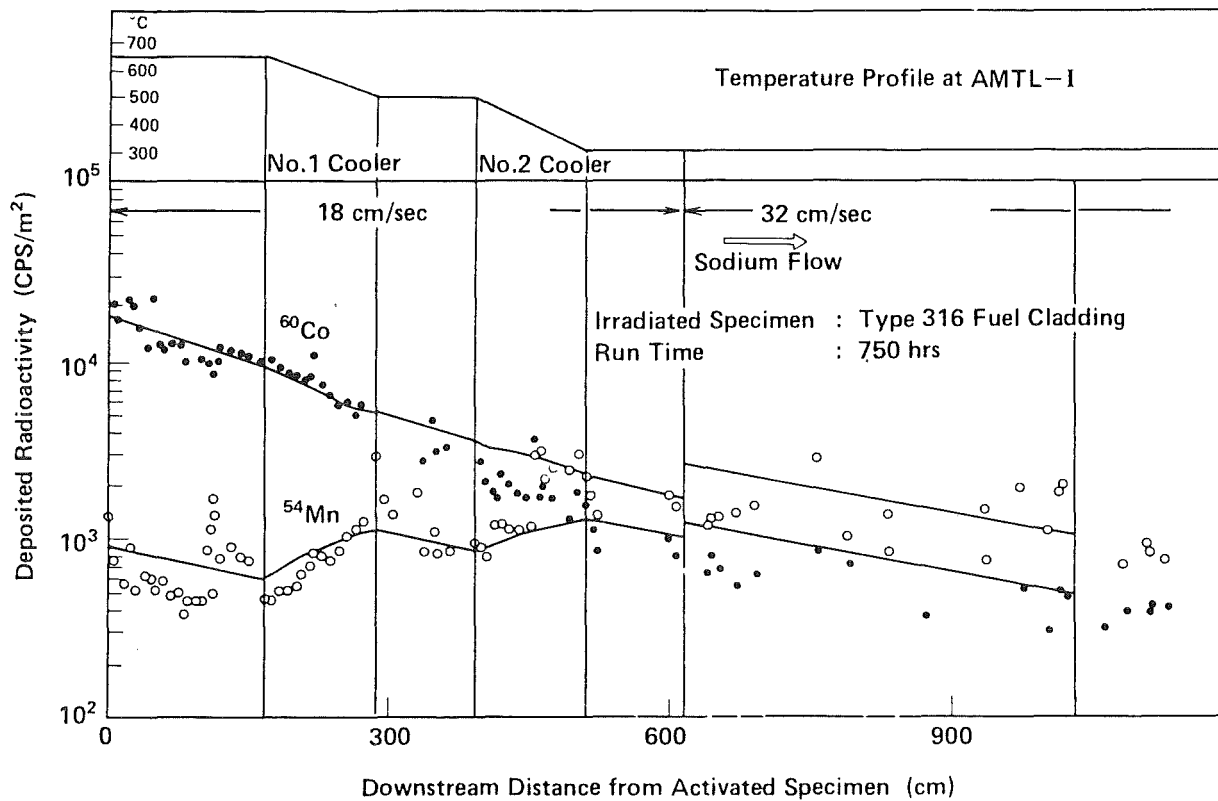


Fig. 11 Comparison between Experimental and Calculated Distribution of <sup>60</sup>Co and <sup>54</sup>Mn Deposits on Piping Wall throughout AMTL-I Main Flow Circuit.

to the order of magnitude lower solubility of cobalt in sodium, the escaping tendency of manganese observed in steel annealing, and the much lower concentration of cobalt than manganese in the steel.

Computer Code for Estimating Radioactive Corrosion Product Transfer in LMFBR Primary Circuits

The PSYCHE code can be applied to estimating radioactive CP transfer in LMFBR primary circuits and the resulting radiation fields exterior to piping and components for the general case of a loop type system. For the radiation field calculation the modified QAD-CG code is used. This code was improved from evaluating the JOYO data, which is named as JOANDARC (JOYO Active Nuclide Dose Assessment and Radiation Control). Fig. 12(a) and (b) shows the flowchart for stable or active CP transfer and radiation field calculation. The density of each deposited radioisotope at chosen coordinate points is converted to dose rate by using the JOANDARC code.

This code uses a data library consisting of conversion coefficient data relating the density of each radioisotope to its dose rate at a given position.

The procedure is to divide the calculating (i.e. operating) time interval into many smaller steps, during each of which the concentration of the species in the bulk sodium is assumed to be constant. The correlations tabulated in Table 1 are applied to each time step, and the resulting concentration is used as the initial value in the next step. In this manner a simple mass balance around the circuit is maintained, although not perfectly. This code is an improvement over previous approaches that use the zero concentration in sodium, overestimating release in both LMFBR primary circuits and experimental sodium loops. An inventory calculation of the species released or deposited in each time step at each region along the circuit is executed by

$$I_{nl} = I_{n-1,l} \exp(-\lambda(t-(n-1)\Delta t)) + J_{nl}(1-\exp(-\lambda(t-(n-1)\Delta t)))/\lambda \quad (22)$$

$$I_{0l} = \begin{cases} 0 & \text{for active release, or} \\ i_0 & \text{for active deposition, and stable release or deposition;} \\ t = 0 & \end{cases} \quad (23)$$

where  $I_{nl}$  ( $\text{Ci}/\text{cm}^2$ ) is release or deposition inventory in time step  $n$  at region  $l$ , and  $\Delta t$  is the step interval (s).

The calculation can be executed for the eight activated and seven parent stable isotopes shown in Table 2(a), and the ten nuclear reactions for production of the active species shown in Table 2(b). For the  $^{58}\text{Co}$  and  $^{181}\text{Ta}$ , the double neutron capture process is taken into consideration because of their very large capture cross sections. The mass transfer of each of the species in sodium is tentatively classified as manganese or cobalt type, as shown in Table 2(c)

Fig. 13 shows a typical LMFBR primary loop system, which primarily consists of core and heat transport systems, the latter including main and overflow (purification) systems. In the core region the expression for release with neutron activation is applied to either bulk corrosion or deposition, and in heat transport systems the expression for deposition is used. The maximum number of loops is applicable to four which are identical or not.

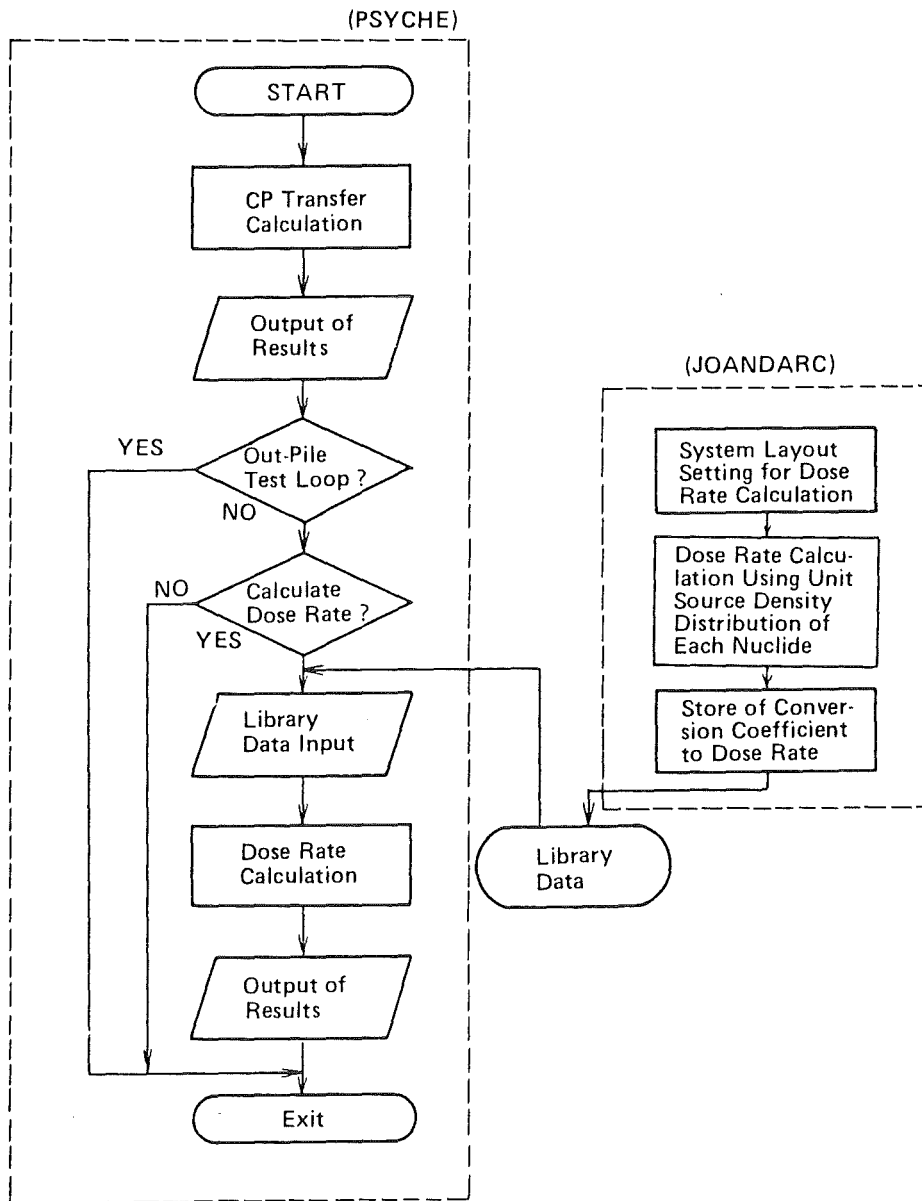


Fig. 12(a) Flowchart for Corrosion Product Transfer and Dose Rate Calculation.

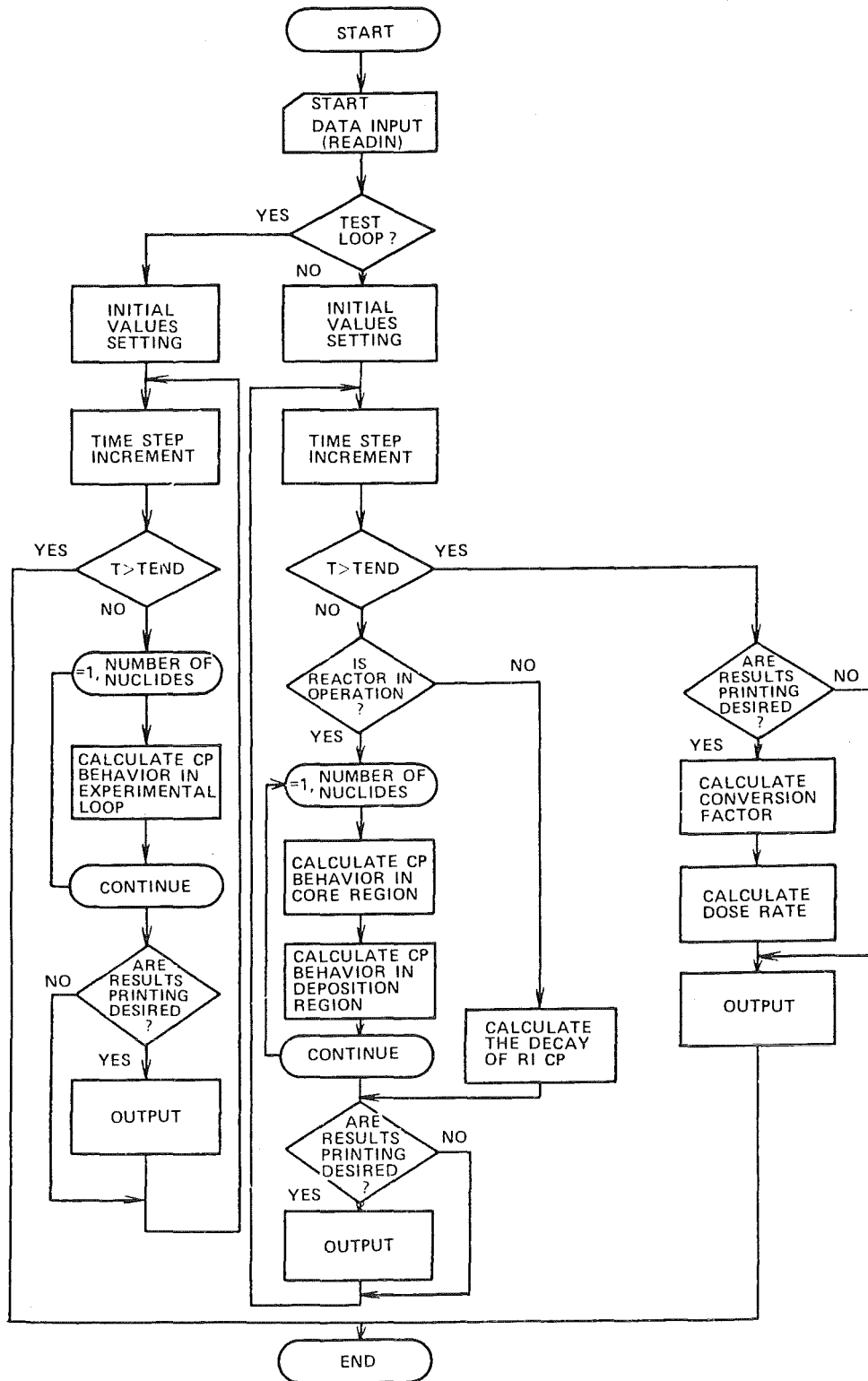


Fig. 12 (b) Flowchart for Corrosion Product Transfer Calculation (PSYCHE).

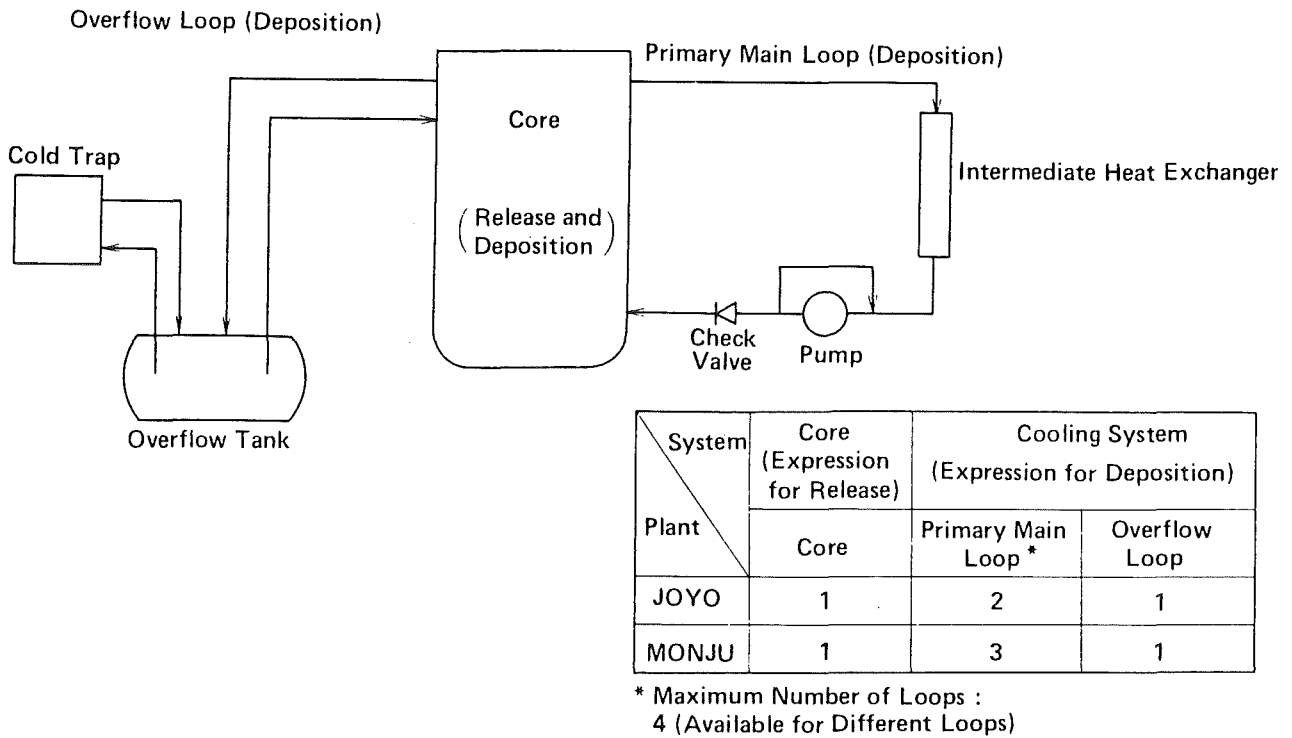


Fig. 13 Diagram of Typical LMFBR Primary System for Evaluating CP Transfer.

For calculating CP production and transfer, the core and heat transport system are divided into smaller regions in which conditions (i.e. region geometry, sodium temperature and flow, and neutron flux in core etc.) can be regarded as identical. The maximum number of regions is 200 for the core and 100 for the heat transport system. The geometry for each region is modelled as a cylinder, in which the sodium and material properties are regarded as constant.

The CP transfer calculation assumes constant reactor power during operation, and takes into consideration the radioactive decay of the active species during down time. This code is also applicable to the restart of a plant after a change such as that MK-1 to -II at JOYO. The effect of materials changed by refuelling can be taken into consideration through the periodic interval input data.

The calculation described above provides the following results :  
(a) the release inventory of the stable or active corrosion products, either total or for a region of interest in experimental sodium loops or LMFBR primary circuits, (b) the deposition distribution in the piping and components of the heat transport system, and in the core, (c) the concentration

profile in the structural or core materials, and (d) the concentration in sodium, etc..

The dose rate is given by

$$D_m = \sum_n \sum_{\ell} f_{n\ell} D_{n\ell m} \quad (24)$$

where  $D_m$  is the dose rate at position  $m$  (mR/h),  $D_{n\ell m}$  is the dose rate (mR/h) at point  $m$  from nuclide  $n$  of unit deposit density ( $1 \mu\text{Ci}/\text{cm}^2$ ) in region  $\ell$ , and  $f_{n\ell}$  is the deposit density of nuclide  $n$  in the source region  $\ell$  ( $\mu\text{Ci}/\text{cm}^2$ ).

The JOANDARC code uses the QAD-CG code as the starting point to evaluate the dose rate in three dimensions, and is based on the point kernel method. For improving the calculational accuracy, the following modifications are made ; (a) the geometrical modelling for the piping and components, and their layout is detailed considering their inter-arrangements, (b) the inter shielding effects between the components are taken into account, and (c) the contribution of each radioisotope and component as a contributor to the dose rate can be expressed in the output, etc.. Capo's polynomial expression for the Goldstein-Winkins values is applied as the buildup factor. The geometrical model for the active source and the positions of points for calculating the dose rate are expressed in Cartesian, cylindrical or polar coordinates. Shielding is composed of seven kinds of elemental structures, i.e. a rectangular parallelepiped, a right cylinder, a triangular piped etc. A complicated shielding structure can thus be simulated.

Using PSYCHE, the calculated values for radioactive CP distribution and the resulting radiation fields in the primary circuit of JOYO have been compared with those measured. It was found that the ratio of calculated/measured values was 0.5 to 2 for the  $^{54}\text{Mn}$  or  $^{60}\text{Co}$  deposits. These results are described in detail in the accompanying paper [12].

### Discussion and Conclusions

Theoretical expressions for a solution - precipitation model are given for release or deposition of corrosion product nuclides in LMFBR primary circuits and experimental sodium loops. The zero concentration assumption for release used by previous workers was improved by introducing a simple



mass balance throughout the circuit by a numerical procedure. The difference between the oxygen dependence of  $^{60}\text{Co}$  and  $^{54}\text{Mn}$  was including assuming that adsorbed oxygen at steel surfaces would activate the dissolution into sodium for weakly leached species, i.e. cobalt isotopes etc..

The parameters needed to predict radioactive CP transfer in LMFBR circuits were developed by fitting the model to the data from sodium loop experiments on active or stable manganese or  $^{60}\text{Co}$  transfer. The data included experimentally determined release rates from cladding, the concentration profile in the steel and the downstream effect for deposition, and the deposition distribution throughout loop. Comparison with experimental release or deposition data enabled the following conclusions to be drawn :

- (a) The effective diffusion coefficients for manganese or cobalt isotopes in type 304 or 316 steel derived from sodium loop experiments is an order of magnitude higher than those obtained from diffusion experiments. These higher values may result from unknown factors in our analysis ; e.g. the high deposition rate on the precipitated layer on the steel surface, and the partial or complete formation of a ferrite phase.
- (b) Analysis of the downstream effect in  $^{60}\text{Co}$  deposition confirmed the tentative suggestion of previous workers that the mechanism controlling  $^{60}\text{Co}$  transfer is diffusion through the boundary sublayer in the flowing sodium (i.e.  $K' \approx k'$ ). This explains why  $^{60}\text{Co}$  mass transfer is highly sensitive to sodium velocity and decreases with distance downstream. On the other hand, the  $^{54}\text{Mn}$  deposition measurements suggest that the controlling mechanism is probably an intermediate case between diffusion control in the liquid and reaction-control at the steel surface. As the sodium temperature or flow is increased, manganese transfer shifts toward control by reaction at the steel surface (i.e.  $K \approx k_p'$ ). Temperature of flow decrease moves the control toward diffusion in the liquid (i.e.  $K' \approx k'$ ).
- (c) In this model it is considered that the driving force for mass transfer is the difference between the interfacial concentration of the species of interest in the sodium and that in equilibrium with the steel surface,  $C_i/\beta$  or  $C_i/\beta'$ . Tendency for  $^{60}\text{Co}$  to be retained more strongly in the steel and to be more sensitive to the oxygen concentration than  $^{54}\text{Mn}$  is attributed to the higher chemical partition parameter for cobalt (oxygen dependent,  $\beta' = \beta/\theta'$ ), than for manganese (oxygen independent,  $\beta$ ). The chemical partition parameter for cobalt,  $\beta = \beta'\theta'$ , is higher by about

one order of magnitude than that for manganese.  $\beta'$  for cobalt (oxygen dependent) increases with a decrease in the oxygen concentration. In general, the chemical partition parameters for the species are related to their solubilities in sodium and their chemical affinities in the steel.

- (d) The super-stoichiometric release of  $^{54}\text{Mn}$  and sub-stoichiometric release of  $^{60}\text{Co}$  often observed in sodium loop experiments are interpreted as follows. In the equation for net release from steel surfaces undergoing

$$\text{bulk corrosion [eq.(1)], } J = D \left. \frac{\partial C}{\partial x} \right|_{x=0} + uC_i, \text{ for the super-stoichiometric}$$

release case,  $^{54}\text{Mn}$ , the first term at the right side (i.e. diffusion term) has high positive values (i.e. effusion from the interior of the steel), which may be primarily due to the low values of  $\beta$  for manganese. Low values of  $\beta$  are likely related to the relatively high solubility of Mn in sodium. The second term expresses release accompanying recession of the steel surfaces. For the sub-stoichiometric release case,  $^{60}\text{Co}$ , the diffusion term in eq.(1) has negative values, indicating diffusion of cobalt into the steel through the surface which is undergoing bulk corrosion. Consequently, the net release of  $^{60}\text{Co}$  can be smaller than the amount which accompanies recession of the steel surface. This effect is primarily due to the high values of  $\beta'$  for cobalt, which are likely related to its very low solubility in sodium.

- (e) The differences between the deposition behavior of  $^{54}\text{Mn}$  and  $^{60}\text{Co}$  often observed in sodium loop experiments are primarily due to differences in the overall mass transfer coefficients and chemical partition parameters for manganese and cobalt.  $^{60}\text{Co}$  deposition is controlled by diffusion through the boundary sublayer in the flowing sodium, because of the very high values of  $k_p'$ . In the equation for net deposition onto steel surfaces undergoing bulk deposition or corrosion [eq.(1) opposite in sign],

$$J = -D \left. \frac{\partial C}{\partial x} \right|_{x=0} \pm uC_i \text{ (the plus sign indicates bulk deposition and the}$$

minus sign bulk corrosion), for net deposition of  $^{60}\text{Co}$ , the diffusion term plays a very important role, particularly in the higher temperature region immediately downstream from the active source. Thus, the decrease in  $^{60}\text{Co}$  concentration in sodium downstream from the active source can become the most important factor affecting its deposition distribution, becoming predominate over the increase in bulk deposition at low temper-

atures. At high temperatures,  $^{54}\text{Mn}$  deposition is probably controlled by interfacial reaction, because values of  $k_p'$  for manganese are relatively small. The deposited manganese diffuses into the steel. The steel surface does, however, undergo bulk corrosion. At low temperatures, deposition is probably controlled by diffusion through the boundary sublayer in the flowing sodium and governed by bulk deposition. This phenomenon may explain why  $^{54}\text{Mn}$  deposition is often observed to increase at low temperatures.

- (f) The release of nuclides from steel is predicted to approach stoichiometric relationships asymptotically in experimental loops, but not necessarily in LMFBR cores. In the former case, the interfacial receding velocity for bulk corrosion,  $u_c$ , is obtained from the steady state corrosion rate. The rate of interface movement for bulk deposition,  $u_d$ , is an adjustable parameter which can be obtained by fitting model calculations to the available data for mass transfer in experimental loops and LMFBR primary circuits.

The computer code developed for a solution - precipitation model is named PSYCHE, and can be applied to estimating radioactive CP transfer and resulting radiation fields around piping and components in LMFBR circuits. The code consists of subprograms for the source term and for the radiation field calculations linked together.

#### Acknowledgement

This paper is published by permission of the Power Reactor and Nuclear Fuel Development Corporation. The authors gratefully acknowledge the leadership of N. Sekiguchi when this study was initiated at PNC Japan.

References

1. N. Sekiguchi, K. Iizawa, H. Atsumo, "Behaviour of Corrosion Product from Irradiated Stainless Steel in Flowing Sodium", Proc. Specialists' Meeting on Fission and Corrosion Product Behaviour in Primary Circuits of LMFBRs, Dmitrovgrad (1975) p.82.
2. W.F. Brehm, "Effect of Oxygen in Sodium upon Radionuclide Release from Austenitic Stainless Steel," *ibid.* (1975) p.186.
3. W.F. Brehm, L.E. Chulos, J.C. McGuire, A.C. Leaf, R.P. Colburn, "Techniques for Studying Corrosion and Deposition of Radioactive Materials in Sodium Loops", *Ibid.* (1975) p.172.
4. M.V. Polley, G. Skyrme, "An Analysis of Radioactive Corrosion Product Transfer in Sodium Loop Systems", *J. Nucl. Mtls.*, Vol.75 (1978) p.226.
5. W.L. Kuhn, "Activated Corrosion Product Radiation Levels in the FFTF Heat Transport System Cells and Closed Loop System Modules", HEDL-TME 76-10, September 1977.
6. F. Oberhettinger, L. Badii, *Tables of Laplace Transforms* (Springer-Verlag, New York Heidelberg Berlin, 1973).
7. A.F. Smith, "The diffusion of Chromium in Type 316 Stainless Steel", CEGB-report RD/B/N 2625, 1973, and A.F. Smith, R. Hales, "Diffusion of Manganese in Type 316 Austenitic Stainless Steel", CEGB-report RD/B/N 2756, 1973.
8. R.P. Anantatmula, J.M. Lutton, M.B. Hall, "Diffusion of Radionuclides in Type 304 and Type 316 Stainless Steels at 534°C", Private Communication, 1981.
9. I.H. Newson, K.T. Claxton, R.W. Dawson, P. Hawtin, "Studies of Radioactive Corrosion Product Release and Deposition in the Harwell Active Mass Transfer Loop", Second Int. Conf. on Liquid Metal Technology in Energy Production (CONF-800401-p2), Richland, 1980.
10. R.E. Treybal, *Mass Transfer Operations* (McGraw-Hill, New York, 1965).
11. A. Maruyama, S. Nomura, M. Kawai, S. Takani, Y. Ohta, H. Atsumo, "Recommended Equation for Corrosion Rate of Austenitic Stainless Steels in Liquid Sodium at Elevated Temperature", *J. of the Atomic Energy Soc. of Japan*, Vol.26, No.4 (1984) p.327.
12. K. Iizawa, S. Suzuki, M. Tamura, S. Seki, T. Hikichi, "Study on Radioactive Corrosion Products Behaviour in Primary Circuits of JOYO", Specialists' Meeting on Fission and Corrosion Products Behaviour in Primary Circuits of LMFBRs, Karlsruhe, 1987.

Table 1 Summary of Proposed Expressions for Analysis of Stable and Active Corrosion Product Transfer in Sodium Loop System

| C o s e                                       |   | Assumption for Steady Source in Sodium   | Concentration in Sodium<br>$C'(y)$ or $C'(y,0)$ , (ML <sup>-3</sup> )                           | Concentration in Steel<br>$C(x,y,t)$ , (ML <sup>-3</sup> )  | Mass Flux<br>$J(y,t)$ , (ML <sup>-2</sup> T <sup>-1</sup> ) |
|---|---|--|---|---|---|
| Release                                       | Stable Corrosion in Experimental Sodium Loop or LMFB Core             | $\frac{\partial C'(y,t)}{\partial t} = 0$  | * $\frac{C_0}{\beta} - \left\{ \frac{C_0}{\beta} - C'(0) \right\} e^{-\frac{4K'y}{v\delta}}$    | $C_0 + \left\{ \frac{K'}{D} C'(y) - hC_0 \right\} G(x,t)$   | $\frac{K'}{\beta} C(0,y,t) - K'C'(y)$                       |
|   | Active Corrosion in Experimental Sodium Loop                          | $\frac{\partial C'(y,t)}{\partial t} = -\lambda C'(y,t)$   | ** $\frac{C_0}{\beta} - \left\{ \frac{C_0}{\beta} - C'(0,0) \right\} e^{-\frac{4K'y}{v\delta}}$ | $\left[ C_0 + \left\{ \frac{K'}{D} C'(y,0) - hC_0 \right\} G(x,t) \right] e^{-\lambda t}$   | $\frac{K'}{\beta} C(0,y,t) - K'C'(y,0)$                     |
|   | Active Corrosion in LMFB Core   | $\frac{\partial C'(y,t)}{\partial t} = 0$  | * $\frac{C_0}{\beta} - \left\{ \frac{C_0}{\beta} - C'(0) \right\} e^{-\frac{4K'y}{v\delta}}$    | $C_0 e^{-\lambda t} + \frac{K'}{D} C'(y) F(x,t) - hC_0 e^{-\lambda t} G(x,t) + \frac{R}{\lambda} (1 - e^{-\lambda t}) - hRH(x,t)$ | $\frac{K'}{\beta} C(0,y,t) - K'C'(y)$                       |
| Characteristic Function                       | { upper sign :<br>bulk corrosion<br>lower sign :<br>bulk deposition } | $h = \frac{u}{D} \left( \frac{K'}{\beta u} + 1 \right)$ $F(x,t) = \frac{u \left( \frac{K'}{\beta u} + \frac{1}{2} \right) \sqrt{D(\lambda + u^2/4D)}}{2(Kh/\beta - \lambda)} \exp \left\{ \left( \sqrt{\frac{1}{D}(\lambda + u^2/4D)} + \frac{u}{2D} \right) x \right\} \operatorname{erfc} \left\{ \frac{x}{2\sqrt{Dt}} + \sqrt{(\lambda + u^2/4D)t} \right\} + \frac{u \left( \frac{K'}{\beta u} + \frac{1}{2} \right) \sqrt{D(\lambda + u^2/4D)}}{2(Kh/\beta - \lambda)} \exp \left\{ - \left( \sqrt{\frac{1}{D}(\lambda + u^2/4D)} + \frac{u}{2D} \right) x \right\} \operatorname{erfc} \left\{ \frac{x}{2\sqrt{Dt}} - \sqrt{(\lambda + u^2/4D)t} \right\}$ $- \frac{u \left( \frac{K'}{\beta u} + \frac{1}{2} \right)}{Kh/\beta - \lambda} \exp(-\lambda t + hx + \frac{Kht}{\beta}) \operatorname{erfc} \left\{ \frac{x}{2\sqrt{Dt}} + u \left( \frac{K'}{\beta u} + \frac{1}{2} \right) \sqrt{\frac{t}{D}} \right\}$ $G(x,t) = \frac{1}{2h} \operatorname{erfc} \left( \frac{x}{2\sqrt{Dt}} + \frac{u}{2\sqrt{D}} + \frac{D\beta'}{2K'} \exp \left( -\frac{ux}{D} \right) \right) \operatorname{erfc} \left( \frac{x}{2\sqrt{Dt}} - \frac{u}{2\sqrt{D}} \right) - \frac{\beta u}{Kh} \left( \frac{K'}{\beta u} + \frac{1}{2} \right) \exp \left( hx + \frac{Kht}{\beta} \right) \operatorname{erfc} \left\{ \frac{x}{2\sqrt{Dt}} + u \left( \frac{K'}{\beta u} + \frac{1}{2} \right) \sqrt{\frac{t}{D}} \right\}$ $H(x,t) = -\frac{1}{2\lambda h} e^{-\lambda t} \operatorname{erfc} \left( \frac{x}{2\sqrt{Dt}} + \frac{u}{2\sqrt{D}} \right) - \frac{\beta D}{2\lambda K'} \exp \left( -\lambda t + \frac{ux}{D} \right) \operatorname{erfc} \left( \frac{x}{2\sqrt{Dt}} + \frac{u}{2\sqrt{D}} \right)$ $+ \frac{u \left( \frac{K'}{\beta u} + \frac{1}{2} \right) \sqrt{D(\lambda + u^2/4D)}}{2\lambda(Kh/\beta - \lambda)} \exp \left\{ \left( \sqrt{\frac{1}{D}(\lambda + u^2/4D)} + \frac{u}{2D} \right) x \right\} \operatorname{erfc} \left\{ \frac{x}{2\sqrt{Dt}} + \sqrt{(\lambda + u^2/4D)t} \right\} + \frac{u \left( \frac{K'}{\beta u} + \frac{1}{2} \right) \sqrt{D(\lambda + u^2/4D)}}{2\lambda(Kh/\beta - \lambda)} \exp \left\{ - \left( \sqrt{\frac{1}{D}(\lambda + u^2/4D)} + \frac{u}{2D} \right) x \right\} \operatorname{erfc} \left\{ \frac{x}{2\sqrt{Dt}} - \sqrt{(\lambda + u^2/4D)t} \right\}$ $+ \frac{\beta u \left( \frac{K'}{\beta u} + \frac{1}{2} \right)}{(Kh/\beta - \lambda) \left( \pm u - K'/\beta' \right)} \exp \left( -\lambda t + hx + \frac{Kht}{\beta} \right) \operatorname{erfc} \left\{ \frac{x}{2\sqrt{Dt}} + u \left( \frac{K'}{\beta u} + \frac{1}{2} \right) \sqrt{\frac{t}{D}} \right\}$ |   |   |   |
|   |   | Stable Deposition in Experimental Sodium Loop or LMFB Primary Circuits   | $\frac{\partial C'(y,t)}{\partial t} = 0$   | * $\frac{C_0}{\beta'} + \left\{ C'(0) - \frac{C_0}{\beta'} \right\} e^{-\frac{4K'y}{v\delta}}$                                    | $C_0 + \left\{ \frac{K'}{D} C'(y) - hC_0 \right\} S(x,t)$   |
| Active Deposition in Experimental Sodium Loop | $\frac{\partial C'(y,t)}{\partial t} = -\lambda C'(y,t)$              | ** $C'(0,0) e^{-\frac{4K'y}{v\delta}}$   | $K'C'(y,0) T(x,t) e^{-\lambda t}$   | $K'\eta(t) C'(y,0) e^{-\lambda t}$<br>where, $\eta(t) = 1 - \frac{K'}{\beta} T(0,t)$  |   |
| Active Deposition in LMFB Primary Circuits    | $\frac{\partial C'(y,t)}{\partial t} = 0$                             | * $C'(0) e^{-\frac{4K'y}{v\delta}}$  | $K'C(y) U(x,t)$   | $K'\chi(t) C'(y)$<br>where, $\chi(t) = 1 - \frac{K'}{\beta} U(0,t)$   |   |
| Deposition                                    | { upper sign :<br>bulk corrosion<br>lower sign :<br>bulk deposition } | $h = \frac{u}{D} \left( \frac{K'}{\beta u} - 1 \right)$ $S(x,t) = \frac{1}{2u \left( \frac{K'}{\beta u} + 0 \right)} \exp \left[ + \frac{ux}{D} \right] \operatorname{erfc} \left( \frac{x}{2\sqrt{Dt}} + \frac{u}{2\sqrt{D}} \right) + \frac{1}{2u \left( \frac{K'}{\beta u} - 0 \right)} \exp \left[ - \frac{ux}{D} \right] \operatorname{erfc} \left( \frac{x}{2\sqrt{Dt}} - \frac{u}{2\sqrt{D}} \right) - \frac{K' - 1}{\beta u + 2} \exp \left( hx + \frac{Kht}{\beta} \right) \operatorname{erfc} \left\{ \frac{x}{2\sqrt{Dt}} + u \left( \frac{K'}{\beta u} + 2 \right) \sqrt{\frac{t}{D}} \right\}$ $T(x,t) = \frac{1}{2u \left( \frac{K'}{\beta u} + 0 \right)} \exp \left[ + \frac{ux}{D} \right] \operatorname{erfc} \left( \frac{x}{2\sqrt{Dt}} + \frac{u}{2\sqrt{D}} \right) + \frac{1}{2u \left( \frac{K'}{\beta u} - 0 \right)} \exp \left[ - \frac{ux}{D} \right] \operatorname{erfc} \left( \frac{x}{2\sqrt{Dt}} - \frac{u}{2\sqrt{D}} \right)$ $- \frac{K' - 1}{u \left( \frac{K'}{\beta u} + 0 \right) \left( \frac{K'}{\beta u} + 1 \right)} \exp \left\{ \frac{ux}{D} \left( \frac{K'}{\beta u} + 1 \right) + \frac{u^2 t}{D} \left( \frac{K'}{\beta u} - 0 \right) \left( \frac{K'}{\beta u} - 1 \right) \right\} \operatorname{erfc} \left\{ \frac{x}{2\sqrt{Dt}} + u \left( \frac{K'}{\beta u} + 2 \right) \sqrt{\frac{t}{D}} \right\}$ $U(x,t) = \frac{u \left( \frac{K'}{\beta u} + 2 \right) \sqrt{D(\lambda + u^2/4D)}}{2 \left( -\frac{Kh}{\beta} - \lambda \right)} \exp \left\{ \left[ \left( \sqrt{\frac{1}{D}(\lambda + u^2/4D)} + \frac{u}{2D} \right) x \right] \right\} \operatorname{erfc} \left\{ \frac{x}{2\sqrt{Dt}} + \sqrt{(\lambda + u^2/4D)t} \right\} + \frac{u \left( \frac{K'}{\beta u} + 2 \right) \sqrt{D(\lambda + u^2/4D)}}{2 \left( \frac{Kh}{\beta} - \lambda \right)} \exp \left\{ - \left[ \left( \sqrt{\frac{1}{D}(\lambda + u^2/4D)} + \frac{u}{2D} \right) x \right] \right\} \operatorname{erfc} \left\{ \frac{x}{2\sqrt{Dt}} - \sqrt{(\lambda + u^2/4D)t} \right\}$ $- \frac{u \left( \frac{K'}{\beta u} + 2 \right)}{Kh/\beta - \lambda} \exp \left\{ -\lambda t + \frac{ux}{D} \left( \frac{K'}{\beta u} + 1 \right) + \frac{u^2 t}{D} \left( \frac{K'}{\beta u} - 0 \right) \left( \frac{K'}{\beta u} - 1 \right) \right\} \operatorname{erfc} \left\{ \frac{x}{2\sqrt{Dt}} + u \left( \frac{K'}{\beta u} + 2 \right) \sqrt{\frac{t}{D}} \right\}$  |   |   |   |

Nomenclature: D: Diffusion Coefficient in Steel (L<sup>2</sup>T<sup>-1</sup>), K': Overall Mass Transfer Coefficient (LT<sup>-1</sup>), β': Chemical Partition Parameter (β or β/θ'; θ' Dimensionless Oxygen Concentration in Sodium)  
 u: Interfacial Velocity (Bulk Corrosion or Deposition Rate) (LT<sup>-1</sup>), C'(0) or C'(0,0) Concentration of Stable or Active Species in Sodium at Zero Downstream Position (ML<sup>-3</sup>)  
 λ: Decay Constant (T<sup>-1</sup>), R: Radioisotope Production Rate in Core Materials (ML<sup>-3</sup>T<sup>-1</sup>)

Table 2(a) Analyzing Stable or Active Nuclides in PSYCHE Code

(Stable Nuclide)

| I.D. | Nuclide           |
|------|-------------------|
| 1    | $^{50}\text{Cr}$  |
| 2    | $^{54}\text{Fe}$  |
| 3    | $^{58}\text{Fe}$  |
| 4    | $^{58}\text{Ni}$  |
| 5    | $^{60}\text{Ni}$  |
| 6    | $^{59}\text{Co}$  |
| 7    | $^{181}\text{Ta}$ |

(Active Nuclide)

| I.D. | Nuclide           |
|------|-------------------|
| 1    | $^{51}\text{Cr}$  |
| 2    | $^{54}\text{Mn}$  |
| 3    | $^{55}\text{Fe}$  |
| 4    | $^{59}\text{Fe}$  |
| 5    | $^{58}\text{Co}$  |
| 6    | $^{60}\text{Co}$  |
| 7    | $^{59}\text{Ni}$  |
| 8    | $^{182}\text{Ta}$ |

Table 2(b) Nuclear Reactions for Active Nuclide Production:

| I.D. | Nuclear Reaction  |
|------|---|
| 1    | $^{50}\text{Cr} (n, \gamma) ^{51}\text{Cr}$                               |
| 2    | $^{54}\text{Fe} (n, \alpha) ^{51}\text{Cr}$                               |
| 3    | $^{54}\text{Fe} (n, p) ^{54}\text{Mn}$                                    |
| 4    | $^{54}\text{Fe} (n, \gamma) ^{55}\text{Fe}$                               |
| 5    | $^{58}\text{Fe} (n, \gamma) ^{59}\text{Fe}$                               |
| 6    | $^{58}\text{Ni} (n, p) ^{58}\text{Co} (n, \gamma) ^{59}\text{Co}$         |
| 7    | $^{59}\text{Co} (n, \gamma) ^{60}\text{Co}$                               |
| 8    | $^{60}\text{Ni} (n, p) ^{60}\text{Co}$                                    |
| 9    | $^{58}\text{Ni} (n, \gamma) ^{59}\text{Ni}$                               |
| 10   | $^{181}\text{Ta} (n, \gamma) ^{182}\text{Ta} (n, \gamma) ^{183}\text{Ta}$ |

Table 2(c) Category for Mass Transfer in Sodium Loop System

| Species* | Chemical Partition Parameter | Overall Mass Transfer Coefficient              |
|----------|------------------------------|--|
| Mn       | $\beta^{**}$                 | $K' = \frac{k'k_p^{**}}{k+k_p}, (k' \sim k_p)$ |
| Ni       |                              |  |
| Ta       |                              |  |
| Co       | $\beta'^{***}$               | $K \approx k'^{***}, (k' \ll k_p)$             |
| Fe       |                              |  |
| Cr       |                              |  |

\* for Either Stable or Active

\*\* Manganese Type

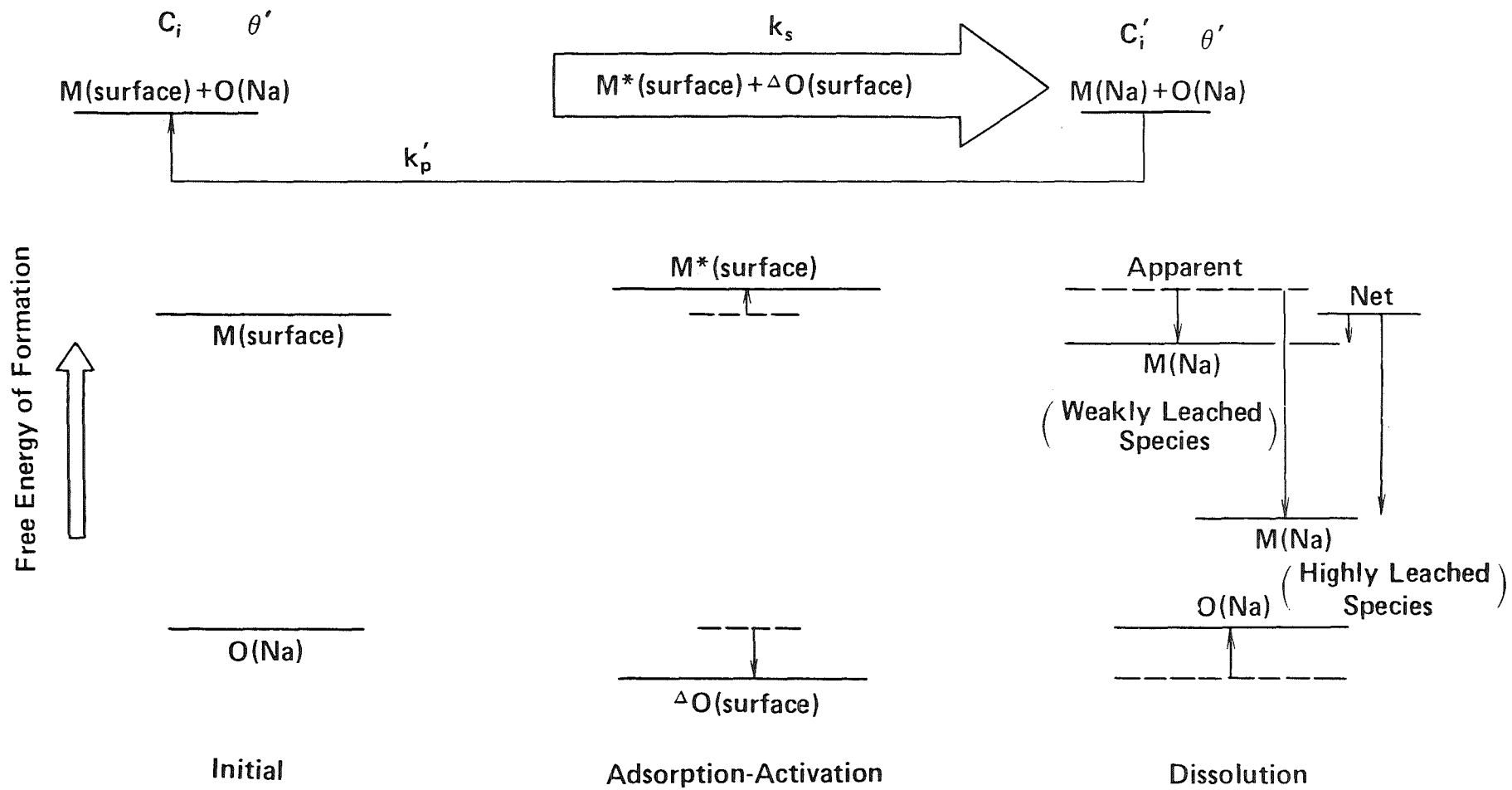
\*\*\* Cobalt Type

## Summary of Model Parameters

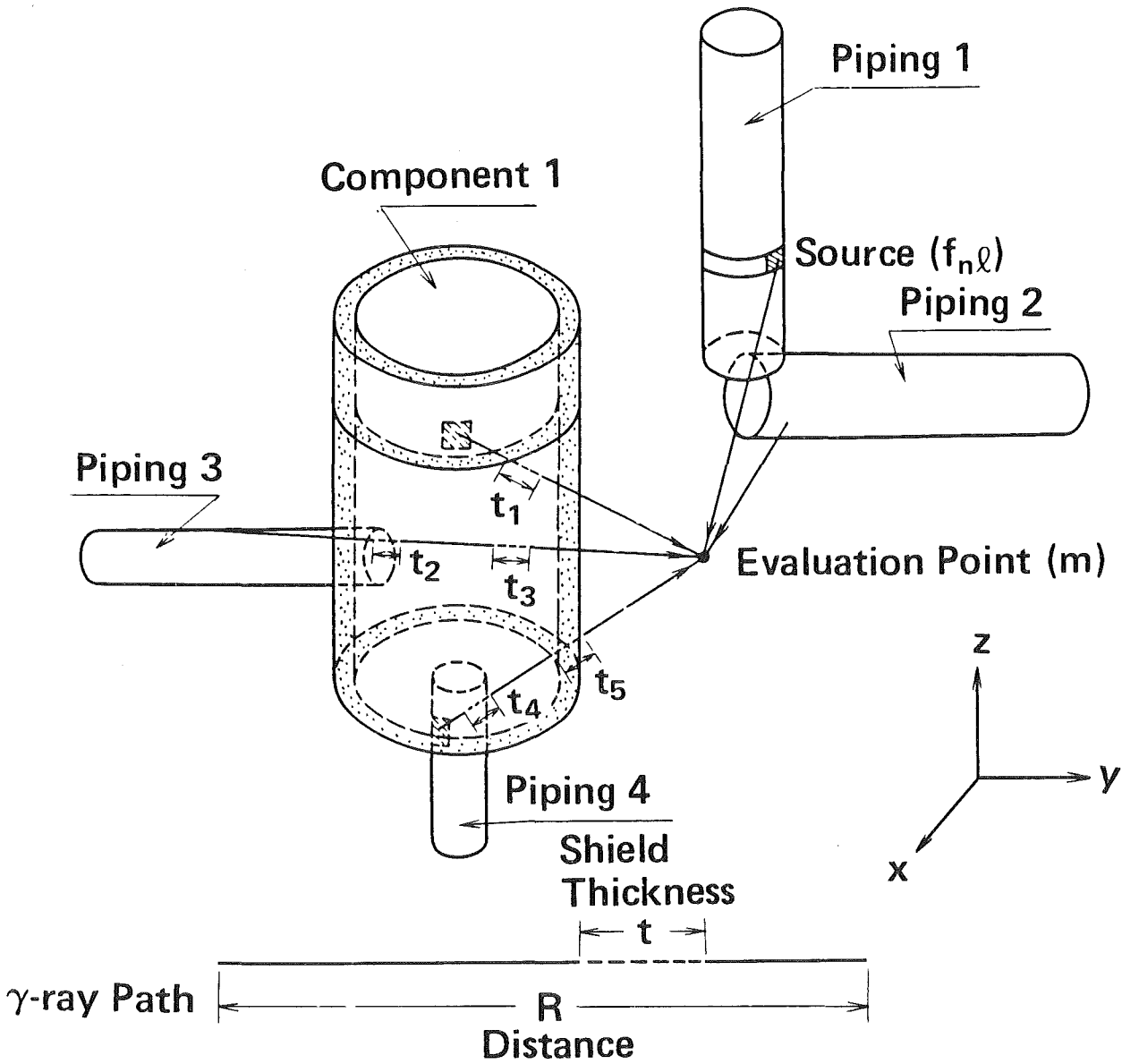
| Symbol<br>(unit)          | Nomenclature  | Expression   |
|---------------------------|---|--|
| D<br>(cm <sup>2</sup> /s) | Effective Diffusion Coefficient in Steel  | $D = 1.32 \times 10^{-4} \exp\left(-\frac{42.1}{RT}\right)$  |
| u<br>(cm/s)               | Interfacial Velocity for Bulk Corrosion (u <sub>c</sub> ) or Deposition (u <sub>d</sub> ) | $u_c = 3.17 \times 10^{-12} \cdot O_X'^{0.803}$ $\times \exp\left(12.63 - \frac{22.0}{RT} - 0.00591 \frac{L}{d}\right)$ $u_d = 3.17 \times 10^{-14} \times 4.02 \exp\left(\frac{2.29}{RT}\right)$                                      |
| β or<br>β' = β/θ'         | Chemical Partition Parameter  | for Manganese Type<br>$\beta = 1.58 \times 10^8 \exp(2.13/RT)$ for Cobalt Type<br>$\beta' \theta' = 9.93 \times 10^9 \exp(1.69/RT), \theta' = X'/12$   |
| K'<br>(cm/s)              | Overall Mass Transfer Coefficient   | for Manganese Type<br>$K' = \frac{k', k'_p}{k' + k'_p}$ $k'_p = 5.05 \times 10^{-3} \exp(3.46/RT)$ for Cobalt Type<br>$K' \simeq k = 0.023 \text{Re}^{0.83} \text{Sc}^{\frac{1}{3}} D'/d$ $D' = 5.1 \times 10^{-4} \exp(-0.032/K_B T)$ |

where,  $R = 1.987 \times 10^{-3}$  Kcals/deg·mol and  $K_B = 8.617 \times 10^{-5}$  eV/deg





## Oxygen Adsorption-Metal Activation Hypothesis



$$D_m = \sum_n \sum_{\ell} f_{n\ell} D_{n\ell m} \quad (24)$$

$$D_{n\ell m} = K_n \frac{B_n e^{-\mu_n t_{\ell m}}}{4\pi R_{\ell m}^2} \quad (25)$$

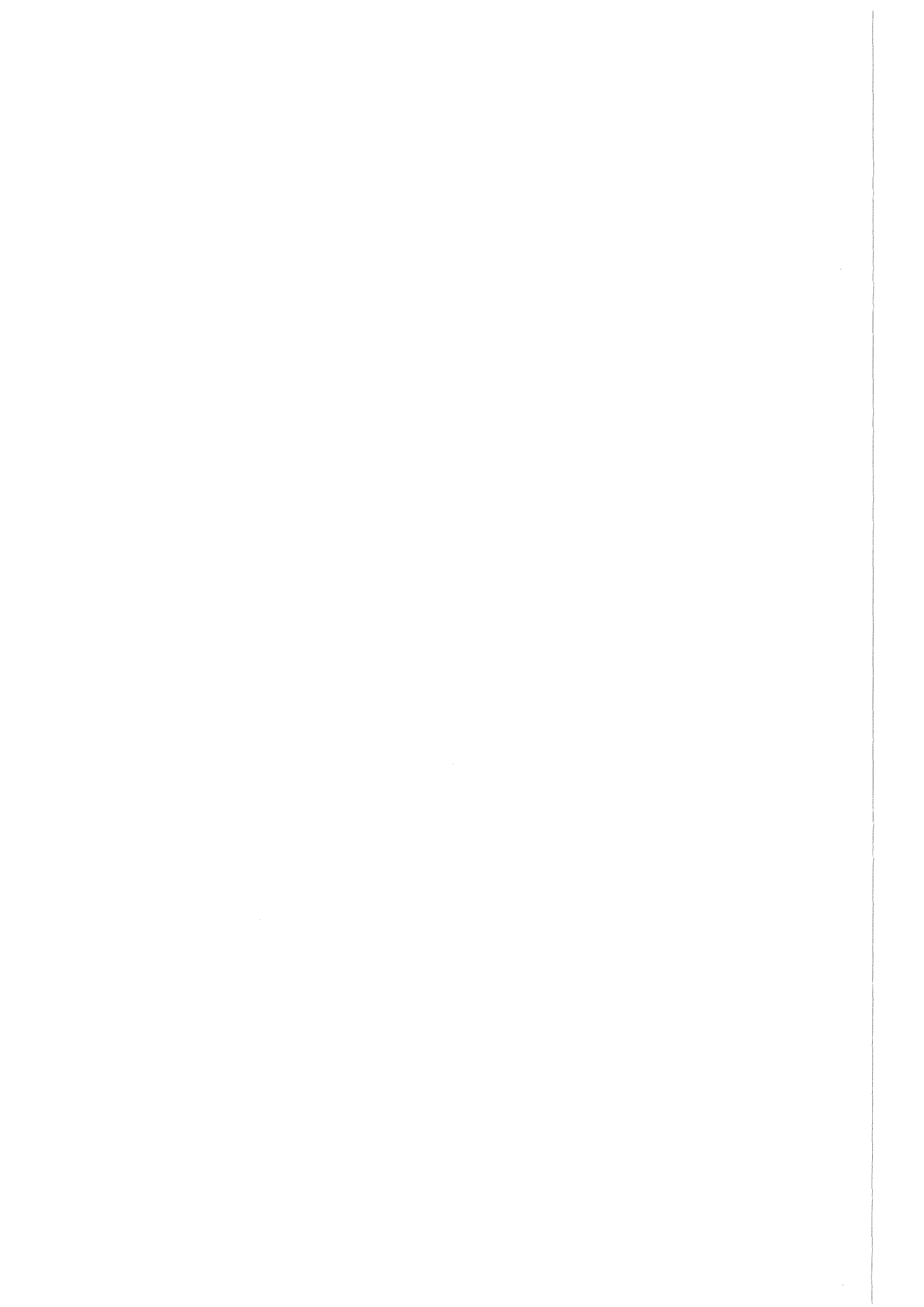
$\mu_n$  = Absorption Coefficient

$B_n$  = Buildup Factor

$K_n$  = Conversion Factor

$f_{ne}$  = Deposit Density

## Dose Rate Calculation Model



## Study on Radioactive Corrosion Products Behaviour in Primary Circuits of JOYO

Katsuyuki Iizawa\*, Soju Suzuki\*, Masaaki Tamura\*  
Seiichi Seki\* and Takayoshi Hikichi\*\*

\* O-arai Engineering Center,  
Power Reactor and Nuclear Fuel Development Corporation,  
4002 Narita-cho, O-arai-machi, Higashi Ibaraki-gun,  
Ibaraki-ken, 311-13 Japan

\*\* Energy Research Laboratory, Hitachi, Ltd.,  
1168 Moriyama-cho, Hitachi-shi, Ibaraki-ken, 316 Japan

Abstract

In the drained primary system of an LMFBR, CP radionuclides are the main radioactive sources during normal operation with no breached fuel. They therefore are of great importance in maintenance and repair operations in the plant which involve primary circuit components and piping, and in sodium removal and liquid waste processing facilities.  $^{54}\text{Mn}$  is found to be the dominant radionuclide in the primary circuit components and piping of a sodium-cooled fast breeder reactor ; in JOYO the radioactivities of  $^{54}\text{Mn}$  deposits were ten times more than those of  $^{60}\text{Co}$  deposits,  $^{58}\text{Co}$  being detected in very small quantities, in the out-of-reactor primary circuits. On the other hand,  $^{60}\text{Co}$  and  $^{58}\text{Co}$  were found to be the dominant radionuclides, followed by  $^{51}\text{Cr}$  and  $^{54}\text{Mn}$ , in the liquid waste from the washing of fuel assemblies following refuelling operations in JOYO.

Radioactive CP deposition and distribution, and the resulting radiation fields along the JOYO primary circuit piping have been measured. The measurement results have been compared with calculations for estimating radioactive CP behaviour and the resulting radiation fields in an LMFBR primary circuit using a computer code which is named PSYCHE. The deposited radioactivity of CPs calculated by using PSYCHE agreed well with the measured results within a factor of 0.5 ~ 2. The gamma dose rate distribution calculated from the PSYCHE results reproduced measured values within a factor of 0.6 ~ 2 over the piping system, using the JOANDARC modification of the QAD-CG code. Using these verified codes, a prediction of radiation levels for future plant operation, and an evaluation of methods for the reduction of radioactive CPs have been conducted. Consequently, it was predicted that the radiation levels will be 70 to 120 mR/hr near the primary circuit piping after  $10^5$  MWd of cumulative reactor output for JOYO, and that the most promising control measure is the installation of CP traps containing a specific getter for  $^{54}\text{Mn}$ , i.e. pure nickel, inside reactor fuel assemblies.

## Introduction

During normal operation of a sodium-cooled fast breeder reactor, activation products like activated sodium, radioactive CPs, and tritium are released into the primary coolant. The transport and deposition of radioactive CPs in particular builds up radiation fields near the primary circuit piping and components. The radiation complicates maintenance and repair work, and contributes significantly to the radiation burden of plant personnel. The development of methods to estimate and control the release and deposition of radionuclides, and radiation fields they cause, will contribute to reducing downtime and expense for maintenance and repairs, exposure of personnel to radiation, and plant operating costs.

R & D work and plant examination have been conducted at the PNC experimental fast reactor JOYO to develop methods to estimate the release and deposition of radioactive CPs, and the radiation fields they cause in primary circuit piping and components of an LMFBR. Our first effort was to characterize radioactive CP behaviour in order to estimate the radiation fields and evaluate potential control methods, and to verify the behaviour model and code for calculating radioactive CP transfer in LMFBR primary circuits and the radiation fields due to them. The model and code are called the solution-precipitation model and PSYCHE, respectively, and are described in the accompanying paper [1]. This program was named the "ALPHABET" program, based on its organization, which consists of Admistration and four working groups, i.e. Behaviour Analysis, Control, Decontamination and Elimination working groups. This paper gives some information obtained from the measurement and analysis of radioactive CP deposits, and the radiation fields due to them in the primary sodium circuit piping and components of JOYO. Additional information obtained from the characterization of radioactive CPs observed in sodium removal equipment, from fuel assemblies, or from other sodium components is referred to in this paper.

The most important corrosion product radionuclides are  $^{54}\text{Mn}$  and  $^{60}\text{Co}$ . These are the main contributors to radiation fields in the vicinity of primary circuit piping and components. Other observed radionuclides are  $^{58}\text{Co}$ ,  $^{51}\text{Cr}$ ,  $^{59}\text{Fe}$ ,  $^{182}\text{Ta}$ ,  $^{110\text{m}}\text{Ag}$ , and  $^{65}\text{Zn}$  etc.. These radionuclides are produced in fast reactor cores by  $(n, \gamma)$  and  $(n, p)$  reactions on the constituents and impurities in the stainless steel in fuel cladding and subassembly wrappers, a small but significant fraction of the radionuclides is released by corrosion (i.e. surface loss) of the activated core materials

and by solid diffusion of nuclides out of the materials into the circulating sodium. The released radionuclides transfer with the sodium and deposit in the primary piping and components, and in core assemblies.

In the primary sodium systems of JOYO, radionuclide deposition and distribution in the piping, and the resulting radiation fields near the piping and components have been measured. To date, in the primary sodium circuits of JOYO with the sodium drained into the dump tank, only  $^{54}\text{Mn}$  and  $^{60}\text{Co}$  have been found in significant quantities, and  $^{58}\text{Co}$  in very small amount. This is a surprising observation, since  $^{58}\text{Co}$  should be the activated radionuclide produced in the greatest quantity in the fuel cladding in fast cores. Average radiation levels of up to 70 mR/hr have been measured in the cells. No fission products have been found, since no significant operation with breached fuel has yet occurred.

The measurement results have been compared with calculations for estimating radioactive CP behaviour and the resulting radiation fields in an LMFBR primary circuit using a computer code which is named PSYCHE [1]. The comparison makes it possible to verify the analytical method and the accuracy of the calculations. The deposited activities of radioactive CPs calculated by using PSYCHE agreed well with the measured results, within a factor of 0.5 ~ 2. The gamma dose rate distribution calculated with PSYCHE was reproduced successfully, within a factor of 0.6 ~ 2, over the piping system, using JOANDARC, which is a modification of the QAD-CG code. Using the verified code, PSYCHE, estimations of conditions during future operation of JOYO and MONJU, and the examination of methods for reducing the amount of radioactive CPs have been conducted.

#### Characterization of Radioactive Corrosion Products in JOYO

Radioactive CPs are produced, transported, and deposited in the plant systems of an LMFBR as shown schematically in Fig. 1. A wide variety of radioactive CPs are released from reactor cores to out-of-reactor primary sodium systems. The most prevalent nuclides are  $^{54}\text{Mn}$  and  $^{60}\text{Co}$ .  $^{54}\text{Mn}$  is particularly interesting, since the activity of deposited  $^{54}\text{Mn}$  is about ten times higher than that of  $^{60}\text{Co}$ , and  $^{54}\text{Mn}$  migrates throughout the primary circuits.  $^{58}\text{Co}$  is found in very small quantities in the out-of-reactor primary sodium circuits of JOYO, notwithstanding it should be the most prevalent activated species in fuel cladding. This apparent anomaly probably

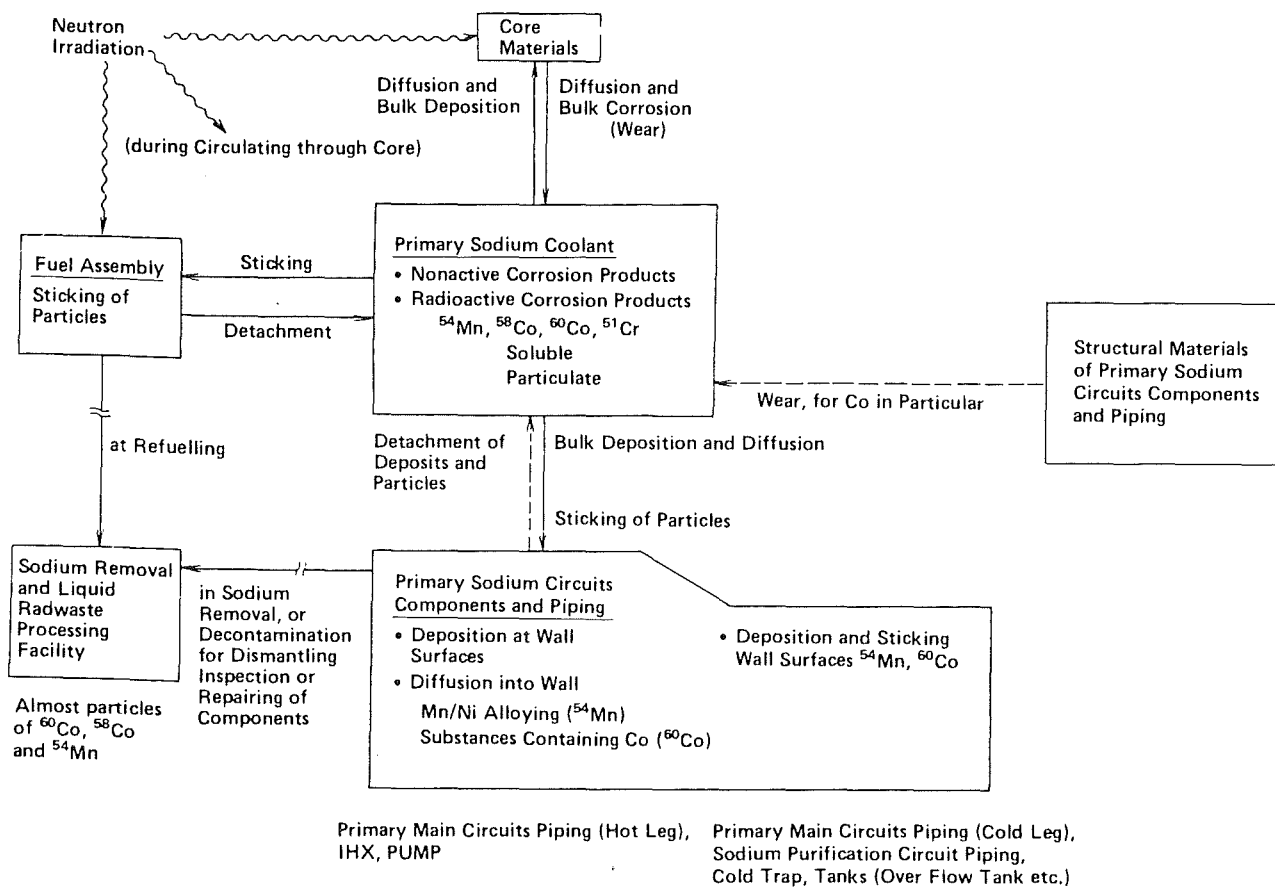


Fig. 1 Radioactive Corrosion Products Behaviour in Primary Circuits of LMFBRs.

results from the combination of the following three phenomena. First, the depletion of the target nuclide ( $^{58}\text{Ni}$ ) for the  $^{58}\text{Ni}(n, p)^{58}\text{Co}$  reaction by the selective leaching of nickel from the fuel cladding by the sodium. Second, the tendency for  $^{58}\text{Co}$  to deposit on core subassembly surfaces. This isotope is produced mostly in the central region of the core ( $^{60}\text{Co}$  is produced more generally throughout the core). Because cobalt generally deposits only a short distance downstream from the release site, a large fraction of the  $^{58}\text{Co}$  never leaves the core region. Third, the burn-up of  $^{58}\text{Co}$  before it leaves the neutron field, to produce  $^{59}\text{Co}$ . The cross sections for this latter process,  $^{58}\text{Co}(n, \gamma)^{59}\text{Co}$ , are large, 1900 b and 7000 b for thermal neutron capture  $\sigma_{\gamma}$  and resonance integral  $I_{\gamma}$ , respectively.

$^{182}\text{Ta}$  is produced from the Ta impurity in the minor-alloying element Nb in fuel cladding.  $^{110\text{m}}\text{Ag}$  and  $^{65}\text{Zn}$  are produced from the trace impurities Ag and Zn in core and structural materials. These metals are quite soluble in the liquid sodium, so they are drained with the sodium into the dump tank. They have never been detected in the sodium-drained piping and components of JOYO, but have been found in sodium samples.



Some information on radioactive CPs in a sodium-cooled fast reactor was obtained from investigating the radioactivity in the liquid waste produced during sodium removal from fuel assemblies and sodium components. The dominant radioactive sources are corrosion products. Of these radioactive CPs,  $^{60}\text{Co}$ ,  $^{58}\text{Co}$ ,  $^{54}\text{Mn}$  and  $^{51}\text{Cr}$  are the most prevalent, in the form of small, insoluble particles. They are removed from the surface of fuel cladding or sodium components into the water during sodium removal. For the case of JOYO,  $^{60}\text{Co}$ ,  $^{58}\text{Co}$  and  $^{51}\text{Cr}$  were more prevalent than  $^{54}\text{Mn}$  in the liquid waste produced from washing fuel assemblies. Conversely,  $^{54}\text{Mn}$  was more prevalent than  $^{60}\text{Co}$ ,  $^{51}\text{Cr}$  and  $^{58}\text{Co}$  in the waste from washing the main pump internals, as shown in Table 3. For the latter case,  $^{58}\text{Co}$  was a very small fraction, in agreement with the observation in the out-of-reactor primary circuit piping.

It can be seen that the driving force for mass transfer of the constituent elements of steel, or their radionuclides, between steel and sodium is the difference between the concentration in the sodium at the interface

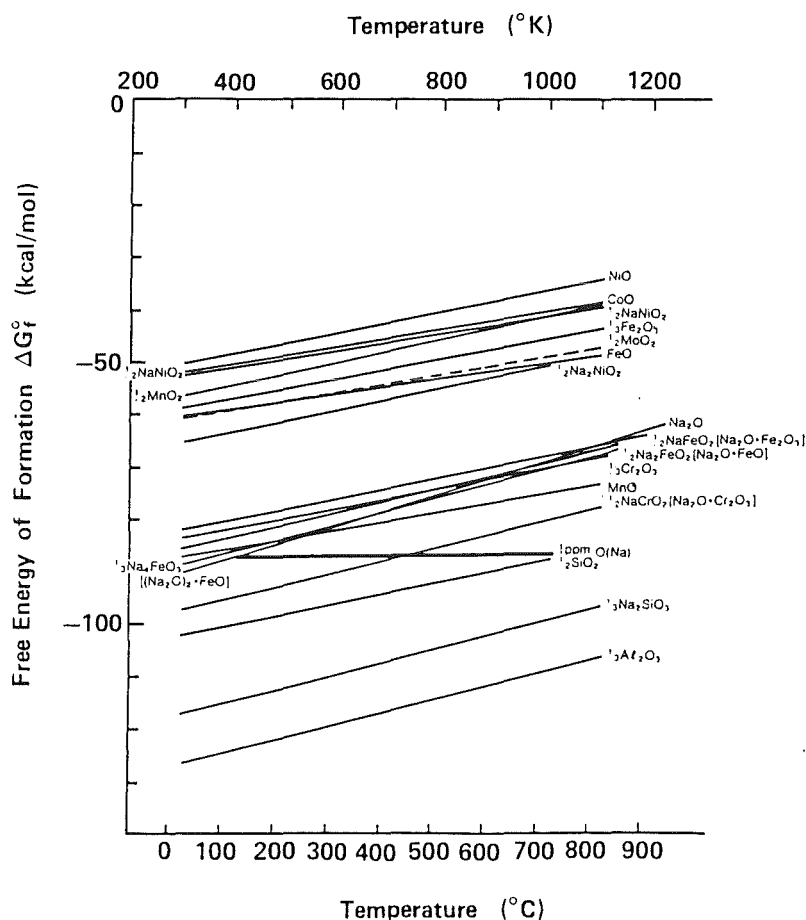


Fig. 2 Free Energy of Formation of Transition Metal Oxides

and that in equilibrium with the system wall surfaces (base metals or deposits). Fig. 2 [2] shows that transition metal oxides or double oxides with sodium are unstable in cold-trapped sodium. Therefore the corrosion product species in the sodium must be in the form of atomic or molecular species other than the oxides or double oxides. Unfortunately we have not yet determined their chemical forms. However apparently manganese is largely incorporated in nickel-manganese rich species [3]. The solubility curves in sodium are shown for Ni, Mn, Co, Fe and Cr in Fig. 3 [4]. The solubility curve for manganese is similar to that for nickel, while that for cobalt is an order of magnitude below manganese or nickel. The observations above could give the background for explaining why manganese isotopes are released more freely than cobalt isotopes from steel. A direct explanation is not obvious, however, because the curves shows the solubility of each metal in sodium for the pure metal binary systems, but not for the sodium and alloy multiplex systems. It may well be that the equilibrium concentration in sodium of the species which contains the alloy constituent element is considerably lower than the solubility of the pure metal.

The release of radioactive CPs in sodium systems shows some striking aspects. Sodium loop experiments [5, 6] have shown that corrosion product species are either selectively leached or retained in the steel, e.g.  $^{54}\text{Mn}$  release is often super-stoichiometric, while  $^{60}\text{Co}$  is often substoichiometric. The concentration at the steel surface is therefore either reduced or increased, and the element in question diffuses towards or away from the surface. Selective leaching can be interpreted as follows:  $^{54}\text{Mn}$  is released into sodium from the surface as well as through bulk corrosion (i.e. surface loss) by diffusing towards the surface from the interior of steel, whereas the release accompanying bulk corrosion is of more importance for  $^{60}\text{Co}$  because of its tendency to be retained in steel.

Brehm [6] showed that  $^{60}\text{Co}$  or  $^{58}\text{Co}$  release was a sensitive function of the oxygen concentration in the cold-trapped sodium, but that for  $^{54}\text{Mn}$  was not. The oxygen effect conflicts with the free energy data for the transition metals oxides mentioned above. The accompanying paper [1] shows that the oxygen effect can be interpreted by assuming that adsorbed oxygen at the solid metal surface activates the dissolution of the weakly leached species, e.g. cobalt isotopes.

Corrosion products are transported and deposited in the out-of-reactor primary circuits as well as in the reactor core. The difference between  $^{54}\text{Mn}$  and  $^{60}\text{Co}$  deposition behaviour has been observed in sodium loop experi-

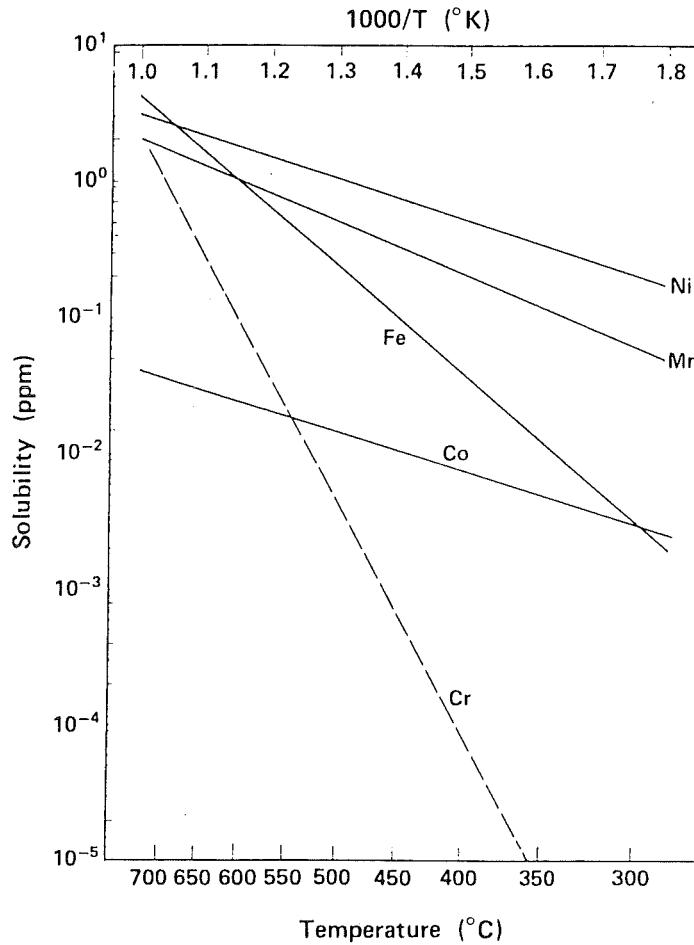


Fig. 3 Solubility of Transition Metals in Sodium.

ments [5].  $^{54}\text{Mn}$  tends to migrate throughout a sodium loop, whereas  $^{60}\text{Co}$  tends to deposit close to the active source. This latter behavior is likely to be true for  $^{58}\text{Co}$  also. Corrosion products are known to diffuse into the base metal following deposition onto sodium system wall surfaces. In this case, corrosion product radioactivity remains in the bulk deposits at the surface and in the base metal. In the hot leg,  $^{54}\text{Mn}$  and  $^{60}\text{Co}$  diffuse into the base metal. In the cold leg,  $^{54}\text{Mn}$  will be the dominant radionuclide. It will largely be present in semiadherent manganese and nickel-rich deposits, with very shallow penetration into the base metal. Silicon-rich deposits are often found in the cold leg, resulting from the release of silicon from the core and structural materials. It appears that the release and deposition behaviour of nickel is similar to that for manganese. Chromium release behavior resembles that for manganese, although chromium deposition behaviour is rather similar to that for cobalt. Particulate corrosion product behaviour (transport, sticking and detachment) is a very complex phenomena which may be clarified by long term plant experience.

In the JOYO plant, local enhancement of radiation fields has been observed near the main pump overflow column and dump tank, etc. which are static sodium regions. This enhancement is related to particulate radioactive CP behaviour. In an LMFBR core both release and deposition of radioactive CPs involve the following circumstances in the core: geometrical factors of fuel assemblies and core structures, neutron flux and nuclear reaction cross sections, and sodium system conditions and concentrations of radioactive CP species in the sodium.  $^{54}\text{Mn}$  and  $^{58}\text{Co}$  formed by fast neutron (n, p) reactions are predominantly produced and released in the driver fuel region.  $^{51}\text{Cr}$  also shows a similar tendency, because the contribution of intermediate energy neutrons is of relatively more importance. On the other hand  $^{60}\text{Co}$  is produced and released in the whole core (both driver and blanket fuel regions), where the contribution of resonance neutron capture at 132 eV is very important in a fast core. For  $^{58}\text{Co}$  production the burn-up effect is interesting because of its very large thermal neutron cross section and resonance integral. Thus, it seems that  $^{58}\text{Co}$ ,  $^{54}\text{Mn}$  and  $^{51}\text{Cr}$  (especially  $^{58}\text{Co}$ ) are more likely than  $^{60}\text{Co}$  to deposit in the reactor core regions (e.g. upper or lower gas plenum, and blanket regions). The largest amounts of radioactive CPs are found in the main primary circuit (out-of-reactor and in-core regions), with smaller quantities in purification circuits and the cold trap.

#### Measurements of Radioactive Corrosion Products in Primary Circuits of JOYO

In April 1977, the sodium cooled experimental fast reactor JOYO achieved initial criticality with a first stage MK-I core (the fast breeder core). After  $2.8 \times 10^4$  MWD operation, the core was changed to the current MK-II core (the fast flux irradiation bed with stainless steel reflectors) in November 1982.

The nominal power of the JOYO MK-II core is 100 MWt. Each operating cycle consists of 45 days full power operation and 15 days shut down for refueling. By the end of 1986, 12 MK-II duty cycles had been completed. Various irradiation tests to develop FBR fuels and reactor structural materials were performed during this period.

There are two (A and B) main circuits and one auxiliary circuit in the JOYO primary cooling system. Approximately 120 tons sodium is circulated in them with constant total flow rate (about 2200 ton/hr). Reactor inlet

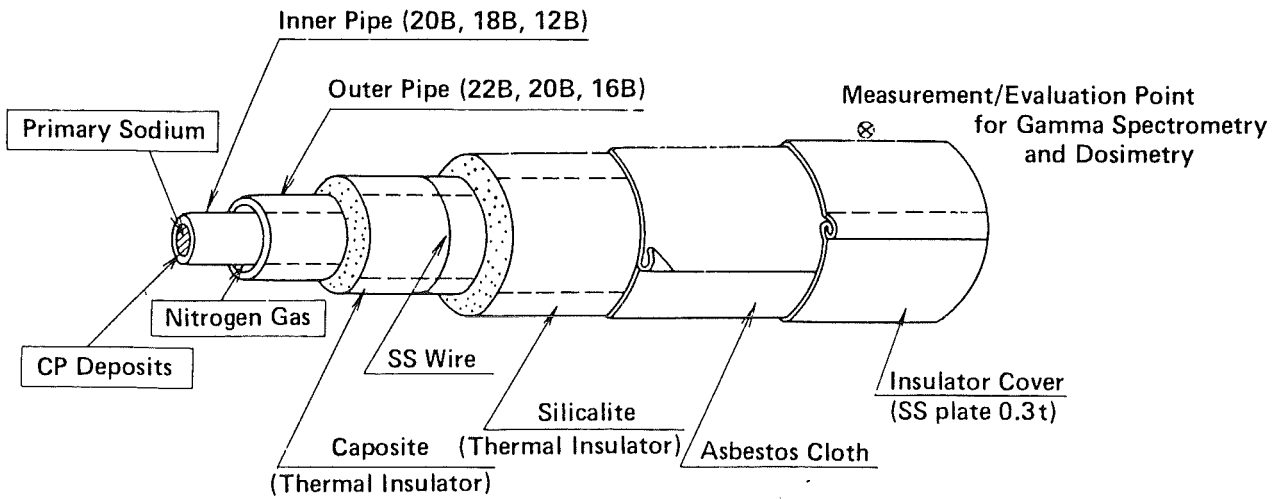


Fig. 4 Geometrical Layout for Measurement Points and Sodium Piping

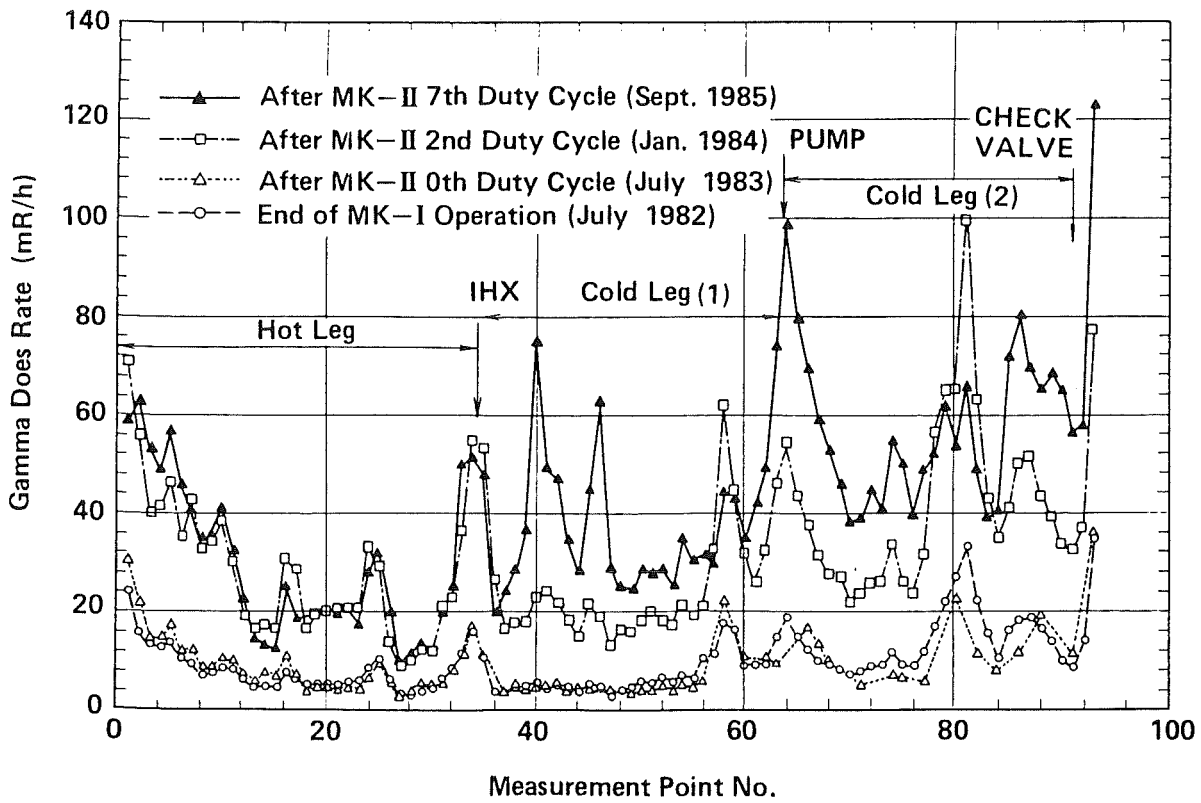


Fig. 5 Measured Gamma Radiation Levels along JOYO Primary Main Circuit Piping (A) after Sodium Draining.

and outlet temperatures are 370°C and 500°C at full power, respectively. All of the primary piping and components are completely isolated with the concrete wall shield, since primary sodium is strongly activated by neutron capture in the core.

During annual plant inspections, to prevent the hazard of radiation from long-lived  $^{22}\text{Na}$ , all primary sodium in the main circulating loops is drained into a sodium tank. Under these conditions, the spatial dose rate distribution is dominated by the radioactive CPs which have deposited on inner surfaces of primary piping and components. It was pointed out earlier that most personnel exposure comes from these CPs. The evaluation and prediction of CP behaviour in primary circuits is therefore essential from the view point of man-rem saving. These techniques have been developed both with measurements and calculations.

In every annual inspection, gamma dose rates from radioactive CP depositing on inner surfaces of the primary main circuits were measured by using calcium sulfate ( $\text{CaSO}_4$ ) thermoluminescent dosimeters (TLDs). Small portable ionization chambers were also employed for some of the measurements.

Gamma dose rate distribution near the piping was measured in detail for 93 locations, at one meter intervals along loop (A) from the outlet to the inlet of the reactor vessel. For each location TLDs were placed every 90 degrees around the thermal insulator cover. The geometrical layout for measurement points and sodium piping is illustrated in Fig. 4. Results from the measurements for loop A are shown in Fig. 5. The average dose rates for a Hot Leg, Cold Leg (1), and Cold Leg (2) are also given in Fig. 12 as a function of cumulative reactor output. Here, these legs are as follows ;

Hot Leg : piping between the reactor vessel outlet and IHX  
(intermediate heat exchanger),

Cold Leg (1) : piping between the IHX and primary main sodium pump, and

Cold leg (2) : piping between the sodium pump and check valve.

As Fig. 12 shows, the gamma dose rate for the MK-I core gradually rose in proportion to the cumulative reactor output, but a rapid increase in the dose rate occurred after the start of MK-II core operation.

Radioactive CP deposits on inner surfaces of primary main piping were measured at the 14 locations shown in Fig. 6, using a Ge solid state detector system. The geometrical conditions for the measurements was almost the same as those for gamma dose rate above described.

As an example of the resulting gamma spectra, that for location CP001 is given Fig. 8. In this measurement, only  $^{54}\text{Mn}$  and  $^{60}\text{Co}$  could be measured. Other radioactive nuclides expected in residual sodium, such as  $^{58}\text{Co}$ ,  $^{51}\text{Cr}$  and  $^{59}\text{Fe}$ , and  $^{22}\text{Na}$ , were present in amounts lower than the detection limit of the CP measurement system. It can be concluded that the gamma dose rate around the primary circuit piping and components after draining the sodium is determined by those two CP nuclides.

The system employed in these CP measurements was calibrated by the use of a piping mockup with two planar type standard gamma sources,  $^{54}\text{Mn}$  and  $^{60}\text{Co}$ , as shown in Fig. 7, so that absolute amounts of CP deposits could be obtained from the gamma spectra. The amount of deposit at each location is tabulated in Table 1, along with cumulative reactor output. The average values for each leg are also given in Fig. 11, compared with the calculated ones.

It can be seen that  $^{54}\text{Mn}$  activity is about 10 times greater than  $^{60}\text{Co}$  activity for any location. In these measurements, a rapid increase of CP activity was found again after the start of MK-II core operation, as expected from the results of gamma dose measurements. The most significant increase was for  $^{54}\text{Mn}$  activity in the Cold leg (2) between MK-II second duty cycle and seventh duty cycle.

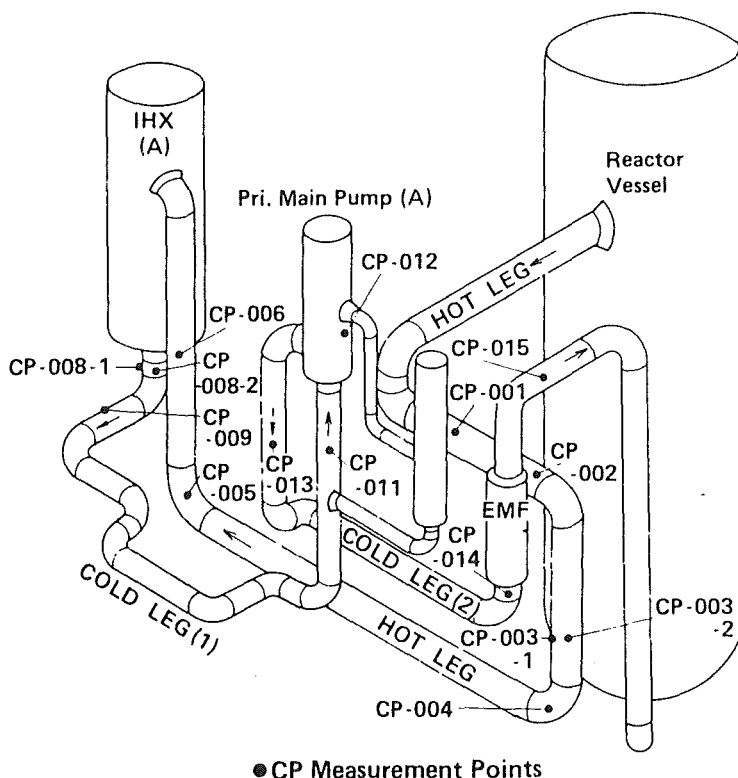


Fig. 6 Measurement Points for CP Deposits.

Comparison of Measurement Results with Calculational Estimation of  
Radioactive Corrosion Product Transfer in Primary Circuits of JOYO

The measurement results have been compared with the calculations for estimating radioactive CP transfer and the resulting radiation fields in the JOYO primary circuits, using the computer code PSYCHE, which is described in the accompanying paper [1]. The PSYCHE code consists of two subprograms, for source term and radiation field calculations, linked together. Source term calculations for radioactive CP transfer are done on the basis of a solution-precipitation model which was originally advanced by Polley and Kuhn, and has been improved in some points by Iizawa. The radiation levels are calculated using the QAD-CG code modified by evaluating the JOYO data. The modified code is named as JOANDARC.

For analyzing radioactive CPs in an LMFBR, data on activation in the core, and plant system and operating conditions are required. For the JOYO case, the difference in core constitution between the MK-I and MK-II cores must be considered. The MK-I active core region consisted of drivers and adjacent blankets, whereas the MK-II core contains drivers and adjacent reflectors. Therefore, calculations must be carried out two for both kinds of core in the reactor. The releases of  $^{54}\text{Mn}$ ,  $^{60}\text{Co}$ ,  $^{58}\text{Co}$  and  $^{51}\text{Cr}$  are

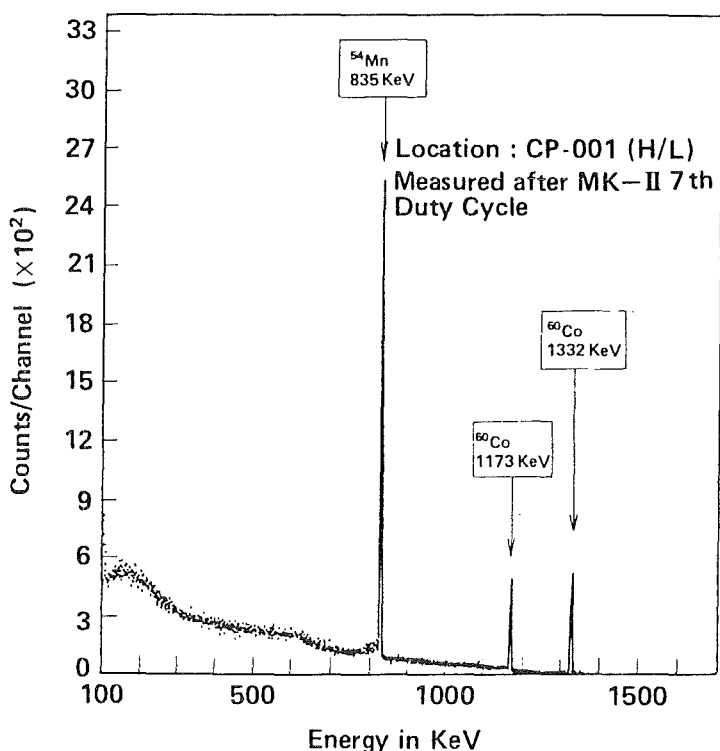


Fig. 8 Typical Gamma Ray Spectrum.



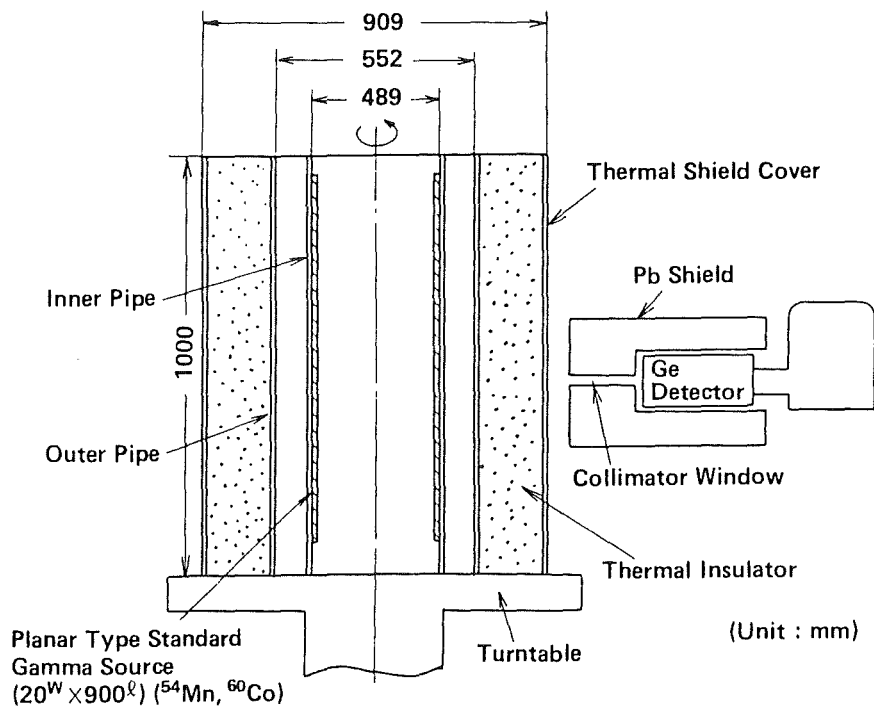


Fig. 7 Piping Mock-up Arrangement for CP Measurement System Calibration (Vertical Cut).

calculated; only  $^{54}\text{Mn}$ ,  $^{60}\text{Co}$  and  $^{58}\text{Co}$  are considered for predicting radiation levels.

In this study, the broad group neutron cross sections and neutron fluxes of 21 groups are applied to the radionuclide production rate calculations in core materials. The 21 group cross sections data were prepared by the procedure described in reference [8]. The neutron fluxes and cross sections of 21 groups are more appropriate than those of 20 groups to calculate the  $^{60}\text{Co}$  production by  $^{59}\text{Co}(n, \gamma)^{60}\text{Co}$ . In this process, the thermal and epithermal energy regions become important, especially the resonance capture at 132 eV. The low energy regions are more exactly considered in the 21 group calculation.

The radionuclide activation and release calculations are performed by dividing the whole core into 56 and 38 regions with cylindrical symmetry for the MK-I and -II cores, respectively. In each of the subregions the requisite data for the calculations (i.e. neutron fluxes and cross sections of 21 groups, equivalent hydrodynamic and geometrical diameter, region length, heat flux and conductivity, and sodium temperature and velocity) are given as input. The broad group cross sections are divided into 5 and 6 regions for the MK-I and -II cores, respectively. The temperatures at the fuel cladding surfaces, and the temperature increases along the various kinds of subassemblies are calculated by using the Lubarsky-Kaufman thermal conductivity expression.

For the out-of-reactor primary sodium systems, the intermediate heat exchanger (IHX), main pump, check valve (C/V) and cold trap are presented as geometrical models. For calculating the transport and deposition behaviour of radioactive CPs, the IHX model is divided into 5 ideally isothermal regions, and the main sodium circulating piping is divided to 4 regions, i.e. the hot leg (H/L), and cold legs(1), (2), and (3) (C/L (1), (2), and (3)). C/L (1), (2), and (3) are located between the IHX and main pump, main pump and check valve, and check valve and reactor vessel inlet, respectively. The overflow circuit is divided into the cold trap and 8 regions in the piping. The equivalent hydrodynamic and geometrical diameter, and the sodium temperature and velocity must be identified as inputs for each of the regions. Each region in the piping is moreover divided into subregions for the dose rate distribution calculations. Sodium flow rates of 1100 t/hr and 10 t/hr are chosen for the main and overflow circuits, respectively. For the oxygen concentrations in sodium, the average value obtained from the chemical analysis of sodium samples is used.

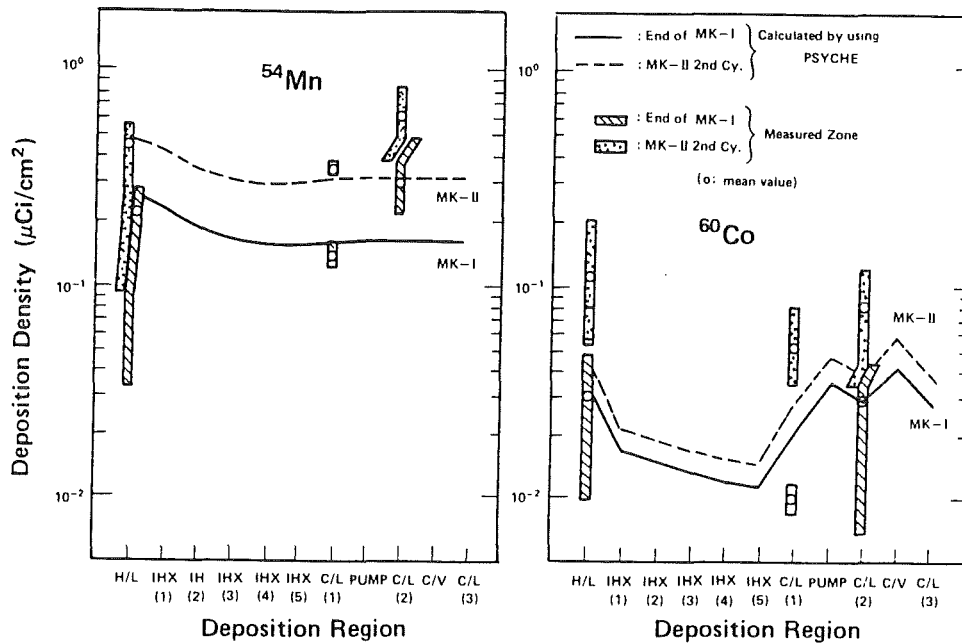


Fig. 9 Comparison of Measured vs. Calculated Deposition and Distribution of  $^{54}\text{Mn}$  and  $^{60}\text{Co}$  in JOYO Primary Main Circuit Piping (A) with MK-I or II Core

( This was made before reactor startup after cooling of 103 or 41 days following MK-I 6 th Duty Cycle or MK-II 2 nd Duty Cycle Operation, respectively. )

These values are 2.5 and 2.0 ppm for the MK-1 and -II phases, respectively.

The actual operating time and down time is considered in the source term calculations. The effective full power days at the each cycle are presented by converting to 75 and 100 MWd for the MK-I and -II cores, respectively. The effects of refuelling are considered for each phase.

The calculations of radioactive CP behaviour in primary sodium system of JOYO are performed by using the model parameters presented in the accompanying paper [1]. The chemical partition parameter for cobalt isotopes ( $\beta'$ ) and the bulk deposition rate ( $u_d$ ) were obtained by improving values based on loop experiments, by including the calculated-to-measured for deposition and dose rate distribution in JOYO.

The measured and calculated results for  $^{54}\text{Mn}$  and  $^{60}\text{Co}$  deposition and distribution in the primary piping of JOYO are compared in Fig. 9. The radioactivities of  $^{54}\text{Mn}$  deposits are about ten times higher than those of  $^{60}\text{Co}$  deposits. Table 2 shows the calculated versus measured results for  $^{54}\text{Mn}$  and  $^{60}\text{Co}$  deposits within the H/L, C/L(1) and (2). It can be seen that the calculated results using PSYCHE show reasonable agreement with the measured values within a factor of 0.5 ~ 2 for both  $^{54}\text{Mn}$  and  $^{60}\text{Co}$ . The

measured and calculated results are shown for  $^{54}\text{Mn}$  or  $^{60}\text{Co}$  buildup within the H/L, C/L(1) or (2) in Fig. 11, including predictions for future operation. These results seem reasonable, except that the measured result for  $^{54}\text{Mn}$  in C/L(2) is higher than that calculated, while the activity in the H/L is lower than that calculated. The measured and calculated results for radiation levels exterior to the primary sodium piping and components of JOYO after the MK-II second duty cycle are compared in Fig. 10. It can be seen that the measured values are successfully reproduced within a factor of 0.6 ~ 2 by the calculations. The contributions of  $^{54}\text{Mn}$ ,  $^{60}\text{Co}$  and  $^{58}\text{Co}$  to the radiation level are estimated to be about 54%, 34% and 12%, respectively, by the calculations using PSYCHE linked to JOANDARC. The increase in measured values in the inlet or outlet piping of the main pump above those calculated can be attributed to influences from radioactive CP deposits in the overflow column of the pump. The higher measured values in the inlet or outlet piping of the reactor vessel may result from streaming gamma rays from the activated reactor vessel wall. These phenomena cannot be reproduced in these calculations. The increases in the measured and calculated values at points No. 15, 25, 42, 52 and 73 etc. show the geometrical effects of elbows in the piping system.

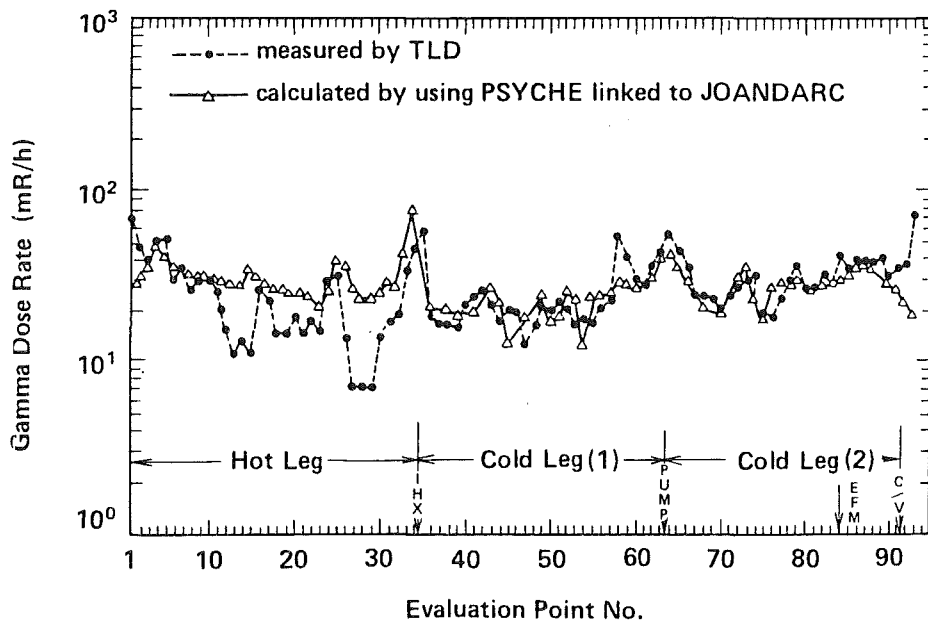


**Fig. 10 Comparison of Measured vs. Calculated Gamma Radiation Levels along JOYO Primary Main Circuit Piping (A) after 41 days Cooling Time Following MK-II 2nd Duty Cycle Operation (Cumulative Reactor Output,  $3.95 \times 10^4$  MWd).**

Estimation for Plant Operation in Future Program and Examination of Methods for Reducing Corrosion Product Activity

Radioactive corrosion products and the resulting radiation field buildup in JOYO MK-II and MONJU future operation are predicted by using PSYCHE. For the JOYO case the total inventories of  $^{54}\text{Mn}$  and  $^{60}\text{Co}$  in the out-of-reactor primary circuits will reach 26.5 and 1.0 Ci, respectively, after 45 days cooling time following the 17th duty cycle in the MK-II phase (cumulative reactor output :  $1.07 \times 10^5$  MWd). Six Ci of  $^{54}\text{Mn}$  radioactivity, 25% of the inventory, will be trapped in the cold trap, while cold trapping is not expected for  $^{60}\text{Co}$ . The radiation levels near primary piping and components will be almost all from  $^{54}\text{Mn}$  and  $^{60}\text{Co}$ . The contribution of  $^{54}\text{Mn}$  to the radiation level will be three times that of  $^{60}\text{Co}$ . The radiation level will reach 300 mR/hr near the IHX inlet nozzle, and will be 70 to 120 mR/hr near the other regions. Fig. 12 shows the prediction of dose rate

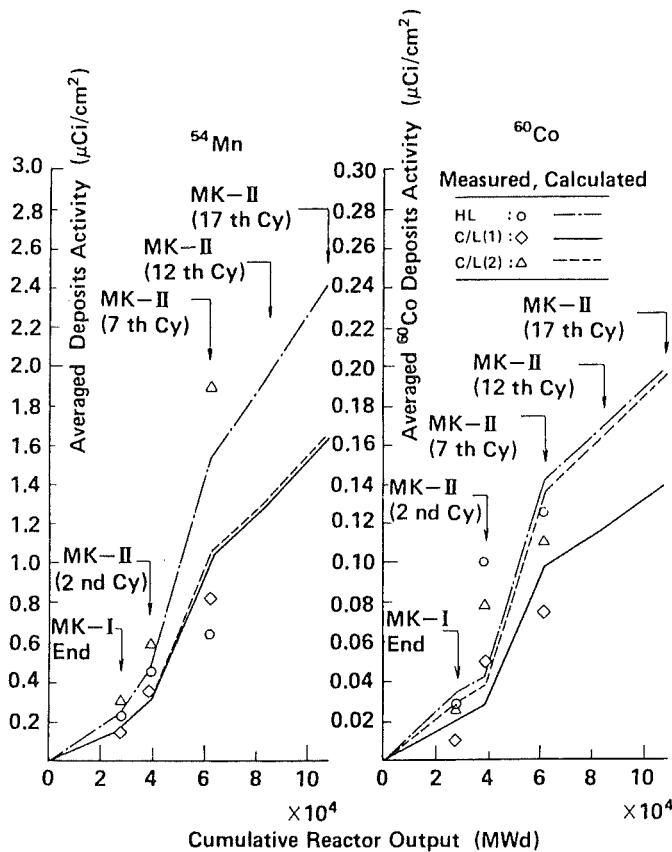
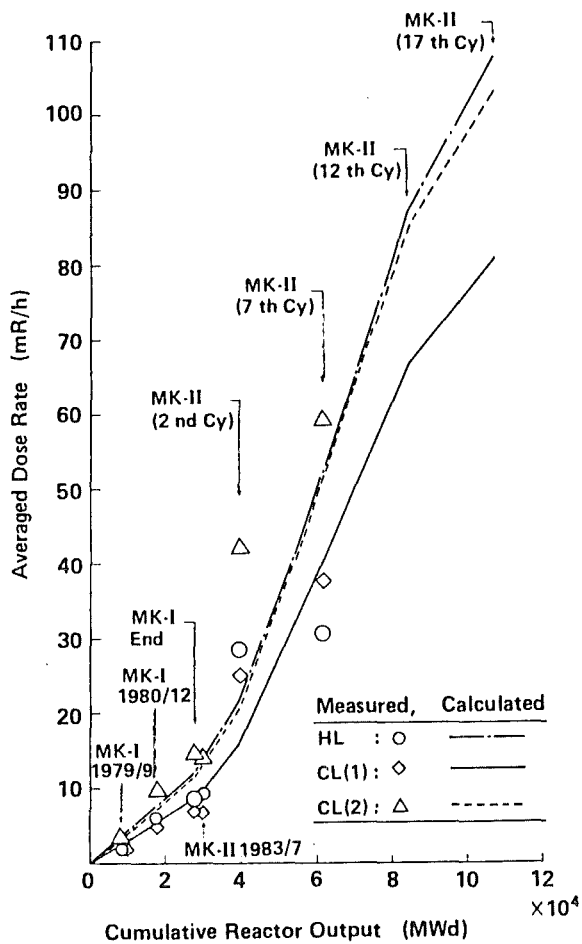


Fig. 11 Comparison of Calculated vs. Measured  $^{54}\text{Mn}$  and  $^{60}\text{Co}$  Buildup in JOYO Primary Main Circuit Piping (A).



buildup near each leg, compared with the measured values. For the MONJU case the predicted radiation levels due to radioactive corrosion products after the 5th and the last (57th) cycle operation are shown in Figs. 13(a) and (b) for various maintenance locations. The contribution of  $^{54}\text{Mn}$  to radiation levels will become dominant. There is no substantial difference between the two cases, because the  $^{54}\text{Mn}$  inventory will nearly have reached the saturated value after the 5th operation. The radiation levels at the surface of the piping will reach 600 to 900 mR/hr, while they will be below

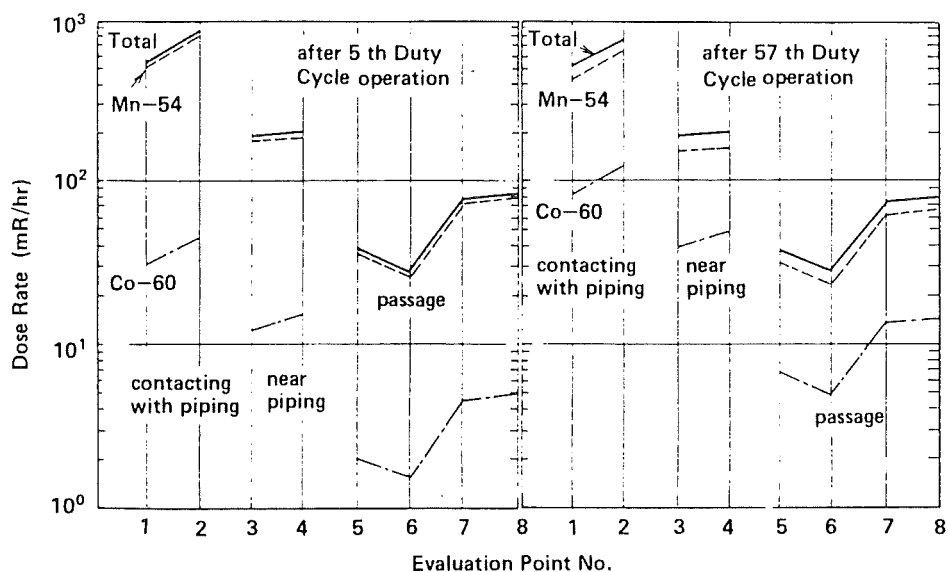


Fig. 13(a) Prediction of Radiation Levels in MONJU-HTS Cell

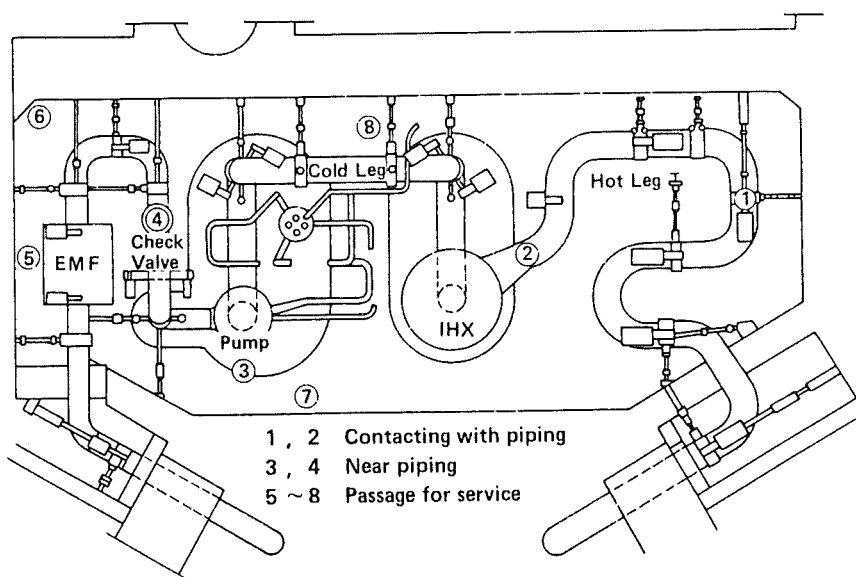
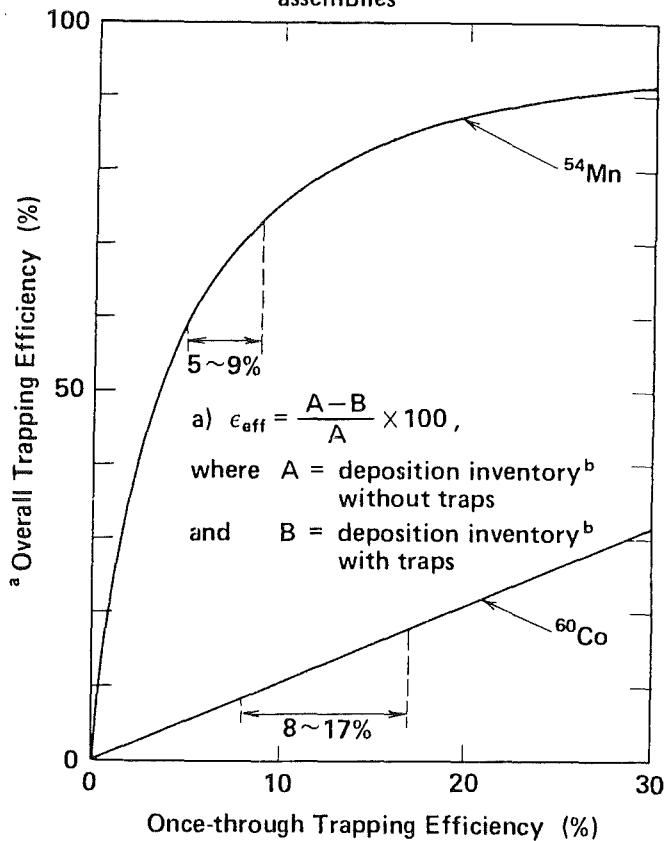


Fig. 13(b) Plan View of MONJU-HTS Cell Layout and Evaluation Points for Dose Rate.

100 mR/hr near the service passage in the heat transport system cell.

The effects of the concentration of oxygen in sodium and of the presence of cobalt impurity in core materials on the radiation levels are predicted and evaluated, using PSYCHE. The radiation level reached at an oxygen concentration of 2 ppm would be 30% and 20% below that at 5 ppm for JOYO MK-II and MONJU, respectively. The radiation levels at cobalt impurity levels 0.01% in fuel cladding and of 0.1% in subassembly wrappers would be similar to those at a cobalt level of 0.01% in both fuel cladding and subassembly wrappers, while the activity of <sup>60</sup>Co deposits in the out-of-reactor primary circuits would increase by 66% and 150% for JOYO MK-II and MONJU respectively. The control of oxygen or cobalt impurity levels is not seen as an effective means of controlling radiation levels. This conclusion results from the fact that <sup>54</sup>Mn is the dominant radionuclide, and its release is insensitive to oxygen concentration.

candidate form : many bored nickel blocks  
 installation : inside all driver and blanket fuel assemblies



|                                   | Nuclide          | Reduction Percentage (%) |
|-----------------------------------|------------------|--------------------------|
| <sup>b</sup> Deposition Inventory | <sup>54</sup> Mn | 63                       |
|                                   | <sup>60</sup> Co | 14                       |
|                                   | <sup>58</sup> Co | 8                        |
|                                   | <sup>51</sup> Cr | 12                       |
| <sup>c</sup> Dose Rate            |                  | 53                       |

b) in out-of-reactor primary circuits components and piping  
 c) at piping surface of IHX inlet nozzle

Fig. 14 Prediction of the Effect of Installing CP Traps in an LMFBR Plant.



The most promising control measures are the development of CP radionuclide traps [7]. Radioactive CPs can be largely confined to the core area by using CP traps. A CP trap is a device designed to be incorporated inside reactor fuel assemblies, and containing a specific getter for  $^{54}\text{Mn}$ , the most prevalent and troublesome of the gamma-emitting irradiation products. The specific getter is pure nickel. The trap is mounted in the fuel subassembly directly above the fuel pins. In this study the effect of installing the traps is predicted and evaluated for MONJU by using PSYCHE. A candidate form of the trap is made of many bored nickel blocks. Fig. 14 shows the correlation between effective, or overall trapping efficiency, and once-through trapping efficiency for  $^{54}\text{Mn}$  or  $^{60}\text{Co}$ , installing the candidate form of trap in all the driver and blanket fuel subassemblies. A large effective efficiency of 60 to 70% for  $^{54}\text{Mn}$  can be expected, even at relatively small once-through efficiency of 5 to 9%, estimated from our work in progress. On the other hand, overall efficiency will be about equal to once-through efficiency for  $^{60}\text{Co}$ . These results are attributed to the different characteristics of radioactive CPs behaviour of Mn and Co. In the primary system  $^{54}\text{Mn}$  essentially recirculates, but that  $^{60}\text{Co}$  mostly deposits during the first pass. Installing the traps would reduce by 60% and 10% respectively, the radioactivity from  $^{54}\text{Mn}$  and  $^{60}\text{Co}$  deposited in the out-of-reactor primary circuits. The radiation levels would be halved, because  $^{54}\text{Mn}$  will be the dominant radionuclide.

#### Discussion and Conclusions

In the drained primary system of an LMFBR, CP radionuclides are the main radioactivity sources during operation with no breached fuel. They assume in great importance in maintenance and repair operations in the plant involving components and piping in the primary circuits, and in sodium removal and liquid waste processing facilities.  $^{54}\text{Mn}$  is found to be the dominant removal radionuclide in components and piping of the primary circuits of a sodium-cooled fast breeder reactor ; in the out-of-reactor primary circuits of JOYO the radioactivities of  $^{54}\text{Mn}$  deposits were ten times higher than those of  $^{60}\text{Co}$  deposits, and  $^{58}\text{Co}$  was detected only in very small quantities. Similar relationships aspects for these radionuclides were observed in the liquid waste from washing of the main pump internals. On the other hand,  $^{60}\text{Co}$  and  $^{58}\text{Co}$  were found to be the dominant radio-

nuclides, followed by  $^{51}\text{Cr}$  and  $^{54}\text{Mn}$ , in the liquid waste from washing of fuel assemblies in JOYO.

It seems likely that these results are primarily due to the selective release and deposition behaviour characteristic of CP radionuclides in a sodium-steel system:  $^{54}\text{Mn}$  release is often found to be super-stoichiometric while cobalt isotope release is often found to be sub-stoichiometric, with the nuclides being retained in the steel;  $^{54}\text{Mn}$  deposition shows a tendency of migrating throughout a sodium system, while cobalt isotopes show a tendency of depositing immediately downstream from the active source.

What is more, it is a very interesting observation in our study that  $^{58}\text{Co}$  is found in very small quantities in the out-of-reactor primary circuit components and piping notwithstanding it may be the most abundant nuclide generated in fuel cladding. This apparent anomaly may be explained by considering the depletion of  $^{58}\text{Ni}$  (the target nuclide) caused by the super-stoichiometric leaching of nickel at metal surfaces in the core, the tendency of  $^{58}\text{Co}$  to deposit on surfaces in the core subassemblies, and the burn-up of  $^{58}\text{Co}$  caused by its very large neutron capture cross section. Analysis by the PSYCHE code predicts that 70 to 80% of the  $^{58}\text{Co}$  which is released will deposit in the core region, compared to only 30 to 50% of the  $^{60}\text{Co}$ .

For the primary circuit piping of JOYO, the corrosion product radionuclide ( $^{54}\text{Mn}$  and  $^{60}\text{Co}$ ) distribution calculated by using PSYCHE agreed well with measured results within a factor of 0.5 to 2. The gamma dose rate distribution calculated by using PSYCHE linked to JOANDARC reproduced the measured values within a factor of 0.6 to 2 over the piping system. We conclude that the analysis methods for radioactive corrosion product behaviour, and resulting radiation levels using PSYCHE and JOANDARC, have been verified. The accuracy of the calculations should be improved by comparison with results to be measured in the future; bulk deposition rates ( $u_d$ ) and chemical partition parameters for cobalt isotopes ( $\beta'$ ) are model parameters which should be investigated in particular.

Using these verified codes, a prediction of radiation levels for future plant operation can be obtained. For the JOYO case of cumulative reactor output of  $1.07 \times 10^5$  MWd, the radiation levels will reach 300 mR/hr near the IHX inlet nozzle, while they will be 70 to 120 mR/hr near other regions in the primary circuit piping. The contribution of  $^{54}\text{Mn}$  to radiation levels will be three times that of  $^{60}\text{Co}$ . For the MONJU case after saturation, the radiation levels at the surface of primary circuit piping will reach

600 to 900 mR/hr, while they will be below 100 mR/hr near the service passage in the heat transport system cell.

Based on calculations using the PSYCHE code, control of oxygen in the sodium and reduction of cobalt impurity in core materials are not effective means of controlling radiation levels. The most promising control measure is the installation of CP traps containing a specific getter for  $^{54}\text{Mn}$ , i.e. pure nickel, inside reactor fuel assemblies. Installing of the traps would reduce by 60% and 10%, respectively, the  $^{54}\text{Mn}$  and  $^{60}\text{Co}$  radioactivities deposited in the out-of-reactor primary circuits, reducing the radiation levels by half.

#### Acknowledgement

This paper is published by permission of the Power Reactor and Nuclear Fuel Development Corporation. The authors gratefully acknowledge the contributions of Dr. J. Horie, Hitachi Division, Hitachi Engineering Co., Ltd.

References

1. K. Iizawa, T. Kikuchi, I. Nihei, J. Horie, "Calculational Model and Code for Corrosion Products Transfer in Sodium Systems", Specialists' Meeting on Fission and Corrosion Products Behaviour in Primary Circuits of LMFBRs, Karlsruhe, 1987.
2. Bin Jenn Shaiu, P.C.S. Wu, P. Chiotti, "Thermodynamic Properties of the Double Oxides of Na<sub>2</sub>O with the Oxides of Cr, Ni and Fe", J. Nucl. Mtls., Vol.67 (1977) p.12, etc.
3. R.P. Colburn, "Characterization of Corrosion Product Deposits in Sodium Systems", Specialists' Meeting on Sodium Removal and Decontamination, Richland, IWGFR-23, 1978.
4. Edited by H.V. Borgstedt, Material Behavior and Physical Chemistry in Liquid Metal Systems (Plenum Press, New York and London, 1982)
5. N. Sekiguchi, K. Iizawa, H. Atsumo, "Behaviour of Corrosion Product from Irradiated Stainless Steel in Flowing Sodium", Proc. Specialists' Meeting on Fission and Corrosion Product Behaviour in Primary Circuits of LMFBRs, Dimitrovgrad (1975) p.82.
6. W.F. Brehm, "Effect of Oxygen in Sodium upon Radionuclide Release from Austenitic Stainless Steel", Ibid. (1975) p.186.
7. J.C. McGuire, W.F. Brehm, "A Radionuclide Trap for Liquid-Metal-Cooled Reactors", Nucl. Technology, Vol.48 (1980) p.101.
8. S. Suzuki, K. Iizawa, N. Ohtani, T. Kobayashi, J. Horie, H. Handa, "Measurement and Calculation of Radiation Sources in the Primary Cooling System of JOYO", Topical Conference on Theory and Practices Radiation Protection and Shielding, Knoxville, Tennessee, 1987.

Table 1 Measured CP Deposits on Inner Surfaces of JOYO Primary Main Circuit Piping (A)

(unit :  $\mu\text{Ci}/\text{cm}^2$ )

| Region                           | Measurement Point<br>(see Fig. 6) | End of MK-I Core Operation               |         | After MK-II 2nd Duty Cycle               |        | After MK-II 7th Duty Cycle              |        |
|----------------------------------|-----------------------------------|--|---------|--|--------|---|--------|
|                                  |                                   | Mn-54                                    | Co-60   | Mn-54                                    | Co-60  | Mn-54                                   | Co-60  |
| Hot Leg                          | CP-001                            | 0.529                                    | 0.0472  | —  | —      | 0.738                                   | 0.148  |
|                                  | CP-002                            | 0.399                                    | 0.0270  | 0.539                                    | 0.0725 | 0.772                                   | 0.0917 |
|                                  | CP-003-1                          | 0.0613                                   | 0.0609  | 0.102                                    | 0.191  | 0.173                                   | 0.155  |
|                                  | CP-003-2                          | 0.205                                    | 0.0298  | 0.292                                    | 0.0870 | 0.461                                   | 0.0776 |
|                                  | CP-004                            | 0.532                                    | 0.0472  | 0.616                                    | 0.114  | 0.920                                   | 0.112  |
|                                  | CP-005                            | 0.480                                    | 0.0407  | 0.566                                    | 0.111  | 0.796                                   | 0.225  |
|                                  | CP-006                            | 0.356                                    | 0.0129  | 0.447                                    | 0.0488 | 0.684                                   | 0.0653 |
| Cold Leg(1)                      | CP-008-1                          | 0.159                                    | 0.0116  | 0.364                                    | 0.0771 | 0.724                                   | 0.100  |
|                                  | CP-008-2                          | 0.166                                    | 0.0107  | 0.356                                    | 0.0603 | 0.721                                   | 0.0979 |
|                                  | CP-009                            | 0.207                                    | 0.00857 | 0.389                                    | 0.0331 | 0.826                                   | 0.0640 |
|                                  | CP-011                            | 0.199                                    | 0.00949 | 0.407                                    | 0.0321 | 0.999                                   | 0.0359 |
| Cold Leg(2)                      | CP-013                            | 0.265                                    | 0.00688 | 0.621                                    | 0.0356 | 1.462                                   | 0.0411 |
|                                  | CP-014                            | 0.606                                    | 0.0430  | 0.915                                    | 0.124  | 2.733                                   | 0.146  |
|                                  | CP-015                            | 0.268                                    | 0.0321  | 0.436                                    | 0.0806 | 1.489                                   | 0.143  |
| Cumulative Reactor Output (Date) |                                   | 2.789 × 10 <sup>4</sup> MWd (Dec., 1981) |         | 3.949 × 10 <sup>4</sup> MWd (Nov., 1983) |        | 6.168 × 10 <sup>4</sup> MWd (May, 1985) |        |

Table 2 Comparison of Calculated vs. Measured Values for Deposition of Mn-54 and Co-60 on Inner Surfaces of JOYO Primary Main Circuit Piping (A)

| Nuclide                   | <sup>a</sup> Region | End of MK-I Operation       |                  | After MK-II 2nd Cycle       |                  | After MK-II 7th Cycle       |                  |
|---------------------------|---------------------|-----------------------------|------------------|-----------------------------|------------------|-----------------------------|------------------|
|                           |                     | <sup>b</sup> Measured       | <sup>c</sup> C/E | <sup>b</sup> Measured       | <sup>c</sup> C/E | <sup>b</sup> Measured       | <sup>c</sup> C/E |
| <sup>54</sup> Mn          | H/L                 | 0.366                       | 1.18             | 0.427                       | 1.07             | 0.644                       | 2.39             |
|                           | C/L(1)              | 0.183                       | 1.14             | 0.379                       | 0.89             | 0.818                       | 1.26             |
|                           | C/L(2)              | 0.380                       | 0.53             | 0.657                       | 0.53             | 1.895                       | 0.55             |
| <sup>60</sup> Co          | H/L                 | 0.038                       | 1.21             | 0.104                       | 0.42             | 0.125                       | 1.14             |
|                           | C/L(1)              | 0.010                       | 2.12             | 0.051                       | 0.54             | 0.075                       | 1.31             |
|                           | C/L(2)              | 0.027                       | 1.07             | 0.080                       | 0.49             | 0.110                       | 1.24             |
| Cumulative Reactor Output |                     | 2.789 × 10 <sup>4</sup> MWd |                  | 3.949 × 10 <sup>4</sup> MWd |                  | 6.168 × 10 <sup>4</sup> MWd |                  |

<sup>a</sup> H/L: hot leg from reactor vessel outlet to IHX, C/L(1): cold leg from IHX to sodium pump and C/L(2): cold leg from sodium pump to check valve

<sup>b</sup> mean value in unit of  $\mu\text{Ci}/\text{cm}^2$

<sup>c</sup> Calculated/Measured: Comparisons were made before reactor startup, after cooling of 103, 41 or 46 days following end of the MK-I operation, or MK-II 2nd or 7th Duty Cycle operation, respectively.

Table 3 Radioactivities in Sodium Removal Liquid Waste

| Item   |                     | Washing for Fuel Assemblies     |                                 | Washing for Pump Internals     |
|--|---------------------|---------------------------------|---------------------------------|--------------------------------|
|  |                     | High Level                      | Low Level                       | Condensed Steam                |
| Radioactivity Concentration and Percentage<br>$\mu\text{Ci}/\text{cm}^3$ , (%) | Na-22               | $6.8 \times 10^{-6}$<br>( 0.1)  | —                               | $4.9 \times 10^{-3}$<br>( 0.2) |
|  | Cr-51               | $1.3 \times 10^{-3}$<br>(19.0)  | $2.4 \times 10^{-4}$<br>(14.9)  | $2.0 \times 10^{-1}$<br>( 9.4) |
|  | Mn-54               | $5.9 \times 10^{-4}$<br>( 8.6)  | $1.1 \times 10^{-4}$<br>( 6.8)  | 1.49<br>(68.9)                 |
|  | Co-58               | $1.7 \times 10^{-3}$<br>(24.9)  | $3.3 \times 10^{-4}$<br>(20.5)  | $3.8 \times 10^{-2}$<br>( 1.8) |
|  | Co-60               | $2.7 \times 10^{-3}$<br>(39.6)  | $8.8 \times 10^{-4}$<br>(54.7)  | $4.0 \times 10^{-1}$<br>(18.6) |
|  | <sup>a</sup> others | $5.3 \times 10^{-4}$<br>( 7.8)  | $5.0 \times 10^{-5}$<br>( 3.1)  | $2.3 \times 10^{-2}$<br>( 1.1) |
|  | Total               | $6.8 \times 10^{-3}$<br>(100.0) | $1.6 \times 10^{-3}$<br>(100.0) | 2.16<br>(100.0)                |

<sup>a</sup>  $^{59}\text{Fe}$ ,  $^{99}\text{Mo}$ ,  $^{99\text{m}}\text{Tc}$ ,  $^{124}\text{Sb}$  and  $^{182}\text{Ta}$

■ Comparison of Calculated-to-Measured Results for Deposition and Dose Rate Distribution in JOYO

Agreement within factors of 0.5 to 2 for radioactive CP deposition distribution, and of 0.6 to 2 for dose rate distribution over piping system.

■ Prediction of Radiation Levels in Future Plant Operation

- For JOYO at cumulative reactor output of  $1 \times 10^5$  MWd : radiation levels of 300 mR/hr near IHX and of 70 to 120 mR/hr near other regions in primary piping.
  - For MONJU after saturation : radiation levels of 600 to 900 mR/hr at primary piping surfaces and below 100 mR/hr near service passage in HTS-cell.
- Estimation of Effect of Methods for Reducing Radioactive CPs
- Reduction of oxygen concentration in sodium and cobalt impurity in core materials only a little effective in controlling radiation levels.
  - Most promising measures are CP traps containing getter made of pure nickel and installed inside fuel assemblies.

# Conclusions

## ■ Main Radioactivity CPs in JOYO

- In primary sodium circuit ;  $^{54}\text{Mn}$  activity level is ten times higher than that of  $^{60}\text{Co}$ , and  $^{58}\text{Co}$  present in very small amounts.
- In liquid waste from washing of fuel assemblies ;  $^{60}\text{Co}$  and  $^{58}\text{Co}$  are dominant radio-nuclides, followed by  $^{51}\text{Cr}$  and  $^{54}\text{Mn}$ .

## ■ Selective Release and Deposition Behaviour of CPs in Sodium Systems

- Super-stoichiometric release of  $^{54}\text{Mn}$  and sub-stoichiometric release of  $^{60}\text{Co}$
- Tendency for  $^{54}\text{Mn}$  deposition to migrate throughout sodium system ;  
Tendency for cobalt isotopes to deposit immediately downstream from active sources.

## ■ Apparent Anomaly of Very Small Amount of $^{58}\text{Co}$ in Primary Circuits

Results from depletion of  $^{58}\text{Ni}$  (target nuclide) at core material surfaces, tendency of  $^{58}\text{Co}$  to deposit on core subassembly surfaces, and burn-up effect of  $^{58}\text{Co}$ .





PROGRAMME OF WORK AT INDIRA GANDHI CENTRE FOR ATOMIC

---

RESEARCH (IGCAR) REGARDING ACTIVITY TRANSPORT IN

---

SODIUM SYSTEMS

---

R.P. Kapoor      D.S. Mitragotri      G. Periaswami <sup>+</sup>)

1.0 INTRODUCTION:

---

The Reactor Research Centre (RRC) now renamed the Indira Gandhi Centre for Atomic Research (IGCAR) was formally established at Kalpakkam in 1971 with the objective of carrying out research and development in the area of fast reactors and the associated fuel cycle.

The principal facility at this centre is FBTR, a test reactor which not only provides operational experience in this area of reactor technology but also serves as a test bed for developing fuels and materials for future reactors. FBTR is a sodium-cooled, plutonium-fuelled loop type fast reactor designed to produce 40 MW of thermal power and 13 MW of electrical power. While FBTR is similar in design to the French test reactor Rapsodie, it incorporates a sodium-heated steam generator and turbo-generator not provided in the French reactor and uses a mixed carbide of uranium and plutonium as a fuel for driving the reactor. FBTR Attained criticality in October, 1985.

The R&D work directed towards reactor engineering, sodium technology, fuels and materials at this centre is carried out in various laboratories namely Reactor Engineering, Material Science, Metallurgy, Radio-Chemistry, Fuel Reprocessing, Safety Research and Instrumentation.

It is generally recognised that a knowledge of radionuclide transport in sodium circuits of fast reactors is essential for evaluating system contamination, for detecting fuel pin failure, for evaluating the con-

<sup>+</sup>) Indira Gandhi Centre for Atomic Research,  
Kalpakkam, India

sequences of reactor operation with failed fuel pins and for estimating radionuclide release into the environment. Radionuclides released to the coolant in the core get transported to components outside the core and deposit there. Many of these radionuclides are long lived giving rise to high radiation fields thus complicating repair and maintenance procedures which lead to longer downtime.

## 2.0 OBJECTIVES:

---

Realising the importance of this activity, a committee was setup at the Centre to give recommendations on the programme of work to be carried out on radioactivity transport in sodium systems. The specific areas of work identified are listed here.(1)

- ° To study the release behaviour of fission products into sodium from carbide fuel simulated to different burnups for the following radionuclide: Cs-137, I-131, Sr-90, Ce-144 and Ba/La-140.
- ° To generate data on the leaching of fuel materials into sodium from different types of fuel pin defects for the prototype fast reactor fuels.
- ° To develop and test radionuclide traps for the following radioactive species: Mn-54, Co-60 & 58, Cs-137 and Ba/La-140.
- ° To study the volatilization of Cs-137 from sodium into the cover gas space.
- ° To study the diffusion of Cs-137 and Mn-54 into the steel surface.
- ° To study the deposition behaviour of the following radionuclides in cold traps: Mn-54, Cs-137, I-131, Co - 60 & 58 and Zn - 65.
- ° To develop mathematical models for describing release, transport and deposition of radionuclides in sodium systems; validation of these models by controlled clean experiments in the active sodium loops; application to the reactor system.

### 3.0 AVAILABLE FACILITIES:

---

#### 3.1 Fast Breeder Test Reactor (Fig.1)

---

With the completion of all physics experiments upto a power level of 500 KW(th) and also the completion, in parallel, of the balance commissioning activities related to the steam generators and the steam water system, FBTR will enter the MW range of power operation during the later half of 1987. The primary circuit piping and components have easier accessibility as a result of the loop type configuration and will be utilized as a test bed towards carrying out the necessary monitorings/samplings. Such generation of data on radionuclides will serve the following functions:

- ° Feed back to designers to validate their models
- ° Investigation into the possibilities of controlling /modifying the transport behaviour by observing the performance of specific radionuclide traps.
- ° Modifications in operating procedures so as to reduce dose levels for operation/maintenance personnel in case access is required to the cells having primary components.

To generate the information on the transport of radionuclides, the following methodology will be used:

- ( i) External monitoring of circuit piping and components, insitu, after draining of sodium by Ge(Li) detector will be carried out to get information on the type and extent of a particular radionuclide.
- ( ii) Radiation fields in the shielded cells will be measured.
- (iii) Accumulation of radionuclides deposited in cold trap will be monitored more frequently by Ge(Li) detector. This component is not drained before monitoring.
- ( iv) Sodium sampling device incorporated in the design of FBTR has a provision to draw 10 cc of sample in a square cup from 50 cm below the sodium level in the reactor vessel (Fig.2). Under all modes

of reactor operation, sodium samples can be taken. These samples will be utilized for monitoring the fission and corrosion product radionuclides in primary sodium.

- ( v) A provision exists in the purification circuit of primary sodium to have flow through bypass (Fig.2). The bypass circuit can be utilized for the following:
- To have a representative sample of primary sodium by incorporating a flow through sampler.
  - To utilize the bypass for testing the efficacy of various types of radionuclide traps, filter devices etc.
  - To sample sodium for monitoring particulates.

### 3.2 Activity Deposition Loop (Fig.3)

In pursuing the specific areas of work for the programme outlined in para 2.0, a sodium loop has been designed and is being erected in an area of 3.8 x 3 metres on a two-stage platform. The loop is constructed with SS 304 and is envisaged to have a circulating sodium inventory of 60 kg. Input of heat takes place in the heater vessel with U-shaped, mineral-insulated heaters (9 x 4.5 Kw) and the heat is rejected with a Na - air, finned tube heat exchanger with forced air cooling. With an operating temperature of 500 - 550°C, a temperature difference of upto 150°C can be achieved. The loop is driven by a 15 gpm e.m. pump and includes a cold trap, plugging indicator and e.m. flowmeters.

The loop piping is generally of 1 inch sch.40, SS 304 and incorporates hot and cold test sections of 1.5 metre lengths of smaller bore (1/2 inch, sch.40) pipe. The test sections permit linear velocities of sodium upto 5 m/s. The heater vessel has provision of a sample port for placement of radioactive source specimen in the heater zone itself.

Operation of the loop is envisaged to involve both (i) isothermal conditions with high velocities (5 m/s) in the test sections and (ii) non-isothermal conditions, with  $\Delta T$  (max) of 150°C with low sodium velocities (1.4 m/s), to enable separate evaluation of the influencing

parameters. Greater attention will be directed to study the aspect of deposition of radioactivities. Radioactivity migration is monitored externally with a gamma ray spectrometer. Initial studies envisaged also include those dealing with the behaviour of Mn-54 with and without radionuclide traps and the leaching behaviour of uranium carbide containing fission product/s premixed in the pellet.

### 3.3 Radioactive sodium chemistry loop (Fig.4)

This loop consists of two major parts namely the main loop for activity transport studies and the auxiliary loop consisting of cold trap, various on-line impurity monitors and samplers to have better characterisation of the sodium chemistry.

The main loop has a figure of 8 configuration with the main loop heat exchanger at the junction of the hot and the cold leg. This configuration helps in reducing both heating and cooling loads so that it can be located in a radioactive laboratory with once through ventilation. The hot leg consists of a heater and main test section. The cold leg has a sodium to air heat exchanger with variable speed air blower to control the cooling rate, an e.m. pump of capacity 2 Cu.m/hr at 4 bars and a flowmeter.

The main loop is constructed out of 25 NB Sch.40 SS 304 and 316. The cold leg operates at a temperature of 350°C and hot leg at 550°C. The total sodium hold up in the loop is 140 kg. Velocities of the order of 6 to 7 m/sec. can be achieved in the test section. Defected fuel pins and clad specimen will be located here for studying fission product and activation product release behaviour.

The loop has provisions for purifying the dump tank sodium, incorporation of on-line meters (oxygen, hydrogen and carbon) and an overflow sampler of the TNO harp type. The cold trap is so designed that the carbon trap for caesium-137 can be located between the economiser and the crystaliser.

This is a more versatile loop and can be utilized for generating data on leaching of fuel material, release of fission products and their transportation and deposition in the circuit, for development of radionuclide traps and also for testing on-line sodium monitors.

#### 4.0 RELATED WORKS:

The following work related to fission and corrosion product behaviour in primary circuits of LMFBRs has been carried out in the Centre:

- ° A FORTRAN-IV program (CHANDY) to compute the evolution of the fission products in a fission reactor by solution of the related coupled first order inhomogeneous differential equations.
- ° Solubility of Mn-54 in sodium has been established. This is an important data required for modelling Mn-54 transport in sodium. This follows the following equation(2):

$$\text{Log } S(\text{ppm}) = 3.6406 - 2601.73/\text{TK} \quad (549 \text{ K to } 811 \text{ K})$$

- ° The fact that oxygen in sodium plays an important role on activity release and transport indicates that there is an interaction between these nuclides and oxygen possibly by formation of ternary compounds. Experiments to prepare these compounds and establish their thermodynamic parameters has been undertaken.(3)
- ° Work related to the standardization of procedures for measurement of radionuclides in sodium and development of on-line monitors for impurities in sodium.
- ° Work on the calculation of various nuclides from reactor core by adopting the solution precipitation model developed at UK.

#### 5.0 CONCLUSION:

Although only initial R & D work on this topic has been attempted at IGC so far, a clear definition of the objectives has emerged at the centre now. With the completion of the two activity transport loops by the end of 1987 and with the entering of FBTR operation in the MW range in the later half of 1987, the centre is on the verge of embarking on a strong R&D programme in this field.

ACKNOWLEDGEMENT:

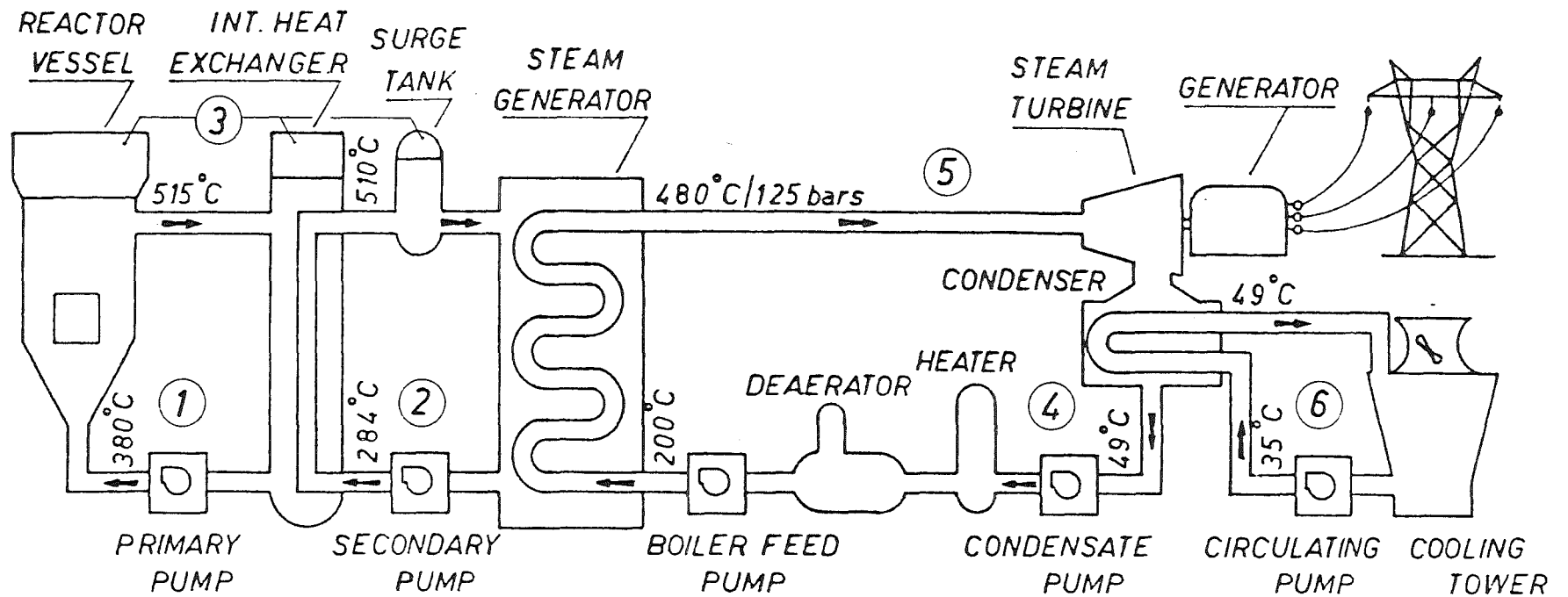
The authors are thankful to Shri K.P.N. Murthy, Shri B. Prahalad, Shri Mohan Das and Shri V. Ganesan for actively participating in the formulation of this programme of work at IGCAR. The authors are also thankful to Shri S.R. Paranjpe, Director, Reactor Group, Dr. D.V. Gopinath, Head, HASL, Dr. C.K. Mathews, Head, Radio-Chemistry Programme and Shri M.K. Ramamurthy, Head, Reactor Operations Division for fruitful discussion and constant encouragement.

REFERNCE:

1. Report of sub-committee for programme of work at IGCAR regarding Activity Transport in Sodium Systems - Aug. 1987 (Internal Report)
2. Solubility of Manganese and Iron in sodium -  
G. Periaswami, S. Rajan Babu, V. Ganesan & C.K. Mathews.  
  
International Seminar on Materials Behaviour & Physical Chemistry in Liquid Metals, Karlsruhe 1981
3. Role of ternary compounds of oxygen in corrosion of stainless in liquid sodium -  
T. Gnanasekaran et.al.  
  
International Conference on Corrosion Science and Technology, Calcutta Feb. 1985.

mvr:





- ① - PRIMARY SODIUM (TWO LOOPS)
- ② - SECONDARY SODIUM (TWO LOOPS)
- ③ - ARGON COVER GAS
- ④ - CONDENSATE FEED WATER
- ⑤ - STEAM
- ⑥ - CONDENSER COOLING WATER

**Fig-1 FBTR SCHEMATIC FLOW DIAGRAM**

# FAST BREEDER TEST REACTOR

## OBJECTIVES :—

- *To Gain Experience in construction & operation of LMFBR's*
- *To Serve as Test Bed for development of fuels & Structural materials*

## MILESTONES:—

1. *Core loaded with Steel & Nickel Sub-assemblies - Jan.'84*
2. *Sodium filled in Sec. storage tank - May'84*
3. *Purification of Secondary Sodium - Dec.84*
4. *Preheating of primary system - Apr.'85*
5. *Filling of Sodium in primary system - July'85*
6. *CRDM Tested in Sodium - Aug'85*
7. *Source loaded in Reactor - 28 Sept.85*
8. *Fuel loading & approach to Criticality - 20 Oct'85*

*cont*

9. *First Criticality - 18 Oct.'85 At 22.02Hrs*
10. *Low power Reactor Physics  
experiment - Jan'86*
11. *Steam generator modules  
Connected to East loop - June'86*
12. *Steam generator modules  
Connected to West loop - Oct'86*
13. *Sodium filled in flooding tanks - Dec'86*
14. *Replacement of primary pumps - Dec'86*
15. *Second Criticality - March'87*
16. *Intermediate Power Physics  
experiment (upto 500kw) - Presently On*

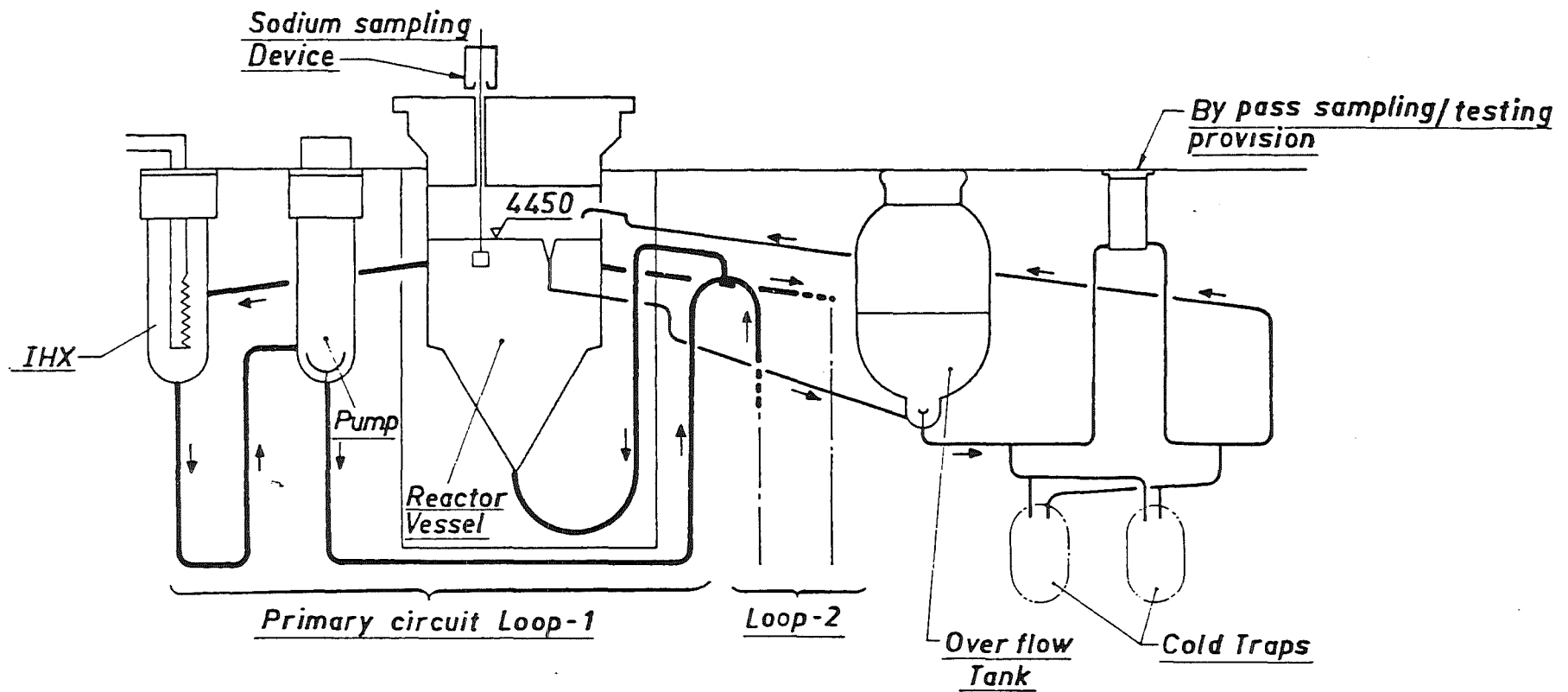


Fig-2 LOCATION OF SAMPLING IN PRIMARY CIRCUIT

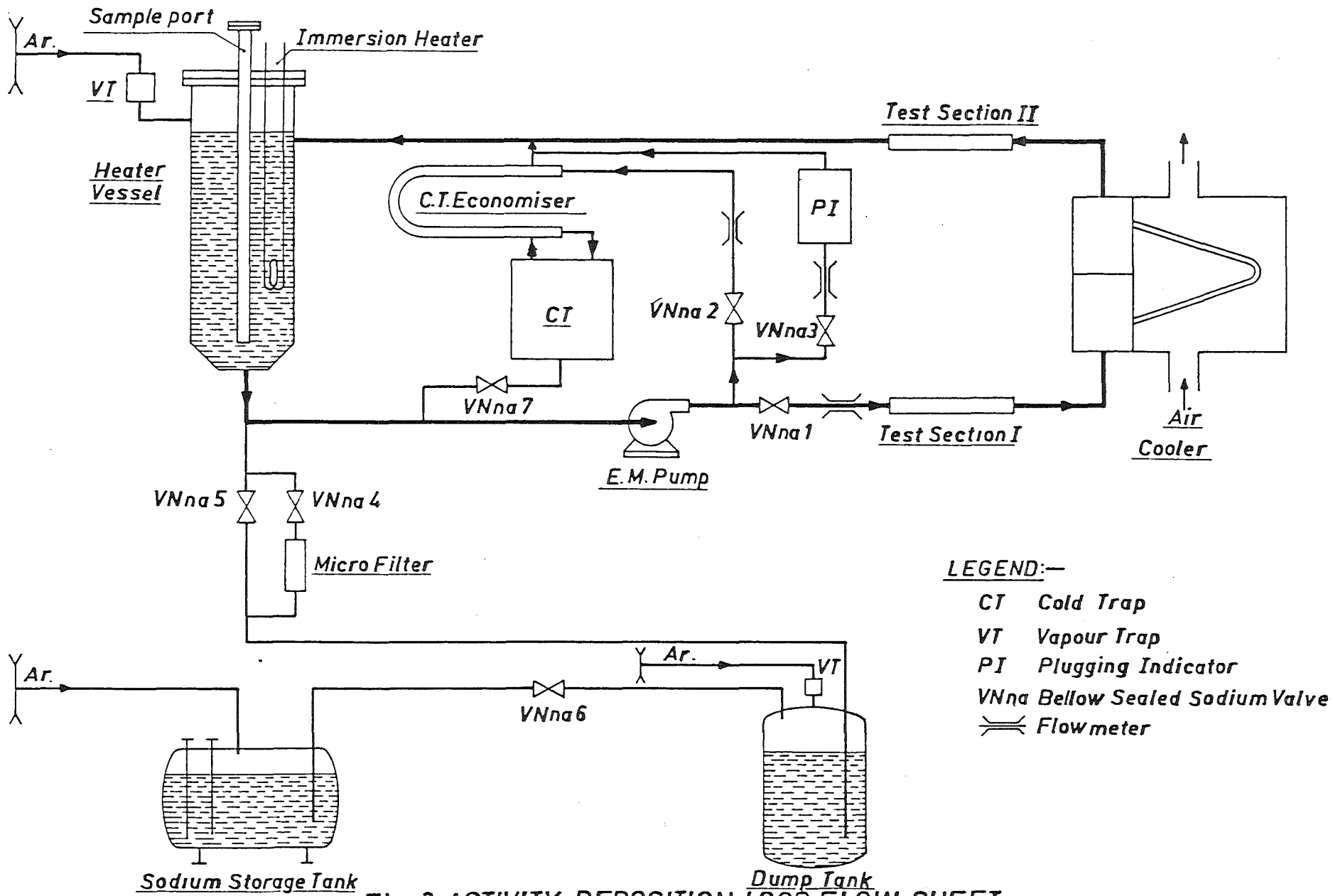


Fig-3 ACTIVITY DEPOSITION LOOP FLOW SHEET

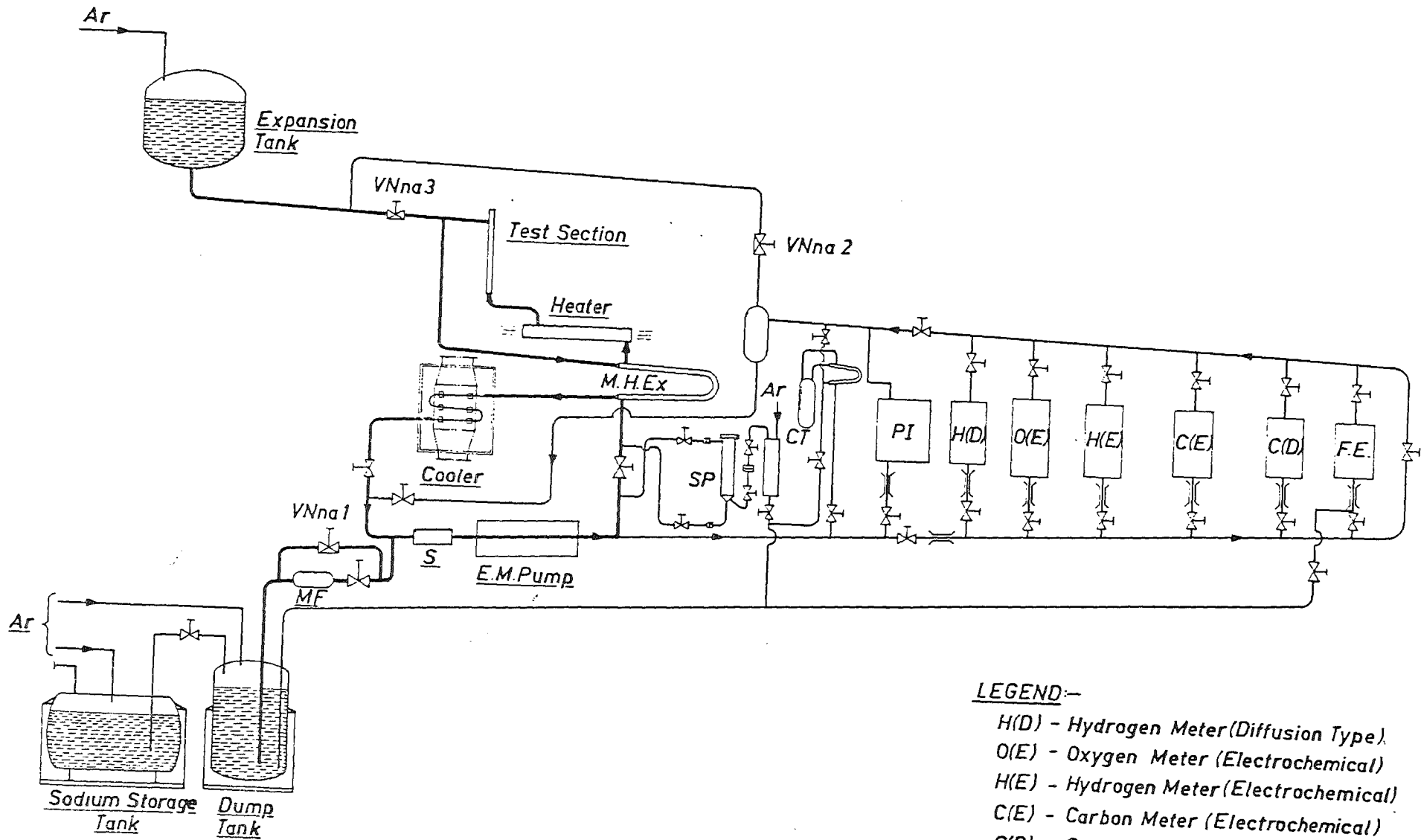
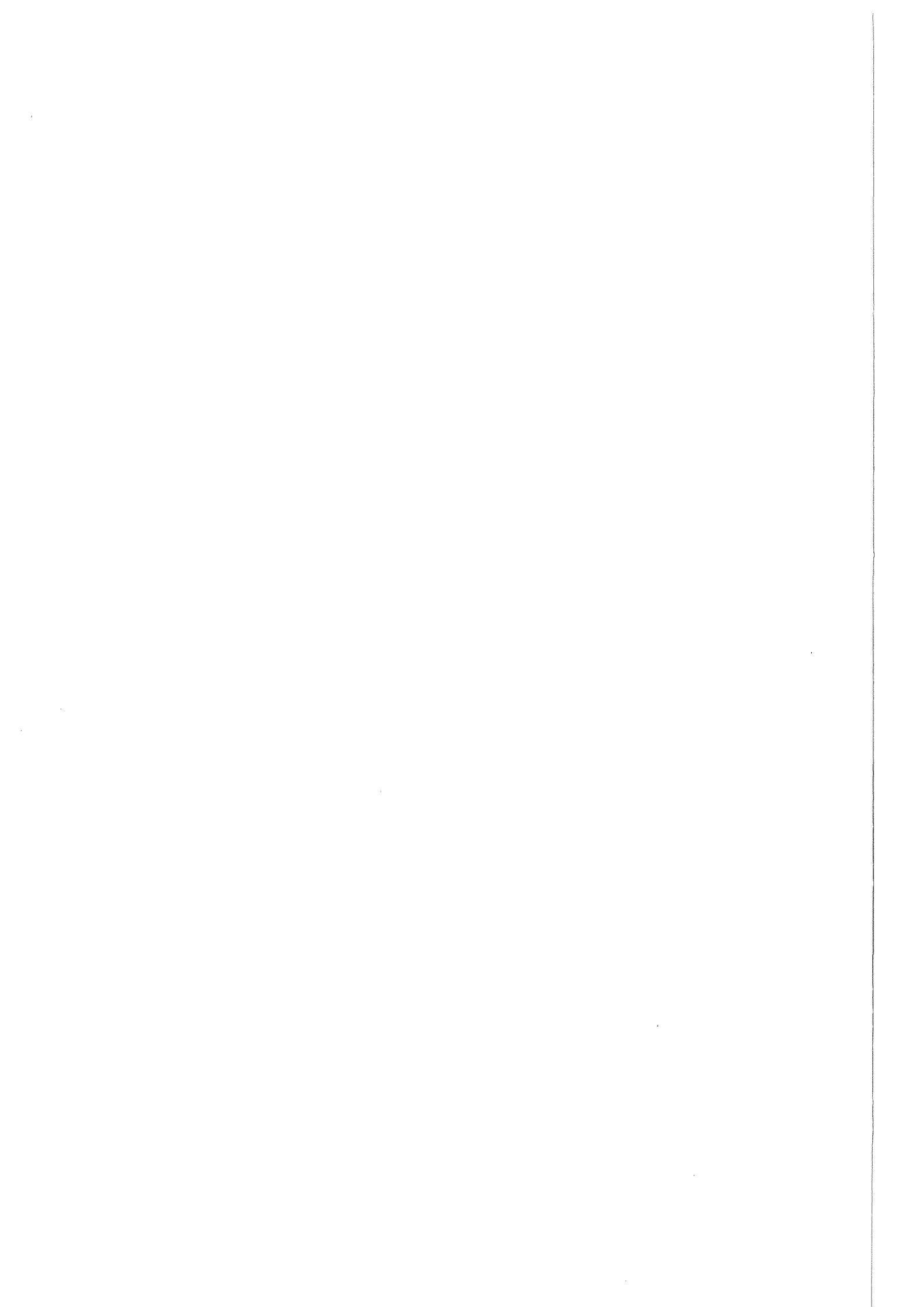


Fig-4 RADIOACTIVE SODIUM CHEMISTRY LOOP

**LEGEND:-**

- H(D) - Hydrogen Meter (Diffusion Type)
- O(E) - Oxygen Meter (Electrochemical)
- H(E) - Hydrogen Meter (Electrochemical)
- C(E) - Carbon Meter (Electrochemical)
- C(D) - Carbon Meter (Diffusion Type)
- F.E. - Foil Equilibration Port



CALCULATED MODEL OF RADIOACTIVE FISSION AND  
CORROSION PRODUCT ACCUMULATION AND DISTRIBUTION  
IN A FAST REACTOR SODIUM COOLANT CIRCUIT

Kizin V.D., Konyashov V.V.

Research Institute of Atomic Reactors,  
Dimitrovgrad, USSR

Abstract

A simple calculation procedure of radioactive products accumulation and distribution in a primary circuit has been developed on the basis of experimental investigations at the BOR-60 reactor. Common knowledge on the impurity products transfer at the liquid-solid and liquid-gas phase boundary is taken. Use is made of the typical in reactor physics relationships for the description of the products transition to the equipment surfaces, of fission products release, metal corrosion and others. Satisfactory agreement of the calculation data with the experimental ones has been obtained.



A sufficiently simple calculation procedure of radioactive products accumulation and distribution in a primary circuit and of gamma-ray fields from the equipment has been developed on the basis of experimental investigations at the BOR-60 reactor. Physical knowledge on impurity products distribution and transfer at the liquid-solid and liquid-gas phase boundary is taken. Use is made of typical in reactor physics relationships for the description of products transition to the equipment surfaces, of fission products release, metal corrosion and others. However for different periods of reactor operation that distinguish in their characteristics a satisfactory agreement of the calculation data with the experimental ones has been obtained.

In the suggested procedure radionuclides accumulation in the primary circuit as a result of the irradiated materials corrosion is described by the equation:

$$\frac{dA}{dt} = n \alpha k_s S [1 - \exp(-\lambda t)] \sum_E \varphi(E) \sigma(E) - \lambda A \quad (1)$$

where  $n$  is the nuclear density of the target;

$S$  is the surface area of core materials;

$\alpha$  is the element part moving to the coolant at corrosion rate equal to  $K_s$ ;

$\lambda$  is the decay constant;

$\varphi(E)$  is the neutron flux density of the energy group  $E$ ;

$\sigma(E)$  is the nuclide-target activation cross-section for the group  $E$  neutrons.

Considering the process of corrosion as a multistage heterogeneous one, which depends on the rate of oxygen in sodium diffusion to steel surface, one should use Eq. /2/ for calculation of the steel corrosion rate:

$$k_s = 81_{-44}^{+98} \exp[(-25600 \pm 1450)/RT] (C_{[O]S} / C_{[O]V})^{1,2 \pm 0,14} C_{[O]V}^{1,2 \pm 0,14}, \quad (2)$$

where  $C_{[O]S}$  is the oxygen content in sodium by steel surface;

$C_{[O]V}$  is the oxygen content in sodium volume;

R is the universal gas constant;

T is the temperature.

Ratio  $(C_{[O]S} / C_{[O]V})^{1,2}$  depends on the hydrodynamics parameters. It is shown in the experiment /2/ that the value of this ratio under the laminar mode of flow ( $Re \leq 1 \cdot 10^4$ ) changes proportionally with  $Re^{0,5}$ ; in a turbulent flow with  $Re = 10^4 - 10^5$  is in proportion to  $Re^{0,8}$  and at great rates of the flow does not depend on the flow rate, i.e.

$(C_{[O]S} / C_{[O]V})^{1,2} = (\frac{Re}{10^5})^{0,5}$  with  $Re \leq 10^4$ ,  $(\frac{Re}{10^5})^{0,8}$  with  $Re = 10^4 - 10^5$  and 1 with  $Re > 10^5$ .

The foundation of the calculation procedure for gaseous and volatile fission product release is the diffusion from structural fuel areas and escape from the open surface during fission /3,4/. It is rather difficult to calculate the release rate of radionuclides from the fuel pin into the coolant, hence it is usually taken as a factor determined by the experiment. The impurity substances transfer from the primary circuit to the surface through laminar sub-layer  $\delta$

$$- \frac{dm}{dt} = DS(C_c - C_o) / \delta, \quad (3)$$

where m is the amount of impurities in a coolant;

D is the diffusion coefficient;

S is the surface area;

$C_c$  is the concentration of atoms in the coolant;

$C_o$  is the concentration of atoms in a wall layer of  $\delta$  thickness;

t is the time.

In this case the rate of the impurity quantity change in the coolant is described by the equation:

$$\frac{dN_c}{dt} = Q - \mathcal{D}S(C_c - C_o)/\delta - \lambda N_c, \quad (4)$$

where  $N_c$  is the amount of radioactive impurities in the coolant;

$Q$  is the source of radioactive impurities;

$\lambda$  is the decay constant.

Changing the second member of the right part we'll get the equation:

$$\frac{dN_c}{dt} = Q - wN_c + \gamma N_s - \lambda N_c, \quad (5)$$

where  $w = \mathcal{D}S/(\delta V_c)$ ;  $\gamma = \mathcal{D}/(\delta \tau)$ ;  $N_c = C_c V_c$ ;  $N_s = C_s S$ ;

$C_o = C_s/\tau$ ;

$N_s$  is the amount of radioactive impurities in deposits;

$C_s$  is the surface concentration of radioactive impurities;

$V_c$  is the coolant volume.

$w$  and  $\gamma$  constants characterize the rate of impurities inflow from the coolant to the surface and outflow.

In a first approximation  $\gamma$  constant is inversely proportional to the distribution coefficient  $K$  determined in the experiments ( $K = C_s/C_c$ ). On the other hand,  $C_o = kC_c$  for small concentrations where  $k$  is the coefficient characterizing the surface ability to adsorb particular impurities. As:

$$C_o = C_s/\tau \quad \text{and} \quad C_c = C_s/K, \quad \text{then} \quad \tau = K/k \quad \text{and} \quad \gamma = Dk/(\delta K).$$

The values of adsorption and desorption constants depend on temperature and circuit hydraulic parameters. The dependence of the diffusion coefficient on temperature is expressed by the exponential law:  $D = D_o \exp[-Q_o/RT]$ , where  $D_o$  is the preexponential factor;  $Q_o$  is the diffusion activation energy. The laminar sub-layer thickness is determined from equation of the type:  $\delta = m \text{Re}^n$ , where  $m$  and  $n$  are the constants;  $\text{Re}$  is the Reynolds number. For pipelines  $m = 64,2$  and  $n = 7/8 / 5/$ .

The distribution coefficient  $K_d$  is usually presented as  $K_d = \exp(A/T+B)$ , where  $A$  and  $B$  are the constants deter-

mined in the experiments. Thus,

$$\omega = D_o \exp(-Q_o/RT) \frac{S}{V} \frac{Re^{7/8}}{64.2}; \quad \gamma = D_o \exp(-Q_o/RT) \frac{Re^{7/8}}{64.2} \exp\left(\frac{A}{T} + B\right).$$

Similarly one can describe the process of the gaseous and volatile product transfer into the circuit cover gas (reactor, pumps, heat exchangers). This process can have a considerable influence on the concentration of some nuclides in the circuit.

A dynamic equilibrium is set up at the sodium-gas interface. Gaseous radionuclides dissolved in sodium will enter the gas from the coolant flow through the surface laminar sub-layer. Gas flow diffusing through the laminar sub-layer of  $\delta_g$  thickness can be found by the expression:

$$q = \frac{D}{\delta_g} (C_c - C_o) = \frac{D}{\delta_g} (C_c - G_o C_g),$$

where  $C_g$  is the concentration of radionuclide atoms in the cover-gas,  $G_o$  is the Henry coefficient,

$C_o$  is the concentration of radionuclide atoms at the interface of phases. The above is true in the assumption that fission gas concentration  $C_o$  in the coolant at the sodium-gas interface is in equilibrium with the concentration of the corresponding atoms in cover-gas. This equilibrium is characterized by Henry coefficient ( $C_o = G_o C_g$ ). Then the equations of fission gas material balance can be written as:

$$\frac{dN_c}{dt} = Q - \frac{D}{\delta_g} (C_c - C_g G_o) S - \lambda N_c; \quad \frac{dN_g}{dt} = \frac{D}{\delta_g} (C_o - C_g G_o) S - \lambda N_g, \quad (6)$$

where  $S$  is the surface of the sodium-gas interface.

Note that  $C_c = N_c/V_c$ ;  $C_g = N_g/V_g$ .

Having denoted  $\alpha = DS/\delta_g V_g$  and  $\beta = DS G_o/\delta_g V_g$  the set of equations (6) will be written in the form:

$$\frac{dN_c}{dt} = Q - \alpha N_c + \beta N_g - \lambda N_c; \quad \frac{dN_g}{dt} = \alpha N_c - \beta N_g - \lambda N_g. \quad (7)$$

The values of leakage ( $\alpha$ ) and capture ( $\beta$ ) constants are proportional to the sodium-gas interface <sup>area</sup> and depend on turbulence of the coolant flow. It is possible to determine the values of leakage constants by having measured the activity of radionuclides in the reactor and pump

cover-gas and having substituted the measured activity values of three isotopes of one element in Eq.(7).

For a stationary case  $dN_c/dt = 0$ ;  $dN_g^R/dt = 0$ ;  $dN_g^P/dt = 0$ , where R is the reactor index, P is the pump index.

For the BOR-60 reactor  $\beta^R \ll \alpha^R$  and  $\beta^P \ll \alpha^P$  and the set of equations (7) will get the form:

$$\begin{aligned} N_c &= Q/(\lambda + \alpha^R + 2\alpha^P); \\ N_g^R &= \alpha^R N_c / \lambda; \\ N_g^P &= \alpha^P N_c / \lambda; \\ \bar{\tau} &= T_{1/2} / \ln 2 = 1/(\alpha^R + 2\alpha^P), \end{aligned} \tag{8}$$

where  $\bar{\tau}$  is the average time of fission gas in the coolant;

$T_{1/2}$  is the period of fission gas semielimination from the coolant.

The last set of equations can be written in the activity units in the form:

$$\begin{aligned} A^R &= \alpha^R Q / (\lambda + \alpha^R + 2\alpha^P); \\ A^P &= \alpha^P Q / (\lambda + \alpha^R + 2\alpha^P). \end{aligned} \tag{9}$$

For the BOR-60 reactor  $\alpha^R = 0,1$ ;  $\alpha^P = 0,01$ ,  $\bar{\tau} = 8$  hs were determined by  $^{133}\text{Xe}$ ,  $^{135}\text{Xe}$ ,  $^{85}\text{Kr}$ ,  $^{88}\text{Kr}$ ,  $^{23}\text{Ne}$  concentrations when all fuel pins have been intact. For the calculation of sodium purification it is more convenient to use an approximate equation:

$$\frac{dN_c}{dt} = Q - \nu N_c - \lambda N_c, \tag{10}$$

where  $\nu$  is the purification constant, which value is found with the help of the expression:

$$\nu = \frac{1}{t_c} \ln \left[ 1 - \frac{\omega}{G} (1 - E) \right];$$

$t_c$  is the time of the coolant movement in the circuit;

$G$  is the complete coolant flow rate.

In general the set of equations describing the distribution of fission products in the primary circuit of the loop-type sodium coolant reactor has the form of:

$$\frac{dA_x^{ci}}{dt} = \frac{A_{x-1}^{ci}}{\tau_{x-1}} + \Delta a_x^i + \gamma_x^i A_x^{si} + \beta_x^i A_x^{gi} + \lambda^{i-1} A_x^{c,i-1} - (\omega_x^i + \alpha_x^i + \nu^i + \lambda^i + \tau_x^{-1}) A_x^{ci};$$

$$\frac{dA_x^{si}}{dt} = \omega_x^i A_x^{ci} + \lambda^{i-1} A_x^{s,i-1} - (\gamma_x^i + \lambda^i) A_x^{si};$$

$$\frac{dA_x^{gi}}{dt} = \alpha^i A_x^{ci} + \lambda^{i-1} A_x^{g,i-1} - (\beta_x^i + \lambda^i) A_x^{gi};$$

$$\frac{dA_p^i}{dt} = \gamma^i \sum_x A_x^{ci} + \lambda^{i-1} A_p^{i-1} - \lambda^i A_p^i,$$

where  $\lambda^i$  is the inflow rate of  $i$  radionuclide from the failed fuel pin;

$x$  is the region number.

For corrosion products the form of equations will be similar. The source of corrosion products should be taken into account in all regions.

Analysis of the calculation results reveals that only for the corrosion product release calculation from the reactor core surfaces where large changes of temperature take place it is necessary to divide the core into regions for the more correct corrosion rate calculation. Other circuit regions do not demand such a detailed division.

Table I gives the comparison of the fission gas activity results calculated by this procedure and of the experimental ones in the primary circuit of BOR-60. For nongas fission products the reliable experimental data have been obtained merely for the long-lived nuclides  $^{137}\text{Cs}$ ,  $^{131}\text{I}$ ,  $^{140}\text{Ba}$ ,  $^{95}\text{Nb}$ , which determine the coolant and the deposit activity (Table 2). The data disagreement for  $^{95}\text{Nb}$  is associated with a considerable dependence of the activity level upon the operation time of the failed fuel pin reactor.

The values of the used constants are given in Table 3. The distribution coefficients have been obtained at BOR-60.

The results of corrosion product calculation in the BOR-60 primary circuit are shown in Table 4.

This procedure has been used to calculate the fission product release fractions of the BOR-60 and BN-350 fuel elements. The maximum fuel temperature in the BOR-60 fuel pins is considered to be 2500 K and in BN-350 - not more than 1800 K. In the latter case zones of large equiaxed

grains and column crystals are absent which has a considerable effect on the gaseous and volatile long-lived fission products release from the fuel (table 5).

There have also been carried out calculations on the corrosion product accumulation in the BN-350 circuit. The total amounts of  $^{54}\text{Mn}$  and  $^{60}\text{Co}$  activity in its primary circuit after 2000 days of operation at 1000 Mw(t) power were equal to 50 and 6,5 TBk, and at 650 Mw (t) power - 5,5 and 0,7 TBk respectively. The latter values were close to the experimental ones during the first period of the BN-350 operation.  $^{54}\text{Mn}$  and  $^{60}\text{Co}$  distribution in the circuit has proved to be different from that calculated with the help of the temperature dependant distribution coefficient obtained in the BOR-60 circuit. At BN-350 the surface activity of  $^{54}\text{Mn}$  is higher on the pipeline before heat exchanger than after it. It may be explained by the low temperature of sodium in pipelines at the outlet from the reactor and the high sorption of  $^{54}\text{Mn}$  on their surfaces, i.e. the  $^{54}\text{Mn}$  and, perhaps, other nuclides distribution coefficient dependence on temperature may differ from that accepted in the calculation model and its experimental verification is required. The same may be said about a higher deposit of  $^{60}\text{Co}$  in the heat exchanger.

On the whole the calculation and experimental values were in substantial agreement.

Thus, the suggested model allows to calculate corrosion and fission products in the coolant, in surface deposits on the equipment, cover gas activity, etc. The code written on the basis of this procedure takes into account parameter changes of the reactor plant during its operation, history of the reactor operation, the overloads of fuel subassemblies.

Table 1

Fission gas activity in the primary circuit of BOR-60

| Nuclide           | Equilibrium distribution, GBk |                             |                      |                    |  |
|-------------------|-------------------------------|-----------------------------|----------------------|--------------------|--|
|                   | Coolant                       | Cover gas of the reactor/6/ |                      | Cover gas of pumps |  |
|                   | Calcul.                       | Calcul.                     | Experim.             | Calcul.            |  |
| $^{85m}\text{Kr}$ | 3,7                           | 3                           | 3,5-6                | 0,1                |  |
| $^{88}\text{Kr}$  | 5,6                           | 2,6                         | 1,9-4                | 0,08               |  |
| $^{133}\text{Xe}$ | 75                            | 1450                        | $(1-1,4) \cdot 10^3$ | 48                 |  |
| $^{135}\text{Xe}$ | 50                            | 65                          | 45-80                | 2,2                |  |

Note: There is one failed fuel pin in the centre of the core; reactor power is 40 Mw.



Table 2

Nuclides activities in the primary circuit of the BOR-60 reactor  
(on a per-one failed fuel pin basis)/7/

| Nuclide           | Coolant,<br>MBk/kg |          | Pipeline before heat ex-<br>changer, MBk/m <sup>2</sup> |          | Pipeline after heat ex-<br>changer, MBk/m <sup>2</sup> |          |
|-------------------|--------------------|----------|---|----------|--|----------|
|                   | Calcul.            | Experim. | Calcul.   | Experim. | Calcul.  | Experim. |
| <sup>95</sup> Nb  | 0,04-0,2           | 0,04-0,1 | 7-150   | 4-40     | 20-350   | 20-110   |
| <sup>131</sup> I  | 4,3                | 3,7      | -   | -        | -  | -        |
| <sup>137</sup> Cs | 7,5                | 7,5      | -   | -        | -  | -        |
| <sup>140</sup> La | 0,1                | 0,04     | 7,5   | 4-15     | 230  | 110-220  |

Table 3

Constants used in calculations

| Nuclide           | $K_p, \text{ cm}$     |                       | A    | B     |
|-------------------|-----------------------|-----------------------|------|-------|
|                   | $330^\circ \text{ C}$ | $500^\circ \text{ C}$ |      |       |
| $^{95}\text{Nb}$  | 200                   | 50                    | 3800 | -1    |
| $^{140}\text{La}$ | 500                   | 30                    | 7710 | -6,6  |
| $^{54}\text{Mn}$  | 200                   | 20                    | 6300 | -5,15 |
| $^{60}\text{Co}$  | 10                    | 3                     | 3300 | -3,2  |

Table 4

Surface activity of corrosion products on the BOR-60  
primary circuit equipment, GBk/m<sup>2</sup> /7/.

| Nuclide          | Date     | Pipeline before heat exchanger |          | Heat exchanger |          | Pipeline after heat exchanger |          |
|------------------|----------|--------------------------------|----------|----------------|----------|-------------------------------|----------|
|                  |          | Calcul.                        | Experim. | Calcul.        | Experim. | Calcul.                       | Experim. |
| <sup>54</sup> Mn | III.1973 | 0,1                            | 0,2      | 0,25           | 0,25     | 0,7                           | 0,4      |
|                  | III.1974 | 0,15                           | 0,8      | 0,4            | 0,2      | 1,4                           | 1,5      |
|                  | X.1975   | 0,2                            | 0,15     | 0,55           | 0,4      | 2,0                           | 2,2      |
| <sup>60</sup> Co | III.1973 | 0,04                           | 0,07     | 0,08           | 0,5      | 0,1                           | 0,2      |
|                  | III.1974 | 0,07                           | 0,07     | 0,2            | 0,7      | 0,25                          | 0,2      |
|                  | X.1975   | 0,15                           | 0,11     | 0,4            | 0,9      | 0,5                           | 0,4      |

Table 5

Calculation and experimental (in brackets) values of fission products release rates into the coolant from failed fuel pins, % /6,8/

| Reactor | $^{85m}\text{Kr}$ | $^{87}\text{Kr}$ | $^{88}\text{Kr}$ | $^{133}\text{Xe}$ | $^{135m}\text{Xe}$ | $^{135}\text{Xe}$ | $^{131}\text{I}$ | $^{137}\text{Cs}$ |
|---------|-------------------|------------------|------------------|-------------------|--------------------|-------------------|------------------|-------------------|
| BOR-60  | 1,2<br>(0,5-0,8)  | 0,7<br>(0,2-0,3) | 0,3<br>(0,1-0,2) | 6,4<br>(4-5)      | 4,9<br>(3,3)       | 2,5<br>(1-2,5)    | 6,7<br>(2-9)     | 40<br>(20-40)     |
| BN-350  | 0,7<br>-          | 0,5<br>-         | 0,3<br>-         | 3<br>(2,5)        | 2,2<br>-           | 1,2<br>-          | 3<br>-           | 3,5<br>(3)        |

## REFERENCES

1. Influence of Flow Rate and Oxygen Content in Sodium on Steel Corrosion / Kraev N.D., Zotov V.V., Starkov O.V., et al., in Coll.: Technology and Corrosion Problems in Sodium Coolant and Shielding Gas, Dresden, Academy of Sciences of the GDR, z k-337, 1977, vol.1, p.57.
2. Corrosion of Construction Materials in Liquid Alkaline Materials / Nevzorov B.A., Zotov V.V., Ivanov V.A., et al. Ed. Nevzorov B.A., M., Atomizdat, 1977.
3. Lastman B., Radiative Phenomena in Uranium Dioxide, Transl. from Engl., Ed. Sokul'sky Yu.I., Kushakovsky V.I., Michunov L.V., M., Atomizdat, 1964.
4. Samsonov B.V., Sulaberidze V.Sh., Gas Evolution from Oxide Nuclear Fuel (Analytical Review), RIAR V-16, Dimitrovgrad, 1977.
5. Dick E.P., Determination of the Interwashing Period and Supercritical Parameters for the Washing Boilers on the Basis of Deposit Formation Studies. In Book: Water-Chemical Mode and Water Treatment at Powerful Boiler Electrical Stations and Thermal Electrical Centres. / Ed. Shtrob A.S., M.-L., Energiya, 1965, p.207.
6. Krasnoyarov N.V., Konyasnov V.V., Polyakov V.I., Chechetkin Yu.V., Fission Gas Release from BOR-60 Defected Fuel Pins, Atomnaya Energiya, vol.38, is.2, 1975, pp.67-71.
7. Radioactivity of Long-Lived Nuclides in BOR-60 Primary Circuit during Operation with Some Defected Fuel Elements Present in the Core, Preprint/Gryazev V.M., Kizin V.D., et al., RIAR P-5(299), Dimitrovgrad, 1977.
8. Study of BN-350 Protection/ Bakumenko O.D., Kulakovsky M.Ya., Tverdovsky N.D., et al., Report 5-th Internat. Conf. on Reactor Protection, Knoxville, 1977.

STUDY OF RADIONUCLIDE DISTRIBUTION IN BOR-60

V.D.Kizin, N.V.Krasnoyarov, V.I.Polyakov,

E.K.Yakshin

Research Institute of Atomic Reactors, Dimitrovgrad,

USSR

Abstract

The research results of radioactive corrosion and fission products distribution in the primary circuit of the BOR-60 fast test reactor are considered. The distribution coefficients between a coolant and equipment surface are obtained for significant radionuclides.

During BOR-60 operation the radioactive product distribution between media (gas, sodium, surface) and on the primary loop equipment (pipeline, pump, heat-exchanger) was systematically investigated.

To learn the behaviour of the significant radionuclides, their contribution to gamma dose rate from separate units of equipment when maintaining and repairing, to obtain data for development of design procedures and methods of coolant purification as well as pipeline and equipment decontamination were the essential investigation objects.

BOR-60 is a test loop-type reactor. The reactor is very convenient to investigate the radioactive products behaviour in the primary circuit. For the whole reactor operation the significant radionuclide concentration changes of coolant and surface were periodically measured. Included in Table 1,2 are some data on dynamics of the primary circuit surfaces contamination with fission and corrosion products.

A considerable information about the fission

Table 1

BOR-60 primary circuit contamination with radioactive products

| Year | An equivalent <sup>x)</sup> contamination of core with fuel, g |                          | Cover-gas activity, TBk/m <sup>3</sup> |                       | <sup>137</sup> Cs activity in sodium, KBk/g of sodium |                          |
|------|--|--------------------------|--|-----------------------|---|--------------------------|
|      | Increase per a campaign  | At the end of a campaign | Increase per a campaign                | At the end of a camp. | Increase per a campaign                               | At the end of a campaign |
| 1981 | 0.4  | 3.2                      | 3.5                                    | 4.1                   | 90  | 340                      |
| 1982 | 1.6  | 4.2                      | 2.7                                    | 3                     | 25  | 260                      |
| 1983 | 1.1  | 3.8                      | 1.1                                    | 1.2                   | 50  | 260                      |
| 1986 | 0  | 2.9                      | 2.6                                    | 3.3                   | 30  | 680                      |

x) Contamination of core with fuel was calculated by readings of delayed neutron detectors



Table 2

Average values of surface contamination in BOR-60 circuit, GBk/m<sup>2</sup>

| Nuclide           | Reactor operation period | Surface activity, GBk/m <sup>2</sup>    |                |   |
|-------------------|--------------------------|---|----------------|---|
|                   |                          | Pipeline from reactor to heat-exchanger | Heat-exchanger | Pipeline from heat-exchanger to reactor |
| <sup>95</sup> Nb  | 1972-1975                | 0.6                                     | 1.5            | 1.0                                     |
|                   | 1976-1981                | 0.7                                     | 0.8            | 3.8                                     |
|                   | 1982-1985                | 3.8                                     | not meas.      | 10.7                                    |
| <sup>140</sup> La | 1972-1975                | 0.2                                     | 0.9            | 2.2                                     |
|                   | 1976-1981                | 0.7                                     | 1.0            | 15                                      |
|                   | 1982-1985                | 0.7                                     | not meas.      | 19                                      |
| <sup>54</sup> Mn  | 1970-1971                | 0.1                                     | 0.2            | 0.4                                     |
|                   | 1972-1975                | 0.1                                     | 0.3            | 0.9                                     |
|                   | 1976-1981                | 0.2                                     | 0.4            | 3.4                                     |
|                   | 1982-1986                | 0.15                                    | not meas.      | 4.0                                     |
| <sup>60</sup> Co  | 1970-1971                | 0.04                                    | 0.35           | 0.2                                     |
|                   | 1972-1975                | 0.06                                    | 1.3            | 0.2                                     |
|                   | 1976-1981                | 0.1                                     | 0.5            | 0.3                                     |
|                   | 1982-1986                | 0.2                                     | not meas.      | 0.25                                    |

products behaviour is known to have been obtained at BOR-60. The fact that the reactor is made use of testing the fuel elements including the damaged ones favoured it.

Recent years the use is made of the mixed vibropack uranium-plutonium fuel (MVF) at BOR-60. As evidenced by the data listed in Table 1 levels of BOR-60 primary circuit contamination with the fission products did not worsen in comparison with levels of reactor operation period with uranium oxide fuel.  $^{137}\text{Cs}$  release rate from the failed fuel elements was roughly reduced about 4 times (Table 3). It seems to be a result of the fuel and fuel elements characteristics. The rupture development in MV fuel element claddings is believed to occur more slowly than in the pellet fuel elements.

In the last period  $^{137}\text{Cs}$  activity in coolant was increased as sodium was not decontaminated from it. At the end of 1986  $^{137}\text{Cs}$  activity has been reduced by a factor of 6 with the help of carbon traps /1/.

Table 3

$^{137}\text{Cs}$  release from failed elements of BOR-60

| Parameter  | Period     |            |           |
|--|------------|------------|-----------|
|  | 1971-1975  | 1981       | 1982-1986 |
| Mean value of $^{137}\text{Cs}$ release from fuel element, % | $24 \pm 6$ | $27 \pm 8$ | $6 \pm 2$ |

The activity change of other significant radioactive products ( $^{95}\text{Nb}$ ,  $^{140}\text{La}$ ,  $^{54}\text{Mn}$ ,  $^{60}\text{Co}$ ) is presented in Table 2. There took place a flattening of  $^{60}\text{Co}$  surface activity in the pipeline before and after a heat-exchanger. The contrary is the case for  $^{54}\text{Mn}$ . In recent years surface activity of  $^{54}\text{Mn}$  before and after the heat-exchanger increased by a factor of 1.5-2 but there was increase by a factor of 3-5 after it. The latter can be associated with increase of the fuel element claddings temperature of 20-40°C, ramping the reactor power and developing the core surface by a factor of 1.1-1.5 because of the growing number of fuel elements and height of their active part.

In recent period of the reactor operation  $^{95}\text{Nb}$  and  $^{140}\text{La}$  activities in deposition was increased. MVFA were under resource test and the opportunity of the prolonged fuel elements operation was under study.

The basic radionuclides all but  $^{137}\text{Cs}$  are mainly in depositions (Table 2): in the heat-exchanger, in the pipelines after the heat-exchanger, in the pump. There is non-uniform distribution of  $^{95}\text{Nb}$  and  $^{60}\text{Co}$  in the heat-exchanger: on the heat-exchanger inlet with a primary sodium stream the activity increases abruptly, then smoothly decreases to the heat-exchanger outlet. The value of the  $^{60}\text{Co}$  surface activity for this region is 2-20 times as high as that of the pipelines/2/.

In 1973 the radionuclide distribution on surfaces of a recessed part of the circulating pump is known /3/

Table 4

Surface activity of nuclides on recessed part of pump, GBk/m<sup>2</sup>

| Description                     | Radionuclide     |                  |                  |                   |                   |
|---------------------------------|------------------|------------------|------------------|-------------------|-------------------|
|                                 | <sup>54</sup> Mn | <sup>60</sup> Co | <sup>95</sup> Nb | <sup>140</sup> La | <sup>137</sup> Cs |
| Running wheel and skirt of pump | 0.9              | 0.2              | 8.3              | 6.4               | 2.5               |
| Displacer:                      |                  |                  |                  |                   |                   |
| - lower part                    | 0.5              | 0.2              | 3.2              | 0.6               | 4.6               |
| - middle part                   | 0.5              | 0.1              | 1.0              | 0.3               | 4.6               |
| - sodium-level area             | 0.02             | 0                | 0                | 0                 | 37                |
| - cover-gas                     | 0                | 0                | 0                | 0                 | 0.2               |

Table 5

Distribution coefficients of radionuclides between sodium and metal surface in primary circuit and reactor loop, cm

| Surface                           | Tempera-<br>ture, °C | Nuclide          |                  |                  |                   |                   |
|-----------------------------------|----------------------|------------------|------------------|------------------|-------------------|-------------------|
|                                   |                      | <sup>54</sup> Mn | <sup>60</sup> Co | <sup>95</sup> Nb | <sup>140</sup> La | <sup>137</sup> Cs |
| Samples in<br>test loop           | 310                  | 21               | 2.1              | 8                | 70                | 0.09              |
| Pipeline before<br>heat-exchanger | 500                  | 4-20             | 2-5              | 50               | 30-60             | 2.0               |
| Pipeline after<br>heat-exchanger  | 330                  | 200-300          | 10-20            | 200-300          | 500-600           | 2.2               |

to have been studied (Table 4).  $^{54}\text{Mn}$  was distributed nearly uniformly along all the surface to be in contact with the coolant. There was mainly  $^{60}\text{Co}$ ,  $^{95}\text{Nb}$ ,  $^{140}\text{La}$  in a region of the running wheel. There was caesium in a region of fluctuation of sodium level. It were only the caesium radionuclides which were recorded in a cover-gas region.

Distribution of radionuclides between the coolant and equipment surfaces of the primary circuit is one of the most important processes for the nuclear-reactor safety. The distribution coefficients defining this process were obtained for fast reactors mostly in test loops. At BOR-60 there was presented a good opportunity to verify as far as the data of the test loop measurement correlated with those obtained for the reactor equipment. The BOR-60 test loops were filled with coolant of the primary circuit. The loop sodium temperature is sustained at the temperature level of the reactor pipeline located after the heat-exchanger. The first circuit materials are identical with those of the loop. In spite of this the trial stainless steel samples failed within the loop for 90-1000 hours have revealed the results which considerably distinguished from the reactor ones. (Table 5).

Obtained from on-line measured activity in course of reactor shutdown (the sodium temperature is 220-230°C) the caesium distribution coefficient was  $2.0 \pm 0.7$  cm. Hence when reactor is shutdown there is up to 30 % caesium on surfaces in the first circuit at BOR-60 (a cold trap

is no account). The distribution coefficient obtained in loop tests would provide essentially lower value of caesium activity in depositions: at the same temperature the BOR-60 first circuit pipelines would contain less than 4 % of radioactive caesium /4/.

There is presented the most part of caesium in a cold trap. After entering oil in the coolant in 1976 caesium quota has been increased in trap up to 90 % of its total amount in circuit and preserved this level for next years /5/. Measurements revealed that other radioactive products concentrated in a cold trap too: 99 % of  $^{131}\text{I}$ , 85% of  $^{65}\text{Zr}$ , 20% of  $^{60}\text{Co}$ . There is a negligible activity of  $^{95}\text{Zr}$ ,  $^{140}\text{La}$ ,  $^{54}\text{Mn}$  in trap /6/.

On the whole the study revealed that if the number of failed fuel elements in the reactor core does not exceed 0.1-0.2 % then the gamma dose rate from fission products will not exceed that of corrosion  $^{54}\text{Mn}$ ,  $^{60}\text{Co}$ ,  $^{58}\text{Co}$  and activation ( $^{22}\text{Na}$ ,  $^{110m}\text{Ag}$ ,  $^{65}\text{Zn}$ ) nuclides. In this case the dose rate from equipment for the mentioned nuclides <sup>is 30-40</sup>  $\mu\text{mR}/\text{c}$  /2/. The reactor being operated. such levels do not make difficulty in maintenance and repair of equipment. While carrying out laborious maintenance works (replacement of electrical heating, cables, etc) the radioactive corrosion products are needed to be removed from circuit. While long-term operating with the failed fuel elements  $^{137}\text{Cs}$  could make the main contribution to gamma fields. However the problem of fast reactor sodium coolant contamination with caesium radionuclides

has been solved by developing and using of the special carbon traps in BOR-60.



REFERENCES:

1. The removal of caesium from the fast reactor primary sodium coolant. N.V.Krasnoyrov, V.I.Polyakov, A.M.Sobolev, E.K.Yakshin.- in Proc. 3 Int. Conf. of Liquid metal engineering and technology, LNES, London, 1984, v.3, p.185.
2. BOR-60 primary circuit radiation level/ V.D.Kizin, E.S.Lisitsyn, V.I.Polyakov, Yu.V.Chechetkin,- Atomnaya energiya, v.44, is.6, 1978, p.492.
3. Long-lived nuclide radioactivity in first circuit of BOR-60 while working failed fuel elements. Preprint RIAR/ V.G.Gryazev, V.D.Kizin, E.C.Lisitsyn, V.I.Polyakov, Yu.V.Chechetkin.- RIAR P-5 (299), Dimitrovgrad, 1977.
4. Caesium depositions on circuit surface when circulating of sodium coolant/ V.D.Kizin, N.V.Krasnoyrov, V.I.Polyakov, D.I.Starodhukov- Atomnaya energiya, v.61, is. 5, Nvember 1986, p.371.
5. Caesium nuclide behaviour while decontaminating of sodium coolant with cold and special traps : Preprint/ V.D.Kizin, N.V.Krasnoyrov, V.I.Polyakov, A.M.Sobolev- RIAR- 33(548).- Dimitrovgrad, 1982.
6. Radioactive addition trapping by BOR-60 cold trap: Preprint/ V.D.Kizin, E.S.Lisitsyn, G.I.Poznyak, V.I.Polyakov, Yu.V.Chechetkin-RIAR P-2(296), Dimitrovgrad, 1977.

MEASUREMENTS OF FISSION PRODUCTS AND ACTIVATED CORROSION  
PRODUCTS IN THE PRIMARY SODIUM CIRCUIT OF THE PROTOTYPE  
FAST REACTOR

L MASON B Sc, GRSC; E A TREVILLION PhD, C Chem MRSC; N S MORRISON LRSC and K B STEELE; UKAEA, DNPDE, Dounreay, Thurso, Caithness, Scotland, KW14 7NL

T H GREEN B Sc, Ph D; TAYLOR WOODROW; Winfrith, UK

INTRODUCTION

1. In an effort to understand the release and distribution of fission products and activated corrosion products in the primary circuit of the PFR a series of measurements have been undertaken in various parts of the reactor. These have included
  - (a) Sampling and analysis of primary circuit sodium
  - (b) Monitoring of the reactor vault using gamma spectrometry
  - (c) Measurements of dose rates in the Intermediate Heat Exchangers (IHxs) using Thermoluminescence Dosimetry (TLD)
  - (d) Measurements of dose rates and isotopic distribution in the primary cold trap by TLD, gamma spectrometry and deposit sampling and analysis
  - (e) Measurement of dose rate and isotopic distribution on components removed from the reactor
  
2. The high levels of Na<sup>24</sup> in the primary pool during operation have resulted in measurements being made during reactor shutdown after a suitable delay to allow for Na<sup>24</sup> decay. Thus measurements have been adventitious and it has not been possible to monitor on a continuous basis the increases in circuit contamination resulting from the production and release of activated corrosion products and fission products.

3. The note reviews the results of measurements made since 1980, concentrating almost exclusively on those isotopes of most interest (Cs134, Cs137, Mn54, Co60 and Zn65). The data are not yet sufficiently comprehensive to allow a proper assessment of existing models for the release and distribution of these isotopes but serve as a useful guide to expected levels in a working reactor.

#### PRIMARY SODIUM SAMPLING

4. Primary sodium samples have been obtained either directly from the primary sodium circuit or indirectly from reactor fuel transfer buckets via the Irradiated Fuel Cave (IFC).

#### SAMPLING FROM THE REACTOR FUEL TRANSFER BUCKET

5. Dip samples of primary sodium are obtained from reactor fuel transfer buckets in the IFC using a wire frame which supports four nickel crucibles lined with silica inserts (Figure 1). The silica inserts are used to reduce the preferential deposition of radionuclides onto the nickel crucibles. The sampler assembly is lowered into the reactor fuel transfer bucket containing the primary sodium, at a temperature of approximately 130°C, allowed to heat soak and fill with primary sodium for fifteen minutes, then removed and allowed to cool.

#### SAMPLING DIRECTLY FROM THE PRIMARY SODIUM CIRCUIT

6. Direct dip sampling of primary sodium is carried out using a 'torpedo' containing ten nickel crucibles lined with silica inserts (Fig 2).
7. The sampler assembly is lowered into the primary sodium circuit through a roof penetration in sector 7/3 above Intermediate Heat Exchanger (IHX) 2A tray. The exercise is normally carried out at least two weeks after the reactor shutdown when the inherent activity of the primary sodium, due to the activation product sodium 24, is reduced sufficiently to allow bagging techniques to be used. The 'torpedo' remains in the primary sodium for a period of two hours before being lifted into the reactor roof to allow the

sodium to solidify. The 'torpedo' is then transferred into a stainless steel transit container, within the bag above the reactor roof.

8. The samples of primary sodium are subsequently taken directly into solution by reaction with methanol, acidified with hydrochloric acid, evaporated to dryness and finally dissolved in one normal nitric acid to give a sodium concentration of approximately  $50 \text{ g litre}^{-1}$ . The resulting solutions are analysed by alpha spectrometry, gamma spectrometry and Inductively Coupled Plasma (ICP) emission spectroscopy.
9. A summary of the data obtained by gamma spectrometry for sodium 22, manganese 54, cobalt 60, zinc 65, caesium 134 and caesium 137 since mid 1980 is presented in Table 1 and Figures 3, 4 and 5.
10. The results for sodium 22 show the predicted steady increase with the cumulative PFR thermal power history, the most recent data indicating a primary circuit sodium 22 level of approximately  $405 \text{ n Ci g}^{-1}$  (Na).
11. The caesium 137 level in the primary sodium increased slightly up to the middle of 1981, most likely because of the defect failed fuel pin experiment which was removed from the reactor in September 1981. From mid 1982 to the beginning of 1984 there was a significant decrease in caesium 137 level which is thought to reflect the removal of caesium from the primary sodium circuit by the operation of the primary cold trap. The caesium 137 level showed a marked increase from the beginning of 1984 onwards reflecting the series of fuel pin failures (1) encountered in the PFR core during this period. The caesium 134 level was apparently relatively steady from the end of 1980 to the beginning of 1984, possibly as the measurements were close to the detection limit for the radionuclide and were thus not reflecting any real trend. From the beginning of 1984 the caesium 134 level showed a marked increase, again reflecting the series of fuel pin failures encountered in the PFR core during this period.
12. The available data on zinc 65 in the primary sodium is inconsistent with any predictable trend. The operation of

the primary cold trap loop from mid 1982 to the beginning of 1984 may have reduced the zinc 65 level in the primary sodium below the detection limit.

13. Levels of Mn54 showed an approximately steady increase from December 1980 until June 1985. Levels in the December 1985 sample, however, were apparently lower even allowing for the decay which resulted as a consequence of the delay in analysing this particular set of samples (the figures in Table 1 are as measured; allowing for the delay time in analysis an estimate of around 1.3 nCi/g is obtained for the level at the time of sampling). No Mn54 was seen in the most recent set of samples. It is not clear at this stage why Mn54 levels have apparently decreased.
14. In the case of Co60 the extreme variability of results (even within a particular set of sodium samples, See Table 2) suggests perhaps that Cobalt is present in particulate form. However, even the highest level of Co60 measured (PNa23, 45nCi/gNa equivalent to  $4 \times 10^{-5}$  ug/g) is below that predicted for the solubility limit at 550°C (0.016 ug/g (Na) ref 2). This suggests that either the cobalt 60 is not in a readily soluble form or that the available solubility data on cobalt is incorrect.
15. There has been no evidence for the presence of uranium or plutonium, above background, in any of the primary sodium samples analysed to date.

#### PFR VAULT GAMMA SPECTROMETRY

16. The bottom of the PFR reactor vessel has been routinely monitored during reactor shutdowns by gamma spectrometry to observe any changes in radionuclide distribution below the diagrid.
17. A collimated intrinsic germanium detector is aligned with the reactor core centre line and connected through its associated electronics to a multi channel analyser (ND 6 MCA). A typical gamma spectrum is obtained with a live time count of between eighteen and twenty-four hours. The background gamma spectrum is estimated by moving the detector out of the direct shine path of the reactor vessel.

18. The results are corrected for relative detector efficiency factor, abundance and background. As yet no correction for geometry has been undertaken because of the relatively complex geometry in question. As a consequence it is not possible to measure the radionuclide concentrations absolutely and results have therefore been expressed as a ratio relative to sodium 22. The results obtained since 1979 when the measurements were first undertaken, are summarised in Table 3.
  
19. The trends in caesium 134 and caesium 137 level noted in the primary sodium samples are, in general, confirmed by the PFR vault measurement. Ratios relative to Na22 from the middle of 1981 to December 1986 (Table 3 and Fig 6) are in reasonable agreement with those observed in sodium samples (Table 4) apart from measurements made during the Reload 10 shutdown in December 1985. In this case the Cs137:Na22 ratio in the sodium samples is much higher than that indicated in the reactor vault measurement. The result suggests that the Cs137 measurement in the sodium sample is high since it does not agree with either the vault scan result or Cs137 trends in primary sodium samples. The reason for this apparently anomolous result has not yet been established. Small differences in measured ratios for the remainder of the samples taken during this period compared to the vault scans may reflect different geometry and attenuation factors (as a result of the reactor vessel) for Cs137 compared to Na22 in the latter.
  
20. The data on Mn54 and Co60 from the scans shows some variability but much less than that observed in sodium samples. Although the isotope:Na22 ratios show no increasing trend overall (apart from two results for Mn54 in Reloads 10 and 11), in real terms the absolute levels of Mn54 and Co60 are increasing because Na22 levels have increased over the period (See Table 1). The isotope:Na22 ratios in the scans are much higher than those observed in the sodium samples. This may reflect either increasing Mn54 and Co60 levels in the diagrid structure itself as a result of increased activation or increasing deposition of Mn54 and Co60 particulate material on the bottom of the reactor vessel.

## INTERMEDIATE HEAT EXCHANGER MONITORING

### THERMOLUMINESCENCE DOSIMETRY

21. Thermoluminescence Dosimetry (TLD) has been used to monitor activity build-up in the IHXs because of the difficulty in obtaining gamma spectra at the temperatures pertaining (greater than 250<sup>o</sup>C). This has been possible by virtue of the presence of a one inch nominal bore tube which penetrates 11 metres vertically into the reactor and 2.5 metres into the IHX tube bundle. Two types of TLD's have been used, calcium fluoride and pre-dosed quartz (silicon dioxide). Calcium Fluoride was used initially. However, this material performs best at temperatures up to 250<sup>o</sup>C, although it can be used up to 290<sup>o</sup>C with poorer results. In view of these temperature limitations and the increase of typical shutdown temperatures to around 300<sup>o</sup>C, pre-dosed quartz was looked at as an alternative. Evidence suggests that this material can be used at temperatures up to 550<sup>o</sup>C, although tests at Dounreay have only been carried out at temperatures up to 350<sup>o</sup>C. The various measurements obtained in the IHX to date are summarised in Figure 7. This shows the measured dose rate as a function of distance below the top tubeplate of the IHX (3,4).
  
22. The most recent dose rate profile is similar to those previously obtained but a factor of 3 higher, peaking at about 10 m Sv h<sup>-1</sup> one hundred centimetres below the top tube plate. Reference 3 notes that the observed activity profile in the PFR IHXs is not consistent with existing predictions based on the deposition of Mn54 and Co60 and suggests that another isotope and/or kinetic mechanism may be responsible. Although further speculation is not justified until the isotope responsible for the activity peak is firmly identified, reference 3 does suggest that caesium, resulting from fuel failures in the PFR core, may be responsible, possibly associated with carbonaceous deposits resulting from an oil spillage early in the life of the reactor. In this context it is worth noting that during cleaning and decontamination of the PFR charge machine caesium has been shown to be mainly associated with carbonaceous deposits resulting from the use of carbon containing freezing agents on the charge machine bearings (5).
  
23. More recent work has concentrated on the development of a gamma spectrometry technique which can be used at temperatures of 250-300<sup>o</sup>C. Initial experiments used a caesium iodide crystal connected to a small photomultiplier contained in a glass vacuum flask, within a stainless steel container. The assembly was lowered into IHX 2B monitoring

thimble at a temperature of 270°C. The high temperature gamma spectra obtained (4) were heavily degraded, however, as a result of relatively high radiation levels causing the caesium iodide crystal and the photomultiplier to saturate.

24. An improved high temperature gamma spectrometer utilising a bismuth germanate crystal was subsequently used and identified caesium 137 and sodium 22 in the ratio of 4 to 1. Further work will be carried out later this year in order to verify the result.

#### PRIMARY COLD TRAP LOOP

25. When a primary cold trap basket was removed in 1982 the opportunity was taken to sample sodium and sodium oxide/hydride deposits found in the bottom of the vessel. The results indicated that the caesium 137 level was much higher than would have been expected from primary sodium samples. At that time the typical primary sodium caesium 137 concentration was approximately  $89 \text{ n Ci g}^{-1} (\text{Na})$ . In comparison the primary cold trap samples had a concentration of between 1000 - 1200  $\text{n Ci g}^{-1} (\text{Na})$  of Cs 137.
26. In order to confirm the apparent removal of caesium by the primary cold trap loop, TLD was used to measure the dose rates down the central thimble of the replacement basket during the Reload 9 and 10 shutdowns. The measurements were made fourteen days after the reactor was shutdown to ensure that dose rates were not affected by Na24.
27. Dose rates measured in the Reload 9 shutdown (June 1985) were in the range  $10\text{-}200 \text{ mSvhr}^{-1}$ . Similar measurements during the Reload 10 shutdown in December 1985 were in the range  $10\text{-}120 \text{ mSvhr}^{-1}$ . There are no previous measurements with which to compare these results directly but it can be noted that they are significantly higher than measurements made by conventional techniques in the cold trap basket removed in 1982. In this case dose rates were typically less than  $10 \text{ mSvhr}^{-1}$ . The most recent measurements may reflect higher Cs137, 134 levels as a result of recent fuel failures.



28. In an effort to understand these increasing dose rates an attempt was made during the Reload 10 shutdown to identify specific radionuclides by inserting a gamma spectrometer (as per Section 23) down the central thimble. Although a badly degraded spectrum was obtained, there were indications that caesium 137 was the dominant radionuclide present (cobalt 60 was also present but to a lesser extent).
29. The mechanism for caesium removal in the primary cold trap loop is not known with any certainty. The element is not cold trappable in the normally accepted manner since it is completely miscible with liquid sodium at temperatures as low as 100°C. However, caesium has a propensity for absorption on a variety of surfaces and it is possible that the removal mechanism from the primary sodium depends upon the presence of carbon, sodium oxide or sodium chromite in the cold trap vessel.

#### REACTOR COMPONENT MONITORING

30. Two PFR Argon Gas Blanket (AGB) sodium aerosol filters have been removed from the clean-up plant, one in 1982 the other in 1984 (6). In both cases the main radionuclide present was caesium 137 which gave rise to radiation fields of 30 m Sv hr<sup>-1</sup> gamma generally and 130 m Sv hr<sup>-1</sup> at 'hot spots' (nominally the cooler regions of the aerosol filter).
31. The more surprising observation was the presence of manganese 54 and cobalt 60. The relatively high volatilities of caesium and zinc (zinc 65 was also identified in the aerosol filter) are understood but currently there is no obvious explanation for the behaviour of manganese and cobalt.
32. The phenomenon of Co60 and Mn54 deposition in gas spaces has been noted previously, however. Thus such deposition has been reported in France (7) and was observed during the removal of a carbon meter rig from the primary circuit of PFR in 1982. Further work is required to establish the transport mechanism.

ESTIMATES OF CAESIUM RELEASE FROM FAILED FUEL PINS IN THE PFR

33. The data on primary sodium circuit caesium 137 burdens up to June 1985 has been used to compare predicted and measured primary sodium circuit caesium 137 inventories following fuel pin failures (Table 5) (1). The comparison is made on the basis of estimates from the FISPIN code that a fuel pin irradiated to 10% burn-up contains 45 Ci of caesium 137. The estimates assume that gas leakers' did not release caesium 137.
34. When using Table 5 it should be noted that the primary sodium circuit was cold trapped between the June 1982 and January 1984 measurement of the caesium 137 level. The January 1984 caesium 137 level has, therefore, been used as a base line for subsequent failures. Cold trapping during the period January 1985 to September 1985 may also have mitigated the caesium 137 level measured in June 1985.
35. The results indicate:
- (a) The failures PFR1, PFR2 and the defect pin experiment released 37.5% of their calculated caesium 137 inventory. If it is assumed that the 'gas leakers' in PFR2 also contributed to the caesium 137 release, this figure reduces to 22%.
  - (b) For the failures PFR5 and PFR6 the percentage caesium 137 release was around 20% assuming one fuel pin failure in PFR5 and twelve in PFR6. For two fuel pin failures in PFR5 this figure reduces to 19% and for three fuel pin failures to 18%. These represent conservative estimates since almost certainly they would have been higher in the absence of cold trapping.

CONCLUSIONS

36. Primary sodium sampling and analysis since 1980 has indicated, in general, increasing Cs137 and Cs134 levels in the primary circuit of PFR. These increasing levels reflect the fuel pin failures experienced on the plant during this period. There has been no evidence for the presence of uranium or plutonium above background.

37. Gamma spectrometry in the reactor vault has, in general, reflected the results for Cs137 and Cs134 observed in the primary sodium samples.
38. Gamma spectrometry and TLD in the primary circuit cold trap suggests that some of the caesium released to the primary circuit from fuel failures has been deposited in this region.
39. Estimates of Cs137 levels in the primary circuit suggest that between 18 and 37% of a fuel pin Cs137 inventory is released during fuel failures. The data at the higher end of the range is thought to be more reliable and it is therefore suggested that 35% is taken as a working assumption until more precise data becomes available.
40. Dose rate measurements in the IHXs are not consistent with current models for Mn54 and Co60 deposition. There is evidence for suggesting that Cs137 may be responsible for observed activity profiles.
41. Caesium contamination levels on components removed from the PFR may be as much a consequence of the presence carbonaceous deposits as of activity in the coolant.
42. Gamma spectrometry in the reactor vault indicates higher levels of Co60 and Mn54 relative to Na22 than are observed in primary sodium samples. These higher levels may be due to either activation of the diagrid structure or to deposition of particulate material below the diagrid.
43. Co60 and Mn54 have been observed in areas of components exposed only to sodium vapour. The transport of these isotopes in the vapour phase is not understood and further work is required to elucidate the mechanism.

**ACKNOWLEDGEMENTS**

The authors wish to thank the UKAEA for permission to publish this paper and acknowledge the efforts and assistance of Mr T S Peat in the high temperature gamma spectrometry work.

REFERENCES

1. GREGORY, C V; LENNOX, T A and TREVILLION, E A. An Assessment of Fuel Cladding Failure Experience at PFR.

Conference on 'Fast Breeder Systems: Experience gained and Path to Economical Power Generation'. Richland, Washington, 13-17 September 1987, to be published.

2. PELLET C R and THOMPSON R. 'Liquid Metal Engineering and Technology' Oxford 9-13 April 1984.

3. VOICE, E H. Measuring Activity in the Intermediate Heat Exchangers of the Prototype Fast Reactor.

Third International Conference on 'Liquid Metal Engineering and Technology'. Oxford, 9-13 April 1984.

4. GREEN T H and PEAT T S. Unpublished work 1986.

5. WHITLOW W H, SHAW R L, MASON L, ROBERTSON C M. Sodium cleaning and decontamination of the PFR fuel charge machine.

Third International Conference on 'Liquid Metal Engineering and Technology'. Oxford 9-13 April 1984.

6. MASON, L; TREVILLION, E A and MELHUISE, K R. A Review of the Operational Experience with the PFR Sodium Aerosol Filters.

International Working Group on Fast Reactors. Specialists' Meeting on 'Heat and Mass Transfer in the Reactor Cover Gas'. Harwell, England, 8-18 October 1985.

7. KREMSER, J and LACROIX, A. Some Aspects of Sodium Technology issued from the Operating Experience of Rapsodie and Phenix.

Second International Conference on 'Liquid Metal Technology in Energy Production'. Champion, Pennsylvania, 3-6 May 1976.

TABLE 1

PFR PRIMARY SODIUM SAMPLE GAMMA SPECTROMETRY RESULTS  
 (ABSOLUTE RADIONUCLIDE CONCENTRATIONS)

| Radionuclide<br>Sample | Sodium 22<br>n Ci g <sup>-1</sup> (Na) | Manganese 54<br>n Ci g <sup>-1</sup> (Na) | Cobalt 60<br>n Ci g <sup>-1</sup> (Na) | Zinc 65<br>n Ci g <sup>-1</sup> (Na) | Caesium 134<br>n Ci g <sup>-1</sup> (Na) | Caesium 137<br>n Ci g <sup>-1</sup> (Na) |
|------------------------|--|---|--|--------------------------------------|--|--|
| PNa 10<br>(21/12/1980) | 147                                    | 0.56                                      |  |                                      | 0.79                                     | 8.9                                      |
| PNa 11<br>(18/04/1981) | 129                                    | 0.37                                      | 1.0                                    | 0.29                                 | 0.56                                     | 9.2                                      |
| PNa 12<br>(04/07/1981) | 143                                    |   | 8.1                                    | 0.80                                 | 0.76                                     | 13.2                                     |
| PNa 13<br>(20/05/1982) | 183                                    | 0.75                                      | 2.9                                    |                                      | 0.71                                     | 12.5                                     |
| PNa 18<br>(06/01/1984) | 182                                    | 1.2                                       | 1.0                                    | 1.2                                  | 0.60                                     | 6.4                                      |
| PNa 21<br>(20/06/1985) | 265                                    | 3.1                                       |  |                                      | 43                                       | 135                                      |
| PNa 22<br>(18/12/1985) | 295                                    | 0.80                                      | 0.90                                   |                                      | 59                                       | 318                                      |
| PNa 23<br>(15/12/1986) | 405                                    |   | 45*                                    |                                      | 30                                       | 137                                      |

\* Particulate Co60 (?)

TABLE 2  
VARIATION OF COBALT 60 CONCENTRATION  
WITHIN A PRIMARY SODIUM SAMPLE

| Radionuclide<br>Sample   | Cobalt 60<br>n Ci g <sup>-1</sup> (Na) |
|--------------------------|--|
| PNa 23/1<br>(15/12/1986) | 2.2                                    |
| PNa 23/2                 | 7.7                                    |
| PNa 23/3                 | 45                                     |

TABLE 3  
PFR VAULT GAMMA SPECTROMETRY RESULTS  
(RADIONUCLIDE RATIOS RELATIVE TO SODIUM 22)

| Radionuclide<br>Scan         | Sodium 22<br>* | Manganese 54<br>* | Cobalt 60<br>* | Zinc 65<br>* | Caesium 134<br>* | Caesium 137<br>* |
|------------------------------|----------------|-------------------|----------------|--------------|------------------|------------------|
| Reload 1<br>(April 1978)     | 1.00           | 0.31              | 2.64           |              |                  |                  |
| Reload 2<br>(December 1978)  | 1.00           | 0.34              | 3.22           |              |                  |                  |
| Reload 4<br>(September 1979) | 1.00           | 0.50              | 1.56           |              |                  | 0.34             |
| Reload 4<br>(October 1979)   | 1.00           | 0.47              | 1.49           |              |                  | 0.42             |
| Reload 4<br>(January 1980)   | 1.00           | 0.49              | 1.85           |              |                  | 0.51             |
| Reload 5<br>(September 1981) | 1.00           | 0.52              | 1.58           |              |                  | 0.05             |
| Reload 5<br>(October 1981)   | 1.00           | 0.50              | 1.57           |              |                  | 0.05             |
| Reload 6<br>(March 1982)     | 1.00           | 0.50              | 1.63           |              |                  | 0.08             |
| Reload 7<br>(November 1983)  | 1.00           | 0.48              | 2.10           |              |                  | 0.04             |
| Reload 8<br>(December 1984)  | 1.00           | 0.42              | 1.65           |              |                  | 0.06             |
| Reload 9<br>(June 1985)      | 1.00           | 0.48              | 1.55           |              | 0.07             | 0.40             |
| Reload 10<br>(December 1985) | 1.00           | 0.77              | 1.31           |              | 0.05             | 0.23             |
| Reload 11<br>(July 1986)     | 1.00           | 0.83              | 1.03           | 0.02         | 0.04             | 0.26             |

\* Raw data corrected for background, relative detector efficiency factor, and abundance finally expressed as a ratio relative to sodium 22 (= 1.00)



TABLE 4

PFR PRIMARY SODIUM SAMPLE GAMMA SPECTROMETRY RESULTS

RADIONUCLIDE RATIOS RELATIVE TO SODIUM 22)

| Radionuclide<br>Sample | Sodium 22 | Manganese 54 | Cobalt 60 | Zinc 65 | Caesium 134 | Caesium 137 |
|------------------------|-----------|--------------|-----------|---------|-------------|-------------|
| PNa 10<br>(21/12/1980) | 1.00      | 0.00(4)      |           |         | 0.00(5)     | 0.06        |
| PNa 11<br>(18/04/1981) | 1.00      | 0.00(3)      | 0.00(8)   | 0.00(2) | 0.00(4)     | 0.07        |
| PNa 12<br>(04/07/1981) | 1.00      |              | 0.06      | 0.00(6) | 0.00(5)     | 0.09        |
| PNa 13<br>(20/05/1982) | 1.00      | 0.00(4)      | 0.02      |         | 0.00(4)     | 0.07        |
| PNa 18<br>(06/01/1984) | 1.00      | 0.00(7)      | 0.00(5)   | 0.00(7) | 0.00(3)     | 0.04        |
| PNa 21<br>(20/06/1985) | 1.00      | 0.01         |           |         | 0.16        | 0.51        |
| PNa 22<br>(18/12/1985) | 1.00      | 0.00(3)      | 0.00(3)   |         | 0.20        | 1.08        |
| PNa 23<br>(15/12/1986) | 1.00      |              | 0.11*     |         | 0.07        | 0.34        |

\* Particulate Cobalt 60?

TABLE 5

## SUMMARY OF PFR FAILED FUEL PIN EVENTS

| Date                  | Event                 | Number of Failed Fuel Pins    | Peak Pin Burn-Up (%) | Predicted Caesium 137 Inventory of Failed Fuel Pins (Total) (Ci) | Cumulative Predicted Primary Sodium Circuit Caesium 137 Inventory (Ci) | Measured Primary Sodium Circuit Caesium 137 Inventory (Ci) |
|-----------------------|-----------------------|-------------------------------|----------------------|--|--|--|
| October 1978          | PFR 1                 | 2                             | 1.2                  | 10.8   | 10.8   |  |
| February 1979         | PFR 2                 | 1*                            | 2.3                  | 10.35  | 21.15  |  |
| 1978 - September 1981 | Defect Pin Experiment | 1                             |                      | 7.6  | 28.75  |  |
| June 1982             |                       |                               |                      |  |  | 10.8   |
| October 1983          | PFR 3                 | N/A                           |                      |  |  |  |
| January 1984          |                       |                               |                      |  |  | 6.0  |
| April 1984            | PFR 4                 | Not Examined                  | 0                    | N/A  |  |  |
| August 1984           | PFR 5                 | Not Examined<br>1 Pin Assumed | 3                    | 13.5   | 42.25  |  |
| April 1985            | PFR 6                 | 12 <sup>+</sup>               | 10.8                 | 583.2  | 625.45   |  |
| June 1985             |                       |                               |                      |  |  | 121  |

\* In addition there were two 'gas leakers' identified

<sup>+</sup> Identified by post irradiation examination to date

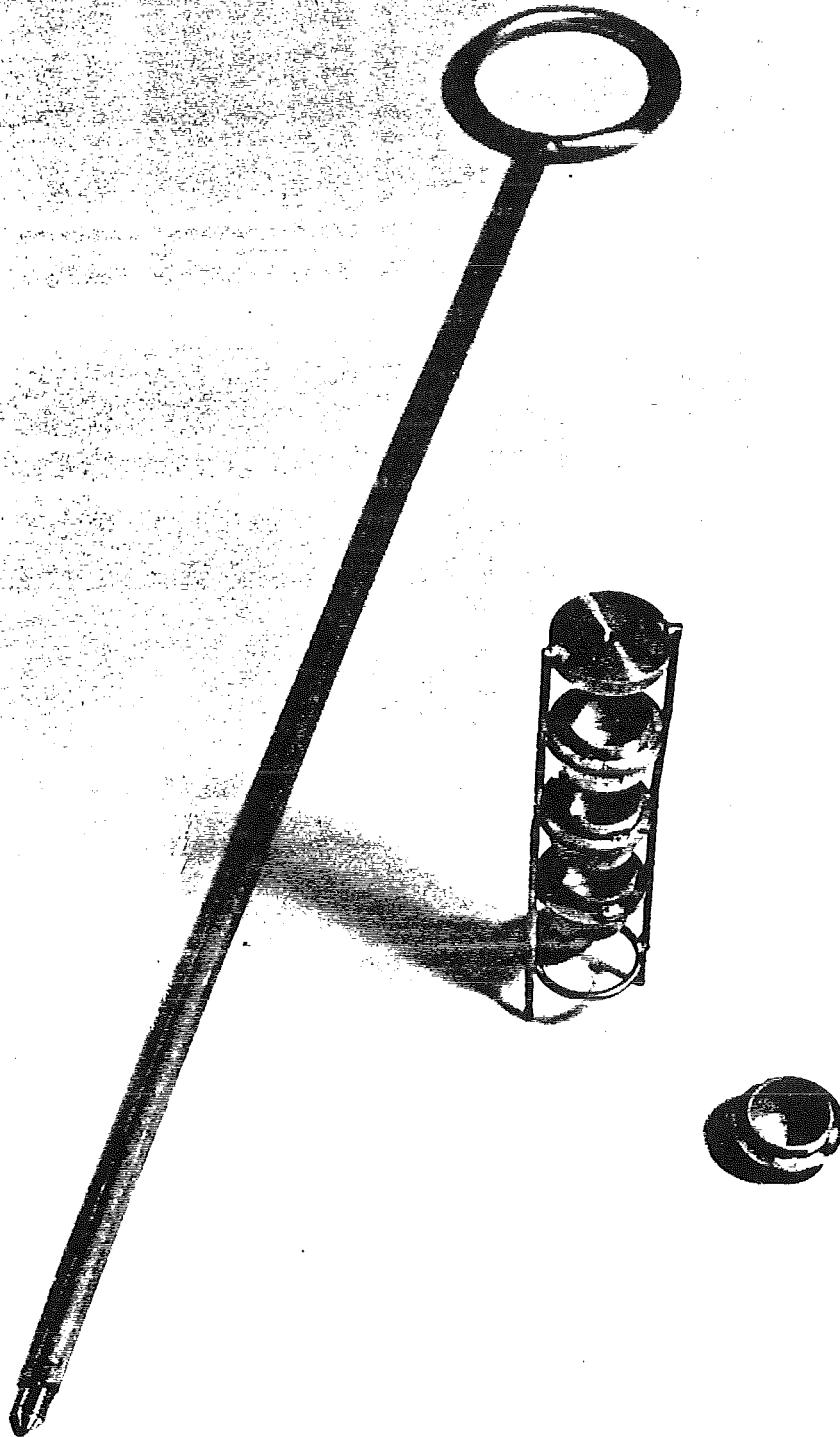


FIG.1 P.F.R. FUEL TRANSFER BUCKET  
SODIUM SAMPLER

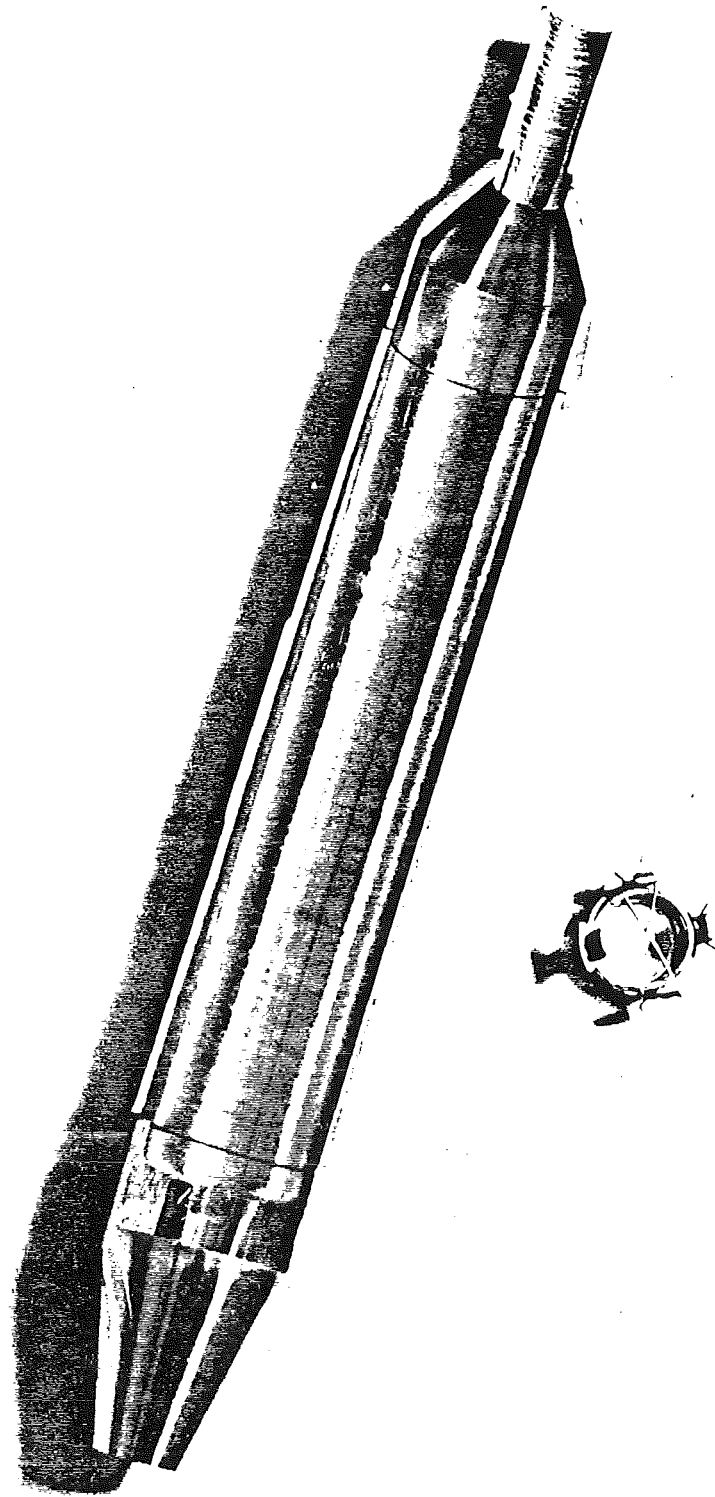


FIG.2 P.F.R. SODIUM SAMPLER "TORPEDO"

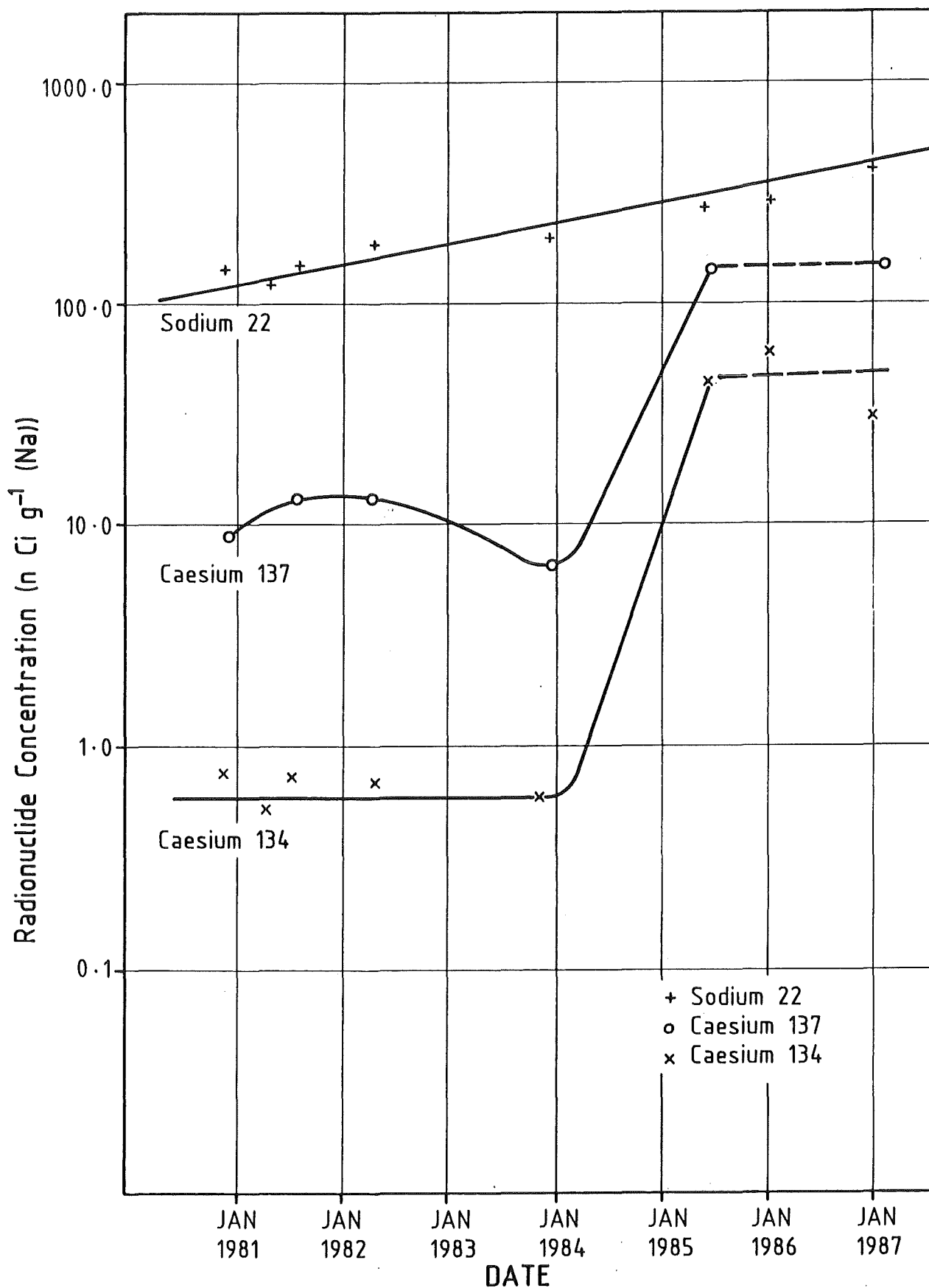


FIG.3 P.F.R. PRIMARY SODIUM SAMPLE  
GAMMA SPECTROMETRY RESULTS  
(Sodium 22, Caesium 134 & Caesium 137)

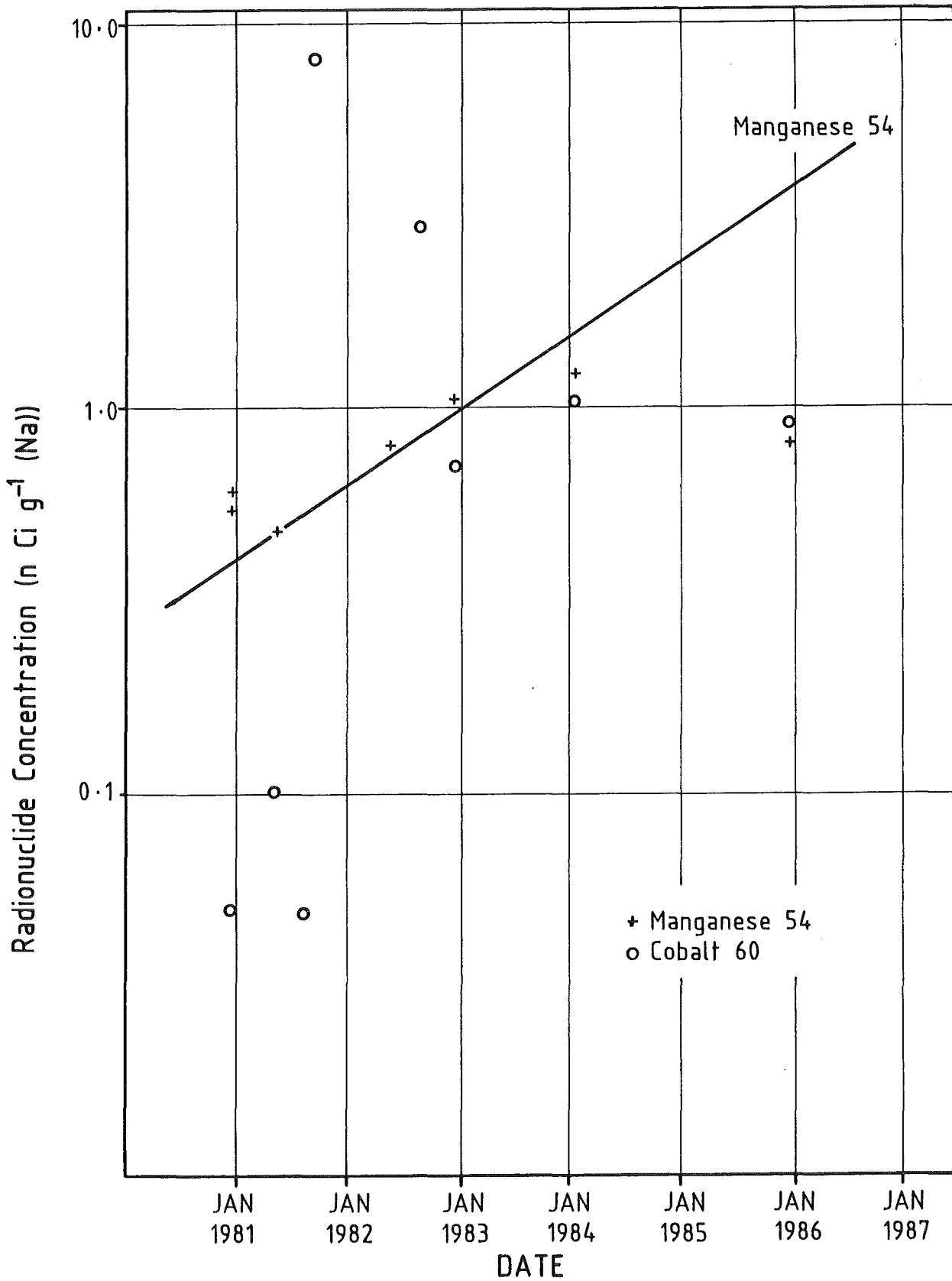


FIG.4 P.F.R. PRIMARY SODIUM SAMPLE  
GAMMA SPECTROMETRY RESULTS  
(Manganese 54 and Cobalt 60)

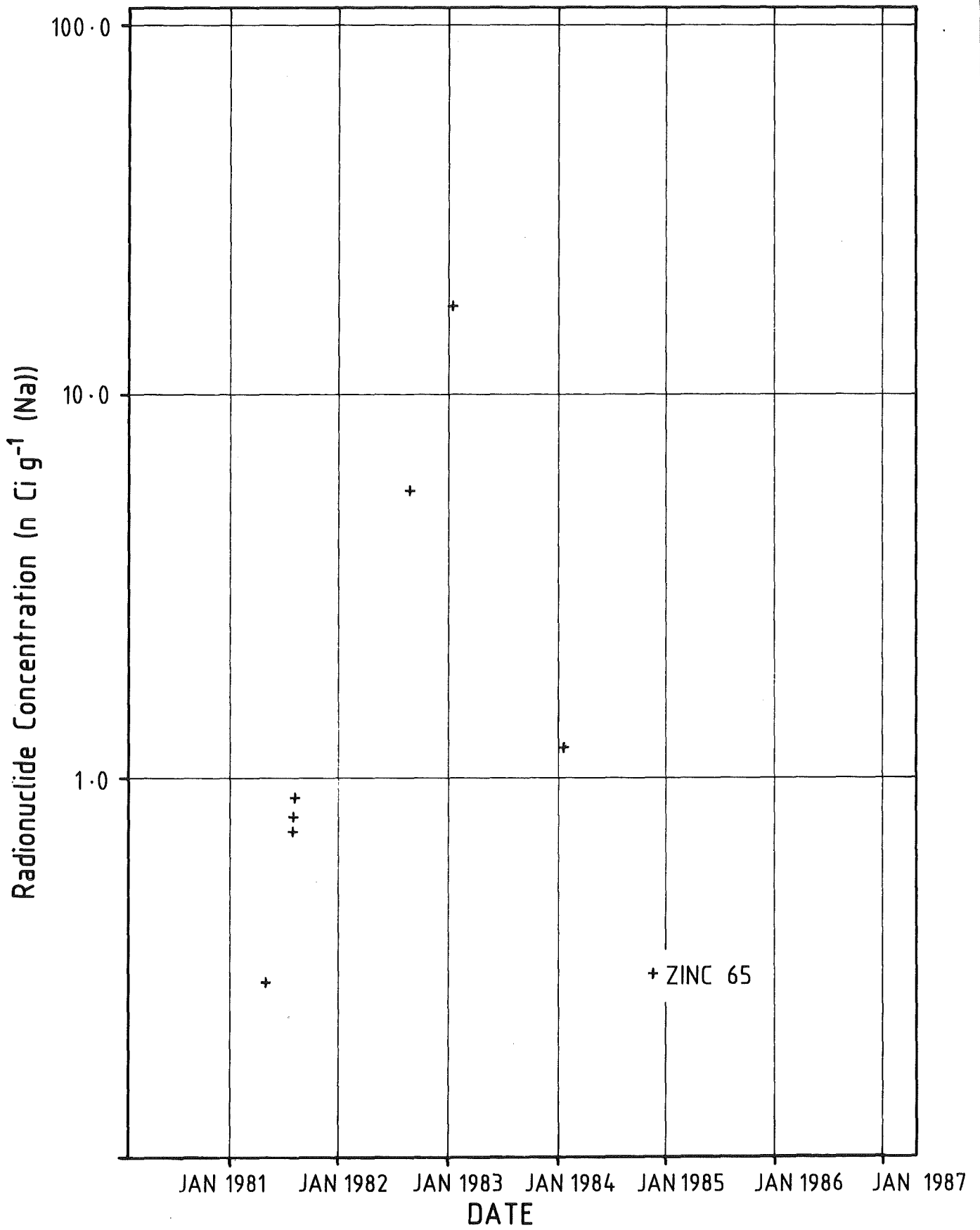


FIG.5 P.F.R. PRIMARY SODIUM SAMPLE  
GAMMA SPECTROMETRY RESULTS  
(Zinc 65)

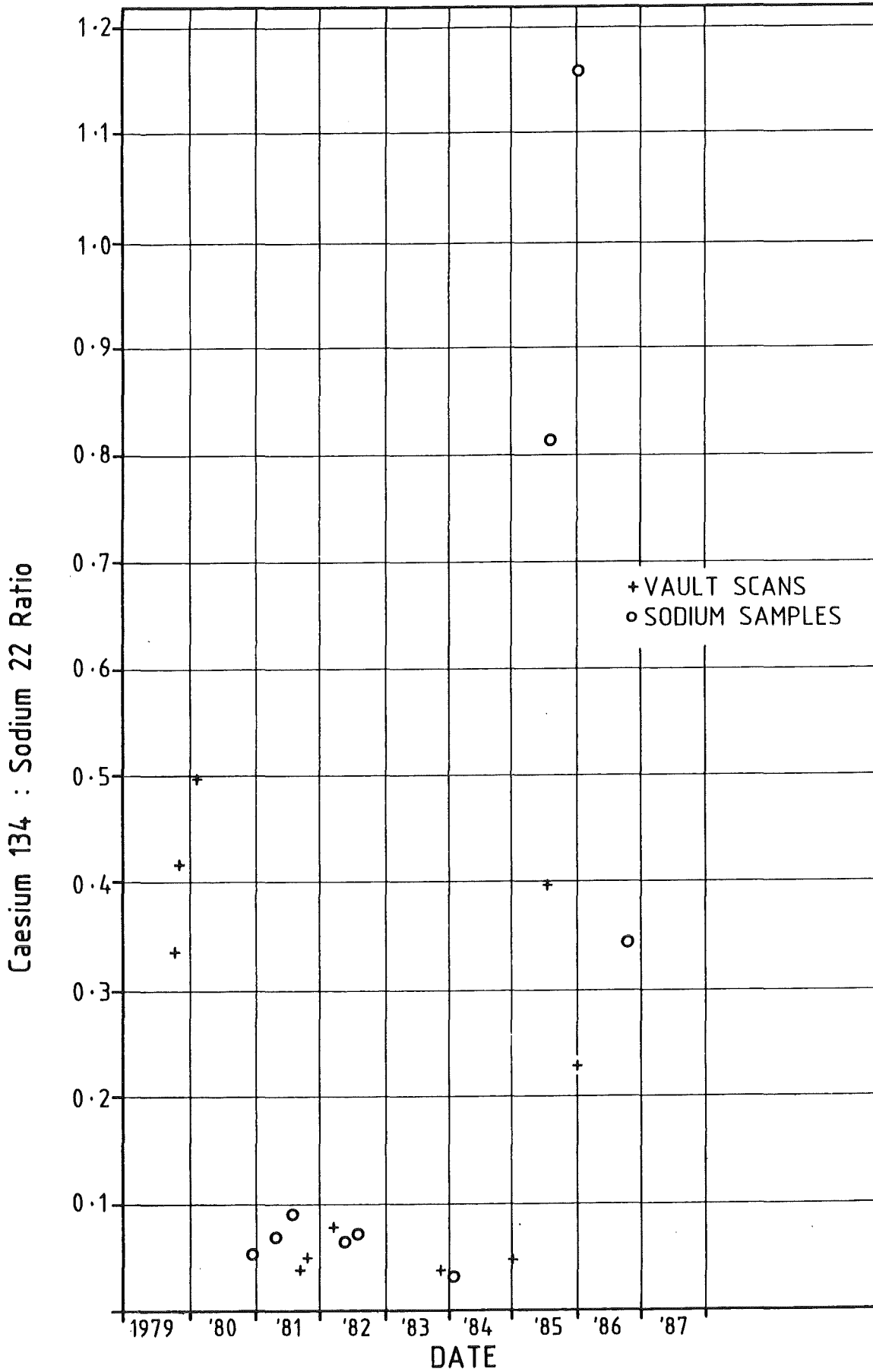


FIG.6 P.F.R. VAULT & PRIMARY SODIUM SAMPLE GAMMA SPECTROMETRY RESULTS (Radionuclide Ratio Relative to Sodium 22)



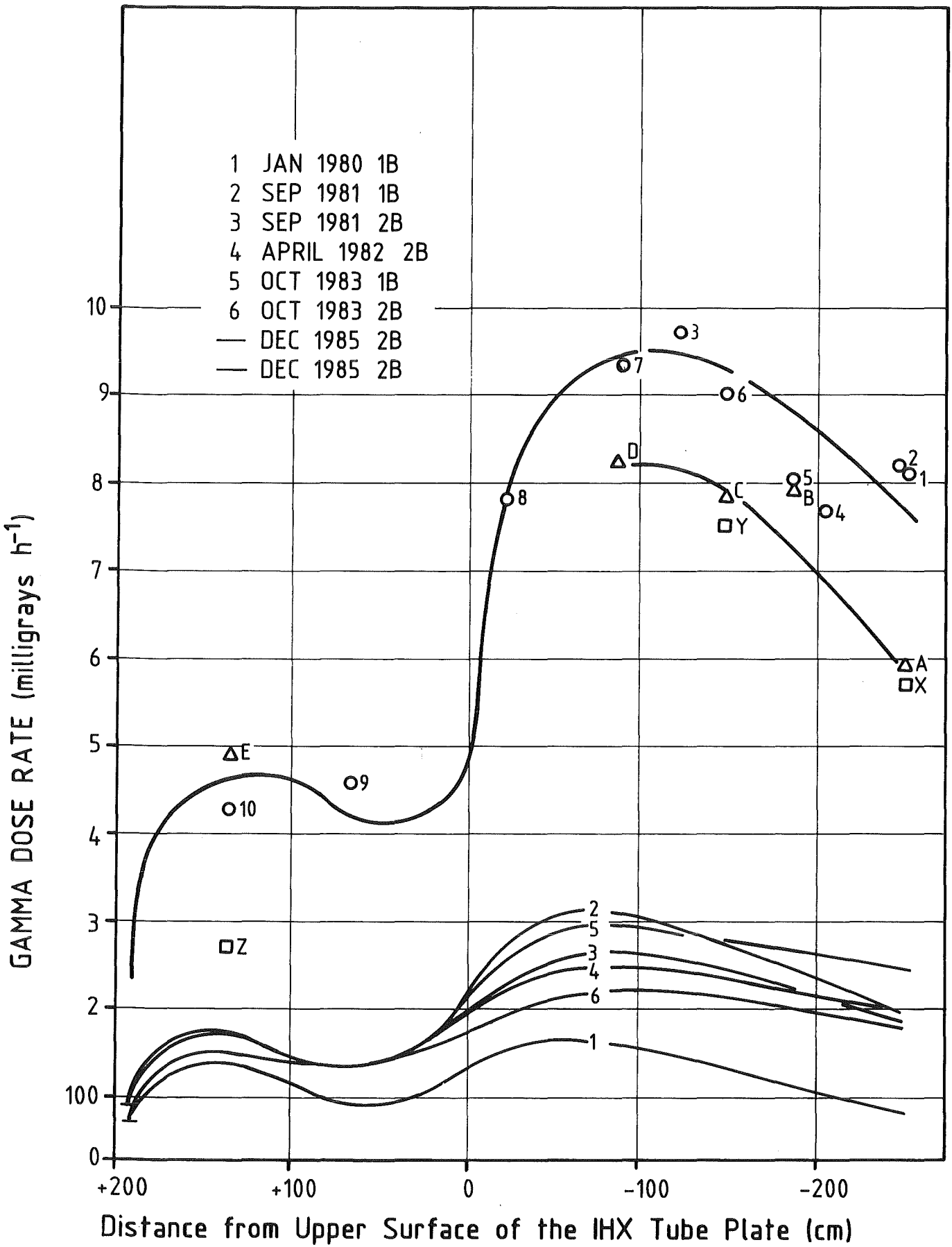


FIG.7 P.F.R. INTERMEDIATE HEAT EXCHANGER THERMOLUMINESCENCE DOSIMETRY RESULTS

Paper presented at an IAEA Specialists' Meeting on  
Fission and Corrosion Product Behaviour in Primary Circuits of LMFBRs,  
Karlsruhe, Federal Republic of Germany, May 5-8, 1987

On the chemistry of defective fuel pins in LMFBRs

by

M A Mignanelli, P E Potter

Chemistry Division, Harwell Laboratory, Oxon OX11 0RA, UK

#### Abstract

The various chemical reactions which can occur between sodium and irradiated oxide fuel are discussed in detail in terms of the individual oxide and fission product systems. We also discuss the contamination of the primary circuit by dissolved fission product species and particulate matter. Reference is made to observations on failed fuel in operating reactors and loops and to some laboratory experiments which are providing information on the release of fuel and fission product species into liquid sodium; the subsequent fate of these species is described. The formulation of a computer code which models the behaviour of failed fuel is considered.

#### 1. Introduction

This paper is concerned with the chemical changes which can occur on failure of fuel pins and the consequences of such failures for the contamination of the primary circuit by fuel and fission product species. In the first part of this paper, we shall summarise the essentials of the chemistry of the reactions of sodium with urania, plutonia, and urania-plutonia solid solutions. We shall also discuss the effects of the presence of dissolved fission product cations, such as those of the lanthanides on the reaction of urania-plutonia with sodium.

In an operating fuel pin, migration of oxygen, fuel and fission product species can occur due to the steep temperature gradients. As a result of this temperature gradient fission products elements will be found in the colder regions of the fuel pin such as the fuel-clad gap and their quantities and chemical constitution will depend on the conditions of irradiation of the fuel.

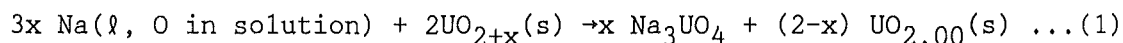
When the cladding is breached, any sodium which enters a pin could react both with the matrix of the fuel, a solid solution of urania-plutonia containing dissolved fission product cations, and with the fission product compounds in the fuel-clad gap. Such reactions can lead to the contamination of the primary circuit.

In the final part of the paper we shall discuss, in more detail, aspects of the consequences of these reactions, some of our experimental and modelling studies as well as observations in reactor systems.

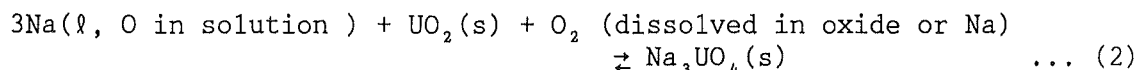
2. The reactions of liquid sodium with the components of oxide fuel

2.1 Reactions with urania:

An isothermal section of the ternary phase diagram Na-U-O is shown in Fig.1 and the equilibrium phase field of major interest is that containing  $UO_2(s)$ ,  $Na(l, O \text{ in solution})$  and  $Na_3UO_4(s)$ .#. The overall reaction involving hyperstoichiometric urania can be represented by



and the equilibrium reaction is



The threshold O:U ratio for the reaction is very close to 2.00 and the threshold oxygen concentration in sodium is  $< 1 \text{ wppm}$  at 1073K [1]. A detailed study on the effect of increasing the O:U ratio and the oxygen content of the sodium on this reaction has been reported [2]. The kinetics of the reaction between liquid sodium and pellets of hyperstoichiometric urania has been investigated over the temperature range 723K to 1173K and the mechanism of the reaction proposed [2].

It should be noted that for the reaction between sodium and hyperstoichiometric urania ( $UO_{2+x}$ ), different mechanisms occur at low and high temperatures. The more destructive reaction between sodium and pellets of urania<sub>2</sub>, can possibly be attributed to the formation of the low-density product sodium monoxide ( $Na_2O$ ) within the grain boundaries at temperatures less than 400°C. This has been observed when the reactants are in contact during the initial period of heating up to the final reaction temperature. As the temperature is raised ( $>450^\circ\text{C}$ ), the thermodynamically more stable sodium uranate ( $Na_2UO_4$ ) is formed. The reaction of sodium with pellets of hyperstoichiometric urania, without the reactants being in contact prior to attaining the reaction temperature, results in swelling which corresponds almost to the calculated value for the formation of  $Na_3UO_4$ .

It was also shown that pellets of stoichiometric urania do not undergo a destructive reaction when in contact with sodium which contains a significant amount of oxygen. A layer of reaction product tends to be loosely held to the surface of the pellet and consists of a high proportion of the phase  $Na_3UO_4$ .

The equilibrium oxygen potential  $\bar{G}_{O_2}^{eq}$  for reaction (2) is given by

$$\bar{G}_{O_2}^{eq} = \Delta_f G^0 [Na_3UO_4(s)] - \Delta_f G^0 [UO_2(s)] - 3\bar{G}[Na(l)] \dots (3)$$

where  $\Delta_f G^0 [Na_3UO_4(s)]$  and  $\Delta_f G^0 [UO_2(s)]$  are the Gibbs energies of formation of  $Na_3UO_4$  and  $UO_2$  respectively and  $\bar{G}[Na(l)]$  is the partial molar Gibbs energy of liquid sodium which, because of the small quantities of oxygen present, can be taken as zero.

---

# s and l represent the solid and liquid states.

The values for the equilibrium oxygen potential for the Na-U-O system were obtained from measurements with an EMF cell. The cell was based on a thoria-yttria electrolyte and the EMF was measured with a slurry of Na(l), UO<sub>2</sub>, and Na<sub>3</sub>UO<sub>4</sub> at one electrode and a mixture of In and In<sub>2</sub>O<sub>3</sub> as the reference electrode. The oxygen potential can be expressed by the equation

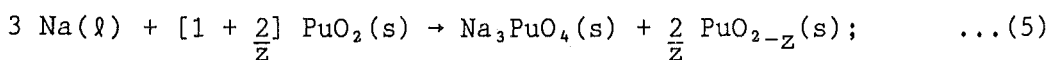
$$\bar{G}_{O_2} \text{ (J mol}^{-1} \text{ O}_2\text{)} = -949789 + 253.1 T \quad \dots(4)$$

for which the estimated uncertainty, including the error in the values for  $\Delta_f G^\circ[\text{In}_2\text{O}_3(\text{s})]$  is  $\pm 2.7 \text{ kJ mol}^{-1} \text{ O}_2$ . These data are in good agreement with those determined by Adamson et al [3]. These experimentally determined values of  $\bar{G}_0$  for the phase field Na(l), UO<sub>2</sub>(s), Na<sub>3</sub>UO<sub>4</sub>(s) are all more negative than the values calculated from the Gibbs energies of formation, although the partial molar entropies of oxygen ( $\bar{S}_0$ ) are identical. It is possible therefore that the discrepancy could be due to a small error in the experimentally determined value for the enthalpy of formation of Na<sub>3</sub>UO<sub>4</sub>.

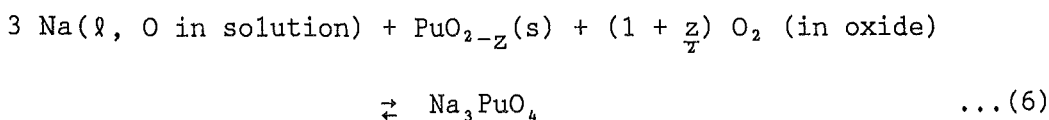
In addition to a possible isothermal section of the Na-U-O phase diagram shown in Fig.1, a predominance area diagram for the system is shown in Fig.2. This latter diagram indicates the regions of existence of the phases of the system in terms of the thermodynamic potentials of oxygen and sodium. Thus if the sodium pressure is set at one temperature, we can immediately determine the conditions required to form the various ternary phases. For example, for the formation of NaUO<sub>3</sub>, we require progressively increasing potentials of oxygen with decreasing pressures of sodium. Thus if the vapour pressure of sodium is set at a lower temperature in a region of the fuel the potential of oxygen which is required for the formation of the phase NaUO<sub>3</sub> at a higher temperature can readily be obtained.

## 2.2 Reactions with plutonia

When sintered pellets of plutonia reacted with liquid sodium at 700°C for 24 hours considerable swelling of the pellets occurred due to the formation of the compound Na<sub>3</sub>PuO<sub>4</sub> [4]. This compound is isomorphous with Na<sub>3</sub>UO<sub>4</sub> with a slightly smaller lattice parameter [Na<sub>3</sub>PuO<sub>4</sub>, a<sub>0</sub> = 0.486 nm [4], a<sub>0</sub> = 0.488 nm [5], Na<sub>3</sub>UO<sub>4</sub> a<sub>0</sub> = 0.479nm]. The remaining phases were a mixture of PuO<sub>2</sub> and PuO<sub>1.61</sub> which formed by the disproportionation of hypostoichiometric plutonia [PuO<sub>2-z</sub>] [3]; the proportion of these phases suggested that the threshold plutonium valency for reaction was between 3.45 and 3.55. Subsequent studies with powders of plutonia heated with liquid sodium at 580-680°C for 120 hours indicated that the threshold valency of plutonium was ca.3.0. We have measured [6, 7] the partial molar Gibbs energy of oxygen for the phase field appropriate to the overall reaction



for which the equilibrium reaction is given by



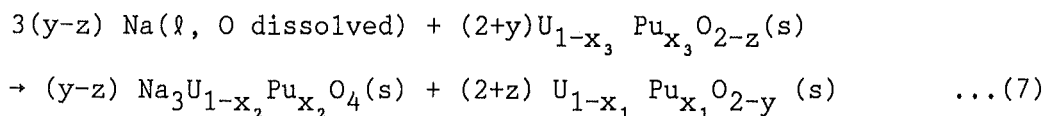
The determination of  $\bar{G}_0$  was made using an EMF cell based on a thoria-yttria electrolyte; the EMF of the cell was measured with a slurry of Na(l), Na<sub>3</sub>PuO<sub>4</sub>, and PuO<sub>2-z</sub> at one electrode, and a mixture of In and In<sub>2</sub>O<sub>3</sub> as the reference electrode.

Measurements of oxygen potential were made with two separate batches of PuO<sub>2</sub> powder (run I and run 2) the results of which are shown in Fig.3.

These two sets of data are not in agreement within the experimental uncertainty and the source of the discrepancy is not clear. Our data for  $\bar{G}_0$  for the three-phase field are compared with data for  $\bar{G}_0$  of the binary plutonium-oxygen system in Fig.3. The observation that the oxide is reduced by liquid sodium to the hexagonal structured Pu<sub>2</sub>O<sub>3</sub> phase indicated that the data for  $\bar{G}_0$  of the binary system extrapolated from the measurements of Woodley [8] and Atlas and Schlehman [9] are inconsistent with our measurements. Our data are more compatible with the determinations of  $\bar{G}_0$  of Martin and McIver [10], for this binary system.

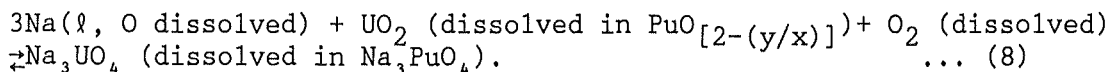
### 2.3 Reactions with urania-plutonia solid solutions

For this system, the overall reaction can be expressed by



We showed earlier [1] that when the three condensed phases  $\text{U}_{1-x_1} \text{Pu}_{x_1} \text{O}_{2-y}(\text{s})$ ,  $\text{Na}_3 \text{U}_{1-x_2} \text{Pu}_{x_2} \text{O}_4(\text{s})$  and Na(l) given in the

overall reaction above are in equilibrium, then the equilibrium reactions can be considered in terms of the separate reactions for the uranium and plutonium components of the system. The equilibrium reaction for the uranium component is:



The valency of plutonium in the oxide solid solution is 2 [2-(y/x)]

It was shown that the oxygen potentials in the phase field of the quaternary system could be expressed in terms of those for the analogous phase field in the ternary uranium system, namely:

$$\bar{G}_2^{\text{q}}(\text{quaternary system}) = \bar{G}_2^{\text{t}}(\text{ternary system}) + RT \ln \left( \frac{a_{\text{Na}_3\text{UO}_4}}{a_{\text{UO}_2}} \right) \quad \dots(9)$$

Where  $a_{\text{Na}_3\text{UO}_4}$  and  $a_{\text{UO}_2}$  are the thermodynamic activities of Na<sub>3</sub>UO<sub>4</sub> and UO<sub>2</sub> in the respective solid solutions. If  $a_{\text{Na}_3\text{UO}_4}$  and  $a_{\text{UO}_2}$  are

identical, then the oxygen potential of the relevant phase field will be the same in both systems. Also, if the solutions were ideal then  $a_{\text{Na}_3\text{UO}_4} = 1-x_2$  and  $a_{\text{UO}_2} = 1-x_1$  and if there were no segregation of

uranium and plutonium cations in the two solid solutions, then the oxygen potential for the quaternary system would be identical to that for the ternary uranium or plutonium systems. If, however, the solid solutions deviated from ideality then  $a_i = \gamma_i x_i$  where  $a_i$ ,  $\gamma_i$  and  $x_i$  are the activity, activity coefficient, and mole fraction of component  $i$  of the solid solution. We earlier considered the solid solutions as regular, and thus  $RT \ln \gamma_i = E_i (1-x_i)^2$  where  $E_i$  is the interaction parameter, and

$$\bar{G}_2^{\text{O}_2} \text{ (quaternary system)} = \bar{G}_2^{\text{O}_2} \text{ (ternary system)} - E_1 X_1^2 + E_2 X_2^2 + RT \ln \frac{1-x_2}{1-x_1} \quad \dots(10)$$

where  $E_1$  and  $E_2$  are regular solution interaction parameters for the U-Pu oxide and the Na uranoplutonate solid solutions. We earlier examined the influence of the variation of the uranium and plutonium concentrations and of the values of the interaction parameters on the calculated values of  $\bar{G}_2^{\text{O}_2}$ . It was noted that the effects of these variations gave values for  $\bar{G}_2^{\text{O}_2}$  which were generally within the estimated uncertainties in the values of  $\bar{G}_2^{\text{O}_2}$  for the uranium system;  $\pm 4.2 \text{ kJ.mol}^{-1} \text{O}_2$ . Only if the interaction parameter for the oxide solid solution ( $E_1$ ) were  $< -17 \text{ kJ}$  or if Pu were greatly segregated into the sodium uranoplutonate, would the values of  $\bar{G}_2^{\text{O}_2}$  lie outside the band of values for the uranium system.

The measurements which have been made of the variation of  $\bar{G}_2^{\text{O}_2}$  with temperature for the three-phase fields are shown in Fig.4 using EMF cells with thoria-yttria electrolytes. The data of Woodley and Adamson for a solution with  $\text{Pu}/(\text{U}+\text{Pu}) = 0.25$  in the temperature range 1073-1273K, are in good agreement with the measured values of  $\bar{G}_2^{\text{O}_2}$  for the urania system. Our measurements are for the two solid solutions with  $\text{Pu}/(\text{U}+\text{Pu})$  ratios of 0.3 and 0.7 respectively. The values of  $\bar{G}_2^{\text{O}_2}$  for the solution with  $\text{Pu}/(\text{U}+\text{Pu}) = 0.3$  are close to the values for the urania system; ca.  $5 \text{ kJ.mol}^{-1} \text{O}_2$  more positive, and for the solution with  $\text{Pu}/(\text{U}+\text{Pu}) = 0.7$  the values of  $\bar{G}_2^{\text{O}_2}$  were ca.  $5 \text{ kJ.mol}^{-1} \text{O}_2$  more negative than those for the urania system. There were also some small differences in the slope or partial entropy ( $\bar{S}_2^{\text{O}_2}$ ) of the system; these differences however are not pronounced.

The determinations of  $\bar{G}_2^{\text{O}_2}$  for the solid solutions of urania-plutonia with  $\text{Pu}/(\text{U}+\text{Pu}) = 0.11, 0.15$  and  $0.30$  using an EMF cell in the temperature range 1023-1323K indicated that the oxygen potential of these solid solutions at a given temperature was determined solely by the average valency of the plutonium cations and was not dependent on the plutonium concentration. These conclusions were supported by later studies using mainly thermogravimetric techniques with some measurements using EMF cells for solid solutions with  $\text{Pu}/(\text{U}+\text{Pu}) = 0.10, 0.25$  and  $0.40$  in the temperature range 1273-1473K, but the absolute values of  $\bar{G}_2^{\text{O}_2}$  are very different.

We should find that at least in the range of plutonium concentrations with  $\text{Pu}/(\text{U}+\text{Pu})$  ratios between 0.1 and 0.4 that the threshold Pu valency for the appropriate three phase field of the quaternary system Na-U-Pu-O should be constant. We have seen that the data for  $\bar{G}_2^{\text{O}_2}$  for the quaternary system could deviate from those

for  $\bar{G}_2^q$  of the ternary Na-U-O system if there were marked departures from ideality in the oxide solid solution. The analysis of the data carried by Woodley [8] and by Rand and Markin [11] suggest that deviations from ideality are not large; for example at 1273K with an average Pu valency of 3.60,  $Y_{PuO}$  was estimated to be 1.087 [8] and at 1150K,  $Y_{PuO_{1.5}}$  was 1.26 [11]<sup>8</sup>. The magnitude of these deviations is such that the values of  $\bar{G}_2^q$  for the quaternary system should not deviate from those of the ternary system.

We have found that this relationship is not appropriate to the pure plutonia system for which the threshold valency of plutonium is 3.0 compared to the values estimated here which are considerably greater than 3.0.

Our recent assessment [12] of the measurements of the lattice parameter of the oxide solid solution phase in equilibrium with liquid sodium and sodium uranoplutonate and of measurements of the swelling of dense pellets of the mixed oxide solid solution have indicated that:

- i) the threshold plutonium valency decreases with increase in temperature in the range 673-1073K.
- ii) the threshold plutonium valency most probably decreases for a given temperature with increase of plutonia concentration of the solid solution.
- iii) the values of the threshold valency derived from measurements of the swelling of dense pellets of urania-plutonia solid solutions on reaction with liquid sodium and those derived from lattice parameters of the remaining oxide phase were in acceptable agreement. Similar trends were observed although there is considerable scatter in the derived values of plutonium valency.
- iv) the values of the threshold plutonium valency derived from lattice parameters of the remaining oxide phase depend upon the relationship employed between lattice parameter and composition of the solid solution.

The values of lattice parameter for the solid solution obtained using a uranium-plutonium alloy or carbon to reduce the oxide are different from those of the solution prepared by reduction in hydrogen. This difference was explained [13] in terms of different concentrations of uranium and plutonium in the metal or carbide phases from that of the 'fully reduced' oxide with which they are in equilibrium. Because of the effects of segregation in the oxides containing a second metal or carbide phase, we have chosen to use the data for lattice parameters of the oxide reduced in hydrogen for the determination of the threshold plutonium valency. The relationship which we have used to determine this threshold plutonium valency ( $V_{Pu}$ ) from a given value of lattice parameter ( $a$ , nm) is:

$$V_{Pu} = 0.4 + \frac{0.72993}{x} [(1-x) 5.4707 + 5.396x - a] \quad \dots(11)$$

When comparing data for the threshold plutonium valency obtained from the determination of lattice parameters of the residual oxide phase it is essential that the same relationship between composition and lattice parameter is employed, otherwise marked discrepancies will appear. There is clearly a need for more detailed experimental determinations of the variation of lattice parameter of the solid solutions with composition.

We now return to the measurements of  $\bar{G}_{O_2}^q$  and in order to obtain values of the threshold plutonium valency from these measurements, we require the relationship between oxygen potential and O/(U+Pu) ratio of the solid solution for different plutonia concentrations at the appropriate temperatures. There is disagreement in the data for this relationship which leads to considerable uncertainty in the values for the threshold Pu valency. This is illustrated in Fig.5, in which the variation of  $\bar{G}_{O_2}$  for the oxide solid solution obtained by Woodley [8] Woodley and Adamson [14] and Martin and McIver [10] are given. The data of Woodley and Adamson have been extrapolated below 1273K, and those of Martin and McIver were measured over the range 1023-1323K. The disagreement in these data is unsatisfactory and further experimental measurements would be helpful for obtaining consistency. With a solid solution containing 30 mol % plutonia at 1096K, the derived values of threshold Pu valency can be either  $3.3 \pm 0.1$  [10] or  $3.7 \pm 0.1$  [8] compared with a value of  $3.44 \pm 0.04$  obtained from our assessment of the data on swelling of pellets of the oxide solid solution on reaction with liquid sodium. The assessment tends to give some support to the measurements of Martin and McIver.

From Fig.5 it can be seen that the data of Martin and McIver do not support the observation that the threshold plutonium valency decreases with increasing temperature; this observation is however supported by the extrapolated data of Woodley and Adamson.

Measurements of  $\bar{G}_{O_2}$  for hypostoichiometric urania-plutonia solid solutions with  $Pu/(U+Pu) = 0.2$  have been reported by Mari et al [15] and Ewart et al [16]. Measurements were made using an EMF cell technique on solutions with oxygen to (U+Pu) ratios of 1.995, 1.985, and 1.964 in the temperature range 800-1300K. The solutions were prepared by coprecipitation and the desired O:(U+Pu) ratio was obtained by reduction at 1473, 1573 and 1673K for 6 hours. Coprecipitation was the method used by Martin and McIver but Woodley obtained the solution using both coprecipitation and mechanical blending of the powders. The data of Mari et al [15] support the measurements of Woodley; subsequent studies by Ewart et al [16] indicated however that the temperature dependence of  $\bar{G}_{O_2}$  may be influenced by the method of preparation. For example, Ewart et al found that at 1350K, successive temperature cycling of the specimen resulted in a lowering of the oxygen potential  $\bar{G}_{O_2}$  and an increase in the entropy ( $S_{O_2}$ ).

Finally in this section on the phase equilibria of this quaternary system it should be noted that we require further information on the threshold Pu valency for solid solutions with concentrations  $Pu/(U+Pu) > 0.4$ . We wish to determine why the threshold Pu valency



decreases with increasing Pu concentration. It should be noted that for solid solutions of urania and ceria, at a given temperature,  $G_{O_2}$  of these solutions is not solely determined by the Ce valency, but also by the Ce concentration [17]. In these solutions with Ce/(U+Ce) ratios up to 0.5, at a given value of  $G_{O_2}$ , the valency of Ce decreases as the Ce concentration increases. If this were a feature of the urania-plutonia solid solutions then for solutions with Pu/(U+Pu) ratios of  $> 0.4$ , we might expect to find a decrease in the threshold Pu valency for reaction with liquid sodium with increase in Pu concentration; we know that for the pure Pu system, the threshold valency is 3.0. There is still a discrepancy for solutions with plutonia concentrations up to 40 mol %, as  $G_{O_2}$  the solid solution is only dependent on the Pu valency and thus the threshold Pu valency for the reaction of liquid sodium with the oxide solid solution should not vary with composition of the solution. We found, however, that the threshold Pu valency obtained from measurements of the swelling of pellets and the lattice parameter of residual oxide give an indication that the thresholded Pu valency increases with increasing Pu concentration.

#### 2.4 The influence of dissolved fission product cations on the reaction of liquid sodium with fuel oxides

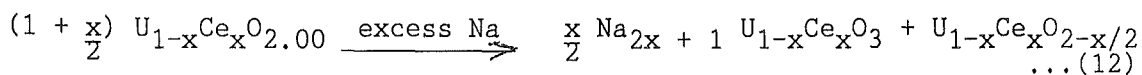
We have discussed the conditions under which liquid sodium would react with urania, plutonia, and urania-plutonia solutions. We have considered our understanding of the thermodynamic aspects of such reactions, further comments on the kinetics and mechanisms of the reactions will be given later. Such knowledge is essential for describing the consequences of failure of fuel which has only been in the core of the reactor for a comparatively very short time. We have also to consider the consequences of burn-up and with the desirability of obtaining significantly greater than 10% burn-up of the actinoid atoms, we have to examine the effects of the presence of considerable quantities of fission products on the reactions of fuel with sodium. In this section we shall briefly describe some of our preliminary experimental studies on the effects of the presence of additional cations in the urania-plutonia lattice on the reactions with liquid sodium.

We have studied experimentally the reactions between liquid sodium and urania-ceria solid solutions [18]. We have found that the reaction between sintered pellets of stoichiometric urania-ceria solid solution with ceria contents between 20 and 80 mol % at 750°C for 50 hr could be interpreted as complete reduction of the cerium cations to the trivalent state. The interaction of liquid sodium with sintered pellets of cerium oxides in the temperature range 400 to 800°C resulted in the formation of the ternary compound  $NaCeO_2$ ; the remaining oxide phase was  $CeO_{1.5}$ . [19].

For the solid solutions containing 3-20 mol % ceria, it was found that the extent of reaction was determined by the amount of ceria present and the average valency of the cerium cations. The effect of the addition of 4-valent cerium cations to urania is to raise

the thermodynamic potential of oxygen and hence exceed the threshold value for reaction with sodium. A pellet of stoichiometric urania-ceria containing 15 mol% ceria reacts destructively with sodium; the reaction took place at 400°C in less than 1 hour, although no reaction was observed at 200°C. The presence of 3 mol% ceria also provided sufficient oxygen to the system for reaction which was confined to the periphery of the pellet. The complete reduction of the solid solution in hydrogen prevented any reaction with sodium.

From the evidence of X-ray powder photographs, the additional phase present was a quaternary compound. The values of the lattice parameters for the reduced ceria-uranium solid solution indicate that the ceria content of this solution is the same as that of the oxide. This quaternary compound has a tetragonal structure, and in the composition range 20-80 mol% ceria, the reaction could be expressed by:



These results possibly indicate that the presence of cerium as a fission product cation in urania or urania-plutonia could result in additional reaction with sodium.

We have also reacted some spheres of sintered doped urania-plutonia with liquid sodium; the spheres were of 800 μm diameter and 98% theoretical density. Their composition was  $U_{0.63}Pu_{0.27}Fp_{0.10}O_2$  with  $0.1Fp = Ba_{0.010} La_{0.009} Ce_{0.020} Pr_{0.008} Nd_{0.023} Zr_{0.003}$

After reaction with sodium at 850°C for 48hr, the spheres remained intact and a volume swelling of ca. 13% occurred. X-ray powder photographs showed only the presence of the reduced oxide phase with a face centred cubic structure and lattice parameter  $a_o = 0.54464 \pm 0.0004$  nm; the lattice parameter of the unreacted oxide was  $a_o = 0.54371 \pm 0.0002$  nm. The presence of the cations had caused an additional volume swelling of ca. 4%.

If the increase in swelling were a result of the further reduction of the oxide, this is not reflected in the increase in the lattice parameter of the oxide product phase relative to the pure oxide system (0.5437 nm to 0.5446 nm for the doped oxide, and 0.5450 nm to 0.5470 nm for the pure oxide).

When the reaction was carried out at 450°C for 170h, a volume swelling of ca. 8.3% was obtained. It would appear therefore that the rate of reaction is also influenced by the presence of these additional cations in the oxide lattice, since negligible swelling was observed with urania-plutonia solid solutions at this temperature.

The results from these studies on the reactions of liquid sodium with urania-plutonia containing fission product cations show that the inclusion of these cations can cause an increase in reaction rate, increased swelling and break-up of pellets. Our results in terms of swelling and temperature are less pronounced than those of Housseau et al [5].

Some measurements of the oxygen potential ( $\bar{G}_{O_2}$ ) of the phase field with liquid sodium, and the doped spheres were made using the same EMF technique as described earlier. The spheres were crushed before placing into the EMF cell with liquid sodium. The variation of the measured values of  $\bar{G}_{O_2}$  with temperature are shown in Fig.6. It will be noted that there is considerable scatter in these data. Problems were encountered in obtaining a constant value with time for the EMF of the cell at each temperature; it seems likely, therefore that the values which are presented may not be true equilibrium values of  $\bar{G}_{O_2}$ . At the higher temperatures, the effect of this drift was to approach values of  $\bar{G}_{O_2}$  for the urania-plutonia system.

The variation of  $\bar{G}_{O_2}^{\text{eq}}$  with temperature for the phase field Na(l),  $Ce_2O_3(s)$ ,  $NaCeO_2(s)$  has been determined [20] using the same EMF cell method as described earlier, and this variation can be expressed by:

$$\bar{G}_{O_2}^{\text{eq}} \text{ (J.mol}^{-1}O_2\text{)} = -848070 + 223.4 T. \quad \dots (13)$$

These data are also shown in Fig.6, and are considerably more positive than those for the Na(l),  $UO_2(s)$  and  $Na_3UO_4(s)$  phase field.

When urania-ceria solid solutions react with liquid sodium, it seems likely that the first phase to form will be  $Na_3UO_4$ ; there may be some solubility of Ce cations in this phase. With addition of oxygen, the solid solution would be oxidised until the four-phase field Na(liquid), urania-ceria solid solution,  $Na_3UO_4$  and  $NaCeO_2$ ; at an oxygen potential close to that for the formation of  $NaCeO_2$  from liquid sodium and ceria is reached. Further oxidation would result in the further oxidation of the solid solution and the formation of other ternary or quaternary compounds.

### 3. The reactions of liquid sodium with irradiated fuel

The possible chemical state of the fission product elements in irradiated fuel is shown in Table 1. Oxygen will migrate to the colder regions of the fuel and the more volatile fission product elements or species will be found in the fuel clad gap or plenum of the pin. In addition to the rare gases krypton and xenon, appreciable quantities, of the elements rubidium and caesium, bromine and iodine, selenium and tellurium and possibly molybdenum will be found in the fuel clad gap. We shall consider only the reactions of the fission products with the significant yields namely, caesium, iodine and tellurium within the fuel-clad gap. In addition to the reactions of the fission product elements with the fuel we have to consider their reaction with the components of the cladding.

The dissolution of the cations of the fission product elements in the urania, plutonia solid solution, particularly the lanthanides for which the predominant valency is 3, would result in an increase in oxygen potential at a given anion:cation ratio. So that charge neutrality is maintained; uranium cations would be oxidised to the 5-valent state. Woodley [21] has carried out some determinations

of the effects of the cations of Y, Ce, Pr, Nd and Ce dissolved in  $U_{0.75}Pu_{0.25}$  oxide on  $Go_2$ . Concentration levels up to those which simulate irradiation up to 10% burn-up of the heavy atoms for temperatures 1173, 1273 and 1373K were examined. Woodley's conclusions were that; for a given hypostoichiometry,  $Go_2$  increases linearly with simulated burn-up, and the rate of increase, increases with initial stoichiometry. At 1173K,  $Go_2$  increases more rapidly with added cation concentration than at 1273 and 1373K for which the rates of increase for a given stoichiometry are essentially identical.

In addition to this effect of irradiation, the presence of other fission product elements will influence the change of  $Go_2$  with burn-up as will the steep temperature gradients within the operating fuel. The centre temperature of the fuel will be  $>2000^\circ C$  and that of the fuel surface ca.  $800^\circ C$ . The temperature gradients will result in transport of both oxygen, the actinide elements and the fission product elements along the gradients. The amounts of the fission product elements which would be found in the fuel-clad gap and in the plenum will be very dependent on the operating conditions of the fuel, for example, the rating, the power history, and the burn-up. Such aspects of fission products release were considered by Fuerstein et al [30] in their review.

We are modelling the chemical constitution of the fission product elements in the fuel clad gap. The physical parameters of the operating fuel pin are obtained using the TRAFIC Code [23] and with these parameters the changes in chemical constitution with burn-up are modelled using the code SOLGASMIX [24]. SOLGASMIX calculates the position of chemical equilibrium by minimising the total Gibbs energy of the system, and some preliminary calculations of the constitution of a fast reactor fuel have been presented earlier [25].

With a knowledge of the chemical state of the fission product elements in the fuel, we can then consider the likely effects of a breach of the cladding and the reactions of irradiated fuel with liquid sodium. The value of  $Go_2$  in the gap will determine the compounds which are formed, or alternatively we can consider that the formation of some compounds will determine the value of  $Go_2$  and act effectively as a buffer against a rise in  $Go_2$  with burn-up of the heavy atoms.

We have examined the conditions of  $Go_2$  under which the groups of compounds could be formed. These have been plotted as Ellingham diagrams in Fig.7 and Fig.8.

We shall now consider the effects of sodium ingress on the compounds in the fuel clad gap. Of the phases given in Table I those that are to be found in the gap would be some of the following:  $Cs_2UO_{3.5}$ ,  $Cs_2UO_4$ ,  $Cs_2Te$ ,  $Cs_2MoO_4$ , Te and I. Additionally the phases  $Cs_4CrO_4$ ,  $Cs_3CrO_4$ ,  $Cs_2CrO_4$  could be found. The exact constitution would depend on  $Go_2$  and temperature.

We have seen that the stabilities of these phases with respect to excess sodium in Figs. 7 and 8, would result in the decomposition of the Cs uranates and chromates to form  $\text{Na}_3\text{UO}_4$  or  $\text{NaCrO}_2$ . Na and Cs are completely miscible in the liquid state [26, 27]. At the temperatures of the coolant between 450 and 650°C, it is most probable that  $\text{Cs}_2\text{Te}$  would dissolve in liquid sodium; there is considerable solubility of Te in Cs (> 10 at % at 300°C) [28]. The phase diagram of the Na-Te system suggests that there could be up to 15 at % Te solubility at 650°C [29], although the subsequent measurements of Walker [30] give a much lower solubility; 0.23 at % Te at 650°C.

Recent determinations of the thermodynamic parameters of  $\text{Cs}_2\text{Te}$  [31, 32] have shown that this compound is very stable and before other tellurides could be formed with, for example, the cladding the thermodynamic activity of tellurium would have to increase and this could be achieved by an increase of the oxygen potential. Relatively high tellurium potentials are required for the formation of tellurides of the fission product element Pd [33, 34] and the main components of the cladding and structural materials, chromium, iron and nickel [35-40]. CsI will also dissolve in liquid sodium. The available data on the solubility of halogens in the alkali metals has been reviewed by Barker [41]. At 833K, the solubility of NaI in Na is ca. 0.2 mol%, and for CsI in Cs is ca. 25 mol %.

Any Cs chromates formed by reaction of Cs with the cladding would also not be stable in the presence of liquid sodium and result in the release of Cs to the liquid sodium.

We also note, however, that any molybdenum in the form of  $\text{Cs}_2\text{MoO}_4$  would be stable with respect to sodium, provided that the thermodynamic data assessed for  $\text{Na}_2\text{MoO}_4$  are reliable [42].

We have already considered the effects of the ingress of sodium on the changes of the chemical constitution of the fission product species in the fuel-clad gap. The outer region fuel matrix will also react with sodium to form essentially a sodium uranoplutonate. These reactions will result in contamination of the primary coolant by dissolved fission product elements and by particulate materials. Some of the dissolved and particulate materials will be found on the surfaces of the primary circuit.

We shall now discuss aspects of the contamination of the primary circuit and make some comments on our laboratory programme aimed at providing information to aid our modelling of all aspects of the failure of fuel. We also briefly comment on published information on failed fuel and on 'in-reactor' experiments which study the phenomena. On failure of the cladding some fuel which has a very low solubility in sodium will be released to the primary circuit in the form of particulate material. Such release could be due to mechanical effects at the time of failure of the cladding, the reaction of sodium with the fuel containing sufficient oxygen, and reaction of the fuel exposed to the sodium coolant containing sufficient oxygen to react with the fuel.

#### 4. The release of fuel particles from a defected fuel pin

##### 4.1 Release on pin failure

The release of fuel particles at the moment of clad failure could be envisaged for pins having a higher internal gas pressure than the coolant pressure. During the depressurisation process loose fuel dust could be ejected from the pin. The quantity and particle size distribution of the emitted fuel will depend on the burn-up of the fuel (ie internal gas pressure), irradiation history and the nature of the failure. Tests performed on LWR fuel cans, involving the pressurisation of cans at 900°C [43] resulted in a maximum release of  $UO_2$  dust of 0.04% of the total fuel inventory. Less than 3% of this released material had a particle size of less than ca. 15 $\mu$ m diameter.

##### 4.2 Release due to the initial sodium-fuel reaction

The mechanism of the reaction of sodium with the fuel containing oxygen in excess of the threshold amount, involves the rapid penetration of the grain boundaries of the fuel matrix by the coolant [4]. The distance of the reaction front into the fuel pellet is determined by the radial oxygen and temperature gradients. The sodium uranoplutonate reaction product accumulates at the grain boundaries in a matter of hours [4] at the temperatures likely to be encountered in the fuel. The resultant swelling forces the grains apart and weakens the fuel structure in the affected regions. Erosion of the reacted fuel by the flow of sodium can occur, particularly near the site of the defects.

The effect of the variation with temperature of the threshold of plutonium valency for reaction of the urania-plutonia solid solution with sodium [12] can result in further contamination of the coolant when the thermal conditions of the failed fuel pin change. This is particularly true for the storage of failed fuel pins in an internal position within the primary vessel of the reactor. During the early stages of storage, the temperature gradient established by high decay heat will not be as severe as that during the irradiation. It is possible, therefore, that inner regions of the fuel that contain excess oxygen available for reaction, but were at high temperatures in the reactor core, could react with the coolant. As the decay heat reduces, so the temperature of the fuel will approach that of the coolant temperature in the storage position. This reduction in temperature and associated increase in the threshold plutonium valency for reaction could result in the decomposition of a proportion of the sodium uranoplutonate. The further weakening of the grain boundaries due to this change could be an additional source of contamination by fuel particles.

##### 4.3 Release due to oxygen contamination of the coolant

The threshold concentration of oxygen in sodium below which reaction would not occur is derived from the values of threshold oxygen potential and oxygen solubility. The discrepancies that exist in the values for oxygen solubility [1] mean that the threshold concentration at a particular temperature can only be

expressed as a range of concentrations. The extrema of the threshold oxygen concentration at 650°C are 0.1 and 1 wppm, most probably below the likely level of the oxygen content in the coolant. It would appear therefore that unless the oxygen content of the coolant is reduced further to below these levels, the sodium can act as a large source of oxygen for further reaction between sodium and fuel.

The mechanism for the reaction of the fuel with sodium containing excess oxygen is different from that in which the oxygen is supplied by the fuel [4]. The reaction product builds up on the surface of the fuel exposed to the coolant. The product layer is loosely adhered to the surface and can be eroded by the coolant flow. As the supply of oxygen is not limited in this reaction, the kinetics are controlled by the rate of diffusion of sodium ions through the layer of sodium uranoplutonate.

#### 4.4 Laboratory studies on the release of fuel particles

There is very little information on the extent of contamination of the coolant by fuel particles or the contribution to the contamination by fuel due to the individual mechanisms described above. Data on the total contamination of the sodium circuit have been obtained from various in-pile experiments on defected fuel pins [44]. However, studies to provide information on the influence of flow rate, the level of oxygen contamination, temperature of fuel and surface area of exposed fuel have not been performed. At Harwell Laboratory, a small sodium loop has been installed in a glove-box in order to study the erosion of particles from urania-plutonia pellets. The loop is constructed of stainless steel and incorporates an electromagnetic pump and an yttria-doped thoria oxygen sensor; the oxygen content in the sodium is set by a cold trap. The first test has just been started and will run for several months.

Preliminary tests to investigate the extent of release of particulate material in static sodium systems have been performed. These experiments were also conducted to determine the release of Cs, Te and I species from a simulated defected small pin. Sintered pellets of urania-plutonia were loaded into a stainless steel tube and elemental Cs, Te and I were added. The tube was welded closed and heat treated to ensure that an equilibrium chemical state of the added simulants with the fuel was achieved. The pins were then defected and given a second heat treatment in a sealed can containing liquid sodium. The amounts of release of Cs, Te and I from the defected pin into the sodium after nine days at 800°C were approximately 0.77, 0.55 and 0.11 of the initial inventory. The analysis of urania-plutonia in the sodium has shown that the release of fuel particles from the pin is very small ( $\sim 1.4$   $\mu\text{g}$  of oxide) and that  $\sim 60\%$  of the released material had settled to the bottom of the reaction can.

#### 5. Failed pin experience in reactors and in-pile experiments

Much detailed information has been published concerning the behaviour of failed fuel pins in reactors and in-pile experiments of fuel pins with engineered defects. Such experience up to 1980

has been reviewed [44]. Since that assessment further in-pile tests have been performed in the EBR-II reactor (RBCB tests - Run Beyond Cladding Breach) [45] and in the SILOE facility [46]. In the following sections rather than report the results from all of these tests in detail, the trends in behaviour of failed fuel pins of low and high burn-up will be discussed.

### 5.1 Fuel pin failure at low burn-up

Failures of fuel pins early-in-life are likely to involve only small defects in the clad. The extent of the sodium-fuel reaction for fuel of low burn-up will depend on the initial O:U+Pu ratio and the plutonium concentration of the solid solution. With the data for the variation of the threshold plutonium valency with Pu concentration, for fresh fuel of initial O:U+Pu ratio of 1.98, the maximum fuel swelling (ie  $\frac{\Delta V}{V} \times 100$ ) would be  $\sim 3\%$  and  $7\%$  for plutonium concentrations of 0.2 and 0.3 respectively. Such swelling is unlikely to impose sufficient strain on the clad to cause an extension of the original defect. The amount of volatile fission products and fuel released to the coolant would be limited due to the low surface areas of fuel exposed; in the absence of secondary cracks the flow of sodium within the pin would be restricted. The results from in-pile tests using fresh fuel show that only slight pin deformation occurs and the contamination of the primary circuit is minimal. In the case of pin hole defects (20.5 nm diameter hole), the formation of sodium uranoplutonate was restricted to the site of the defect. The SILOE defect pin test C1 [46] was run for 200 days without defect extension or any fuel loss. A similar defect test was also performed with fuel at  $\sim 2.8\%$  BU (test RS-5 [47]) and the results were consistent with the previous tests.

The presence of a larger initial defect (ie an engineered slit) in a fresh fuel pin however does result in easier access of the sodium into the pin and a significant release of the volatile fission products (eg 40%, 10% and 3% release of the Cs, I and Te inventory in the pin) [44]. The release of fuel particles from the pin would be very small ( $< 40$  mg) and it should be possible to continue reactor operation up to ca. 3% burn-up. In-pile tests on fuel at ca. 4% burn-up have shown that significant extension of the original defect and the formation of secondary cracks can occur which result in an increase in fuel loss (EBR II tests, RBCB-2 [45] and SILOE test KS-1 [46]).

### 5.2 Fuel pin failures at high burn-up

The changes in chemical constitution of the fuel and fission product elements as the irradiation proceeds and the changes in mechanical properties of the cladding influence the behaviour of failed fuel pins at high burn-up. The extent of deformation of the pin is enhanced over that for a failure at low burn-up due to a number of factors: these factors are (a) the fuel is more 'oxidising', (b) the clad is less ductile, (c) certain fission products can influence the extent and kinetics of the reaction and (d) the oxygen in the coolant can participate in the reaction.



The overall effect of the increased sodium-fuel reaction and the reduction in ductility of the cladding is a tendency for considerable extension of the original defect and the formation of secondary cracks. As more fuel surface is exposed, so the extent of release of fission products and fuel particles is increased.

A number of in-pile tests on irradiated fuel pins have been performed to simulate the effect of pin failures at high burn-up. In all cases, the extension of the original defect and the fuel loss from the site of the defect was greater than for fuel pins at low burn-up (eg EBR-II tests RBCB 1, 2, 3 and XY-2 [45]; SILOE tests 53, 54, RS1, C2 and PSL [46]). The post-irradiation examination results from these tests show that a layer of sodium uranoplutonate forms along most of the fuel column. The increase in volume due to the reaction is accommodated either by an increase in diameter of the pin (with the possibility of crack formation) or by a reduction in the size of the central void or by both. In most cases the regions where maximum diameter increases were observed, were confined to the axial extent of the defects; a typical increase in diameter is ca. 12% at 10% burn-up.

As mentioned above, the extent of release of the volatile fission products and particulate material is dependent on the amount of fuel exposed to the sodium and also on the flow of sodium within the pin. The ranges of release of Cs, Te and I are 80-100%, 20-50% and 10.20% respectively of the initial inventory [44]. The weight of fuel released from the defect tests also varies considerably. A release rate of ca.  $1 \times 10^{15}$  atoms  $\text{cm}^{-2} \text{s}^{-1}$  can be obtained from an analysis of the SILOE test 54 [44] and the B9D test performed in the General Electric Test Reactor (GETR) [47]. The maximum release from a fuel pin that has been determined was 1.5g from the SILOE 54 test; releases of 100mg are typical for a pin at 10% burn-up.

6 The development of a code to describe the behaviour of a failed fuel

The development of a code that models the physical and chemical behaviour of a defected pin is required in order to relate the signals derived from the failed fuel detection system with the evolution of a breach in the cladding. Such a code will require information from:

- i) Studies of the sodium-fuel reaction and fission product systems.
- ii) Out-of-pile tests on irradiated fuel.
- iii) Detailed monitoring of failed fuel in the reactor.
- iv) Post-irradiation examination of intact and failed fuel pins.

### 6.1 The calculation of the chemical constitution of a failed fuel pin

The chemical constitution of a breached pin can be determined by calculating the equilibria for various regions of the pin with sodium as an additional component using the code SOLGASMIX [24]. The extent of fuel swelling at each location due to the formation of sodium uranoplutonate, which will probably contain some fission product ions, is determined from the number of moles of the reaction product formed in each chosen radial segment of the fuel. The kinetics of the sodium-fuel reaction will be governed by the results obtained from laboratory experiments [4]. The internal stress on the clad due to the increases in fuel volume could result in the extension of the original defect. The extent of this effect will depend on the burn-up of the fuel and the mechanical properties of the clad. An evaluation of the clad diametral strains and defect evolution can be obtained with the code TRAFIC [23].

The release of radionuclides from the defected pin is considered in two parts; the release of the fission product elements (eg Cs, Te, I) in the gap [see section 3] and the release of fuel particulate matter. The amount of the fission product elements that is in the gap and which could be released would depend on the chemical state of those species after sodium has equilibrated with the fuel, their solubility in sodium and the sodium flow through the pin. There are limited data on the release rates of fuel particles from the surface of exposed fuel and more information is required. The experimental programme being carried out at Harwell Laboratory using small sodium loops is intended to provide information on the release of fuel and fission products to the primary coolant as well as information on their behaviour on the surfaces of the primary circuit.

### Summary and Conclusions

A detailed discussion of the reactions between sodium and oxide fuel has been given. There are still some discrepancies in the thermodynamic data for the urania-plutonia system. Further studies are required on thermodynamic and kinetic aspects of the effects of fission product cations dissolved in urania-plutonia solid solutions on reactions with liquid sodium.

The development of a computer code to model the behaviour of fuel on failure and the consequences of failure requires information on the reactions of sodium with the matrix of the fuel and with the fission product species in the fuel-clad gap of a pin. Such reactions are likely to lead to some contamination of the primary circuit in the form of particulate material or dissolved fission product species.

The significance of our small-scale laboratory experiments for the provision of information on the contamination of the primary circuit is described. Observations on failed fuel from operating reactors and in-pile loop experiments provide essential information for the input to a model which will describe the mechanical, physical and chemical behaviour of the fuel. Some of these observations and future requirements have been discussed.

### Acknowledgements

A part of the assessment was carried out under study contracts from the Commission of the European Communities (Contract Nos. EC1.909-B7222-82-UK and EC1-1267-B7222-84-UK).

## References

1. M G Adamson, M A Mignanelli, P E Potter, M H Rand. J. Nucl. Mater. 27 (1981) 203.
2. M G Mignanelli, P E Potter. J. Nucl. Mater. 114 (1983) 168.
3. M G Adamson, E A Aitken, D W Jeter. Proc. Intern. Conf. on Liquid Metal Technology in Energy Production, Champion, PA 1976. CONF-760503-P2, 866.
4. M A Mignanelli, P E Potter. J. Nucl. Mater. 125 (1984) 182.
5. M Housseau, G Dean, J-P Marcon, J-F Marin. Report CEA-N-1588 (1973).
6. M A Mignanelli, P E Potter. Liquid Metal Engineering and Technology. BNES, London 1984 pp.117-122.
7. M A Mignanelli, P E Potter. J. Nucl. Mater. 130 (1985) 289.
8. R E Woodley. J. Nucl. Mater. 96 (1981) 5.
9. L M Atlas, B J Schlehman. McMillan, Proc. 3rd. Int. Conf. on Plutonium. Inst. Metals, London 1965 p.838.
10. T L Markin, E J McIver. *ibid* p.845.
11. M H Rand, T L Markin. Thermodynamics of Nuclear Materials 1967. IAEA Vienna 1968 pp.637-650.
12. M A Mignanelli, P E Potter. J. Less Common Metals 121 (1986) 605.
13. P E Potter. 'Behaviour and Chemical State of Irradiated Ceramic Fuels'. Panel Proceedings Series IAEA, Vienna 1974 p.115.
14. R E Woodley, M G Adamson. J. Nucl. Mater. 82 (1979) 65.
15. C M Mari, S Pizzini, L. Manes, F. Toci. J. Electrochem. Soc. 124 (1977) 1831.
16. F T Ewart, L Manes, H J Matzke, C M Mari, F Toci, R Schreiber. J. Nucl. Mater. 81 (1979) 185.
17. D I R Norris, P Kay. J. Nucl. Mater. 116 (1983) 184.
18. M A Mignanelli, P E Potter. J. Nucl. Mater. 118 (1983) 130.
19. M A Mignanelli, P E Potter, M G Barker. J. Nucl. Mater. 97 (1981) 213.
20. M G Barker, S Frankham. Private Communication (1985).
21. R E Woodley. J. Nucl. Mater. 74 (1978) 290.
22. H Feuerstein, A J Hooper, F A Johnson. Atomic Energy Review (IAEA) 17 No.3 (1979) 697.
23. J R Matthews. UKAEA report. AERE-R 10818 (rev). 1984.

24. G Eriksson. Chem. Scrp. 8 (1975) 100.
25. M A Mignanelli, P E Potter. Science and Technology of Fast Reactor Safety. BNES. London 1986 vol.I p.53.
26. P E Potter, M H Rand. Handbook of Thermodynamic and Transport Properties of Alkali Metals. (ed. R W Ohse). Blackwell Scientific Publications, 1985. IUPAC Ch.9.1 p.915.
27. P E Potter, M H Rand. Ibid. Ch.9.3 p.941.
28. M G Adamson, J E Leighty. J. Nucl. Mater. 114 (1983) 327.
29. M Hansen, K Anderko. Constitution of Binary Alloys. 2nd edition Genium Publishing Corp. 1985 p.1006.
30. R A Walker. Ph.D Thesis, University of Birmingham 1968.
31. E H P Cordfunke, W Ouweltjes. J. Chem. Thermodyn. To be published.
32. E H P Cordfunke, W Ouweltjes, J C van Miltenburg, A Schuijff. J. Chem. Thermodyn. To be published.
33. H Ipser, W Schuster. J. Less Common Metals 125 (1986) 183.
34. H Ipser, Z Metallkunde 73 (1982) 151.
35. H Ipser, K L Komarek, K O Klepp. J. Less Common Metals 92 (1983) 265.
36. K O Klepp, K L Komarek. Mh. Chemie 103 (1972) 934.
37. H Ipser, K L Komarek, H Mikler. Mh. Chemie 105 (1974) 1322.
38. H Ipser, K O Klepp, K L Komarek. Mh. Chemie. 111 (1980) 761.
39. H Ipser, K L Komarek. Ibid 105 (1974) 1344.
40. M Eltenberg, K L Komarek, E Miller. J. Solid State Chem. 1 (1970) 583.
41. M G Barker. Handbook of Thermodynamic and Transport Properties of Alkali Metals (ed. R W Ohse). Blackwell Scientific Publications, 1985. IUPAC. Ch.8.5 p.905.
42. T B Lindemer, T M Besmann, C E Johnson. J. Nucl. Mater. 100 (1981) 1978.
43. R A Lorenz, J L Collins, A P Malinanskas, O L Kirkland, R L Towns. In Report NUREG/CR-0772 (1981).
44. M Tetenbaum. Report EPRI NP.1609 (1980).
45. J D B Lambert, R V Strain, K C Gross, G L Hofman, R P Colburn, M G Adamson, S Ukai. Nuclear Fuel Performance, BNES, London 1985 p.77.
46. H Plitz, H Kleykamp, P Weimar, J P Hairion, R Languille, P Cecchi. Science and Technology of Fast Reactor Safety, BNES, London 1986, Vol.1 p.393.
47. P E Bohaboy, C N Craig, G L Stimonell, G I Regimbal, P E Novak. Report GEAP-13925 (1972).

TABLE I

The chemical state of fission products in irradiated urania breeder and urania-plutonia solid solution fuel

| <u>Fission Product Elements</u> | <u>Likely Chemical State</u>  |
|---------------------------------|---|
| Kr, Xe                          | Elemental state.  |
| Y, La-Eu and actinides          | Oxides which dissolve in host matrix.   |
| Ba, Sr                          | Oxides which can dissolve to a limited extent in the fuel and also form separate phases<br>$Ba_{1-x} Sr_x [Zr_{1-w-y-z} Mo_w U_y Pu_z] O_3$               |
| Br, I                           | Single phase halide solution.<br>$Cs_{1-x} Rb_x Br_{1-y} I_y$   |
| Rb, Cs                          | $Cs_{1-x} Rb_x Br_{1-y} I_y$ and compounds analagous to<br>$Cs_2UO_4$ and $Cs_2UO_{3.56}$<br>e.g. $(Cs_{1-x} Rb_x)_2 (U_{1-y} Pu_y) O_4$                  |
| Se, Te                          | Single phase chalcogenide solution.<br>$(Cs_{1-x} Rb_x)_2 Se_{1-y} Te_y$  |
| Zr, Nb                          | Some dissolution in host matrix, see also Ba,Sr group.  |
| Mo, Tc, Ru, Rh, Pd              | Usually single phase alloy, sometimes two phase. Some Mo can oxidise to $MoO_2$ and also form a compound analagous to $Cs_2MoO_4 - (Cs_{1-x} Rb_x) MoO_4$ |
| Ag, Cd, In, Sn, Sb              | Fission yields low; alloyed.  |



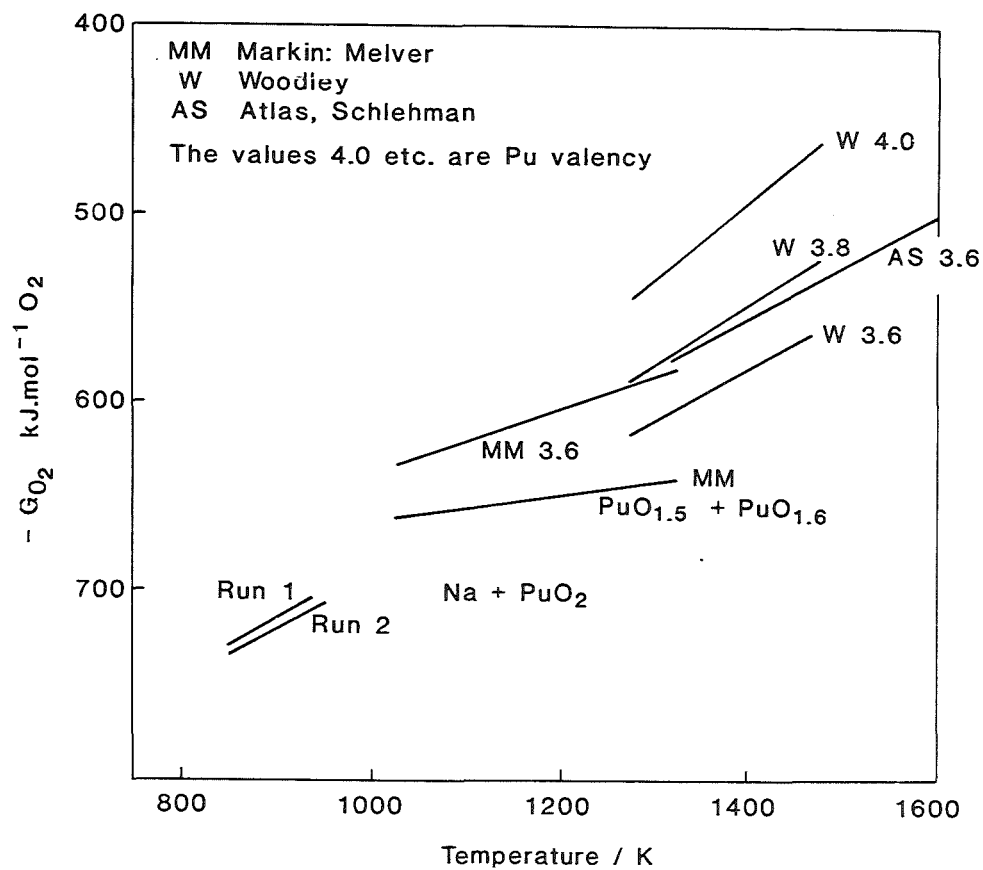


Fig. 3.  $\bar{G}_{O_2}$  for the sodium-plutonia reaction and for the plutonium-oxygen system

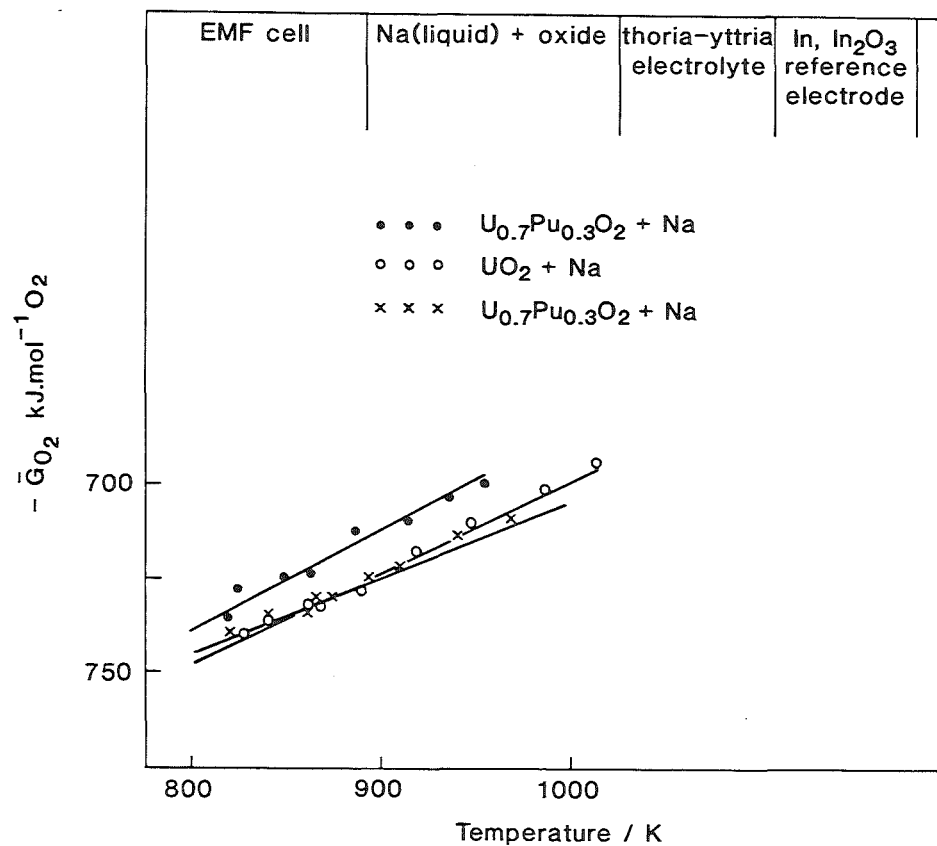


Fig. 4. The experimentally determined variation of  $\bar{G}_{O_2}$  with temperature for sodium-urania and sodium-urania-plutonia

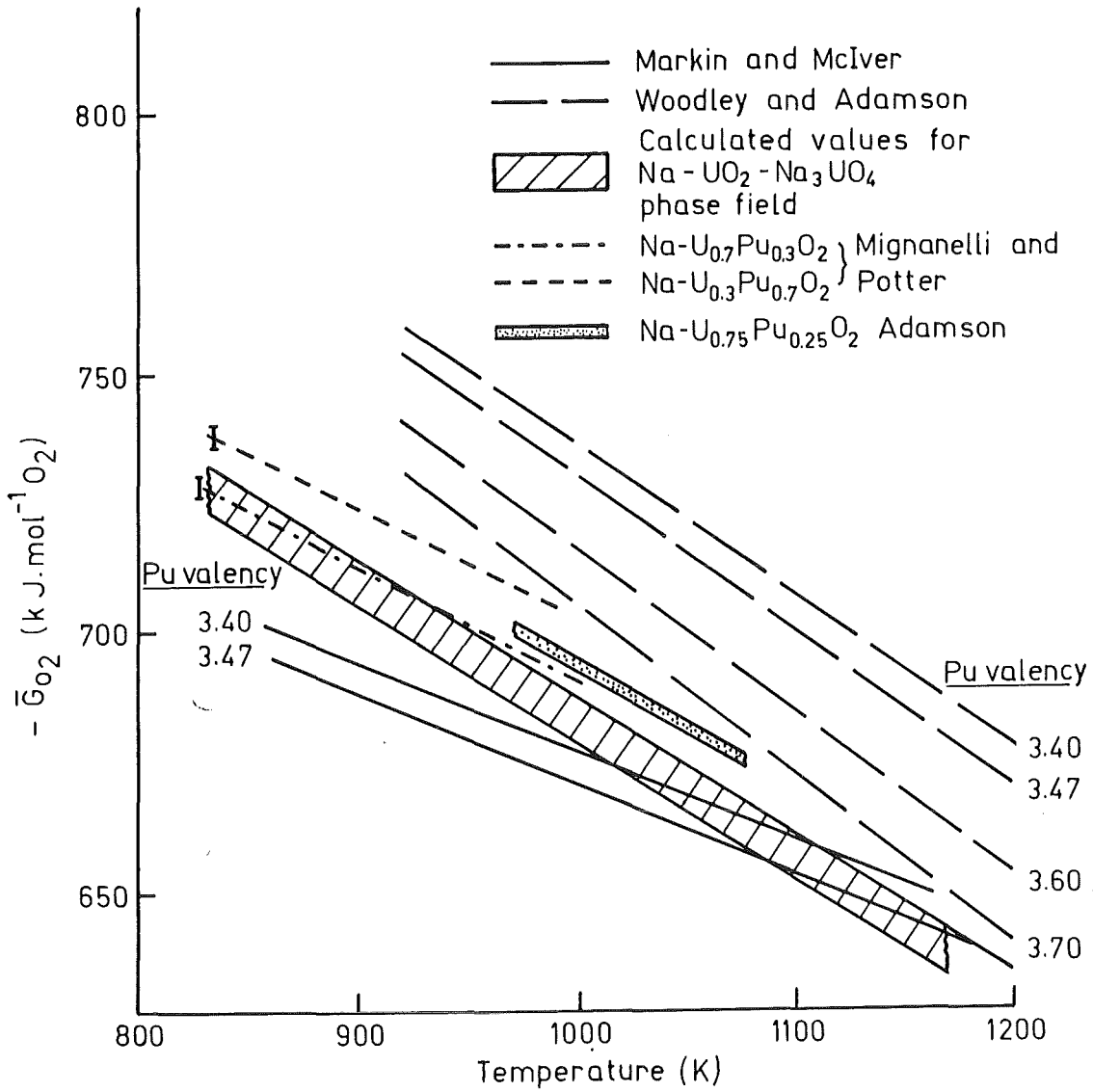


FIG.5: A comparison of oxygen potentials for the sodium-urania and sodium-urania-plutonia systems with those for the urania-plutonia system.



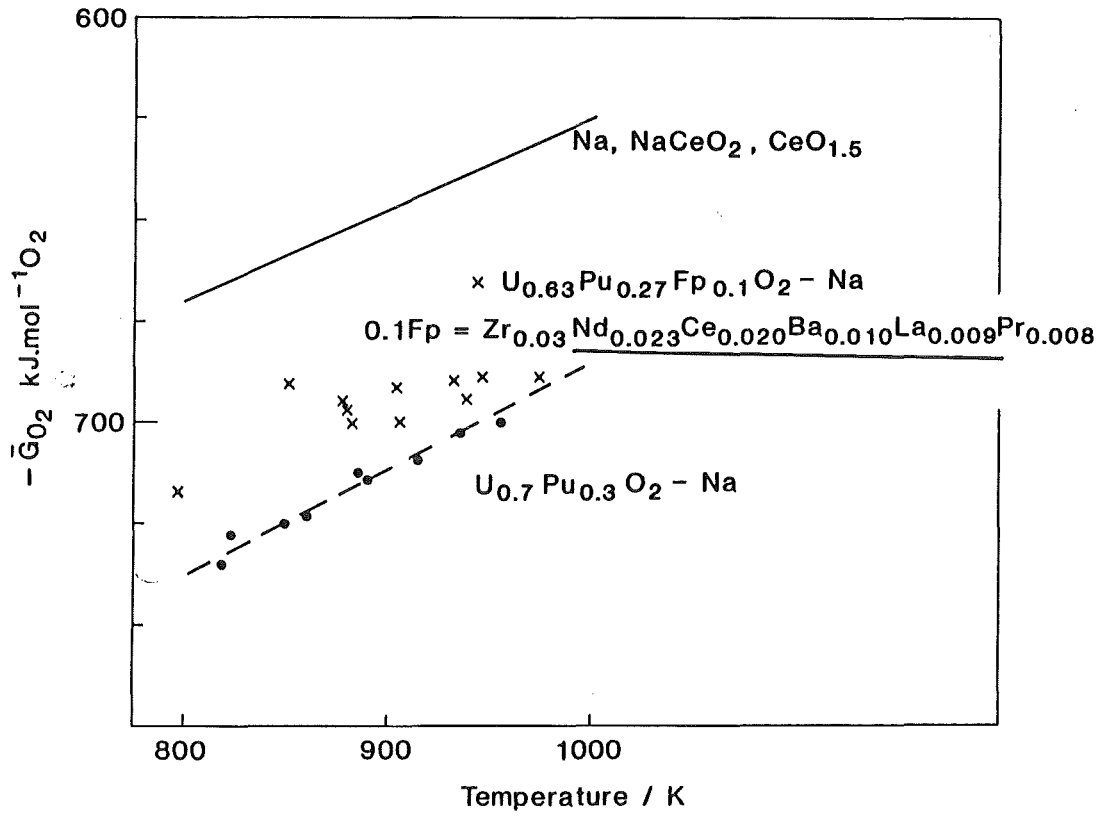


Fig. 6.  $\bar{G}_{O_2}$  for the sodium-ceria, sodium-urania-plutonia and sodium-urania-plutonia with the addition of fission product cations (Fp)

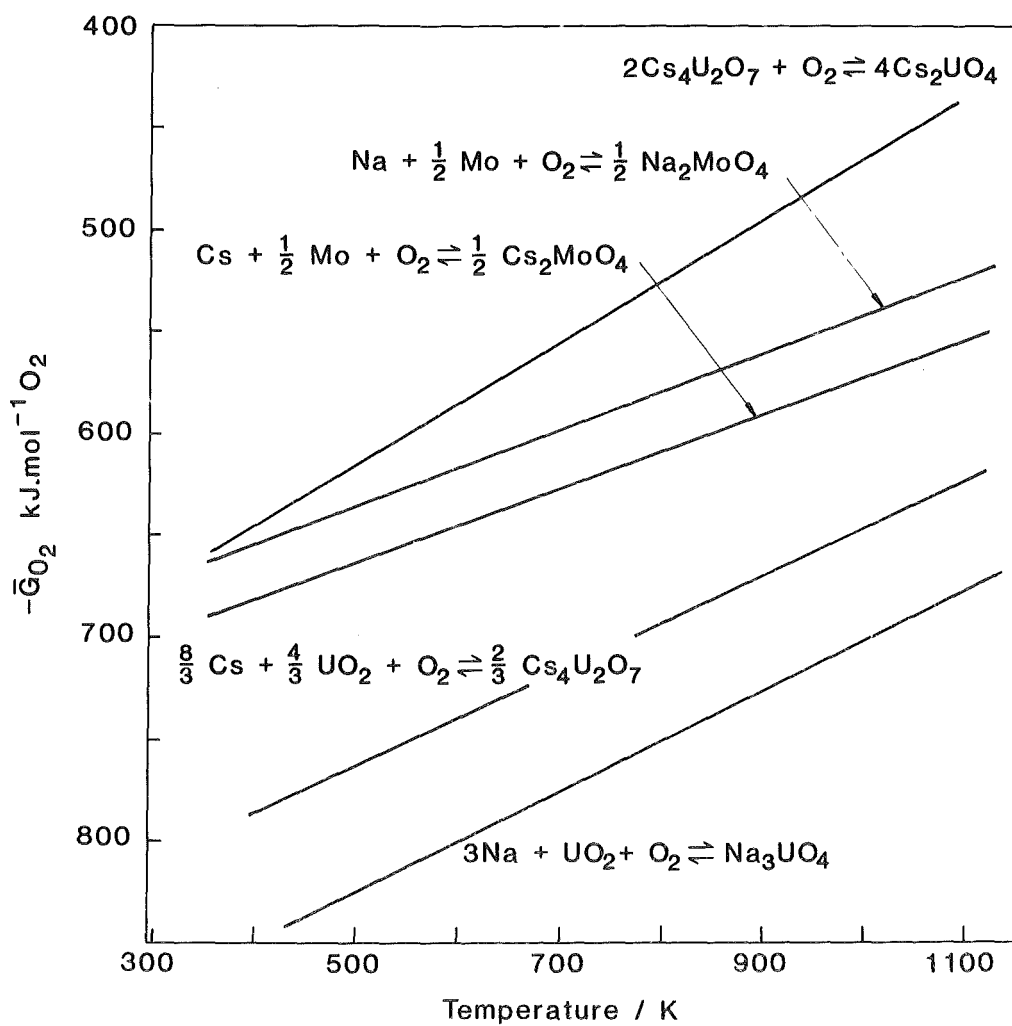


Fig. 7. Stabilities of Caesium and Sodium Uranates and Molybdates

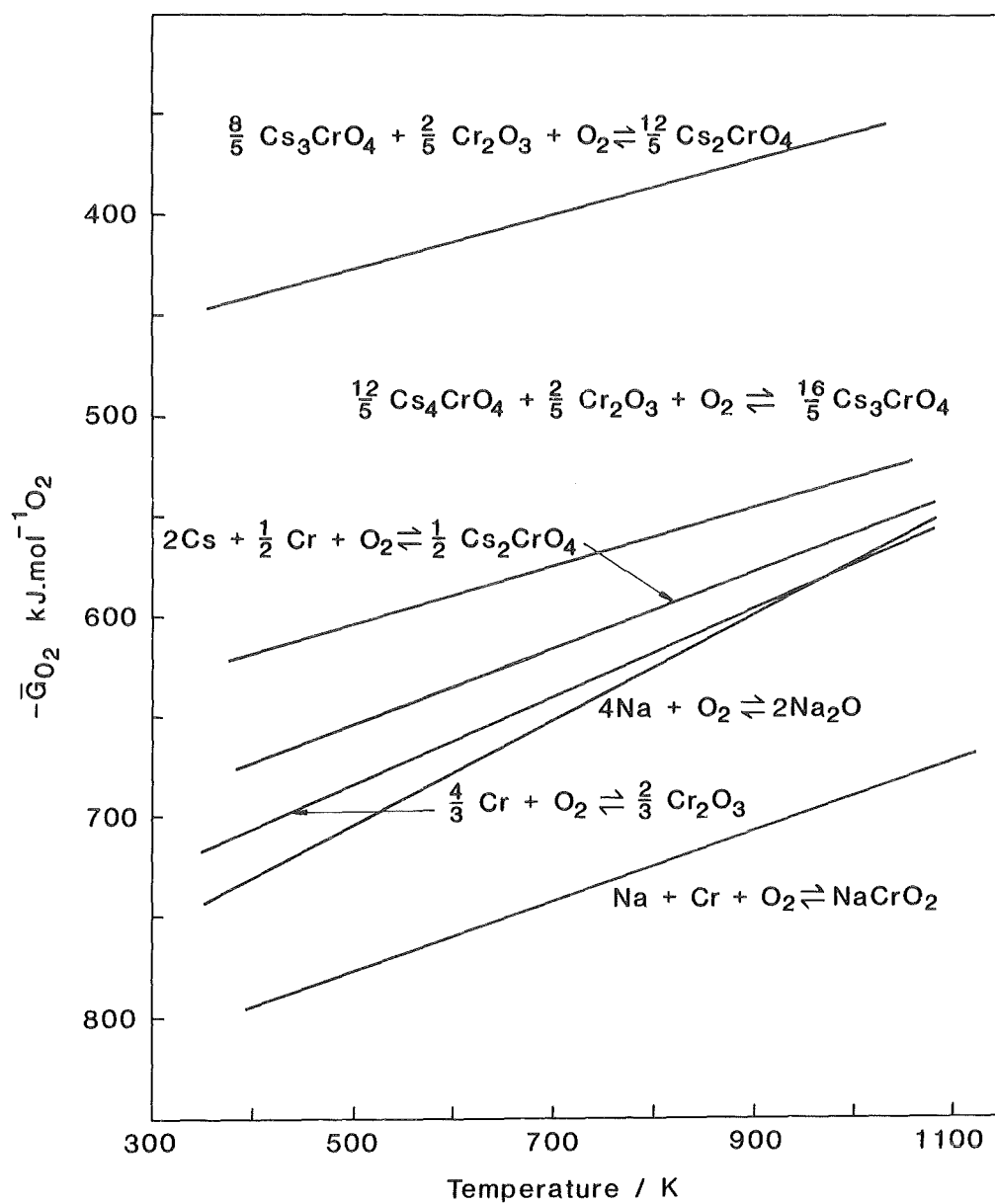


Fig. 8. Stabilities of Caesium and Sodium Chromates





METHODS FOR MEASUREMENT OF GAMMA-EMITTING NUCLIDE  
ACTIVITIES IN A FAST REACTOR CIRCUIT

V.I. Polyakov

Research Institute of Atomic Reactors,  
Dimitrovgrad, USSR

A b s t r a c t

Considered are the errors in the nuclide activity measurements in the sodium-coolant circuit. It has been shown that the best representativity of the nuclide activity measurements in sodium sampling is achieved while using flowing samplers, short time for sodium circulation and its specific activity measurement in a sampler in the "point" geometry. When measuring radionuclide activity in the reactor components and piping without sampling it is recommended to use the shielded gamma-spectrometers with collimators as well as simple analytical expressions to calculate a relative efficiency of monitoring. The error in the methods suggested doesn't exceed 12-22 %.

To make proper decision on the reactor performance, on the maintenance date as well as on the development and test of the models for calculation of the radionuclides build-up and distribution within the circuit it is necessary to ensure reliability of monitoring their activity in all the technological media ; in sodium, gas, and in the deposits onto the piping and equipment. Representativity of monitoring , that is the confirmity between values for the nuclide specific activities measured in the samples and those in the observed section of the sodium coolant circuit, doesn't always satisfy the requirements of investigators. The activity values for cobalt, zirconium, barium, fuel etc measured, for example, in the parallel samples of sodium may differ by an order of magnitude.

The methods and instruments are discussed for sampling sodium coolant, for activity measurements in both sodium and deposits on the piping and equipment without sampling which have been used in the BOR-60 plant and made possible to improve the representativity of the analysis.

#### I. Methods for Sampling and Measurement of Activity in Samples

Over the first years of the BOR-60 reactor operation the sodium coolant sampling has been carried out just from

the reactor vessel into the metallic sample-glasses of 30, 70 and 200 cm<sup>3</sup> volume. A glass comprised the closing cap and central metallic pin with a head adjustable to the bar grip in the reloading machine. It has been found that the specific activities of cerium, barium, zirconium, niobium nuclides in the samples taken from the upper layer of coolant are usually from 10 to 100 times of those taken from the depth. Inside a sampler the fission products are also distributed ununiformly (Table 1).

The activity in a smear from the outer surface of a glass is enriched with the niobium, cesium, antimony nuclides ten times of the sodium samples. It results in overestimating the levels of the fission product activities measured on gamma-spectrometry of the glass as a whole.

Non-uniformity of the nuclides distribution in the reactor vessel and in the non-flowing type samplers causes high errors in calculations of the coolant nuclide activities. When testing the different types of the flowing samplers with the delivery and discharge tubes and the sample-collector inside them the ten-fold difference was observed in the nuclide specific activity values obtained with the samplers made of various metals, and with those made of the same material, the difference in <sup>60</sup>Co, <sup>124</sup>Sb, <sup>182</sup>Ta, <sup>54</sup>Mn, <sup>110m</sup>Ag, <sup>65</sup>Zn activities amounted 1.2 - 1.5 /1/.

In spite of the complicated design of the samplers comprising inner sample-collectors they do not offer the desired reproducibility of the analyses. While comparing, for example, the results from measurements of the <sup>137</sup>Cs specific activities in the BN-6000 primary sodium samples with those from measurements in the spectrometric loop of the same reactor, they differ by a factor of two.

We managed to obtain essentially higher reproducibility of the results from measurements of the sodium sample activities at the BOR-60 plant using the flowing tube-samplers installed into the primary bypass. The samplers made of a stainless steel tube of 32 mm or 16 mm in diameter are placed into the loop section with a seal of the "sphere (stainless steel) along cone (annealed copper)" type. Sealing is provid-



Table 1

Specific activities of nuclides in two sodium samples taken simultaneously from the reactor vessel, relat. units

| N u c l i d e                | $^{22}\text{Na}$ | $^{110\text{m}}\text{Ag}$ | $^{137}\text{Cs}$ | $^{134}\text{Cs}$ | $^{95}\text{Nb}$ | $^{125}\text{Sb}$ |
|------------------------------|------------------|---------------------------|-------------------|-------------------|------------------|-------------------|
| in 70 g glass :              |                  |                           |                   |                   |                  |                   |
| - near central metal.pin     | 1                | 0.28                      | 5.6               | 0.44              | 0.09             | 0.15              |
| - in the middle of radius    | 1                | 0.33                      | 0.57              | 0.06              | 0.17             | 0.26              |
| - near the outer wall        | 1                | 0.32                      | 1.8               | 0.13              | 0.12             | 0.27              |
| in 200 g glass :             |                  |                           |                   |                   |                  |                   |
| - near central metal.pin     | 1                | 0.33                      | 5.8               | 0.42              | 0.10             | 0.28              |
| - in the middle of radius    | 1                | 0.28                      | 1.4               | 0.10              | 0.09             | 0.25              |
| - near the outer wall        | 1                | 0.30                      | 9.0               | 0.71              | 0.11             | 0.27              |
| - a smear from outer surface | 1                | 0.93                      | 200               | 18                | 35               | 20                |

ed by means of the sleeve nuts, after that the samplers are shut with thermal insulation and equipped with leak detectors. The operating experience has demonstrated that the probability for sodium leak is negligible. The merits of the tube-samplers are in the ease of fabrication, installation and removal as well as in feasibility for measurement of the activity in the whole volume without sodium melting. This permits the nuclides redistribution inside a sampler not to be taken into account and the average value for the nuclide specific activity to be obtained.

Representativity of sampling was verified by comparing the results with those from continuous relative measurements of the nuclide specific activity in the loop obtained with the help of the continuous monitoring device (Table 2).

While measuring the activity with the removable tube-samplers without sodium melting the error in the cesium activity in the coolant was 12 - 16 %. The error in measurements of the specific activities of other nuclides dissolved in the coolant ( $^{110m}\text{Ag}$ ,  $^{65}\text{Zn}$ ) didn't exceed 10 % but still it remained high for nuclides which tend to deposit on the walls ( $^{95}\text{Zr}$ ,  $^{95}\text{Nb}$ ,  $^{140}\text{Ba}$ ,  $^{140}\text{La}$ ,  $^{54}\text{Mn}$ ,  $^{60}\text{Co}$ ). When increasing both the time for sodium circulation and sodium velocity, and when decreasing the temperatures the deposits on the sampler walls grow. That is why a relative control of changes in the nuclide activity in the coolant is possible only in the case of identical sampling. According to paper /1/ to achieve an equilibrium activity in the deposits the 4-hour sodium cycling is sufficient. But based on our results one should say that accumulation of activity in the deposits continues for hundreds of hours (Fig.1).

Therefore, the effect of nuclides deposited onto the walls on the results of the sample analyses can be diminished by reducing the time for sodium circulation through a sampler. An optimum time sufficient for reliable substitution of sodium in the delivery tube up to a sampler which provides a minimum of deposits is about 0.2 to 1 h.

The deposit samples taken from the piping and equipment surfaces offer even lower representativity than those

T a b l e 2

<sup>137</sup>Cs specific activity in BOR-60 coolant

| Date of sampling                      | 1982  |       |       | 1983  |       |       | 1984  |       |       |       |
|---------------------------------------|-------|-------|-------|-------|-------|-------|-------|-------|-------|-------|
|                                       | 25.11 | 01.12 | 16.12 | 07.01 | 03.02 | 04.02 | 12.02 | 22.02 | 08.03 | 23.03 |
| Sodium samples, kBk/g                 | 210   | 300   | 320   | 230   | 260   | 240   | 330   | 350   | 350   | 400   |
| Continuous measurements, relat. units | 210   | 280   | 270   | 200   | 260   | 260   | 330   | 310   | 330   | 380   |

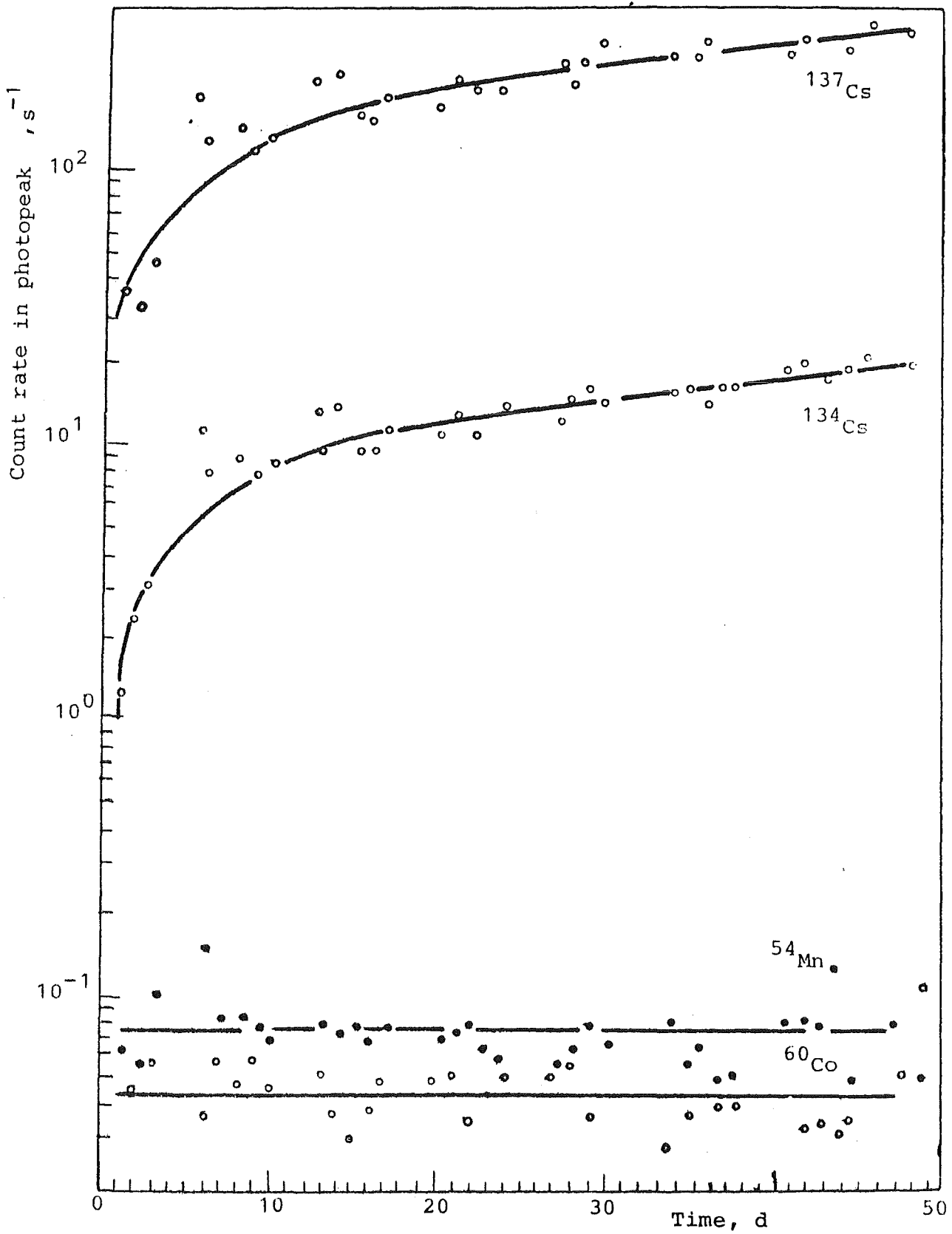


Fig.1 Accumulation of nuclides on stainless steel

from sodium coolant. Imperfection of taking smears and scrapers off the removable components is associated with variations in the fraction of the monitored activity, and primarily, with the nonuniformity in the nuclide distribution. On the surface of the removable section of the BOR-60 pump, for instance, the activity of  $^{54}\text{Mn}$ ,  $^{140}\text{Ba}$  and  $^{95}\text{Nb}$  varied from 10 to 100 times and that of  $^{137}\text{Cs}$  - to  $10^3$  times at sites spaced from each other within 0.5 - 1 m /2/. One should also take into account that the presence of sodium residual film and the formation of the nuclide chemical compound can result in the difference between the isotopic content of activity in a smear and that on the surface studied. That is why the sampling of the surface deposits presents only appraisal results, and as for more precise data or changes in the nuclide surface activity on the circuit components, they can be obtained by spectrometer scanning with a collimator.

The gas sampling usually presents no difficulties but the difference in the activity levels inside the remified gas plenums increases the error in the total activity estimation. At the BOR-60, for example, the activities of  $^{133}\text{Xe}$ ,  $^{135}\text{Xe}$ ,  $^{87}\text{Kr}$ ,  $^{88}\text{Kr}$  and  $^{41}\text{Ar}$ ,  $^{23}\text{Ne}$  were, respectively, 4 - 5 and 500-1000 times less inside the pump plenums than those in the reactor cover gas /2/. The gas activity was also found to be different in various gas plenums of the BN-600.

Together with the errors in the analyses of the nuclide activities in the gas, sodium and deposit samples arising from the uncontrolled processes of their redistribution within the medium being sampled, they also occur when measuring the activity in the samplers if their dimensions exceed those of a detector. It is possible to determine the efficiency of monitoring of the extended sources in the case of similarity in geometry of measurements; for example, a sample filled with the water solution of the reference sources. At the BOR-60 plant the simpler calibration method is used.

When melting sodium out of a sampler or when sampling sodium out of a sampler the degradation in representativity is observed due to nuclide nonuniform distribution along a radius. This can be avoided if the activity is defined

throughout a sampler by gamma-spectrometry (without melting sodium out of a sampler) and if it is placed in a "point" geometry, that is at a distance which is 10-20 times the dimensions of a sampler. Taking into account the energy dependence of the detector monitoring efficiency,  $\mathcal{E}_p(E)$ , (Fig. 2, curve 2) under these conditions the efficiency of monitoring for a sampler,  $\mathcal{E}_s(E)$ , is determined in relative units by introducing a correction for gamma-ray absorption /3/ :

$$\mathcal{E}_s(E) = \mathcal{E}_p(E) e^{-\mu_{Fe} \cdot t} \left[ 1 - \frac{8}{3\pi} \mu_{Na} R + \frac{1}{2} \mu_{Na} R^2 - \frac{32}{45\pi} \mu_{Na}^3 R^3 \right], \quad (1)$$

where  $t$  is the thickness of the sampler wall,

$R$  is the sampler radius,

$\mu_{Fe}, \mu_{Na}$  are the coefficients for gamma-quantum attenuation in ferrum and sodium.

The ratio obtained (Fig. 2, curve 3) is normalized according to the relation of  $^{22}\text{Na}$  photopeak area within the spectrum of a sampler to its specific activity (curve 1). Such a calibration error is combined with those in values for a reference sample activity (3 %), in the photopeak area estimates (2-4 %), in measurements of the sample mass (0.5 %) and, finally, with those in the energy dependence (12 %). The total error doesn't exceed 20 %, that is quite tolerable for all practical problems.

## 2. Non-sampling measurements of the nuclide activities in the extended sources

The reactor vessel, the separable components (pumps, heat exchangers), the piping are the extended sources the yields of gamma-quanta from which can be calculated analytically or on a computer. To measure the nuclide activities in such sources the gamma-spectrometric detectors are used in the shield with a "narrow" collimator, and for calibration it is convenient to apply simple analytical expressions /4/.

When measuring the nuclide activities in the components it is necessary to make calculations of the radiation fluxes towards a detector from various elements of source volume visible from different points of a detector taking into

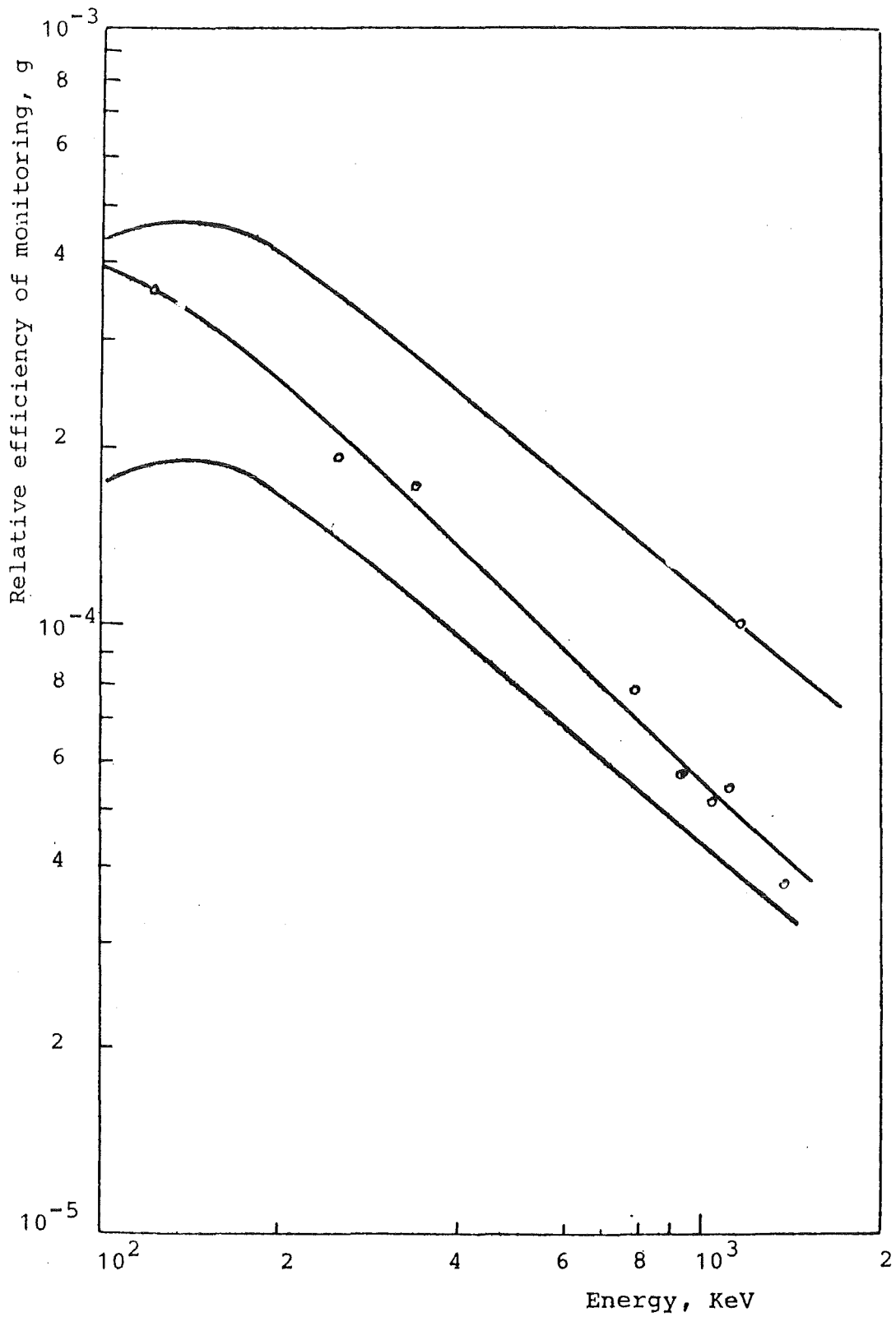


Fig.2 Calibration of Ge(Li) detector in measuring nuclide activities from extended sources (sodium sampler)

account the expansion of the "visible" volume as a result of leakage of radiation. It has been suggested to apply the notion of relative efficiency of monitoring, r.e.m.,  $\mathcal{E}^*(E)$ , which can be determined as the relation of a number of the pulses monitored by a detector,  $n$ , with energy  $E$ , to the specific,  $A_m$ , volumetric,  $A_v$ , surface,  $A_s$ , linear,  $A_l$  activities :

$$\mathcal{E}^* = \frac{n}{A_i} ; \quad A_i = A_m, A_v, A_s, A_l. \quad (2)$$

To calculate the r.e.m. from the sources of optional shapes the expression is given in the integrated form :

$$\mathcal{E}^* = \iint_S ds \iiint_V \frac{\rho dV}{4\pi x^2} (1 - e^{-\mu_d x_d}) e^{-\mu_s x_s - \mu_{sh} x_{sh} - \mu_c x_c} \quad , \quad (3)$$

where  $x$ ,  $x_d$ ,  $x_s$ ,  $x_{sh}$ ,  $x_c$  are, respectively, the distance between a detector and the source partial volume, the length of the gamma-quanta path in a detector, source, shield and collimator material ;

$\mu_d$ ,  $\mu_s$ ,  $\mu_{sh}$ ,  $\mu_c$  are the coefficients for attenuation of gamma-quanta in the materials of, respectively, a detector, a source, shield, collimator ;

$ds$ ,  $dV$  are the elements of integration according, respectively, to the detector surface and the source volume. The analytical calculations of all the distances,  $x_i$ , and the integration limits for each particular geometry of measurements are very tedious. That is why it is of good practice to use a set of simple analytical expressions instead of computations to determine the r.e.m.

For narrow angles of collimation the following expressions have been obtained from equation (3) :

- for the point source at the collimator axis

$$\mathcal{E}^* = \mathcal{E}_p \frac{a^2}{4b^2} \left( 1 + \frac{2}{\mu_c b} + \frac{6}{\mu_c^2 b^2} \right) \exp(-\mu_{sh} t); \quad (4)$$

- for the plane source

$$\mathcal{E}_s^* = \mathcal{E}_p \frac{\pi a^4}{4L^2} \left[ 1 - \frac{3a^2}{4b^2} \left( 1 - \frac{a^2}{2L^2} \right) \right] \left( 1 + \frac{4}{\mu_c L} + \frac{12}{\mu_c^2 L^2} \right) \exp(-\mu_{sh} t); \quad (5)$$

- for the linear source

$$\mathcal{E}_l^* = \mathcal{E}_p \frac{a^3}{2bL} k \left( 1 + \frac{1}{\mu_c L} + \frac{2}{\mu_c b} + \frac{2}{\mu_c^2 L^2} + \frac{6}{\mu_c^2 b^2} \right) \exp(-\mu_{sh} t); \quad (6)$$

where  $k = 1$  at  $b = L$ ,  
 $k = 0.9$  at  $b = 15L$ ,  
 $k = 0.85$  at  $b/L = \infty$ ;



- for closely spaced cylindrical source ( $b < b' = LR/a$ )

$$\mathcal{E}_{V1}^* = \mathcal{E}_P \frac{\pi a^4}{4\mu_s L^2} (1 - e^{-2\mu_s R}) e^{-\mu_{sh} t} \left(1 + \frac{4}{\mu_c L} + \frac{12}{\mu_c^2 L^2}\right); \quad (7)$$

- for the surface cylindrical source ( $b < b'' = 2LR/a$ )

$$\mathcal{E}_{S1}^* = \frac{\pi a^4}{4L^2} (1 + e^{-2\mu_s R}) e^{-\mu_{sh} t} \left(1 + \frac{4}{\mu_c L} + \frac{12}{\mu_c^2 L^2}\right); \quad (8)$$

- for the source spaced far away from the cylindrical source ( $b > b' = LR/a$ )

$$\mathcal{E}_{\cdot 2}^* = \mathcal{E}_P \frac{0.85\pi a^3 R}{4bL\mu_s} (1 - e^{-2\mu_s R}) e^{-\mu_{sh} t} \left(1 + \frac{1}{\mu_c L} + \frac{2}{\mu_c b} + \frac{2}{\mu_c^2 L^2} + \frac{6}{\mu_c^2 L^2}\right); \quad (9)$$

- for the surface cylindrical source ( $b > b'' = 2LR/a$ )

$$\mathcal{E}_{S2}^* = \mathcal{E}_P \frac{0.85\pi a^3 R}{2bL} (1 + e^{-2\mu_s R}) e^{-\mu_{sh} t} \left(1 + \frac{1}{\mu_c L} + \frac{2}{\mu_c b} + \frac{2}{\mu_c^2 b^2} + \frac{6}{\mu_c^2 b^2}\right), \quad (10)$$

where  $\mathcal{E}_P$  is the photoefficiency of the detector monitoring,

$R$  is the source radius,

$a$  is the collimator radius,

$L$  is the collimator length,

$b$  is the distance between a detector and a point,

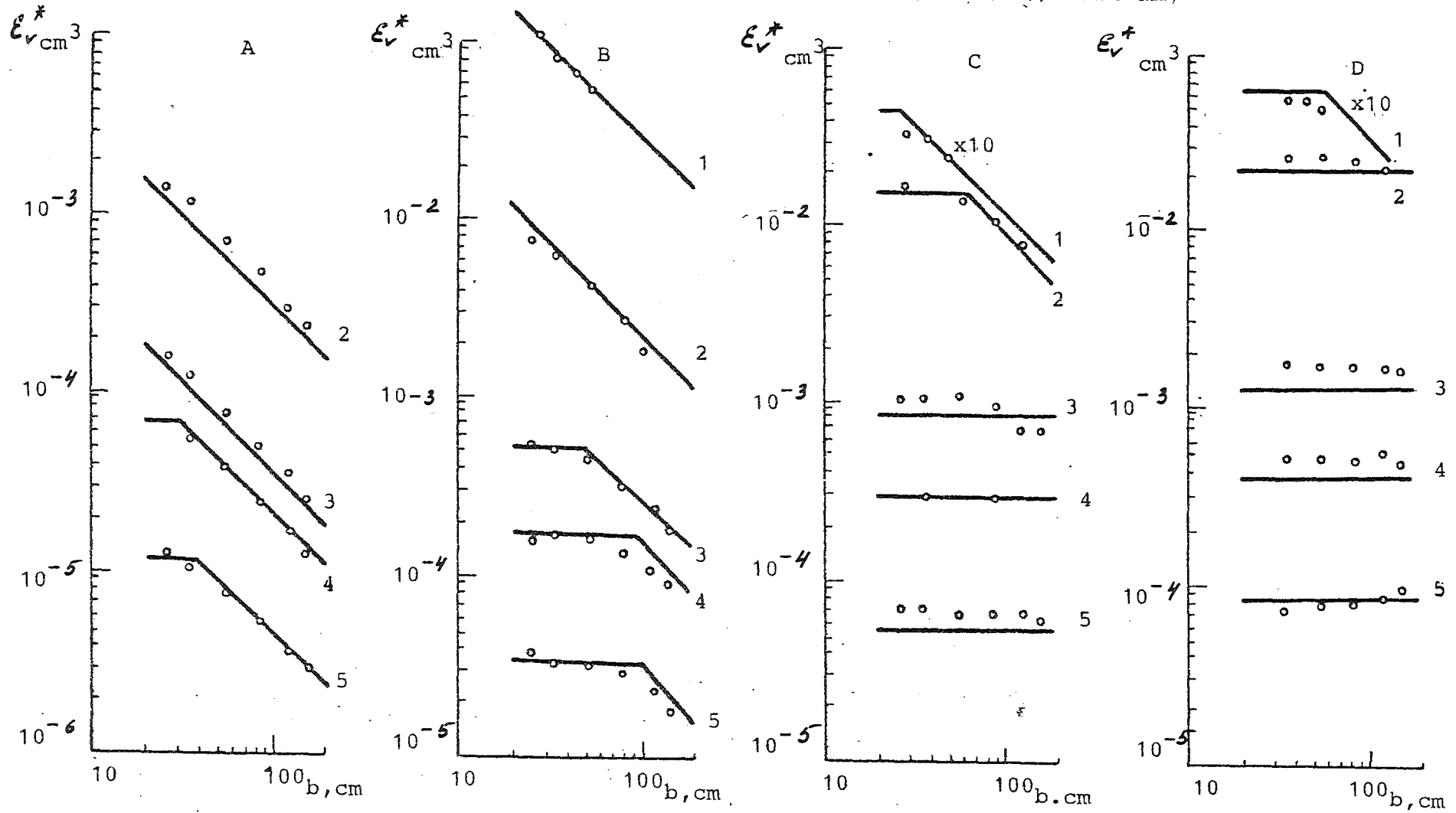
linear sources and an axis of a cylindrical one.

To define experimentally the limits of both applicability and a maximum error for the approximate expressions obtained a series of tests has been carried out with various detectors, collimators of 150 and 250 mm length and 5, 10, 20 and 50 mm in diameter, with the volume and surface cylindrical sources of 16, 50, 121 and 255 mm in diameter and distances from 25 to 170 cm between a source and a detector, with iron shield from 1 to 5 cm thick and with gamma-quanta energies from 142 to 1333 KeV. The error in the value for the r.e.m. was mainly a function of that in the data for specific activity of the solution, and amounted 9-14 %.

Figs. 3 and 4 present the examples of the experimentally defined r.e.m. for the cylindrical sources as compared to the theoretical values obtained from equations (7 - 10).

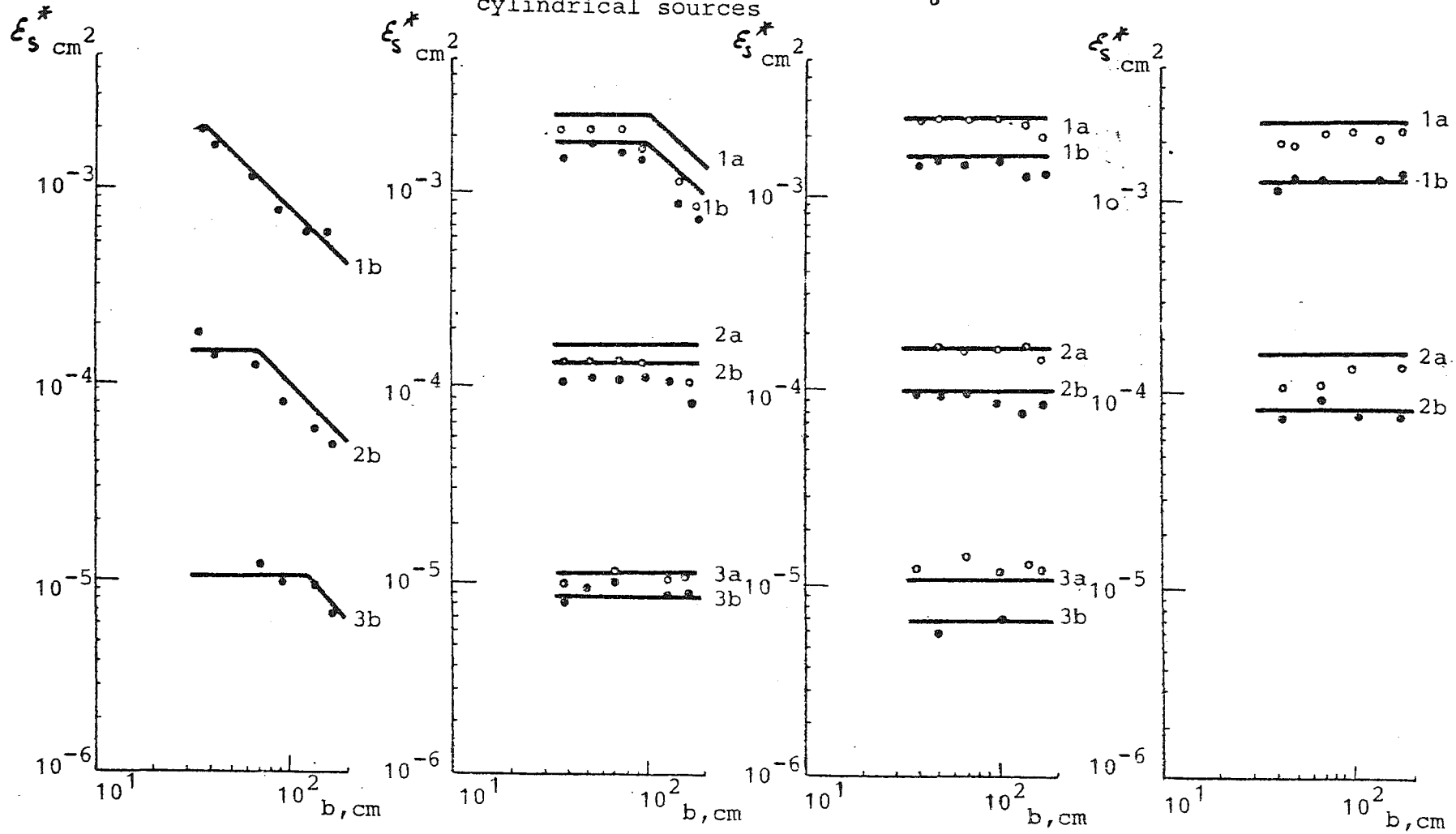
Within the considered range of the parameters variation the analytical expressions offer satisfactory accuracy. A mean disagreement between the experimental and theoretical data for all the sources and geometries lies within the

Fig.3 Relative efficiency of monitoring radiation from volume cylindrical sources of  $^{137}\text{Cs}$  ( $E=662$  KeV), NaI(Tl)  $\phi 70 \times 70$  mm,



Sources A :  $2R=1.6$ ,  $t=0.21$ . B:  $2R=5.0$ ,  $t=0.31$ . C:  $2R=12.1$ ,  $t=0.57$ . D:  $2R=25.5$ ,  $t=0.58$  cm.  
 Collimators 1:L=15,  $a=5.0$ , 2:L=15,  $a=2.1$ , 3:L=15  $a=1.0$ , 4:L=25,  $a=1.0$ , 5:L=15  $a=0.5$  cm  
 ——— calcul. accord. to (7,9),  $\circ$  experim.

Fig.4 Relative efficiency of monitoring radiation from surface cylindrical sources



Source :  $^{141}\text{Ce}$  (142 KeV) a)  $\circ$  - the source without selfabsorption, b)  $\bullet$  - the source with selfabsorption. The rest symbols as in Fig.3. Calcul. accord. to (8,10).

range of the experimental errors and amounts 12 % for the volume and 22 % for the surface cylindrical sources. And only in the case of  $b$  approaching to  $b'$  and  $b''$  the error increases up to 30-40 %.

The procedure initially suggested and experimentally tested with the scintillation detectors was further applied to the measurements with the semiconductor Ge(Li) detectors/5/.

The efficiency of Ge(Li) detector monitoring for given collimation conditions is estimated experimentally. For this purpose the energetic calibration of the detector is performed which is normalized according to the photopeak area ( $n_p$ ) of the point calibration source with the activity  $A$ , located at the collimator axis

$$\mathcal{E}_p^*(E) = \frac{n_p}{A \gamma} , \quad (11)$$

where  $\gamma$  is the gamma-quanta yield.

By substituting (11) to (3) one can determine the efficiency of the detector monitoring

$$\mathcal{E}_p(E) = \frac{4 n_p b^2}{A \gamma a^2 \left( 1 + \frac{2}{\mu_c b} + \frac{6}{\mu_c^2 b^2} \right)} , \quad (12)$$

which is then used in expressions (7 through 10) to calculate the relative efficiency of monitoring radiation from volume and surface cylindrical sources.

To measure the nuclide activities in the sodium coolant a simpler procedure for normalizing the r.e.m. is applied which doesn't require the use of the calibration sources with due regard for the photopeak area and sodium-22 and its known specific activity.

The surface activity of the nuclides in the piping is derived from Eqs. 9-10.

$$\mathcal{E}_{s1}^* = \mathcal{E}_{v1}(E) \cdot \frac{(1 + e^{-2\mu_s R}) R}{(1 - e^{-2\mu_s R})} \mu_s \quad (13)$$

The non-sampling measurements of the nuclide activities in the piping and equipment using the above expressions is feasible if it is known that the particular nuclide is distributed uniformly either along the source volume or along its surface. It is known that together with  $^{22}\text{Na}$  and  $^{24}\text{Na}$  nuclides,  $^{110m}\text{Ag}$ ,  $^{23}\text{Ne}$  are uniformly distributed in the coolant;  $^{60}\text{Co}$ ,  $^{95}\text{Zr}$  -  $^{95}\text{Nb}$ ,  $^{140}\text{Ba}$  -  $^{140}\text{La}$  nuclides are found

practically only in the deposits, and the other nuclides are observed in both sodium and deposits ;  $^{137}\text{Cs}$ ,  $^{134}\text{Cs}$  nuclides being to a greater degree in sodium and  $^{54}\text{Mn}$  - on the walls. While measuring the specific activity of cesium in piping the estimated photopeak area is composed of the count rates from the surface and volume sources and while evaluating the efficiency of monitoring from Eq. (9), the value for the specific activity,  $A_m$ , is turned to be higher than that measured in sodium samples,  $(A_m)_{\text{samp}}$ . If the volume activity of a nuclide in the coolant is obtained from sampling then its surface activity can be derived from the results of the non-sampling measurements of the photopeak area,  $n$ , according to the expressions 9 and 10 for the relative efficiency of monitoring :

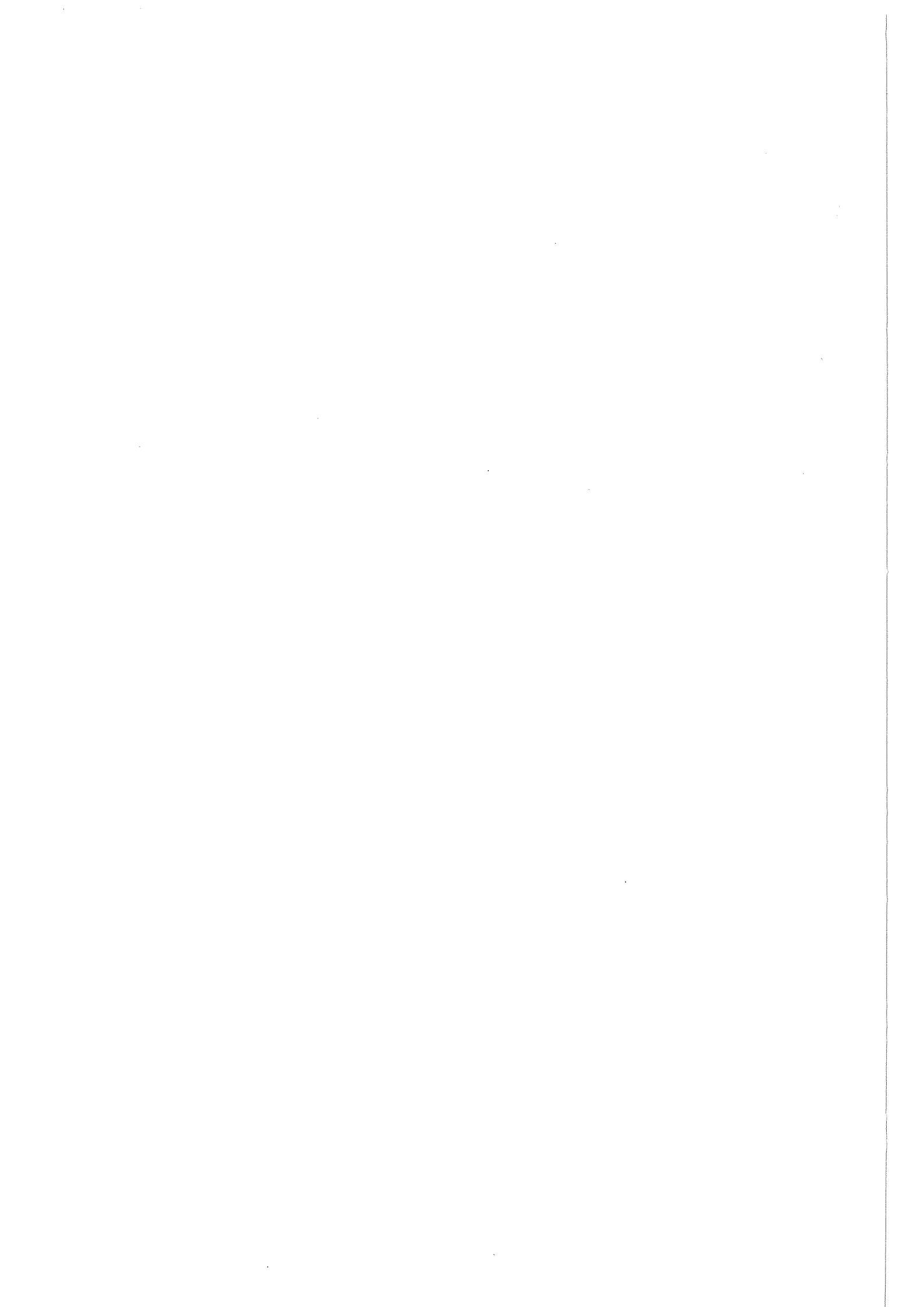
$$A_s = \frac{n - \epsilon_v^* (A_m)_{\text{samp}} \rho_{\text{Na}}}{c_s^*} \quad (14)$$

### C o n c l u s i o n s

The methods for measuring the activity from gamma - emitting sources considered above improve the representativity and accuracy of the analyses. The best representativity of sodium-coolant sampling and nuclide activity measurements is achieved when applying the flowing samplers, short cycling period and by measuring specific activity in a sampler without melting sodium out in a "point" geometry. In the non-sampling measurements of the radionuclide activities in the reactor piping and equipment one can use both the gamma-spectrometers in the shield with collimators and the simple analytical expressions to calculate the relative efficiency of monitoring. The experimental tests of the methods within a wide range of the parameter variations have shown that the error in the monitoring doesn't exceed 12 - 22 %.

#### REFERENCES

1. Stamm H.H. Sorption of radionuclides on sodium sampling vessels. - Proc.Int.Conf. on Liquid Metal Technology in Energy Production, Champion - CONP - 760503 - PI - USA, ERDA, 1976, p. 271.
2. Kizin V.D., Lisitsyn E.S., Polyakov V.I., Chechetkin Yu.V. BOR-60 Primary Circuit Radiation Level. Atomnaya energiya 44, 6 (1978) , p.492.
3. Gorshkov G.V. Penetrating radiation from radioactive sources. The Second Edition, added and revised. Nauka, Leningrad, 1967, p. 54.
4. Polyakov V.I., Chechetkin Yu.V. Determination of Gamma-Emitting Isotope Concentrations in Extended Sources without Sampling, Preprint RIAR, P-123, Melekes, 1971.
5. Kizin V.D., Polyakov V.I., Chechetkin Yu.V. Non-sampling analysis of radiation level in the liquid metal fast reactor circuit. In coll. "APP Radiation Protection and Safety" Ed.Yu.A. Egorov. M., Energoizdat, 1982, 246.



# Filtration Experiments of the KNK II Primary Sodium

H. H. Stamm  
Kernforschungszentrum Karlsruhe  
Institut für Radiochemie

and

K. Ch. Stade  
Kernkraftwerk-Betriebsgesellschaft m.b.H.  
Eggenstein-Leopoldshafen

Federal Republic of Germany



## **Filtration Experiments of the KNK II Primary Sodium**

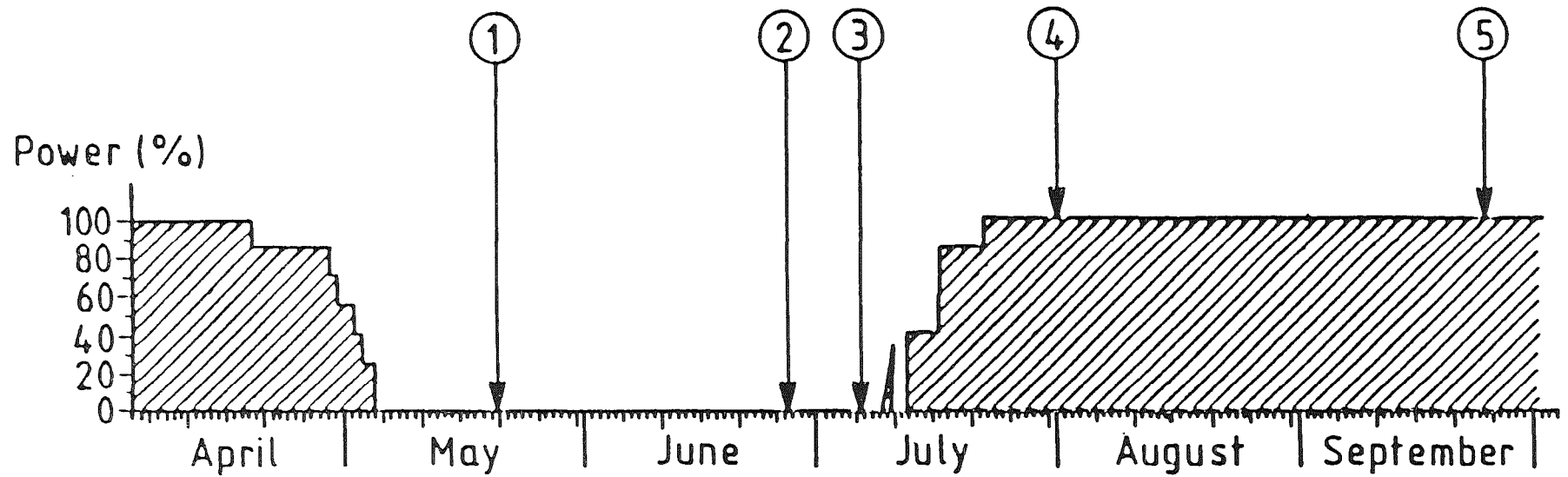
### **OBJECTIVE OF THE EXPERIMENTS**

**Determination of particles in the KNK primary sodium**

- a) Particle concentration in the primary sodium**
- b) Distribution of the particle size**
- c) Chemical composition of the particles**
- d) Possible correlation between the particle size or particle concentration and drift of the sodium outlet temperature during operation of the core KNK II/2**

---

**KBG**



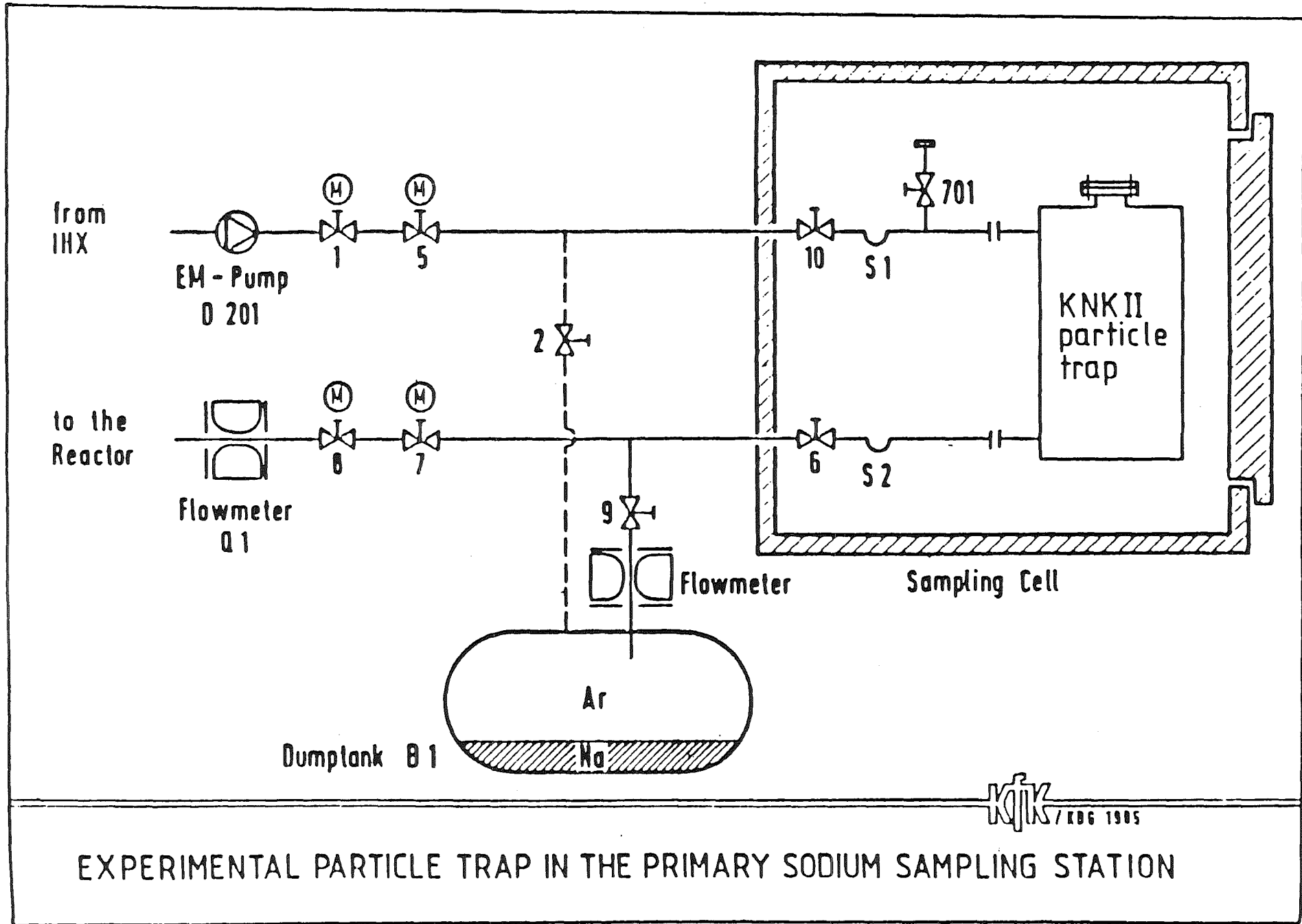
FILTRATION SAMPLES WITH THE KNK  
PRIMARY SODIUM SAMPLER 1985

- DEVICE, KNK II particle trap (modified primary sodium sampler with different sintered metal filters)
- NUMBER OF TESTS: 5 (during April up to September 1985)
- TEST PARAMETERS:
  - operating time: 1 - 24 hours
  - sodium temperature: 220 - 330 C
  - sodium flow through the particle trap: 0.1 - 0.85 cubic-meter/h
  - total volume filtered sodium: 1.2 - 13.2 cubic-meter (60% of the entire primary sodium inventory)
  - dimension of sintered metal filter:
    - diameter: 30 mm
    - thickness: 2 and 5 mm
    - porosity: 30 - 50% (ca. 5-10 micron mesh size)

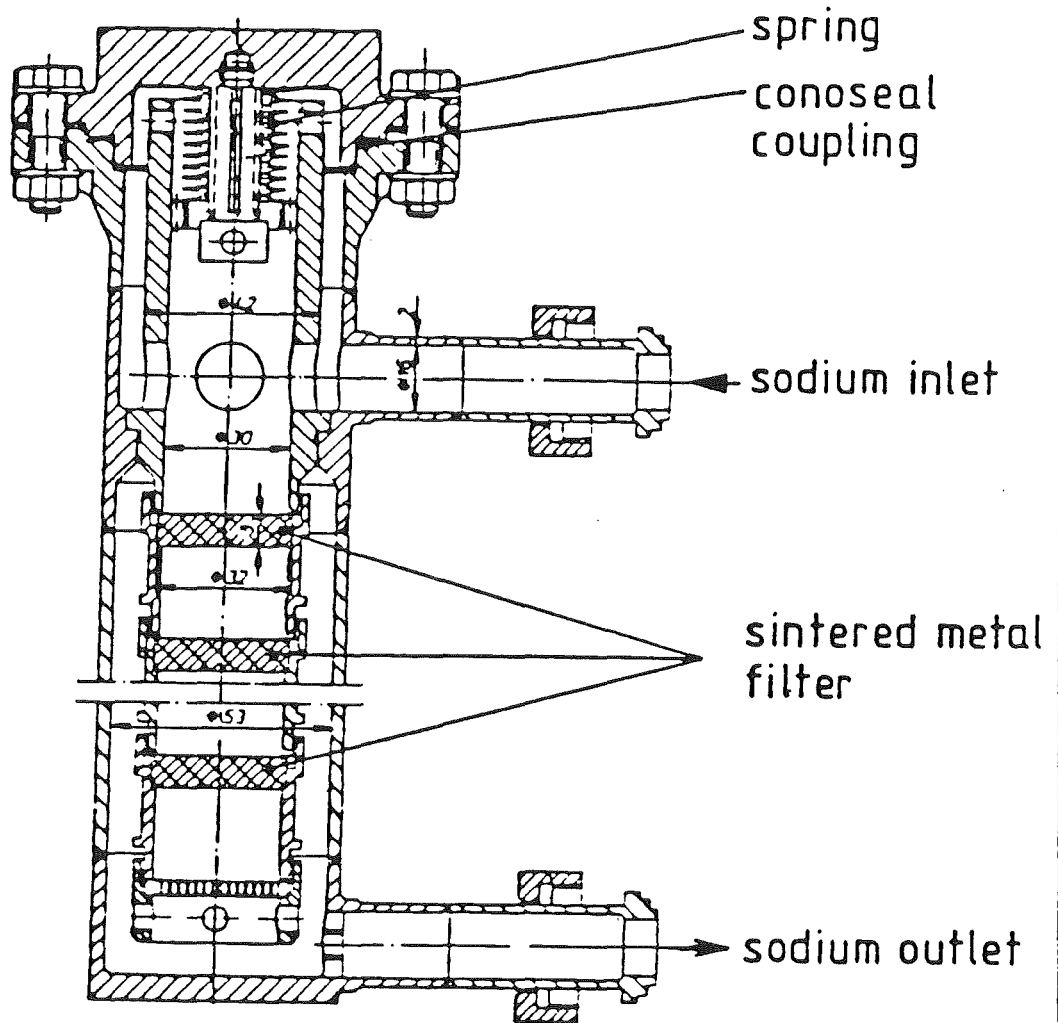
PROBLEM OF THESE TESTS: From hydraulic reasons particles with a size greater than 100 micron are not transported to the sodium sampling system

**KBG**

First tests in the primary sodium sampling system (with and without reactor operation)



EXPERIMENTAL PARTICLE TRAP IN THE PRIMARY SODIUM SAMPLING STATION



KNK II PARTICLE TRAP

- Location: fuel rod adapter at the core position YG-403 after removal of the fuel subassembly (all tests were performed during reactor shut down from December 1985 up to February 1986)
- Filtration device: Chemical sieve filter with wire screen, removeable fixed in a modified fuel rod adapter
- Mesh size: 300 micron (5 tests)  
160 micron (4 tests)  
11 micron (2 tests)
- Additional parameters:
  - o sodium temperature: 210 - 400 C
  - o operating time: 1 - 435 hours
  - o fluid velocity: 6.82 - 6.88 kg/sec
  - o sodium flow through the core:
    - a) constant at 1021 m<sup>3</sup>/h (ca. 100%)
    - b) verified between 320 and 1021 cubic-meter/h

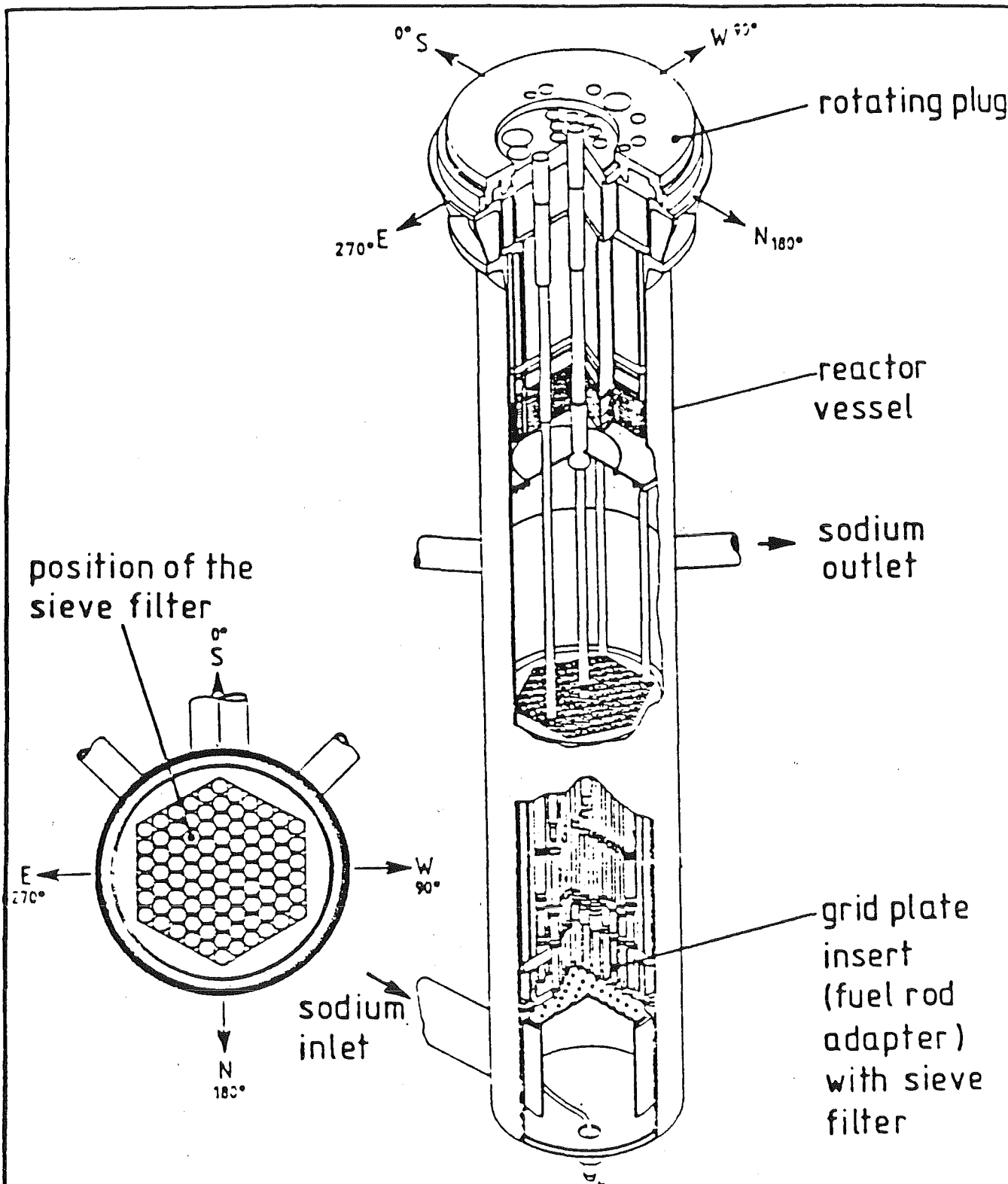
**KBG**

Filtration of the primary sodium near the sodium inlet  
of the KNK core

- Location: fuel rod adapter at the core position YG-403 after removal of the fuel subassembly (The experiment was performed in February 1986 during reactor shutdown)
- Experimental device: short mock-up bundle removable fixed in a modified fuel rod adapter
  - o Number of pins: 37
  - o Number of spacer grids (Mk-II): 2
- Operating time: 289 hours
- Sodium temperature: 400 C
- Sodium flow rate through the core: 1021 cubic-meter/h

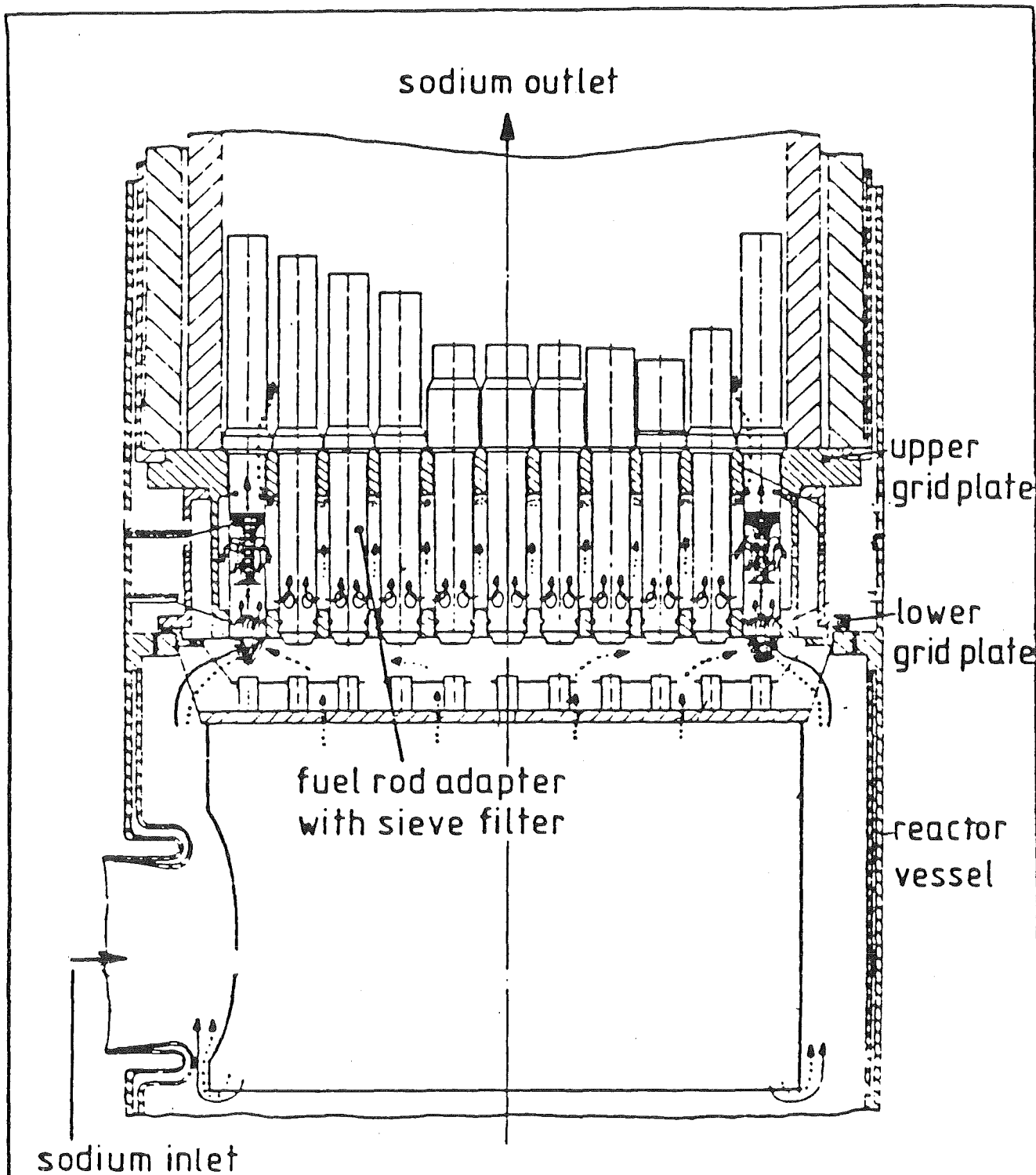
**KBG**

**Particle deposition experiment with a short mock-up bundle**

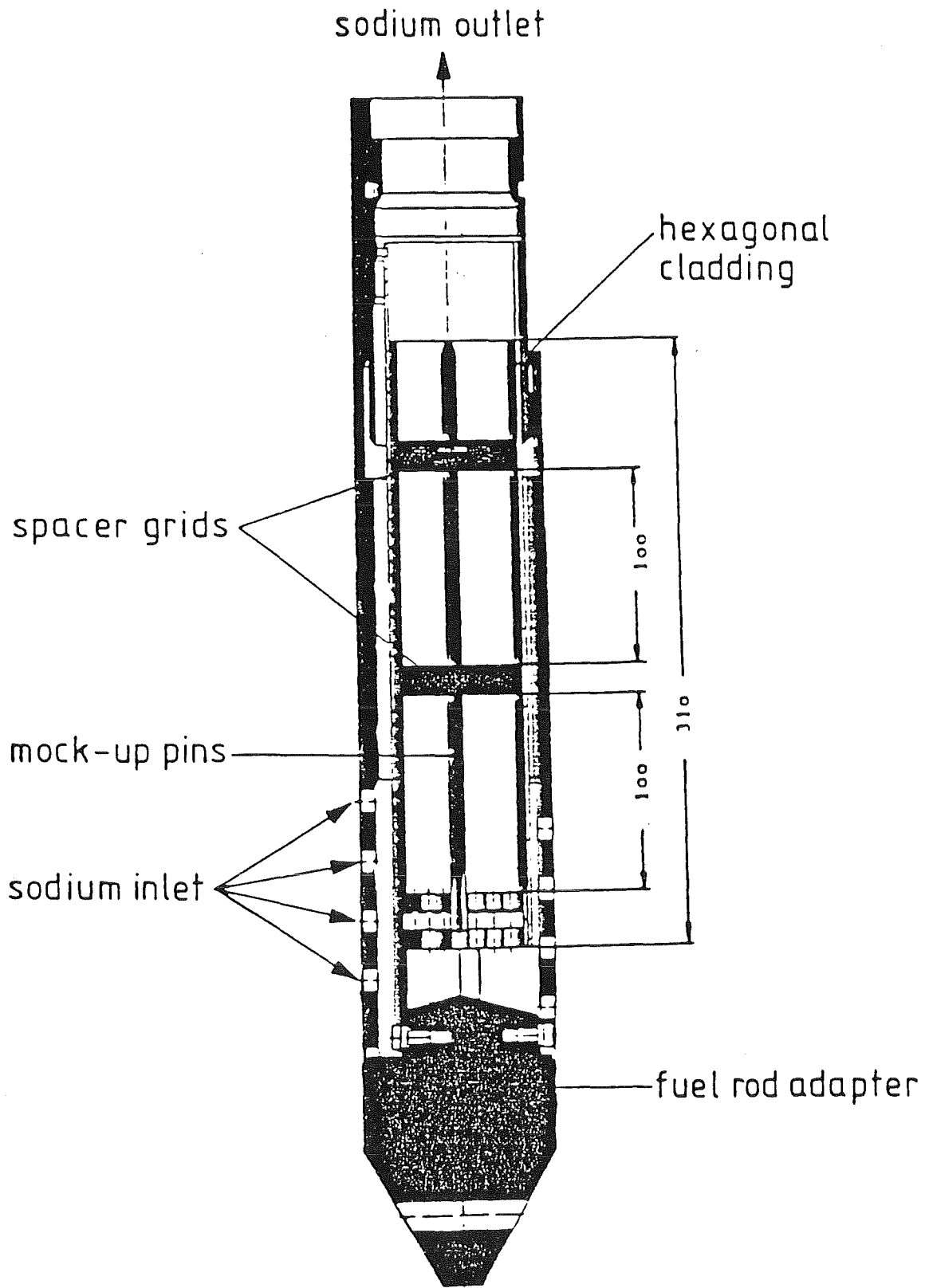


POSITION OF THE SIEVE FILTER IN  
THE KNKII REACTOR VESSEL

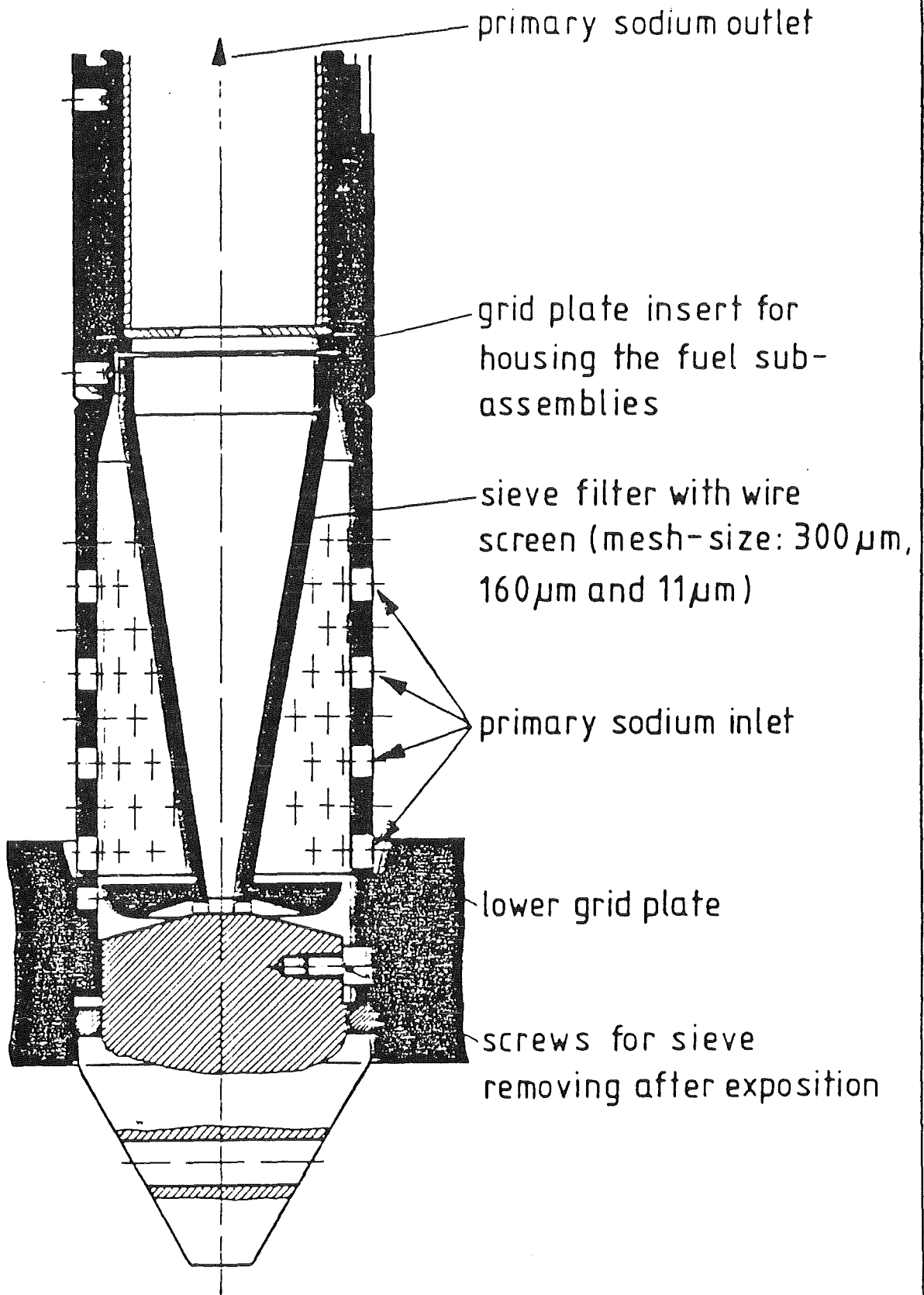




LOWER PART OF THE KNCII REACTOR VESSEL  
WITH POSITION OF THE SIEVE FILTER



SHORT MOCK-UP BUNDLE FOR PARTICLE DEPOSITION EXPERIMENTS



GRID PLATE INSERT WITH SIEVE FILTER

- Removal of sodium by solution with alcohol (ethylen-glycol-monobutyl-ether) and neutralization of the solution with water and nitrid acid
- Filtration of the solution through a combination of filters consisting of wire mesh (300 and 100 micron) and membrane filters (Typ NUCLEPore, 0.4 micron pore size)
- Ultrasonic cleaning of the sieve filter with In-nitrid acid
- Filtration of the solution through the same combination of filters

#### Chemical Analysis of the separated particles

- gamma spectroscopy
- electron spectroscopy chemical analysis (ESCA)
- raster electron microscope (REM)
- X-ray spectroscopy and X-ray diffraction (XES)
- microprobe analysis

**KBG**

Separation of the filtered particles after exposure

SUMMARY OF THE FILTRATION EXPERIMENTS WITH THE CONICAL SIEVES

| Test-<br>Number | Operating<br>Time<br>(h) | Filter<br>Mesh<br>Size<br>( $\mu\text{m}$ ) | Gamma-Dose<br>Rate<br>(mR/h) | Sodium<br>Temperature<br>(centigrade) | Sodium Flow<br>through the<br>Core<br>(m <sup>3</sup> /h) | Particle<br>Amount<br>(mg) | Particle<br>Concentration<br>( $\mu\text{g}/\text{kg Na}$ ) |
|-----------------|--------------------------|---|------------------------------|---------------------------------------|---|----------------------------|---|
| 1               | 1                        | 300   | 40                           | 212                                   | 1021  | 13, 77                     | 0, 58   |
| 2               | 1                        | 160   | 80                           | 210                                   | 1021  | 18, 11                     | 0, 73   |
| 3               | 22                       | 300   | 85                           | 210                                   | 1021  | 18, 98                     | 0, 035  |
| 4               | 22                       | 160   | 70                           | 210                                   | 1021  | 32, 73                     | 0, 081  |
| 5               | 118                      | 160   | 130-200                      | 210                                   | 1021  | >18, 49                    | >0, 008   |
| 6               | 22                       | 160   | 60-80                        | 220                                   | 320-1021  | 25, 22                     | 0, 048  |
| 7               | 435                      | 300   | 150-250                      | 400                                   | 1021  | 34, 97                     | 0, 003  |
| 8               | 22                       | 300   | 30                           | 210                                   | 1021  | 33, 83                     | 0, 081  |
| 9               | 22                       | 300   | 30                           | 220                                   | 320-1021  | 14, 07                     | 0, 028  |
| 10              | 1                        | 11  | 180                          | 220                                   | 1021  | 151, 11                    | -----   |
| 11              | 85                       | 11  | 400                          | 220                                   | 1021  | 172, 35                    | -----   |

## Results of the experiments

- Total particle mass obtained by the particle trap experiments varies between 5.1 and 61 mg (corresponds to 4.8 up to 18.4 micro-gram/kg Na).
- Total particle mass obtained by the sieve experiments varies between 13.8 and 33.8 mg (mesh size: 300 and 160 micron) of 151 and 172 mg (mesh size: 11 micron). This corresponds to 0.05 up to 0.7 micro-gram/kg Na.
- The filtered particle mass depends not from the operating time.
- Morphology of the separated particles was characterized by single particles, agglomerates of particles and fibrous particles.
- The predominant group of particles (99%) were single particles and agglomerates
- More than 80 - 95% of the particles were less than 100 micron in diameter
- The maximum of the size distribution for the particles less than 100 micron was between 0.7 and 1.5 micron in diameter

KBG

## Results of the experiments (continued)

- The chemical makeup of these particles is very complex
- .. Single particles and agglomerates consist of Fe, Cr and Ni with different composition. The main part was Cr as oxidized compound.
- Some particles of Ca and Si were found.
- Small amounts of metallic particles consisting of Fe or Fe-Ni-alloy were isolated.
- The fibrous particles are 20 - 50 micron in diameter and 0.5 - 1 cm in length
- The chemical analysis of these fibrous particles showed 2 types of fibers:
  - a) brittle fibers consisting of Ca, Al, Si, Mo and O
  - b) flexible fibers consisting of Al, Si, Mo and O

KBG

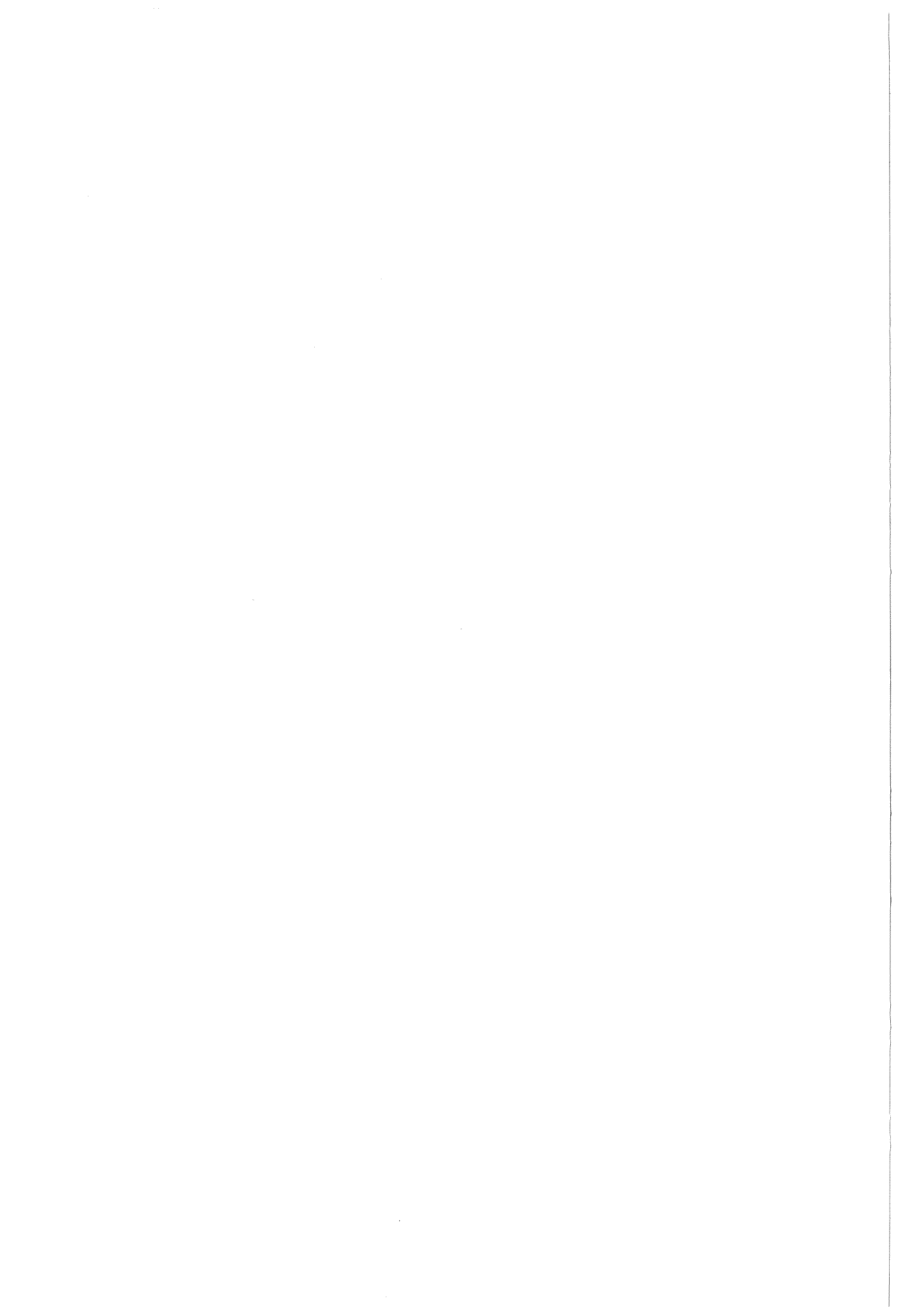
## Conclusions of the experiment

1. The separated particles of the KNK primary sodium are a result of a normal corrosion rate by using ferritic and austenitic steels in sodium.
2. Similar particle distributions and concentrations were found in primary circuits of other breeder plants (EBR-II et al)
3. The experimental results of the particle concentration in the KNK primary sodium were lower than the theoretical calculation. Based on a corrosion rate of 0.5 micron/y for austenitic steels and a corrosion rate of 1.5 mg/square-cm y for a ferritic steel used in KNK as structure material a equilibrium particle concentration of 1.066 mg/kg Na was calculated.
4. The experimental results of particle size are not in agreement with theoretical calculation of the BACCHUS code

---

KBG





RADIOCHEMICAL SURVEILLANCE  
OF KNK PRIMARY SODIUM

by

H. H. Stamm  
Kernforschungszentrum Karlsruhe  
Institut für Radiochemie

and

K. Ch. Stade  
Kernkraftwerk-Betriebsgesellschaft m.b.H.  
Eggenstein-Leopoldshafen

Federal Republic of Germany

## 1. INTRODUCTION

KNK II is an experimental, sodium-cooled fast breeder reactor, located in the nuclear research center KfK near Karlsruhe/Germany. The reactor was operated until 1974 with a thermal core (KNK I) to demonstrate the reliable operation of a sodium-cooled nuclear power plant for electricity generation.

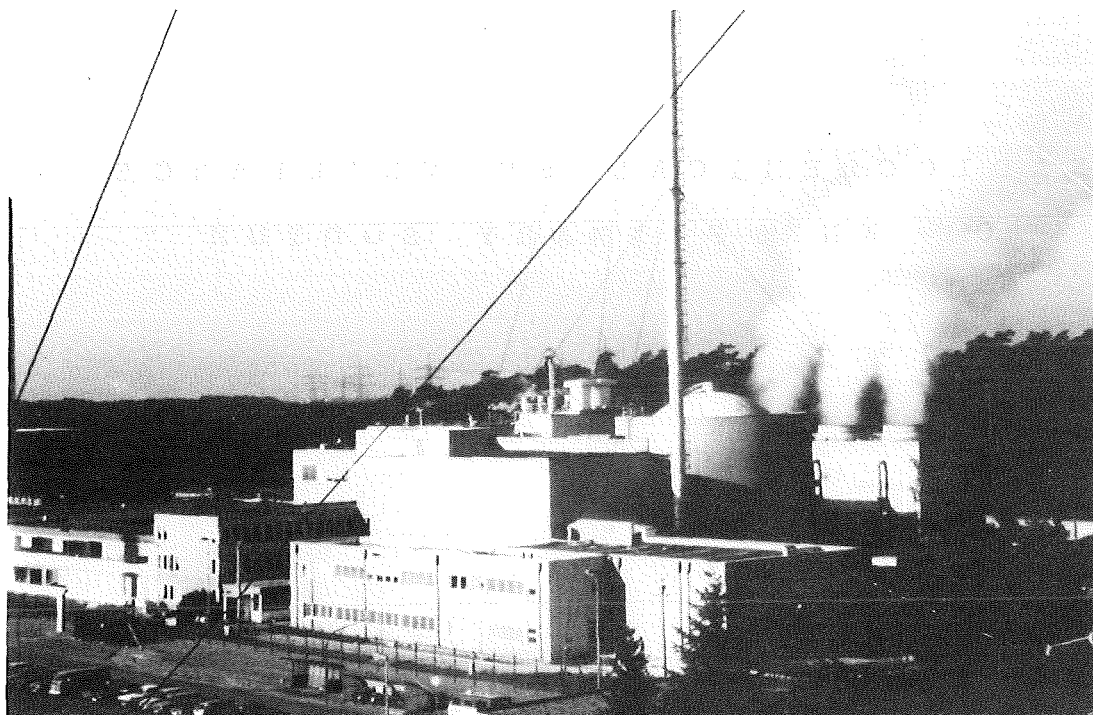


Fig. 1: KNK test reactor

The plant was converted into a fast breeder reactor (KNK II) from 1974 up to 1977. The commissioning of KNK-II was started in October 1977 with the first core KNK II/1 (1). After 400 effective full power days (EFPD) and a maximum fuel burnup of 100000 MWd/t the reactor was shut down in August 1982. After replacing the total KNK II/1 core by the second fast core KNK II/2, the plant went into operation again in August 1983. In August 1986 nearly 400 EFPD were achieved with the second core KNK II/2. It is foreseen to extend the operation up to 720 EFPD with the core KNK II/2. KNK II is widely used as an experimental facility. Therefore, the operation mode of the plant is governed by the experimental program rather than by energy production. Radionuclides and other impurities in the primary sodium were determined for plant surveillance as well as for an extensive radiochemistry program. This experimental radiochemistry program includes investigations of radionuclide deposition on pretreated surfaces under flowing sodium and development of new methods for trapping of radionuclides from primary sodium. Aim of this work is to minimize the radiation exposure associated with maintenance and repair work.

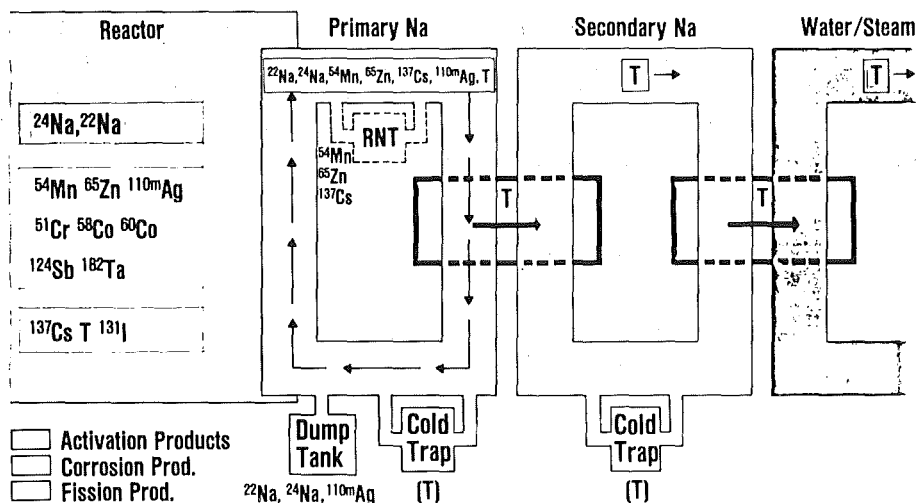


Fig. 2: Radionuclides in LMFBR coolants

A contamination of the primary loops of sodium cooled reactors with long-lived radionuclides (2) may be caused

- a/ by impurities in the circulating sodium, activated by neutrons when passing the core region,
- b/ by activated corrosion products of the primary system wall materials including fuel claddings, and
- c/ by fission products released into the sodium coolant from failed fuel elements.

The primary coolant of every sodium-cooled nuclear reactor is highly radioactive due to Na-24 (half-life: 15.03 hours), generated by neutron irradiation of natural sodium. But even after shutdown and after sufficient time for decay of this radionuclide (for instance 20 half-lives = 12.5 days), admission to certain parts of the plant for inspection, maintenance and repair work may be restricted because of gamma radiation from long-lived system contamination.

## 2. PRIMARY SODIUM SAMPLING

KNK is a loop-type fast breeder reactor. The primary circuit consists of two loops. The total amount of primary sodium is 32.1 tons; 21 tons of these are circulating in the reactor vessel and in the primary circuits, the rest remains in the dump tank. Table 1 shows the main operating parameters.

Table 1: KNK II operating parameters

|                         | Primary Circuit                 | Secondary Circuit   |
|-------------------------|---------------------------------|---|
| Power                   | 58 MW <sub>th</sub>             | 21.4 MW <sub>el</sub>   |
| Volume of Sodium        | 32.3 t                          | 51.5 t  |
| Pumping Rate            | 498 t h <sup>-1</sup>           | 451 t h <sup>-1</sup>   |
| Hot Leg Temperature     | 527°C                           | 504°C   |
| Cold Leg Temperature    | 360°C                           | 322°C   |
| Cold Trap Flow Rate     | 1m <sup>3</sup> h <sup>-1</sup> | 1m <sup>3</sup> h <sup>-1</sup><br>(5m <sup>3</sup> h <sup>-1</sup> ) |
| Pipe Structure Material | Ferritic Steel <sup>x)</sup>    | Ferritic Steel <sup>x)</sup>  |
| Reactor Vessel Material | Ferritic Steel <sup>x)</sup>    | <sup>x)</sup> stabilized with 0.1% Nb                                 |

An absolute necessity for the determination of radionuclides in primary sodium is a reliable and representative sodium sampling procedure. That means first of all that the total sample composition has to remain unchanged until the analytical work starts. Because of the very low solubility of most of the impurities in liquid sodium at low temperatures, this is the main problem of sodium sampling. Normally sodium samplings are taken at the cold leg temperature ( ~ 360 ° C). Cooling down to room temperature is necessary before the sample can be removed from the sampling station. Segregation to outer layers of the sample and deposition of radionuclides on the walls of sampling vessels are observed.

Several different sampling systems including the "tube-flow-through" method, the "overflow" method and the "on-line-distillation" sampling have been tested to overcome these problems.

The "overflow" method has proved to be the most reliable procedure (3).

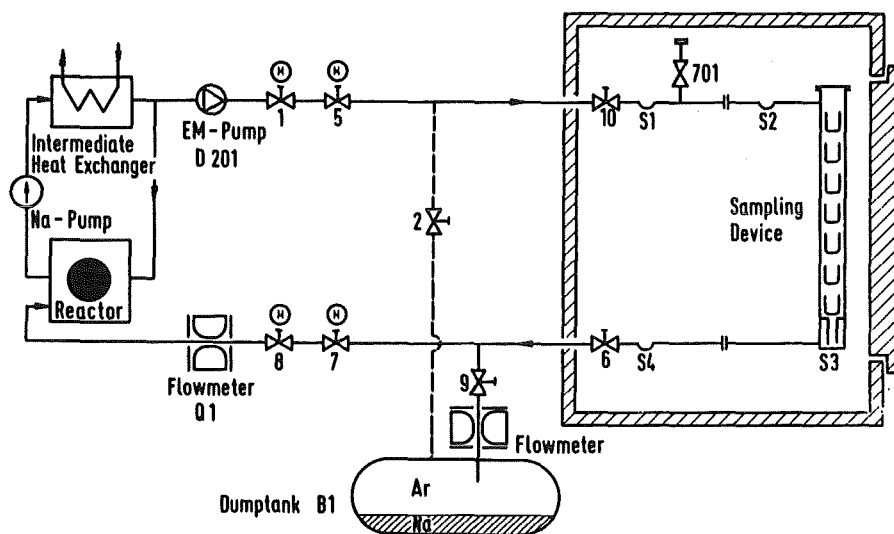


Fig. 3: KNK II primary sodium sampling station (PSSS).

At KNK II, an "overflow" sampler of primary sodium is located parallel to one of its two primary heat transfer loops. The sampling loop branches off from the main primary loop 2 after the intermediate heat exchanger; that restricts sampling temperatures at full power operation to 320 °C and during down-times of the reactor to 200 °C. A vertical sampling tube may contain up to seven crucibles (20 mm high, 20 mm diameter) with capacities of four to five grams of sodium each. The sodium return pipe passes an electromagnetic flow meter before reentering the reactor vessel. To get the sodium flowing through the sampling station, the valves 1, 5, 6, 7, 8, and 10 have to be opened, and the electromagnetic pump has to be activated. After the intended flushing time (normally 4 hours), valves 1, 5, 7 and 8 are closed, valves 9 and 2 are opened, and the excess sodium flows into the primary dump tank. About 30 grams of sodium are left in the seven crucibles inside the sampler. They contain 72 GBq Na-24 at full power operation of the plant; this corresponds to a  $\gamma$ -dose rate level of 4 Sv. Since the sampling tube cannot be removed unless the radiation level has dropped down below a 0.25 mSv level, it is necessary to wait for about 20 half-lives (12.5 days) of Na-24, before the lead shielded sampling cell may be opened.

After cooling down to room temperature, freeze seals in the siphons S2 and S3 are protecting the samples during transfer from the sampling station to the laboratory. The crucibles are removed from the crucible holder inside an inert gas glove box. So far, about 200 primary sodium samples were taken during 15 years of operation without significant problems. Only once the primary sodium sampling inlet pipe had to be replaced so far because of a leak. A failure in the control of the electrical trace heating was responsible for this leak.

### 3. PROCESSING OF SODIUM SAMPLES AND EVALUATION OF RADIONUCLIDES

The further processing of the sodium-filled crucibles depends on the analytical aim. No processing at all is necessary when gamma emitting radionuclides have to be determined by means of gamma spectrometry (most frequent determination). In that case each crucible is enclosed in a small, gastight plastic container and transferred to the counting room.

When a determination of alpha- or beta-emitting radionuclides is necessary, the bulk sodium has to be removed from the crucible as a first step. The easiest way of removing metallic sodium from its non-volatile impurities is vacuum distillation. Still inside the argon glove box, the amount of sodium in each crucible is determined by weight, and each sample is placed separately into a glass distillation flask. The closed distillation flasks are evacuated to a pressure below  $6 \times 10^{-8}$  bar. The heating has to be done very carefully in order to avoid spattering. High frequency induction heating has proved to be superior to direct resistance heating.

Fig. 4 shows a typical distillation set-up with the high-vacuum pump (right), the water-cooled transmitter with the Cu high-frequency coil, the control and power supply unit, and finally (to the left) the plotter, which records the temperature of a Fe/constantan thermocouple in the crucible. In Fig. 5 the distillation flask is shown in detail, containing the sampling crucible and the thermocouple, in front of the transmitter unit and inside the water-cooled high-frequency Cu coil. At the KNK chemistry laboratory an equipment is provided permitting a parallel treatment of four sodium samples.

As long as metallic sodium is boiling, the temperature of the crucible stays within a region of  $350^{\circ}$  to  $370^{\circ}$  C, depending on the quality of the vacuum. A thermocouple indicates the end of the distillation process, when the temperature of the crucible starts to rise again. The high-frequency generator is switched off, and after cooling to room temperature the sample is ready for further chemical operations like dissolving the non-volatile residue in a suitable acid or else. Again, the residue and the inner crucible wall have to be treated as a whole.

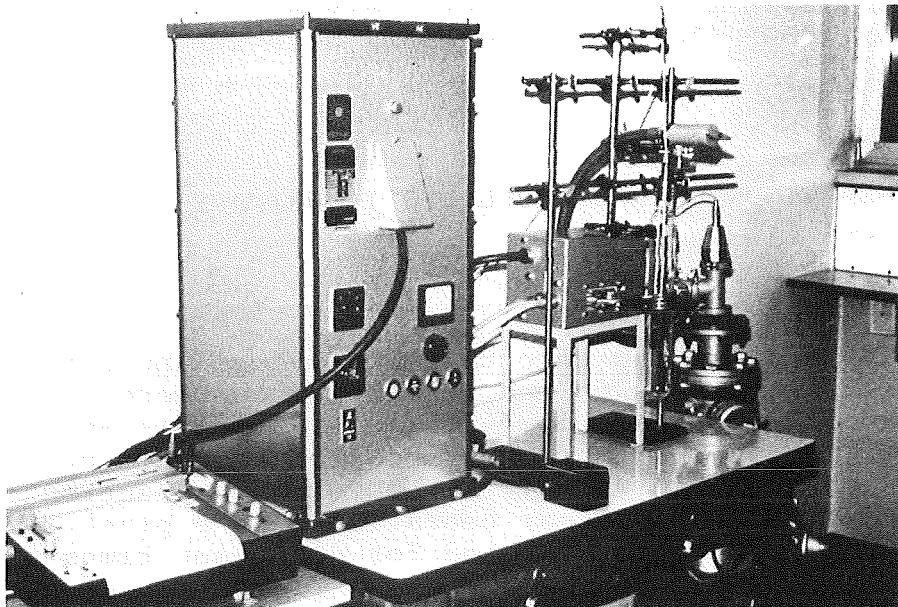


Fig. 4: Induction heated vacuum distillation of sodium

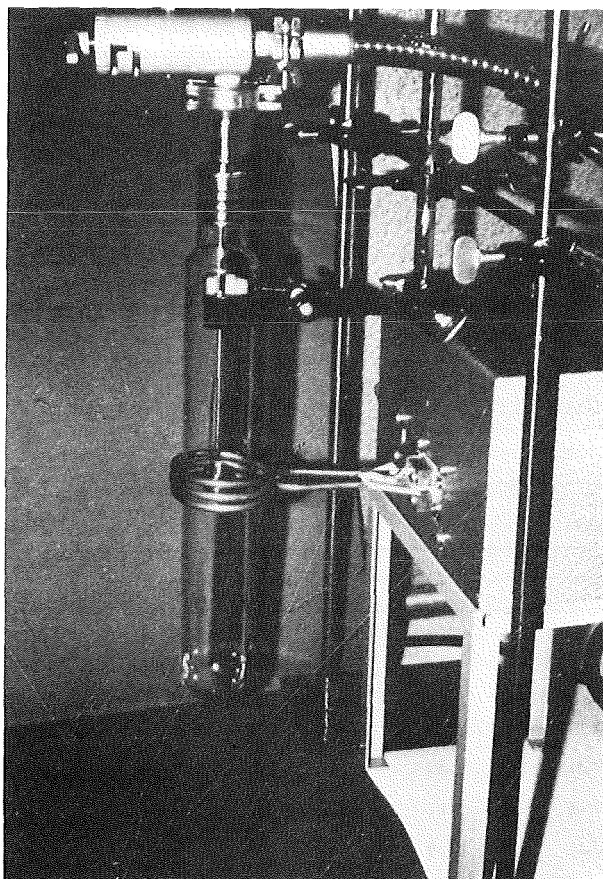


Fig. 5: Distillation flask with crucible in the high-frequency coil



During distillation losses are possible for chemical species with a vapour pressure similar to that of metallic sodium.

The gamma activity of sodium samples is assayed with Ge(Li) detectors attached to multichannel analysers. The evaluation is done on-line by a PDP 11/34 microcomputer with the Canberra program SPECTRAN-F.

#### 4. BEHAVIOUR OF RADIONUCLIDES IN PRIMARY SODIUM

##### 4.1 KNK I

After filling sodium into the primary cooling circuits of KNK I, metallic impurities in the primary sodium were determined by neutron activation analyses (6). The aim of this analytical program was to get informations about possible sources of radionuclides in the primary sodium which will be formed by neutron irradiation of the sodium during nuclear operation of the plant. 9 primary samples were taken and irradiated for different times (27.5 d, 60.5 d and 96.1 d) in the reactor FR-2, a former research reactor of the Karlsruhe Nuclear Research Center. Fe, Cr, Co, Sb, Zn, Ag and Hg were measured. Zn (3.7 ppm), Ag (0.1 ppm) and Hg (0.02 ppm) had a rather homogeneous distribution, while Fe (1.6 - 48 ppm), Cr (0.3 - 35 ppm), Co (0.004 - 0.06 ppm) and Sb (0.05 - 1.15 ppm) varied considerably from one sample to another. The measured concentrations of Fe and Cr were higher than the calculated values using the solubility equations; therefore it had to be assumed, that Fe and Cr were mainly suspended in the primary sodium in form of small particles. With the exception of Fe and Cr mean activity concentrations in the primary sodium were calculated for the activation of Zn, Sb, Ag and Hg after 100 effective full power days of KNK operation and after 14 days decay time (7).

The measured activity concentrations from January 1973 up to August 1974 (end of KNK I operation after 153 effective full power days) are given in Table 2.

Table 2: Radionuclides in KNK I primary sodium

| Date of Sampling   | January 1973 | May 1973 | January 1974 | August 1974 |
|--------------------|--------------|----------|--------------|-------------|
| Radionuclide       | kBq/gNa      |          |              |             |
| <sup>22</sup> Na   | 0.79         | 2.59     | 3.49         | 9.84        |
| <sup>54</sup> Mn   | 0.38         | 0.59     | 1.41         | 10.32       |
| <sup>65</sup> Zn   | 78.16        | 200.15   | 135.05       | 743.70      |
| <sup>110m</sup> Ag | 0.31         | 1.33     | 1.55         | 5.25        |
| <sup>124</sup> Sb  | 0.46         | 0.63     | 0.52         | 0.93        |
| <sup>182</sup> Ta  | 0.47         | 0.89     | 0.78         | 5.55        |
| <sup>140</sup> Ba  | —            | —        | —            | 0.81        |

Na-24, resulting from  $\text{Na-23}(n,\gamma)\text{Na-24}$ , was the predominant activity in the primary sodium during plant operation. The saturation value at full power was 9.25 GBq/g Na.

As expected, Na-22 generated by  $\text{Na-23}(n,2n)\text{Na-22}$  increased with the KNK I operating time. Late in August 1974, Na-22 had attained a specific activity of 9.6 kBq/g Na.

The activity concentration of Zn-65 was surprisingly high in each sodium sample. Further experiments (4) showed, however, that Zn-65 and on a somewhat lower level Mn-54 are strongly absorbed to the walls of the nickel sampling crucibles, which means a certain restriction in the validity of the values given for Zn-65 and Mn-54 in Table 2. From these experiments it had to be concluded that nickel crucibles are not suitable for Na sampling, if radionuclides, especially Zn-65 and Mn-54, are to be measured in primary sodium. Therefore, stainless steel crucibles are used at KNK II for radionuclide determination.

Extensive investigations have been performed in order to find the source of Zn in the KNK system. The original sodium filling had a Zn content between 1 and 4 ppm. 130 ppm were found in the KNK structure material. The main source was probably a zinc chromate protective coating used to cover the external surfaces of the ferritic pipes prior to the assembling. Obviously, small amounts of this paint had entered also the internal surfaces of the pipes. A further source was an oil leakage into the primary sodium from one of the primary sodium pumps; the oil was stabilized with zinc-dithiophosphate. Nevertheless, there has to be another Zn source, which is still delivering Zn into the primary sodium.

The source of the Ag-110m activity in the KNK primary sodium is not known. The increase of the Ag-110m activity depended only on the operation time of the plant.

The same increase with the irradiation time was observed for the Sb-124 activity in the primary sodium. The source of the Sb-124 activity is not well known. Possibly, the use of MOLYKOTE (containing antimony trisulfide) as slipping coating at the bearing rings at the bottom of the subassemblies caused this activity.

The low-alloyed ferritic steel used at KNK as material of reactor vessel and primary piping is Nb-stabilized; because of the chemical similarity, Nb is always accompanied by certain amounts of Ta.

Ta-182 is the  $(n,\gamma)$  activation product of Ta-181 (99.998% of natural Ta). Because of its long half-life (115 days) and its hard gamma radiation, it contributed much to the dose rate in the primary cell during maintenance periods at KNK I.

KNK I was operated without fuel failure. Therefore, Cs-137 as the most important fission product in primary circuits of sodium-cooled reactors, was never found in sodium samples taken from the primary sodium during KNK I operation. Trace amounts of Ba-140/La-140 were found only when the reactor was in full power operation for a long period (8). These low activities of Ba-140/La-140 originated from a fuel element surface contamination with small amounts of fuel ("tramp uranium"). Later, small amounts of Cs-137 were found in the primary cold trap of KNK I when this component was removed from the plant (9).

A high enrichment of Zn-65 was observed in samples of condensed sodium taken from the annulus gap between reactor vessel and the rotating plug.

## 4.2 K N K I I

### 4.2.1 Activation Products

-----

The complete primary sodium inventory of KNK I was used again in the operation of KNK II, the fast breeder version of KNK, with its first (KNK II/1) and its second (KNK II/2) core.

Like in KNK I, Na-24 is the predominant activity in the primary sodium during reactor operation of KNK II. The measured saturation value of Na-24 was 2.5 GBq/g Na during 100% reactor operation at KNK II/1, and 2.2 GBq/g Na at KNK II/2. This is about 4 times lower compared to KNK I, caused by higher fractions of fast neutrons in both KNK II core versions.

As expected, the Na-22 activity in KNK II is higher compared to KNK I, depending strongly on the reactor operation time. Until the end of the KNK II/1 operation the specific activity of Na-22 had increased to 21 kBq/g Na. With the second fast core, 400 effective full power days of operation were achieved in Mai 1986; the Na-22 activity had increased to 25 kBq/g Na at that time.

Mn-54 is the most prominent radioactive corrosion product in the KNK II primary sodium. It is formed by the Fe-54(n,p)Mn-54 reaction. The behaviour of Mn-54 in anisothermal sodium loops is very complex. It is still not completely known in which chemical form manganese is transported by sodium. Mn-54 in the KNK primary sodium was not simply depending on the plant operation time like the activity concentrations of more soluble radionuclides. The KNK experience is indicating that Mn-54 plates out from the sodium very rapidly when the sodium temperature is decreased from 520 °C to 200 °C. This deposition of manganese is not completely reversible when the sodium temperature is increased again.

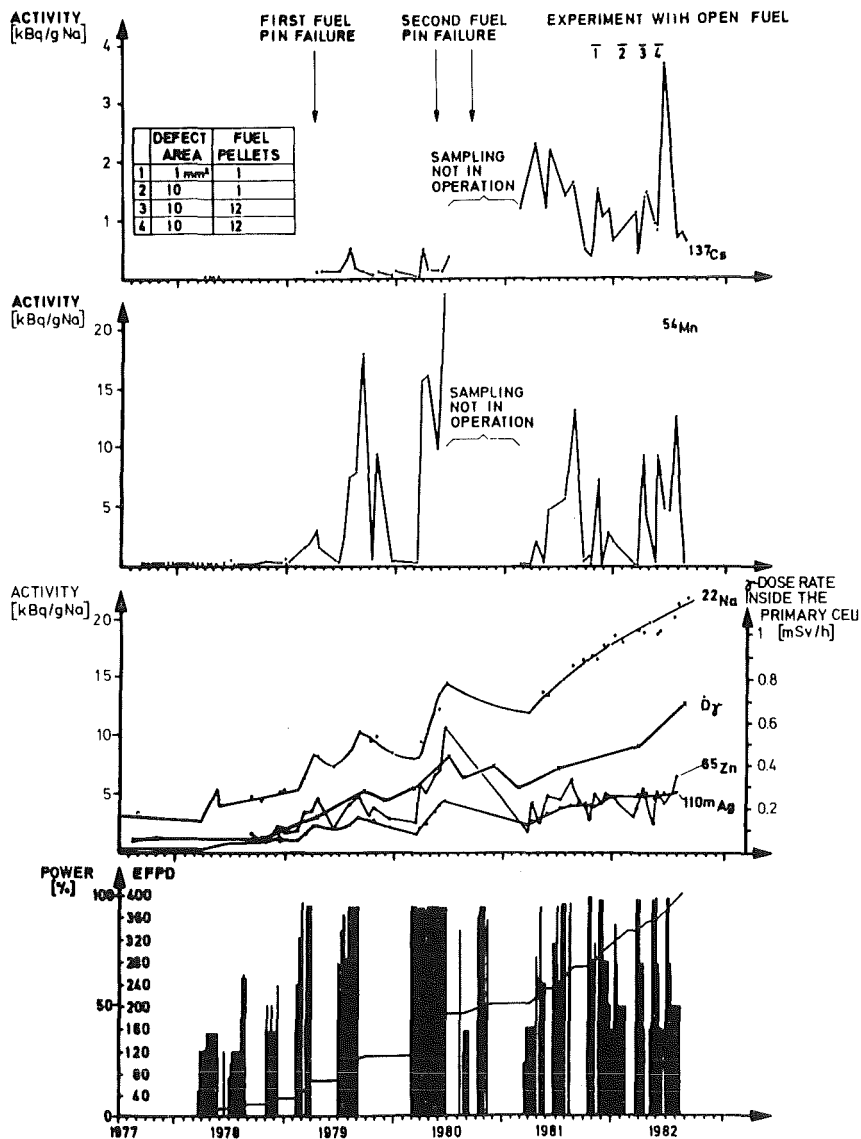


**Fig. 6:** Primary coolant activity, dose rate and effective full power days (EFPD) vs. operating time of KNK II/1

Like in KNK I,  $\text{Zn-65}$ ,  $\text{Ag-110m}$  and  $\text{Sb-124}$  were growing again with a nearly linear dependency of the operating time.

$\text{Co-60}$  was found in some sodium samples in very small quantities only (0.02 - 0.11 kBq/g Na). It is well known that  $\text{Co-60}$  is deposited preferentially in the hot part of the primary system.

Because of the much lower thermal neutron flux, the  $\text{Ta-182}$  activity was negligible at KNK II.

$\text{Co-58}$ , formed by an  $\text{Ni-58}(n,p)$ -reaction was measured occasionally in some samples only.

#### 4.2.2 Fission products

-----

As already mentioned, no fuel failure occurred during operation of KNK I. During operation of KNK II, six fuel failures have been detected so far. Two of these cladding failures happened during operation with the first fast core, four of them in the second fast core. With some of these fuel failures, KNK II was operated for several weeks at full power. As a result, fission products were released into the primary sodium. Zr-95/Nb-95, Ru-103, Ru-106, I-131, Te-132/I-132, Cs-134, Cs-136, Cs-137, Ce-141 and Ce-144 were detected by gamma spectrometric measurements. Cs-137, always accompanied by some Cs-134 and Cs-136, was the major contribution of fission products to the KNK II primary sodium activities. Until May 1987, the Cs-137 activity in the primary coolant had increased to 34 kBq Cs-137/g Na.

The release fractions of Cs-137 from the two fuel failures during KNK II/1 operation were 5.2 and 10%, respectively, after radiochemical measurements in the primary sodium. The release fraction of Cs-137 from the third failure was nearly 25%. The release fractions of this radionuclide from the fourth and the fifth fuel failure may be significantly higher. The Cs-137 behaviour in the primary coolant was characterized by a reversible, temperature depending deposition on the inner walls of the piping and the components of the primary circuit. On the other hand, Cs-137 was enriched in the condensed sodium in certain parts of the cover gas system, especially in the gaps between the rotating plug and the reactor vessel, and in the cover gas plenums of the primary sodium pumps. Enrichment factors for Cs-137/Na-22 up to 1000 were obtained compared to the cesium concentration in the bulk primary sodium.

I-131 was measured in the primary sodium after each fuel failure (max. value: 38 kBq/g Na). Because of its behaviour in flowing sodium (formation of NaI as stable compound) and its short halflife it was never a problem regarding the KNK II operation.

Released fuel was never found as particles in the KNK II primary sodium after the usual sodium sampling procedure (see 4.2.4, from p. 14). However,  $\alpha$  activity was detectable after extraction into TOPO/Xylene at a level of 1 Bq/g Na. Only Pu-isotopes are estimated by this procedure ( $\alpha$  gas counting).

#### 4.2.3 Reproducibility of radionuclide evaluation

-----

The KNK primary sodium sampling station may house up to seven crucibles; therefore it was possible to investigate the reproducibility of the whole sampling and measurement procedure, and to check the influence of the crucible material (glass, steel, Ni) on the results (10). These experiments indicated that samplings at higher sodium temperature (> 300 C) are providing better reproducible results than Na samplings at 200 C.

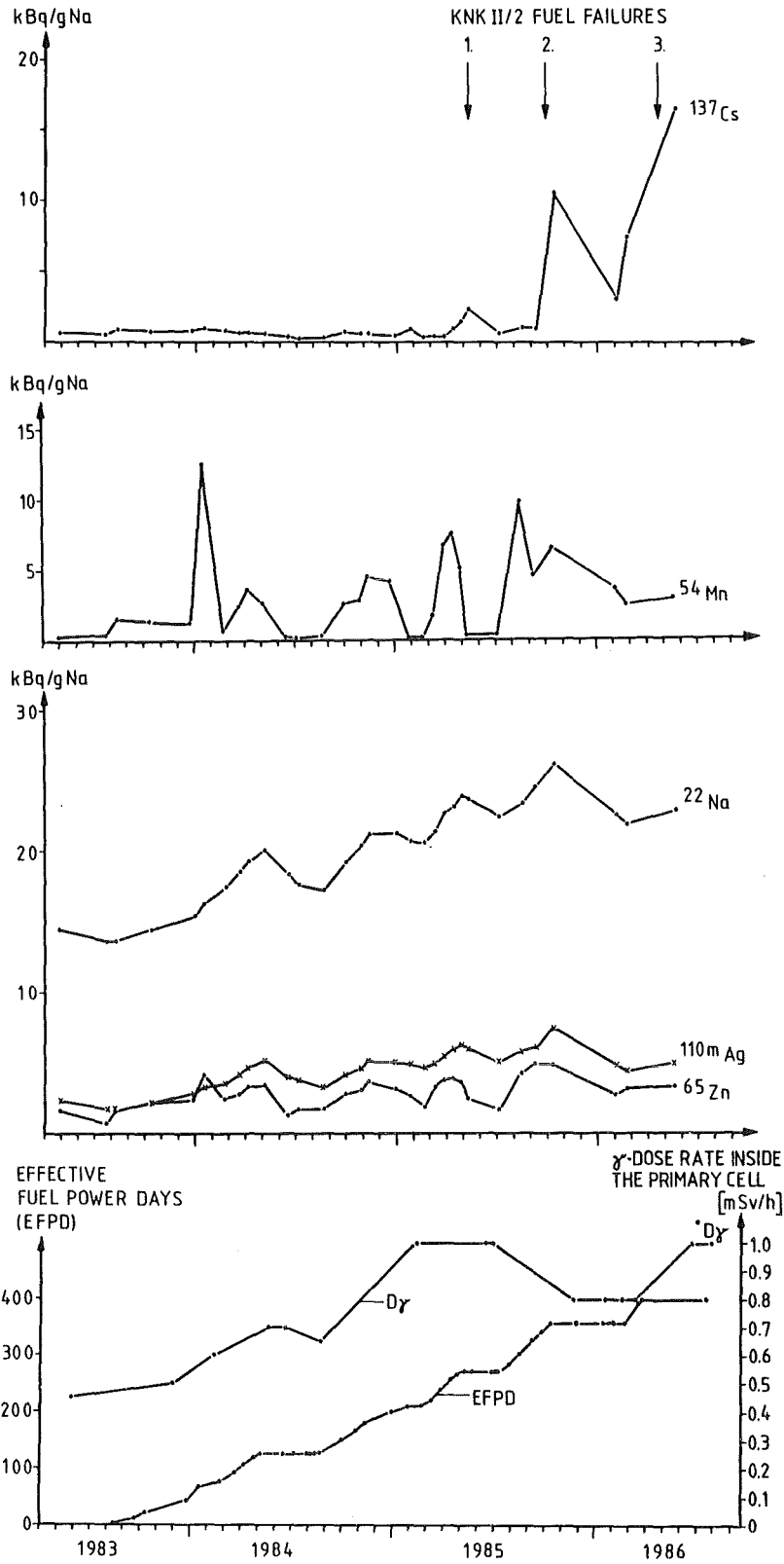


Fig. 7: Primary coolant activity, dose rate and effective full power days (EFPD) vs. operating time KNK II/2

Table 3 demonstrates the statistical evaluation of a sampling procedure with 7 stainless steel crucibles from KNK primary sodium at 200°C after a fuel failure had occurred. Table 4 compares the results of statistical treatments for crucibles made of glass or of stainless steel, respectively, for sampling procedure at 200°C, and at more than 300°C.

The following conclusions have been drawn from table 4:

One crucible per sampling will be sufficient for the determination of radionuclides readily soluble in liquid sodium (Na-24, Na-22, Ag-110m, Sb-124). Several crucibles should be used for the determination of radionuclides of lower solubilities (Co-58, Fe-59, Co-60, Ta-182) or of low activity concentrations. Their results should be treated finally with statistical methods.

No chemical inert crucibles are known so far. The measured activity concentrations of Na-22, Ag-110m, Sb-124 and Cs-137 seemed always to be higher in glass crucibles than in stainless steel crucibles. On the other hand, stainless steel crucibles gave higher values of Zn-65 and Mn-54 than glass crucibles. These differences increased with increasing temperature, indicating chemical reactions rather than adsorption on the crucible walls. Stainless steel crucibles should be avoided for determination of Mn-54 at 300°C and above.

Table 3: Radionuclides in 7 stainless steel crucibles (sampling from 200°C sodium); statistical treatment of the results

| Crucible No.                         | 1     | 2      | 3      | 4     | 5     | 6     | 7     | $\bar{x}$ | s     | RSD(%) |
|--------------------------------------|-------|--------|--------|-------|-------|-------|-------|-----------|-------|--------|
| Na content[g]                        | 4.389 | 5.361  | 4.611  | 4.933 | 4.513 | 4.255 | 3.935 | 4.571     | 0.465 | 10.2   |
| <sup>22</sup> Na                     | 24.0  | 23.5   | 24.0   | 23.5  | 23.8  | 23.9  | 23.9  | 23.8      | 0.22  | 0.9    |
| <sup>54</sup> Mn                     | 0.35  | 0.24   | 0.31   | 0.29  | 0.36  | 0.29  | 0.34  | 0.31      | 0.04  | 14     |
| <sup>58</sup> Co                     | 0.61  | -      | 0.04   | -     | -     | 0.07  | 0.01  | -         | -     | -      |
| <sup>60</sup> Co                     | 0.058 | 0.040  | 0.061  | 0.045 | 0.058 | 0.048 | 0.057 | 0.052     | 0.008 | 15     |
| <sup>65</sup> Zn                     | 2.29  | 3.10   | 2.12   | 2.82  | 2.85  | 2.42  | 2.44  | 2.58      | 0.35  | 14     |
| <sup>110m</sup> Ag                   | 6.01  | (6.81) | (4.53) | 6.06  | 6.27  | 6.18  | 6.02  | 6.11      | 0.11  | 1.9    |
| <sup>113</sup> Sn                    | 0.07  | 0.08   | 0.08   | 0.06  | 0.07  | 0.09  | 0.09  | 0.077     | 1.11  | 14     |
| <sup>124</sup> Sb                    | 0.42  | 0.59   | 0.47   | 0.50  | 0.57  | 0.46  | 0.44  | 0.49      | 0.065 | 13     |
| <sup>131</sup> I                     | 38    | 19     | 35     | 31    | 30    | 28    | 31    | 30.3      | 6.0   | 20     |
| <sup>132</sup> Te(a)                 | 4.7   | 1.9    | 4.2    | 3.9   | 3.2   | 3.4   | 4.1   | 3.6       | 0.9   | 25     |
| (b)                                  | 4.9   | 2.1    | 4.6    | 4.0   | 3.7   | 3.4   | 4.7   | 3.9       | 0.97  | 25     |
| <sup>134</sup> Cs                    | 0.061 | 0.064  | 0.081  | 0.086 | 0.072 | 0.068 | 0.073 | 0.072     | 0.009 | 12     |
| <sup>136</sup> Cs                    | 0.48  | 0.52   | 0.58   | 0.63  | 0.59  | 0.48  | 0.62  | 0.56      | 0.063 | 11     |
| <sup>137</sup> Cs                    | 1.8   | 2.0    | 2.3    | 2.6   | 2.4   | 2.0   | 2.2   | 2.2       | 0.27  | 13     |
| <sup>137</sup> Cs/ <sup>136</sup> Cs | 3.8   | 3.8    | 3.9    | 4.1   | 4.1   | 4.1   | 3.5   | 3.9       | 0.22  | 6      |
| <sup>137</sup> Cs/ <sup>134</sup> Cs | 29    | 31     | 28     | 30    | 34    | 30    | 30    | 30.3      | 1.89  | 6      |

Table 4: Relative standard deviations (RSD in %) of analyses for radionuclides in KNK primary sodium samples

| Sampling crucibles<br>Sampling temperature | Glass |       | Stainless steel |       |
|--|-------|-------|-----------------|-------|
|  | 200°C | 330°C | 200°C           | 320°C |
| Na-22                                      | 0.9   | 1.0   | 0.4             | 0.6   |
| Mn-54                                      | 25    | 10    | 23              | 16    |
| Co-60                                      | 48    | 36    | -               | -     |
| Zn-65                                      | 10    | 6.5   | 17              | 4.8   |
| Ag-110m                                    | 1.2   | 0.6   | 4.8             | 2.5   |
| Sb-124                                     | 73    | 2.2   | -               | 1.1   |
| I-131                                      | -     | 14    | -               | 18    |
| Cs-137                                     | 18    | 17    | 32              | 14    |

#### 4.2.4 Particles

-----

Because of some analytical results (high values of metals like Fe), particles were suspected in the KNK primary sodium for several years. However, it was never possible to isolate particles from the 4 grams of sodium in a sampling crucible. The amount of particles should be very low, therefore, and unevenly distributed in the circulating primary coolant.

In order to catch particles from a considerable larger volume of sodium, small magnets were exposed at first in the sampling station. Small amounts of ferromagnetic particles could be washed from the magnets afterwards, their main component was Fe besides small amounts of Cr. In 1985, a filter unit was first exposed to the flowing sodium, containing a sintered stainless steel filter disk. A similar filter was used successfully earlier to catch particles from the EBR-II primary sodium (11). With the filter unit (Fig.8) it was possible, to remove a surprising variety of particles from the KNK primary sodium (12). An energy dispersive X-ray spectrometer, attached to a scanning electron microscope, identified particles which contained

- iron besides small amounts of Cr and even less Ni,
- chromium besides small amounts of iron,
- silicon (probably silicates),
- calcium and magnesium, and
- arbitrary mixtures of these components.



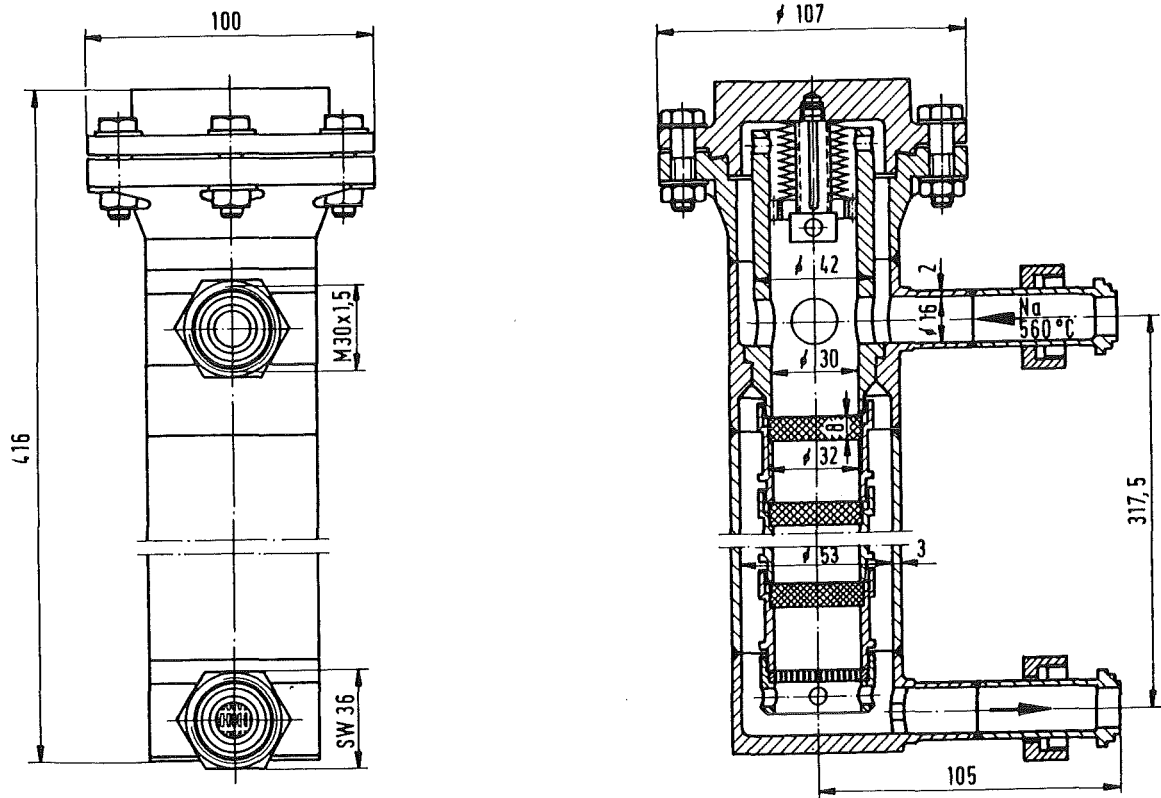
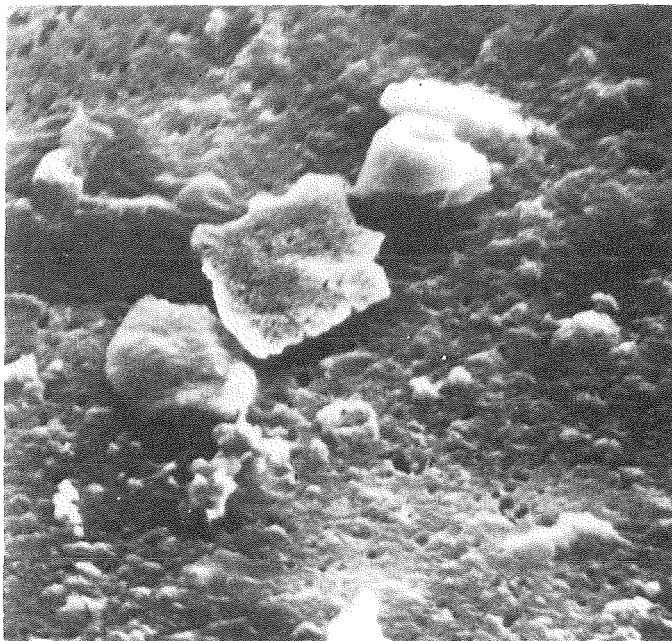


Fig. 8: Filter unit for the KNK primary sodium sampling station

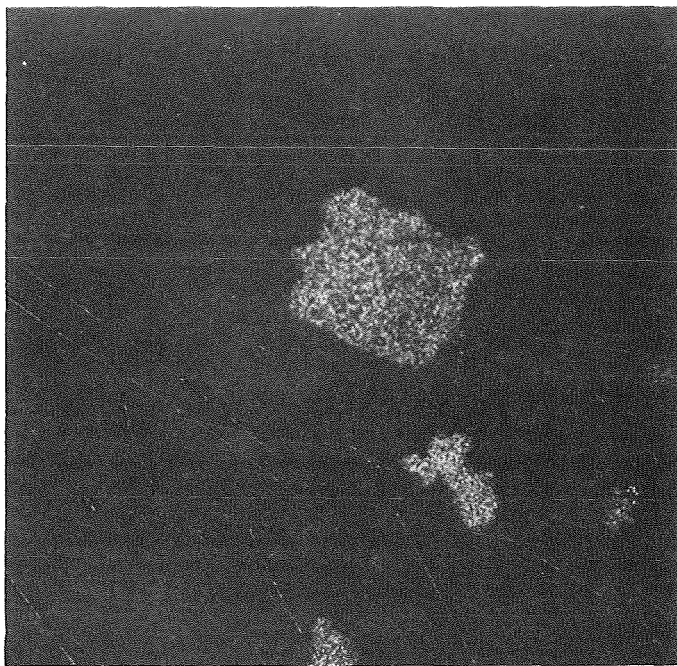
Fig. 9 shows a secondary electron image (SEI) of some particles from KNK primary sodium, Fig. 10 the X-ray distribution of iron of the very same filter section. Clearly visible are particles with a high Fe content (visible in Fig. 9 as well as in Fig. 10) and particles of a different composition (visible only in Fig. 9). It was not possible to find correlations between the morphology of particles and their chemical composition.

As expected, all particle samples were radioactive. Besides the  $\gamma$ -activities of activation and fission products (in addition to the fission products already detected in primary sodium: Zr/Nb-95, Ru-103, Ru/Rh-106, Ce-141 and Ce/Pr-144),  $\alpha$ -activity from washed-out fuel was measured.



10  $\mu$ m

Fig. 9: SEI of particles from KNK primary Na



10  $\mu$ m

Fig. 10: X-ray distribution of Fe in particles  
(same filter area)

Table 5 gives a compilation of the amounts of filtered particles in eight experiments and the  $\alpha$ -activity measured on the filter disks. Again, no correlation was possible between  $\alpha$ -activity and mass or form of the particles.

Table 5: Alpha activities and particle masses on sintered metal filters

| Sintered Metal Filter | Alpha Activity (Bq) | Particle Mass (mg) | Through-put ( $m^3Na$ ) | Concentration ( $mg/m^3Na$ ) |
|-----------------------|---------------------|--------------------|-------------------------|------------------------------|
| 1                     | 2040                | 61.0               | 13.2                    | 4.6                          |
| 2                     | 15000               | 24.5               | 2.0                     | 12.2                         |
| 3                     | 45000               | 28.5               | 4.2                     | 6.8                          |
| 4                     | 300                 | 5.1                | 1.2                     | 4.3                          |
| 5                     | 23                  | 14.2               | 0.85                    | 16.7                         |
| 6                     | 2100                | 44.9               | 4.1                     | 10.9                         |
| 7                     | 1100                | 27.9               | 14.1                    | 2.0                          |
| 8                     | 200                 | 14.1               | 1.0                     | 14.1                         |

In addition, filtration experiments were accomplished during downtimes of the plant with mesh filter sieves in the lower fuel element grid plate. Similar particles were found on the sieves with a slightly different size distribution.

## 5. GAMMASPECTROMETRIC MEASUREMENTS ON PRIMARY COMPONENTS

### 5.1 Measurements in the primary cell

Because some radionuclides are plating out on the walls of the primary components, the radionuclide determination in the primary sodium samples is not sufficient for a complete description of the system contamination development. For this reason, gamma spectrometric measurements have been performed on the components and pipes of the primary circuit of KNK I/II during reactor down-times (13, 14). Fig. 11 indicates the usual measuring location on both loops.

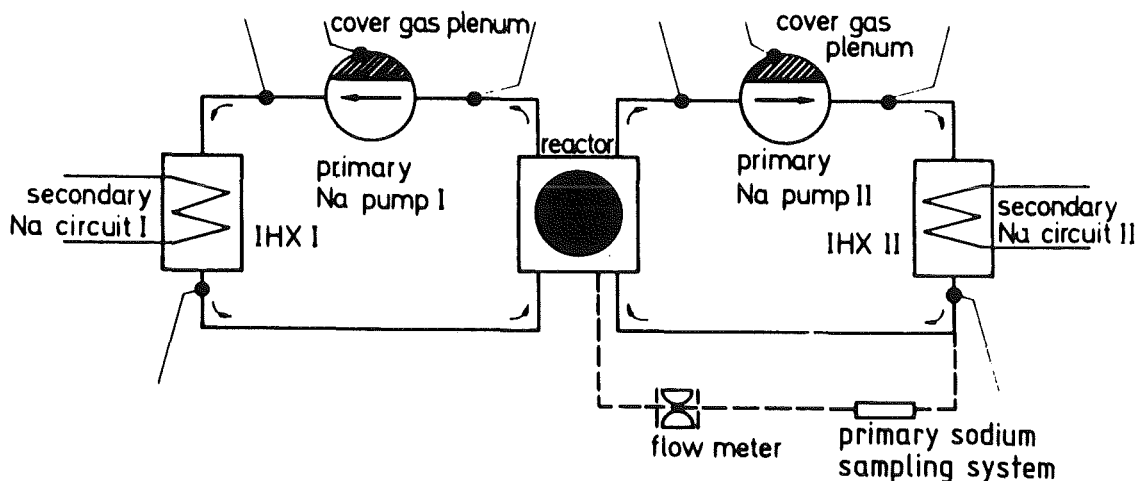


Fig. 11: Measuring locations in the KNK primary cell

All components of the primary system are located in a so-called primary cell, a gastight concrete cell lined with steel sheet on the inner surface. During reactor operation this primary cell is closed and filled with gaseous nitrogen. After shutdown, the Na-24 activity has to decay for about 20 half-lives before the primary cell can be opened and air vented.

During a shutdown period in July 1974 and again after termination of the KNK I operation, first on-line gamma measurements in the primary cell were performed using transportable gamma spectrometers.

In the sodium filled primary loop Na-22, Mn-54, Ag-110m, Zn-65, Ta-182 and traces of Co-60 were detected. After draining of the sodium from the primary loop only Mn-54, Co-60, Zn-65 and Ta-182 were found; Ag-110m was completely drained with the sodium (and of course - Na-22) into the dump tank. As illustrated by Fig. 12, Ag has a high solubility in sodium (15). No deposition or adsorption of Ag-110m on the walls of the KNK primary loops was observed.

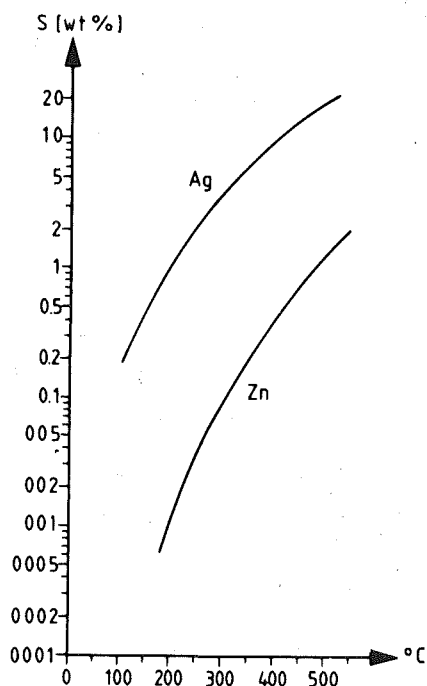


Fig. 12: Solubilities of Ag and Zn in Na  
from T.D. Claar, *Reactor Technology* 13, 124-146 (1970)

So far, five measurement campaigns have been performed in the primary cell:

- 1974 after 153 effective full power days (EFPD) of KNK I,
- 1981 after 82 EFPD of KNK II,
- 1983 after 400 EFPD of KNK II,
- 1984 after 527 EFPD of KNK II, and
- 1985 after 680 EFPD of KNK II.

Table 6: Deposited activities in the KNK II primary system after 680 effective full power days

| COMPONENT                                       | ACTIVITY DEPOSITION (kBq/cm <sup>2</sup> )   |                  |                  |                  |                   |                   | DOSE RATE D <sub>γ</sub> (mSv/h) |                |  |
|---|--|------------------|------------------|------------------|-------------------|-------------------|----------------------------------|----------------|--|
|   | <sup>54</sup> Mn   | <sup>65</sup> Zn | <sup>58</sup> Co | <sup>60</sup> Co | <sup>182</sup> Ta | <sup>137</sup> Cs | sodium filled                    | sodium drained |  |
|   |  |                  |                  |                  |                   |                   |                                  |                |  |
| HOT LEG BETWEEN REACTOR OUTLET AND PRIMARY PUMP | 28.4   | 0.46             | 3.21             | 1.73             | 1.82              | not detectable    | 1.9                              | 0.50           |  |
| INLET OF INTER-MEDIATE HEAT EXCHANGER           | 37.5   | 0.62             | 3.38             | 1.39             | 1.79              | not detectable    | 1.9                              | 0.55           |  |
| OUTLET OF THE INTERMEDIATE HEAT EXCHANGER       | 113.9  | 5.62             | 0.90             | 0.46             | 3.66              | 4.10              | 3.2                              | 1.20           |  |
| KBG/IA  | DEPOSITED ACTIVITIES IN THE KNK II PRIMARY LOOP AFTER 680 EFFECTIVE FULL POWER DAYS WITH KNKII/1 AND KNKII/2 |                  |                  |                  |                   |                   |                                  |                |  |

Table 6 (16), shows the deposited activities after 680 effective full power days of KNK II on significant locations in the primary loop. The highest deposited activity on all 3 positions was Mn-54. As expected, the highest deposition of Mn-54 was found at the outlet of the intermediate heat exchanger. Additional measurements on the primary pumps indicated a strong enrichment of Cs-137 and Zn-65 in the cover gas plenum. Maximum dose rates of 7 mSv/h were measured at these points. As long as the primary system was filled with sodium, Na-22, Ag-110m, Mn-54 and Zn-65 were the dominating radio-nuclides. Again, draining of the primary sodium transferred Na-22 and Ag-110m completely into the dump tank. This lowered the γ-dose rate by a factor of 2 to 3 compared to the sodium filled systems.

## 5.2 Measurements on components removed from the primary system

### Valves

-----  
 During the conversion of KNK I into KNK II all shutoff and regulating valves of the primary circuits were removed for repair (exchange of the top section of the valves) and inspection. The disks of the valves are as the whole system made of ferritic steel, however, in addition partially coated by a layer of COLMONOY-6. The Mn-54 activity on the COLMONOY coated surfaces was 20 to 30 times higher compared to the uncoated surfaces; the Zn-65 activity was about 10 times higher (13).

Pumps

1984 one of the primary sodium pumps was removed after 65000 h operating time at 200°C sodium temperature and 25000 h operating time at 520°C. After dismantling a  $\gamma$ -dose rate of 70 mSv/h was measured on the hydrostatic bearing of the pump. The surface of the hydrostatic bearing is coated with a layer of COLMONOY, a Ni-based alloy. The reason for the high dose rate was a rather high adsorption of Mn-54 of this layer. Fig. 13 demonstrates the decontamination effect of the inertgas/steam cleaning on the pump. The left diagram shows the results of a gammaspectrometric scanning of the pump after removal from the housing, the right diagram after cleaning with N<sub>2</sub>/steam. Zn-65 and Cs-137 were completely removed by the washing procedure, especially in the region above the sodium level where these radionuclides formerly governed the dose rate. However, the treatment had almost no influence on the distribution of Mn-54 and Co-60.

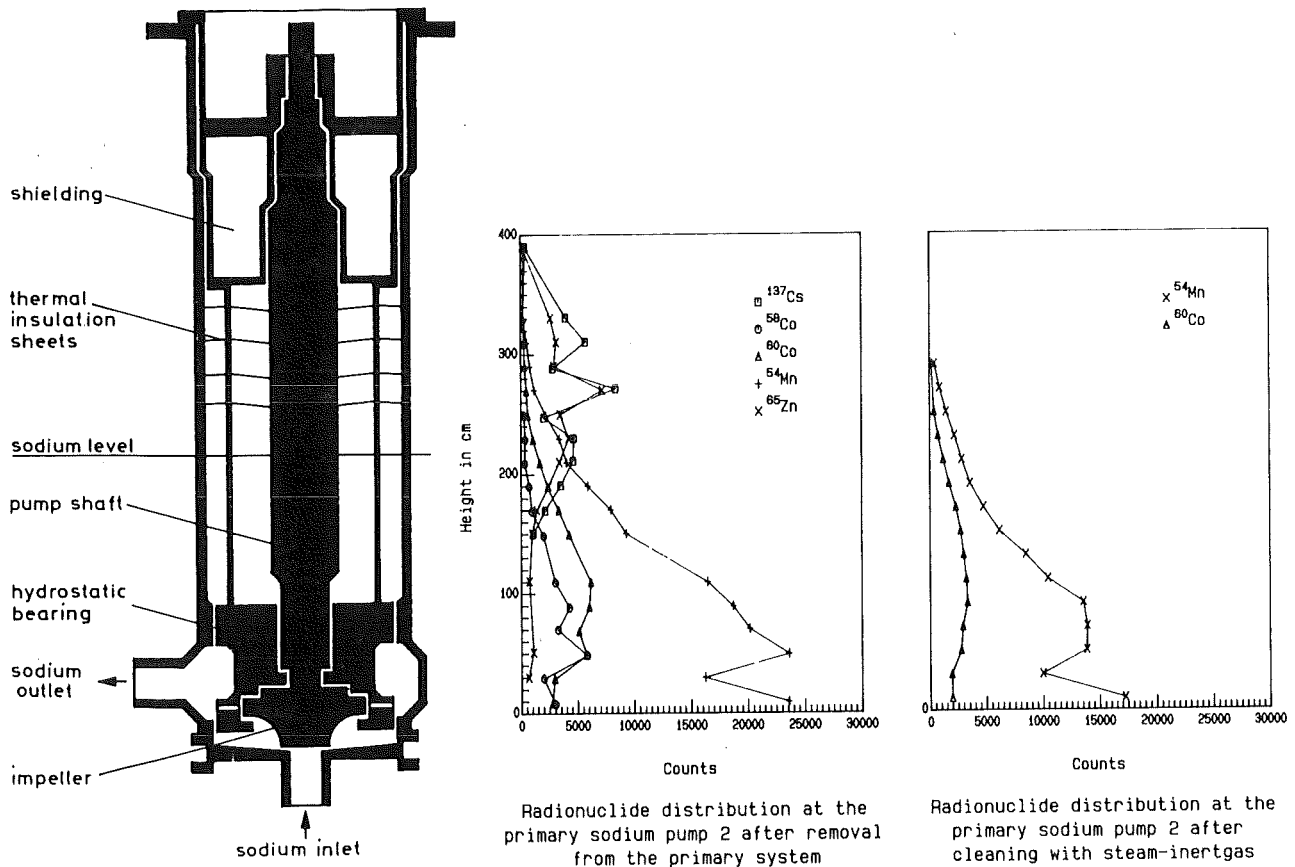


Fig. 13: Effect of an inertgas/steam treatment on the radionuclide distribution on a primary Na pump

### Cold Traps

The cold traps of KNK are made of a special, ferritic steel, as the whole KNK system. Only few spare cold traps are available. It is, therefore, very expensive to replace a cold trap by a new unit. This is the reason why saturated KNK cold traps are removed from the system, and cleaned with the aim of a requalification for a re-use. Three primary cold traps have been removed from the primary purification circuit so far (9). The third cold trap was disconnected from the system during February 1985. The component was gamma-spectrometrically scanned with a high-purity Ge-detector. Fig. 14 shows a gamma spectrum measured at a location with a high dose rate (1700 mr/h). It is clearly to be seen that Mn-54, Zn-65 and Cs-137 are the crucial radionuclides.

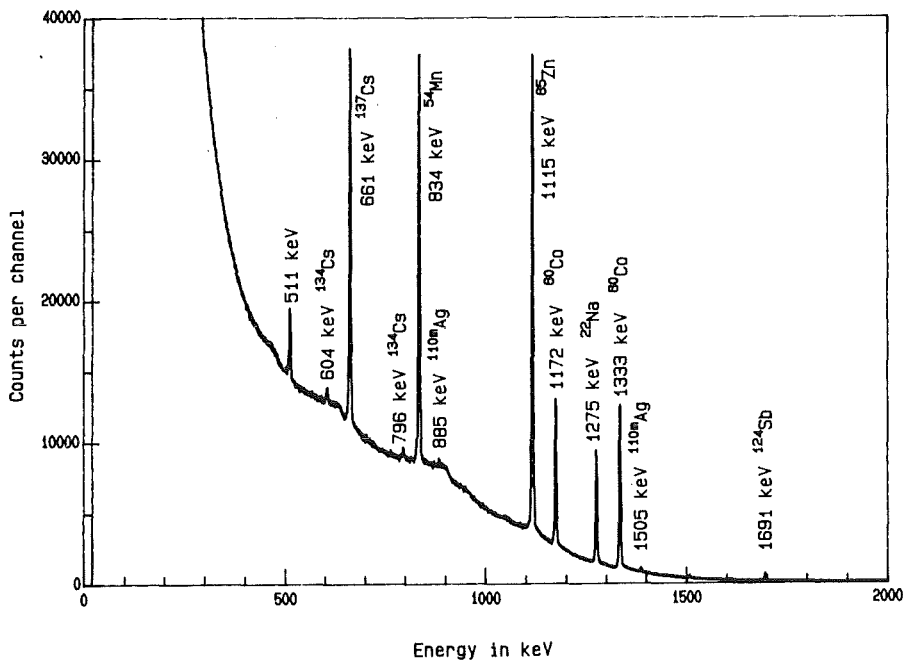


Fig. 14: Gamma spectrum of radionuclides in a KNK primary cold trap



## 6. REMOVAL OF RADIONUCLIDES FROM THE KNK PRIMARY SODIUM

Cleaning of the primary sodium of KNK and of all the other liquid metal cooled fast breeder reactors is accomplished by cold traps in special purification loops. These cold traps are removing non-radioactive impurities like sodium oxide and sodium hydride from the primary and secondary sodium with a good efficiency.

Cold traps are almost ineffective for the removal of radionuclides from liquid sodium, however, because these are present in very small amounts only, completely soluble in the liquid sodium even at cold trap temperatures.

For several years now, an extensive investigation program is performed in order to develop special radionuclide traps. It was obvious from the beginning that it will be not possible to have one single, efficient trap for all kinds of radionuclides because of their different chemical properties. Therefore, it was necessary to select those radionuclides which contribute most to the gamma dose rate in the primary cell during reactor downtimes. As long as an LMFBR is operated without fuel element failures ("clean core"), the activation products Mn-54 and Zn-65 are of most concern (Na-22 and Ag 110m are drained completely into the dump tank with the sodium). After one or more fuel cladding failures, Cs-137 becomes more and more important because of its high release fraction, its long half-life, and its excellent solubility in hot, flowing sodium.

Zn-65 and Cs-137 are of additional importance because of their enrichment (compared to Na-22) in cover gas areas. So, emphasis was laid on radionuclide traps for Mn-54, Zn-65 and fission product cesium.

### 6.1 Screening Tests

From experience with the sorption of Mn-54 and Zn-65 on the walls of Ni crucibles in the KNK primary sodium sampling station it was concluded that Nickel is a promising material for radionuclide traps for the removal of Mn-54 and Zn-65 (17). Using a special sample holder in the primary sodium sampling station, a lot of screening tests were performed in search for other, possibly more effective trap materials (18). Table 7 shows results of such a screening test. Six elemental metal samples were exposed in the PSSS to the flowing primary sodium at 200 °C for fifty hours. Only Zn-65 indicated a selective sorption on Ni, and much more on Cu. The deposited activities of Mn-54 exhibited a material-independent down-stream decrease. Additional experiments in the laboratory sodium loop NATAN confirmed the outstanding sorption of Zn-65 on copper (19), but Mn-54 was not removed from the flowing sodium. Because Ni displayed a satisfactory sorption of both crucial activation products, Zn-65 and Mn-54, this material was chosen for the first radionuclide trap at KNK II.

Table 7: Sorption of radionuclides (Bq/cm<sup>2</sup>) on metal coupons from flowing sodium (200 °C) in 50 hours

| Position  | 2   | 3   | 4     | 5   | 6   | 7   |
|-----------|-----|-----|-------|-----|-----|-----|
| Material  | Co  | Ni  | Cu    | Ti  | Zr  | Hf  |
| Cr - 51   | 24  | -   | -     | 16  | 22  | -   |
| Mn-54     | 155 | 150 | 148   | 73  | 83  | 58  |
| Fe - 59   | 14  | -   | -     | -   | -   | -   |
| Co - 58   | 47  | 4.1 | -     | 2.2 | 3.5 | 3.1 |
| Co - 60   | 72  | 4.8 | 10    | 23  | 3.0 | 3.2 |
| Zn - 65   | 235 | 820 | 30414 | 10  | 40  | 14  |
| Ag - 110m | 13  | 58  | 31    | -   | 78  | 2.2 |
| Sb - 124  | 3.3 | -   | -     | 5.6 | 4.4 | -   |
| Ta - 182  | 53  | 17  | 162   | 161 | 182 | 202 |
| Cs - 137  | 4.1 | 3.0 | 10.0  | 5.6 | 6.7 | 6.7 |

## 6.2 Radionuclide trap for the removal of Mn-54 and Zn-65

A first radionuclide trap -using Ni, too- was developed at Richland, and successfully tested at EBR-II (20, 21). This trap is included into the fuel element sodium exit, and acts as a real hot-leg trap. At KNK, experimental radionuclide traps were connected to the primary system in the PSSS (Fig. 3, pg. 4) instead of the sampling device. These traps were filled with Ni pall rings. Fig. 15 shows the real trap (stainless steel) besides a plastic model, showing the pall ring packing inside.

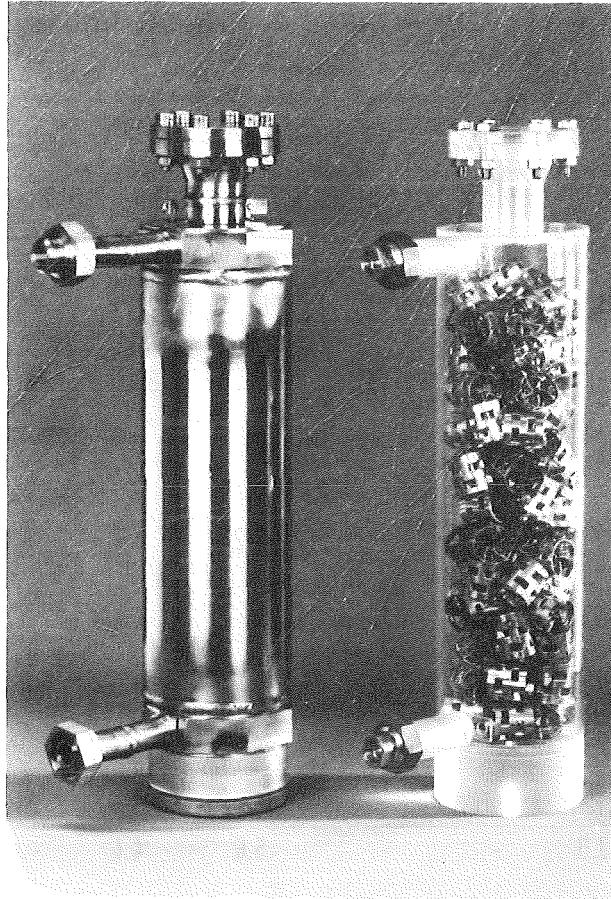


Fig. 15: KNK radionuclide trap and plastic model

The very promising results of such radionuclide traps for the removal of Zn-65 and Mn-54 with Ni pall rings as packing have been reported elsewhere (22).

### 6.3 Radionuclide trap for the removal of Cs

Again, a first radionuclide trap for the removal of the most important fission product, Cs-137, was developed and successfully tested at EBR-II (23). The packing of this trap was "RVC", reticulated vitreous carbon. In a series of laboratory experiments the same material was compared to the Cs sorption properties of other carbonaceous materials (24). Finally, three Cs traps, filled with 3 different carbonaceous materials, were successfully tested in the KNK primary sodium sampling station.

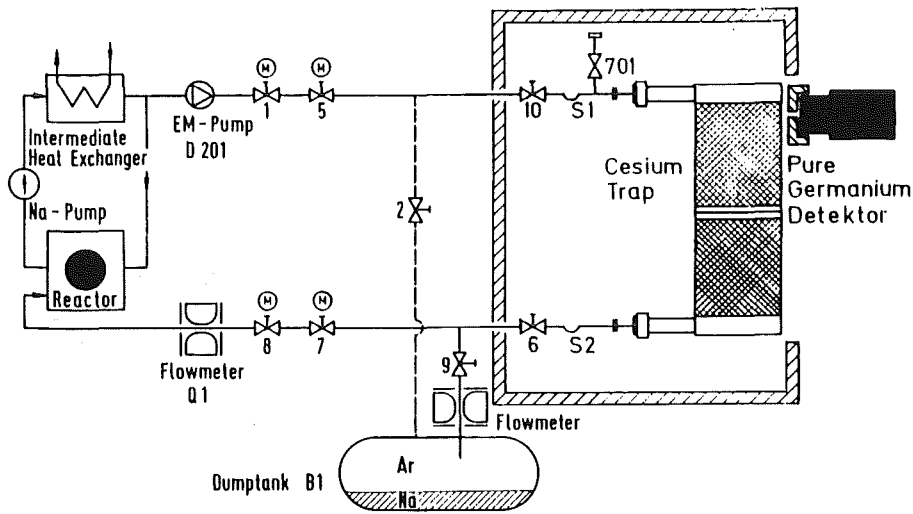


Fig. 16: Experimental Cs trap in the KNK II primary sodium sampling station

Fig. 17 shows the increase of Cs-137 activities in the traps B 705 and B 706 during loading of these traps.

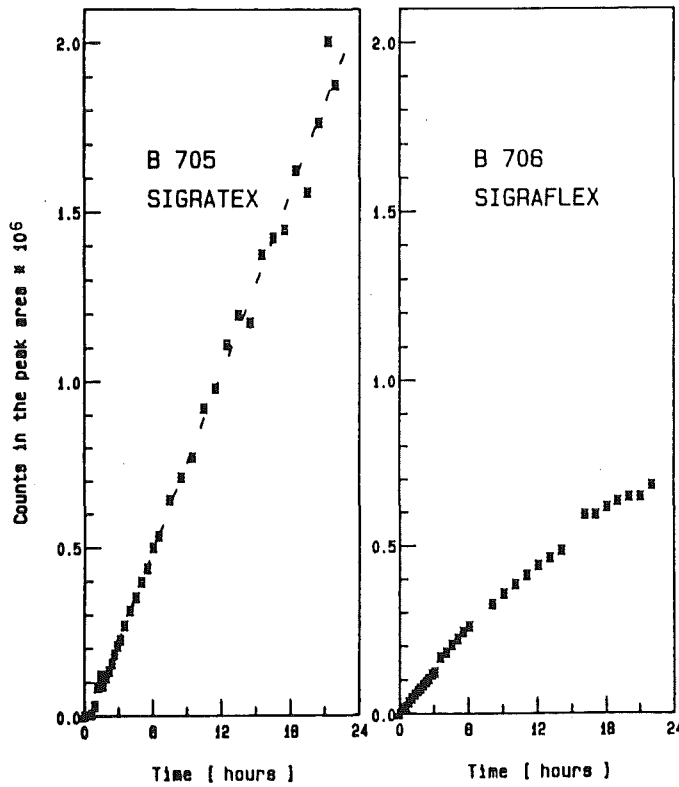


Fig. 17: Increase of the Cs-137 activities in the traps B 705 and B 706 during loading

Again, the results of these experimental Cs traps have been reported (25). An operational cesium trap in the KNK II primary purification circuit is in preparation. The trap is expected to be operational in 1988.

## 7. SUMMARY AND CONCLUSIONS

Radiochemical surveillance of the KNK primary sodium has been performed now for 15 years of reactor operation (= 953 effective full power days). The overflow method used for sodium sampling proved to be reliable. Different crucible materials have to be used for different analytical tasks. The amount of radionuclides in the primary system has not given any restrictions to plant operation at any time.

On-line gamma spectrometry on piping and components of the primary circuits was accomplished in reactor downtimes. Activity depositions on the walls were dominated by Ta-182 after KNK I operation. Main deposited activities at KNK II were Mn-54 ("clean core") and -after operation with failed fuel- Cs-137, in cover gas areas together with Zn-65.

Efficient experimental radionuclide traps for the removal of Mn-54, Zn-65 and Cs-137 from the primary coolant were tested successfully.

The dose rates on primary pipes and components (after decay of Na-24!) of KNK I and KNK II were lower by an order of magnitude compared to water-cooled nuclear reactors. This is in good agreement with experiences from LMFBR's in other countries. The resulting average yearly accumulated personal dose rate was 0.211 man-Sv at KNK, compared to 3.92 man-Sv (26) at German light-water-cooled power reactors.

8. REFERENCES

- (1) H.H. Stamm, K.Ch. Stade, H. Richard  
SODIUM CHEMISTRY AT KNK  
Proc.2nd Int. Conf. Liquid Metal Technology in Energy  
Production  
pp. 16-30 to 16-37; Richland, WA; April 20 - 24, 1980  
CONF-800401-P2
- (2) H. Feuerstein, A.J. Cooper, F.A. Johnson  
MECHANISM OF RELEASE OF RADIOACTIVE PRODUCTS INTO LIQUID-  
METAL COOLANTS, THEIR TRANSPORT WITHIN THE CIRCUITS AND  
REMOVAL FROM LMFBRs  
Atomic Energy Review 17, No.3, 697-761 (1979)
- (3) J.M.F. Rohde, M. Hissink, L. Bos  
EQUIPMENT FOR SAMPLING SODIUM  
J.Nucl.Energy 24, 503-508 (1970)
- (4) H.H. Stamm  
SORPTION OF RADIONUCLIDES ON SODIUM SAMPLING VESSELS  
Proc.Int.Conf. Liquid Metal Technology in Energy Production  
pp. 271-277; Champion, PA; May 3 - 6, 1976  
CONF-760503-P1
- (5) H.H. Stamm  
RADIOACTIVE MATERIALS IN PRIMARY CIRCUITS OF LMFBRs  
SOURCES - TRANSPORT - REMOVAL  
pp. 39-73 in H.M. Kottowski (Ed.), "Safety Problems Related  
to Sodium Handling in Liquid Metal Fast Breeder Reactors and  
Large Test Facilities", Ispra (Varese)/Italy, Nov. 12-14, 1980  
Harwood Academic Publishers, ISBN: 3-7186 0087-0
- (6) H.H. Stamm  
ACTIVATION ANALYSIS OF METALLIC SODIUM  
Proc.Int.Conf. Liquid Alkali Metals  
pp. 65-69, BNES, Nottingham, April 4 - 6, 1973
- (7) H.H. Stamm, H. Clauss, K. Nolte  
AKTIVIERUNGSANALYTISCHE BESTIMMUNG VON METALLISCHEN VERUN-  
REINIGUNGEN IN KNK-PRIMARNATRIUM  
Z. Analyt. Chem. 266, 337-340 (1973)

- (8) H.H. Stamm  
RADIONUKLIDE IM KNK-PRIMÄRSYSTEM  
Reaktortagung Nürnberg 1975, Compacts pp. 730-733
- (9) K.Ch. Stade, E. Zimmermann, J. Schindewolf  
CLEANING AND REQUALIFICATION OF KNK PRIMARY COLD TRAPS  
Proc.3rd Int.Conf. Liquid Metal Engineering and Technology  
Vol.2, pp. 407-412, BNES, Oxford, April 9 - 13, 1984
- (10) H.H. Stamm, K.Ch. Stade  
MONITORING OF RADIONUCLIDES AND METALLIC IMPURITIES IN THE  
KNK II PRIMARY SODIUM  
pp. 285-292 in W.S. Lyon (Ed.) "Analytical Spectroscopy"  
Proc.26th Conf.Analyt.Chem. in Energy Technology  
Knoxville, TN, October 11 - 13, 1983 ELSEVIER 1984
- (11) Charles R.F. Smith, J.T. Holmes  
PURITY OF EBR-II SODIUM: 1967 - 1974  
Report ANL-75-26 (Dec. 1975)
- (12) H. Clauss, H.D. Hanke, H.H. Stamm, H. Wild  
UNTERSUCHUNGEN AN PARTIKELN AUS DEM PRIMÄRNATRIUM DER  
KOMPAKTEN NATRIUMGEKÜHLTEN KERNREAKTORANLAGE KNK II  
Kurzreferate (Abstracts) GDCh-Vortragstagung Nuklear-  
chemie, Regensburg, 29.09. - 02.10.1986
- (13) H.H. Stamm, K.Ch. Stade  
CORROSION PRODUCT BEHAVIOUR IN THE PRIMARY CIRCUIT OF  
THE KNK NUCLEAR REACTOR FACILITY  
pp. 36-62 in Summary Rep. IAEA-IWGFR Specialists' Meeting  
"Fission and Corrosion Product Behaviour in Primary Cir-  
cuits of LMFBRs", Dimitrovgrad, USSR, Sept. 8 - 11, 1975
- (14) H.H. Stamm, H.D. Hanke, H. Clauss, K.Ch. Stade  
KNK II COMPONENT CONTAMINATION MEASUREMENTS BY  
GAMMA SPECTROMETRY  
Proc.3rd Int.Conf. Liquid Metal Engineering and Technology,  
Vol. 3, pp. 131-136, BNES, Oxford, April 9 - 13, 1984
- (15) T.D. Claar  
SOLUBILITY OF METALLIC ELEMENTS IN LIQUID SODIUM  
Reactor Technology 13, 124-146 (1970)
- (16) U. Quandt, Interatom, private communication



- (17) H.H. Stamm  
SORPTION VON RADIONUKLIDEN AUS NATRIUM AN METALL-OBERFLACHEN  
Atomwirtschaft 22, 639-640 (1977)
- (18) H.H. Stamm, H.D. Hanke, H. Clauss  
REMOVAL OF RADIONUCLIDES FROM LIQUID SODIUM BY SORPTION ON  
METALLIC SURFACES  
Proc.2nd Int.Conf. Liquid Metal Technology in Energy Production  
pp. 17-58/17-66, Richland, WA, April 20 - 24, 1980  
CONF-800401 P2
- (19) H.H. Stamm, C.R. Venkatasubramani, unpublished
- (20) J.C. McGuire, W.F. Brehm  
A RADIONUCLIDE TRAP FOR LIQUID-METAL-COOLED REACTORS  
Trans. Am. Nucl. Soc. 30, 189-190 (1978)
- (21) J.C. McGuire, US-Patent 4.088.533 (1978)
- (22) H.H. Stamm, H. Clauss, H.D. Hanke  
FIRST TEST OF A RADIONUCLIDE TRAP AT KNK II  
Proc.3rd Int.Conf. Liquid Metal Engineering and Technology  
Vol. 3, pp. 137-142, Oxford, April 9 - 13, 1984
- (23) W.H. Olson, W.E. Ruther  
CONTROLLING CESIUM IN THE COOLANT OF THE EXPERIMENTAL BREEDER  
REACTOR II  
Nuclear Technology 46, 318-322 (1979)
- (24) N. Hanebeck, Interatom, unpublished
- (25) K.Ch. Stade, H.H. Stamm, H. Clauss, H.D. Hanke,  
N. Hanebeck, R. Tusche  
STATUS OF CESIUM REMOVAL FROM PRIMARY SODIUM IN THE  
GERMAN LMFBR PROGRAM  
Proc. Int. Top. Meeting on Fast Reactor Safety,  
Vol. 1, pp. 197-204, Knoxville, TN, April 21 - 25, 1985
- (26) H.J. Schroeder  
OPERATIONAL RADIATION PROTECTION AND MONITORING PROGRAMME  
IAEA Interregional Training Course on "Safety Analyses"  
Oct. 29 - Dec. 13, 1984, SKT, Kernforschungszentrum Karlsruhe  
Federal Republic of Germany

| <u>LIST OF FIGURES</u>  | Page |
|---|------|
| 1) KNK Test Reactor   | 1    |
| 2) Radionuclides in LMFBR coolants  | 2    |
| 3) KNK II primary sodium sampling station PSSS  | 4    |
| 4) Induction heated vacuum distillation of sodium   | 6    |
| 5) Distillation flask with crucible in the HF coil  | 6    |
| 6) Primary coolant activity, dose rate and effective full power days vs. operating time of KNK II/1 | 10   |
| 7) Primary coolant activity, dose rate and effective full power days vs. operating time of KNK II/2 | 12   |
| 8) Filter unit for the KNK primary sodium sampling station  | 15   |
| 9) SEI of particles from KNK primary Na   | 16   |
| 10) X-ray distribution of Fe in particles (same filter area)  | 16   |
| 11) Measuring locations in the KNK primary cell   | 18   |
| 12) Solubilities of Ag and Zn in Na (from T.D. Claar)   | 19   |
| 13) Effect of an inertgas/steam treatment on the radionuclide distribution on a primary Na pump     | 21   |
| 14) Gamma spectrum of radionuclides in a KNK primary cold trap                                      | 22   |
| 15) KNK radionuclide trap and plastic model   | 25   |
| 16) Experimental Cs trap in the KNK II primary Na sampling station                                  | 26   |
| 17) Increase of the Cs-137 activities in the traps B 705 and B 706 during loading                   | 26   |

LIST OF TABLES

|  | Page |
|--|------|
| 1) KNK II operating parameters   | 3    |
| 2) Radionuclides in KNK I primary sodium   | 7    |
| 3) Radionuclides in 7 stainless steel crucibles,<br>(sampling from 200 °C sodium), statistical<br>treatment of the results | 13   |
| 4) Relative standard deviations (RSD in %) of<br>analyses for radionuclides in KNK primary<br>sodium samples               | 14   |
| 5) Alpha activities and particle masses on<br>sintered metal filters   | 17   |
| 6) Deposited activities in the KNK II primary<br>system after 630 effective full power days                                | 20   |
| 7) Sorption of radionuclides (Bq/cm <sup>2</sup> ) on metal<br>coupons from flowing sodium (200 °C) in 50 hours            | 24   |

Transport Behavior of Cs and I in Sodium Vapor Trap

Hiroshi Taki\*, Koji Hata\* and Katsuyuki Iizawa\*\*

\* Mitsubishi Atomic Power Ind. Inc., O-miya, Saitama, Japan

\*\* O-arai Engineering Center, Power Reactor and Nuclear Fuel Development Corporation, O-arai, Ibaraki, Japan

Abstract

In an LMFBR, Cs and I radioisotopes would be released from failed fuel into the primary sodium coolant and subsequently they would be vaporized into cover gas system.

In this work, experimental study on transport and trapping for Cs-134 and I-131 in the vapor trap system were conducted. The experimental apparatus was consisted of reflux type mist trap (R/T), filter type vapor trap (F/T), and backup filter (B/T). They were connected in series, simulating to the primary cover gas system of an LMFBR.

The results were as follows;

- (1) Cs-134 was trapped at the lower temperature region in R/T, but they gradually moved to the downstream and some amounts of them broke out through the R/T.
- (3) These Cs which broke out through the R/T were trapped at the upstream region in the following F/T, and they hardly move anymore. Total trapping efficiency of R/T and F/T for Cs was nearly equal to 100%.
- (3) All amount of I were trapped at the higher temperature region in the R/T.
- (4) Sodium was mainly trapped at the higher temperature region in the R/T, and its trapping efficiency for sodium was higher than 99%. Through both the vapor traps (R/T and F/T), sodium was perfectly trapped.
- (5) The apparent distribution coefficient for Cs and I were obtained to be;

$$K_d (\text{Cs-Na}) = 2.0 \sim 3.6 \times 10^2 \quad (\text{at } 529^\circ\text{C})$$

$$K_d (\text{I -Na}) = 1.4 \times 10^{-1} \quad (\text{at } 580^\circ\text{C})$$

- (6) The substantial transfer ratio for sodium was obtained to be;

$$F = 0.13 \sim 0.38 \quad (\text{at } 480 \sim 580^\circ\text{C})$$

## 1. Introduction

Cs and I radioisotopes, produced by the fission of fuel material, are important fission products from the stand point of radiological protection during the reactor operation, maintenance works, and of plant safety evaluation, since they have high potential hazard, i.e., "high fission yields", "high mobility", "long half lives", and "high volatility".

These radioisotopes released to the primary sodium are vaporized from gas-liquid surface, and are entrained in argon gas flow and deposited on the primary cover gas system. These transport might increase some problems on the radiological protection. Thus it is necessary to understand more exactly the behavior of these radioisotopes in the primary cover gas system.

In this work, experimental study on transport and trapping behavior for Cs and I in sodium vapor traps was carried out.

## 2. Experiment

### 2-1. Experimental Apparatus

Fig. 1 shows the flow diagram of the test apparatus which was consisted of the sodium system and the cover gas system. The sodium system was consisted of sodium charge and drain line, vaporization tank (V/T), and argon gas atmosphere glove-box. The cover gas system, which was composed of reflux type mist trap (R/T), filter type vapor trap (F/T), and backup filter (B/T), was connected to the V/T.

The construction of R/T is shown in Fig. 2. The R/T was made of Type 304 stainless steel tube ( $\phi 34$  mm OD,  $\phi 28$  mm ID, 411.25 mm length), containing three kinds of stainless steel meshes (20, 40, 90 mesh-size). Each mesh was packed in the order of 20, 40 and 90 mesh-size from gas inlet side.

The construction of F/T is shown in Fig. 3. The F/T was made of Type 304 stainless steel tube ( $\phi 34$  mm OD,  $\phi 28$  mm ID, 320 mm length), containing also three kinds of stainless steel meshes (90, 120, 160 mesh-size). Each mesh was packed in the order of 90, 120, and 160 mesh-size from gas inlet side.

The B/T was made of Type 304 stainless steel canister ( $\phi 60.5$  mm OD,  $\phi 54.9$  mm ID, 97.5 mm height) which contained an active carbon.

## 2-2. Procedure

### (1) Radioactive sodium preparation

The sodium system was first heated, then the sodium, containing a certain amount of Cs-134 or I-131, was charged in V/T.

### (2) Cover gas system conditioning

Then the cover gas system conditioned and controlled for the experiments as; V/T... 529°C at Cs-134 tests, 580°C at I-131 tests, R/T, gas inlet region ... 460°C, R/T, gas outlet region... 200°C. These conditions were simulated to an LMFBR's vapor trap system. Sodium sampling was performed for the measurement of Cs-134 or I-131 activity, when temperature equilibrium was established over the cover gas system.

### (3) Argon gas circulation

The gas circulation pump was then started to circulate through the cover gas system with bubbling in V/T. The flow rate was 0.5ℓ/min which meant 2.2 ~ 3.5 cm/sec of linear velocity in R/T and F/T.

### (4) Detection and analysis

Cs-134 or I-131 activity was measured by scanning NaI scintillation counter with collimator, placed at the outside of both R/T and F/T every 2 hrs. One test running was lasted to 10 ~ 50 hrs.

After each test run, the cover gas system was disassembled and the deposited (attached) sodium at each region of their mesh-size section was dissolved into solution. Cs and I activities and sodium, accumulated in each vapor trap were measured and examined by Ge-detector and chemical analysis.

## 2-3. Results

### (1) Distribution of Cs-134 in the cover gas system

Accumulation and distribution profile of Cs-134 were obtained by NaI scintillator scanning. They are shown in Figs. 4, 5 for R/T and F/T respectively. As can be seen from Fig. 4, Cs-134 activities were trapped at the lower temperature region in R/T, but they were gradually moved to the downstream. After 12 hrs' gas circulation, some of them were broken through R/T. This is observed clearly from Fig. 5, where the Cs-134 activities in the upstream region of F/T begin to increase after 12 hrs' gas circulation. Fig. 6 shows the distribution for Cs between each section of the vapor traps after 50 hrs' test run. In consequence of the break-through from R/T,

26.8% of total trapped Cs-134 was trapped in the connection parts (tube fitting) between the R/T and the F/T.

The total Cs-134 trapping efficiency of R/T and F/T was nearly equal to 100%.

(2) Distribution of I-131 in the cover gas system

Table 1 shows the measurements of the I-131 activities in each section of R/T after 50 hrs.' test run. All amount of I-131 were trapped at the R/T tube.

(3) Distribution of sodium in the cover gas system

Table 2 summarizes the results of chemical analysis for sodium accumulated in each section of every vapor traps. This table shows that sodium was mainly trapped at the higher temperature region (460 ~ 300°C) in the R/T, and its trapping efficiency for sodium was 99.9% which can be substantially even as 100%.

### 3. Discussion

#### 3-1. Distribution of Cs-134 and I-131 in the Cover Gas System

Temperature profile through R/T is plotted in Fig. 7. From this figure, it is shown that there was about 100°C of large temperature drop at the region of 120 ~ 180 mm from the entrance of the mesh-packed region. It is suggested that the Cs-134 activity peak appeared at this region after 2 hrs.' gas circulation would be caused by this large temperature drop. According to the works of some researchers<sup>(1)</sup>, it had been reported that cesium was vaporized from cesium-sodium solution as an elemental (atomic) form and was deposited in the lower temperature region, irrelevant to sodium deposition.

On the other hand, those Cs, trapped at the upstream region in F/T, were hardly moved anymore, because the temperature was too low at the 90 mesh region in F/T, of 40°C.

I-131 were detected at the R/T tube, though distribution of I-131 in this region was not clearly obtained. None of I-131 was detected at the downstream mesh region in R/T nor in F/T. According to the papers of some other workers<sup>(1)</sup>, it was reported that I was vaporized from I-Na solution as NaI and deposited at the higher temperature region in a thermally gradiented deposition tube. All amounts of I-131 were trapped at the upstream region from mesh inlet.

### 3-2. Equilibrium Vaporization of Cs-Na, I-Na

The Cs-134 and the I-131 were perfectly trapped with R/T + F/T and R/T, respectively. Since total amounts of Cs-134, I-131 and sodium vaporized, were negligible small, the concentration of Cs-134 and I-131 in Cs-Na or I-Na solution in V/T were constant.

We defined the apparent distribution coefficient for Cs-134 and I-131 as;

$$K_d(\text{Cs-Na}), K_d(\text{I-Na}) = \frac{A_V}{A_L} \dots\dots\dots (1)$$

- K<sub>d</sub>: apparent distribution coefficient for Cs-134 or I-131
- A<sub>L</sub>: concentration of Cs-134 or I-131 in the liquid phase
- A<sub>V</sub>: concentration of Cs-134 or I-131 in the vapor phase,  
which is equal to the concentration in the trapped sodium

By substituting the experimental results into equation (1), the apparent distribution coefficient were calculated, as follows.

$$K_d(\text{Cs-Na}) = 2.0 \sim 3.6 \times 10^2$$
$$K_d(\text{I-Na}) = 1.4 \times 10^{-1}$$

Fig. 8 and Fig. 9 show  $K_d(\text{Cs-Na})$  and  $K_d(\text{I-Na})$  obtained our experiments and the  $K_d(\text{Cs-Na})$ ,  $K_d(\text{I-Na})$  values from other workers' (2)(3) are also presented in Figs. 8, 9. Referred values of  $K_d(\text{Cs-Na})$ ,  $K_d(\text{I-Na})$  plotted there, were theoretical values or experimental results which had been obtained with omitting the deposition effect on the pipe wall through the transport. Our experiments were carried out to make more practical estimation of Cs and I activities behavior which would be more likely occurred in the primary cover gas system of an LMFBR. In our experiments which simulated to plant system, vaporized Cs-134, I-131, and sodium were transported by circulation gas flow with repeating deposition and vaporization. The difference between our work and the referred works, shown in Figs. 8, 9, were caused from these deposition and vaporization effects.

Our results may be more realistic for plants, considering the practical operation of the primary cover gas system.



### 3-3. Transfer Ratio and Distribution for Na

We defined the transfer ratio for sodium by the following equation.

$$F_{Na} = \frac{N_{av} \text{ (deposited)}}{N_{aT} \text{ (transported)}} \dots\dots\dots (2)$$

$N_{av}$ : Amount of sodium trapped in the vapor traps

$N_{aT}$ : Amount of transported sodium obtained by estimation with saturated vapor pressure in the V/T

By substituting the experimental results into equation (2),  $F_{Na}$  were obtained to be 0.13 ~ 0.38. It was considered that, the reduction of  $F_{Na}$  was caused by the deposition on pipe wall between V/T and R/T. Fig. 10 shows the amount of sodium by experimental measurement (regional analysis of each vapor trap) and theoretical calculation from vapor pressures. Theoretical calculations were conducted on the basis that the sodium was trapped perfectly depending on the difference of saturated vapor pressures for each discrete temperature region of R/T. Fig. 10 shows that calculated value is higher than that of measured at 20 mesh region. But except this region, the calculated value is lower than that of measured in almost over the regions. The difference would be caused by some refluxed sodium flow against to argon gas stream.

Thus, it was considered that the deposition of sodium was also dependent on the difference of saturated vapor pressure.

### 4. Conclusion

In this work, some trapping test were conducted by using a simulated cover gas system of an LMFBR, and accumulation and distribution of Cs, I, and Na in every vapor traps (R/T, F/T, and B/T) were investigated.

The test results were as follows:

- (1) Cs-134 was trapped largely at the lower temperature region (300°C to 200°C) in R/T, and it was moved gradually to the downstream of R/T with running time and finally it broke through R/T. On the other hand, all amounts of I-131 were trapped at the higher temperature region in R/T.
- (2) Cs-134, which was broken through R/T, was almost trapped at the upstream region in F/T.
- (3) Through both the vapor traps of R/T and F/T, sodium was perfectly trapped.
- (4) The apparent distribution coefficient and sodium transfer ratio were obtained to be:

$Kd(\text{Cs-Na}) = 2.0 \sim 3.6 \times 10^2$ ,  $Kd(\text{I-Na}) = 1.4 \times 10^{-1}$ ,  $F_{\text{Na}} = 0.13 \sim 0.38$ .

(5) In this work, more practical informations were obtained. These results may be suitable for practical estimation on design and its analysis of the LMFBR cover gas system.

(6) The practical estimation would be made by the following equation.

$$\begin{aligned} & [\text{Cs or I}], \text{ transported to every vapor traps (Ci/sec)} \\ & = [\text{flow rate of cover gas}] (\text{m}^3/\text{sec}) \times [\text{distribution coefficient: } Kd] \\ & \times [\text{concentration of Cs and I in sodium}], (\text{Ci}/\text{m}^3) \quad (3) \end{aligned}$$

#### References

- (1) A. W. Castleman, Jr., I. N. Tang and R. A. Mackay: FISSION PRODUCT BEHAVIOR IN SODIUM SYSTEMS, BNL 10727, 1966.
- (2) B. D. Pollock, M. Silverberg and R. L. Koontz: Vaporization of Fission Products from Sodium, ANL-7520, pp. 549 - 554, 1968.
- (3) W. P. Kunkel, B. D. Pollock, J. Guon, G. B. Zwetig, M. Silberberg and S. Berger: LMFBR Fission Product Contamination and Control Studies-A Status Report, AI-AEC-12687, 1968.

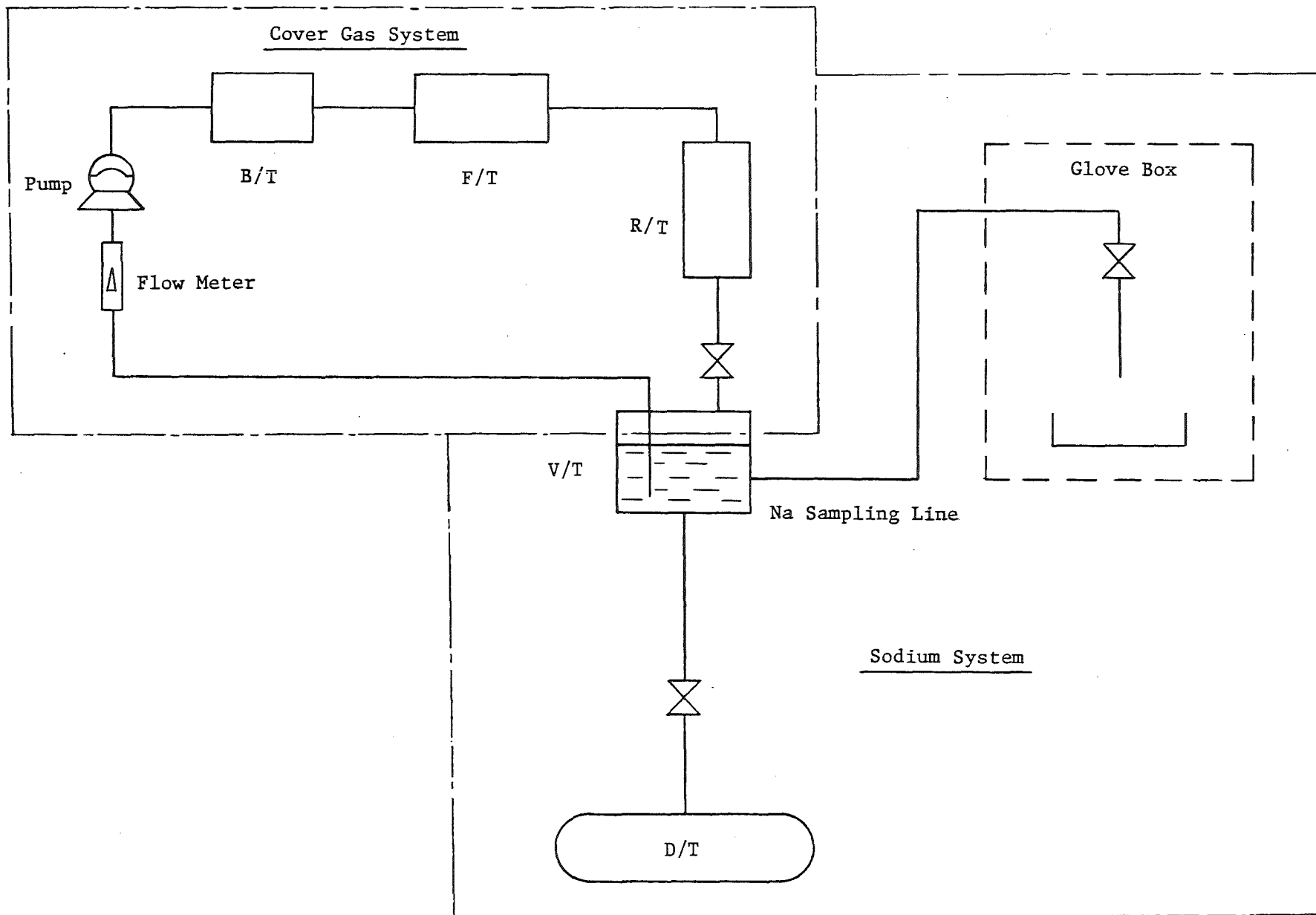


Fig. 1 Flow Diagram

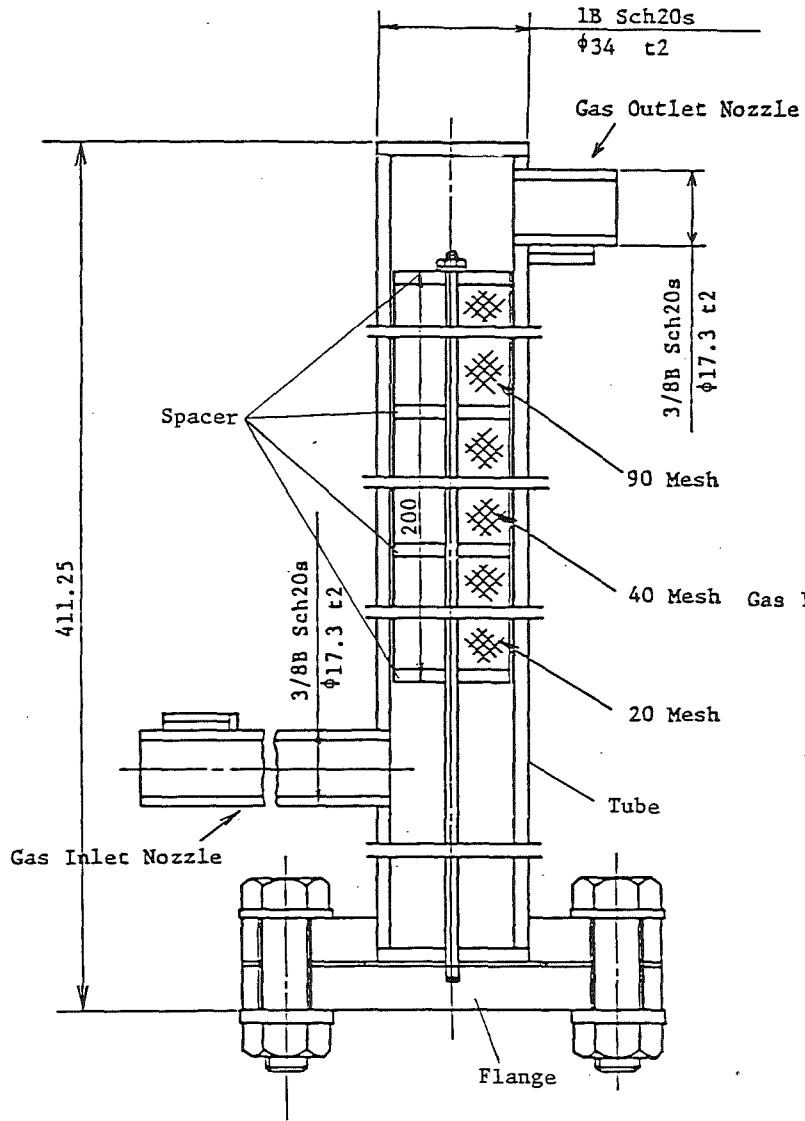


Fig. 2 R/T

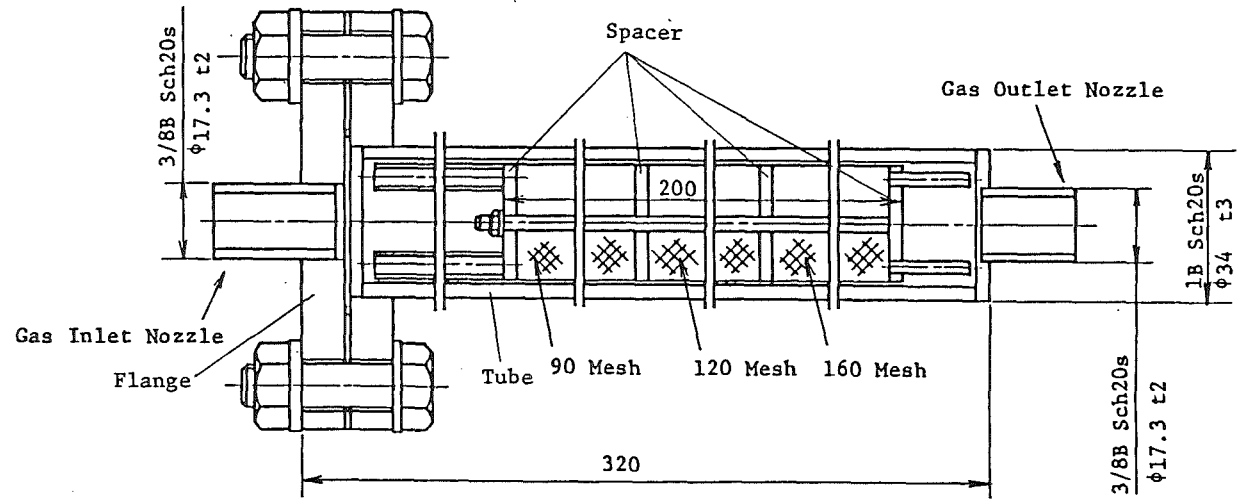


Fig. 3 F/T

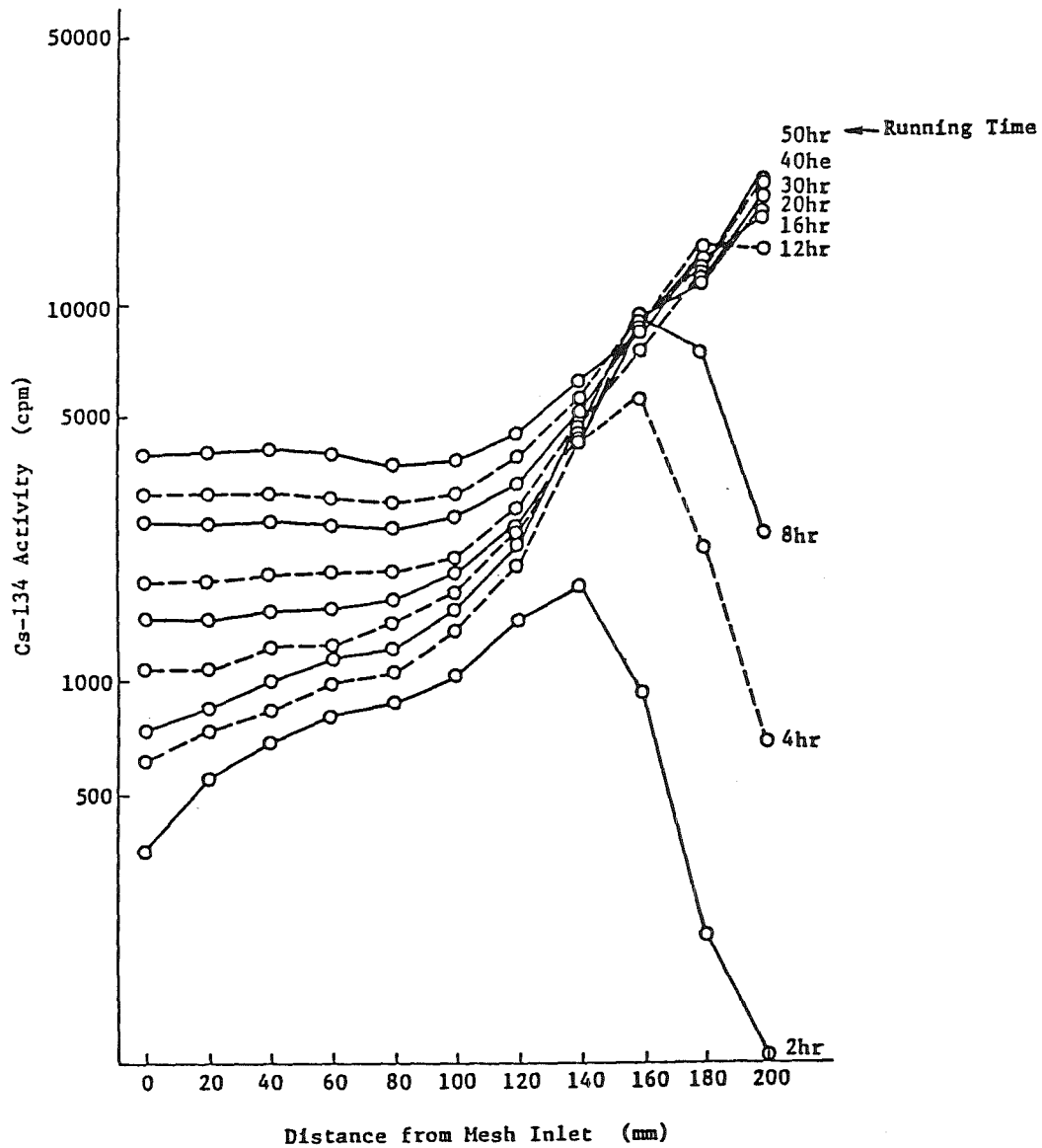


Fig. 4 Distribution of Cs-134 in R/T

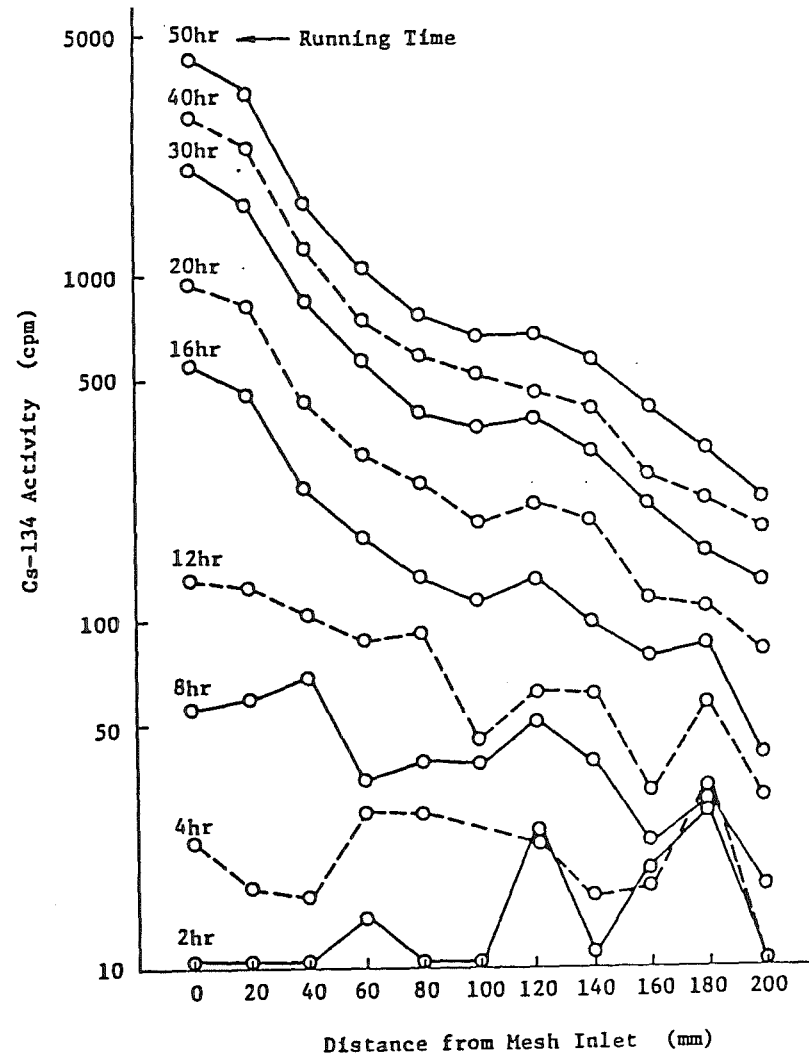


Fig. 5 Distribution of Cs-134 in F/T

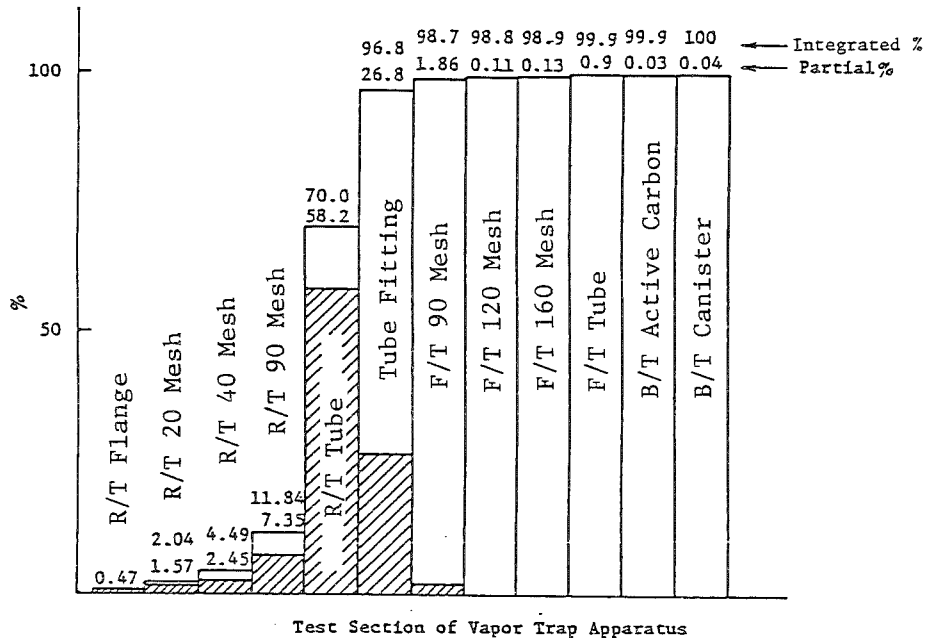


Fig. 6 Distribution of Cs-134 in Vapor Trap Apparatus after Test Run (50 hrs Test)

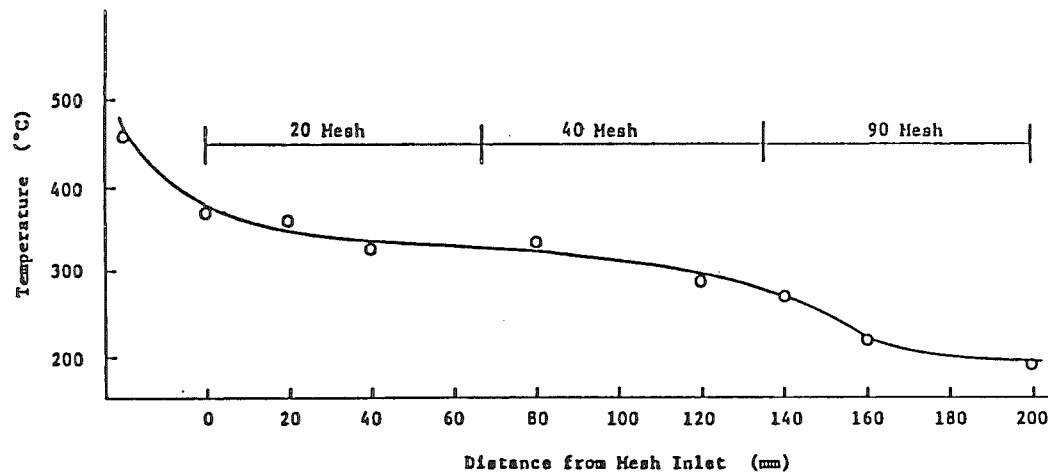


Fig. 7 Axial Temperature Distribution in R/V

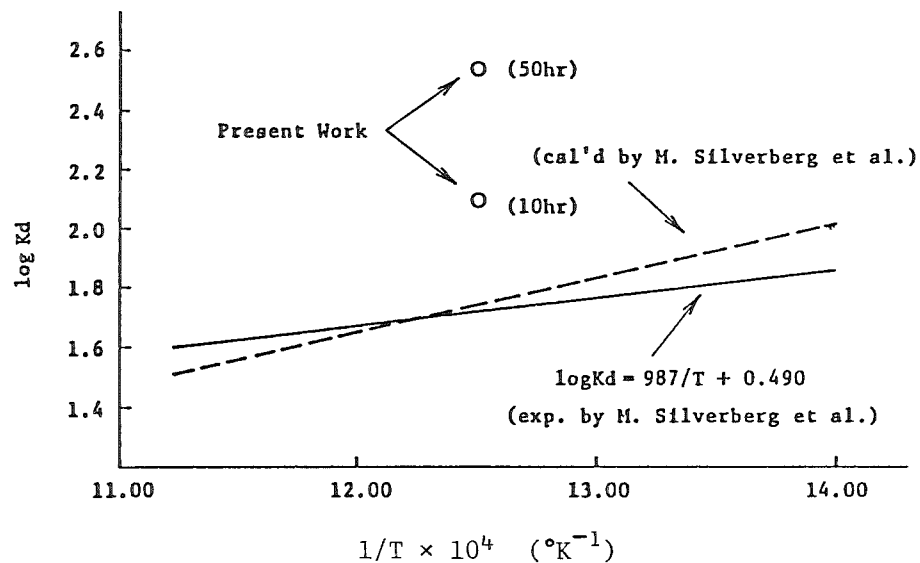


Fig. 8 Distribution Coefficient for Cs-Na System

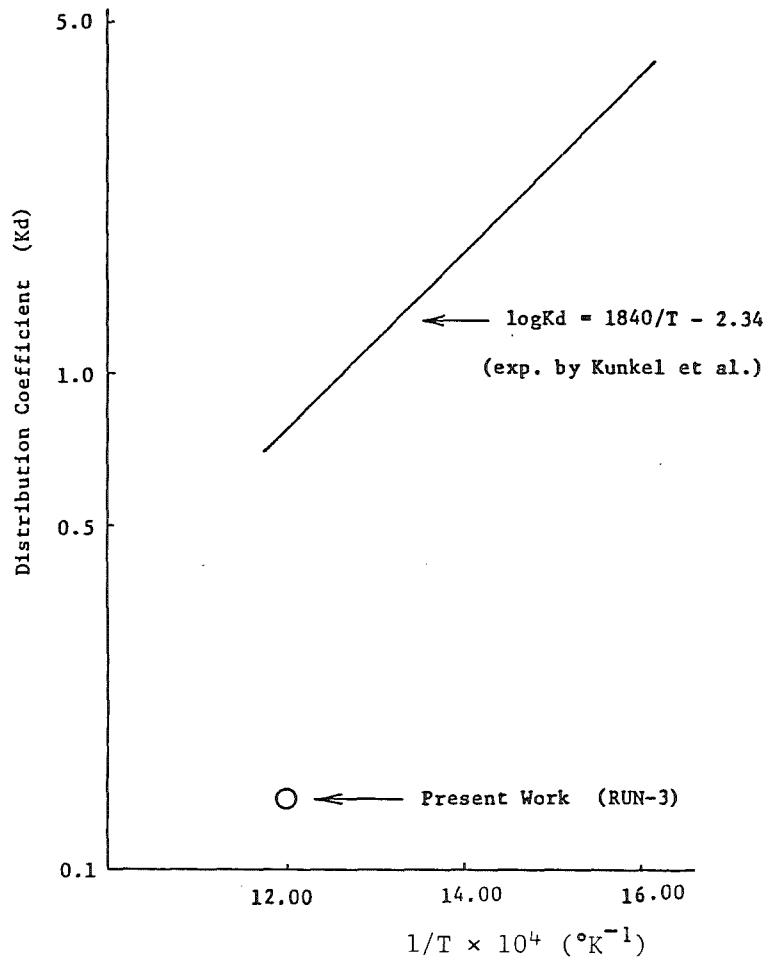


Fig. 9 Distribution Coefficient for NaI-Na System

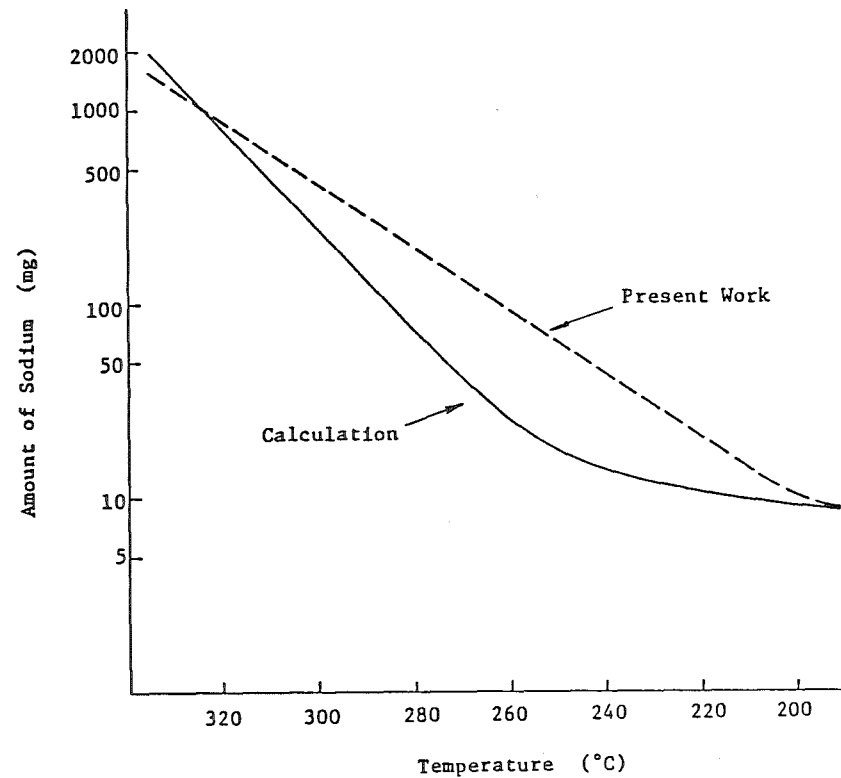


Fig. 10 Distribution of Sodium in R/T

Table 1 I-131 Distribution in R/T

(20 hrs Test)

| Test Section | I-131 Activity (RUN-1) (μCi) | I-131 Activity (RUN-2) (μCi) | I-131 Activity (RUN-3) (μCi) |
|--------------|------------------------------|------------------------------|------------------------------|
| R/T Flange   | * N·D                        | * N·D                        | * N·D                        |
| R/T 20 Mesh  | * N·D                        | * N·D                        | * N·D                        |
| R/T 40 Mesh  | * N·D                        | * N·D                        | * N·D                        |
| R/T 90 Mesh  | * N·D                        | * N·D                        | * N·D                        |
| R/T Spacer   | * N·D                        | * N·D                        | * N·D                        |
| R/T Tube     | * N·D                        | * N·D                        | $9.1 \times 10^{-3}$         |

\* Less than Detection Limit

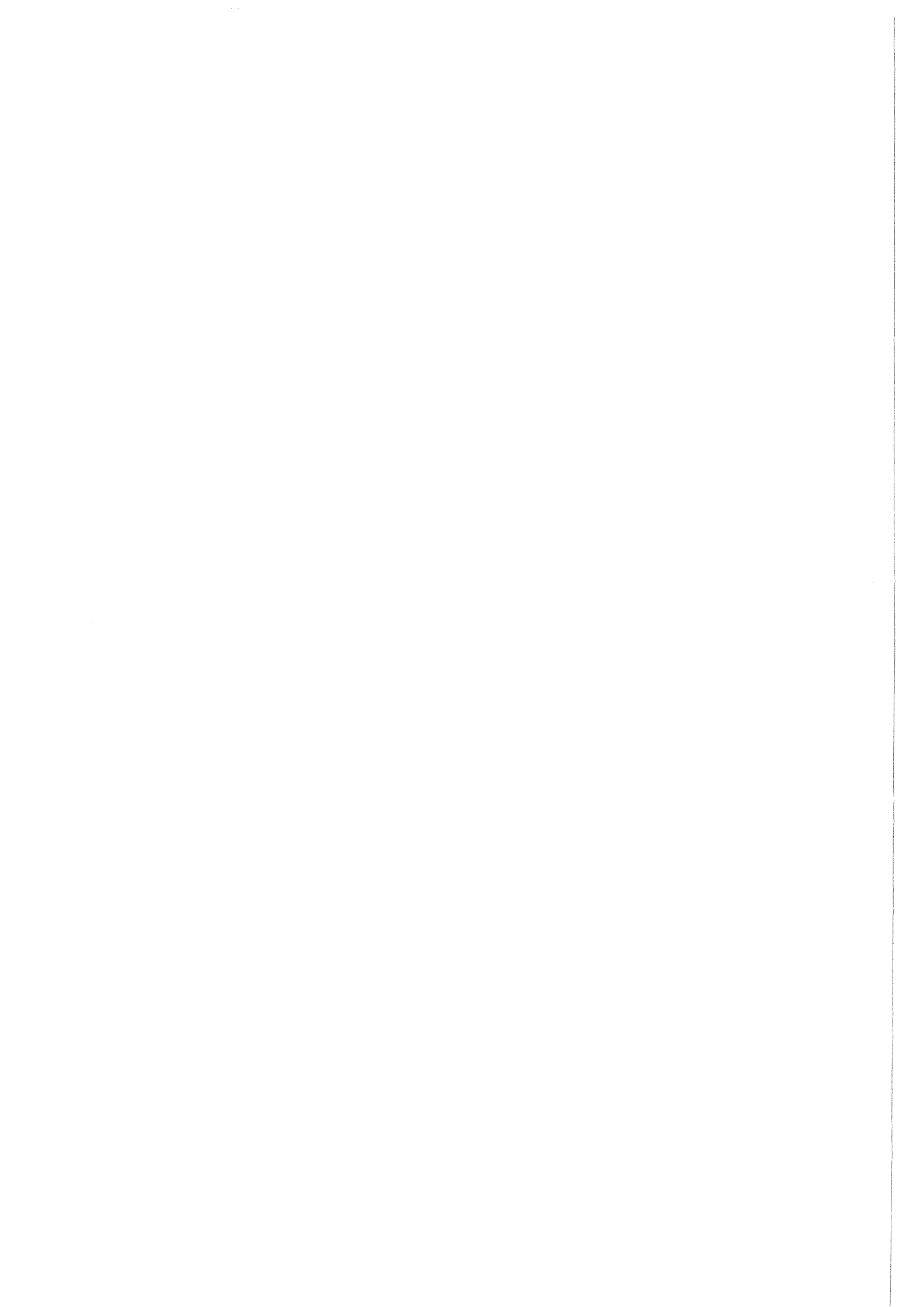
Table 2 Amount of Sodium in Test Section

(50 hrs Test)

| Test Section | Amount of Sodium (mg) | % of Amount |            |
|--------------|-----------------------|-------------|------------|
|              |                       | Fractional  | Integrated |
| R/T Flange   | 5.8                   | 0.4         | 0.4        |
| R/T 20 Mesh  | 899.3                 | 62.8        | 63.2       |
| R/T 40 Mesh  | 156.8                 | 10.9        | 74.1       |
| R/T 90 Mesh  | 9.6                   | 0.7         | 74.8       |
| R/T Tube     | 360.0                 | 25.1        | 99.9       |
| Tube Fitting | 0.06                  | 0.004       |            |
| F/T 90 Mesh  | 0.28                  | 0.020       |            |
| F/T 120 Mesh | 0.26                  | 0.018       |            |
| F/T 160 Mesh | 0.09                  | 0.006       |            |
| F/T Tube     | 0.04                  | 0.003       |            |
| B/T          | * N·D                 |             |            |
| Total        | 1432.23               | 100         | 100        |

\* Less than Detection Limit





Fission and corrosion product behaviour in primary circuits of LMFBR's

A W THORLEY

1. INTRODUCTION

This paper reviews work undertaken in the UK to further our understanding of corrosion and fission product behaviour in sodium cooled fast-reactor systems. The review essentially up-dates the UK paper on the same subject which was presented at Dimitrovgrad in 1975. Briefly it covers the following topics.

Development of models to describe the corrosion and deposition of radioactive material eg  $^{54}\text{Mn}$ ,  $^{58}\text{Co}$  and  $^{60}\text{Co}$  in reactor primary circuits.

Estimates of release and deposition of radioactive corrosion products (Mn, Co).

Behaviour of fission products, notably  $^{137}\text{Cs}$ , and fissile material following fuel pin failure.

Results from experimental programmes

In-reactor measurements.

2. RELEASE AND DEPOSITION OF ACTIVE CORROSION PRODUCTS IN SODIUM

2.1 Theoretical Background

The modelling studies in the UK have been directed towards rationalising the different behaviour of  $^{54}\text{Mn}$  and  $^{60}\text{Co}$ ,  $^{58}\text{Co}$  in sodium systems. The model developed by Polley and Skyrme(1) at BNL considers the released material to be dissolved as opposed to particulate species and in the model the mass transfer of species of interest between sodium and steel is characterised by an expression derived by equating the mass flux  $J$  to three relationships, namely, transfer across the laminar boundary layer, absorption and desorption at the steel surface, and diffusion in the steel. These are respectively for net release;

$$J = k(c_i' - c') \quad (1)$$

$$J = k_d c_i - k_a c_i' \quad (2)$$

$$J = D(\partial c / \partial x)_{x=0} + u c_i \quad (+ \text{ for bulk corrosion, } - \text{ for bulk deposition}) \quad (3)$$

where  $c$  and  $c'$  are the concentrations in the steel and bulk sodium respectively, the subscript  $i$  refers to interfacial values at  $x = 0$ ,  $u$  is the magnitude of the interfacial velocity and  $k_a$  and  $k_d$  the absorption and desorption mass transfer coefficients. For net deposition, if  $J$  is the magnitude of the mass flux, the relationships are identical but opposite in sign (Fig 1).

Equations 1 and 2 are modified to accommodate an effective mass-transfer coefficient  $K$  and a dimensionless chemical partition coefficient  $\beta$ . Beta is small for species which are highly soluble and large for specimens which are relatively insoluble. Another dimensionless parameter used in the model is the parameter  $A = K/\mu\beta$  ( $\mu$  is viscosity) which determines the

release/deposition behaviour of the solute of interest. The introduction of  $K$  and  $\beta$  provides the boundary condition at the interface, namely;

$$D(\partial c/\partial x)_{x=0} = (K/\beta \pm u) c_i - K c' \quad \begin{array}{l} \text{- for bulk corrosion} \\ \text{+ for bulk deposition} \end{array} \quad (4)$$

In the case of release from fuel pins Polley and Skyrme calculate the concentration profile in the steel by solving the relevant diffusion equation:

$$D \frac{\partial^2 c}{\partial x^2} + u \frac{\partial c}{\partial x} - \lambda c + R = \frac{\partial c}{\partial t} \quad (5)$$

where  $R$  is the rate of production of the species of interest by neutron activation and  $\lambda$  is the decay term. The boundary condition at the interface is given by equation (4) and the steel is assumed to be effectively of infinite thickness. The specific inventory  $I$ , the mass released or deposited per unit area and which remains undecayed after an exposure time  $t$ , is given by:

$$I = \int_0^t J(t') \exp [-\lambda (t - t')] dt' \quad (6)$$

For calculating release rates zero concentration of the radioactive species is assumed in the turbulent sodium core. When  $A < 1$  release is hypostoichiometric, thus cobalt isotopes  $^{59}\text{Co}$  and  $^{60}\text{Co}$  have been found to be selectively retained when activated stainless steel is corroded by sodium. When  $A > 1$  release is hyperstoichiometric ie selective leaching occurs as with  $^{54}\text{Mn}(2,3,4,5,6,7)$ . Polley and Skyrme loosely interpret  $A < 1$  or  $A > 1$  as indicating whether the species are more or less 'soluble' in sodium than the bulk steel consisting basically of iron, chromium and nickel. It is not possible at present to calculate cobalt inventories from an exact analytical formula, and calculated stoichiometric inventories have to be multiplied by selective retention factors which have been determined experimentally.  $A$  is generally in the range 0.1 to 1 for  $\text{Co}$ .  $^{54}\text{Mn}$  inventories are calculated from a solution to the diffusion equation in steel assuming zero concentration at the interface.

The diffusion equation(6) has been solved for the case of a corroding surface or one subjected to bulk deposition and the solutions simplified in a number of ways in order to determine which mechanism operates under different conditions. A number of possible mechanisms have been identified.

For  $A < 1$  deposition is always controlled by diffusion across the sodium laminar boundary layer. By taking appropriate values for  $A$  for release and deposition Polley and Skyrme's model would predict that  $^{60}\text{Co}/^{58}\text{Co}$  deposition is laminar boundary layer controlled. Work carried out in the Harwell Active Mass Transfer Loop on the release and deposition of corrosion products from an irradiated stainless steel specimen exposed to circulating sodium strongly supports this view; see later.

Making the inverse assumption for  $^{54}\text{Mn}$  that  $A > 1$  then it would be expected that the high temperature deposition of  $^{54}\text{Mn}$  is characterised by solid state diffusional control. At lower temperatures where there is bulk deposition, a "co-precipitation" mechanism is predicted with an effective mass transfer coefficient  $K_{\text{eff}} = \mu\beta$ . However, the possibility cannot be dismissed that  $\beta$

for  $^{54}\text{Mn}$  may increase very rapidly with decreasing temperature causing enhanced deposition at low temperatures under conditions of laminar boundary flow control. Distinguishing between these two mechanisms for  $^{54}\text{Mn}$  deposition on cold surfaces may be difficult.

Thus the model for  $^{54}\text{Mn}$  would predict (i) no velocity dependence in high temperature regions, (ii) little change with temperature in the hot parts of the circuit because the rise in  $\beta$  will be opposed by the fall in  $\sqrt{D}$ , (iii) rapid rise in deposition in the cold parts of the circuit due to the rise in  $\beta$ , (iv) possible velocity dependence and downstream effect in the cold region due to variation in  $\mu$ . These findings are broadly in line with experimental observations.

## 2.2 Behaviour of Different Isotopes

The three main corrosion product isotopes of concern are  $^{58}\text{Co}$ ,  $^{60}\text{Co}$  and  $^{54}\text{Mn}$ .  $^{58}\text{Co}$  activity arises from the nickel content of stainless alloys used for cladding and wrappers. Estimates of corrosion product activity inventories present after one year show that  $^{58}\text{Co}$  is the largest contributor to the total and its gamma energy of 0.81 MeV would make  $^{58}\text{Co}$  a major contributor to external dose rates from components ex-reactor. Because of its modest half life (71 days) the inventory of released  $^{58}\text{Co}$  achieves equilibrium within a year.

$^{60}\text{Co}$  on the other hand is derived solely from the inactive cobalt and  $^{60}\text{Ni}$  content of alloy steels used in the core or from Stellites used for sub-assembly rubbing or wear pads. Because of the long half life of  $^{60}\text{Co}$  the average release rate of radioactivity during one year in a 4-batch fuel management system is only 6.3% of the estimated equilibrium value. However, equilibrium in the primary sodium is rapidly achieved in spite of the long half life for  $^{60}\text{Co}$  because removal processes to surfaces dominate. Build up on surfaces is considered to be effectively governed by a constant concentration in bulk sodium and by local mass transfer coefficients.

The corrosion product activity of Manganese 54 is typified by its high generation and release rate from core steels, long half life and high gamma energy. Its behaviour has received extensive study because diffusion in cladding enhances release to sodium above stoichiometric expectations, and the possible diffusion into IHX steels at lower sodium temperature renders decontamination difficult if not impossible without removing metal from surfaces. Equilibrium in primary sodium is rapidly achieved in spite of the long half life for  $^{54}\text{Mn}$  because again removal processes to surfaces are considered to dominate. Build up on surfaces is, therefore, governed by an effectively constant concentration of  $^{54}\text{Mn}$  in bulk sodium and by local mass transfer coefficients which, unlike those for  $^{58}\text{Co}$  and  $^{60}\text{Co}$ , are adjusted to accommodate the well-established and significant effect of temperature on Mn deposition (see laboratory experiments later). However, because more experimental work is required to improve our understanding of  $^{54}\text{Mn}$  behaviour it is necessary, for present purposes, to use effective liquid phase mass transfer coefficients which correspond to practical observations.

## 2.3 Assessment of Radionuclide Transport in LMFBR's

In order to obtain estimates of deposited radioactivity on critical components such as IHX's and pumps Tanner(8) has assumed that the primary circuit contains a well mixed volume of sodium (V) bounded by areas  $A_1$ ,  $A_2$ ,  $A_3$  etc, associated with local mass transfer coefficients  $K_1$ ,  $K_2$ ,  $K_3$  etc, determined by flow, geometry and sodium properties. Material is introduced

at a constant rate  $R$  and decays with a time constant  $\lambda$ . The steady uniform concentration in sodium is  $M/V$  where  $R = M(\lambda + \frac{\Sigma AK}{V})$ . It is easily shown that  $\lambda \ll \frac{\Sigma AK}{V}$  hence the concentration is  $R/\Sigma AK$ . The deposition rate at the  $i$ th surface is therefore  $RK/\Sigma AK$  per unit area per unit time. The model assumes a constant concentration of released material and therefore does not consider the possibility of concentrations changing in series and parallel flow arrangements due to desaturation or down stream effects. Modifications have been suggested to accommodate situations where sidestreams and changing concentrations exist in reactor plant. However this type of model has not been fully developed and for computational purposes transport to surface is considered to be governed by local mass transfer coefficients which are calculated from the well known mass-transfer relationship:

$$K^1 = 0.023 \cdot \frac{D}{d} \cdot (Re)^{0.8} (Sc)^{0.4} \quad (7)$$

where  $D$  is the diffusion coefficient of the species in sodium (generally taken to be the self-diffusion coefficient)

$d$  is the hydraulic diameter

$Re$  is Reynolds number

$Sc$  is Schmidt number

Computer assisted calculation of activity levels on PFR primary circuit components, in particular the intermediate heat exchangers have been undertaken by the UKAEA and CEGB. The main stages of the calculations are as follows; a calculation of the rate of production  $R$  of each nuclide, a calculation of recession velocities as a function of temperature and oxygen content or saturation temperature, a determination of the volumetric release rates by multiplying the above by the appropriate areas, assumptions on the enhancement/retention factors for  $^{54}\text{Mn}$ ,  $^{60}\text{Co}$  and  $^{58}\text{Co}$  and thence the equilibrium activity release rates, a calculation of the average activity release rate which depends on the residence time of the fuel, and identification of the areas for deposition and a definition of the appropriate mass transfer coefficients for each area, and finally a calculation of the activity of each nuclide on the component of interest. Fig 2 summarises the results of typical calculations.

#### 2.4 Factors Which Can Effect Model Predictions

Although current models assume that corroded material is first dissolved by high temperature sodium and then transported to the cooler parts of the system some consideration is still being given to the possibility that in certain parts of the fuel pin or in positions downstream of the core, material could be removed from the component surface in the form of particulates due to oxidation of the steel surface. Information from test loops (see later) has identified for example that such processes can occur just down-stream of the high temperature part of the loop system where the sodium is sufficiently saturated, with respect to nickel, to prevent the well known gamma to alpha iron transformation (ferrite layer formation). Under these conditions it seems the material is more susceptible to internal oxidation especially in regions where the chemical activity of oxygen in sodium starts to increase as the temperature decreases.

In terms of modelling the behaviour of these particles it seems their deposition behaviour can best be described as being controlled by inertial projection through a viscous sub-layer (particle dynamics) rather than by turbulent diffusion. Models which describe this type of behaviour are available; see reference 8 and 9. Also more detailed information concerning

the diffusion behaviour of particles in fluid streams and their resuspension when flow rates provide shear stress values greater than the combined aerodynamic forces, gravity and intermolecular adhesive forces is provided in UK refs 10 to 14.

Thus particles entering the sodium stream from oxidised or damaged surfaces outside the core could pass through the core to become activated. Once activated these particles, depending on their size, will deposit at certain critical velocities in different parts of the system to form layers of deposited material whose final thickness will be dependent upon their mechanical stability in flowing sodium. On the other hand if re-suspension of particles occurs then secondary particles (still radioactive) can deposit in other areas of the plant. Also if the resuspended material contains more than one particle then its terminal velocity may prevent it circulating in the system, especially when it enters slow flow regions of the reactor such as below the diagrid. Under these circumstances particle suspensions containing active material could be present below the core, especially in pool-type systems.

### 3. BEHAVIOUR OF FISSION PRODUCTS AND FISSIONABLE MATERIAL

According to Potter (15) fuel clad failures in normal operation of a reactor can be essentially described in three groups according to their size:

1. Small pin-hole failures with no ingress of sodium. Such failures may result in the release of gaseous and volatile fission products.
2. Larger holes which allow sodium to enter the free volume within a fuel pin but with little exchange of sodium except during transients of temperature and power. Some fission products will dissolve in sodium and be released relatively slowly to the primary circuit by diffusion to the breach and then through it into the circuit. Reactions between sodium and the fuel and breeder will take place and the amount of oxygen in the sodium which logs a pin may be reduced by these reactions, and
3. Larger holes and splits through which the coolant may freely pass. Sodium/fuel reactions will occur with products entering the sodium as particulate material, releasing non-soluble fission products as well as those in (1) and (2) above.

The potentially hazardous fission products released from failed fuel may be classified according to the way in which they escape and interact with sodium.

- |    |   |                                     |            |
|----|---|-------------------------------------|------------|
| 1) | Noble gases; Kr, Xe   | )                                   |            |
| 2) | Cs, Rb  | ) Soluble                           | ) Volatile |
| 3) | I, Te, Sb, Sn, Ag.  | ) Limited solubility.)              |            |
| 4) | Ba, Sr.   | ) Soluble but stable oxide formers. |            |
| 5) | Other fission products; lanthanides, Zr, Nb, Ru, Mo and fuel; |                                     |            |
|    | very low solubilities and released probably as particles.     |                                     |            |

Current UK views on how these various elements may behave in sodium circuits are summarised as follows:

Caesium 137/134/136

$^{137}\text{Cs}$  is not a gamma emitter: it is accompanied by  $^{137}\text{mBa}$  which is. Because of the long half life of  $^{137}\text{Cs}$  (30 years),  $^{137}\text{mBa}$  is always present once caesium has been released from failed fuel. The build up towards equilibrium in the fuel is slow and after one year (the average residence time for fuel) the  $^{137}\text{Cs}$  inventory is 2.25% of the equilibrium value. In the event of pin failure and if a 4-batch fuel management scheme is used then this amount of  $^{137}\text{Cs}$  is released four times per calendar year (ie fractional release for each batch is 100% and release is assumed to occur at a uniform smoothed rate). Build up in the primary circuit is slow: surface concentrations remain in equilibrium with the bulk sodium concentration and are related to the local surface to volume partition coefficient,  $K$ , for the area increment  $A$ . For modelling the time of first fuel failure is arbitrarily set at 9 months after first full power operation. Hot core surfaces are not considered to be sinks for caesium. Additional sources of radioactivity also arise from the presence of  $^{134}\text{Cs}$  and  $^{136}\text{Cs}$  which have half lives of 2.07 years and 13 days respectively(16). The distribution of these isotopes in the primary circuits of LMFBR's is assumed to follow the same pattern as  $^{137}\text{Cs}$ .

As regards Cs behaviour in sodium systems thermodynamic arguments indicate that Cs should be present in sodium as the metal rather than as the oxide or halide salts. Caesium and sodium are miscible in all proportions at temperatures of interest. Caesium distributes between steel surfaces and sodium in a manner which depends fairly strongly on temperature and, supposedly, on surface condition. The apparent distribution coefficient ( $K^1$ , cm) can be as large as unity at 330°C (fig 3) and this would imply that about 97% of caesium could remain in the primary sodium. This in turn would leave caesium activities contributing about 10% of the surface gamma dose from major components. Variation in the oxygen level in sodium is not thought to affect caesium distribution behaviour at interfaces, but caesium, contrary to more recent UK observation (see later), is thought to be retained on sodium oxide surfaces in cold traps. Cold trap operation could, therefore, influence the amount of caesium available for distribution at surfaces.

The technical problems with caesium arise from the further observations that it may diffuse into steels and that it is strongly retained on graphite and charcoal. In addition there is speculation that Cs could concentrate in a sodium boundary layer adjacent to the interface rather than as a discrete Cs phase at the interface.

The very wide range of caesium partition coefficients reported in the literature and referred to in Fig 3 indicates a confused state of affairs although there seems to be clear evidence that the overall partition has a negative temperature coefficient. A change in temperature from 150 to 550°C generally reduces  $K$ , the ratio of surface concentration to concentration in bulk sodium, by an order of magnitude(17)(18). However there are variations in slope which could be attributed to changes in the condition of the steel surface.

### Iodine 131

Iodine 131 is a short-lived soluble fission product (half-life 8 days), whose equilibrium is rapidly attained in fuel and it is assumed that once core equilibrium is established there is continuous release to primary sodium at a rate, equivalent to an iodine release fraction of unity. This assumption probably holds even as early as the end of the first full power year. Similarly, it can be expected that a rapid approach to equilibrium will occur in primary sodium and on surfaces exposed to sodium. It is assumed however

that hot core surfaces, ie fuel cladding and wrappers above the level of the top of the lower axial breeder, are not sinks for iodine as these surfaces are corroding at a significant rate. Iodine is thus distributed between the remaining surfaces and primary sodium: provided that its concentration in sodium is everywhere below saturation the local surface concentrations will be proportional to  $K$  (cm), the local surface/volume partition coefficient.

Measurements of  $K$  for iodine have been reported by Allan (19) and Shimojima (20). Both studies showed a strong temperature dependence with  $K$  at reactor pool temperatures about 30 times greater than at the core mean outlet temperature. Allan's data Ref 19 also gives iodine (as sodium iodide) solubility data in sodium. At cold trap temperature (160°C) the solubility is  $9.6 \times 10^{-3}$  ppm: at 140°C,  $2.9 \times 10^{-3}$  ppm: at 120°C,  $7.7 \times 10^{-4}$  ppm. It is at least possible therefore that enough iodine will be present in primary circuits to cause FP iodine, as and when it appears, to distribute between the primary cold trap and the rest of the circuit. Therefore, calculation of surface iodine 131 concentrations using Allan's partition data and ignoring possible precipitation in the cold trap is likely to yield maximum estimates. Some iodine 131 will be retained in the cold trap by partition between steel mesh surfaces, existing deposits and sodium, although this process could be affected by sodium oxide deposition on cold surfaces and trapping efficiency.

#### Tellurium 132

This short-lived soluble fission product is accompanied by I 132 which is a strong gamma emitter with a half life of 78 hours. Equilibrium in fuel is rapidly attained and it is assumed that there is continuous release to sodium of 100%. Tellurium is considerably more soluble than iodine in sodium (21). Like iodine therefore its distribution in the primary circuit will depend on local values of the surface to volume partition coefficient. Hot core surfaces are again excluded as sinks. Some values for  $K$  have been derived by Shimojima (20) and these are used in UK estimates although there is considerably more scatter in these data than for iodine, measured in the same loop. Some Te activity would be expected to partition between cold steel mesh surfaces and sodium, provided these surfaces are not masked by sodium oxide.

#### Zirconium/Niobium 95

This fission product pair has half lives (64 days, 35 days) which ensure that the inventory in fuel is almost at equilibrium at one year. The fractional release from failed pins is taken to be 1%. Given the half lives above, the equilibrium inventory in primary sodium would in any case be established virtually within the first year of operation with failed fuel because processes removing Zr/Nb to surfaces, as well as decay, serve to accelerate the approach to equilibrium.

The Zr/Nb pair are supposed to be present in sodium as highly insoluble oxides and hence the partition coefficient procedure used for iodine, tellurium and caesium cannot be used to determine the overall distribution between sodium and surfaces. It is a common observation, however, that Zr/Nb deposit preferentially on surfaces: one possible model, depending on particle size, to account for this behaviour would use a mass transfer coefficient  $K'$  (based on the Chiltern-Colburn heat and mass transfer analogy) to determine transport to the sodium/steel interface, where Zr/Nb is thereafter supposed to be irreversibly bound.

#### Barium-Lanthanum 140



This fission product pair is treated in almost exactly the same manner as Zr/Nb95. It is included because of the high gamma energy of La140 and the high chain yield for mass number 140. Fractional release from failed pins of peak rating is taken to be 1%. Ba and La are supposed to be present in primary sodium as insoluble oxides and their transport to surfaces is held to be governed by local mass transfer coefficients. However, it is postulated that Ba/La is preferentially retained when it arrives at cold surfaces and that there is a reduced sticking probability on hot surfaces. For calculational purposes this is equivalent to a reduction in the local mass transfer coefficient. At intermediate temperatures smoothed coefficients are chosen. The effect of this adjustment is to reduce the quantity  $\Sigma AK^1$  but, this has comparatively little effect on the calculation of deposition on cold surfaces.

As with Zr/Nb activity, the concentration of Ba/La remaining in sodium is small. The inventory of Ba/La140 is thus entirely distributed over surfaces.

#### 4. DATA FROM EXPERIMENTAL PROGRAMMES

##### 4.1 Non-active Studies

Corrosion. The corrosion behaviour of fuel element cladding materials in liquid sodium has largely been studied in out-of-pile loops at RNL Risley. Design equations are now available for the UK choice of fuel cladding, which is Type M316 stainless steel, and also for materials of similar composition. These equations relate the corrosion rate of the material to sodium temperature, oxygen level, sodium velocity or Re No, time and position in the isothermal zone of the loop(22). It is concluded from these and other studies(23) that under steady state operating conditions corrosion is only important in terms of release of material but not in its effect on mechanical properties. Fuel element performance in PFR will establish whether these conclusions are correct.

Corrosion data obtained, in different types of loop arrangement and the Large Mass Transfer Loop(24) since the Dimitrovgrad meeting, have now tended to confirm the earlier corrosion values obtained in small loops with single holder geometries (see Ref 25). The effect of temperature on the corrosion rate of stainless steel for example is in broad agreement in all loop systems irrespective of specimen arrangement as long as comparisons are made in that part of the circuit where the temperature is increasing. Also the presence of heat flux in the corrosion test section of the LMT Loop does not appear to significantly affect the corrosion rate of the steels as long as metal temperature and not sodium temperature is used in the estimates of corrosion loss. It has been found, however, that corrosion losses extend beyond the core section of the loop and it is felt that components such as the neutron shield rods will make a contribution to the burden of corrosion products in reactor plant. (See Fig 4 for details of corrosion effects).

Overall we find the oxygen impurity level in the sodium remains one of the critical factors in controlling the rate of bulk release of both austenitic and ferritic steel into flowing sodium environments and depending upon the level it is possible to change from intergranular type corrosion at high levels to straight forward dissolution of alloying elements at low levels.

In many respects these extremes of corrosion behaviour plus the possibility that at intermediate oxygen levels (say 7-30 ppm) a mixture of the two processes may occur still makes it difficult to present a unified model to describe the corrosion behaviour of stainless steel in liquid sodium. The

problem is also exacerbated by the fact that although better data for the solubility of iron in sodium have been provided by AERE (see later) the values are too high to support current UK models for the corrosion of iron in sodium (26) unless the sodium is extremely saturated with iron before it enters the test section. Nevertheless the values obtained, coupled with the strong dependency of iron corrosion rates on oxygen level(27), suggest that some intermediate step, based on the formation of a solvated complex, may be rate-controlling at the iron-sodium interface(27). This possibility requires further study.

In terms of present and future designs of LMFBRs it can be argued that the effect of oxygen level per se on corrosion behaviour in the hot parts of the fuel cladding becomes less of a problem because of the large inventories of sodium used and the concomitant lower oxygen potentials in these systems. Under these conditions dissolution processes may start to predominate and it is for this reason our current programme is putting more emphasis on the mass transfer behaviour of steel materials in very low oxygen (1-3ppm) sodium environments.

Deposition. In the UK studies are in hand at AERE and RNL to establish a suitable model which best describes the deposition processes which may occur in LMFBRs. It has already been established that particle size plays a major role in the deposition behaviour of corroded material released from surfaces down stream of the corrosion zone in pumped sodium loops(28)(24)(29), and depending on size, transport of material to the wall of a conduit may be controlled in the liquid phase by precipitation, diffusion, turbulent eddies providing sufficient angular momentum to particles or gravity settling. Once the species reach the wall it is tentatively assumed (although the point is still under investigation), that in most instances sticking probabilities are high (~ unity) and that particles are not subject to bounce or lift-off which can be a feature of deposit behaviour in certain gaseous environments.

Experimental work so far undertaken at RNL to determine deposition coefficients from weight change values for corroded material deposited in both the small loops and the large mass transfer loop has identified that the bulk of the corrosion products deposited in the cooler parts of the small test loops are primarily steel particles which have been removed from oxidised surfaces in the hot parts of the test loop. The size (~ 2 $\mu$ m) and composition of the particles are consistent for example with the size and composition of the corroded material from these positions. For further details see Refs (24), (30), and Figs 4 and 5. Also examination of specimens removed from the deposition part of the large mass transfer loop shows that the weight gains observed in the IHX region are a combined effect of surface oxidation and the deposition of small particles which vary in size (average size 1-2 $\mu$ m). The composition of the particles also varies and depending upon the period of exposure, the composition can range from particles rich in nickel and manganese to particles which have high iron and chromium contents (see Ref 23).

Deposition coefficients obtained for the deposited materials are illustrated in Fig 6, where it is seen that the deposition behaviour in the two different loop geometries is more consistent with momentum controlled particle transport than say mass-transport in the liquid phase. The apparent temperature dependence for the deposition of Ni-Mn particles(24) is of interest and more work is being directed towards establishing whether or not this material forms by precipitation in the cooler parts of the loop.

#### 4.2 Radioactive Studies

### Corrosion and Deposition Studies in the Harwell Active Mass Transfer Loop

The Harwell Active Mass Transfer Loop (AMTL)(fig 7) has been used to study the problem of corrosion of steels in the high temperature high velocity sodium regions of the loop (up to 600°C and 6m/sec respectively), followed by deposition of corrosion products in lower temperature, lower velocity regions. The loop has the facility for using radioactive tracers, e.g.  $^{60}\text{Co}$ ,  $^{58}\text{Co}$ ,  $^{59}\text{Fe}$ ,  $^{54}\text{Mn}$ ,  $^{51}\text{Cr}$ , to provide valuable insight into the mechanism of deposition of species, as well as the transport and distribution of various species round the loop.

Since the Dimitrovgrad meeting experiments to measure the release and deposition of corrosion products from an irradiated steel specimen exposed in a high temperature sodium loop have been reported at the 1980 Richland and 1984 Oxford Conferences (29)(31). In the first series of tests nickel, stainless steel and pure iron specimens were placed on either side of the source to obtain data on corrosion rates and activity deposition. The tubular specimens were exposed to sodium flowing at 6m/sec and 585°C and downstream the sodium was cooled to 370°C by passage through a 7m long simulated heat exchanger tube in which deposition occurred.

Deposition ( $^{54}\text{Mn}$  and  $^{60}\text{Co}$ ) on the nickel specimen upstream of the irradiated source was of the order of 100 times that on the adjacent steel specimen. The measured corrosion rates of the stainless steel specimens over the 2287 hour run agreed well with the RNL corrosion data. Counting of the irradiated specimens showed that  $^{54}\text{Mn}$  removal was hyperstoichiometric and  $^{60}\text{Co}$  sub-stoichiometric with selective release factors of 1.34 and 0.95 respectively, and a very high affinity was shown by the released  $^{54}\text{Mn}$  for the nickel specimens.

Analysis of the deposition patterns of  $^{60}\text{Co}$  and  $^{58}\text{Co}$  along the heat exchanger showed that Co deposition was governed by its mass transfer rate through the flowing sodium layer. The downstream dependence yielded a value for the diffusivity of cobalt in sodium of  $3 \times 10^{-4} \text{ cm}^2 \text{ s}^{-1}$  at the mean temperature of 478°C. The  $^{54}\text{Mn}$  deposition increased by approximately a factor of 14 down the length of the heat exchanger (fig 8).

In the second series of tests several SS tubular specimens of 6.4mm bore were placed in a test section for a period of 2756 hrs through which sodium flowed at 585°C and 6.1 m/s. The central specimen was irradiated and released radioisotopes, notably  $^{60}\text{Co}$ ,  $^{58}\text{Co}$  and  $^{54}\text{Mn}$ , into the sodium. These isotopes, and other inactive corrosion products, were again deposited immediately following the test section on the 7m long, single pipe, air cooled heat exchanger of 17.2mm bore in which the sodium was cooled to 370°C.

The Mn and Co isotope deposition patterns were quite different. The Co deposited preferentially on hot, corroding, surfaces immediately following the irradiated specimen; while  $^{54}\text{Mn}$  deposited preferentially on the colder regions of the heat exchanger. Analysis of the Co deposition pattern confirmed earlier work (ref 29) showing that deposition was controlled by mass transfer through the flowing sodium boundary layer, the mass transfer coefficient being calculable from standard correlations (fig 9). From this result it was shown possible to predict the Co deposition round the loop. The  $^{54}\text{Mn}$  deposition pattern supported the theory of Polley and Skyrme (ref 1) which suggests that the ratio of adsorption to desorption rates at the sodium/metal interface (which is dependent on temperature) governs  $^{54}\text{Mn}$  deposition. The measured stainless steel specimen corrosion rates again

agreed reasonably with the predictive equation of Thorley (ref 32) based on RNL data.

### Studies Using the Small Active Loop at RNL Risley

Deposition experiments are being carried out at RNL Risley in a small pumped sodium loop (fig 10) using irradiated specimens of pure iron as a source of activated corrosion products;  $^{59}\text{Fe}$  and  $^{54}\text{Mn}$ . Initially the loop was operated with a  $T$  of  $450^\circ\text{C}$  at which temperature minimal dissolution would be expected. Nevertheless appreciable deposition of  $^{54}\text{Mn}$  and  $^{59}\text{Fe}$  was observed at the entrance to the heat exchanger within 24 hrs suggesting mechanical removal from the source.  $T$  was subsequently raised to  $650^\circ\text{C}$  and the loop ran for 97 days with a  $\Delta T$  of  $95^\circ\text{C}$ . Maximum deposition of  $^{59}\text{Fe}$  occurred at the inlet to the deposition tube, whereas  $^{54}\text{Mn}$  deposition peaked about one quarter of the way down the tube and then fell continuously to approximately one half of the maximum at the outlet, figs 11 and 12. Deposition of  $^{59}\text{Fe}$  at any particular point in the heat exchanger increased linearly with time whereas  $^{54}\text{Mn}$  deposition increased only parabolically with time, suggesting possible solid state supply limitations at source or alternatively a balance between deposition and release processes. In the second run the sodium velocity in the deposition tube was increased from 0.43 to 0.63m/sec and the temperature gradient reduced to approximately  $35^\circ\text{C}$ . It was found that although the time dependent behaviour of both  $^{59}\text{Fe}$  and  $^{54}\text{Mn}$  was similar to the first test, in the second test the initially observed peak of  $^{54}\text{Mn}$  one quarter of the way down the deposition tube was not observed. The build-up of the manganese isotope increased approximately linearly in the downstream direction with a sharp cut-off at the exit of the tube.

Estimates of the deposition constant for  $^{59}\text{Fe}$  for the first run are in reasonable agreement with mass transfer coefficients obtained from Sherwood and downstream correlations. The deposition of  $^{54}\text{Mn}$  does not seem to fit a diffusion controlled process and some other process is thought to be affecting its movement to the wall of the deposition tube during the initial stages of the experiment. A mass balance of the corroded and deposited species also indicated that the  $^{59}\text{Fe}$  was, within the limits of measurement, approximately in balance whereas the amount of deposited  $^{54}\text{Mn}$  was in excess. This latter observation is consistent with  $^{54}\text{Mn}$  behaviour identified in other loop systems and further supports the view that its release is hyperstoichiometric from steel surfaces. It is also interesting to record that when the minimum temperature of the main circuit was changed to different positions along the deposition tube the  $^{54}\text{Mn}$  deposition profile followed this change (fig 13), although the cold trap in the circuit was also attracting the Mn.

More recent work on the small active loop has concentrated upon investigating the efficiency of  $^{54}\text{Mn}$  removal from the sodium using nickel foil and filter assemblies. The filtration experiments, using filters made from stainless steel, molybdenum and tantalum which were also used to try and collect products for subsequent examination, were unsuccessful and it was noticed that with filters placed just up-stream of the specimens that the deposition profiles for the two isotopes were identical to profiles obtained in the absence of filters. The insertion of nickel into the loop sodium, which had a measured Mn content of ~2ppm, however provided an excellent sink for  $^{54}\text{Mn}$  and it was established by changing the velocity of the sodium that the rate of take up of  $^{54}\text{Mn}$  by the nickel appeared to be diffusion controlled in the liquid phase (fig 14).

In the current series of tests which use irradiated stainless steel specimens with pre-formed ferrite layers on their surfaces the intention is to establish whether the mass-transfer behaviour of  $^{59}\text{Fe}$  and  $^{54}\text{Mn}$  follows a similar pattern to that already observed for pure iron specimens. So far preliminary results indicate that the deposition behaviour of material removed from this type of surface is different see ref 33. Further tests are in hand, at controlled oxygen levels, to confirm these initial findings.

#### Studies to improve our understanding of Cs behaviour in LMFBR's

Since the earlier BNL work by Evans and Watson(18) and Watson and Gwyther(34); Hooper(BNL) has shown that Cs tends to migrate to the cooler parts of a small loop system and that the migratory process may be associated with the presence of sodium chromite on the steel surfaces. In his experiments Hooper(35) also noted that Cs starts to de-sorb in certain temperature regions due to possible break-down of the oxide as the oxygen level was progressively lowered in the sodium. The main conclusions arising from his experiments were:

Reversible adsorption occurs at Type 316 steel surfaces up to 563°K.

Adsorption becomes negligible with time at temperatures > 563°K.

No preferential adsorption occurred on  $\text{Na}_2\text{O}$  surfaces in the cold trap.

No obvious attraction to carbides in the surface of the steel.

Adsorption coefficient  $K \frac{\mu\text{ci cm}^{-3}}{\mu\text{ci cm}^{-3} \text{ sodium}}$  steel surfaces is  $\log K = -3.3 + \frac{1270}{T}$  (8)

for the temperatures in the range 373 to 563°K.

More recently it has also been found that when 17ppm of  $^{134}\text{Cs}$  was added to the sodium in the Harwell AMTL, this level reduced to approx 10 ppm when the loop was operated with a  $\Delta T$  of 370 to ~600°C for 4000 hrs. Subsequent inspection of the internals of the loop to establish where the Cs had deposited revealed very little Cs on the pipework. Some Cs was found in the cold-trap while the majority was associated with a particulate sludge which had collected in the quiescent regions of the dump tank. Current views are that the Cs plus the particles may have come from corroded surfaces initially covered with sodium chromite. Preliminary values recorded for 'K' on the isothermal return leg of the loop were of the order of 0.003-0.005 for a temperature of 370°C.

Because of the large differences which exist for the partition coefficient, K (fig 3), it has now been decided to use the Harwell AMTL to investigate Cs behaviour in a pumped sodium loop under more realistic conditions.

Consequently an investigation is to be undertaken at AERE to establish the degree of partitioning which occurs between liquid sodium and vapour environments when the sodium is circulated in the Harwell Mass Transfer loop under conditions typical of those anticipated in FBR's. The study will involve experiments to investigate the mass transport of radioactive Cs from a hot sodium pool to the cover gas, as well as its deposition behaviour in various parts of the sodium circuit. Briefly the aim will be to provide mass transport rates as a function of temperature difference between the sodium pool and the cooled roof. The effects of disturbed pool surfaces (roughened surfaces) and gas bubble disentrainment on transport rates will also be investigated. Heat transfer rates through the cooled roof will also be measured using heat flux meters installed in appropriate positions. Details of the type of facility to be used in these studies are illustrated in figs 7 and 15.

Finally it is to be noted that measurements of Zn 65 behaviour have also been undertaken in the AMTL. This work and the non-active zinc studies undertaken at RNL were reported at the IAEA Cover-gas meeting held in Richland, Washington last year.

### Fissile Material

The basic aims of the fissile material programme at AERE are to provide both fundamental and technological data concerning fuel-sodium reactions. The specialist paper provided for this conference describes the experimental studies and modelling of the phase equilibria, thermodynamic characteristics and morphologies of the reactions between liquid sodium and the relevant fuel and breeder materials; urania, urania-plutonia solid solutions with and without the presence of fission product elements.

The paper also highlights that the degree of any contamination of the primary circuit with fuel and fission product elements will depend on the extent of the chemical reactions and on the nature of the rupture of the cladding. There will be a concentration of fission product elements in the gap between fuel and cladding; the amount of these elements and their chemical constitution will depend upon the extent and history of the irradiation of the fuel. Among the phases which could be found in the gap are those based on chromates, uranoplutonates, tellurides and the iodide of caesium and it is considered that it is the constitution of the gap and the reactions of the phases with sodium which allow the release of caesium, tellurium and iodine into the primary circuit. The calculations of chemical equilibria involving these multicomponent phase systems have been carried out using the computer programme SOLGASMIX to obtain the minimum total Gibbs energy for the system.

The increase in volume of fuel when sodium uranoplutonate phases are formed together with the effects of the variation with temperature of the threshold plutonium valency of the urania-plutonia solid solution could result in contamination of the primary circuit with fuel material in particulate form. Some laboratory studies on this aspect of fuel failure are also described.

In the final part the paper deals with the published observations on the chemical aspects of failed fuel and show that the understanding of the systems which we have discussed in the paper can be used to interpret observations made in post irradiation examinations and to develop a model which will describe and predict the chemical consequences of the failure of fuel and breeder pins during operation in a reactor and in storage.

### Solubility Measurements

In support of the mass-transfer programme solubility determinations on metals of direct interest to current models have been undertaken by Thompson at AERE(36)(37)(38). The solubility behaviour of iron in sodium-oxygen solutions has been studied, using a sealed capsule equilibration technique and the radiochemical tracer <sup>59</sup>Fe. The recommended expression obtained is of the form:

$$\log S(\text{Fe}) \mu\text{g/g}_{\text{Na}} = 4.808 \pm 1.064 - \frac{4185 \pm 425}{T} \quad (9)$$

T is temperature in °K

The results also showed that oxygen had only a small effect on iron solubility below ~10% of the oxygen concentration at a particular temperature.

The solubility of cobalt has been studied in the temperature range 400-700°C to provide an expression:

$$\log_{10} S(\text{Co}) \mu\text{g/g}_{\text{Na}} = 0.010 - \frac{1493}{T} \quad (10)$$

T is the temperature in °K.

Finally the solubility of manganese in sodium has been determined using alumina crucibles contained in nickel cans. The following expression was determined over the temperature range 350-750°C.

$$\log S(\mu\text{g/gm}_{\text{Na}}) = 2.325 - \frac{2017}{T} \quad (11)$$

In these experiments the presence of oxygen in sodium was found to increase the amount of Mn in solution at both 450 and 650°C.

### In-reactor Measurements

#### Monitoring for Activated Corrosion Products and Fission Products

When the reactor is at power, ( $n\gamma$ ) reactions in the sodium generate an equilibrium activity of 20mCi  $^{24}\text{Na}$  per gram of sodium leading to gamma dose rates of up to  $2 \times 10^5$  rads per hour. However, the 15 hour half life of  $^{24}\text{Na}$  means that one week after shut down the measurement of  $\gamma$  dose rates of reactor components in situ is feasible provided a suitable dosimeter operating at 250°C is available. Voice(39) has applied high temperature thermoluminescence for this purpose and the latest results obtained using this technique are described in a specialists paper to this meeting.

Periodic sampling of the primary sodium has also allowed estimates to be made of a range of important isotopes. In particular the increase in Cs137 and Cs134 levels as a result of fuel failures has been assessed. Sodium phase fission product and activated corrosion product analyses coupled with the above Thermoluminescence Dosimetry of the IHXs and primary cold trap and gamma spectroscopy in the reactor vault are also providing a better understanding of the behaviour of radioactive constituents in these parts of the reactor system. Results from these measurements are included in the paper.

Gaseous fission products, in particular Xe133 and 135 continue to be monitored in PFR on a continuous basis by gamma spectroscopy as part of the reactor failed fuel detection systems. The installed equipment has operated satisfactorily and has allowed the successful early detection of failures since the first failure event in October 1978. The installed delayed neutron monitoring system on the IHXs and the failed fuel delayed neutron location system have also behaved satisfactorily and have provided valuable data on failure progression.

#### Tritium Measurements

The sustained full power operation of PFR over the past few years has allowed a more detailed study of tritium transport within the reactor system than was previously possible. This has been aided by the commissioning of an on-line tritium monitor on the primary circuit adapted for use from the installed

Harwell Carbon Meter iron membrane. The meter uses a 5% Hydrogen in argon sweep gas and tritium is determined using a proportional counter. Routine monitoring on the secondary sodium circuit is still not possible but occasional measurements have been made using the installed under sodium hydrogen detection system in which the normal argon sweep gas has been replaced by a 5% hydrogen in argon mixture. It is hoped to commission an on line meter on the secondary cold trap loop (SCTL) before the middle of 1987. This will be based on a spare Harwell Carbon Meter membrane currently installed on the SCTL. Tritium continues to be routinely monitored in the reactor hall, turbine hall and steam generating hall using water bubblers and the liquid scintillation counting. In addition steam drum water is monitored by the same technique. Measurements have also been made of the tritium inventory of a number of cold trap baskets and estimates have been made of tritium levels in the primary circuit argon gas blanket and the decay heat removal NaK loops.

With regard to tritium transport models the mechanisms and methods used in current models are broadly accepted and the data accumulated to date on the PFR is being used to empirically validate various aspects of the models. In particular work is directed at evaluating the tritium source term for PFR, assessing permeation coefficients for tritium in the Intermediate Heat Exchangers and Decay Heat Removal Loops and the evaluation of tritium cold trapping rates. Preliminary estimates suggest that the tritium source term for PFR is 10-11.6 Ci per effective full power day operation (efpd) although this figure may be revised in the light of current work to obtain better estimates of cold trapping rates, losses to decay heat removal loops and losses to the primary circuit argon gas blanket. When allowance is made for tritium production in control rods and lithium and boron impurities in steel and sodium it is estimated that between 9.5 and 11.1 Ci/efpd are produced by ternary fission, assuming a 10% release of tritium from control rods. This suggests a ternary fission yield of  $1.2-1.4 \times 10^{-4}$ .

The estimate of ternary fission yield from PFR is at the lower end of the range of literature estimates for fast fission of Pu239 ( $1.4-2.5 \times 10^{-4}$ ). The fact that literature estimates are based on U235 experimental fission data (fast fission of U235 yields about 2.5 times more tritium than thermal fission and this factor has been applied to experimental thermal Pu239 values) has prompted the suggestion that experimental measurements on Pu239 should be made in the UK in the near future.

Work is currently in progress at PFR on the estimation of tritium permeation coefficients for the IHXs. This has involved monitoring increases in secondary circuit tritium levels, following cold trapping, with approximately constant tritium levels in the primary circuit.

#### Assessment of Particulate Behaviour

Because the sodium in the primary circuit of PFR is continuously transferred from and to the pool, it might be imagined that this arrangement would form an effective particle trap. However, about 15% of the sodium flow from each IHX is directed to the bottom of the pool to cool the structure in this region, with the result that considerable mixing of the sodium takes place. As the associated fluid velocities are of the order of 5mm/sec, only iron particles with a diameter of  $> 50\mu$  will, in theory, sediment out during operation, although during shutdown considerable settlement may well occur.

Other areas where deposition of material may occur in the reactor are the inlets to the diagrid, fuel element channels and the intermediate heat



exchanger where the deposition of corrosion products generated in the core may conceivably affect the hydraulic resistance and heat transfer coefficient. Consequently, in order to provide some guidance on the effects of material transport in the PFR primary circuit, facilities have been provided to extract both materials and coolant samples from various parts of the circuit. Also crud filters with mesh sizes 60 to 100 mesh have been removed after the early power runs and are awaiting examination. A fourth unit which was inserted some time later will be removed after some appropriate period of exposure to the coolant.

## SUMMARY AND CONCLUSIONS

### Corrosion of Fuel Element Cladding

Corrosion of stainless steel fuel cladding by sodium has largely been studied in out of pile loops at Risley. It is believed that this phenomenon is reasonably well understood, and under normal operational conditions corrosion is important only in its release of corrosion products to the primary circuit and not in its effect on the mechanical properties of the cladding. Confirmation of this view will be obtained from PFR. An experiment to study clad corrosion in PFR is also under consideration. Source term data for alternative fuel cladding, such as the nickel alloys, are not so comprehensive and therefore more work is required to produce improved design equations for these materials.

### Release and Deposition of Corrosion Products

The processes by which the corrosion products are released and deposited in the primary circuit have been modelled as well as studied in a number of sodium loops, both active and inactive, at Harwell and Risley.

The empirical data obtained from these studies and results from PFR must eventually be extrapolated to demonstration reactor circuits, which may have a different configuration and operating conditions. The mass transfer processes are complex however, and more information is required from working reactors to support our understanding of these processes so that extrapolations can be made with some degree of confidence.

### The Deposition of Fuel and Fission Products

Fuel and fission products released from the fuel pins could remain suspended or dissolved in the coolant, plate out as solids on component surfaces, precipitate or settle out in for example the cold traps or low flow regions of the circuit, be released to the covergas, or transported through the cover gas to other surfaces. Earlier analysis of the DFR cold trap residues provided useful guidance and suggested that the fuel and those fission products which are strong oxide formers remains in suspension and that most of the caesium remains in solution in the circuit. It is expected that further valuable information will be obtained when DFR is decommissioned but this will be qualitative as the DFR circuit differs substantially from those of PFR and future designs. Extended data will be sought from the PFR cold trap, and from a variety of monitoring specimens in the PFR circuit which will eventually be removed and analysed for deposited activity.

Studies of caesium adsorption onto steel have been made, and although the 'plate-out' phenomenon is poorly understood, it is expected on current assumptions for a reference design of reactor eg 100% release that caesium plate-out may be more important compared with the other fission products by

virtue of its relatively higher release rate from fuel pins, and its long half-life. Quantitative calculations suggest however that the circuit activity arising from clad corrosion products will be greater than that provided by fission products released from say 1% of failed fuel pins.

The higher vapour pressure of caesium relative to sodium also suggests that it may concentrate in the vapour phase above the liquid sodium. Therefore, any engineering problems associated with the deposition of 'sodium frost', may be aggravated if the frost includes active caesium. Work programmed at AERE on the AMTL to research in more detail Cs behaviour in liquid sodium and cover gas environments will improve the understanding in this area. Also the studies of the thermodynamics and kinetics of fuel-coolant interactions in flowing sodium environments will provide more realistic release data for fuel pin failure situations.

Specific factors concerning corrosion and fission product behaviour which are considered to require further consideration are as follows:

#### Corrosion Products

Manganese. The assumptions underlying the source term for manganese are considered to be well established and include a factor for enhancement by diffusion. However the chemical and physical forms of manganese following release are obscure. If manganese is associated with particulate material in sodium then its deposition behaviour will depend on particle size which in turn depends on factors other than the form of manganese at the moment of its release. Manganese deposition has been estimated by considering local mass transfer coefficients and assuming complete retention at surfaces in the cooler parts of the circuit. A major factor influencing deposition appears to be temperature and it is a convenience for calculation purposes to adjust relative mass transfer coefficients at different temperatures to accord with observations. The underlying physical processes responsible for different deposition rates at different temperatures must include additional resistances to transfer as well as chemical interaction with other dissolved species eg Ni. Virtually nothing is known about these processes in the case of manganese or any other species in sodium.

Cobalt. The assumptions underlying the source term for cobalt activity ( $^{58}\text{Co}$  and  $^{60}\text{Co}$ ) are not nearly so well established as for  $^{54}\text{Mn}$ . The observation of cobalt retention at the surface of steels corroding in sodium is well authenticated but the underlying physical reasons for this behaviour are not understood, although  $^{60}\text{Co}$  could account for between one-third and one-half of total deposited activity assuming stoichiometric release, whereas sub-stoichiometric release could reduce this accordingly. Similar considerations also apply to  $^{58}\text{Co}$ . In addition the question of what amount of Co leaves the core has to be considered in the light of experience on working reactors. Generally speaking, there does not seem to be such a marked temperature effect on deposition as for Mn and Ba/La, consequently the need for major adjustment of local coefficients to match temperature effects is not pressing. However there is a need to confirm experimentally that cobalt deposition follows the pattern of changes of mass transfer coefficient in other geometries such as pumps, well characterised pipes and ducts. This is a general comment which also applies to insoluble FPs and manganese.

#### Soluble Fission Products

Caesium. Experimental work should aim to provide:

- a. Nuclear data to calculate  $^{134}\text{Cs}$  and  $^{136}\text{Cs}$  content in fuel pins.
- b. Partition Data between steel surfaces and sodium. The effect of surface condition, carbon content, bulk corrosion/deposition rate and flow/geometry regime.
- c. The impact, on the overall caesium balance, of losses to the cover gas and associated surfaces and to the primary cold trap.
- d. Means for deliberately segregating caesium, thus preventing or at least minimising its deposition on surfaces. If carbon traps continue to appear promising then investigate means for retaining carbon and preventing an increase in the chemical carbon activity of sodium.
- e. Means for removing caesium from surfaces. This part of the investigation should be linked to consideration of the treatment and disposal of the decontamination solution - which will contain other nuclides as well as caesium.

Iodine and Tellurium. Estimates suggest that these nuclides will be minor contributors to dose rate even compared to caesium. They have short half lives and the important gamma emitters ( $^{131}\text{I}$ ,  $^{132}\text{I}$ ) could if necessary be segregated at the cold trap.

#### Insoluble Fission Products

Attention should be given to:

- a. The source term, fractional release and whether failures arising from manufacturing defects are randomly distributed over all pins irrespective of rating.
- b. The form of insoluble FPs following release. If these are present as oxides what can be said about particle size and its effect on the liquid phase mass transfer coefficient since values used so far are based on molecular diffusion through the boundary layer. Also, are there other resistances or transfers in the reverse direction, which can govern the overall deposition process?

REFERENCES

1. Polley M V and Skyrme G. *Journal of Nuclear Materials*, 75, 226-237 (1978).
2. Kuhn W L. International Conference on Liquid Metal Technology in Energy Production, Champion, PA, 280-283, May (1976).
3. Brehm W F. Paper 19 at IAEA Specialists Meeting, Dimitrovgrad, USSR, Sept (1975).
4. Menken G and Reichel H. Paper 6, *ibid*.
5. Brehm W F. Paper 18, *ibid*.
6. Brehm W F. International Conference on Liquid Metal Technology in Energy Production, Champion, PA, 263-270, May (1976).
7. Brehm W F, McGuire J C, Colburn R P, Maffei H P, Olsen W H. Second International Conference on Liquid Metal Technology in Energy Production, Richland, Washington, April (1980).
8. Beal S K. Deposition of particles in turbulent flow on Channel or pipe walls. *Nucl. Science and Engineering* 40 1-11, (1970).
9. Friedlander S K and Johnstone H F *Ind. Eng. Chem* 49 1151 (1957).
10. Reeks M W and Skyrme G. The dependence of particle deposition velocity on particle inertia in turbulent flow RD/B/N3515 Nov 1975.
11. Hutchinson P et al. *Chem Eng Sci* 26 419-439 (1971).
12. Reeks M W et al. On the long term re-suspension of small particles by a turbulent flow Part 1. A statistical model CEGB/TPRD/13/0638/N85.
13. Reed J and Reeks M W. CEGB/TPRD/B/0642/N85.
14. Reeks M W et al - Part III - suspension for rough surfaces CEGB/TPRD/B/0640/N85.
15. Potter P E. AERE Unpublished Work.
16. Findley J R. Internal Communication (1975).
17. Cooper M H and Taylor G R. *Nuclear Technology* vol-12. No 1 p.83 (1971).
18. Evans H E and Watson W R. Liquid Alkali metals BNES Conference Nottingham (1973).
19. Allan C G. Liquid Alkali Metals BNES Conference Nottingham (1973).
20. Shimojima et al. IWGFR specialists meeting Dimitrovgrad (1975).
21. Walker R A. *J Nuclear Materials* Vol 34, p.165 (1970).
22. Thorley A W and Tyzack C. Liquid Metals Alkali Conf. BNES Nottingham (1973) pp.257-273.

23. Thorley A W and Jeffcoat P J. Effect of sodium on mechanical properties and structure of fuel cladding alloys. Second Int. Conf, Richland, USA, April 1976 Conf 800401-P2.
24. Thorley A W et al First Int Conf on Liquid Metal Technology in Energy Production Champion Pennsylvania (1976).
25. Thorley A W et al. Second Int Conf., Richland, USA, April 1976 Conf. 800401 - P2.
26. Polley M V and Skyrme G. An analysis of the corrosion of pure iron in sodium loops. Jnl Nucl. Matls. 66 (1977) pp 221-235.
27. Thorley A W. Corrosion of iron in sodium and the influence of alloying elements on its mass transfer behaviour - Proc of a conference on materials behaviour and Physical Chemistry in liquid metal systems - Karlsruhe 1981. Plenum press 1982.
28. Claxton K T and Collier J S. Mass transport of stainless steel corrosion products in flowing liquid sodium Jnl. Brit. Nucl Energy Soc. 12 (1) 63 (9173).
29. Newson I H et al. Studies of radioactive corrosion product release and deposition in the Harwell active mass-transfer loop Second Int Conf. Richland, USA April 1986 Conf 800401 - P2.
30. Thorley A W et al. Mass transfer of steel in pumped sodium loops and its effect on microstructure. Proc of a conference on Model behaviour and Physical chemistry in liquid metal systems - Karlsruhe 1981. Plenum press 1982.
31. Newson I H et al. Studies of stainless steel corrosion transport and deposition in the Harwell AMTL Proc. 3rd Int Conf Liquid Metal Engineering and Technology BNES Oxford 1984, Vol 1.
32. Thorley A W and Sumbler G. RNL internal document.
33. Thorley A W. Corrosion and Mass transfer behaviour of steel materials in liquid sodium Proc 3rd Int Conf Liquid Metal Eng and Technology BNES Oxford 1984, Vol 3.
34. Watson W R and Gwyther J R. The behaviour of radioactive isotopes in liquid metal cooled fast reactors. Part V. Behaviour of Cs 134 Cs 137 and Na 22 in a small stainless steel pumped loop. CEGB/RD/B/N4452.
35. Hooper A J. The behaviour of fission product caesium in LMFBR primary circuits; experiments in a small stainless steel loop containing circulating sodium CEGB. TPRD.B/0935/R.87.
36. Thompson R and Stanaway W P. Sol of metals Fe and Mn in sodium Second Int Conf on Liquid met Tech Richland USA, 1986 Conf 800401 - P2.
37. Thompson R and Stanaway W P. The solubility of transition metals Mn and Co in liquid sodium. Proc of Conf on Materials behaviour and Physical Chemistry in liquid metal systems Karlsruhe 1981 Plenum press 1982.

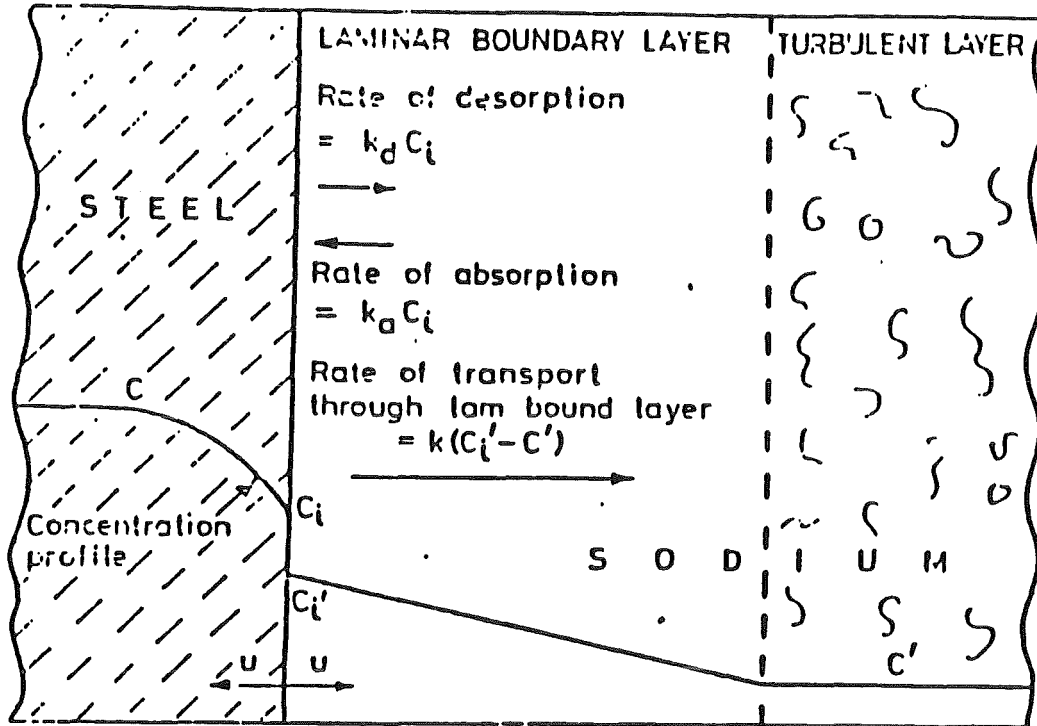
38. Pellet C R and Thompson R. Measurement of transition metal solubilities in liquid sodium; Co, Ni, Cr. Proc 3rd Int Conf Liquid Metal Eng and Technology BNES Oxford 1984, Vol 3.
39. Voice E H. Measuring activity in the intermediate heat exchangers of the prototype fast reactor. Proc 3rd Int Conf on Liquid Metal Eng and Technology BNES Oxford 1984, Vol 1.

#### Acknowledgements

The author acknowledges the assistance provided by Dr E Trevillion (DNE) and Drs M Mignanelle and I Newson (AERE) in preparing certain sections of this paper. Information provided by Mr C Tanner BNFL is also acknowledged.

#### Abbreviations

- DNE = The Dounreay Nuclear Establishment, Dounreay, Caithness, Scotland
- AERE = Atomic Energy Research Establishment, Harwell, Oxon.
- RNL = Risley Nuclear Laboratories, Risley, Cheshire.
- BNL = Berkeley Nuclear Laboratories, Berkeley, Glos.
- PFR = Prototype Fast Reactor, Dounreay.
- DFR = Dounreay Fast Reactor



$k_a$ : mass transport coefficient for adsorption ( $m s^{-1}$ )

$k_d$ : mass transport coefficient for desorption ( $m s^{-1}$ )

$k$ : mass transport coefficient for transport across laminar boundary layer ( $m s^{-1}$ )

$u$ : bulk corrosion / deposition rate ( $m s^{-1}$ )

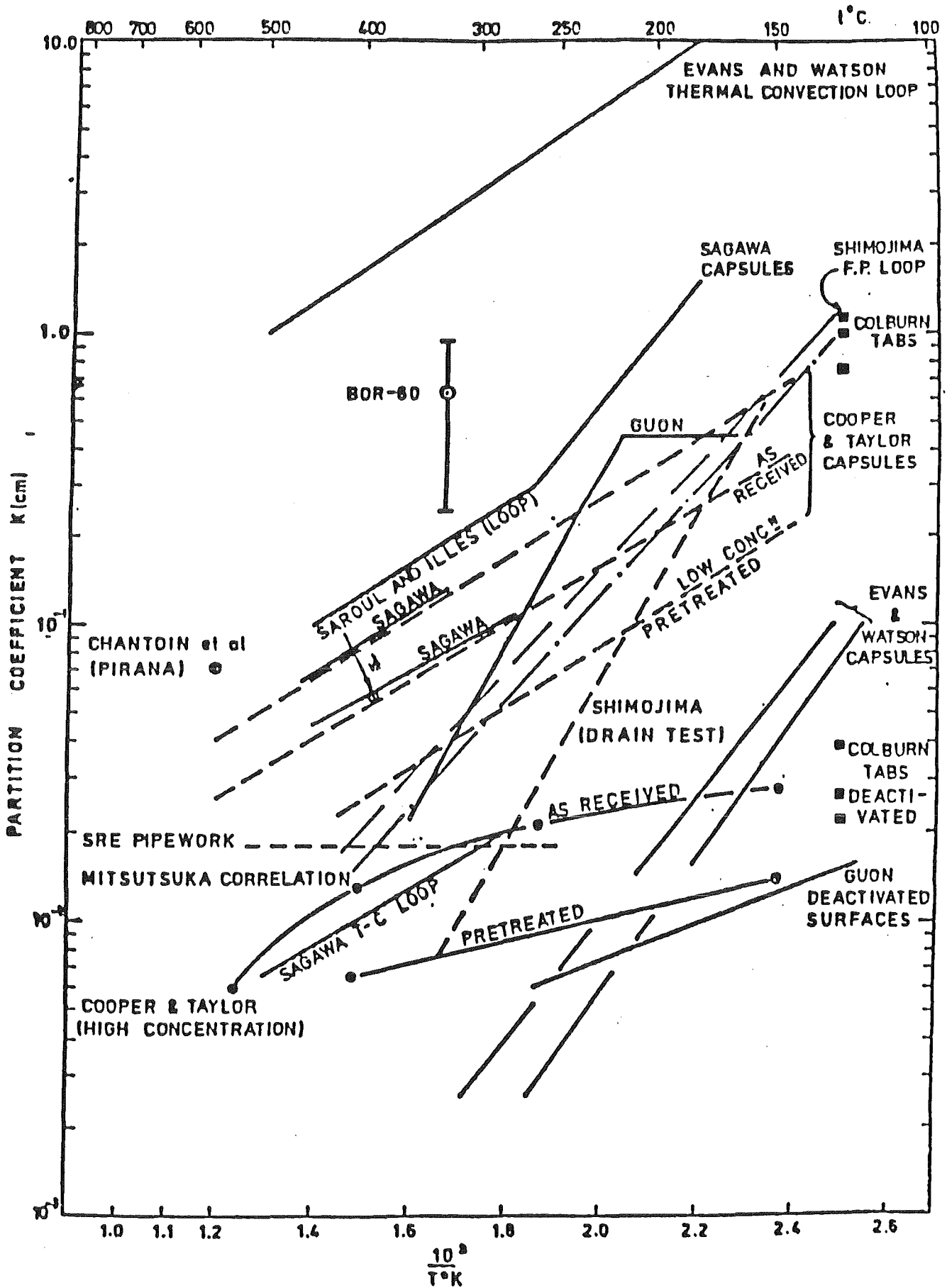
$$\beta = k_a / k_d \quad A = k / u\beta$$

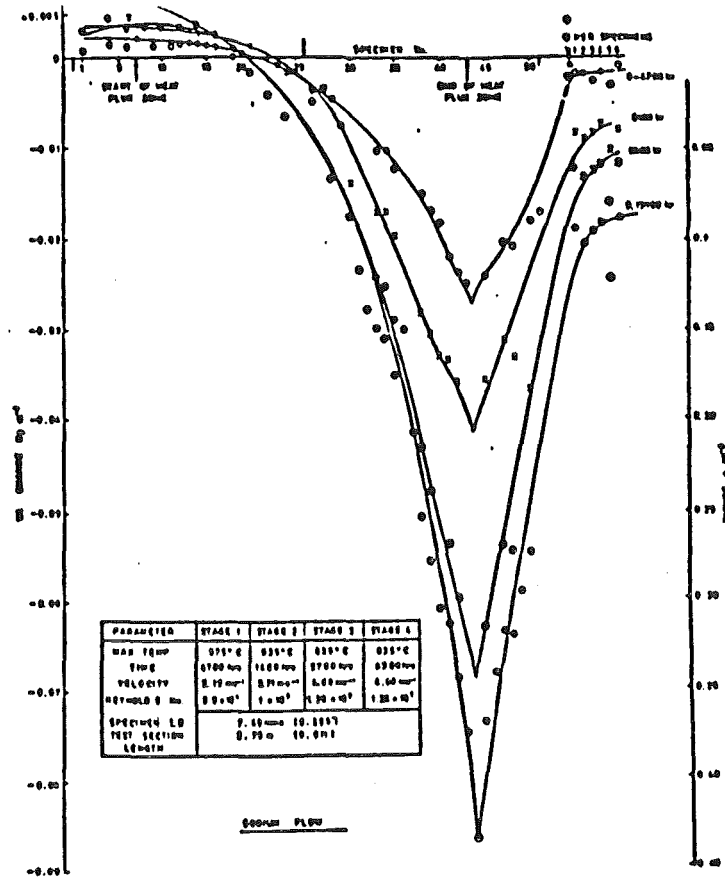
FIG. 1. Kinetics of Corrosion Product Release / Deposition: Interpretation (for Release) of the Parameter  $A = k / u\beta$ .



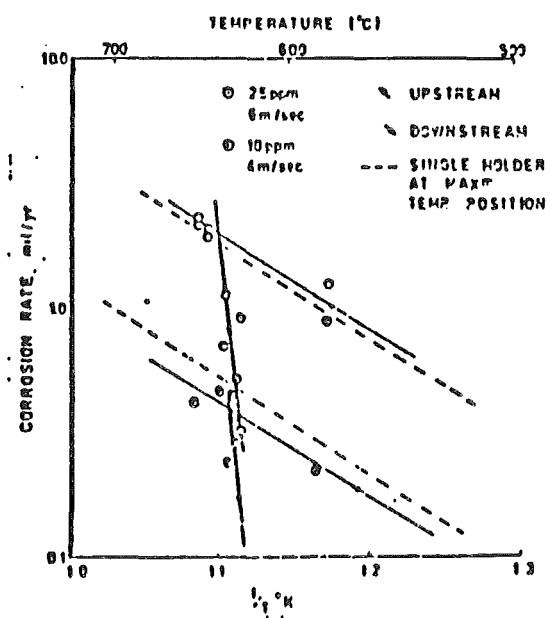


FIG. 3 CAESIUM DISTRIBUTION.



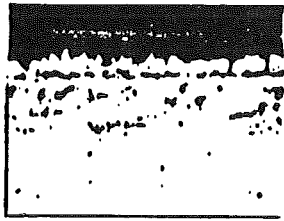


Weight change data in core test section No 2 of the LMT loop in the presence of heat flux.

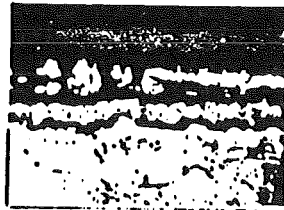


Effect of temperature on upstream and downstream corrosion of stainless steels in RHL loops.

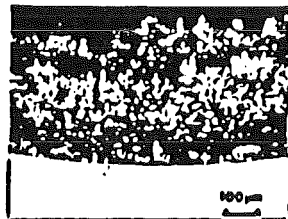
FIG 4 EFFECT OF CERTAIN PARAMETERS ON CORROSION RATE IN LOOPS OF DIFFERENT GEOMETRY.



Sodium Velocity  $0.3\text{m.s}^{-1}$   
Oxygen Level 10ppm



Sodium Velocity  $3\text{m.s}^{-1}$   
Oxygen Level 25ppm



Sodium Velocity  $3\text{m.s}^{-1}$   
Oxygen Level 10ppm

FIG 5 CORROSION/DEPOSITION EFFECTS IN SMALL LOOPS.

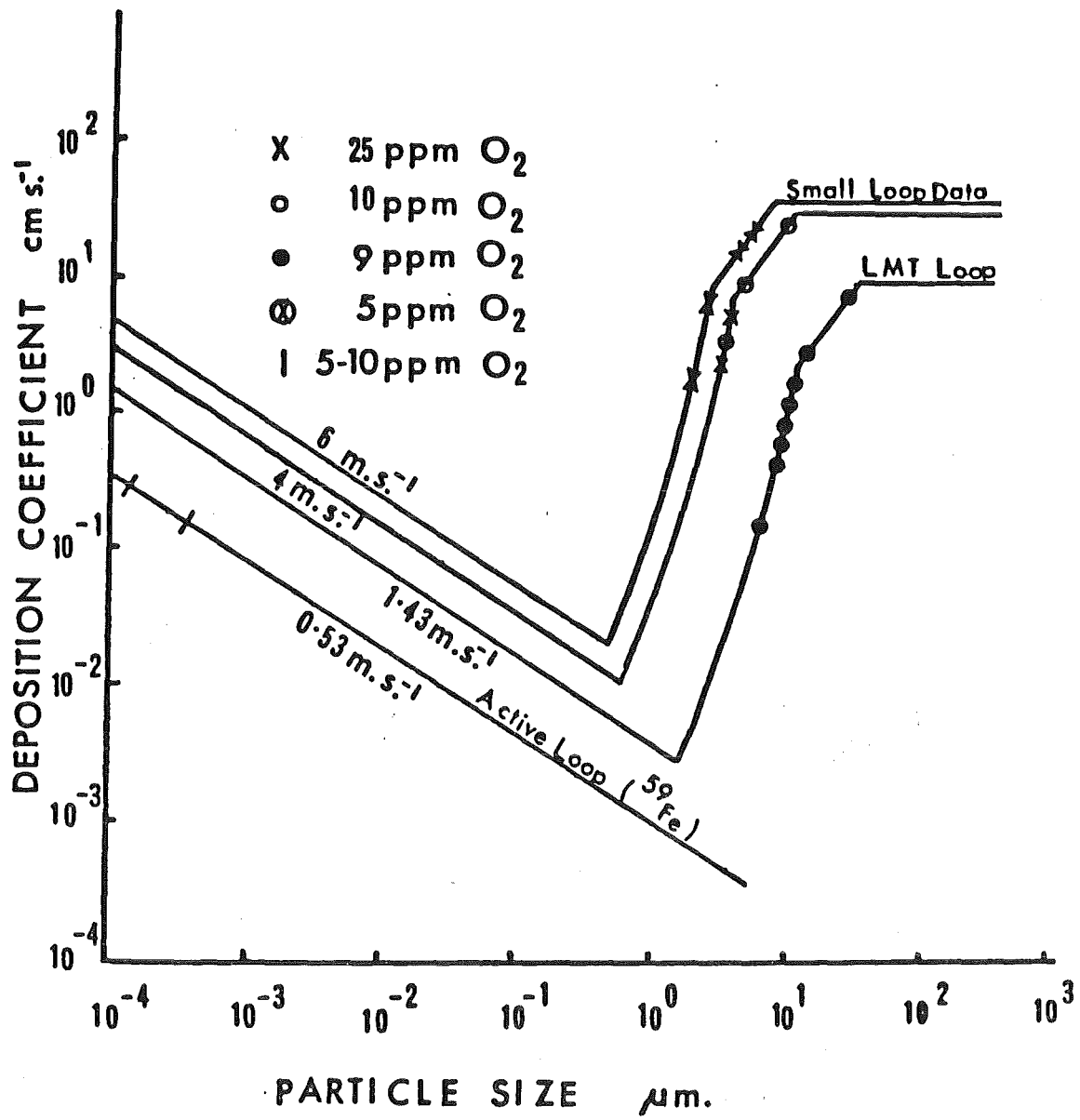


FIG 6. DEPOSITION COEFFICIENTS IN SODIUM LOOPS.

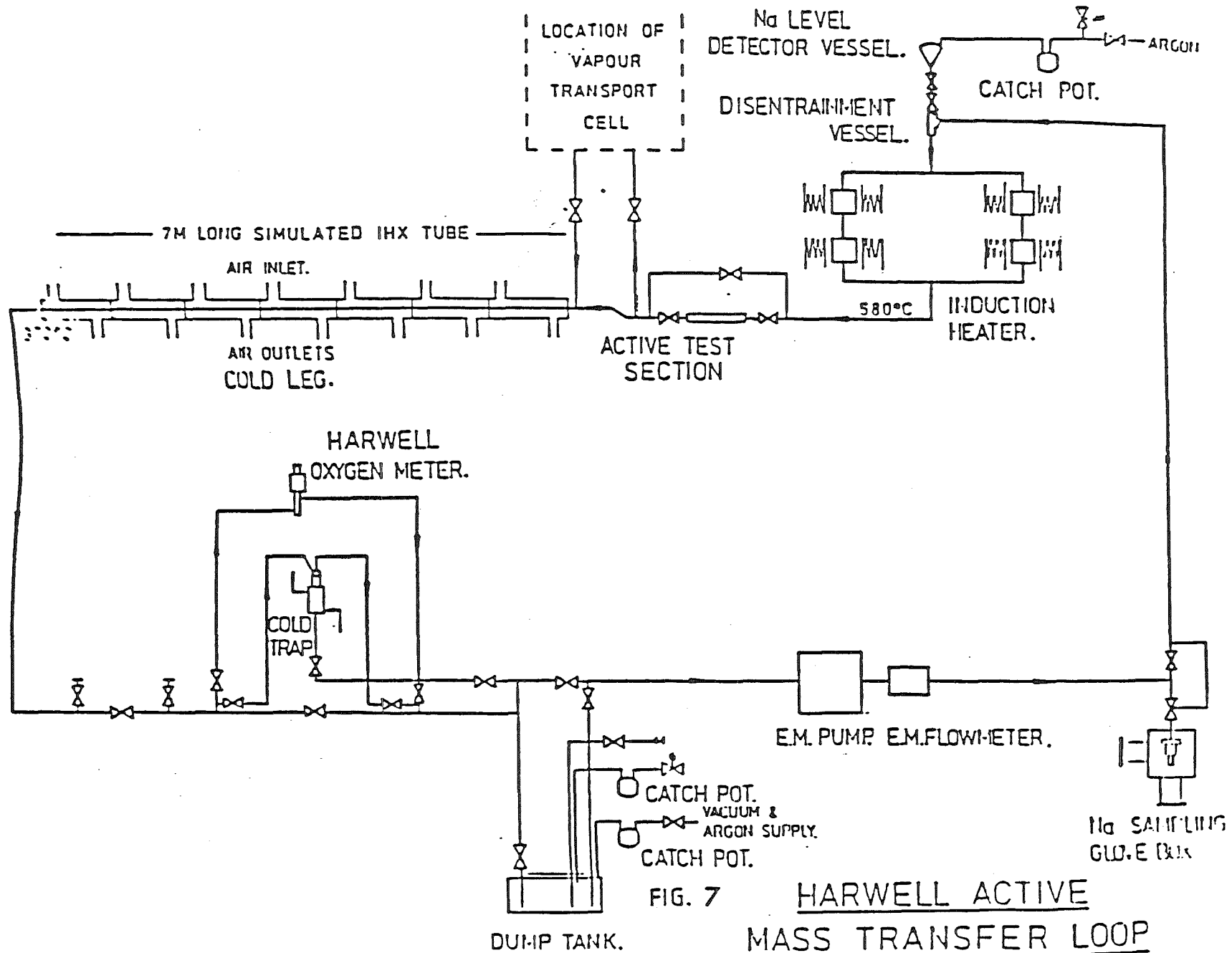


FIG. 7

HARWELL ACTIVE MASS TRANSFER LOOP

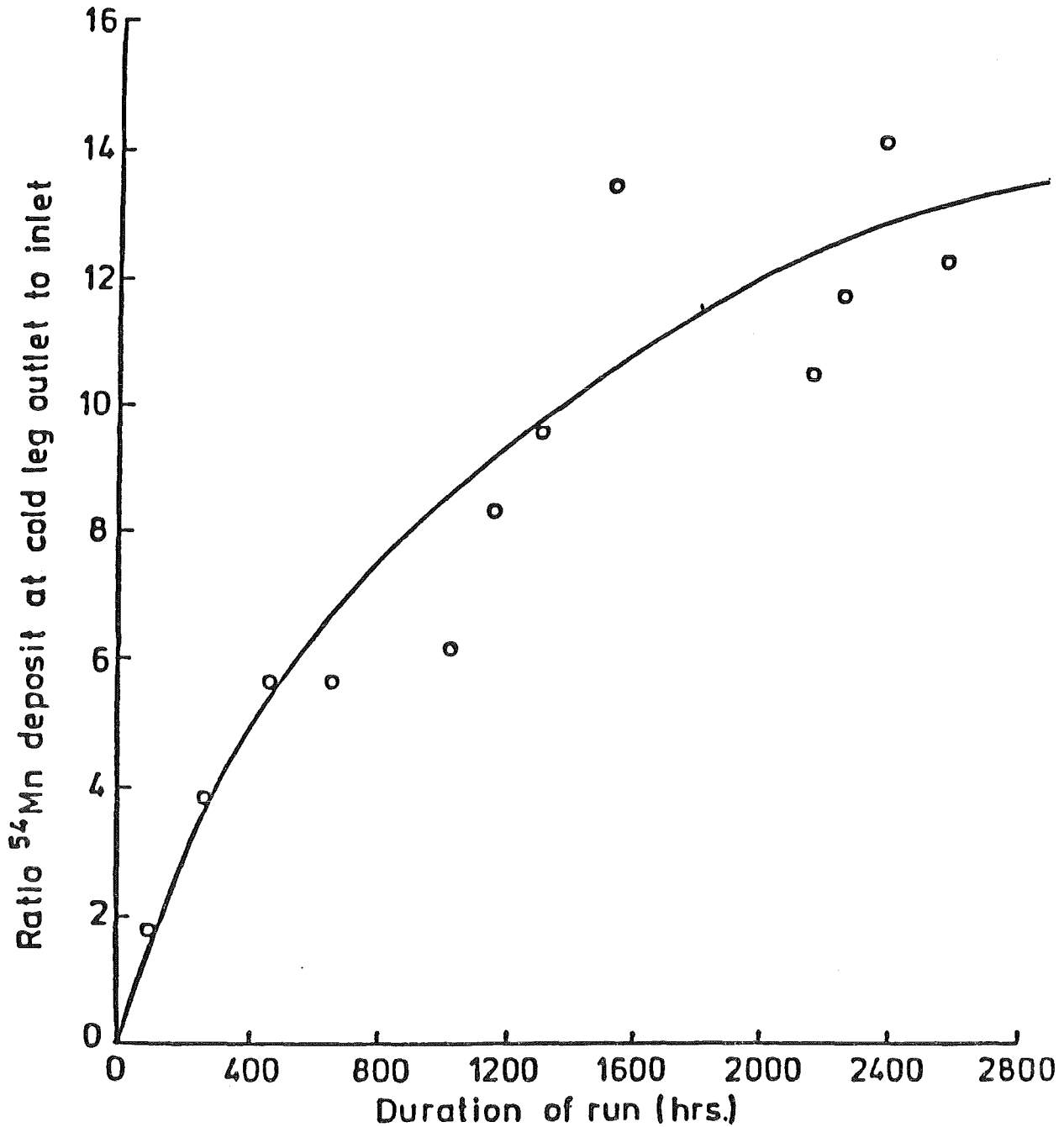


FIG. 8 THE VARIATION WITH TIME OF THE RELATIVE  $^{54}\text{Mn}$  TRACED DEPOSITION BETWEEN COLD LEG OUTLET AND INLET

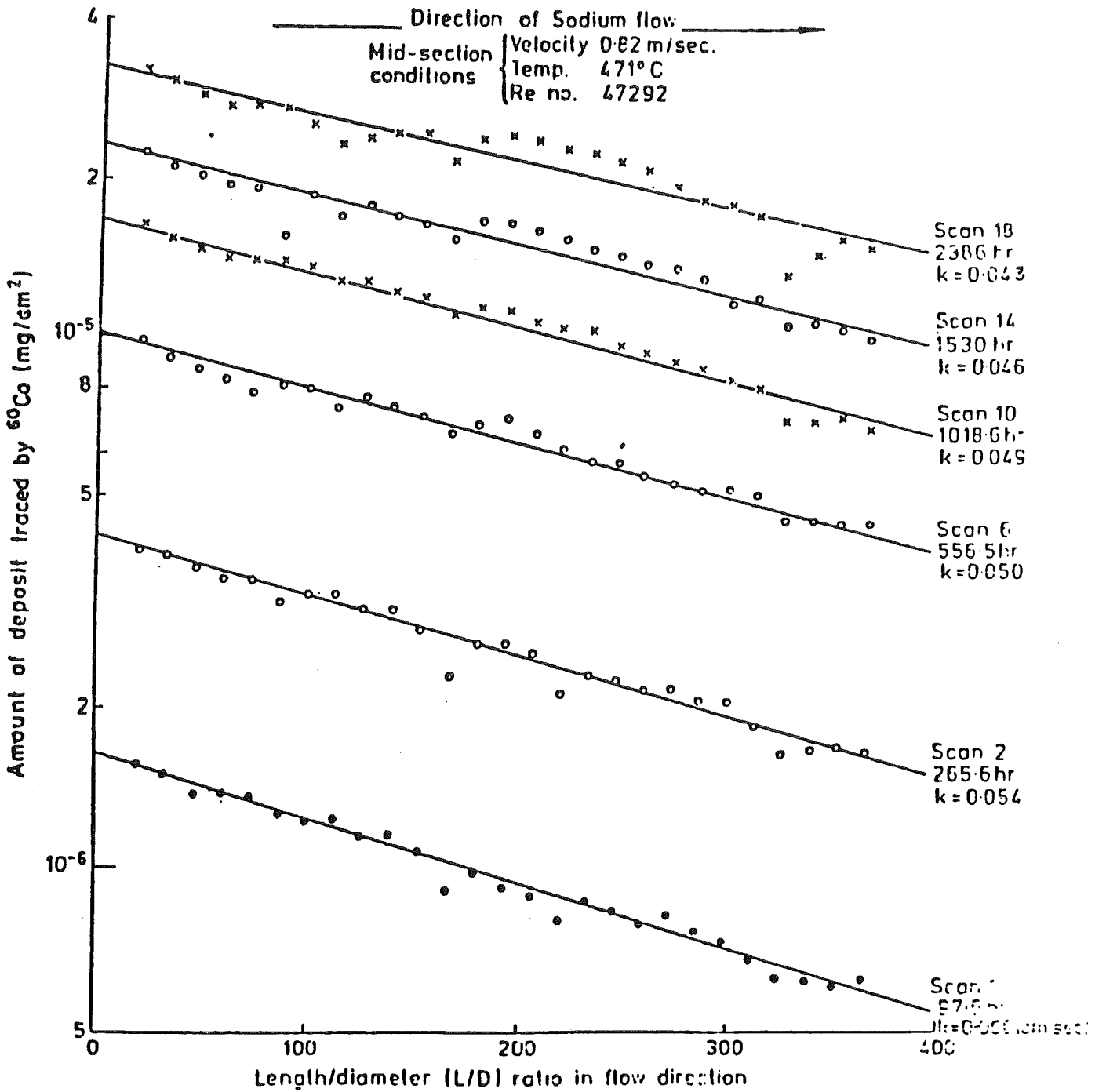


FIG.9 RESULTS OF  $^{60}\text{Co}$  TRACED DEPOSITION MEASUREMENTS ON 'COLD LEG'

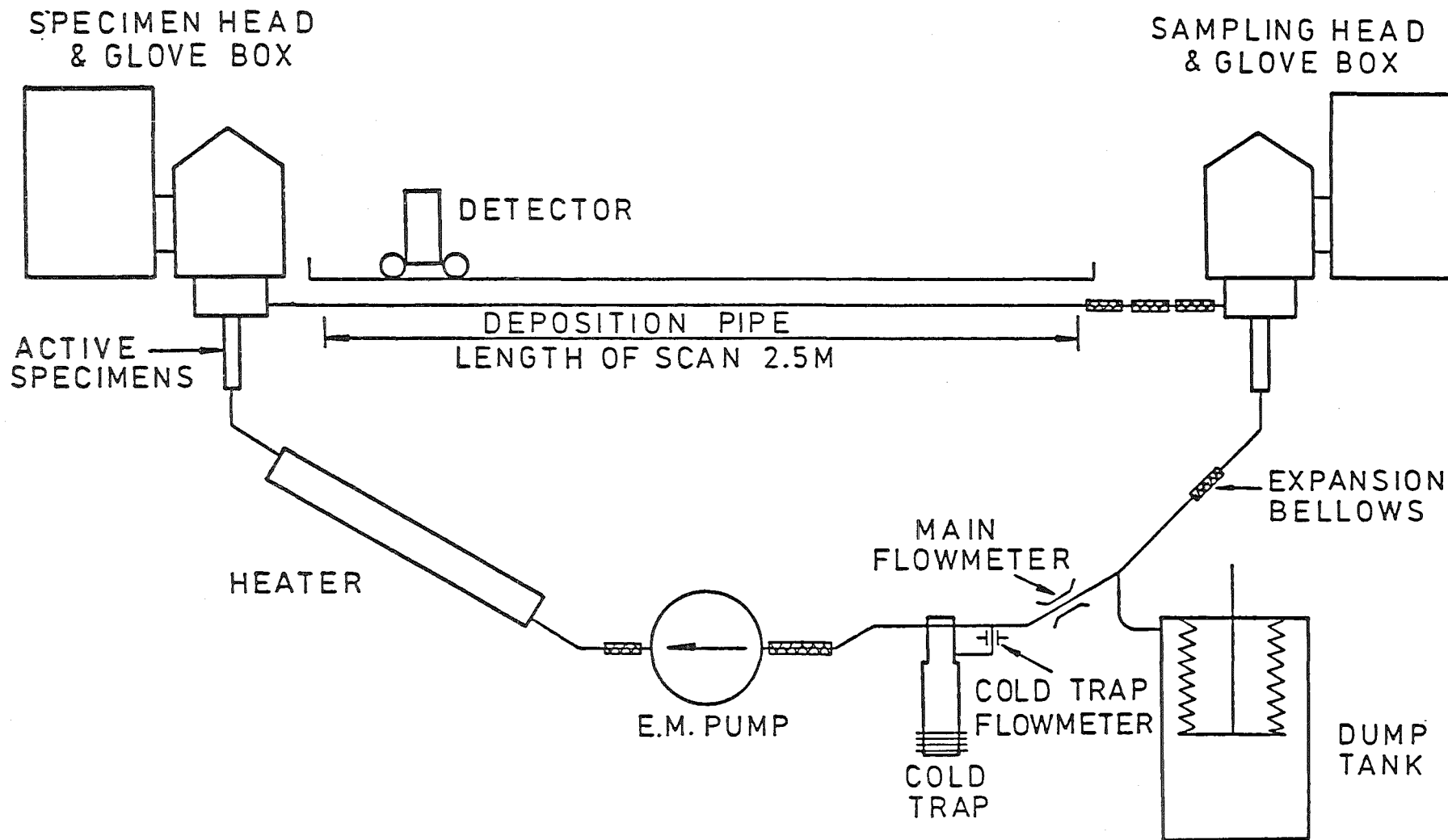


FIG. 10 ACTIVE SPECIMEN RIG



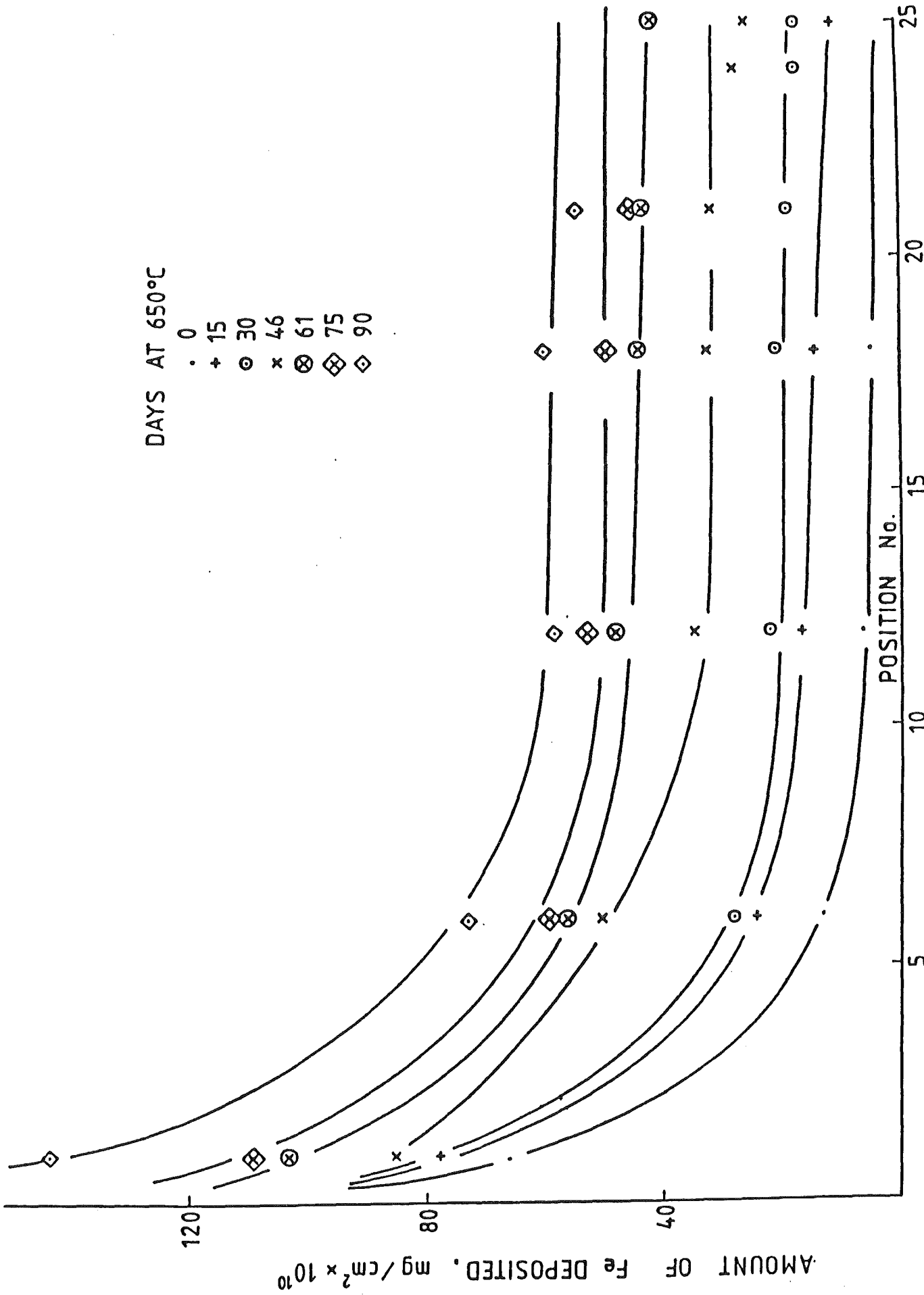


FIG. 11 CORROSION OF IRRADIATED PURE IRON IN LIQUID SODIUM  
POSITION NO. 5 10 15 20 25  
REDUCTION OF COE 11 701 MeV DEAK 1 ALONG PIPE

DAYS AT 650 °C

- 0
- X 10
- ⊙ 22
- ⊗ 39
- + 50
- ⊕ 68
- 97

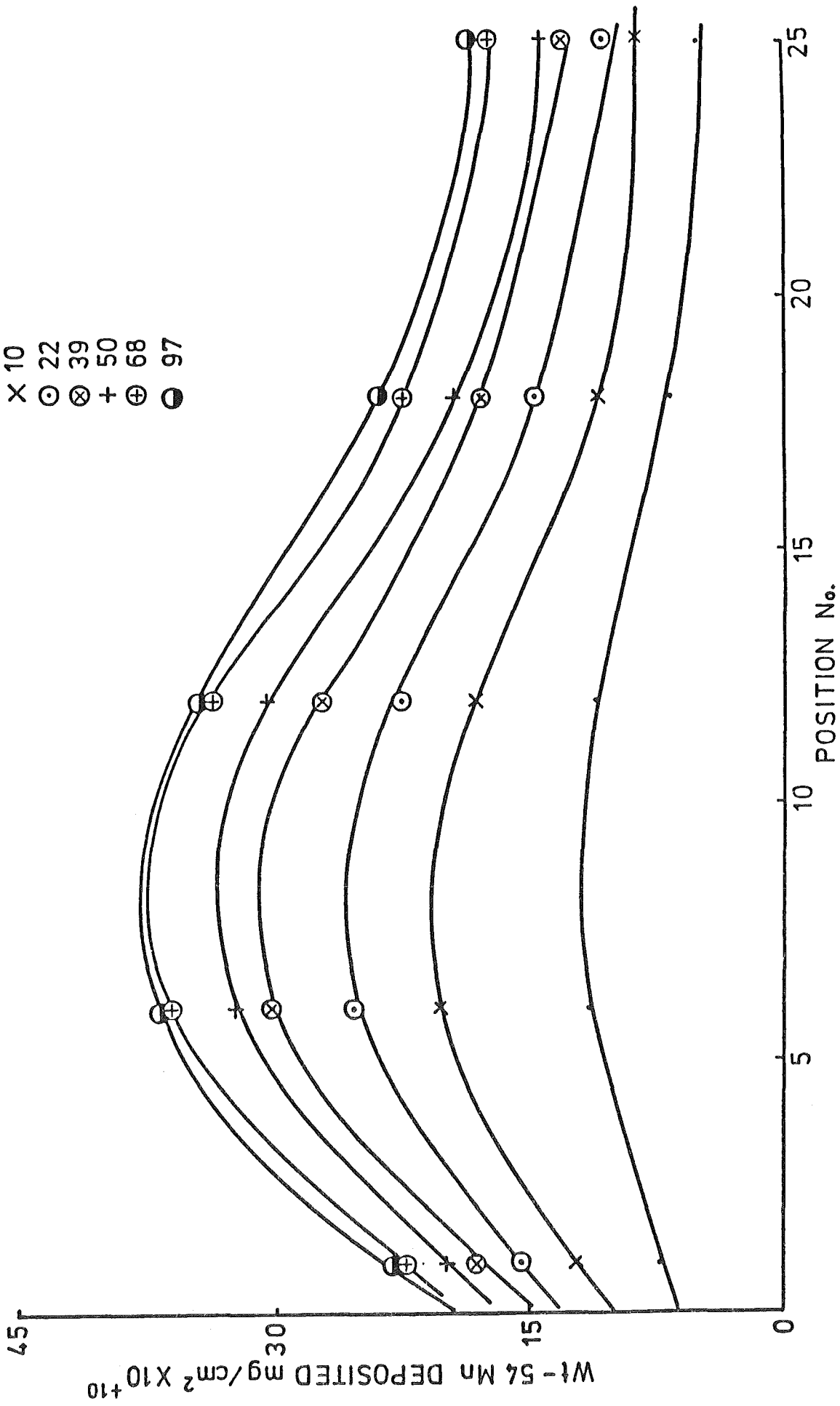


FIG. 12 54Mn DEPOSITION ALONG PIPE

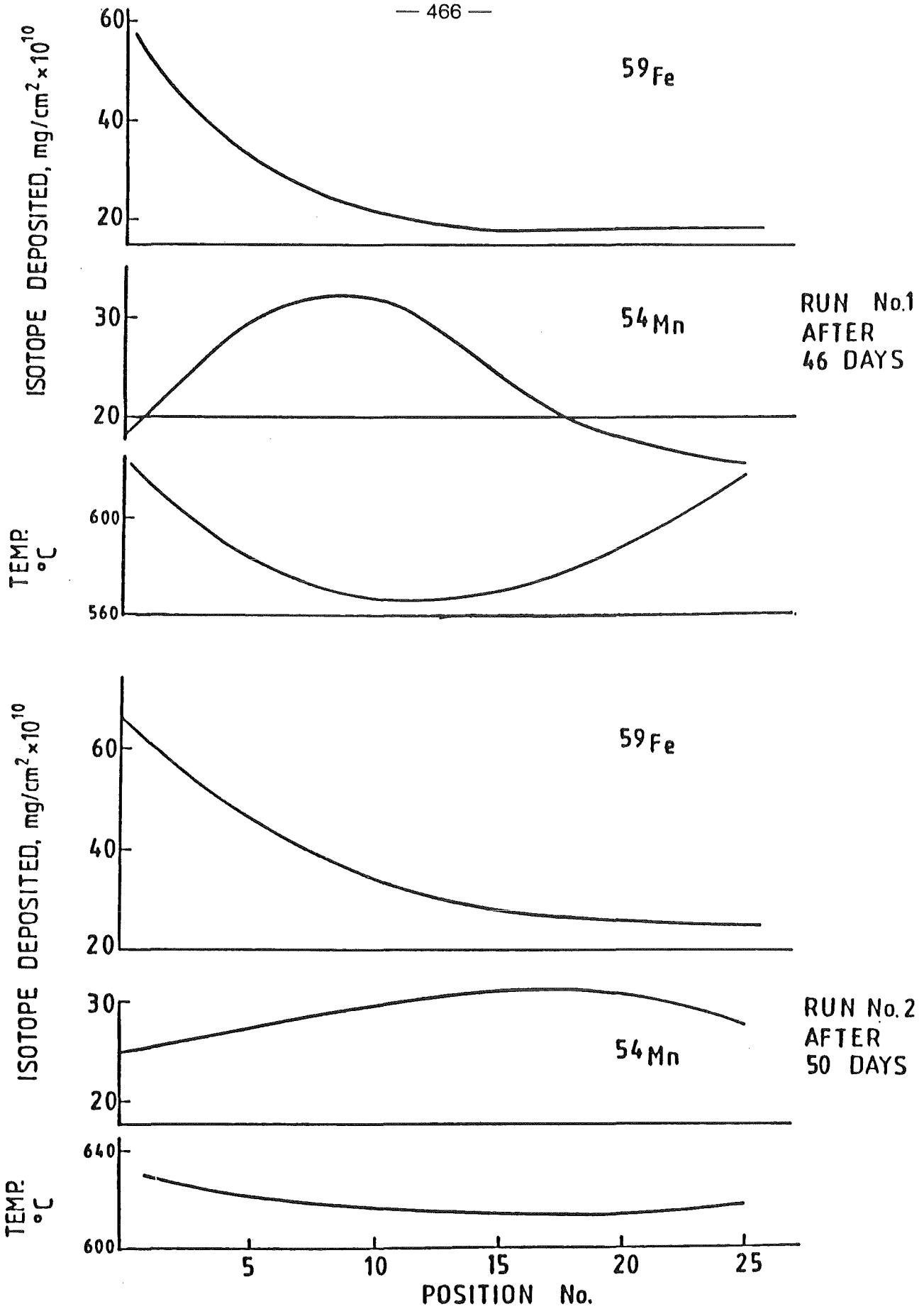


FIG.13 DEPOSITION OF 54-MN AND 59-Fe FROM CORROSION OF IRRADIATED PURE IRON IN DYNAMIC SODIUM AT 650°C

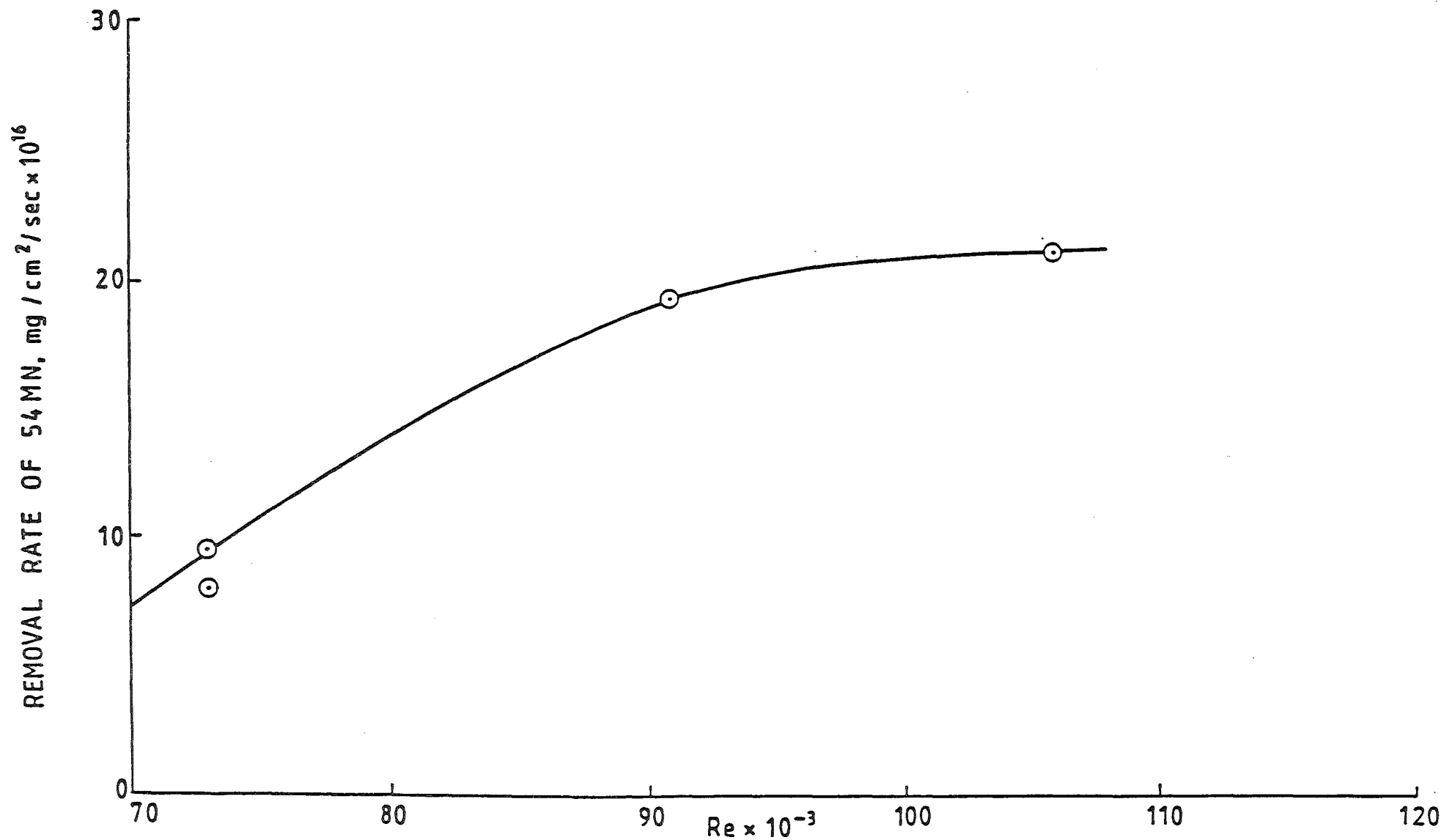


FIG.14 EFFECT OF REYNOLDS NUMBER ON REMOVAL OF 54 MN FROM SODIUM BY NICKEL IN RNL ACTIVE RIG

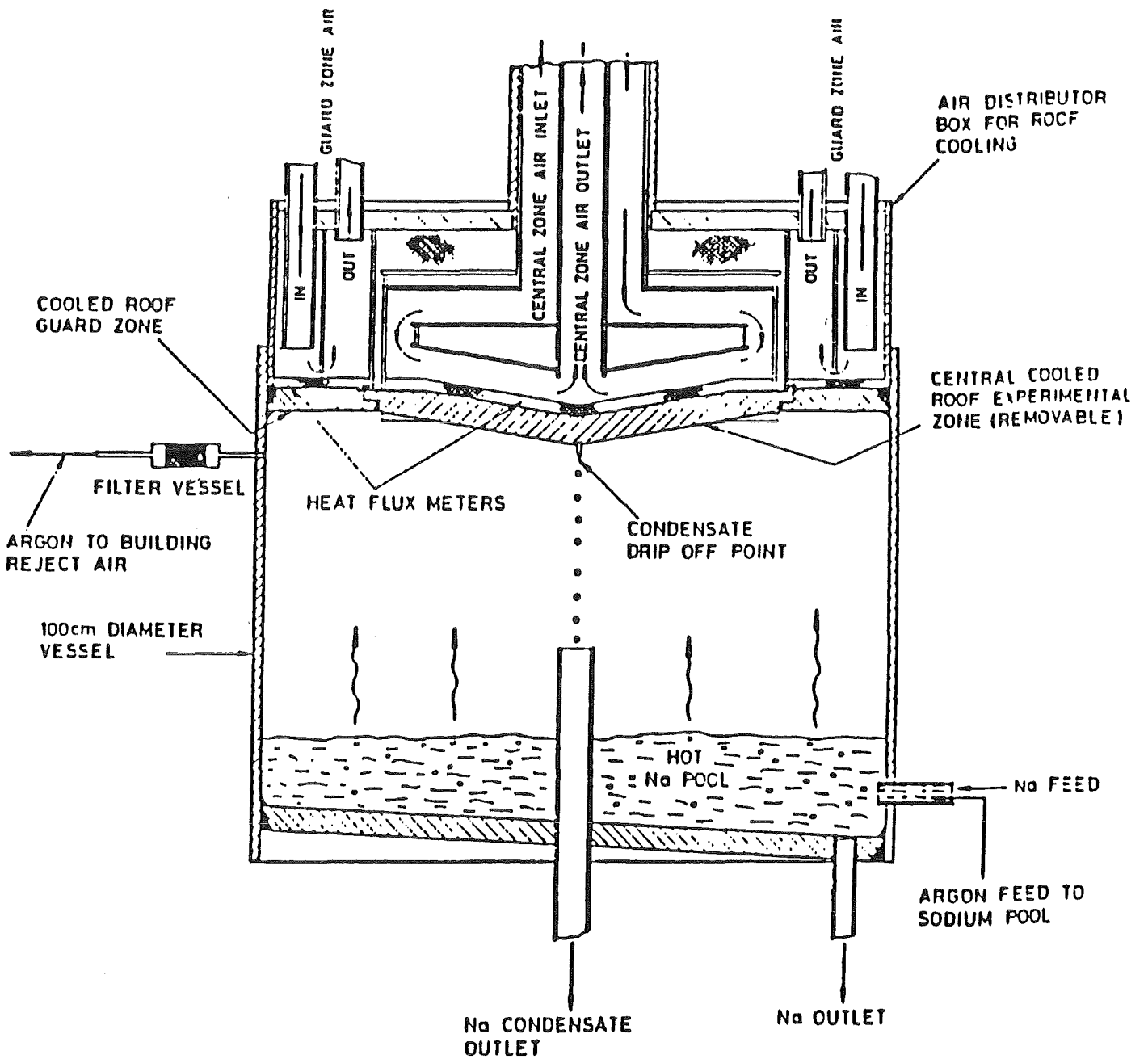


FIG.15 REPRESENTATION OF 100cm DIAMETER VESSEL FOR STUDY OF VAPOUR PHASE TRANSPORT OF RADIOACTIVE SPECIES.

Precipitation Mechanism of Corrosion Products Released  
from Type 304 Stainless Steel in Liquid Sodium

Norikatsu Yokota \*  
Shigehiro Shimoyashiki \*  
Junnosuke Horie \*\*

\* Energy Research Laboratory, Hitachi, Ltd.  
1168 Moriyama-cho, Hitachi-shi, Ibaraki-ken, 316 Japan  
\*\* Hitachi Division, Hitachi Engineering Co., Ltd.  
3-2-1 Saiwai-cho, Hitachi-shi, Ibaraki-ken, 317 Japan

Abstract

To clarify the precipitation mechanism in liquid sodium, precipitation experiments have been done in flowing sodium, while varying the temperatures from 560-670°C. Particles precipitated on Type 304 stainless steel surfaces were analysed regarding their chemical compositions and characteristic shapes.

Corrosion products released from Type 304 stainless steel were grouped into the following three classes: (a) a globular shape having iron as the main component, (b) a hexagonal plate shape having chromium as the main component, and (c) an undefined shape having a chemical composition which included reduced chromium from the stainless steel. The compositions of each type were located on the precipitation line of the Fe-Cr-Ni ternary phase diagram at 560°C. Hence, the elements Fe, Cr and Ni, which were released into the sodium, precipitated, forming particles having the chemical composition along this line.

Critical size of the globular particles was 3 $\mu$ m. When they grew larger than this, crystal growth occurred on the (110) and (100) planes, and particles became chain-like. Critical size of the hexagonal plate particles was 0.3 $\mu$ m. The particle size distribution of all three classes was expressed by a logarithmico-normal distribution with an average diameter of 4 $\mu$ m and a standard deviation of 2.

## 1. Introduction

When radiated fuel claddings and structural materials in an FBR core are corroded by sodium, various radioactive corrosion products are released into liquid sodium of the primary cooling system. Transported by sodium flow, these corrosion products deposit on surfaces of piping and components. It is very important to evaluate their dose rate to ensure reliability of piping and components<sup>(1)-(3)</sup>.

Corrosion products in liquid sodium take two forms, molecular and particulate. Several workers have reported on behavior of molecular corrosion products in non-isothermal loops<sup>(4)-(7)</sup>. However, particulate behavior including its formation mechanism, shape and composition is not as well as known<sup>(4),(7)-(9)</sup>. In FBRs, the structural material of piping and components is austenitic stainless steel which has a good compatibility with liquid sodium. Therefore, corrosion products generated in liquid sodium incorporate iron, chromium and nickel. This report describes a precipitation mechanism of corrosion products in liquid sodium, obtained in experiments, using a sodium loop constructed of stainless steel.

## 2. Experimental

### 2.1 Sodium loop

The sodium loop used in these experiments is shown in Fig.1. This loop was made of Type 304 stainless steel. It consisted of a drain tank, cold trap, heater and test pot. Sodium in the drain tank was pumped up using an electromagnetic pump and circulated through the cold trap, heater and test pot. The cold trap was packed with a stainless steel mesh and was cooled to the desired sodium purification temperature by changing the blower power. A test rig and test pieces were set in the test pot for use in corrosion and precipitation experiments, respectively. The test rig (Fig.2) consisted of a cylinder, heater pin and thermal insulator. The sodium inlet was located at the cylinder bottom and the sodium outlet was formed in the upper end by a baffle plate. When the heater pin was heated, sodium in the cylinder was also heated. Therefore, there was a difference in sodium densities inside of the cylinder and in the test pot. This difference became the motivating force for sodium circulation through the cylinder interior, from the inlet to the outlet. Sodium flow rate was varied by controlling the gap between the baffle plate and cylinder.

Test pieces used for corrosion and deposition experiments were of two types. One for corrosion experiments was 0.3mm thick, 5mm wide and 15mm long. The other for deposition experiments was 0.3mm thick, 20mm wide and 15mm long. Test pieces were set at four positions along the axial direction of the heater pin.

### 2.2 Experimental procedure

Sodium was purified at the cold trap temperature of 120°C and the sealed in the test pot. After being used for 1000 hours, sodium in the test pot was drained into the drain tank. Test pieces were cooled down to room temperature. Any sodium adhering to them was removed by rinsing in alcohol. Furthermore, test pieces were also cleaned using an ultrasonic vibrator to collect the corrosion products particles deposited on the stainless steel surface. The alcohol wash was filtrated through an acetate filter (pore diameter, 0.8 $\mu$ m). Particles collected on the filter were analyzed as to shape and composition using

scanning electron microscopy (SEM) and energy dispersed X-ray (EDX) analysis. Crystal structures of particles were analyzed by X-ray diffraction.

Sodium in the test pot was sampled, using a glass tube, to determine concentrations of Fe, Cr and Ni. Sampled sodium was distilled and the residue was dissolved in a mixture of 50%vol HCl and 50%vol HNO<sub>3</sub>.

### 3. Experimental results

#### 3.1 Precipitated particles on stainless steel

Test pieces attached to the heater pin showed a loss of weight, but particles from these test pieces could not be obtained. On the other hand, test pieces immersed in the test pot at 560°C gained weight during immersion. Weight changes of the two test pieces were measured during cleaning with the ultrasonic vibrator. These results are shown in Fig.3. The weights of test pieces fell with cleaning time, but after 1 hour, they were unchanged. The alcohol wash was filtrated through the acetate filter to collect precipitated particles. Particles collected on the filter were observed by SEM and chemical compositions were analyzed by EDX. The composition results are shown in Fig.4 and typical SEM photos, in Fig.5.

The particles were distinguished as three types: a flaky, undefined shape, a globular shape, and a hexagonal plate shape. The globular shape(Fig.5(a)) which had shap edges, had a polyhedron structure. Particle chemical compositions were different for the three types. The undefined shape particles included reduced chromium from the stainless steel. The globular particles had iron as their main component, while the hexagonal plate particles had chromium as their main component. Chemical compositions of total collected particles are shown in Table 1. Metallic impurity solubilities in sodium and test piece compositionbefore immersion are also listed. For all three types, the main component was iron. In the liquid sodium, iron was detected in the largest amount, followed by nickel.

#### 3.2 Particle size distribution and crystal structure

Particles collected on the acetate filter were dispersed on a glass microscope slide to measure their size distribution. A SEM photograph is shown in Fig.6. The distribution was obtained on the basis of a volume diameter. Precipitated particles showed a logarithmico-normal distribution, with an average diameter of 4μm and a standard deviation of 2.

Crystal structures of the collected particles were determined by an X-ray diffraction method. These results are shown in Fig.7. Type 304 stainless steel, before immersing in sodium, showed diffraction lines for α-Fe and γ-Fe. The particles also showed these same diffraction lines. The broad peak at a lower diffraction angle was for the acetate which was the of filter material.

### 4. Discussion



#### 4.1 Precipitated particle

Relationships between metallic elements of the particles were investigated as shown in Figs.8 and 9. Iron and Cr concentrations were indirectly proportional for both the globular and hexagonal particles. Iron and Ni concentrations were directly proportional for the hexagonal plate particles. The relationship between Fe and Ni in the globular particle was indirect. The globular particle was composed mainly of Fe and Ni. Therefore, the composition of Ni decreased relative to an increased composition of Fe in the globular particles.

Compositions of the three type particles are plotted in the Fe-Cr-Ni ternary phase diagram of Fig.10. Composition of Type 304 stainless steel is also drawn there. The three types appeared in three regions in the phase diagram. Based on data reported by Rivlin and Raynor<sup>(10)</sup>, the Fe-Cr-Ni ternary phase diagram at 560°C was obtained as shown in Fig.11. Superimposing Fig.11 onto Fig.10 gives Fig.12<sup>(11)</sup>. The composition of each particle was then located along the precipitation line of the Fe-Cr-Ni ternary phase diagram. If the test pieces of stainless steel were corroded by sodium, the concentrations of Fe, Cr and Ni in sodium would nearly equal those in the stainless steel. Test pieces set on the heater pin were corroded by sodium and the concentrations of Fe, Cr and Ni in sodium increased along the sodium flow from the inlet to the outlet. When the sodium reached the lower temperature region of the test pieces in the test pot, the concentrations became super saturated and precipitation occurred on the stainless steel. A precipitation mechanism could be explained using the Fe-Ni phase diagram. When Fe and Ni in sodium began to precipitate on the stainless steel (at 560°C), the sodium temperature was decreasing from 670°C and precipitated particles separated into the  $\alpha$ - and  $\gamma$ -phases. Hence, the composition of the precipitated particles was obtained along the precipitation line of the phase boundary between the  $\alpha$ - and  $\gamma$ -phases. This could also be extended to the Fe-Cr alloy. In the Fe-Cr phase diagram, Fe and Cr did not form a solid solution in the solid region and  $\alpha$ -Fe and  $\alpha'$ -Cr were precipitated separately. Hence, the indirect relationship between Fe and Cr in the particles as shown in Fig.8 would be reasonable. Therefore, precipitated particles were composed of  $\alpha$ -phase Fe and  $\gamma$ -phase reduced Cr. These facts were supported by X-ray diffraction analysis which detected  $\alpha$ - and  $\gamma$ -phases in the particles. On the other hand, the hexagonal plate particle had Cr as their main component. From the ternary phase diagram, the  $\alpha'$ -phase was predicted. The Cr crystal structure is bcc or hcp. The Cr rich particles had the hexagonal plate shapes as shown in Fig.5(b). Hence, the Cr rich particle was identified as probably hcp. However, diffraction lines of hcp were not detected. As the main component for all particles was Fe, the amount of Cr was small, and therefore not enough to obtain the X-ray diffraction lines of hcp Cr.

#### 4.2 Particle size distribution and crystal growth

The globular particle as shown in Fig.5(a) was a single crystal. This particle grew on the (110) and (100) planes<sup>(12),(13)</sup>. The particle was about 3 $\mu$ m in diameter. The SEM observations showed that these particles grew into chain-like groups when the diameter exceeded 3 $\mu$ m.

The average particle size was about 4 $\mu$ m as shown in Fig.6. This value was larger than the critical size of 3 $\mu$ m. It was considered that the average particle size was larger because the particles were clustered. The hexagonal plate particles had a 0.3 $\mu$ m in diameter. This was smaller than for the globular particle and the amount of Cr in the total particle composition was one-twentieth that of iron. Therefore, particle size distribution was not affected by the hexagonal plate particles, it was dependent only on the globular particles having Fe as the primary component.

#### 5. Conclusion

Precipitation experiments for corrosion products released from Type 304 stainless steel have been done in flowing sodium while varying the temperature from 560-670°C. The precipitation mechanism was investigated with the results summarized as follows.

(1) Corrosion products were grouped into three classes: (a) a globular shape, having iron as the main component; (b) a hexagonal plate shape, having chromium as the main component; and (c) an undefined shape having a chemical composition which included reduced chromium from the stainless steel. The compositions of each particle type were located on the precipitation line of the Fe-Cr-Ni ternary phase diagram at 560°C. Hence, the elements iron, chromium and nickel, which were released into the sodium, precipitated, forming particles having chemical compositions along this precipitation line.

(2) Critical size of the globular particles was 3 $\mu$ m. When they grew larger than this, crystal growth occurred on the (110) and (100) planes, and particles became chain-like. Critical size of the hexagonal plate particles was 0.3 $\mu$ m. The particle size distribution of all three classes was expressed by a logarithmico-normal distribution with an average diameter of 4 $\mu$ m and a standard deviation of 2.

#### References

- (1) C.A.Erdman, A.B.Reynolds : Nucl. Safety, 16(1975), p.43.
- (2) W.H.Kuhn : Conf. 760503-P1, (1976), p.280.
- (3) M.H.Cooper, G.R.Taylor : Nucl. Eng. Design, 32(1975), p.246.
- (4) T.H.Thorley : Material Behavior and Physics Chemistry in Liquid Metal, edited by H.U.Borgstedt, Plenum Press, NewYork and London(1980), p.5.
- (5) I.H.Newson, K.T.Claxton, R.W.Dawson, P.Hawtin : 2nd Inter. Conf. on Liquid Metal and Tech., Richiland, Washington, April(1980), 5 session.
- (6) J.R.Weeks, H.S.Issacs : Advanced in Corrosion and Engineering, 3(1972), p.207.

- (7) B.H.Kolster : Corrosion, Transport and Deposition of Stainless Steel in Liquid Sodium : 1st Inter. Conf. on Liquid Metal and Tech., Champion, Pa., May (1976).
- (8) H.Schneider : Material Behavior and Physics Chemistry in Liquid Metal, edited by H.U.Borgstedt, Plenum Press, New York and London(1980), p.71.
- (9) R.Tompson : Material Behavior and Physics Chemistry in Liquid Metal, edited by H.U.Borgstedt, Plenum Press, New York and London(1980), p.455.
- (10) V.G.Rivlin, G.V.Raynor : Int. Met. Rev., 21(1980), p.21.
- (11) M.Hanzen, K.Anderko : McGraw-Hill Book Co., New York(1958), p.686.
- (12) T.Kuroda, R.Lacman : J. Crystal Growth, 56(1982), p.189.
- (13) R.Lacman : N. Jb. Miner. Abh., 122(1974), p.36.

Table 1 Chemical compositions of particles and concentrations of metallic elements in sodium

| Term   | Fe   | Cr   | Ni   | Mn   | Unit |
|--|------|------|------|------|------|
| Particles deposited on<br>Type 304 stainless steel     | 96.6 | 0.05 | 3.3  | 0.05 | wt%  |
| Particles deposited on<br>the lower part of heater pin | 86.3 | 4.3  | 6.9  | 2.3  | wt%  |
| Type 304 stainless steel before<br>immersion           | 71.8 | 18.3 | 8.6  | 1.3  | wt%  |
| Metallic elements in sodium                            | 1.28 | 0.18 | 0.41 | 0.02 | ppm  |

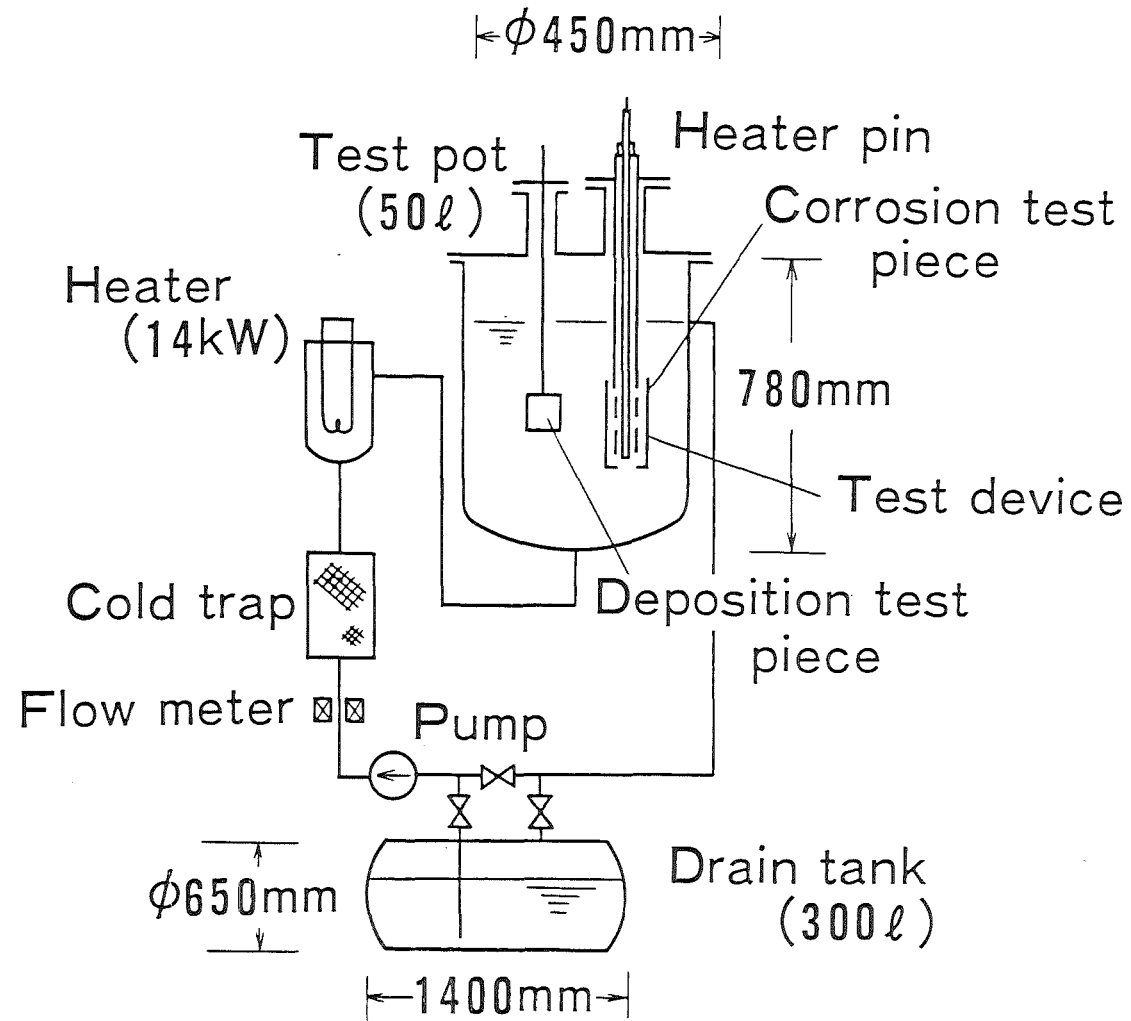


Fig. 1 Sodium loop

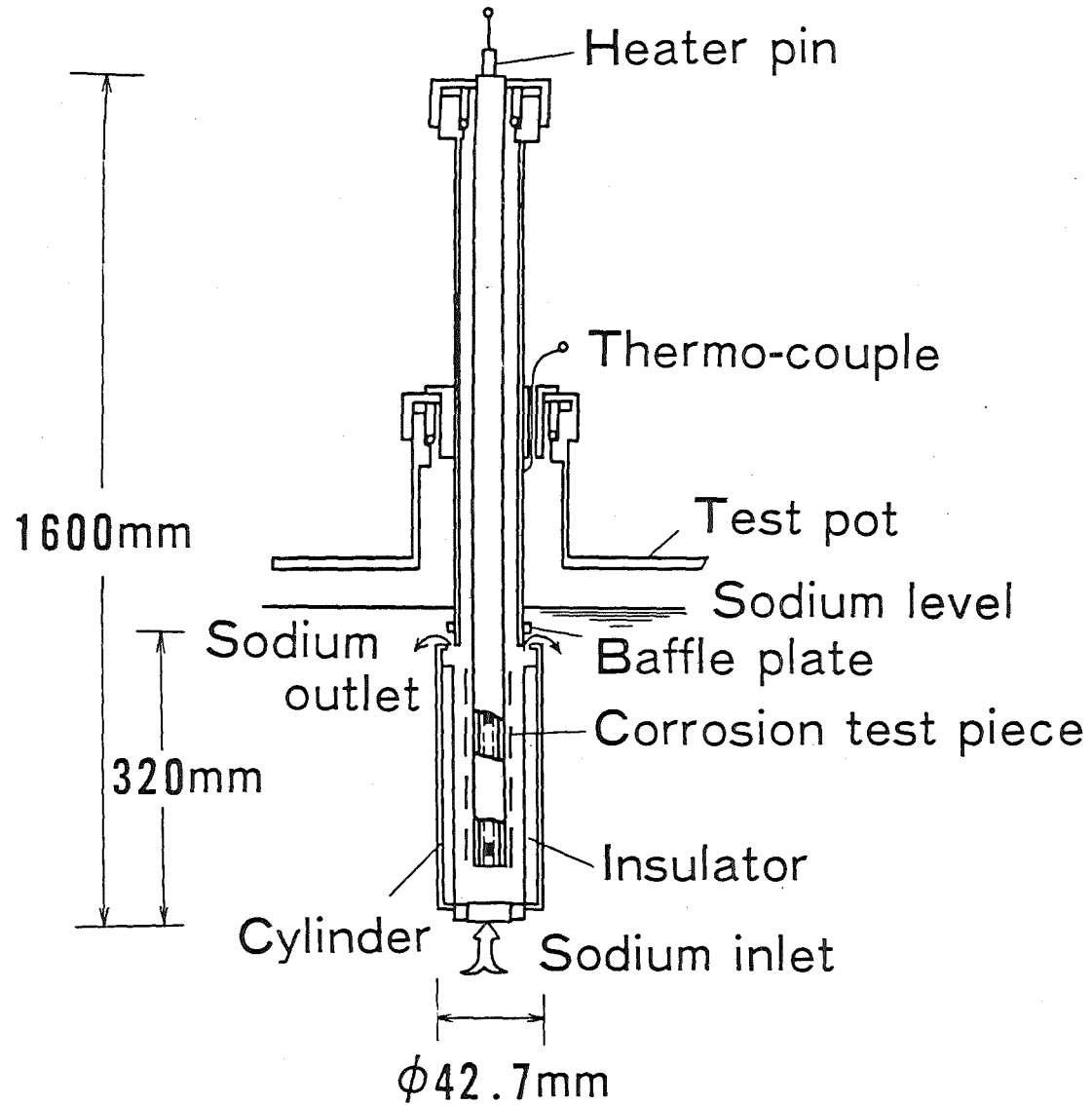


Fig. 2 Test device

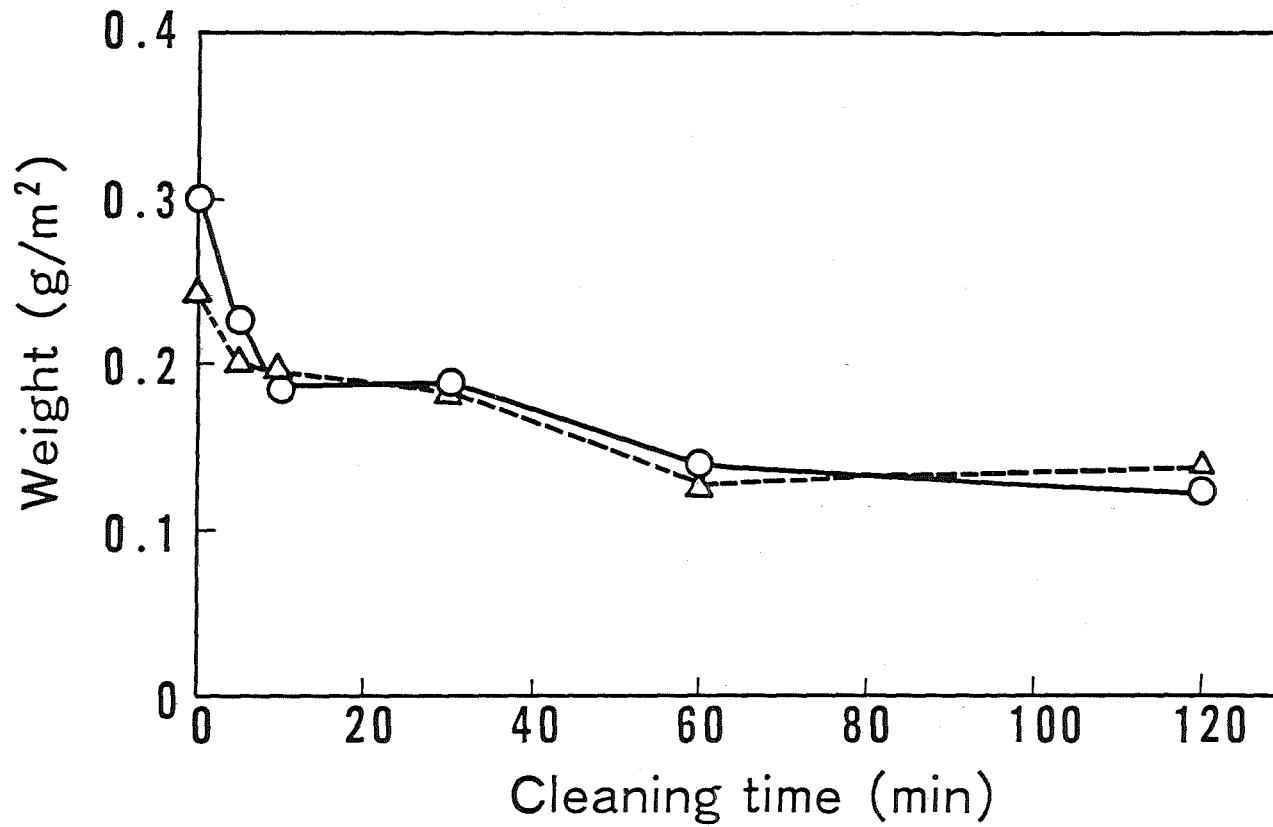


Fig. 3 Weight change of Type 304 stainless steel test pieces with cleaning time in an ultrasonic vibrator

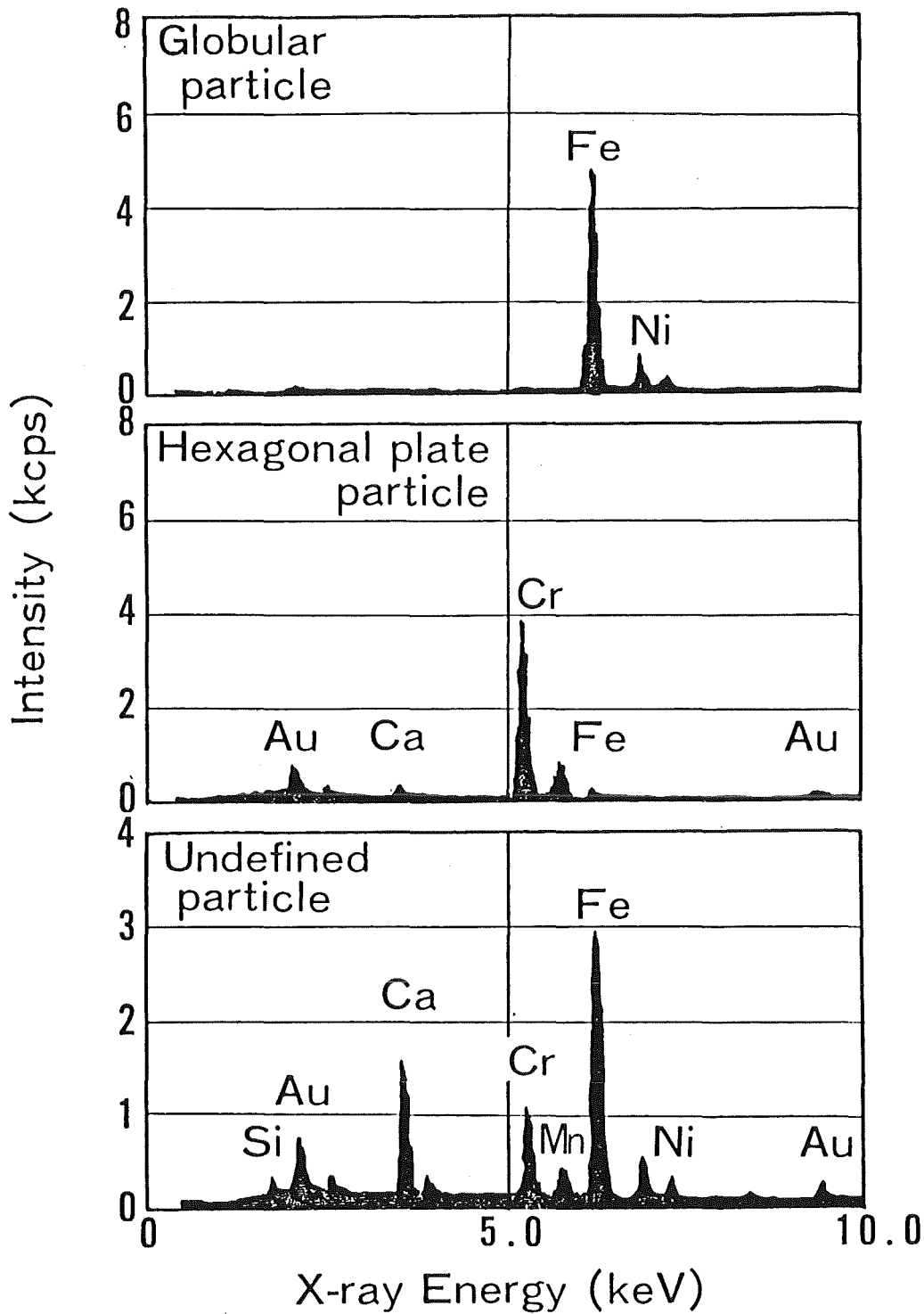
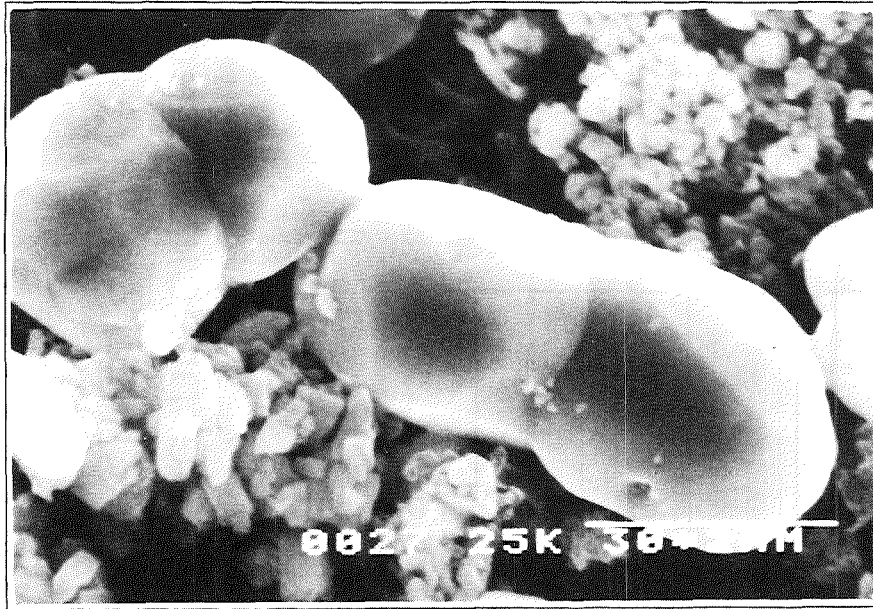
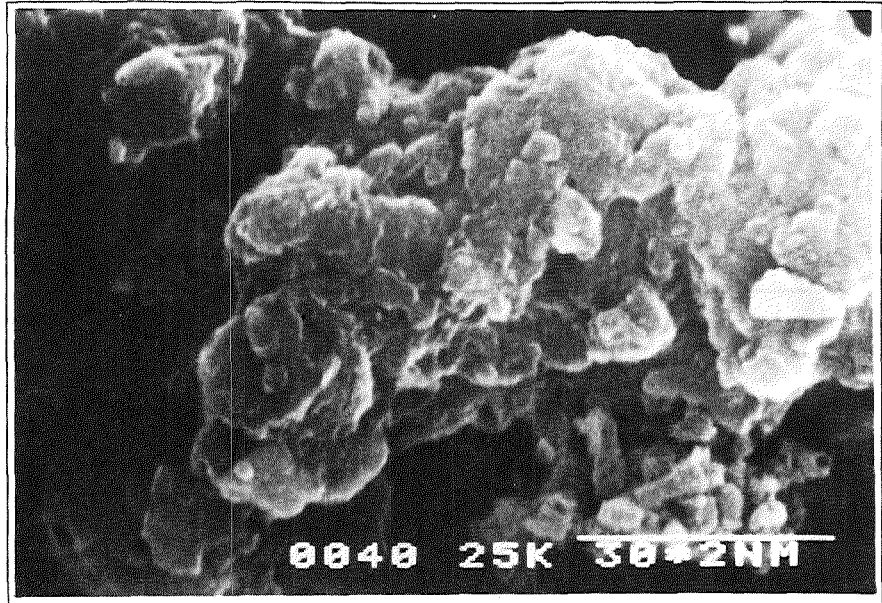


Fig. 4 Compositions of particle precipitated on Type 304 stainless steel surface

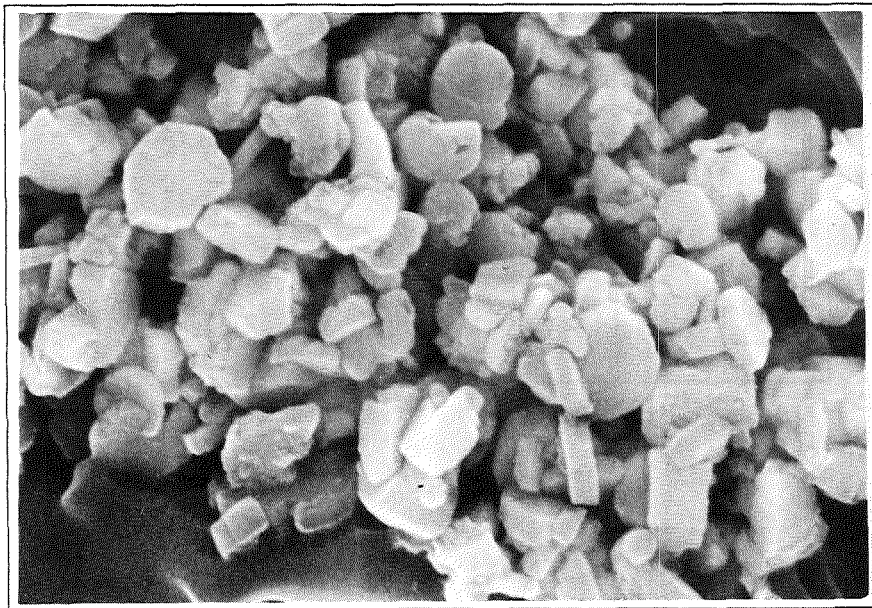




(a) Globular shape  $3 \mu\text{m}$



(c) Undefined shape  $3 \mu\text{m}$



(b) Hexagonal plate shape  $1.5 \mu\text{m}$

Fig.5 Characteristic shapes of precipitated particles

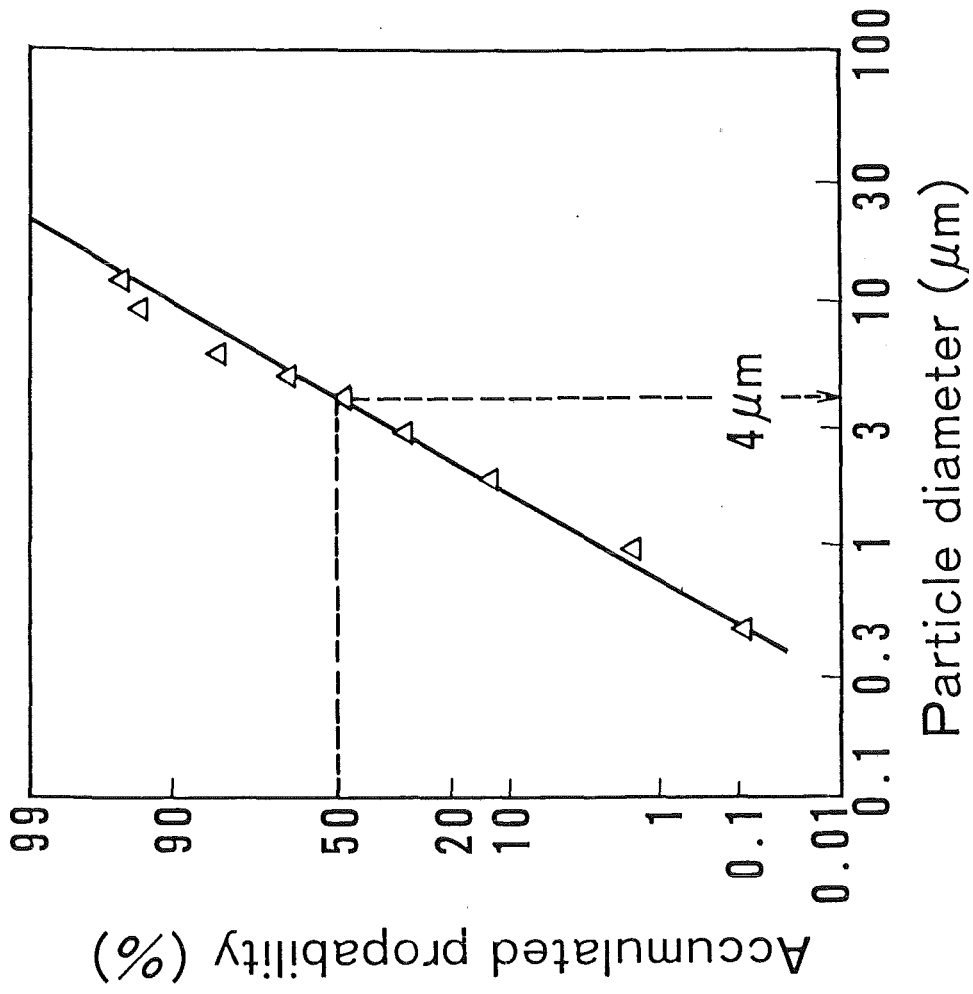


Fig. 6 Particle size distribution

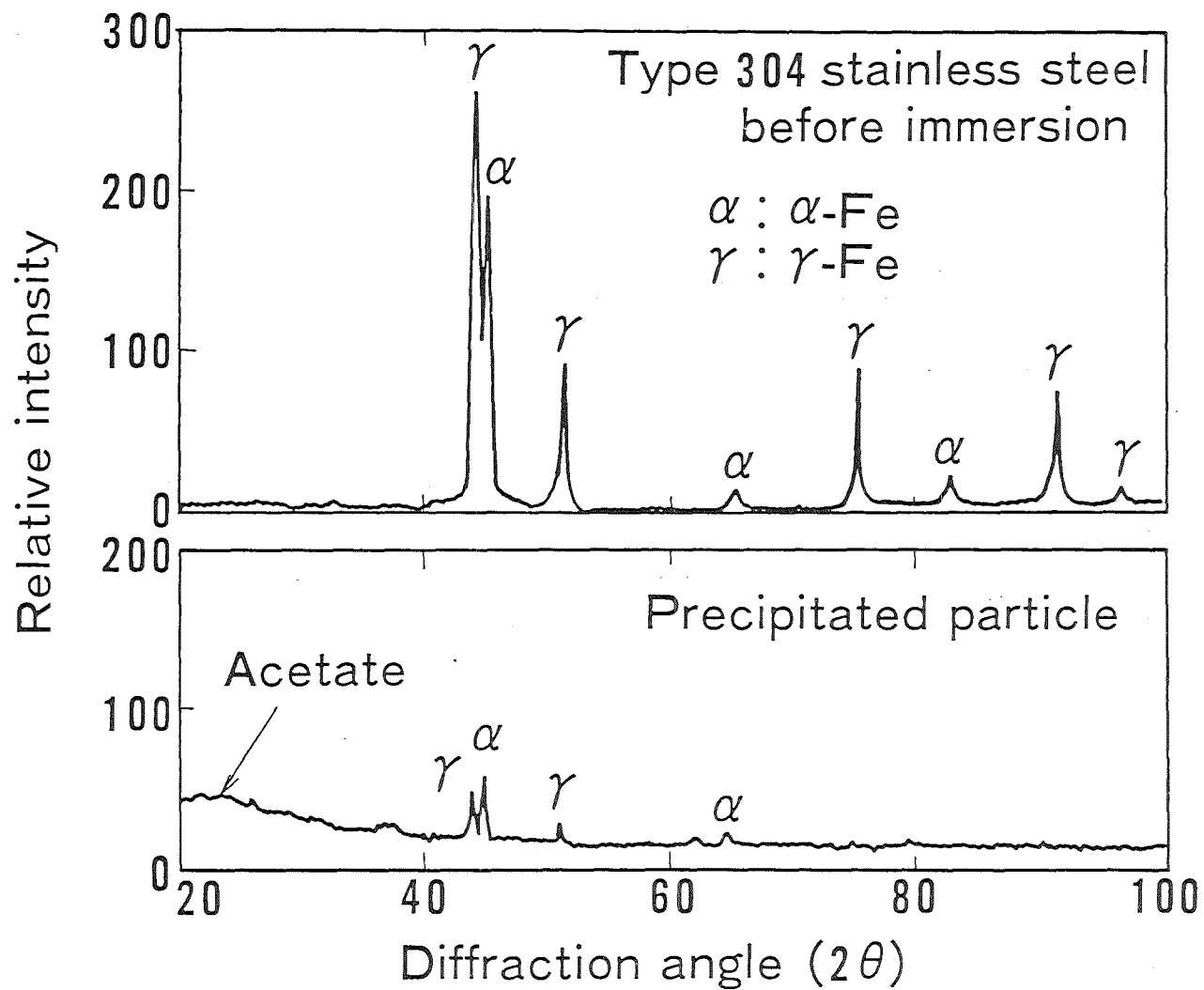


Fig. 7 Crystal structure analysis of precipitated particle and Type 304 stainless steel by X-ray diffraction

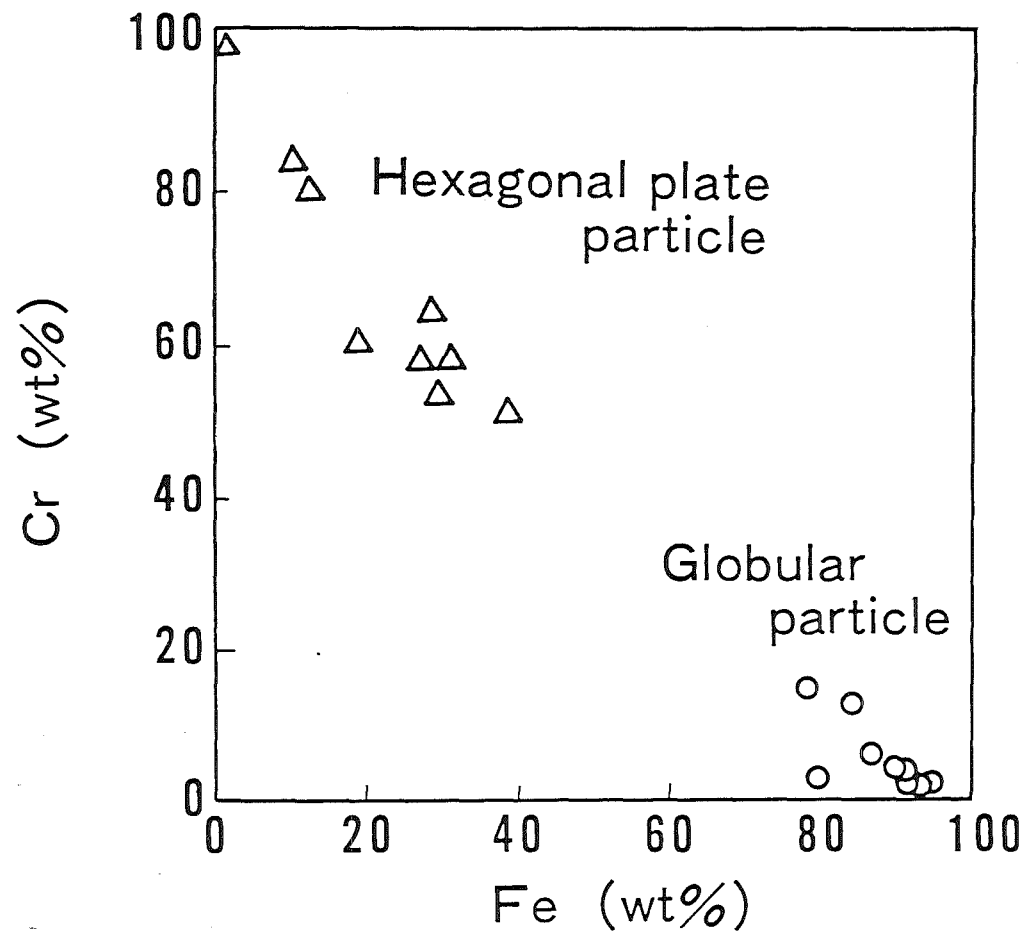


Fig. 8 Correlation between Fe and Cr weight percents in precipitated particles

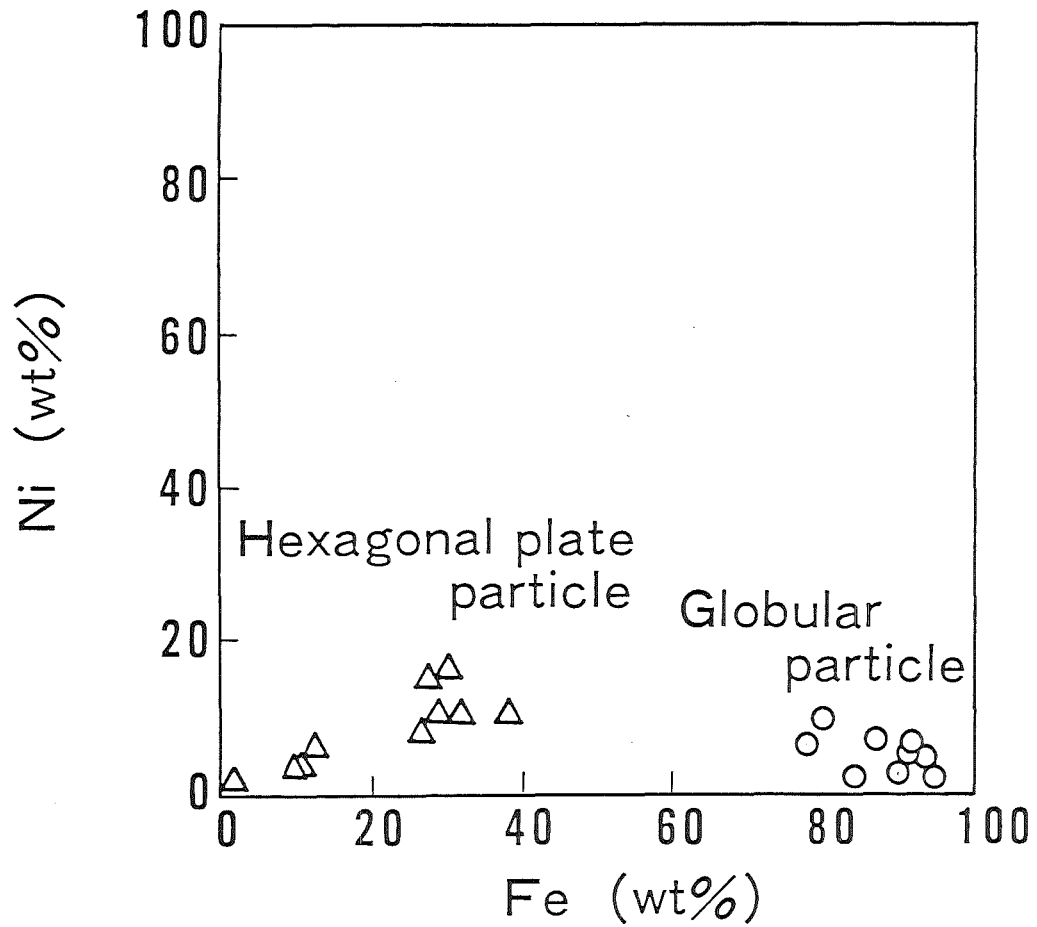


Fig. 9 Correlation between Fe and Ni weight percents in precipitated particles

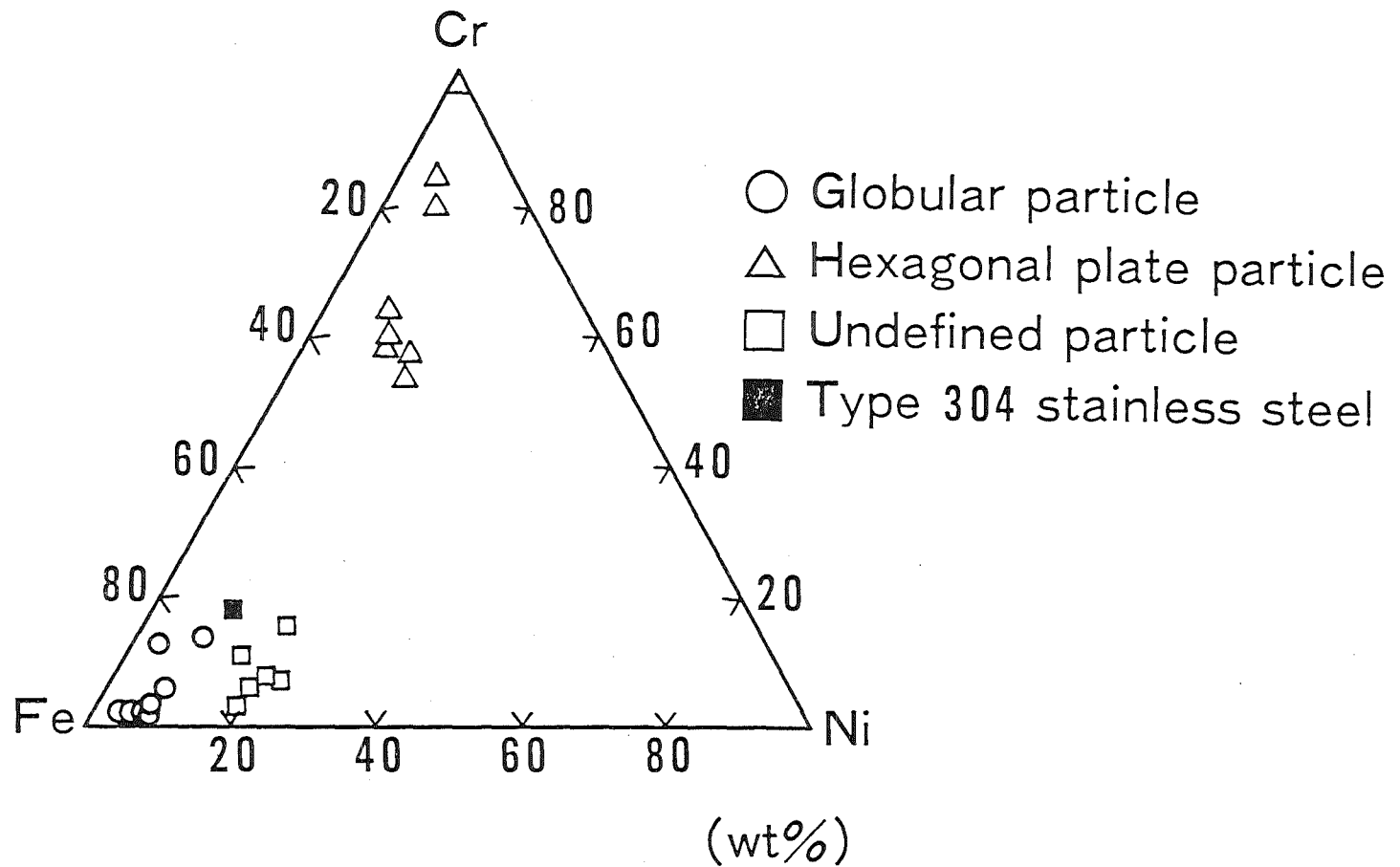


Fig. 10 Plot of chemical composition of precipitated particle in Fe-Cr-Ni ternary phase diagram

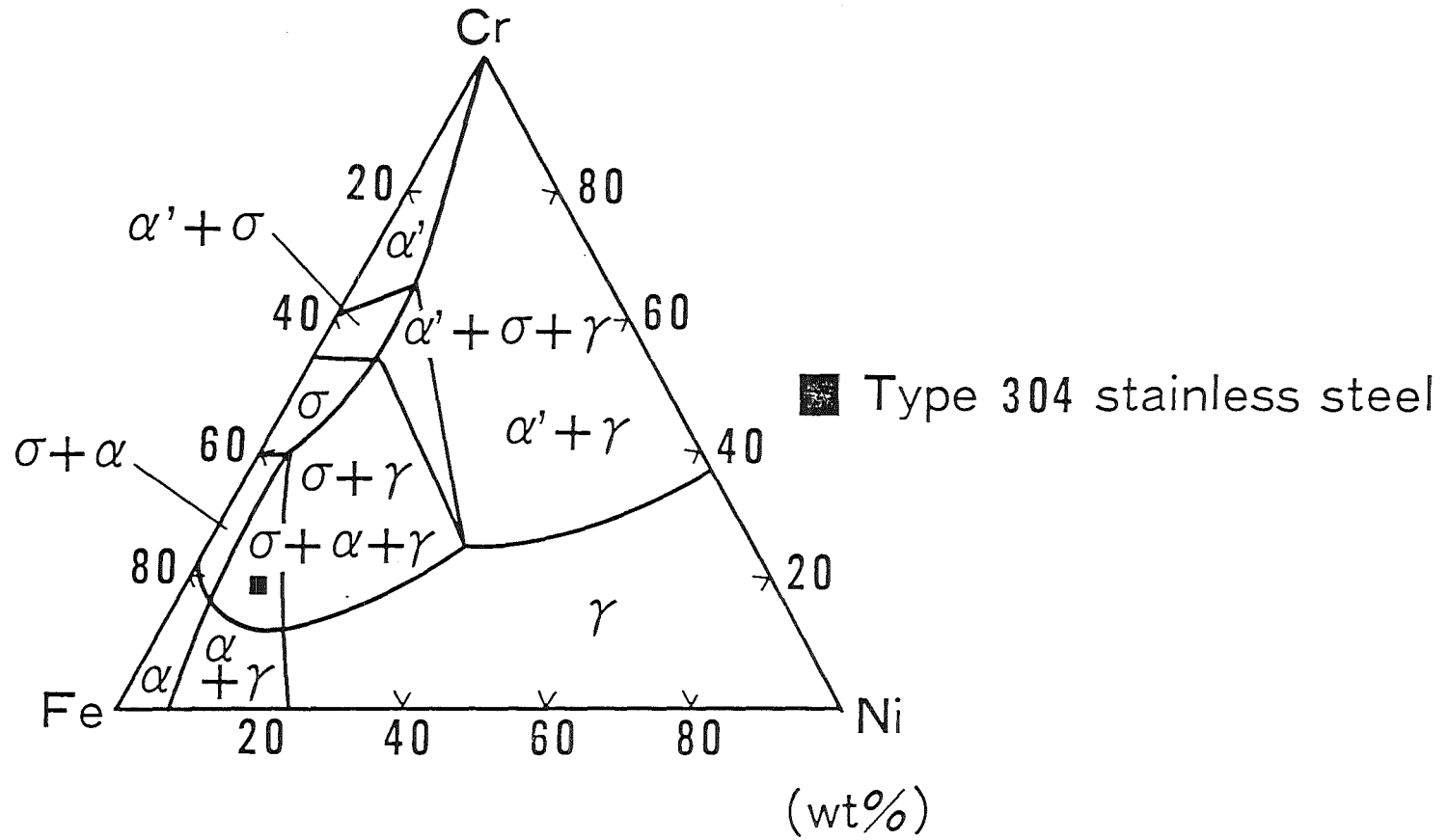


Fig. 11 Cross-section phase diagram of Fe-Cr-Ni ternary system at 560°C

- Globular particle
- △ Hexagonal plate particle
- Undefined particle
- Type 304 stainless steel

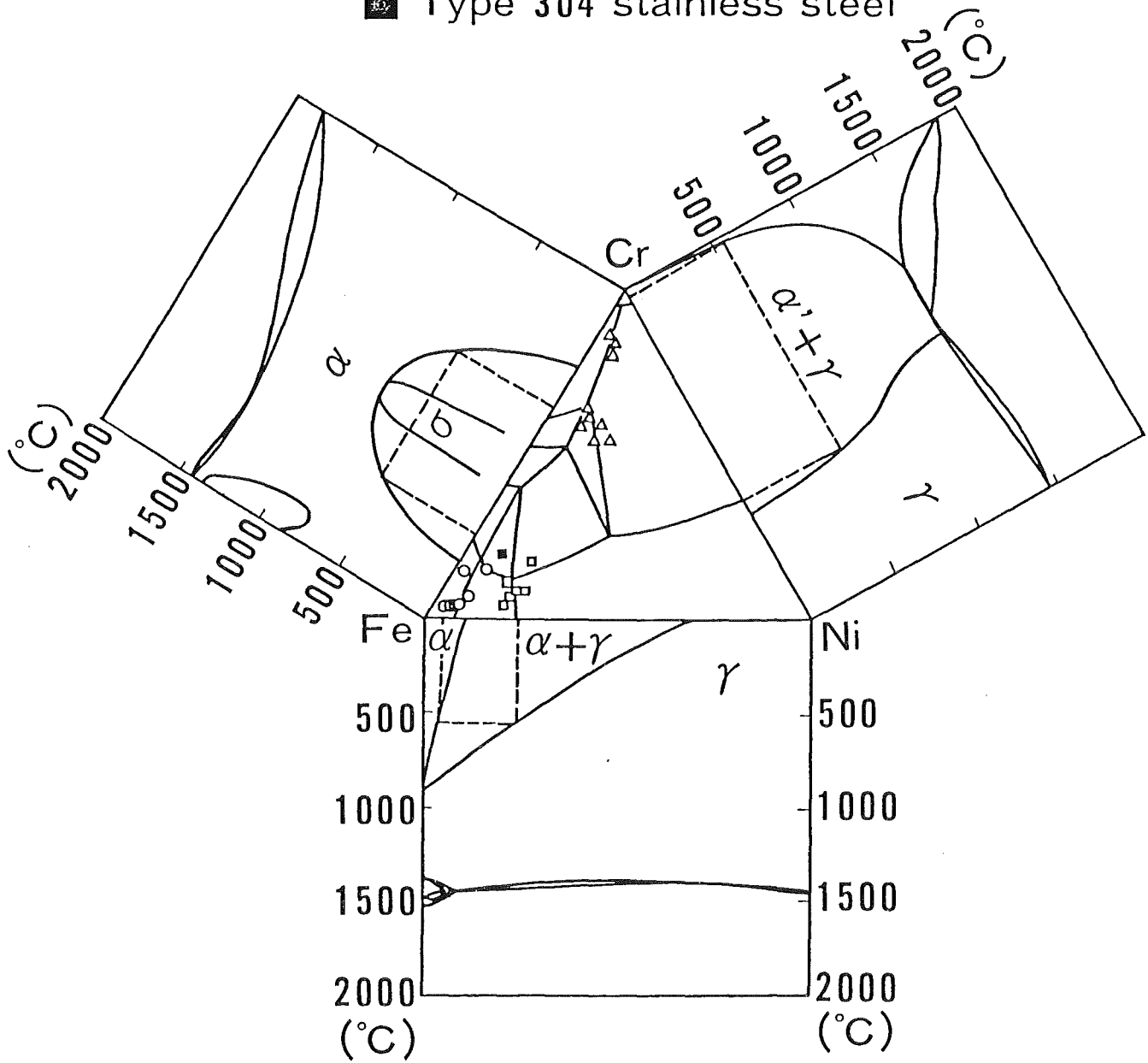


Fig. 12 Precipitation mechanism in Fe-Cr-Ni ternary system